Epigenetic profiling of mouse and human vascular smooth muscle cells, S100β resident vascular stem cells and their lineage-specific progeny *in vitro*

Yusof Shukri Y Gusti, MSc

Under the supervision of Professor Paul A. Cahill

School of Biotechnology

Dublin City University

A thesis submitted for the degree of Doctor of Philosophy

2023

Declaration

I hereby certify that this material, which I now submit for assessment on the programme of study leading to the award of PhD is entirely my own work, and that I have exercised reasonable care to ensure that the work is original, and does not to the best of my knowledge breach any law of copyright, and has not been taken from the work of others save and to the extent that such work has been cited and acknowledged within the text of my work

Name: Yusof Shukri Y Gusti

Student ID No: 17210340

Signed:

Date: 24 -10-2022

Dedication

I dedicate this thesis to my Dad, Shukri Gusti and Mom, Najla Abuzabibah who always showed us (not only me) immense patience, love and support, throughout the trials and tribulations of my studies and provided me and my siblings with what is needed to be educated and successful in life the way we are now.

Acknowledgements

First and foremost, I would like to express my gratitude to Professor Paul Cahill for the opportunity to work in his lab and under his supervision and carry out this work. I would also like to acknowledge him for going above and beyond the call of any supervisor in providing constant encouragement and support throughout this whole process. Next, I would like to thank the members of the VBT lab past and present. In particular, Dr Roya Hakimjavadi, Dr Abidemi Olayinka and Dr Mariana Di Luca for teaching me almost everything I know. To my colleagues Eoin Corcoran, Denise Burtenshaw, Susan Harman, Muhayla Alanazi, Dr Imen Gdara and Dr Michael Kitching. A special and huge thank you to Dr Emma Finlay who helped me a lot in the last chapter of results and guided me through bioinformatics from A to Z.

To the unsung heroes of the School of Biotechnology, the technical staff, I cannot thank you enough for all of the times you bailed me out of seemingly impossible situations. No problem was ever too large that you couldn't fix and every one of you went above and beyond to make life easier for me and all of the other postgrads in the School. Graham, Monica, Deirdre, David, Janice, Teresa, Kasia, Allison and Carmen, my experience over the last five years would have been a lot less enjoyable without your help and generosity.

Finally, I would like to thank my parents again, for working so hard their whole lives to provide me with the opportunity to pursue my education. To my grandmother Faiga Abbas Shitaiwi and to my siblings, Mohammed, Maarib, Badr, Baraa, and Abdulrahman.

Publications and Presentations

Publications

Di Luca M, Fitzpatrick E, Burtenshaw D, Liu W, Helt JC, Hakimjavadi R, Corcoran E, **Gusti Y**, Sheridan D, Harman S, Lally C, Redmond EM, Cahill PA. The calcium binding protein S100β marks hedgehog-responsive resident vascular stem cells within vascular lesions.

NPJ Regen Med. 2021 Mar 1;6(1):10. doi: 10.1038/s41536-021-00120-8. PMID: 33649337; PMCID: PMC7921434.

https://www.nature.com/articles/s41536-021-00120-8

Molony C, King D, Di Luca M, Kitching M, Olayinka A, Hakimjavadi R, Julius LAN, Fitzpatrick E, **Gusti Y**, Burtenshaw D, Healy K, Finlay EK, Kernan D, Llobera A, Liu W, Morrow D, Redmond EM, Ducrée J, Cahill PA. Disease-Relevant Single Cell Photonic Signatures Identify S100β Stem Cells and their Myogenic Progeny in Vascular Lesions.

Stem Cell Rev Rep. 2021 Oct;17(5):1713-1740. doi: 10.1007/s12015-021-10125-x. Epub 2021 Mar 17. PMID: 33730327; PMCID: PMC8446106.

https://link.springer.com/article/10.1007/s12015-021-10125-x

Oral Presentations

A comparison of the epigenetic profile of reprogrammed vascular smooth muscle cells versus stem cell-derived myogenic progeny *in vitro*, 10th Annual SoBT Research, January 2018, Dublin, Ireland.

A comparison of the epigenetic profile of reprogrammed vascular smooth muscle cells versus stem cell-derived myogenic progeny *in vitro*, 12th Annual SoBT Research, January 2021, Dublin, Ireland.

Multimedia video

A comparison of the epigenetic profile of reprogrammed vascular smooth muscle cells versus stem cell-derived myogenic progeny *in vitro*, 11th Annual SoBT Research, January 2019, Dublin, Ireland

Epigenetic profiling of mouse and human vascular smooth muscle cells, S100β resident vascular stem cells and their lineage-specific progeny *in vitro*

Yusof Shukri Y Gusti

Lay Summary:

Epigenetics is the study of the changes that occur in cells caused by the modification of the way the gene expresses itself rather than alteration of the genetic code itself. Despite the same DNA, every cell does not express each gene equally and this can result in different cells with very different functions. Epigenetic alterations are known to play a key role in many disease processes, including diseases of the artery. While there have been extensive studies performed on the epigenetic changes that occur in cells typical of diseased arteries when exposed to stimuli that promote arterial disease, there has been very little information on how arterial stem cells with the vessel wall respond to the same stimuli.

This project investigated the key epigenetic changes that occur in arterial smooth muscle cells and arterial stem cells that have been subjected to the same stimuli that promote arterial disease. The results of this project suggest that similar epigenetic alterations on key genes associated with arterial disease are also present when stem cells are subjected to stimuli that promote arterial disease. These data provide clues about the origin of cells with disease arteries that in the future will enable the development of drugs that target these changes or help identify patients who are at a high risk of developing arterial disease.

Abstract:

DNA methylation/demethylation and histone modifications represent classic interdependent epigenetic mechanisms controlling gene expression. Di-methylation of lysine 4 on histone 3 (H3K4me2) imprinting and DNA demethylase Tet methylcytosine dioxygenase- 2 (Tet-2) binding at lineage-specific gene loci has been proposed as the central epigenetic mechanisms controlling retention of lineage identity and cellular memory of vascular smooth muscle cells (SMCs) during SMC de-differentiation. This study aimed to assess whether similar histone modifications and Tet-2 binding occur at SMC loci in both stem cell-derived SMC-like cells (myogenic progeny) and non-SMCs (adipogenic, osteogenic and vasculogenic progeny) typical of arteriosclerotic lesions. Using mouse and human S100β stem cells exposed to atherogenic stimuli *in vitro,* Tet-2 binding and histone modifications were assessed using quantitative single gene ChIP-PCR assays, genome-wide bulk ChIP-seq analysis, *in-silico* bulk ChIP-seq analysis qRT-PCR mRNA analysis.

Single gene ChIP-PCR analysis revealed that S100β stem cells enrich for H3K27me3 at the SMC *Myh11* locus but lose this mark and acquire the H3K4me2 mark with increased Tet-2 binding when undergoing myogenic differentiation *in vitro,* concomitant with increased expression of the *Myh11* gene. Tet-2 siRNA knockdown attenuated the enrichment of H3K4me2 in response to atherogenic stimuli and reduced *Myh11* gene expression. Adipogenic and osteogenic progeny, but not vasculogenic, also acquire this mark at the *Myh11* locus without a parallel increase in *Myh11* gene expression. Genome-wide bulk ChIP-seq analysis of H3K4me2 and H3K27me3 marks in human S100β cells revealed a similar profile while parallel

in-silico bulk ChIP-seq analysis of published datasets for H3K4 methylation and H3K27me3 marks confirmed these data.

Collectively, these data suggest the presence of the H3K4me2 mark at the *Myh11* locus is not exclusive to de-differentiation of medial SMCs and may reflect the overall 'commitment status' of these cells and ultimately dictate their capacity to proceed and be fully determined and fated down specific lineages.

Table of Contents

Publications and Presentations ..... *v*

Abstract ..... *vi*

List of Figures ..... *xiii*

List of Tables ..... *xxi*

Abbreviations ..... *xxiv*

Units ..... *xxxii*

Chapter 1 ..... *1*

Introduction *1*

1.1 Cardiovascular disease **2**

1.2 Vascular structure **3**

1.2.1 Artery 3

1.2.1.1 The tunica intima 3

1.2.1.2 The Tunica Media 4

1.2.1.3 The Tunica Adventitia 4

1.3 Atherosclerosis **5**

1.4 Subclinical atherosclerosis **7**

1.5 Model Systems for Investigating Subclinical Atherosclerosis **8**

1.5.1 Rodent models 8

1.5.2 Induced Pluripotent Stem Cells (iPSCs) 8

1.5.3 Multipotent Resident Vascular Stem cell 10

1.5.4 Vascular Smooth Muscle cells (SMCs) 10

1.5.5 Adventitial cells 11

1.5.6 Endothelial cells 12

1.6 Current therapies for cardiovascular disease **13**

1.6.1 Surgical Interventions 13

1.6.1.1 Balloon angioplasty 13

1.6.1.2 In-stent restenosis (ISR) 13

1.7 Origin of Neointimal Cells **14**

1.7.1 De-differentiation and reprogrammed SMCs 14

1.7.2 Bone marrow-derived Stem Cells 16

1.7.3 Endothelial cells 16

1.7.4 Resident multipotent vascular stem cells (mVSCs) 16

1.8 Myogenic differentiation **18**

1.9. Phenotypic characteristics of differentiated smooth muscle cells **19**

1.9.1 Transforming Growth Factor-β (TGF-β) signalling pathways 20

1.9.2 TGF-β signalling control of smooth muscle cell differentiation 22

1.9.3 Platelet-derived Growth Factor (PDGF) Signalling 24

1.9.4 PDGF signalling control of smooth muscle cell differentiation 24

1.9.5 Notch signalling pathway 25

1.9.6 Notch signalling control of smooth muscle cell differentiation 27

1.10 Lineage tracing analysis of lesional cells **28**

1.11 Epigenetics **30**

1.11.1 What is Epigenetics? 30

1.11.2 Histone modifications 32
1.11.3 DNA methylation 33
1.11.4 DNA demethylation 34
1.12 The role of histones in differentiated SMCs **34**
1.13 Epigenetic changes during SMC differentiation/de-differentiation **36**
1.14 Epigenetics in stem cells **42**
1.15 DNA methylation and DNA demethylation interaction **42**
1.16 Detection of histone modifications at specific gene loci **44**
1.16.1 Chromatin Immunoprecipitation (ChIP) assay 44
1.16.2 Chromatin immunoprecipitation sequencing (ChIP-Seq) 45
1.16.3 Cleavage under targets and release under nuclease (CUT&RUN) 47
1.16.4 Cleavage under targets and tagmentation (CUT&TAG) 48
1.16.5 ChIP-ChIP 49
1.16.6 The proximity ligation assay (PLA) *in situ* 51
1.17 hypothesis and thesis objectives **51**
Chapter 2 ..... ***56***
Materials and Methods ***56***
2.1 Materials **57**
2.1.1 Primers 57
2.1.1.1 QIAGEN primers 57
2.1.1.2 IDT primers 58
2.1.2 Chemical and Biological agents 58
2.1.3 Antibodies 60
2.1.4 Tissue Culture 62
2.1.4.1 Cell lines 62
2.1.4.2 Growth medium 63
2.1.4.2.1 MOVAS maintenance medium 63
2.1.4.2.2 S100β mVSC maintenance medium 64
2.1.4.2.3 Mouse S100β mVSCs Differentiation medium 64
2.1.4.2.4 S100β SNEP Maintenance medium 66
2.1.4.2.5 Human S100β SNEPs Differentiation media 66
2.2 Methods **68**
2.2.1 Cell culture 68
2.2.1.1 Mouse Aortic Smooth Muscle Cells (MOVAS) 68
2.2.1.2 Isolation and culture of mouse vascular stem cells (vSCs) by explant and sequential seeding following enzymatic dispersion 68
2.2.1.3 Mouse embryonic stem cells (mESC) 72
2.2.1.4 Mouse Aorta 72
2.2.1.5 Human-induced pluripotent stem cells (HiPSCs) 73
2.2.1.6 Generation of HiPSCs-derived NE progenitors (SNEP) 73
2.2.1.7 Human iPSC-derived smooth muscle cells (hSMC) 74
2.2.1.8 Cell Culture Methods 75
2.2.1.9 Cell Subculture and Expansion 75
2.2.1.10 Cryopreservation 75
2.2.1.11 Viable Cell Counting 76
2.2.2 Differentiation 76
2.2.2.1 Myogenic differentiation 76
2.2.2.1.1 Myogenic differentiation of S100β mVSC 76
2.2.2.1.2 Myogenic differentiation of S100β SNEP 77
2.2.2.2 Vasculogenic Differentiation 77
2.2.2.2.1 Vasculogenic Differentiation of S100β mVSC 77

2.2.2.2.2 Vasculogenic Differentiation of S100β SNEP 78
2.2.2.3 Adipogenesis Differentiation 78
2.2.2.3.1 Adipogenesis Differentiation of S100β mVSC 78
2.2.2.3.2 Adipogenesis Differentiation of S100β SNEP 78
2.2.2.4 Osteogenesis Differentiation 79
2.2.2.4.1 Osteogenesis Differentiation of S100β mVSC 79
2.2.2.4.2 Osteogenesis Differentiation of S100β SNEP 79
2.2.3 Transient Transfections 80
2.2.3.1 Short interfering (siRNA) transfection 80
2.2.4 Chromatin immunoprecipitation (ChIP) followed by polymerase chain reaction (PCR) – (ChiP-PCR) 81
2.2.4.1 Chromatin Extraction 81
2.2.4.2 Chromatin Immunoprecipitation (ChIP) 83
2.2.4.3 Real-Time Polymerase Chain Reaction (RT-PCR) 85
2.2.4.4 ChIP fold enrichment normalization 86
2.2.5 Total RNA Extraction from tissue and cultured cell samples. 86
2.2.6 DNA Isolation 87
2.2.7 Quantitation of Nucleic Acid Concentration 87
2.2.9 Real-Time One-Step RT-PCR by QIAGEN 89
2.2.9.1 Relative expression ratio analysis by the REST© tool 92
2.2.10 Immunocytochemistry (ICC) 93
2.2.11 Protein Manipulation 95
2.2.11.1 Protein Storage 95
2.2.11.2 Whole Protein Lysate Extraction 95
2.2.11.3 Preparation of protein from adherent cells samples 95
2.2.11.4 Bicinchoninic acid Protein Assay 95
2.2.11.5 Western blot 96
2.2.12 Running the DNA on 1.5% Agarose gel 98
2.2.13 Oil Red O Dye 99
2.2.14 Alizarin Red S Dye 100
2.2.15 chromatin immunoprecipitation sequencing (ChIP-seq) analysis 101
2.2.15.1 In Silico ChIP-seq 101
2.2.15.2 Human SNEP ChIP-seq 106
2.2.15.2.1 Data quality control 109
2.2.15.2.2 Mapping 111
2.2.15.2.3 Fragment size prediction 113
2.2.15.2.4 Strand cross-correlation (SCC) 113
2.2.15.2.5 Peak Calling 113
2.16 Data Analysis and statistics 114

Chapter 3 116

The level of enrichment of H3K4me2, H3K27me3 and Tet-2 binding at the Myh11 locus in de-differentiated murine vascular smooth muscle cells, resident S100β vascular stem cells and their myogenic progeny in vitro 116

3.1 Introduction: 117

3.2 Strategy 121

3.3 Results 123
3.3.1 De-differentiated mouse aortic SMCs retain the H3K4me2 mark at the *Myh11* locus *in vitro* but it is dramatically reduced compared to differentiated aortic SMCs *in vitro* 123
3.3.2 Mouse mVSCs and MOVAS SMCs express key phenotypic markers 128
3.3.3 Atherogenic stimuli (PDGF-BB, TGF-β1 and Jagged1) differentially regulate H3K4me2 enrichment at the *Myh11* locus concomitant with changes to *Myh11* mRNA levels in mouse de-differentiated SMCs 131

3.3.4 Atherogenic stimuli (PDGF-BB, TGF-β1 and Jagged1) enhance the enrichment of H3K4me2 at the *Myh11* locus and increase *Myh11* mRNA levels in resident mouse S100β mVSCs *in vitro.* 137
3.3.5 Stem cell maintenance media failed to change the H3K4me2 and H3K27me3 mark at the *Myh11* locus or *Myh11* mRNA levels in murine de-differentiated SMCs *in vitro.* 143
3.3.6 The DNA demethylase, Tet-2 regulates H3K4me2 and H3K27me3 enrichment at *Myh11* locus and *Myh11* mRNA levels in de-differentiated aortic SMCs and resident S100β mVSCs *in vitro* 150

3.4 Discussion 169

Chapter 4 185

The level of enrichment of H3K4me2, H3K27me3 and Tet-2 binding at the Myh11 locus in mouse and human S100β mVSCs following myogenic, osteogenic, adipogenic and vasculogenic differentiation in vitro 185

4.1 Introduction 186

4.2 Strategy 190

4.3 Results 191
4.3.1 Adipogenic and osteogenic progeny acquire the H3K4me2 mark at the *Myh11* locus independent of any change in *Myh11* mRNA levels in resident mouse S100β mVSCs *in vitro.* 191
4.3.1.1 Summary: 206
4.3.2 Adipogenic and osteogenic differentiation acquire the H3K4me2 mark at the *Myh11* locus independent of any change in *Myh11* mRNA levels in human iPSC derived S100β SNEP *in vitro.* 206
4.3.2.1 Summary 222

4.4 Discussion 223

Chapter 5 232

Genome-wide bulk ChIP-seq analysis of histone methylation in undifferentiated stem cells before and after myogenic, adipogenic, osteogenic and vasculogenic differentiation 232

5.1 Introduction: 233

5.2 Strategy 237
5.2.1 *In-silico* ChIP-seq analysis of H3K4 methylation histone marks at SMC-specific gene loci from published data in undifferentiated murine and human MSCs and hESCs and their respective myogenic, adipogenic, osteogenic and vasculogenic progeny. 237
5.2.2 Bulk ChIP-seq analysis of H3K4me2 histone marks at the *MYH11* gene locus in undifferentiated hiPSC-derived S100β SNEPs and their myogenic, adipogenic, osteogenic and vasculogenic progeny *in vitro.* 238

5.3 Results 238
5.3.1 *In-silico* genome-wide bulk ChIP-seq analysis confirms the enrichment for H3K4 methylation at the SMC gene loci following myogenic, osteogenic and adipogenic differentiation of mouse MSC *in vitro.* 238
5.3.2 *In-silico* genome-wide bulk ChIP-seq analysis reveals the enrichment for H3K4 methylation at the SMC gene loci following myogenic, osteogenic and adipogenic differentiation of human MSC and human embryonic stem cells (H9 ESCs) *in vitro.* 255
5.3.3 Bulk ChIP-seq analysis reveals the acquisition of the H3K4me2 mark at the *MYH11* locus following myogenic, osteogenic and adipogenic differentiation of hiPSC-derived S100β SNEPs *in vitro.* 271

5.4 Discussion 278

Chapter 6 286

General Discussion 286

6.1. De-differentiated murine vascular SMC-like cells typical of vascular lesions retain the H3K4me2 mark at the *Myh11* locus.....290

6.2. Murine resident vascular S100β mVSCs and spontaneous S100β human iPSC-derived neuroectoderm progenitor stem cells (SNEPs) acquire the H3K4me2 mark at the *Myh11* locus following myogenic differentiation into SMC-like cells typical of vascular lesions. 294

6.3. Murine resident vascular S100β mVSCs and spontaneous S100β human iPSC-derived neuroectoderm progenitor stem cells (SNEPs) acquire the H3K4me2 mark at the *Myh11* locus following adipogenic and osteogenic differentiation into non-SMC-like cells typical of vascular lesions. 297

6.4 H3K4 methylation marks at lineage-specific loci may define commitment of multipotent stem cells before cell fate is determined by transcriptional activity 303

6.5 Future work 306

6.6 Conclusions 308

References 310

Appendices 365

List of Figures

Figure 1.1. Composition of an Artery

Figure 1.2. The deposition of Lipids in the vascular wall alters the integrity of the endothelium

Figure 1.3. Atherosclerotic and Arteriosclerotic lesions

Figure 1.4. In-stent Restenosis

Figure 1.5. Myogenic Differentiation of stem cells to smooth muscle-like cells

Figure 1.6. SMAD/TGF-β Signalling Pathway

Figure 1.7. Notch Signalling Pathway

Figure 1.8. Principal epigenetic mechanisms of gene expression regulation

Figure 1.9. DNA methylation is usually associated with inactive transcription and suppressed gene expression

Figure 1.10. Cartoon depicting epigenetic changes in mature SMCs

Figure 1.11. H3K4me2 interacts with TET2 and mediates TET-dependent gene activation.

Figure 1.12. The chromatin immunoprecipitation (ChIP) assay

Figure 1.13. A comparison between ChIP-seq, CUT&RUN and CUT&TAG assays

Figure 2.1. Adventitial removal

Figure 2.2. Tissue pieces on a CellStart pre-coated 6-well plate

Figure 2.3. Schematic illustration of the seeding step on a CellStart pre-coated 6-well plate after cell enzymatic dissociation

Figure 2.4. Schematic illustration of the seeding steps of the modified enzymatic dispersion protocol

Figure 2.5. siRNA Transfection efficiency by Eoin Corcoran

Figure 2.6. qRT-PCR

Figure 2.7. Isolated rfmVSC3T cells in maintenance media type 1 positively stained for S100β and Nestin proteins, astrocyte, and neuroectoderm markers, respectively by Mariana Di Luca

Figure 2.8. Western Blot. Relative protein expression levels were measured using Western Blot

Figure 2.9. Positive Oil Red O on MSC-derived adipocyte under phase contrast by Eimear Kennedy

Figure 2.10. Positive Alizarin Red S on MSC-derived osteocyte under phase contrast by Eimear Kennedy

Figure 2.11. FastQC report on Galaxy

Figure 2.12. MACS predicted tool

Figure 2.13. MACS2 call peak showing chromosome number start and end of a peak with a Peak score**.**

Figure 2.14. The work flow which was done by Novogene Company Ltd

Figure 2.15. Library construction done by Novogene Company Ltd

Figure 2.16. Sequencing done by Novogene Company Ltd

Figure 2.17. Bioinformatic analysis done by Novogene Company Ltd

Figure 2.18. Quality control of the clean reads after trimming

Figure 3.1. The level of enrichment of H3K4me2 at the *Myh11* locus in aortic tissue, MOVAS SMCs and mESCs

Figure 3.2. The level of enrichment of H3K27me3 at the *Myh11* locus in aortic tissue, MOVAS SMCs and mESCs

Figure 3.3. Ratio of H3K4me2/H3K27me3 levels in Aortic tissue, MOVAS and mESCs

Figure 3.4. Relative expression of *Myh11* mRNA levels in fresh Aorta, MOVAS and mESCs

Figure 3.5. Characterisation of S100β mVSCs and MOVAS

Figure 3.6. The level of enrichment of H3K4me2 at the *Myh11* locus in MOVAS SMCs following treatment with Notch ligand, PDGF-BB and TGF-β1

Figure 3.7. The level of enrichment of H3K27me3 at the *Myh11* locus in MOVAS SMCs following treatment with Notch ligand, PDGF-BB and TGF-β1

Figure 3.8. H3K4me2/H3K27me3 ratio at the *Myh11* locus in MOVAS SMCs following treatment with Notch ligand, PDGF-BB and TGF-β1

Figure 3.9. Expression of *Myh11* mRNA in MOVAS SMCs following treatment with Notch ligand, Jag-1, PDGF-BB and TGF-β1

Figure 3.10. The level of enrichment of H3K4me2 at the *Myh11* locus in S100β mVSCs following treatment with Notch ligand, Jag-1, PDGF-BB and TGF-β1

Figure 3.11. The level of enrichment of H3K27me3 at the *Myh11* locus in S100β mVSCs following treatment with Notch ligand, Jag-1, PDGF-BB and TGF-β1

Figure 3.12. H3K4me2/H3K27me3 ratio at the *Myh11* locus in S100β mVSCs following treatment with Notch ligand, Jag-1, PDGF-BB and TGF-β1

Figure 3.13. Expression of *Myh11* mRNA in S100β mVSCs following treatment with Notch ligand, Jag-1, PDGF-BB and TGF-β1

Figure 3.14. The effect of growth media on the morphological characteristics of MOVAS SMCs
Figure 3.15. The effect of growth media on the level of enrichment of H3K4me2 at the *Myh11* locus in MOVAS SMC
Figure 3.16. The effect of growth media on the level of enrichment of H3K27me3 at the *Myh11* locus in MOVAS SMC
Figure 3.17. The effect of growth media on H3K4me2/H3K27me3 ratio at the *Myh11* locus in MOVAS SMC
Figure 3.18. The effect of growth media on mRNA levels of SMC differentiation markers and stem cell markers in MOVAS SMC
Figure 3.19. The effect of Notch ligand, TGF-β1 and PDGF-BB on Tet-2 binding to the *Myh11* locus in MOVAS SMC
Figure 3.20. The effect of Notch ligand, TGF-β1 and PDGF-BB on Tet-2 binding to the *Myh11* locus in S100β mVSCs
Figure 3.21. Transfection Efficiency of siRNA in S100β mVSCs
Figure 3.22. Tet-2 knockdown in MOVAS SMCs compared to scrambled control
Figure 2.23. Tet-2 knockdown in MOVAS SMCs compared to scrambled control
Figure 3.24. The level of enrichment of H3K4me2 at the *Myh11* locus in Tet-2 siRNA treated MOVAS SMCs compared to scrambled control
Figure 3.25. The level of enrichment of H3K27me3 at the *Myh11* locus in Tet-2 siRNA treated MOVAS SMCs compared to scrambled control
Figure 3.26. The combined H3K4me2/H3K27me3 ratio at the *Myh11* locus in MOVAS SMCs following siRNA knockdown of Tet-2 compared to scrambled control
Figure 3.27. Expression of *Myh11* and *Cnn1* mRNA in MOVAS SMC compared to scrambled control
Figure 3.28. Tet-2 knockdown in S100β mVSCs compared to scrambled control before and following treatment
Figure 3.29. The level of enrichment of H3K4me2 at the *Myh11* locus in Tet-2 siRNA control S100β mVSCs compared to scrambled control and treated S100β mVSCs compared to treated scrambled
Figure 3.30. The level of enrichment of H3K27me3 at the Myh11 locus in Tet-2 siRNA control S100β mVSCs compared to scrambled control and treated S100β mVSCs compared to treated scrambled

Figure 3.31. The combined H3K4me2/H3K27me3 ratio at the Myh11 locus in Tet-2 siRNA control mVSCs compared to scrambled control and treated S100β mVSCs compared to treated scrambled

Figure 3.32. Expression of *Myh11* mRNA in S100β mVSC compared to scrambled control before and following treatment

Figure 3.33. Expression of *Cnn1* mRNA in S100β mVSC compared to scrambled control before and following treatment

Figure 4.1. The effect of lineage-specific differentiation media on the morphological characteristics of S100β mVSCs and their derived progeny

Figure 4.2. S100β mVSCs exhibit adipogenic and osteogenic potential

Figure 4.3. Expression of *Myh11* and *Cnn1* mRNA in S100β mVSCs following growth in their maintenance medium (MM1) compared to mVSCs grown in myogenic differentiation medium

Figure 4.4. Expression of *Alpl* and *Sost* mRNA in S100β mVSCs following growth in their maintenance medium (MM1) compared to mVSCs grown in osteogenic differentiation medium

Figure 4.5. Expression of *Lpl* and *Fabp4* mRNA in S100β mVSCs following growth in their maintenance medium (MM1) compared to mVSCs grown in adipogenic differentiation medium

Figure 4.6. The level of enrichment of H3K4me2 at the *Myh11* locus in S100β mVSCs following growth in their inductive medium (MM1) compared to growth in Endothelial cell medium, Myogenic differentiation medium (RPMI), Adipogenesis differentiation medium and Osteogenesis differentiation medium

Figure 4.7. The level of enrichment of H3K27me3 at the *Myh11* locus in S100β mVSCs following growth in their inductive medium (MM1) compared to cells grown in vasculogenic (endothelial), myogenic (muscle), adipogenic (fat) and osteogenic (bone) differentiation medium

Figure 4.8. H3K4me2/H3K27me3 ratio at the *Myh11* locus in S100β mVSCs following growth in their inductive medium (MM1) compared to cells grown in vasculogenic (endothelial), myogenic (muscle), adipogenic (fat) and osteogenic (bone) differentiation medium

Figure 4.9. Tet-2 fold enrichment at the *Myh11* locus in S100β mVSCs following growth in their maintenance medium (MM1) compared to cells grown in vasculogenic (endothelial), myogenic (muscle), adipogenic (fat) and osteogenic (bone) differentiation medium

Figure 4.10. Expression of *Myh11* mRNA in S100β mVSCs following growth in their maintenance medium (MM1) compared to cells grown in vasculogenic (endothelial), myogenic (muscle), adipogenic (fat) and osteogenic (bone) differentiation medium

Figure 4.11. Expression of *Cnn1* mRNA in S100β mVSCs following growth in their maintenance medium (MM1) compared to cells grown in vasculogenic (endothelial), myogenic (muscle), adipogenic (fat) and osteogenic (bone) differentiation medium

Figure 4.12. The effect of myogenic, adipogenic, osteogenic and vasculogenic differentiation media on the morphological characteristics of S100β SNEPs

Figure 4.13. Osteogenic differentiation of S100β SNEPs

Figure 4.14. Adipogenic differentiation of S100β SNEPs

Figure 4.15. Expression of *MYH11* and *CNN1* mRNA in S100β SNEP following myogenic differentiation

Figure 4.16. Expression of *PECAM-1* mRNA in SNEP following vasculogenic differentiation

Figure 4.17. Expression of *ALPL* and *SOST* mRNA in S100β SNEP following osteogenic differentiation

Figure 4.18. Expression of *LPL* and *FABP4* mRNA in S100β SNEP following adipogenic differentiation

Figure 4.19. The level of enrichment of H3K4me2 at the *MYH11* locus in S100β SNEP following myogenic, vasculogenic, adipogenic and osteogenic differentiation

Figure 4.20. The level of enrichment of H3K27me3 at the *MYH11* locus in S100β SNEP following myogenic, vasculogenic, adipogenic and osteogenic differentiation

Figure 4.21. H3K4me2/H3K27me3 ratio at the *MYH11* locus in S100β SNEP following myogenic, vasculogenic, adipogenic and osteogenic differentiation.

Figure 4.22. TET-2 fold enrichment at the *MYH11* locus in S100β SNEP following myogenic, vasculogenic, adipogenic and osteogenic differentiation

Figure 4.23. The expression of *MYH11* mRNA in S100β SNEP following myogenic, vasculogenic, adipogenic and osteogenic differentiation

Figure 4.24. The expression of *CNN1* mRNA in S100β SNEP following myogenic, vasculogenic, adipogenic and osteogenic differentiation

Figure 5.1. ChIP-seq peak calling for H3K27me3 and H3K4me3 at *Myh11, Cnn1, Tagln* and *Smtn g*ene loci in cultured mouse vascular smooth muscle cells (mVSMC)

Figure 5.2. ChIP-seq peak calling for Input and H3K27me3 at the *Myh11, Cnn1, Tagln* and *Smtn* gene loci in undifferentiated mMSC grown in their maintenance medium

Figure 5.3. ChIP-seq peak calling for H3K4me3 at the *Myh11, Cnn1*, *Tagln* and *Smtn* gene loci in undifferentiated mMSC and mMSCs following myogenic differentiation

Figure 5.4. ChIP-seq peak scores for H3K4me3 at different gene loci *(Myh11, Cnn1, Smtn* and *Tagln*) in mMSC derived myogenic progeny compared to undifferentiated mMSCs

Figure 5.5. ChIP-seq peak calling for H3K4me3 at the *Pecam1* gene locus in undifferentiated mMSC and vasculogenic differentiated mMSC

Figure 5.6. ChIP-seq peak calling for H3K4me1 at *Lpl* gene locus in undifferentiated mMSC and adipogenic differentiated mMSC

Figure 5.7. ChIP-seq peak calling for H3K4me3 at *Sost* gene locus in undifferentiated mMSC and osteogenic differentiated mMSC

Figure 5.8. ChIP-seq peak calling for H3K4me3 at *Myh11, Cnn1, Tagln* and *Smtn* gene loci in undifferentiated mMSC and following vasculogenic and osteogenic differentiation of mMSC

Figure 5.9. ChIP-seq peak calling for H3K4me1 at *Myh11, Cnn1, Tagln* and *Smtn* gene loci in undifferentiated mMSC and following adipogenic differentiation of mMSC

Figure 5.10. ChIP-seq peak scores of H3K4me3 at SMC gene loci (*Myh11, Cnn1, Smtn, Tagln)* and the *Pecam1* locus in mMSC derived vasculogenic progeny compared to undifferentiated MSCs

Figure 5.11. ChIP-seq peak scores of H3K4me3 at SMC gene loci (*Myh11, Cnn1, Smtn, Tagln)* and the *Sost* locus in mMSC derived osteogenic progeny compared to undifferentiated MSCs

Figure 5.12. ChIP-seq peak scores of H3K4me1 at SMC gene loci (*Myh11, Cnn1, Smtn, Tagln)* and the *Lpl* locus in mMSC derived adiopgenic progeny compared to undifferentiated MSCs

Figure 5.13. ChIP-seq peak calling for Input and H3K27me3 at *MYH11, CNN1, TAGLN* and *SMTN g*ene loci in undifferentiated hMSC grown in their maintenance medium

Figure 5.14. ChIP-seq peak calling for H3K4me2 at *MYH11, CNN1, TAGLN* and *SMTN* gene loci in undifferentiated H9 hESCs and following myogenic differentiation of H9 hESCs

Figure 5.15. ChIP-seq peak scores of H3K4me2 at SMC gene loci (*MYH11, CNN1, SMTN, TAGLN)* in H9 hESCs derived myogenic progeny compared to undifferentiated H9 hESCs

Figure 5.16. ChIP-seq peak calling for H3K4me3 at the *CD34* gene locus in undifferentiated hMSC and following vasculogenic differentiation of hMSCs

Figure 5.17. ChIP-seq peak calling for H3K4me1 at the *LPL* gene locus in undifferentiated hMSC and following adipogenic differentiation of hMSCs

Figure 5.18. ChIP-seq peak calling for H3K4me1 at *SOST* gene locus in undifferentiated hMSC and following osteogenic differentiation of H9 hESCs

Figure 5.19. ChIP-seq peak calling for H3K4me3 at SMC gene loci (*MYH11, CNN1, TAGLN* and *SMTN)* in undifferentiated hMSC and following vasculogenic differentiation of hMSCs

Figure 5.20. ChIP-seq peak calling for H3K4me1 at SMC gene loci (*MYH11, CNN1, TAGLN* and *SMTN)* in undifferentiated hMSC and following adipogenic differentiation of hMSCs

Figure 5.21. ChIP-seq peak calling for H3K4me1 at SMC gene loci (*MYH11, CNN1, TAGLN* and *SMTN)* in undifferentiated H9 hESCs and following osteogenic differentiation of H9 hESCs

Figure 5.22. ChIP-seq peak scores of H3K4me3 at SMC gene loci (*MYH11, CNN1, TAGLN* and *SMTN)* and the *CD34* locus for H3K4me3 in hMSC derived vasculogenic progeny compared to undifferentiated hMSCs

Figure 5.23. ChIP-seq peak scores of H3K4me1 at SMC gene loci (*MYH11, CNN1, TAGLN* and *SMTN)* and the *LPL* locus in hMSC-derived adipogenic progeny compared to undifferentiated hMSCs

Figure 5.24. ChIP-seq peak scores of H3K4me1 at SMC gene loci (*MYH11, CNN1, TAGLN* and *SMTN)* and the *SOST* locus in hMSC-derived osteogenic progeny compared to undifferentiated hMSCs

Figure 5.25. ChIP-seq peak calling for Input and H3K27me3 at the *MYH11* locus in undifferentiated S100β SNEP grown in their maintenance medium

Figure 5.26. ChIP-seq peak calling for H3K4me2 at the *MYH11* locus in undifferentiated S100β SNEP and following myogenic differentiation of S100β SNEPs

Figure 5.27. ChIP-seq peak calling for H3K4me2 at the *PECAM1* locus in undifferentiated S100β SNEP and following vasculogenic differentiation of S100β SNEPs

Figure 5.28. ChIP-seq peak calling for H3K4me2 at *SOST* gene locus in undifferentiated S100β SNEP and following osteogenic differentiation of S100β SNEPs

Figure 5.29. ChIP-seq peak calling for H3K4me2 at *LPL* gene locus in undifferentiated S100β SNEP and following adipogenic differentiation of S100β SNEPs

Figure 5.30. ChIP-seq peak calling for H3K4me2 at *MYH11* gene locus in undifferentiated S100β SNEP and following vasculogenic, adipogenic and osteogenic differentiation of S100β SNEPs

Figure 6.1 Non-SMC-like cells (fibroblasts, macrophage -, adipogenic - and osteogenic-like cells) in vascular lesions could arise from SMC that retain the epigenetic profile of H3K4me2 at the *Myh11* locus following progeny differentiation.

Figure 6.2 Non-SMC-like cells (fibroblasts, macrophage -, adipogenic - and osteogenic-like cells) in vascular lesions could arise from S100β resident vascular mVSCs that acquire the epigenetic profile of H3K4me2 at the *Myh11* locus following progeny differentiation.

Figure 6.3 When MSC differentiation requires cell commitment and epigenetic changes before the differentiation of these cells is determined and the transcript level is upregulated for a specific lineage.

Supplementary Figure S1. Optimisation of DNA fragment size

Supplementary Figure S2. ChIP-seq peak calling for H3K4me1 at the *Alpl and Sost* gene loci in undifferentiated mMSC and following adipogenic differentiation of mMSCs

Supplementary Figure S3. ChIP-seq peak calling for H3K4me3 at the *Lpl and Fabp4* gene loci in undifferentiated mMSC and following osteogenic differentiation of mMSCs

Supplementary Figure S4. ChIP-seq peak calling for H3K4me1 at the *ALPL and SOST* gene loci in undifferentiated hMSC and following adipogenic differentiation of hMSCs

Supplementary Figure S5. ChIP-seq peak calling for H3K4me1 at the *LPL and FABP4* gene loci in undifferentiated H9 hESCs and following osteogenic differentiation of H9 hESCs

List of Tables

Table 1.1. The HERP family

Table 2.1. QIAGEN primers

Table 2.2. IDT primers

Table 2.3. Chemical and biological agents

Table 2.4. Antibodies and their corresponding dilutions used in immunocytochemistry.

Table 2.5. Antibodies used in Chromatin Immunoprecipitation

Table 2.6. Commercial cells used during the study

Table 2.7. Tissue and cell-derived cells used during the study

Table 2.8. Growth medium

Table 2.9. RPMI

Table 2.10. MM1

Table 2.11. Endothelial cell medium

Table 2.12. StemPro® Adipogenesis Differentiation

Table 2.13. StemPro® Osteogenesis Differentiation

Table 2.14. Gibco™ Essential 8™ Flex Medium

Table 2.15. DMEM

Table 2.16. Endothelial cell growth medium

Table 2.17. CellStart Dilution for a 6-well plate

Table 2.18. Volume for siRNA Complex Tube setup with Mirus TransIT-X2

Table 2.19. Sonication conditions for each cell line

Table 2.20. ChIP reaction components.

Table 2.21. Preparation of a single Reaction Tube for PCR.

Table 2.22. Cycling Condition Setup for PCR.

Table 2.23. Components supplied in the Rotor-Gene SYBR® Green RT-PCR Kit (QIAGEN, 204174)

Table 2.24. A Table for preparation of reaction tubes for the Rotor-Gene SYBR® Green RT-PCR Kit (QIAGEN, 204174)

Table 2.25. Cycling Condition Setup for the Rotor-Gene SYBR® Green RT-PCR Kit (QIAGEN, 204174)

Table 2.26. 1.5% Agarose gel preparation

Table 2.27. Summary of Peak scores

Table 2.28. mouse MSC ChIP-seq accession numbers

Table 2.29. human MSC ChIP-seq accession numbers

Table 3.1. The level of enrichment of H3K27me3 and H3K27me3 at the Myh11 locus and the level of Myh11 expression in MOVAS SMCs following treatment with Notch ligand, Jag-1, PDGF-BB and TGF-β1 in relation to untreated MOVAS

Table 3.2 The level of enrichment of H3K27me3 and H3K27me3 at the Myh11 locus and the level of Myh11 expression in S100β mVSCs following treatment with Notch ligand, Jag-1, PDGF-BB and TGF-β1 in relation to untreated S100β mVSCs

Table 3.3 The effect of Notch ligand, Jag-1, TGF-β1 and PDGF-BB on Tet-2 binding to the Myh11 locus in MOVAS SMC in relation to MOVAS

Table 3.4 The effect of Notch ligand, Jag-1, TGF-β1 and PDGF-BB on Tet-2 binding to the Myh11 locus in mVSCs in relation to untreated S100β mVSCs

Table 3.5 The level of enrichment of H3K27me3, H3K27me3 at the Myh11 locus and ratio H3K27me3/H3K27me3 in Tet-2 siRNA treated MOVAS SMCs compared to scrambled control

Table 3.6 The level of enrichment of H3K27me3, H3K27me3 at the Myh11 locus and ratio H3K27me3/H3K27me3 in Tet-2 siRNA treated mVSCs at baseline and following atherogenic stimuli compared to scrambled control

Supplementary Table S1 Peak scores for enrichment for H3K4me1 in Undifferentiated mMSC

Supplementary Table S2 Peak scores for enrichment for H3K4me3 in Undifferentiated mMSC

Supplementary Table S3 Peak scores for enrichment for H3K4me3 in myogenic differentiated mMSC

Supplementary Table S4 Peak scores for enrichment for H3K4me3 in Vasculogenic differentiated mMSC

Supplementary Table S5 Peak scores for enrichment for H3K4me1 in Adipogenic differentiated mMSC

Supplementary Table S6 Peak scores for enrichment for H3K4me3 in Osteogenic differentiated mMSC

Supplementary Table S7 Peak scores for enrichment for H3K4me1 in undifferentiated hMSC

Supplementary Table S8 Peak scores for enrichment for H3K4me1 in undifferentiated H9 hESC

Supplementary Table S9 Peak scores for enrichment for H3K4me2 in undifferentiated H9 hESC

Supplementary Table S10 Peak scores for enrichment for H3K4me3 in undifferentiated hMSC

Supplementary Table S11 Peak scores for enrichment for H3K4me2 in Myogenic differentiated hMSC

Supplementary Table S12 Peak scores for enrichment for H3K4me2 in Vasculogenic differentiated hMSC

Supplementary Table S13 Peak scores for enrichment for H3K4me1 in Adipogenic differentiated hMSC

Supplementary Table S14 Peak scores for enrichment for H3K4me1 in Osteogenic differentiated H9 hESC

Supplementary Table S15 Collagenase/Elastase Solution

Abbreviations

Acta2	α-smooth muscle actin
ADAM	A disintegrin and metalloproteinase
ASH2L	Absent, small or homeotic 2-like protein
AIT	Adaptive intimal thickening
Alpl	Alkaline phosphatase
ApoE	Apolipoprotein e deficient mouse model
BAM	Binary Alignment Map
BSA	Bovine Serum Albumin
cDNA	Complementary DNA
CArG	CC(A/T)-rich GG
CC	Cross Correlation
CD34 / 68	Cluster of differentiation 34/68
CGIs	CpG islands
ChIP	Chromatin Immunoprecipitation
ChIP-Seq	Chromatin immunoprecipitation sequencing
ChIP-PCR	Chromatin Immunoprecipitation followed by Polymerase Chain Reaction
CHD	Coronary heart disease

c-Myc	Cellular myelocytomatosis oncogene
Cnn1	Calponin1
CO_2	Carbon Dioxide
Cre	Cyclization recombinase
CPG	Cytosine phosphate guanine
CVD	Cardiovascular Disease
CUT&TAG	Cleavage under targets and tagmentation
CUT&RUN	Cleavage under targets and release under nuclease
DAPI	4',6-diamidino-2-phenylindole
DEPC	Diethylpyrocarbonate
DIT	Diffuse intimal thickening
DMEM	Dulbecco's Modified Essential Medium
DMSO	Dimethyl Sulfoxide
Dmp1	Dentin matrix protein 1
DNA	Deoxyribose Nucleic Acid
dNTP	Deoxynucleoside triphosphate
DNMT	DNA-methyltransferase
DPBS	Dulbecco's Phosphate Buffered Saline

DPY30	Protein DPY-30 homolog
Drop-ChIP	Droplet-based single-cell ChIP-seq
E8	Essential 8
EDTA	Ethylenediaminetetraacetic acid
eGFP	Enhanced green fluorescent protein
ESC	Embryonic stem Cells
EBI	European Biotechnology Institute
ECM	Extracellular matrix
ERT2	Estrogen receptor type 2
Ezh	Enhancer of Zeste
FABP4	Fatty acid binding protein 4
FBS	Fetal Bovine Serum
FGF	Fibroblast Growth Factor
5-hmc	5-hydroxymethylcytosine
5-mc	5-methylcytosine
GAPDH	Glyceraldehyde 3-phosphate dehydrogenase
GTN	Galaxy Training Network
H9 ESCs	Human embryonic stem cells

HBSS	Hank's balanced salt solution
HES	Hairy enhancer of split
HERP	HES-related repressor protein
HF	Heart failure
HDMTs	Histone demethylases enzymes
HMTs	Histone methyltransferase enzymes
HiPSC	Human induced Pluripotent Stem Cells
H3K4me2	Histone 3 lysine 4 di-methylation
H3K27ne3	Histone 3 lysine 27 trimethylation
HPRT	Hypoxanthine phosphoribosyltransferase 1
hPSCs	Human Pluripotent stem cells
ICC	Immunocytochemistry
IGB	Integrated Genome Browser
IgG	Immunoglobulin G
IP	Immunoprecipitation
iPSC	Induced Pluripotent Stem Cells
ISH-PLA	In Situ Hybridization-Proximity Ligation Assay
ISR	In-stent restenosis

KLF4/5	Krüppel-like factor 4/5
LB	Lysis buffer
LDL	Low-density lipoprotein
LDLR	Low-density lipoprotein receptor
LoxP	Locus of x-over, P1
LSD1	Lysine-specific demethylase 1
LPA	Lysophosphatidic acid
Lpl	Lipoprotein lipase
MACS	Model-based Analysis of ChIP-seq
MSC	Mesenchymal Stem Cell
MV	Matrix vesicles
mVSC	Multipotent Vascular Stem Cell
mVSMC	Mouse vascular smooth muscle cells
MM1	Maintenance Medium 1
miRs	MicroRNAs
mRNA	Messenger RNA
Myh10/11	Myosin Heavy-chain 10/11
MYOCD	Myocardin

NE-MM	Neuroectodermal-derived cells maintenance medium
NCBI	National Center for Biotechnology Information
NICD	Notch Intracellular Domain
NECD	Notch Extracellular Domain
NF	Non functional
NGS	Next-generation sequencing
NTMIC	Notch Transmembrane and Intracellular Domain
NEXT	Notch Extracellular Truncation
Oct 3/4	Octamer-binding transcription factor 3 / 4
pA-Tn5	protein A-Tn5 transposase
PBS	Phosphate basic solution
PCR	Polymerase Chain Reaction
PDGF	Platelet-derived Growth Factor
PECAM1	Platelet endothelial cell adhesion molecule 1
PIT	Pathologic intimal thickening
PLA	Proximity ligation assay
Pitx2	Pituitary homeobox 2
PRC2	Polycomb repressive complex 2

QC	Quality control
qRT-PCR	Quantitative real-time Polymerase Chain Reaction
RBP-Jk	Recombination signal sequence-binding protein Jkappa
RCA	Rolling circle amplification
RCP	Rolling circle product
RbBP5	Retinoblastoma binding protein 5
RNA	Ribo-nucleic Acid
RNAi	RNA interference
RIPA	Radioimmunoprecipitation assay
RT	Reverse transcriptase
RPMI	Roswell park memorial institute
S100β	S100 calcium-binding protein β
Sca-1	Stem Cell Antigen-1
SCC	Strand cross-correlation
scChIP-Seq	Single cell ChIP-sequencing
scRNA-Seq	Single cell RNA sequencing
SiRNA	Short interfering RNA
SMAD	Suppressor of mother against Decapentaplegic

SMC	Smooth Muscle Cell
Smtn	Smoothelin
Smtn2	Smoothelin 2
SNEPs	HiPSC-derived S100β human multipotent neuroectoderm progenitor stem cells
Sost	Sclerostin
Sox2/10/17	SRY-box transcription 2/10/17
SRF	Serum Response Factor
TAE	Tris-acetate
TBS-T	1X Tris-Buffered Saline, 0.1% Tween
TET	Ten-eleven-translocation
TGF-β	Transforming Growth Factor Beta
Tagln	Transgelin
TSS	Transcription starting site
VEGF	Vascular Endothelial Growth Factor
WDR5	WD Repeat Domain 5
YFP	Yellow fluorescent protein

Units

oC	Degrees Celsius
cm	centimetre
g	grams
hr	hour
L	litre
M	molar
mg	milligram
min	minute
mL	millilitre
mM	millimolar
nm	nanometre
nM	nanomolar
rpm	revolutions per minute
sec	second
µL	microlitre
µg	microgram
µm	micrometre
µM	micromolar

Chapter 1

Introduction

1.1 Cardiovascular disease

Cardiovascular disease (CVD) refers to diseases of the heart and the peripheral vasculature. Heart diseases, such as myocardial infarction and stroke, occur suddenly before any medical care is available. Many therapeutic interventions to treat such diseases are therefore inapplicable or palliative. The widespread occurrence of CVD relates mostly to lifestyles and modifiable physiological factors. Risk factor modifications have shown a reduction in mortality and morbidity, especially in people with either recognised or unrecognised CVD (De Backer et al., 2003). These diseases can occur and develop problematically in individuals with a genetic predisposition or following the development of atherosclerotic lesions during one's lifetime (Fishbein & Fishbein, 2015).

CVD is the leading cause of morbidity and mortality. This is particularly true in developed countries (Murray & Lopez, 1996; Yusuf et al., 2001). In the past 50 years there has been remarkable and unprecedented progress in addressing CVDs, marked by a large and continuing reduction in CVD-related mortality, however, even with this progress, CVD is still the leading cause of death and disability both in the United States and globally, affecting 85.6 million Americans and accounting for 1 in every 6 healthcare dollars spent (McClellan et al., 2019). In many countries, including the United States, CVDs cause more deaths in women than in men each year (Rosamond et al., 2007; Shaw et al., 2006). On the basis of National Health and Nutrition Examination Survey 2015 to 2018 data, the prevalence of CVD (comprising coronary heart disease (CHD), heart failure (HF), stroke, and hypertension) in adults ≥20 years of age is 49.2% (126.9 million in 2018), this increases with age in both males and females. Most prevalent CVD is hypertension, accounting for about 40%, while other CVDs, such as CHD, HF, and stroke, are responsible for 9.3% (Ss et al., 2021). In 2020, there were 8,744 deaths in Ireland alone caused by CVDs – including CHD, stroke and other circulatory diseases, according to a report by Irish Heart Foundation (https://irishheart.ie/news/decline-in-deaths-from-heart-disease-and-stroke-in-2020/). As people age, aortae can stiffen as a result of the increase in collagen and the decrease in the level of elastin (Johnson et al., 2001). The higher the stiffness, the more the reflected waves are raised as well as the systolic pressure is elevated (Asmar et al., 1988).

1.2 Vascular structure

1.2.1 Artery

In mammals, the vascular system is made up of an intricate network of vessels that transport blood around the body. Arteries carry oxygenated blood, with the exception of pulmonary arteries, away from the heart to a range of different tissues in order to provide the necessary life-sustaining components. An artery is made up of three main layers, to facilitate its function [Figure 1.1]. All layers of the artery are mechanoresponsive and remodel during vascular disease progression (Humphrey et al., 2008).

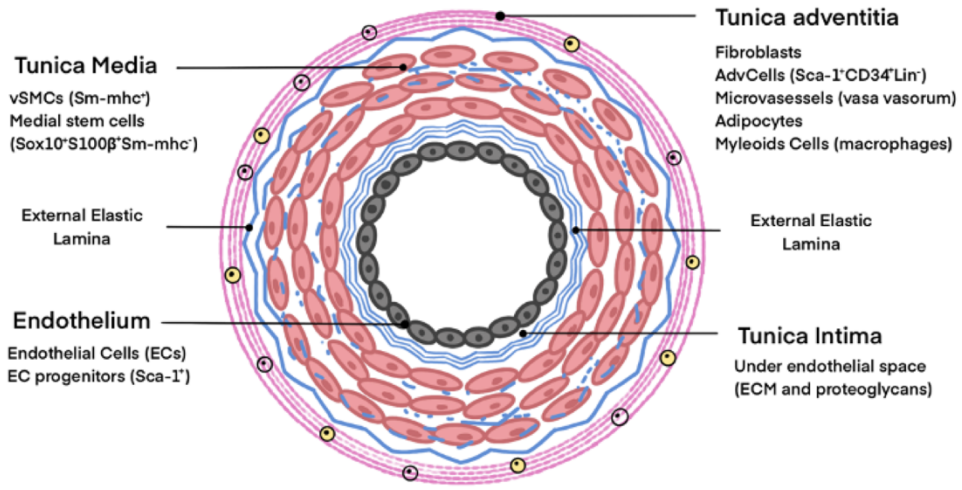

Figure 1.1. Composition of an Artery. Arteries consist of three main layers (i) tunica intima, a single-cell endothelium barrier between the lumen and the artery wall, (ii) a layer of vascular smooth muscle cells (the media), and (iii) the outermost adventitial layer composed primarily of fibroblasts, stem cells and resident macrophages. Adapted in part from Jouda et al., 2022.

1.2.1.1 The tunica intima

The tunica intima is the innermost layer of the artery. It surrounds the lumen and consists of a monolayer of endothelial cells and a sub-endothelial support structure. As the point of contact between the artery and the blood, endothelial cells possess a number of characteristics to maintain normal blood flow and prevent disease development. For example, the smooth, flat structure of these cells allows for frictionless flow of blood through

the vessel to reduce shear stress on vascular cells (Gimbrone et al., 2000). Moreover, endothelial cells are known to express high levels of anti-inflammatory and anti-thrombotic proteins in response to changes in blood flow dynamics (Berk et al., 2001). The endothelial cells are connected to the basal elastic lamina of the tunica media which has additional collagen, proteoglycans and glycans essential for endothelial support and function. These endothelial cells are a critical component of the vasculature due to their direct contact with the lumen, and therefore subjected to blood flow forces and interactions with blood components (Schwartz et al. 1995; Kockx et al. 1995; Catravas et al. 1999).

1.2.1.2 The Tunica Media

The tunica media is the middle layer and consists mostly of vascular smooth muscle cells (SMCs) which contract to narrow the lumen and create pressure for blood flow. The tunica media is separated from tunica intima by a layer of connective tissue and elastic fibres known as the internal elastic lamina (Roostalu et al., 2018). SMCs within this layer are compartmentalised into further layers separated by elastic lamina which provides a fibrous structure that lends rigid support to the tunica media. In addition to these SMCs, the medial layer contains pericytes, proteoglycans and a small population of resident stem cells (Potter et al., 2014; Tang et al., 2012).

1.2.1.3 The Tunica Adventitia

The tunica adventitia is the outermost layer, separated from the tunica media by external elastic lamina and is surrounded by adipose tissue. The adventitia is a collagen matrix that is less rigid than the other vascular layers, and is rich with stem cells, perivascular nerves, adventitial macrophages, mast cells, T cells, microvascular endothelial cells and adipocytes. It is important to note that the adventitia has been implicated in numerous vascular pathologies due to its complex network of interacting cells and biological factors (Majesky et al., 2011).

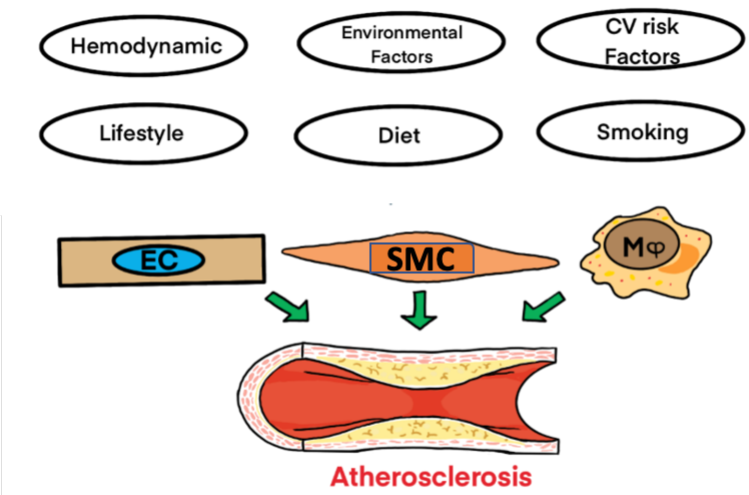

Figure 1.2. The deposition of Lipids in the vascular wall alters the integrity of the endothelium, which also permits the transmigration of circulating monocytes into the SMC layer where they mature further into macrophages and engulf cholesterol. Growth factors and inflammatory mediators are released by activated macrophages promoting the de-differentiation of resident medial SMC from a contractile phenotype to the synthetic state. SMCs migrate and populate the intima and participate in fibrous cap formation through heightened proliferation and extracellular matrix (ECM) synthesis. Severe atherosclerosis can require revascularization procedures to restore blood flow through vessels. Adapted from Lu et al., 2022.

1.3 Atherosclerosis

Atherosclerosis is the underlying pathology, which develops insidiously over years and is usually advanced by the time symptoms occur (De Backer et al., 2003). Atherosclerosis was once viewed as a lipid storage disease (Tesfamariam & Cohen, 1992), although it is known to be a chronic disease of arteries which is defined as acute coronary syndromes, stable or unstable angina, arterial revascularization, stroke, transient ischemic attack, peripheral arterial disease or a history of myocardial infarction presumed to be of atherosclerotic origin (Targets & Targets, 2015). As a consequence, thrombotic events associated with rupture or erosion of instability in plaques can result in mortality (Bennett et al., 2016). Lesions are characterized by the accumulation of cholesterol in the arterial wall together with the accumulation of vascular SMC-like cells [Figure 1.2] (Sanchez & Veith, 1998; Yia-Herttuala et al., 1989). The progression of a simple fatty streak to an advanced neointimal plaque also involves many cell types, including macrophages, endothelial cells, lymphocytes and vascular SMCs. Atherosclerosis develops over several decades of life (Ross et al., 1993).

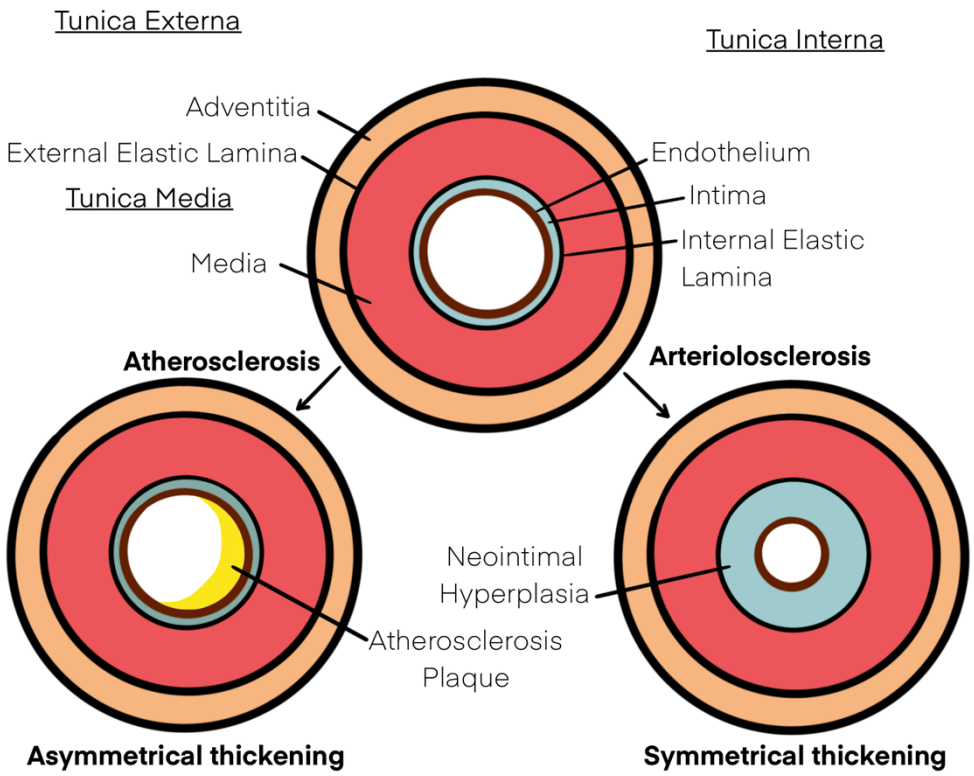

Figure 1.3. Atherosclerotic and Arteriosclerotic lesions. In a pathological artery, the atherosclerotic plaque forms asymmetrically whereas arteriosclerotic lesions are represented by a symmetrical thickness of the intimal layer (Newby & Zaltsman, 2000; Stocker & Keaney, 2004; Wick et al., 2004). Image adapted from https://themedfield.wordpress.com/2020/09/24/arteriosclerosis/.

In atherosclerosis, an activated endothelium with the expression of adhesion molecules appears to be an early event, allowing mononuclear leukocytes, such as T-cells and monocytes, to attach to the endothelium and penetrate the intima (Frostegård et al., 1999). Though not as common as these cells, mast cells, dendritic cells and a few neutrophils and B-cells may also be present in lesions. SMC-like cells, which undergo a change in phenotype to synthetic SMC and migrate into the intima from the media [Figure 1.3], are also purported to be present in lesions. Atherosclerosis is considered an inflammatory disease based on the finding that immunocompetent cells are abundant in atherosclerotic lesions, and also are producing cytokines, especially proinflammatory cytokines (Frostegård et al., 1999).

Monckeberg medial calcific sclerosis is a process that affects only the tunica media of large and medium-sized arteries, without any compromise to the arterial lumen. Arteriolosclerosis affects vessels all over the body and is mostly associated with hypertension and diabetes

mellitus (Fishbein & Fishbein, 2009). However, these will not be discussed in depth in this study.

1.4 Subclinical atherosclerosis

Subclinical atherosclerosis defines the initiation and progression of early atherosclerotic plaques and can be present in a number of forms. Pathologic intimal thickening (PIT) is one of the most widespread forms of subclinical atherosclerosis and is widely reported to give rise to more advanced plaque lesions. It is known for an infiltration of the macrophages, loss of intimal SMCs and the formation of an extracellular lipid pool (Kolodgie et al., 2007). Adaptive intimal thickening (AIT) is generally present from birth and involves only SMCs and the proteoglycan matrix but without immune cell infiltration. AIT is often seen as a precursor to PIT as it allows for increased lipid retention in the vessel wall (Otsuka et al., 2015). There are also multiple, less frequently observed forms of subclinical atherosclerosis which are not progression-prone. One such form is known as an intimal xanthoma (Sakamoto et al., 2018). Intimal xanthomas are mostly composed of fat-laden macrophages and form a “fatty streak” in the vessel wall. They do not share many of the features associated with more advanced atherosclerotic plaques and usually regress over time (Virmani et al., 2000). Diffuse intimal thickening (DIT) occurs at the beginning of the atherosclerosis stage, whereby lipids accumulate in the extracellular space in DIT. Subsequently, macrophages infiltrate into the thickened intima and become foam cells to form an early lesion together with intimal SMCs and extracellular lipids (Nakashima et al., 2007; Tabas et al., 2007). The fatty infiltration is similar to those of DIT, apart from a mild deposition of extracellular lipids in the middle to the deep layer of the intima (Nakagawa & Nakashima, 2018).

In the PIT, a larger amount of extracellular lipids are deposited to form lipid pools in the middle and/or deep layers of the intima. Foamy and non-foamy macrophages accumulate above the lipid pool. SMCs are sparsely arranged throughout the intima. Some SMCs contain lipids in their cytoplasm. The number and density of macrophages are low in DIT and the fatty infiltration, but increase significantly in the fatty streak and PIT, while the number of SMCs is almost the same as that of DIT in the three atherosclerotic lesions. However, the SMC density decreases markedly in fatty streak and PIT compared to the DIT and fatty infiltration. The decrease in SMC density in the inner areas of the fatty streak and PIT correlates with the rise

in the number of macrophages. Meanwhile, the decrease in SMC density in the outer areas of the PIT correlates with extracellular lipid accumulation in lipid pools, as these are localized mainly in the outer areas. Furthermore, this correlation is confirmed by the significant decrease in SMC density within the lipid pool compared to that in the DIT (Nakagawa & Nakashima, 2018).

1.5 Model Systems for Investigating Subclinical Atherosclerosis

Atherosclerosis, as a chronic progressive inflammatory disease, is widely regarded as one of the leading causes of death due to CVD worldwide. A hallmark of subclinical atherosclerosis is the accumulation of SMC-like cells leading to intimal medial thickening, lipid accumulation, plaque formation and the obstruction to blood flow that may result in a heart attack or stroke. Pathological observations in human vessels confirm that early 'transitional' lesions enriched with SMC-like cells called adaptive lesions are routinely present in atherosclerotic-prone regions of arteries driving subclinical atherosclerosis, PIT, lipid retention, and the appearance of a developed plaque (Sakamoto et al., 2018). Several model systems have been developed to generate SMCs for investigation *in vivo* and *in vitro*.

1.5.1 Rodent models

Subclinical atherosclerosis is usually modelled in rodents following surgical interventions through partial ligation of a carotid artery which has been reported to result in either full or partial flow obstruction with resultant hemodynamic perturbations (Korshunov & Berk, 2003). These injury models elicit vascular remodelling patterns characterized by PIT and the formation of non-atherosclerotic AIT intimal lesions that can develop further into more advanced atherosclerotic lesions in apolipoprotein e-deficient mouse model (*ApoE)* gene-deficient mice when placed concurrently on a western diet (Liu et al., 2011).

1.5.2 Induced Pluripotent Stem Cells (iPSCs)

iPSCs are a novel cell type that is derived from somatic cell reprogramming via overexpression of exogenous transcription factors (Zachary & Morgan, 2011). They can be theoretically differentiated into any mature cell type derived from the three primary germ layers, namely ectoderm, mesoderm and endoderm. To date, iPSCs have been successfully differentiated

into many different cell types, including neural cells, lung and airway epithelial cells, cardiomyocytes (Huang et al., 2014) and endothelial cells (Choi et al., 2009; Rufaihah et al., 2011; Taura et al., 2009). In addition, the production of induced endothelial cells is possible by transdifferentiation of adult fibroblasts directly to endothelial cells, bypassing the pluripotent stem cell intermediate (Li et al., 2013; Margariti et al., 2012).

iPSCs are most commonly derived from dermal fibroblasts, although they have also been generated from other cell types, including adipose stromal cells, hepatocytes, gastric epithelial cells, dental pulp stem cells, cord blood cells and peripheral blood mononuclear cells (Koyanagi-Aoi et al., 2013; Tanabe et al., 2013). Octamer-binding transcription factor 3/4 (Oct3/4) is a homeodomain transcription factor, that controls the maintenance and differentiation of pluripotent stem cells. SRY-box transcription 2 (Sox2) controls the expression of Oct3/4 in part. Oct3/4, Sox2 and Nanog homeobox constitute the key transcriptional network for pluripotency. Cellular myelocytomatosis *(c-Myc)* is a proto-oncogene associated with the cause of cancers. It recruits chromatin-modifying proteins which leads to widespread transcriptional activation. It was previously shown that c-Myc is dispensable for reprogramming (Masui et al., 2007) and can be replaced with another type of myelocytomatosis gene, i.e. *L-Myc,* which is deficient in transformation activity (Nakagawa et al., 2008). Krüppel-like factor 4 (Klf4) acts as an oncoprotein or a tumour suppressor in a context-dependent manner, is a downstream target of leukemia inhibitory factor and also activates Sox2 (Nakagawa et al., 2010). Although the precise mechanism is not fully elucidated, the coordination of these reprogramming factors leads to the reprogramming of somatic cells into pluripotency (Niwa et al., 2009).

iPSCs have aberrant DNA methylation profiles compared to embryonic stem cells (ESCs), due to incomplete reversal of lineage-specific methylation patterns, varying de novo methylation patterns during reprogramming and variability in X chromosome inactivation (Kim et al., 2010; Kitai Kim et al., 2011; Liang & Zhang, 2013). Conversely, other analyses of human iPSCs and ESCs have revealed overlapping and non-significant differences in DNA methylation in these two cell types and that the difference between iPSCs and ESCs is no greater than the difference between individual ESC lines (Koyanagi-Aoi et al., 2013; Liang & Zhang, 2013; Maherali et al., 2007). iPSCs seem to be equivalent to ESCs in terms of their ability to

differentiate into mature cell types (Taura, Noguchi, et al., 2009; Xi et al., 2010). The situation is complex and appears to be influenced by donor cell type, the degree of similarity between the parent and target cell types and the iPSC derivation method (Tokumoto et al., 2010).

1.5.3 Multipotent Resident Vascular Stem cell

Mesenchymal stromal stem cells (MSC) and multipotent resident vascular stem cells (mVSCs) have the capacity to develop into several cell types, i.e., adipocytes, myocytes, chondrocytes, and osteocytes (Covas et al., 2008; Huang et al., 2009; Lin et al., 2010; New et al., 2015) following exposure to specific growth factors and other biomolecules in their inductive media (Colazzo et al., 2014). Vascular SMC differentiation was stimulated by the presence of transforming growth factor-β (TGF-β) (Park et al., 2013). Adipocyte genes, such as fatty acid-binding protein (*FABP4*) (Shi et al., 2010) and lipoprotein-lipase (*LPL*) (Wakil, 1989) all play important roles in the formation of fat. When cultured in osteogenic media, MSCs express markers known to be expressed by bone-forming osteoblasts, which are the cells responsible for laying down the matrix and mineral during new bone formation *in vivo* (Huang *et al*., 2007). Osteocyte marker gene expressions, increase following osteogenic differentiation especially sclerostin (*Sost*), dentin matrix protein 1 (*Dmp1*), and fibroblast growth factor 23 (*Fgf23*) (Feng et al., 2006; Poole et al., 2005). Maul *et al* successfully differentiated rat MSCs to endothelial cells and found an incline in expression levels of endothelial-specific genes including prominin 1 and platelet endothelial cell adhesion molecule 1 (*Pecam1*) (Maul et al., 2011).

1.5.4 Vascular Smooth Muscle cells (SMCs)

SMCs provide structural support to hollow organs such as the uterus, bladder, and organs of the gastrointestinal system. In addition, they play a key physiological role in the contractility of blood vessels under normal conditions to maintain normal blood pressure and may be involved in pathological conditions, such as vessel remodelling during disease progression following injury. This subtype is known as SMCs, and its origin is diverse. SMCs are considered to be heterogeneous due to their repertoire of functions and various embryological origins (Gammill & Bronner-Fraser, 2003; Hao et al., 2003; Majesky, 2007; Sinha et al., 2014). These

cells play significant roles in the formation and function of the cardiovascular, respiratory, digestive and urinary systems.

These SMC are the dominating cell type inside the blood vessel wall. They are housed in a matrix of collagen and elastin within the medial layer and facilitate vascular tone by means of vasodilation and vasoconstriction thereby distributing blood flow and regulating blood pressure. They exhibit important phenotypic markers including α-smooth muscle actin (*Acta2)*, myosin heavy chain 11 (Myh11), calponin 1 (Cnn1), smoothelin 2 (Smtn2) and transgelin (Tagln) (Owens et al., 2004). Changes in both extracellular and intracellular tension, alter actin cytoskeletal organisation and regulate cell contraction, migration and survival (Papakonstanti & Stournaras, 2008).

It has been known for several years that SMCs originate from different areas of the embryo during development and contribute to the formation of distinct tissues of the vasculature. They can arise from two main sources: the mesoderm and the neuroectoderm, that is, the ectoderm of the neural crest. Most of the SMCs in the vascular tree are of mesodermal origin such as lateral plate and paraxial mesoderm, and are formed mainly from mesenchyme, which is, a type of connective tissue found during the development of an embryo or from mesothelium via the epithelial to mesenchymal transition. The different embryological origins of the SMCs comprising the tunica media of the aorta include the cranial neural crest from where the aortic arch, ascending aorta and branching carotid arteries are derived, and mesodermal background of the aortic root and annulus and descending (Shi & Chen, 2016).

1.5.5 Adventitial cells

The adventitia contains a highly dynamic population of microvessels, leukocytes, adipocytes, and resident progenitor cells that collectively both maintain the artery wall and respond robustly to many kinds of vascular (Majesky, Dong, Regan, et al., 2011). In some cases, the adventitia can be the main site of pathological change such as in the formation of tertiary lymphoid organs in diseased arteries, fibrotic changes reduce compliance and promote renal damage in hypertension, and as a focus for inflammatory cell accumulation in the development of medial dissections and aneurysms (Galkina et al., 2006; Hu et al., 2004;

Passman et al., 2008; Psaltis et al., 2012). In small vessels, the adventitia and associated perivascular cells are important signalling niches (Gräbner et al., 2009; Guzik et al., 2007; Poduri et al., 2015; Tieu et al., 2009) for bone marrow hematopoietic stem cells (Kramann et al., 2015).

Adventitial stem cell antigen-1 (Sca1) stem cells differentiate into other types of cells participating in vascular lesions, including osteogenic progeny and macrophage colony-forming units (Cho et al., 2013; Psaltis et al., 2012). Studies using lineage tracing analysis have suggested that some of these adventitial Sca1 cells are derived from Myh11 genomic marked differentiated SMCs and are a major contribution to adventitial remodelling (Majesky et al., 2017). Also, the adventitia may play a role in atherosclerosis development and is usually characterized by lymphocyte infiltrates (Campbell et al., 2012).

1.5.6 Endothelial cells

Endothelial cells cover approximately 7 m^2 in an average adult (Cines et al., 1998). In the tunica, intima endothelial cells exist as a semipermeable monolayer. Endothelial cells of all the vessels are of mesodermal origin (Aird, 2007). Endothelial cells play a significant role in the initiation, amplification, and resolution of the inflammatory response. The deregulated inflammatory response implicated in a variety of cardiovascular diseases such as atherosclerosis and hypertension is related to endothelial dysfunction and its resultant vascular remodelling (Cohn et al., 2001; Xiao et al., 2014). Normally, endothelial cells, which form the innermost surface of artery walls, resist adhesion by leukocytes. However, triggers of atherosclerosis, such as consuming a high saturated fat diet, smoking, hypertension, hyperglycaemia, obesity, or insulin resistance, can initiate the expression of adhesion molecules by Endothelial cells, thus allowing the attachment of leukocytes to the arterial wall (Tesfamariam & Cohen, 1992). Endothelial dysfunction is recognized as a key early risk factor for cardiovascular morbidity and mortality (Cohn et al., 2001). In general, vascular endothelial cells maintain blood fluidity, regulate blood flow, control vessel wall permeability and quiesce circulating leukocytes. Blood fluidity is actively maintained by several endothelial-cell-dependent mechanisms that inhibit coagulation throughout the vascular system (Bazzoni & Dejana, 2004).

1.6 Current therapies for cardiovascular disease

Despite having a genetic predisposition, CVD primarily occurs naturally in humans. However, there are numerous measures that can prevent or delay its onset by adopting a healthy lifestyle. These are highly recommended for the normal population and of course patient cohorts who present either early or with advanced CVD symptoms. Medication is also prescribed to relieve symptoms by reducing high blood pressure and high Low-density lipoprotein (LDL) cholesterol levels. Patients with advanced atherosclerotic plaque formation commonly developed in coronary arteries are routinely subjected to surgical and non-surgical intervention. Percutaneous Transluminal Coronary Angioplasty followed by stenting is commonly used in the treatment of advanced CVD (Benjamin et al., 2019).

1.6.1 Surgical Interventions

In very severe cases of CVD, invasive action must be taken to treat the patient. For the treatment of CVD in coronary arteries, bypass grafts have been the method of choice for a number of years. By taking a blood vessel from elsewhere in the body and using it to direct blood flow around the blockage in the coronary artery.

1.6.1.1 Balloon angioplasty

Recently, balloon angioplasty and stenting have become very popular techniques for treating patients with severe atheroma. In balloon angioplasty, once the balloon catheter is in place, the balloon is inflated pushing the atheroma into the vessel wall re-establishing the blood flow [Figure 1.4]. In order to reduce the possibility of elastic recoil a stent is often inserted. A stent is a short metal mesh used to maintain the opening created by the angioplasty. However, this can later lead to a number of other challenges, most notably the occurrence of in-stent restenosis (ISR) due to vessel damage (Farooq et al., 2011).

1.6.1.2 In-stent restenosis (ISR)

ISR also known as clinical restenosis or neointima hyperplasia is characterised by extensive proliferation and migration of SMC-like cells into the intimal space of the stented artery resulting in the formation of a neointima (Indolfi et al., 2003). The process of ISR appears to

be a multi-factorial mechanism involving (i) Biological Factors - resistance mechanisms in cells after they are exposed to therapeutic agents due to their high cytotoxic effect (ii) Arterial Factors - biomechanical forces due to compliance mismatch (iii) Stent Factors - where the stent material, the type of drug, the elution profile and dose are important factors driving neointimal hyperplasia after implantation of a drug-eluting stent (iv) Implantation Factors - failure to correctly expand the obstructed vessel (Farooq et al., 2011), and (v) Molecular Factors - driving neointima hyperplasia including chemokines that trigger an immune response and the activation of SMC-like cells that contribute to lesion formation in response to mitogenic factors such as platelet-derived growth factor (PDGF) and TGF-β1 (Indolfi et al., 2003).

The source of smooth muscle-like cells contributing to neointimal hyperplasia, in general, is a topic of much controversy. The sources reported so far are de-differentiated SMCs (Chappell, 2016), resident vascular stem cells (Tang et al., 2012), bone marrow-derived stem cells (Shimizu et al., 2001) and endothelial to mesenchymal Transition also has been suggested to occur in neointimal thickening associated with transplant atherosclerosis and restenosis (Zeisberg et al., 2007).

Figure 1.4. In-stent Restenosis. Balloon angioplasty is regularly used to widen the lumen of an artery after an atherosclerotic plaque has caused the lumen to narrow. A metal mesh stent can be inserted around the balloon to prevent elastic recoil and re-occlusion of the lumen. However, this can injure the artery wall and cause artery wall hardening and neointima formation which restricts blood flow. This is called in-stent restenosis. Adapted from Yin et al.,2014.

1.7 Origin of Neointimal Cells

1.7.1 De-differentiation and reprogrammed SMCs

SMCs generally exist in the tunica media normally expressing a wide range of SMC markers, including SMC *Myh11*, 22-kDa SMC lineage-restricted protein Tagln, Acta2, Smtn2, Cnn1 and

others (Alexander & Owens, 2011). Following endothelial injury, inflammatory cells infiltrate and secrete various cytokines, which can trigger de-differentiation, migration, and proliferation of medial SMCs (Ross et al., 1999). This process of dedifferentiation and reprogramming is regularly associated with a significant loss in the expression of key SMC differentiation marker genes for a large number of proliferative vascular diseases *in vivo* and *in vitro* (Chamley-Campbell et al, 1981). SMC phenotype is known to be altered by many stimuli such as PDGF, oxidized phospholipids (Mcdonald et al., 2006, 2007), TGF-β1 (Ailawadi et al., 2009; Owens et al., 2004) and retinoic acid (Spin et al., 2005, 2010), appear to act in part through effects upon SMC chromatin structure (Spin et al., 2012). SMC phenotype switching is dictated by transcription factor KLF4. KLF4 factors are expressed in SMCs that are phenotypically modulated and bind to G/C-rich cis-elements found in SMC marker gene promoters. Differentiated SMCs in normal blood vessels do not express KLF4. In contrast, it is rapidly induced following vascular injury (Yan et al., 2008).

Many studies have shown that SMCs in adults respond to injury by expressing genes or gene products (such as tropoelastin, fibronectin, tenascin, cytokeratin 8, and extra domain-A fibronectin) characteristic of earlier developmental states. In addition, genes such as smooth muscle-specific α-actin, desmin, tropomyosin and myosin, which are expressed preferentially in adult cells *in vivo*, are down-regulated when adult cells migrate and divide following injurious stimuli (Stenmark & Mecham, 2002). This behaviour can lead to remodelling of the vascular wall, including stenosis and obliteration of the vascular lumen.

Up to 98% of the cells that are present in the restenosis lesion are primarily vascular SMC-like cells (Shankman et al., 2015). Originally, it was purported by many investigators that these neointimal SMC-like cells originated from differentiated SMCs that switched phenotype to become de-differentiated and began proliferating/migrating to the site of injury to form the neointima. Subsequent lineage tracing studies have provided further compelling evidence in support of SMC switching and re-programming by demonstrating that neointimal SMCs (Herring et al., 2014; Nemenoff et al., 2011; Shankman et al., 2015) and a considerable number of neointimal macrophage-like cells (Shankman et al., 2015) may be derived from 'marked' medial differentiated SMC *in vivo* (Chappell et al., 2016; Cherepanova et al., 2016; Shankman et al., 2015). Research from our group provided evidence that SMCs in culture also

begin to express neural stem markers, such as SRY-box transcription 10 (Sox10), but do not have the same level as multipotent vascular stem cells (Kennedy, Hakimjavadi, et al., 2014; Kennedy, Mooney, et al., 2014).

1.7.2 Bone marrow-derived Stem Cells

There are a few studies that support the role of circulating bone marrow-derived stem cells and hematopoietic progenitor cells in the development of vascular lesions. Most of these studies involved bone marrow transplantation into a mouse which subsequently underwent vessel ligation. A large number of the neointimal cells were then shown to have originated from the donor mouse (Sata, 2003; Shimizu et al., 2001). Some human studies suggested that SMCs in an atherosclerotic lesion may be derived from donor bone-marrow stem cells (Caplice et al., 2003). However, it has also been suggested on a number of occasions that these circulating cells are indeed recruited to the ligation site but do not go on to differentiate into neointimal SMC-like cells (Hoofnagle et al., 2006).

1.7.3 Endothelial cells

In 1997, it was shown that endothelial cells have the ability to transition to an SMC progenitor cell expressing myogenic markers (Deruiter et al., 1997). Later this process of trans-differentiation has been demonstrated on a number of occasions, with the progenitor cell being classed as a mesenchymal stem cell (MSC). This has given rise to the term, endothelial-to-mesenchymal transition, a process which is characterised by the loss of morphological features such as tight junctions and the loss of endothelial markers such as PECAM1 and von Willebrand factor and the gain of mesenchymal markers such as fibroblast-specific protein 1 and vimentin (Chen et al., 2015). Several research suggested that endothelial-to-mesenchymal transition occurs during neointimal hyperplasia and that SMC-like cells in the neointima are derived from cells which have undergone this transition process (Chen et al., 2021; Frid et al., 2002).

1.7.4 Resident multipotent vascular stem cells (mVSCs)

Stem cells can be defined as units of organization of biological systems that are responsible for both the regeneration and development of organs and tissues. These cells are capable of

self-renewal and differentiation into multiple cell lineages (Dulak et al., 2015; Weissman, 2000). Recently, a new paradigm has been proposed where resident mVSCs in the wall of vessels differentiate to the SMC-like cells of the neointima. A population of Sca1-positive cells was discovered in the adventitia layer which could be stimulated to differentiate through a myofibroblast intermediate into an SMC population. It was also shown that these cells can migrate through the media *in vivo* and contribute to the neointima (Sartore et al., 2001; Torsney et al., 2005). Further data from cell fate mapping studies indicated that adventitial stem cells may indeed play a role in lesion formation, but only in cases where severe vessel injury is present (Roostalu et al., 2018). This has been supported by recent lineage tracing and single-cell RNA sequencing (scRNA-Seq) data which indicates that a population of adventitial Sca1 stem cells migrate into the medial layer and differentiate later into SMC-like cells following severe vascular injury to initiate vessel repair (Tang et al., 2020).

Vascular stem cells are most abundant in the adventitia but populations of multipotent cells have also been identified in the tunica media (Tintut et al., 2003). Sca1 cells have been isolated from the medial layer and confirmed their ability to differentiate into both SMC and endothelial cell lineages following appropriate stimulus (Sainz et al., 2006). In 2012, Song Li research group identified a new population of Sca1 cells in the tunica media of rat carotid arteries, termed mVSCs (Tang et al., 2012). Due to the fact that the carotid artery develops from a neuroectodermal lineage (Hempleman & Warburton, 2013), mVSCs were positive for neural crest stem cell markers, such as Sox10, SRY-box transcription 17 (Sox17) and Nestin. Furthermore, this subpopulation of cells expressed the calcium-binding protein S100 calcium-binding protein β (S100β). Although S100β is extensively used as a marker for mature glial cells and astrocytes, it has been shown on multiple occasions to be expressed by several types of neural stem cells (Ihrie & Alvarez-Buylla, 2008; Seri et al., 2004). S100β has also been suggested to contribute to neointima formation following ligation-induced injury (Cao et al., 2017). Furthermore, mVSCs were found to be negative for myogenic markers such as Myh11 and Cnn1 and demonstrated high levels of proliferation and telomerase activity which indicates stemness. This study also carried out lineage tracing to show that, following wire-induced injury, neointimal cells did not arise from the de-differentiation of medial SMCs, but rather mVSCs from medial and/or adventitial (Tang et al., 2012).

Using lineage tracing analysis and single-cell photonic analysis, our group have reported that SMC-like cells in vascular lesions may be originated from an S100β resident vascular stem cell that undergoes myogenic differentiation via the hedgehog signalling pathway (Molony et al., 2021). These data support the theory that mVSCs may contribute, at least to some extent, to the formation of a neointimal lesion following vessel injury. However, in order to understand the exact mechanisms by which these events might occur, further investigation is required regarding the involvement of key signalling pathways that drive mVSCs towards myogenic differentiation, such as PDGF, TGF-β1 and Notch signalling [Figure 1.5].

1.8 Myogenic differentiation

In vitro, TGF-β1 promotes myogenic differentiation of ESCs and the maturation of mural cells by positive regulation of SMC differentiation genes through the Suppressor of mother against Decapentaplegic 2 and 3 (SMAD2 and 3) dependent pathways and the Notch signalling pathway. PDGF is another important modulator of differentiation. PDGF-BB transduces its signal via specific tyrosine kinase receptors, PDGFR-α and PDGFR-β and acts as a potent mitogen. PDGF-BB promotes myogenic differentiation of Sca1+ progenitor stem cells via PDGFR-β-mediated signalling (Rensen, Doevendans and van Eys, 2007).

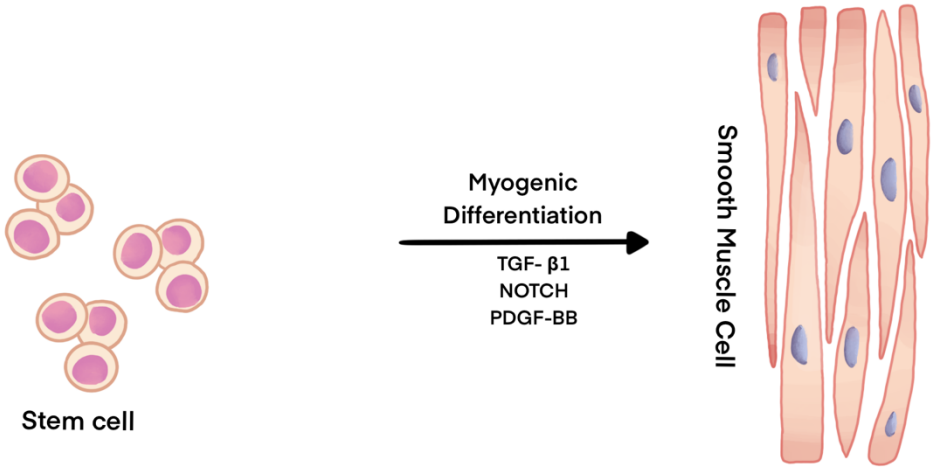

Figure 1.5. Myogenic differentiation of stem cells to smooth muscle-like cells. Vascular stem cell differentiation to smooth muscle cells through signalling molecules TGF-β1, Notch and PDGF-BB.

SMC differentiation can be determined by the level of expression of specific markers of SMC differentiation at messenger RNA (mRNA) and protein levels. These differentiation markers have been divided into early, mid-term and late, according to their appearance during

embryonic development, during restoration of differentiated phenotype of SMC or differentiation of stem cells toward SMCs. For example, during the early stage of differentiation of ESC-derived embryoid bodies, Acta2 is the first to be detected; Mid-term markers are h-caldesmon and Cnn1 followed by myocardin (Myocd), Tagln and Myh11.

1.9. Phenotypic characteristics of differentiated smooth muscle cells

For many years now, SMCs are reported to retain high degrees of plasticity *in vitro* and *in vivo*. They are a unique cell type as they have the ability to switch readily between two phenotypic states contractile and synthetic which all depend on the environmental situation to respond to alterations in blood flow or when a repairment is needed after vascular injury. Any disruption of this balance leads to many CVDs (Rensen, Doevendans and van Eys, 2007). Silenced genes in differentiated SMC acquire modifications associated with a closed chromatin state and transcriptional silencing (McDonald et al., 2006).

The control of SMC differentiation is a complex process that involves the co-operative interaction of many different key factors. Vascular SMC differentiation is determined primarily by serum response factor (SRF) and MYOCD (Chen et al., 2002). They directly promote the differentiation of SMC through binding to CC(A/T)-rich GG(CArG) elements and activation of the corresponding SMC differentiation genes. SRF-MYOCD level and activity dictate the transcriptional switch for a growing number of SMC differentiation genes (Long et al., 2008). A feature that is common of these genes is the presence of a 10-base pair cis-element known as a CArG box (consensus is CCW6GG, where W can be either A or T). These CArG sequences are recognised and bound by SRF and many of the SMC genes are dependent upon SRF activity. SRF recruits several coactivators that regulate the binding of CArG-SRF around those SMC genes to maintain cellular homeostasis. MYOCD, a cardiac- and SMC-restricted gene selectively transactivates CArG-containing contractile genes through a physical association with the Minichromosome maintenance protein 1, Agamous, Deficiens and SRF domain (Wang et al., 2001). SRF-MYOCD is active over genes containing multiple CArG elements, however, the presence of multiple CArG sites does not usually indicate functionality in SRF-MYOCD (Zhou & Herring, 2005) as additional coding information in DNA may attenuate SRF-MYOCD transcriptional activation, through alterations in CArG-SRF

structure, which lead to suboptimal MYOCD binding. The MYOCD role in dictating SMC phenotype is confirmed by loss-and-gain-of-function studies that demonstrate any non-SMC type overexpressing MYOCD is converted into an SMC-like state (Miano, 2015). Also, there are two other known related myocardin genes [Myocardin-related transcription factor A and B] both of which have similar SRF-dependent functions and are widely expressed but are under different control processes than MYOCD (Pipes et al., 2006).

In addition to SRF-MYOCD complexes, microRNAs (miRs) represent another class of regulatory effectors of SMC differentiation (Miano, 2015). The non-coding RNAs function as molecular regulators by decreasing protein levels through mRNA degradation, mRNA deadenylation, or translational repression (Carthew & Sontheimer, 2009). A number of miRs have been defined in SMCs, but the major regulatory effector for differentiation in SMC is the miR-143/145 bicistronic cluster. The miR-145 targets include the KLF4 and KLF5 to direct SMC differentiation and are capable of promoting myogenic differentiation while reducing the proliferative response to growth factors. Furthermore, there are several parallel transcriptional (or post-transcriptional) pathways that control SMC differentiation which includes the histidine-rich calcium-binding protein gene that lacks functional CArG elements but contains a conserved binding site for the Myocyte enhancer factor–2 family of transcription factors (Anderson et al., 2004). Similarly, Heart And Neural Crest Derivatives Expressed 2, SMADs, intracellular Notch receptor domains (NICD) and a great number of zinc finger contains transcription factors have also been implicated in SRF-MYOCD independent control of SMC-specific genes (Bobik, 2006).

1.9.1 Transforming Growth Factor-β (TGF-β) signalling pathways

TGF-β signalling is an important pathway during embryonic development and adulthood that controls cell behaviour such as cell proliferation and differentiation, tissue homeostasis and tissue regeneration. TGF-β signalling consists of two principal pathways namely, the canonical and the non-canonical pathways. The canonical TGF-β signalling transduction is mediated by the activity of the membrane-bound receptors, secreted ligands and the signalling effectors SMAD proteins (Derynck & Zhang, 2003). TGF-β is the prototype of the highly-conserved TGFβ superfamily the TGF-β family of ligand proteins is very extensive, with over 30 members

identified in humans. They are classified into two subfamilies namely the TGF-β-activin-Nodal and the Bone Morphogenic Protein subfamilies. TGF-β family of Serine/threonine kinase receptors consists of two receptor subfamilies defined as type I and type II, which create specific ligand-receptor combinations and thus activate a different signalling pathway. For instance, TGF-β binds exclusively to type I receptors TGFβR1 and TGFβR2. The SMAD family consists of eight proteins that regulate TGF-β signal transduction and thus transcription of the TGF-β target genes. SMAD proteins are activated by type I phosphorylation; however, the SMAD isoform that is activated depends on the ligand-receptor combination. For instance, SMAD2 and SMAD3 are targeted by TGFβR1 (Derynck & Zhang, 2003; Massagué, 2012; Ten Dijke & Hill, 2004).

TGFβ superfamily has the same overall structure, consisting of two extended monomers held together by an intermolecular disulphide bond (Hinck, 2012). All TGFβ monomers incorporate a characteristic 'cysteine knot' structure, composed of three intramolecular disulphide bonds that link six conserved cysteine residues (Hinck & Huang, 2013). There are three TGFβ isoforms that are expressed in mammals (TGFβ 1-3) all of which are localised in major blood vessels during development differently TGFβ1 highly localised to the tunica intima, TGFβ2 restricted to the tunica media and TGFβ3 expressed throughout the whole vessel wall (Akhurst et al., 1990; Millan et al., 1991). In adults, TGFβ1 and TGFβ3 proteins are mainly localised to the arterial intima, with TGFβ1 present in around 50% of the intimal stellate-shaped population of SMC (Bobik et al., 1999). TGFβ is considered part of a large latent complex, consisting of the C-terminal mature TGFβ peptide and N-terminal latency-associated peptide covalently bound to large latent TGFβ binding proteins (Ten Dijke & Arthur, 2007). Latent TGFβ complexes are stabilised by latent TGFβ binding proteins and play a role in facilitating their retention at the cell surface through direct interactions with fibrillin and other extracellular matrices (ECM) proteins (Robertson et al., 2015). while arginyl glycyl aspartic sequences in the latency-associated peptide target latent TGFβ to integrin receptors (Munger et al., 1998).

When TGF-β binds to its receptors, a hetero-tetrameric receptor complex composed of type I and two type II receptor components initiate activation of TGF-β signalling pathway. Thereafter, phosphorylation of type I by type II ensues and the signal is propagated by the

phosphorylation of SMAD2 and SMAD3 effector proteins. These receptor-regulated SMAD proteins form a heterodimeric complex with SMAD4 in the cytoplasm and subsequently translocate to the nucleus where they interact with other DNA-binding transcriptional factors and co-activators essentially cyclic binding protein and p300 to transcriptionally activate target genes [Figure 1.6]. The R-SMAD-SMAD4 trimer can also bind to co-repressors in order to repress the transcription of target genes. Therefore, the promoter targeted by the DNA-binding transcription complex is selected by the initial ligand-receptor combination (Derynck & Zhang, 2003; Massagué, 2012).

Both type I and type II receptors are present in the cell plasma membrane as homodimers preventing signal transduction in the absence of TGF-β ligands. The overall effect of SMAD/TGF-β signalling varies depending on the activity of different ligands, receptors and regulators, as well as contextual determinants that further shape the activity of the SMAD/TGF-β pathway (Derynck & Zhang, 2003; Massagué, 2012).

1.9.2 TGF-β signalling control of smooth muscle cell differentiation

In vitro studies demonstrated that the TGF-β1 isoform played an important role in embryonic-derived SMC development (Sinha et al., 2004, 2014; Wang et al., 2015; Xie et al., 2011). Human pluripotent stem cells (hPSCs: ESCs and iPSCs) were driven towards the SMC phenotype by transitioning through embryological lineage-specific progenitors that involved the treatment of neuroectodermal or (paraxial and lateral plate) mesodermal progenitors with recombinant TGF-β1 protein thus confirming the involvement of TGF-β signalling in SMC maturation from embryonic cells *in vitro* (Cheung et al., 2014).

Various SMC differentiation systems have been used to study the effect of recombinant TGF-β1 *in vitro*. For instance, neural crest cell-derived models (Monc-1 and JoMa1 cells) and mesodermal-derived models (C3H/10T1/2) transition to the SMC phenotype after TGF-β1 treatment, resulting in both expression of the SMC markers and phenotypic changes to the spindle-shaped morphology (Xie et al., 2011). In adult vascular SMCs, TGF-β treatment was associated with reduced proliferation and increased SMC differentiation, favouring the contractile or spindle-shaped morphology (Hao et al., 2003). The TGF-β signalling seems to be

an important mechanism of SMC differentiation and maintenance of stem cells and adult contractile SMCs, respectively (Wang et al., 2015).

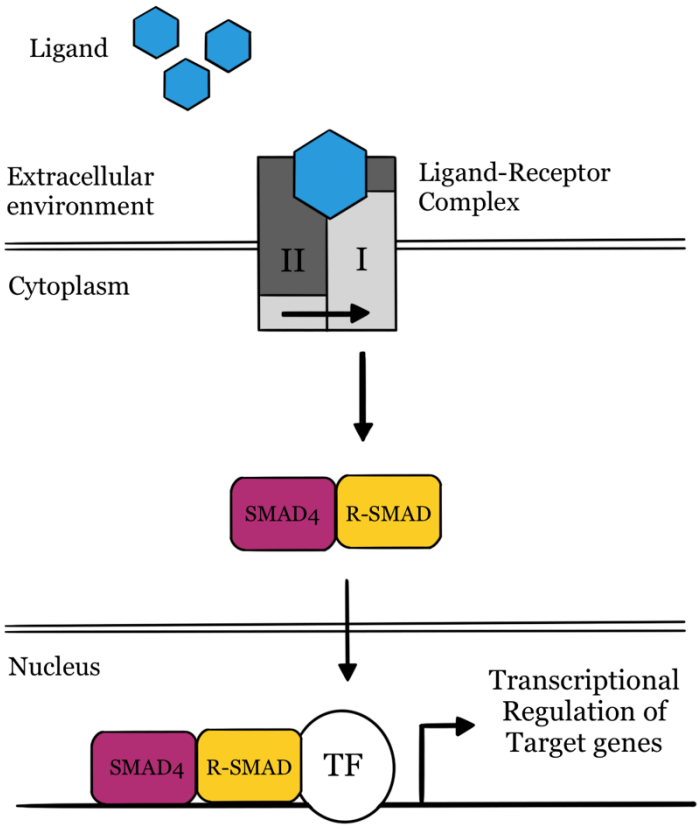

Figure 1.6. SMAD/TGF-β Signalling Pathway. Assembly of the two types I and II receptor components occurs upon binding of TGF-β ligands to the receptors. Subsequently, type I is activated by phosphorylation of type II and TGF-β signalling is activated, which in turn phosphorylates SMAD proteins (R-SMAD). R-SMADs bind to SMAD4 and translocate to the nucleus where the trimer associates with partners transcription factors to activate or repress the transcription of target genes. Image adapted in part from https://www.researchgate.net/publication/330251110_Celastrol_inhibits_colorectal_cancer_through_TGF-b1Smad_signaling/figures?lo=1.

Some of the atheroprotective effects of TGFβ are in part attributed to its capacity for stimulating SMC differentiation by inducing the expression of different mature SMC genes (including ACTA2, TAGLN and MYH11) (Guo, 2012) through SMAD2 and/or SMAD3, which interact with the SMC-specific promoters at putative SMAD binding element (Chen et al., 2003; Hu et al., 2003). TGFβ induces SRF protein expression and enhances its binding activity to CArG elements within the promoters of SMC marker genes (Hirschi et al., 2002). It has been shown that SMAD3 is the primary mediator for TGFβ1-induced TAGLN expression, while

SMAD6 and SMAD7 repress its activation. In addition, the authors illustrated that SMAD3 can bind to a SMAD binding element in the first exon of TAGLN and directly associate with the SRF complex in response to TGFβ1 treatment (Qiu et al., 2003). The synthetic SMC phenotype is induced by TGFβ, stimulating the production and secretion of collagen and proteoglycans by SMCs via direct and indirect interactions with the promoters of these genes (Kubota et al., 2003; Leask & Abraham, 2004; Verrecchia & Mauviel, 2002). However, the effects of TGFβ on SMC behaviour are more variable, with studies previously done showing that TGFβ can both inhibit and stimulate SMC proliferation and migration. This may occur because of the heterogeneous nature of SMCs, as evidenced by the varying gene expression patterns of human SMCs derived from primary atherosclerotic plaques, in-stent stenosis or healthy arteries (Zhang et al., 2002). At the molecular level, these differences are attributing to varying levels of receptor expression, membrane localisation of receptors, availability of intracellular signalling mediators and presence of transcriptional co-regulators within the nucleus (Khan et al., 2007).

1.9.3 Platelet-derived Growth Factor (PDGF) Signalling

PDGF isoforms (PDGF-A, PDFG-B, PDGF-C, PDGF-D, PDGF-AB, PDGF-AA, and PDGF-BB) are strong mitogenic and chemoattractant ligands that are involved in development, inflammation and tissue repair. Their secretion is regulated by platelets and endothelial cells to act on SMCs and mesenchymal-derived cells by binding to their corresponding tyrosine kinase receptors (PDGFR-α and PDGFR-β) (Hellström et al., 1999; Wang et al., 2015; Westermark et al., 1990).

1.9.4 PDGF signalling control of smooth muscle cell differentiation

It has been reported that PDGF signalling may play opposing roles in myogenic differentiation depending on the initial differentiation state of the target cells. In embryonic and adult stem cells, PDGF promotes myogenic differentiation to an SMC-like phenotype (Cheung et al., 2014; Xiao et al., 2007), whereas in differentiated SMCs, PDGF may be responsible for promoting de-differentiation to a more synthetic SMC phenotype (Corjay et al., 1989).

Primary cultures of Sca-1 MSCs undergo myogenic differentiation to SMC lineage following PDGF-BB treatment and increase the expression of ACTA2, TAGLN, CNN1 and MYH11 proteins (Hu et al., 2004). Mouse ESCs-derived Fetal liver kinase positive cells specification towards the SMC phenotype is also governed by PDGF-B/PDGFR-β, while administration of the vascular endothelial growth factor (VEGF) favoured endothelial cell differentiation (Yamashita et al., 2000). However, during adulthood, PDGF isoforms, PDGF-A and PDGF-B, are known to stimulate contractile SMC transition to a more synthetic phenotype *in vitro* as evident by changes in morphology, gene expression profile along with migration and proliferation rates (Rensen, Doevendans and van Eys, 2007). *In vivo,* arterial SMC proliferation contributing to neointima thickening was coordinated by PDGF-B but not PDGF-A in a balloon injury model of rabbit femoral arteries. PDGF-B and PDGFR β were highly expressed in the neointima with trace amounts within the tunica media of injured femoral arteries. Expression of PDGF-B in lesional cells peaked at 7 days concomitant with cell proliferation resulting in the formation of a large neointima by 21 days (Uchida et al., 1996; Wang et al., 2018).

1.9.5 Notch signalling pathway

The Notch signalling pathway plays a significant role in embryonic development and adult life, and controls various mechanisms in the vasculature such as stem cell proliferation, cell-cell interaction and differentiation state (Gazave et al., 2009). A variety of diseases in humans are controlled by the dysregulation of the Notch signalling pathway; thereby, modulation of Notch receptor signalling can serve as a regenerative medicine tool for vascular diseases (Jafar-Nejad et al., 2010). Notch signalling consists of two principal pathways namely, canonical and non-canonical (ligand- or transcription-independent) pathways. Canonical Notch signalling transduction is mediated by the activity of the membrane-bound receptors and ligands in vertebrates. There are four Notch receptors (Notch1-4), four delta-like ligands and two jagged ligands (Jagged1 and II I SMAD4 R-SMAD Cytoplasm transcription factors Nucleus Transcriptional Regulation of target genes Ligand-Receptor complex extracellular environment Ligand SMAD4 R-SMAD Jagged2) found in mammals up to date. The Notch receptors are heterodimers, which consist of a Notch extracellular domain (NECD) subunit non-covalently bound to the transmembrane and intracellular domain (NTMIC) [NECD-NTMIC] (Bray et al., 2016; Kopan & Ilagan, 2009).

Upon receptor-ligand interaction between neighbouring cells, the ADAM (A disintegrin and metalloproteinase) family of metalloproteases initiate a proteolytic cleavage of Notch at site 2 resulting in the release of the extracellular domain from the heterodimer Notch receptor followed by its endocytosis by the ligand-presenting cell. In the Notch-activated cells, a membrane-tethered intermediate known as Notch extracellular truncation (NEXT) is proteolytically cleaved by γ-secretase, a multiprotein complex of cleaving proteases at site 3 and site 4, thus the release of the NICD into the cytoplasm. Subsequently, NICD translocates the nucleus where it interacts with the DNA-binding protein Recombination signal sequence-binding protein Jkappa (RBP-Jk) recruiting the co-activator Mastermind, which in turn recruits the mediator transcription activation complex thus activating transcription of the Notch target genes. Notch target genes include the hairy enhancer of split (HES) and the HES-related repressor proteins (HERP) family (Table 1.1) that act as Notch effectors by negatively regulating the expression of downstream target genes encoding for tissue-specific proteins (Figure1.7)(Bray et al., 2016; Iso et al., 2003; Kopan & Ilagan, 2009).

Table 1.1. The HERP family (Iso et al., 2003).

Abbreviations	**Full Names**	**Species**	**Function**
HERP1, HERP2 & HERP3	HEY-related repressor protein	Mouse, rat, human	Transcriptional repressor
Hesr1, Hesr2 & Hesr3	Hairy/E(spl)-Related	Drosophila, mouse, human	Transcriptional repressor
Hey1, Hey2 & HeyL	Hairy/E(spl)-related with YRPW	Drosophila, mouse, chicken, human	Transcriptional repressor

In the absence of a ligand, the initial cleavage of the Notch receptor by ADAM is prevented by a unique negative regulatory region within the NECD (Kopan & Ilagan, 2009).

Both Notch receptors and ligands are trans-membrane proteins. Receptors are activated in adjacent cells by expressed ligands, which then undergo successive proteolytic cleavages.

NICD translocates to the nucleus where it associates with RBP-Jk. The NICD-RBP-Jk forms a transcriptional complex which activates the expression of the primary Notch target genes, HES and HES-related repressor protein families that act as Notch effectors (Iso et al., 2003).

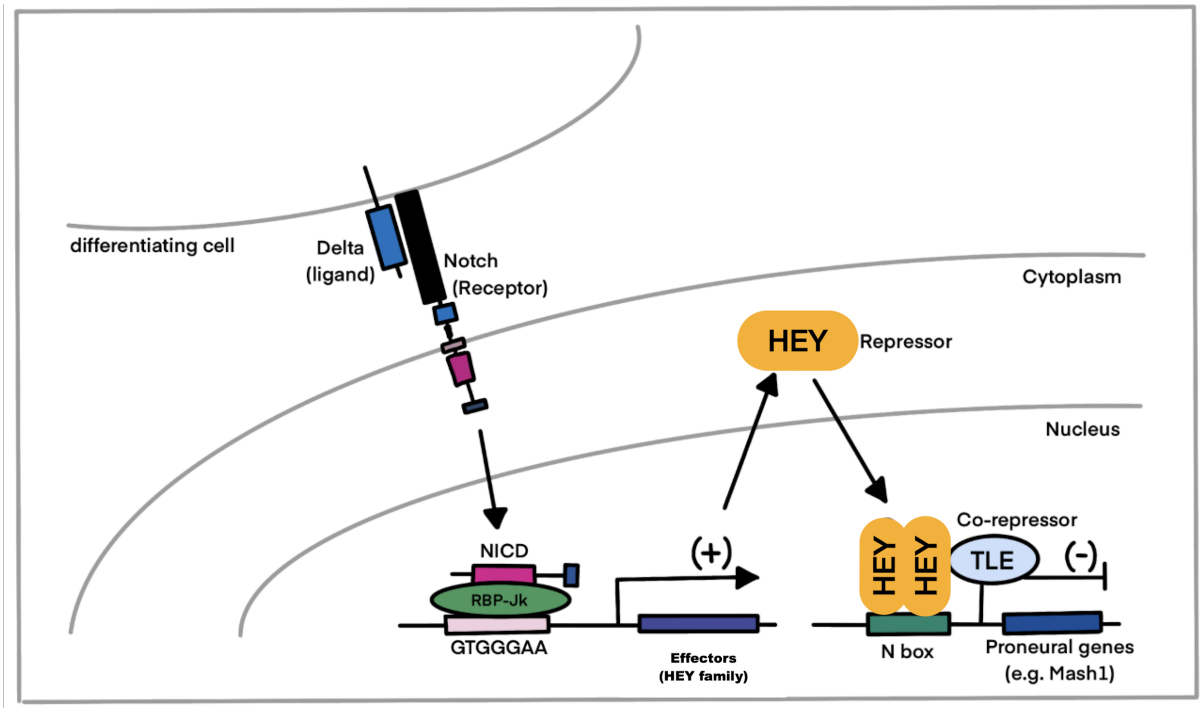

Figure 1.7. Notch Signalling Pathway. The Notch receptor binds to its cognate ligand (Jag-1 in this case) on a neighbouring cell. A conformational change occurs which exposes site 2 which is subsequently cleaved by a metalloprotease called Disintegrin and metalloproteinase domain-containing protein 10. The complex of NECD-Jag- 1 is trans-endocytosed into the ligand-expressing cell. A second cleavage at Site 3 by γ-secretase releases the NICD which translocates to the nucleus and forms a transcription complex with a number of factors, including RBP-Jκ. Expression of target genes such as *Hey1* and *Hey2* is subsequently activated.

1.9.6 Notch signalling control of smooth muscle cell differentiation

There are highly conserved Notch signalling pathway functions in many different developmental and homeostatic processes (Bray et al., 1998). In the canonical ligand-dependent pathway, Notch receptors (Notch1-4) undergo conformational changes upon ligand engagement (e.g. Jagged1, Jagged2, Serrate and Dll4), stimulated by a pulling force on the extracellular fragment of Notch that results from endocytosis of the receptor-bound ligand into the ligand-expressing cell. These conformational changes in the receptor allow for two consecutive proteolytic cleavage events to occur, which release the intracellular region of the receptor into the cytoplasm where it then migrates to the nucleus and induces Notch target gene transcription [Figure 1.7]. However, there is accumulating evidence that other

pathways may also induce Notch signalling. A ligand-independent mechanism of Notch activation is described as a receptor process initiated via cell-internal signals. These signals result in the internalization of Notch into endosomal compartments, where chemical changes existing in this microenvironment result in the conformational modifications required for receptor processing (Bray et al., 2016).

The Notch signalling pathway has an important role in the differentiation and function of SMCs. Many studies have shown that Notch activation promotes differentiation of some SMC cultures but inhibits differentiation in others. Overexpression of constitutively activated form of NICD in human aortic smooth muscle increased the expression of smooth muscle marker genes (*MYH11* and *TAGLN*) (Doi et al., 2006) and Jagged-1 induced Notch activation upregulated contractile protein expression in human SMCs (Boucher et al., 2011; Wang et al., 2015). In contrast, It has been shown that active Notch signalling inhibits SMC differentiation (Morrow et al., 2005; Proweller et al., 2005). However, it promotes SMC differentiation in a population of stem cells. MSCs have also been stimulated to become SMC-like cells via Jagged-1-induced Notch activation (Kurpinski et al., 2010). Studies In both *in vivo* and *in vitro* have reported the importance of Notch activation during SMC specification of neural crest progenitors, and the separation of SMC, and blood cell /endothelial cell progenitors of ventral mesodermal cells (High et al., 2007; Shin et al., 2009; Wang et al., 2015).

1.10 Lineage tracing analysis of lesional cells

Lineage tracing techniques have greatly facilitated the characterization of cell fate. Various lineage tracing techniques include the use of dyes or radioactive tracers labelling (Serbedzija et al., 1989), transfection (Kim et al., 2018), genetic mosaics (Mintz et al., 1965) and genetic recombination (Giangreco et al., 2009). DNA site-specific recombination using the Cyclization recombinase (Cre), a genetic recombination technique, has been widely used to identify cell fate due to the ability to label the cells indelibly with a fluorescent tag (Bruneau, 2008; Driessens et al., 2012). The DNA site-specific recombination system is comprised of a specific promoter-driven Cre recombinase and a STOP codon sequence between two recognition locus of x-over, P1 (LoxP) sites (Metzger et al., 1999) upstream of a reporter gene under the control of a ubiquitous promoter (e.g., Rosa26). In a cell-specific manner, the recombinase

constitutive or inducible (under the control of an estrogen receptor type 2(Cre-ERT2)) is activated and deletes the STOP sequence between the 2 x LoxP sites thereby facilitating indelible genomic marking of a specific cell population with a fluorescent tag (e.g, enhanced green fluorescent protein (eGFP)).

Adult SMCs possess the potential to give rise to diverse phenotypes, through which SMCs from media are purported to be involved in vascular lesion formation (e.g., atherosclerosis). Using *Myh11-CreER/Apoe*$^{-/-}$ mice, it has been reported that macrophage-like cells and MSCs in atherosclerotic lesions are derived from adult SMCs, a process mediated by KLF4 (Shankman et al., 2015). A similar result was observed in a study using *Myh11-CreER*;Rosa26-Confetti mice were a subset of medial-derived SMCs expressing the macrophage marker, Galectin3 during neointima formation (Chappell et al., 2016). Both research groups confirm that medial SMCs can simultaneously form fibrous caps and the plaque core that are respectively characterized by ACTA2^{+} modulated SMCs and macrophage-like cells (Chappell et al., 2016; Feil et al., 2014). However, the lineage tracing efficiency of the inducible CreERT2-LoxP system has been criticized due to its reliance on tamoxifen to induce the Cre-ERT2 which may remain in tissues long after tamoxifen withdrawal and thereby go on to inadvertently mark non-SMCs that acquire SMC differentiation markers (Reinert et al., 2012).

Indeed, the roles of resident stem/progenitor cells in various mouse models of vascular injury have been demonstrated (Kramann et al., 2016; Tang et al., 2012; Wan et al., 2012). As shown in two studies, non-bone marrow-derived progenitors are able to generate SMCs and endothelial cells in allograft mouse model, while minimally participating in neointima formation in femoral artery injury mouse model (Chen et al., 2018; Ni et al., 2019). Lineage tracing analysis has provided compelling evidence for the involvement of (i) stem cell-derived progeny (Kramann et al., 2016; Tang et al., 2012; Wan et al., 2012) in addition to (ii) 'reprogrammed' differentiated SMC (Albarrán-Juárez et al., 2016; Chappell et al., 2016; Herring et al., 2014; Nemenoff et al., 2011), (iii) SMC derived from endothelial-to-mesenchymal transition (Cooley et al., 2014) and (iv) SMC derived from bone-marrow stem cells (Yu et al., 2011) in the formation of intimal thickening as these cells become activated/reprogrammed, differentiate down vascular and myeloid lineages and then dictate, in part, vessel remodelling.

Another way of investigating the origin of these SMC-like cells in the neointima is to examine their stable epigenetic marks which may provide an answer to their origin. Indeed, *in vivo,* the SMC lineage-tracing studies that identified de-differentiation, proliferation and migration of a discrete population of Myh11/Sca1 positive medial SMCs also demonstrated that the enrichment of histone 3 lysine 4 di-methylation (H3K4me2) on the CArG regions of Myocd-regulated SMC genes as a stable ‘‘epigenetic signature’’ of SMC lineage (McDonald et al., 2006).

1.11 Epigenetics

1.11.1 What is Epigenetics?

Epigenetics is defined as inheritable changes in gene expression which occur without any alterations in DNA sequence. In each eukaryotic nucleus, the compacted DNA is named chromatin which is formed by the basic unit that is known as nucleosome. Every nucleosome is formed by histones surrounded by 145-147 pairs of DNA bases. Histone is an octamer composed of four pairs of proteins namely, H3, H4, H2A and H2B. Epigenetics regulation of histone alters chromatin conformation and the accessibility of transcription factors to DNA, which results in the activation or silencing of gene transcription (Luger et al., 1997).

Decades ago it was noticed by many researchers that commonly recognized risk factors (lifestyle, diet and genetic background) do not explain all features of cardiovascular morbidity (Rose et al., 1964). Epigenetic mechanisms have linked the internal genetic landscape and the external environmental influences, thus they might provide better mechanistic insight into the cause of CVD (Ordovás et al., 2010). There are three main mechanisms of epigenetic regulation that are identified [Figure 1.8]. Two of which, namely, DNA methylation and histone modification, have an influence on the type of chromatin structure by regulating patterns of gene expression (Baccarelli et al., 2010). These processes are important to the development and differentiation of distinct cell lineages in the adult organism (Handy et al., 2011). The third mechanism is based on the expression of microRNAs (miRNAs) (Tao et al., 2016) which are short (18–20 nucleotides) non-coding RNAs that bind target mRNAs via partial or complete match of their 3’ untranslated region and lead to their degradation and

post-transcriptional gene silencing. Many human miRNAs loci are located within intronic regions and are capable of exerting epigenetic control upon cell cycle, apoptosis and other crucial biologic processes (Della Vittoria Scarpati et al., 2014; Rouhi et al., 2008). Notably, miRNAs combine with mRNA induce transcriptional repression by recruiting specific argonaute proteins and forming epigenetic remodelling complexes that suppress gene expression by fostering histone and DNA methylation. In addition, long non-coding RNAs which are defined as RNAs longer than 200 nucleotides that are not translated into functional proteins can work in combination with miRNA to regulate gene expression (Duan et al., 2018).

Epigenetics provides an important contribution to the differentiation program of SMCs, since it increases the accessibility of the CArG motifs for SRF binding in SMCs (McDonald et al., 2006). Many genes that characterize SMC phenotypic switching, including the contractile proteins, are regulated at the level of transcription. As such, most research has focused on identifying the transcription factors and promoter elements that drive such responses. Smooth muscle-specific genes are generally regulated by dual CArG elements in their promoter or intronic regions that bind to SRF. SRF can also regulate pro-proliferative genes when bound to growth factor-regulated co-factors (Miano, 2003), smooth muscle- and cardiomyocyte-specific transcriptional co-activator MYOCD, which binds to SRF at CArG elements, and is sufficient to promote the SMC contractile phenotype (Long et al., 2008).

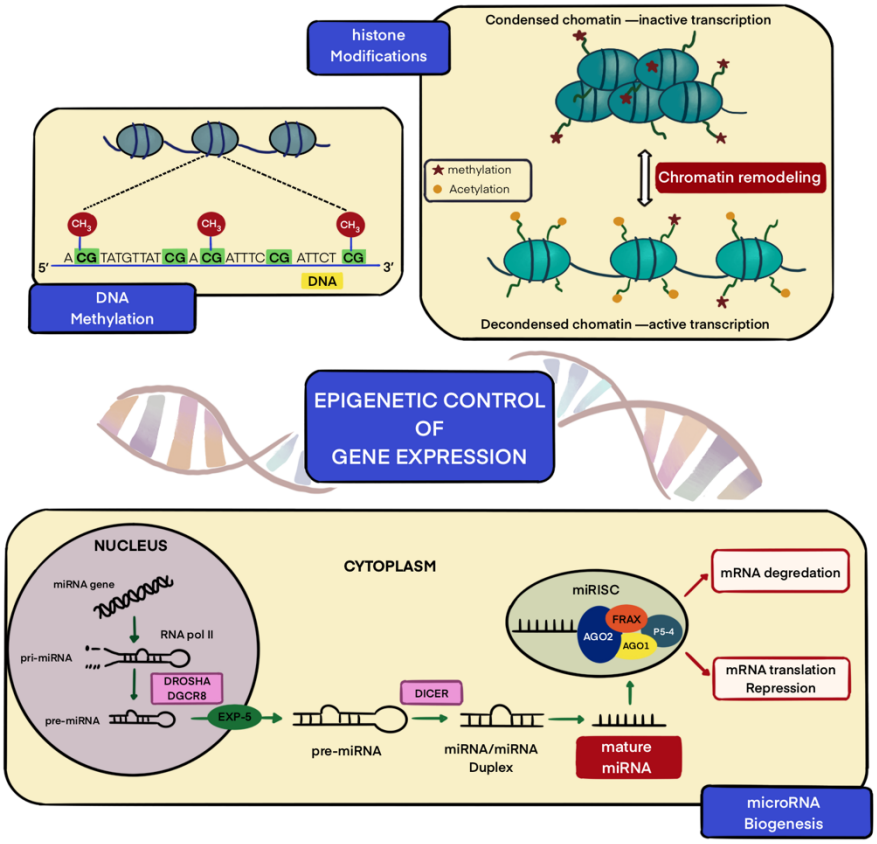

Figure 1.8. Principal epigenetic mechanisms controlling gene expression. DNA methylation, the covalent binding of a methyl group to the 50 carbon of cytosine at cytosine phosphate guanine (CpG) dinucleotide sequences usually inhibits gene transcription if occurring in the gene promoter but it may also promote transcription when localized at a gene exons sites. Epigenetic histone modifications are known to be post-translational changes that involve histone tail residues and influence gene expression by controlling the dynamics of chromatin. Histone tail methylation and acetylation are reported as the main histone epigenetic phenomena as schematically shown in the upper right panel of the Figure. In particular, as reported in a simplified scheme in the Figure, the acetylation of specific lysine residues (i.e. H3K9, H4K12) leads to a decondensed, transcriptionally active chromatin, while histone methylation is usually associated to transcriptional repression, even if di- and trimethylation of lysine 4 of histone H3 (H3K4me2, H3K4me3) may be associated to transcriptionally active chromatin. In the lower panel is reported a simplified scheme of microRNA biogenesis. MicroRNAs are small non-coding RNA fragments, recently classified as epigenetic mechanisms. The biogenesis of microRNAs occurs across nucleus and cytoplasm of the cell, the latter cell environment being the place where mature microRNAs exert their down-regulating effect on gene transcription by leading to target mRNA degradation or by mRNA translation repression. Image adapted from Udali et al., 2012.

1.11.2 Histone modifications

Histone modifications are post-translational modifications of histone protein that regulate a different physiological mechanism. As a result, dysregulation of histones is involved in many diseases and complications (Waggoner et al., 2007). Several types of histone modifications

are known, amongst which acetylation, methylation, phosphorylation, and ubiquitination are the most widely characterised and important in terms of the regulation of chromatin structure and (transcriptional) activity (Sawicka & Seiser, 2012). There are 13 modification sites in histone H2A, 12 modification sites in histone H2B, 21 modification sites in histone H3 and 14 modification sites in histone H4. Each site can either be unmodified or modified. These modifications, especially methylation, acetylation and phosphorylation of histone H3 and H4, regulate the binding of sequence-specific transcription factors to DNA within the context of the intact cells and chromatin. For example, lysine acetylation at the histone N-terminal is able to eliminate the positive charge of histones, allowing negatively charged DNA to separate from them and acquire a transcription-ready configuration. While histone lysine methylation causes transcriptional activation or repression depending on the position of the methylated lysine. There are three different possibilities for each site of the methyl group (mono, di or tri). The outcomes of these modifications can be gene transcription and chromatin relaxation, or as an opposite, chromatin compaction and gene repression (Strahl & Allis, 2000).

1.11.3 DNA methylation

DNA methylation, a pre-transcriptional modification that is characterized by the addition of methyl groups to specific nucleotides, regulates the stability of gene expression states and maintains genome integrity by collaborating with proteins that modify nucleosomes (Urnov & Wolffe, 2001). DNA methylation is the transfer of a methyl group to the 5' position of cytosine. This reaction is due to enzymes called DNA-methyltransferase (DNMT) which target DNA sequences specifically rich in cytosine and guanine nucleotide pairs. There are two types of DNMT, namely DNMT1, which preserves a pattern of a pre-existing methyl after replication of cells, and DNMT3 that methylates unmethylated DNA [Figure 1.9]. In human DNA, cytosine-phosphate-guanine (CpG) regions are concentrated in short CpG-enriched DNA fragments, called CpG islands (CGIs). About 60% of all gene promoters are rich in CGIs, and thus these genes can be epigenetically regulated. (Bernstein et al., 2007; Meissner et al., 2008). Having been characterized as the best epigenetic modification, DNA methylation is linked to gene silencing. Furthermore, it has been shown that certain SMC genes that are regulated by DNA methylation could be associated with SMC phenotypic modulation and the development of vascular diseases (Laukkanen et al., 1999).

In atherosclerosis-prone ApoE-null mice, DNA methylation changes occurred in both peripheral blood leukocytes and the aorta before the formation of vascular lesions (Chen et al., 2001). Changes were shown to contribute to inflammation and promote atherosclerosis (Lund et al., 2004). When normal heart tissue was compared with tissue from patients with heart failure, the diseased tissue showed differential methylation in angiogenesis-related genes, as well as differential expression (Movassagh et al., 2010).

1.11.4 DNA demethylation

The mechanisms of DNA demethylation, albeit controversial, have been described during SMC differentiation and the presumed role of the ten-eleven-translocation (TET) family of enzymes that oxidise 5-methylcytosine (5-mC) to 5-hydroxymethylcytosine (5-hmC) in SMC. Through the repairment pathway of DNA and thymine-DNA glycosylase, 5hmC is converted to unmethylated cytosine, leading to DNA demethylation and gene activation. TET-2 is the predominant isoform in human coronary artery SMC cultures, which is highly enriched in smooth muscle tissues (Ito et al., 2010; Koh et al., 2011). *TET-2* expression increased following myogenic differentiation and was reduced following PDGF-BB-stimulated de-differentiation. Parallel loss-and-gain-of-function studies confirm the role of TET-2 in inducing SMC differentiation genes (*MYOCD, MYH11, ACTA2, and TAGLN*) by modifying histone methylation (H3K4me2) contributing to regulation of these genes (Liu et al., 2013).

1.12 The role of histones in differentiated SMCs

SMC-selective changes in chromatin remodelling contribute to the coordinate activation of CArG-dependent SMC marker genes during differentiation of these cells from ESCs. Enrichment of H3K4me2 on SMC marker genes, including *Myh11, Acta2,* and *Tagln*, in mature SMC and SMC progenitor cells committed to differentiate into SMC. On the contrary, this enrichment was not seen in ESC and non-SMC somatic cells. 5hmC plays an important role in the maintenance of pluripotency, self-renewal, and proper differentiation of ESC during early development. The role of 5hmC in somatic cells is imperfectly understood. However, several studies suggest that 5hmC promotes cell-specific differentiation programs in somatic cells via

the enzyme TET-2 (Dawlaty et al., 2014; Ficz et al., 2011). Furthermore, even with more interrogation, it was demonstrated that H3K4me2 and H4 hyperacetylation of the SM α-actin gene locus in SMCs do not depend on the CArG boxes and thus are also independent of either SRF or myocardin/myocardin-related transcription factor binding (McDonald et al., 2006).

This H3K4me2 epigenetic mark has several important characteristics including (i) enrichment of H3K4me2 on SMC contractile genes, including *ACTA2*, *MYH11*, and *TAGLN* is restricted to the SMC lineage. (ii) H3K4me2 epigenetic signature appears in SMC precursors during all-trans retinoic acid-induced SMC differentiation. (iii) H3K4me2 enrichment on the SMC contractile genes occurs independently of binding of the SRF-MYOCD complex on CArG boxes. (iv) H3K4me2 signature is stably retained on poised SMC marker genes during SMC transient phenotypic modulation *in vitro* and *in vivo* (Gomez et al., 2013).

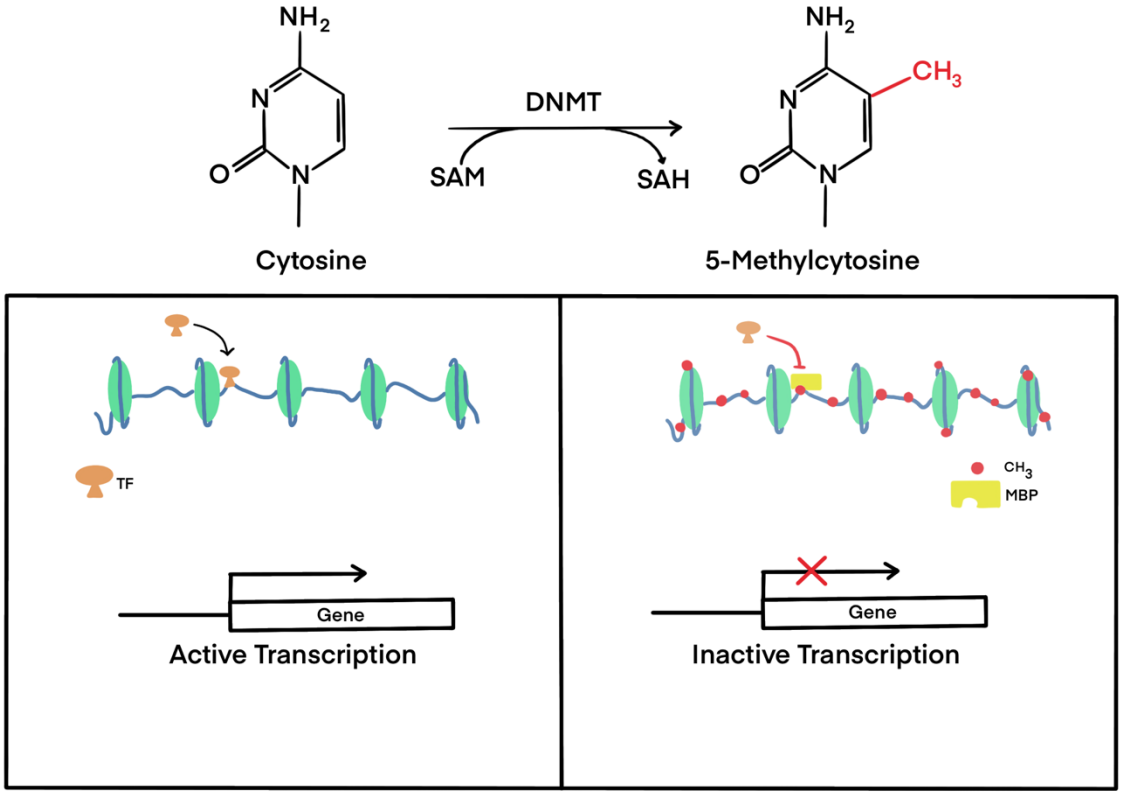

Figure 1.9. DNA methylation is associated with inactive transcription and suppressed gene expression. The figure outlines the molecular mechanism linking DNA methylation and inactive transcription. Cytosine is methylated to 5-mC by DNA methyltransferase (DNMT). Binding of a methyl CpG-binding protein to methylated sequences prevents access to this sequence by transcription factors, thereby suppressing transcription. MBP indicates methyl CpG-binding protein; SAM, S-adenosylmethionine; and SAH, S-adenosylhomocysteine. Image adapted from Zhong et al.,2016.

H3K4me2 is known to be an epigenetic mark that directs progenitor cells toward SMC differentiation, both in normal vascular development and in vascular diseases (McDonald et al., 2006). However, it is unclear how histone methyltransferases, which catalyse the formation of H3K4me2, are specifically addressed to SMC target genes and how the H3K4me2-marked SMC genes switch from a silent to an active state during embryogenesis or adult homeostasis (McDonald et al., 2006). H3K4me2 on the SMC marker genes is known to be a restricted and stable epigenetic signature of the SMC lineage distinguishing SMC from other cell types independently of their state of differentiation. While H3K27 methylation mono, di and tri are markers of transcriptionally silent chromatin (Barski et al., 2007). Non-coding RNAs in the panorama of epigenetic mechanisms also influence SMC development. Among non-coding RNAs, miRNAs are ~22 nucleotide-long non-coding RNA molecules that control gene expression by alternations in the function of mRNAs. Indeed, miR-143 and miR-145 are necessary to keep SMCs in a fully differentiated state (Cordes et al., 2009). Genetic interference with the expression of miR-143/145 in mice reduced the expression of SMC differentiation markers, smooth muscle contractile activity and blood pressure, but caused neointimal lesions in the femoral arteries of these miR143/145 mutant mice (Boettger et al., 2009). The H3K4me2 signature has also been used to further suggest that neointimal SMC-like and macrophage-like cells are derived from differentiated SMCs *in vivo* (Shankman et al., 2015).

1.13 Epigenetic changes during SMC differentiation/de-differentiation

It was assumed that SMCs are not terminally differentiated and can undergo rapid changes in phenotype in response to vascular injury or in various CVDs, including atherosclerosis. However, until recently, the evidence for this was mostly based on inferences from studies in cultured SMC (Alexander & Owens, 2011; Gomez & Owens, 2012; Libby et al., 2011). Treatment of SMC in culture with various growth factors, such as PDGF or basic fibroblast growth factor, oxidized phospholipids resulted in coordinate reductions in expression of SMC marker genes, as well as increased migration, proliferation, and secretion of various ECM proteins and cytokines. This process is collectively referred to as phenotypic modulation or switching (Alexander et al., 2012; Bornfeldt et al., 1994; Kaplan-Albuquerque et al., 2005;

Millette et al., 2005; Pidkovka et al., 2007; Yoshida et al., 2007). The understanding of phenotypic modulation and the fate of phenotypically modulated SMC *in vivo* are confounded by the fact that this process is characterized by downregulation of the SMC marker genes like *Acta2 a*nd *Myh11* making their identification *in vivo* unreliable without rigorous lineage tracing systems. Thus, the paradigm of SMC phenotypic switching during vascular injury and disease has been challenged by studies, suggesting that a significant subset (Gomez & Owens, 2012), if not the majority, of lesion and neointimal cells are of mesenchymal stromal stem cell (Caplice et al., 2003; Sata et al., 2002) or adventitial (Hu et al., 2004) origin and not from SMC.

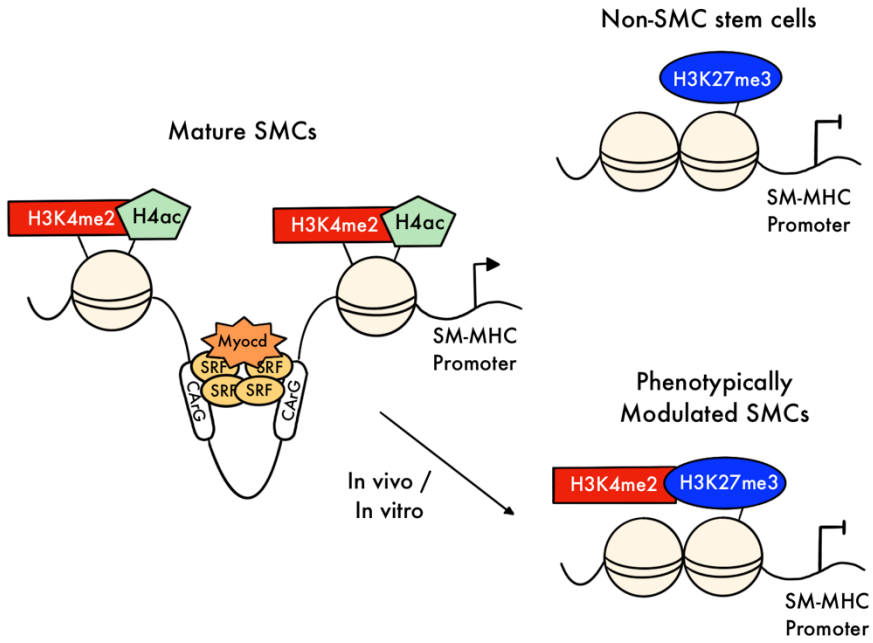

Figure 1.10. Cartoon depicting epigenetic changes in mature SMCs. Diagram summarises the histone methylation and acetylation of the SM-MHC promoter at CArG sites in mature SMCs, phenotypically modulated SMCs and non-SMC stem cells. Adapted from Gomez et al., 2013.

Tang et al, provided a much more profound claim that challenged the conventional dogma that SMCs are the principal source of SMC marker-positive cells within the neointima and concluded that mature SMCs are terminally differentiated (Tang et al., 2012). That group suggested that the primary source of neointimal cells following vascular injury is derived from what they claimed was a medial stem cell population (Tang et al., 2012). However, the main conclusions of this study were strongly refuted in an Editorial from a collective group of authors, who are leaders in the field, on the basis of there being major technical and design flaws in those studies (Nguyen et al., 2013). Several subsequent rigorous lineage tracing

studies refute the major conclusions of Tang et al and provided compelling evidence that SMCs are plastic and exhibit phenotypic switching *in vivo* (Feil et al., 2014; Gomez et al., 2013; Herring et al., 2014; Nemenoff et al., 2011; Shankman et al., 2015).

One particular study using a novel SMC-specific conditional lineage tracing mouse model (ie, *Myh11*-CreERT2 ROSA floxed STOP e yellow fluorescent protein (YFP) mice, designated SMC *YFP +/+* mice) demonstrated that >80% of SMC-derived cells within advanced *ApoE*$^{-/-}$ brachiocephalic artery lesions were marked as originating from medial SMCs but lacked detectable expression of SMC markers, such as Acta2 (Shankman et al., 2015). Moreover, approximately one-third of these cells that were YFP+ but Acta2− expressed multiple markers of macrophages. Thus, the authors argued, previous studies in the field may have misidentified these cells as being monocyte-derived macrophages. Most importantly, these phenotypic transitions of SMC were functionally important, in that SMC-specific conditional knockout of the pluripotency factor Klf4 did not prevent SMC phenotypic switching, but rather altered the nature of the phenotypic transitions, including a marked reduction in SMC-derived macrophage-like cells (Shankman et al., 2015). Another study was conducted using a *Tagln* CreERT2 ROSA floxed STOP LacZ mouse model to show that a subset of SMC-derived cells expresses several macrophage markers, and SMC-derived cells within lesions underwent clonal expansion during atherosclerosis using R26R-Confetti multi color Cre reporter mice (Feil et al., 2014). Further evidence of SMCs being not terminally differentiated and undergo phenotypic transitions during vascular injury repair can be found in studies by Nemenoff et al, who used a conditional *Myh11*CreERT2 ROSA26 LacZ reporter mouse and provided compelling evidence that the majority of neointimal cells after wire-induced injury of the femoral artery are derived from pre-existing differentiated Myh11 SMC. Herring et al, used conditional *Myh11* and *Acta2* creET2 mTmG mice to show that previously differentiated SMC dedifferentiate and constitute the main source of SMC within the neointima after carotid ligation injury (Herring et al., 2014) and to confirm the observations from Nemenoff's previous work (Nemenoff et al., 2011).

Taken together, these studies emphasise the need for reliable identification of SMC-derived cells within intimal lesions after injury or within atherosclerotic lesions. This can be done through the use of rigorous SMC lineage tracing in combination with high-resolution imaging

to ensure the lineage tracing of the gene and markers of cell phenotype are present within the same cell (Caplice et al., 2003; Gomez & Owens, 2012; Iwata et al., 2010).

There is a repertoire of SMC-specific epigenetic histone modifications that are acquired during hESC myogenic differentiation, including H3K4me2 at SMC marker genes such as *ACTA2* and *MYH11*, with MYH11 being the most specific marker of SMC lineage (Manabe & Owens, 2001; McDonald et al., 2006; Miano et al., 1994). Currently, results show that H3K4me2 of these genes is restricted to only SMCs and is absent in non-SMCs. Furthermore, H3K4me2 enrichment of these genes persists when cultured SMCs are induced to undergo phenotypic switching to a less differentiated state [Figure 1.10](McDonald et al., 2006), a process that requires the activation of the hESC pluripotency factor KLF4 both *in vivo* (Salmon et al., 2012) and in cultured cells (McDonald et al., 2006). These results suggest that H3K4me2 at SMC marker gene loci represent a stable epigenetic mark of SMC lineage, at least *in vitro.*

In vivo, Gomez et al, initially used a proximity ligation assay (PLA) to further interrogate H3K4me2 enrichment at the *MYH11* locus in human coronary arteries by detecting the proximity between a biotin-labelled probe targeting the *MYH11* promoter and H3K4me2 at this locus (Gomez et al., 2013). PLA is widely utilized for protein-protein interactions or detection of protein post-translational modifications (Brobeil et al., 2011; Rantala et al., 2011). Consistent with PLA results in small arteries of mice and ChIP results in cultured cells, Gomez et al, found that ACTA2 SMCs in the media of human vessels were the only positive cells for the H3K4me2 mark using the PLA assay [Figure 1.10], while adventitial fibroblasts and endothelial cells were negative. In advanced atherosclerotic lesions, cells that did not express SMC marker genes such as *ACTA2* and *MYH11* were positive for the H3K4me2 mark in human coronary arteries using the PLA assay (Gomez et al., 2013).

To further address the role of H3K4me2 in regulating SMC differentiated state and whether H3K4me2 may serve as a mechanism for maintenance of SMC lineage identity, a targeted epigenome editing strategy consisting of gene-specific demethylation of H3K4me2 on the family of Myocd-dependent gene repertoire has recently been reported by the same research group (Liu et al., 2021). The CArG box-SRF- Myocd complex has been known as a central master regulator of the SMC contractile gene activation. Myocd is a potent myogenic coactivator exclusively expressed in SMC and cardiomyocytes (Chen et al., 2002; Du et al.,

2003; Wang et al., 2001). Myocd functions by forming a complex with SRF recruited to the *cis*-element CArG box CC(A/T)6GG which is present in SMC marker genes including *Acta2*, *Myh11*, *Tagln*, and *Cnn1*. Myocd is required for SMC differentiation during vascular development as suggested by *in vivo* loss-of-function studies (Huang et al., 2008; Li et al., 2003). Besides Myocd, the DNA methylcytosine dioxygenase TET-2 promotes SMC differentiation by preventing DNA methylation at SMC contractile genes (Liu et al. 2019).

A fusion protein linking the nuclear localization signals and the SRF-binding domain of Myocd and the lysine-specific demethylase 1 (LSD1) was engineered to serve as a recruitment and catalytic subunit, respectively. A non-functional editing system Myocd-LSD1/NF containing the catalytically inactive LSD1 was also designed as a control. Data show a significant decrease in H3K4me2 levels on myogenic genes in SMCs expressing Myocd-LSD1 specifically while no noticeable effect was observed in SMCs expressing Myocd-LSD1/NF, suggesting that Myocd-LSD1-induced H3K4me2 demethylation is dependent on LSD1 demethylase activity (Liu et al., 2021).

The same research group delivered lentivirus encoding Myocd-LSD1 or Myocd-LSD1/NF on the right carotid arteries of *Myh11* CreERT2 -YFP mice using pluronic gel application. Upon tamoxifen treatment, Myh11 SMCs were permanently and specifically labelled with YFP using Myh11-Cre-LoxP mice where SMC identity is traced regardless of SMC marker gene expression (e.g., *Acta2* and *Myh11*), which could be altered upon H3K4me2 editing. Myocd-LSD1 was highly expressed in transduced carotid arteries and SMCs following two weeks of virus delivery. While Myocd-LSD1 did not induce significant changes in vessel morphology, a marked reduction in Acta2 and Myh11 expression was observed in YFP-positive SMCs. Importantly, there was a direct association between expression of Myocd-LSD1 (mCherry) positive and reduced Acta2 expression. Expression of Myocd-LSD1 was not associated with a change in SMC proliferation, survival, and apoptosis rate. Thus, the presence of H3K4me2 on the CArG box regions of SMC contractile genes is essential for maintenance of SMC contractile phenotype and function *in vitro* and *in vivo* (Figure 1.11) (Liu et al., 2021).

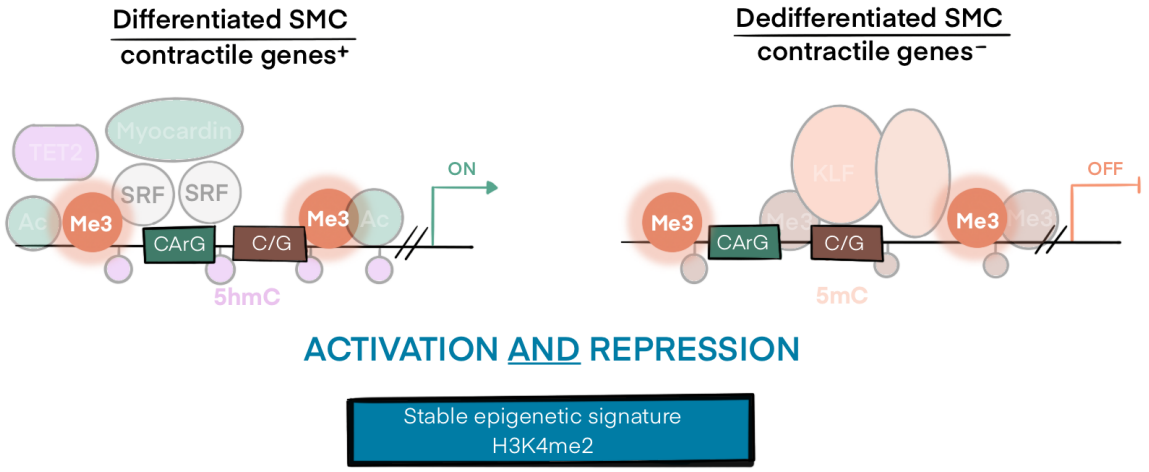

Figure 1.11. H3K4me2 interacts with TET-2 and mediates TET-dependent gene activation. in differentiated SMC Myocd/SRF is binding to the CArG with the presence of TET-2 which demethylase the DNA, thus activation of SMC genes. In the absence of TET-2, KLF binds to the C/G with the presence of DNMT family enzymes which methylate the DNA causing repression of SMC genes. Adapted from Liu et al., 2021

In further follow-up studies, they also investigated the functional consequences of alteration of H3K4me2 distribution on SMC participation in vascular remodelling. Local Myocd-LSD1 lentivirus delivery was performed before carotid ligation was performed. Three weeks after injury, ligated vessels showed high expression of Myocd-LSD1 constructs concomitant with a significant decrease in neointima formation in ligated carotids transduced with Myocd-LSD1 where SMC investment in the neointima was nearly abolished after Myocd- LSD1 delivery. Mechanistically, they argued that Myocd-LSD1 induced loss of SMC migration capacity in response to PDGF-BB. H3K4me2 editing also altered SMC adaptive capacities during vascular remodelling due to the loss of miR-145 expression. There was downregulation of miR-145 in Myocd-LSD1 SMC compared with Myocd-LSD1 /NF and PDGF-BB-treated counterparts. Furthermore, H3K4me2 editing induced a profound alteration of SMC lineage identity by redistributing H3K4me2 toward genes associated with stemness and developmental programs (Liu et al., 2021).

Myocd-LSD1 expression also induced an increase in DNA methylation (5mC) and a simultaneous reduction in DNA hydroxymethylation (5hmC) on *Acta2* and *Myh11* CArG box promoter regions. There was a striking loss of TET-2 recruitment to these loci in Myocd-LSD1

SMC, while the expression of TET-2 was not altered [Figure 1.11] (Liu et al., 2021). Using HA-tag Cleavage under targets and tagmentation (CUT&Tag) sequencing in control or Myocd-LSD1 SMCs expressing HA- TET-2, H3K4me2 editing was associated with a partial loss of TET-2 recruitment in Myocd-LSD1 SMC (Liu et al., 2021). Using PLA the same group found a decrease in the number of H3K4me2/TET-2 interactions in Myocd-LSD1 SMCs, suggesting that a significant subset of these interactions occurs on myocardin-regulated genes impacted by Myocd-LSD1 (Liu et al., 2021).

1.14 Epigenetics in stem cells

The multipotency of stem cells is reduced over time because of gene silencing progression. Genes active in earlier progenitors are gradually silenced at later stages when development is required, and subsets of cell type-specific genes are turned on. This progression occurs as a result of selective expression of transcription factors in concert with classic 'cornerstones' of epigenetics – chromatin remodelling and chromatin modifications, DNA methylation of CpG dinucleotides (Li, 2002; Williams et al., 2006). Thus, its accessibility and positioning within specialized nuclear domains undergo dynamic changes. For example, heterochromatic markers, such as heterochromatin protein 1, as well as heterochromatic histone modifications change their localization from dispersed and very dynamic in ESC to more concentrated distinct loci during cellular differentiation (Meshorer et al., 2006; Meshorer & Misteli, 2006). This suggests that differentiation leads to the restructuring of the chromatin accompanied by the change in the global nuclear architecture which allows the pluripotent nature of the ESC genome to become more condensed. Thus, it is more transcriptionally restrained with maturation of the heterochromatin.

1.15 DNA methylation and DNA demethylation interaction

Aberrant expression of DNMTs, TETs, or their subsequent DNA modifications is involved in various CVDs (Liu et al., 2013; Zhong et al., 2016). However, the interactions between these two family enzymes or their marks and transcription factors in the molecular pathogenesis of these diseases are less well understood. DNA methylation appears to have a pro-inflammatory role (Dunn et al., 2015). It has been shown that transcription factors can guide DNMTs and TETs to particular promoter regions in other cell types including bone marrow-

derived dendritic cells, neurons, and adipocytes (Fujiki et al., 2013; Perera et al., 2015; Yang et al., 2012; Zhang et al., 2015). For example, during inflammation resolution, TET-2 is recruited to *Il-6* promoter (Zhang et al., 2015) which is proatherogenic by promoting inflammatory cell infiltration into the plaque, endothelial dysfunction, SMC proliferation, and uptake of LDL. It has been implicated that TET-2 is a master epigenetic regulator of SMC phenotype, and its expression is inversely correlated with severity of atherosclerosis in human plaques (Liu et al., 2013). In 2017, a study revealed an opposing relationship between TET-2 and DNMT1 in SMCs, with DNMT1 leading to methylation of the TET-2 promoter, suppressing expression of TET-2 and MYOCD. Furthermore, DNMT inhibitors suppressed both atherosclerosis and intimal hyperplasia (Zhuang et al., 2017) and these factors regulate expression of KLF4 and MYOCD (Liu et al., 2013; Zhuang et al., 2017), whether and how TET-2 and DNMTs interact with SMC-specific transcription factors is not yet known but will be important to determine. These studies demonstrate that DNA-modifying enzymes associate with transcription factors in numerous cell contexts, suggesting that perhaps similar associations occur to regulate gene expression in the pathogenesis of CVD (Liu et al., 2013; Zhuang et al., 2017).

TET-2 expression closely correlated temporally with SMC differentiation markers such as Myh11 and Acta2 but inversely correlated with *KLF4* expression (Liu et al., 2013). Liu et al determined that TET-2 is abundantly expressed in multiple SMC-rich murine tissues. In the vasculature, TET-2 was highly expressed in SMCs isolated from the medial layer of normal mouse aorta but decreased with culture in 10% serum, in parallel with Myh11 expression. These levels were partially rescued with rapamycin. Because of the TET proteins enzymatic function in converting 5-mC to 5-hmC (Ito et al., 2010; Koh et al., 2011), 5-hmC levels were measured in SMCs by Genomic dot blot analysis revealing a global increase in 5-hmC levels in differentiated SMCs and reduced 5-hmC levels in dedifferentiated cultures. Liu et al demonstrate that both TET-2 and its 5-hmC product correlate with the SMC differentiated phenotype (Liu et al., 2013).

Tet-2 and 5-hmC expression in murine and human models of vascular injury and disease has also been examined. Intimal hyperplasia of mouse femoral artery following wire-induced injury resulted in reduced Tet-2 levels in the injured medial layer, with only 16% of cells in the

neointima Tet-2 positive after 3 weeks (Liu et al., 2013). The 5-hmC staining and genomic levels closely paralleled *Tet-2* expression patterns suggesting that high Tet-2 and 5-hmC levels are associated with the mature, differentiated SMC phenotype, whereas significant loss of Tet-2 and 5-hmC is characteristic of dedifferentiated SMC. Similar conclusions were made when human coronary artery samples from normal and arteriosclerotic patients were interrogated and assessed (Liu et al., 2013).

In hCASMCs, TET-2 knockdown resulted in a significant reduction in SMC differentiation gene expression and 5-hmC levels. TET-2 is an obligate effector of rapamycin-induced differentiation because TET-2 knockdown prevented rapamycin-induced contractile gene expression and morphology. Moreover, TET-2 overexpression promoted many aspects of differentiation in hCASMCs such as, increased contractile gene levels, elevated global 5-hmC expression, a contractile morphology when stimuli are absent, a downregulation of *KLF4* and other dedifferentiation gene expression levels, and antiproliferative gene expression. Together, these results suggest that TET-2 is both necessary and sufficient for SMC differentiation (Liu et al., 2013).

1.16 Detection of histone modifications at specific gene loci

1.16.1 Chromatin Immunoprecipitation (ChIP) assay

ChIP is a powerful assay by which to follow the protein-DNA interactions involved in these processes (Impey et al., 2004). The assay determines whether a protein-DNA interaction is present at a given location within the genome and also provides an estimation of the density/enrichment of a given factor in that region (Nelson et al., 2006). Along with other techniques, ChIP assays are uncovering an extraordinarily rich and dynamic chromatin environment (Chih et al., 2005; Cosma et al., 1999; Koyanagi et al., 2005; Métivier et al., 2004).

In the ChIP assay, protein-DNA complexes are fixed by cross-linking with formaldehyde (Solomon & Varshavsky, 1985), and the chromatin is sheared either by sonication (Mymryk et al., 1997) or enzymatic methods, into DNA fragment sizes of 200–1,000 base pairs. Using an antibody specific to that protein, complexes containing the factor of interest are immunoprecipitated. DNA is purified from the isolated chromatin, and Polymerase Chain

Reaction (PCR) detects specific genomic regions. Appropriate numbers of PCR cycles are used to confirm that the specific and mock-precipitated DNAs are within the linear range of amplification [Figure 1.12]. Enrichment of a specific DNA locus in immunoprecipitated material, compared to mock precipitation, indicates that the factor of interest interacts with this genomic region, and the intensity of the PCR signal is comparable to occupancy at the binding site (Bernstein et al., 2005; Cawley et al., 2004; Pokholok et al., 2005).

1.16.2 Chromatin immunoprecipitation sequencing (ChIP-Seq)

Transcription factors play a key role in the regulation of gene expression and the re-organization of chromatin by binding to specific genomic loci in a cell type-specific manner, (Gertz et al., 2013; Xie et al., 2013). ChIP-Seq is a popular genomic approach that identifies binding sites in the genome for a protein of interest (Valouev et al., 2008). ChIP-seq can be done on bulk cells and or more recently on a single cell. This technique involves reverse cross-linking of a protein of interest to DNA, followed by fragmentation, immunoprecipitation and parallel sequencing, which permits identification of DNA sequences bound by transcription factors or histones across the genome (Valouev et al., 2008). ChIP-Seq has been widely used, with over 40,000 ChIP-Seq assays of enormous DNA-binding proteins available in public repositories, such as Sequence Read Archive and the Gene Expression Omnibus (Clough et al.,2016). Depending on the availability of these datasets researchers can explore novel questions related to transcriptional response by comparing results of multiple ChIP-Seq datasets.

ChIP-Seq data analysis is a multi-step process that includes obtaining quality control measures, mapping of sequencing reads to a reference genome, peak calling, performing differential binding analysis, annotating sites, and identifying motifs (Bailey et al., 2013). Informatics tools have been developed to perform these tasks (Shin et al., 2013) The ENCODE project produced many ChIP-Seq datasets along with published standards and guidelines that recommend use of biological replicates, specific antibody and input control characteristics, and uniform processing pipelines to analyse ChIP-Seq data of different protein classes (Landt et al., 2012). For example, to confirm whether transcription factor binding sites are associated with corresponding gene transcription, it is recommended that ChIP-Seq experiments include measures of RNA polymerase II occupancy along with the transcription factor of interest

(Mokry et al., 2012). In the absence of RNA polymerase II ChIP-Seq data, genome-wide gene expression results derived from microarray or RNA-sequencing studies with similar treatment conditions as the ChIP-Seq study of interest which can be used to link between transcription factor binding sites and transcriptomic changes.

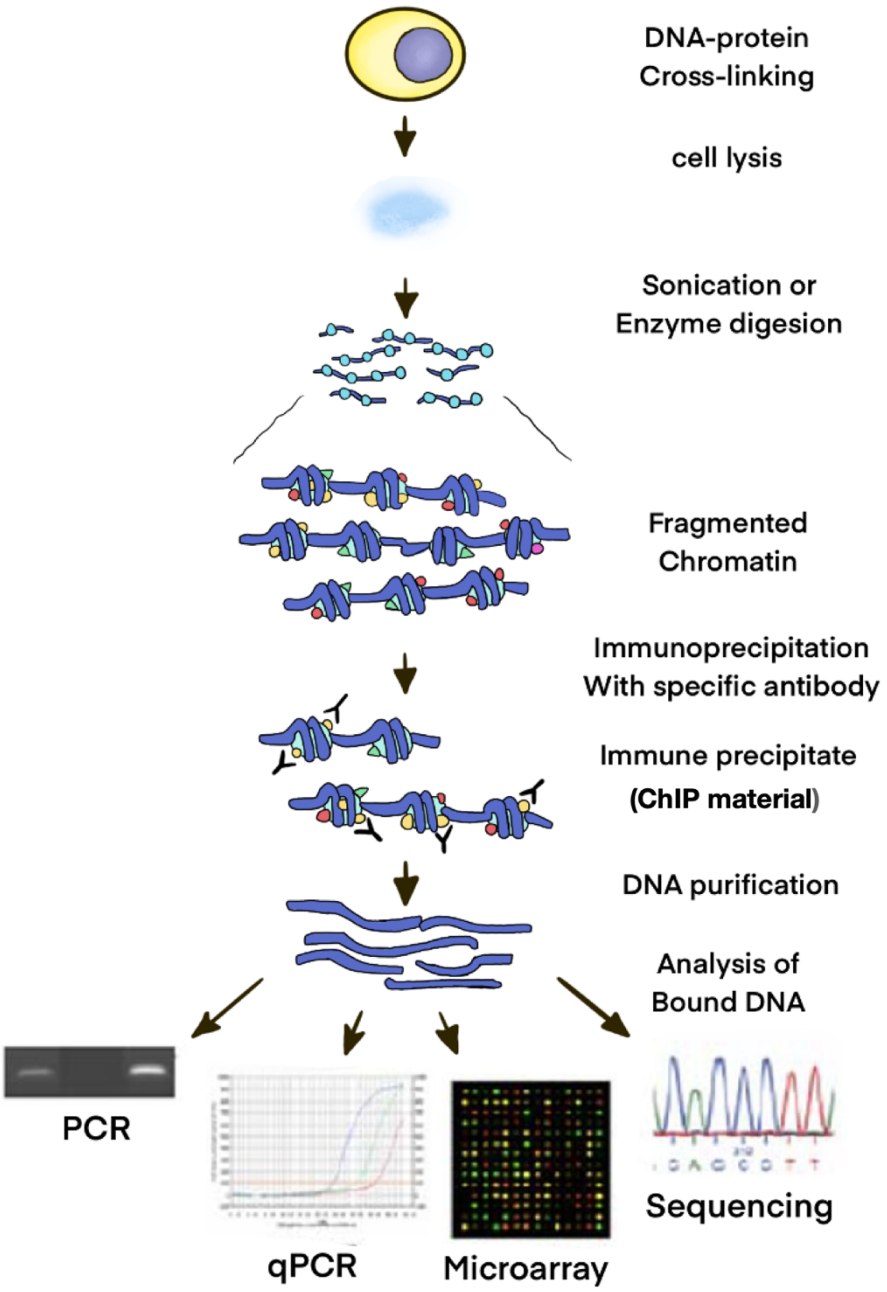

Figure 1.12. The chromatin immunoprecipitation (ChIP) assay. Adapted from Collas et al., 2008.

Software tools to analyse ChIP-Seq data include the R packages chip-seq (Sarkar et al., 2013) and CSAR (Muiño et al., 2011) which perform binding site identification based on aligned data obtained via command-line tools, while Homer (Heinz et al., 2010), seqMINER (Ye et al., 2011) and Sole- Search (Blahnik et al., 2009) are popular tools that focus solely on aspects of downstream analysis. Pipelines that combine existing informatics tools to perform comprehensive ChIP-Seq analyses include ChiLin (Qin et al., 2016) and the ENCODE pipeline *(https://github.com/ENCODE-DCC/chip-seq-pipeline2)*, which consist of Python scripts that integrate steps for sequence data mapping, peak calling, and differential binding analysis (only available in ChiLin). The Galaxy-based platforms Cistrome (Liu et al., 2011) and Nebula (Boeva et al., 2012) are similar cloud-based options, but their computational speed and customization of commands are limited. None of the existing pipelines, however, facilitate analysis of publicly available ChIP-Seq data via automated retrieval of raw sequencing files and phenotype information from public repositories. Hence, an end-to-end ChIP-Seq data analysis pipeline is needed which includes direct access to the growing resource of public datasets in a sophisticated yet straightforward manner. However, ChIP-seq and its variations (Policastro & Zentner, 2018) suffer from low signals, high backgrounds and epitope masking due to cross-linking, and low yields that require large numbers of cells (Policastro & Zentner, 2018; Teytelman et al., 2013). Alternatives to ChIP include enzyme-tethering methods for unfixed cells, such as Cleavage under targets and release under nuclease (CUT&RUN) and CUT&TAG (Skene et al., 2018; Skene & Henikoff, 2017) where a specific protein of interest is targeted *in situ* and then profiled genome-wide (Schmid et al., 2004).

1.16.3 Cleavage under targets and release under nuclease (CUT&RUN)

CUT&RUN is based on Laemmli's Chromatin ImmunoCleavage strategy (Schmid et al., 2004), chromatin protein is mapped by successive binding of a specific antibody, and then tethering a Protein A/Micrococcal Nuclease fusion protein in permeabilized cells without cross-linking (Skene & Henikoff, 2017). Micrococcal Nuclease is activated by calcium, and fragments are released into the supernatant for extraction of DNA, library preparation and paired-end sequencing [Figure 1.13]. Base-pair resolution of specific chromatin components is provided by CUT&RUN, with less cost of genome-wide profiling. Although CUT&RUN can generate high-quality data from as few as 100–1000 cells, it must be followed by DNA end polishing and

adapter ligation to prepare sequencing libraries, which increases the time, cost and effort of the procedure. Moreover, the release of Micrococcal Nuclease-cleaved fragments into the supernatant with CUT&RUN is not suitable for application to single-cell platforms (Mezger et al., 2018; Zheng et al., 2017).

1.16.4 Cleavage under targets and tagmentation (CUT&TAG)

CUT&Tag is a very recent development in enzyme-tethering chromatin profiling technologies that has been the substitution of the Tn5 transposase (Kaya-Okur et al., 2019). The protein A-Tn5 transposase (pA-Tn5) is loaded with mosaic end adapters and activated by magnesium ions, integrates the adapters into nearby DNA and fragments are created which are amplifiable to generate sequencing libraries. Antibody-tethered Tn5-based methods achieve high sensitivity levels due to the high efficiency of tethered Tn5 integration. As Tn5 remains bound following the cut-and-paste tagmentation reaction, fragments are retained within the cell, which makes these methods suitable for single-cell profiling [Figure 1.13]. Indeed, these methods were introduced with proof-of-concept single-cell profiling data, suggesting that this basic strategy represents an important future direction for single-cell chromatin profiling in studies of both development and disease (Kaya-Okur et al., 2020).

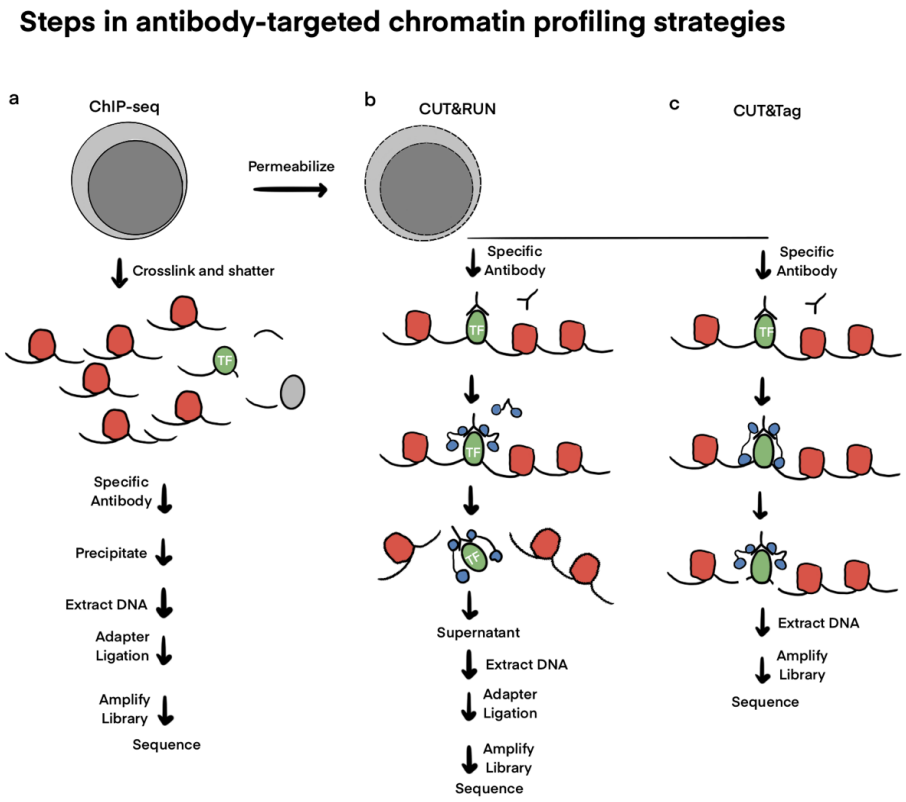

Figure 1.13. A comparison between ChIP-seq, CUT&RUN and CUT&TAG assays. a, ChIP-seq, b, CUT&RUN, c, CUT&Tag. Cells are indicated in grey, chromatin as orange nucleosomes, and a specific chromatin protein in green. Adapted from (Kaya-Okur et al., 2020).

1.16.5 ChIP-ChIP

The ChIP-chip technique was first applied to identify binding sites for individual transcription factors in *Saccharomyces cerevisiae* (Iyer et al., 2001; Ren et al., 2000). Later, also in yeast, a c-Myc epitope protein tagging system was used to map the genome-wide positions of 106 transcription factors (Lee et al., 2002). Other applications have been reported, including the study of DNA, recombination (Gerton et al., 2000), replication (Wyrick et al., 2001), and chromatin structure (Bernstein et al., 2002; Nagy et al., 2003; Robyr et al., 2002).

Generally, cells are grown under the desired experimental condition and fixed with formaldehyde. Formaldehyde crosslinks proteins to each other primarily between the ϵ-amino group of lysine residues and an adjacent peptide bond. Formaldehyde can also form DNA–protein crosslinks, but that only occurs if the DNA is partially denatured to expose the –

CO–NH moiety at position 1 of guanine or the exocyclic amino groups of adenine, guanine, or cytosine. After cross-linking, the extract is sonicated to shear the DNA fragments to the desired size, usually 1 kb or smaller (Kurdistani & Grunstein, 2003).

DNA fragments crosslinked to the protein of interest are enriched in one of three main ways: immunoprecipitation with a protein-specific antibody, immunoprecipitation of a tagged protein using an antibody specific to the tag, and the third way is affinity purification using a tag that obviates the need for antibodies, such as the tandem affinity purification tag (Puig et al., 2001). The formaldehyde crosslinks are later reversed, and the DNA is purified. Immunoprecipitation (IP) reactions with Low DNA yields DNA amplification is a requirement for DNA microarray-based detection. Randomly primed (Bohlander et al., 1992) or ligation-mediated PCR-based methods have been used the most, but a recently described linear amplification method is likely to give higher fidelity results (Liu et al., 2003). Preferably, the IPs can be scaled up economically and amplification can be ignored.

Enriched DNA is labelled with a fluorescent molecule such as Cy5 or Alexa 647. The fluorescent molecule can be introduced directly in the form of a modified nucleotide (Duggan et al., 1999) or by chemical coupling after the introduction of an aminoallyl nucleotide derivative (Xiang et al., 2002). In two-colour array platforms, genomic DNA prepared from IP extract is generally used for referencing and similarly amplified and labelled with a different fluor, such as Cy3 or Alexa 555 (Weinmann et al., 2002). Later the two probes are combined and hybridized into a single DNA microarray. Ideally, to provide a comprehensive and unbiased survey of protein-DNA interactions, the DNA microarrays used in ChIP experiments contain elements that represent the entire genome. The results of the hybridization allow us to identify which segments of the genome were enriched in the IP. Since the location of each array element is known, construction of a genome-wide map of *in vivo* protein–DNA interactions is possible. The resolution of the method depends mainly on two factors: the length of the sheared chromatin enriched by the IP and the length and spacing of the arrayed DNA elements used to detect the IP-enriched fragments (Liu et al., 2002).

1.16.6 The proximity ligation assay (PLA) *in situ*

PLA mechanism allows improved detection of individual proteins or protein complexes, using antibodies with attached DNA strands that participate in ligation, replication, and sequence decoding reactions (Fredriksson et al., 2002; Gullberg et al., 2004). *In situ,* PLA involves a modification of the PLA mechanism allowing highly specific imaging of proteins and protein complexes in tissue samples. *In situ* PLA and its application for imaging proteins, protein interactions and post-translational modifications by microscopy offers an assay with high selectivity and sensitivity (Söderberg et al., 2008). Identification of target molecules depends on two recognition events. Formation of a proper detection complex results in a circular DNA strand creation, which in turn is used to template a localized Rolling circle amplification (RCA) reaction, generating a long single-stranded DNA molecule, rolled up in a ball that can be detected by hybridizing fluorescence-labelled probes (Söderberg et al., 2006). Proximity probes are the binding to a target molecule or complex by two antibodies with attached oligonucleotides followed washes by the addition of two more oligonucleotides that are later ligated into a circular DNA strand, templated by the oligonucleotides attached to antibodies. Then one of the antibody-bound oligonucleotides is used to prime an RCA reaction, which results in the formation of a single-stranded rolling circle product (RCP). The RCP is composed of concatenated complements of the DNA circle, and it is covalently attached to one of the proximity probes. A 1-h RCA by Phi29 DNA polymerase results in a 1000-fold amplification of the 100 nt DNA circle, producing an around 100 kb RCP that forms a bundle of DNA less than 1 µm in diameter, close to the light microscopic resolution. The RCP is visualized by hybridization of fluorescence-labelled complementary oligonucleotide detection probes. Individual RCPs are clearly visible over background as every RCP becomes labelled with several hundred fluorophores (Söderberg et al., 2008).

1.17 hypothesis and thesis objectives

A hallmark of subclinical atherosclerosis is the accumulation of SMC-like and non-SMC (e.g., osteocytes, adipocytes, endothelial cells, macrophages, MSCs) within vascular lesions that may ultimately obstruct blood flow and result in a heart attack or stroke. The source of these cells is an attractive therapeutic target for treating subclinical atherosclerosis but

remains controversial. Several lineage tracing studies suggest that they may be derived following de-differentiation, proliferation and migration of medial SMCs and/or partial differentiation, proliferation and migration of S100β resident vascular mVSCs in response to atherogenic stimuli. The persistence of the H3K4me2 mark at the SMC *Myh11* gene locus despite this gene being transcriptionally silent is a common feature of SMC de-differentiation *in vitro.* It is also present in SMC-like and non-SMCs within lesions to purportedly facilitate de-differentiated SMCs remaining permissive for re-differentiation during reversible phenotypic switching. However, a role for partial differentiation of mVSCs in response to atherogenic stimuli, which are also cell fate mapped to vascular lesions, in dictating the presence of this mark at the *Myh11 l*ocus within lesional SMC-like and non-SMC cells cannot be ruled out.

Hence the central hypothesis to be addressed in this study is that the presence of the H3K4me2 mark at the SMC *Myh11* locus in SMC-like cells and non-SMCs (typical of vascular lesions) in response to atherogenic stimuli is a direct result of partial differentiation of S100β resident mVSCs cells. Moreover, the presence of this mark at the *Myh11* locus is dependent on the activity of the Tet-2 demethylase. Furthermore, the presence of this mark at multiple lineage-specific loci following inductive stimulation may reflect the overall commitment status of multipotent vascular stem cells and dictate their capacity to proceed and be fully determined and fated down specific lineages. In doing so, a greater understanding of the origin of SMC-like cells and non-SMCs with lesions will be revealed based on their epigenetic profile. Targeting the methyltransferase enzymes that mediate these histone modifications in resident vascular stem cells may therefore present as a novel strategy for treating subclinical atherosclerotic disease by modulating the appearance of lineage-specific stem cell-derived progeny within lesions.

Therefore, the aim of this study was to assess whether histone modifications at the SMC *Myh11* locus in both SMC-like cells (myogenic progeny) and non-SMCs (adipogenic, osteogenic and vasculogenic progeny) occur as a result of lineage-specification of S100β mVSCs, rather than or in addition to, de-differentiation of medial SMCs, in response to atherogenic stimuli, and correlate these modifications to *Myh11* gene expression. Using quantitative single gene Chromatin Immunoprecipitation followed by Polymerase Chain Reaction (ChIP-PCR) assays, the extent of histone modifications and the binding of the DNA

demethylase, Tet-2 at the *Myh11* locus was first assessed in response to atherogenic stimuli and correlated with *Myh11* gene expression using quantitative PCR (qRT-PCR) *in vitro*. The cells included undifferentiated mouse and human S100β mVSCs, de-differentiated SMCs, and differentiated aortic SMC and ESCs deployed as controls. In addition, the effects of specific knockdown of the demethylase, Tet-2 on these histone modifications in response to atherogenic stimuli was correlated with changes in *Myh11* gene expression. In order to determine whether the same H3K4me2 mark was present at the *Myh11* locus in cells committed to proceeding down several specific lineages (myogenic, osteogenic, adipogenic and vasculogenic), the level of enrichment of H3K4me2 and Tet-2 binding at this locus in resident S100β mVSCs and hiPSC-derived S100β progenitor stem cells was also assessed by single gene ChIP-PCR assays and correlated with gene expression using qRT-PCR. Subsequent bulk ChIP-seq analysis of histone marks was performed before and after the same lineage-specific differentiation of human S100β progenitor stem cells to confirm the H3K4me2 mark was present at lineage-specific loci and specifically at the *Myh11* locus in these progeny. Finally, *in silico* analysis of bulk ChIP-seq published datasets from mouse and human stem cells before and after lineage-specific differentiation was also performed to confirm whether the same H3K4me mark was present at lineage-specific loci and the *Myh11* locus in all these progeny.

Collectively, these experiments will address whether the presence of the H3K4me2 mark at that SMC *Myh11* locus in cell phenotypes typical of vascular lesions is indicative of differentiation of resident S100β vascular stem cells, and not merely exclusive to de-differentiation of medial SMCs. Moreover, these studies will address whether the presence of this histone mark at multiple lineage-specific loci following differentiation may reflect the overall 'commitment status' of multipotent vascular stem cells and ultimately dictate their capacity to proceed and be fully determined and fated down specific lineages.

In Chapter 3 the following objectives were addressed:

1. To determine the level of enrichment of H3K4me2 and H3K27me3 (epigenetic profile) at the *Myh11* locus in de-differentiated mouse SMC *in vitro* and compare with differentiated mouse SMC isolated from freshly isolated aortic tissue *ex vivo* and

mouse embryonic stem cells (mESC) *in vitro* using single gene ChIP-PCR and correlate with *Myh11* gene expression using qRT-PCR.

2. To determine the effects of atherogenic stimuli on the epigenetic profile at the *Myh11* locus in mouse SMCs using single gene ChIP-PCR and correlate any changes with *Myh11* gene expression using qRT-PCR.

3. To determine the effects of atherogenic stimuli on the epigenetic profile at the *Myh11* locus in resident S100β mVSCs *in vitro* using single gene ChIP-PCR and correlate any changes with *Myh11* gene expression using qRT-PCR.

4. To determine the epigenetic profile at the *Myh11* locus in de-differentiated mouse SMC *in vitro* when cells are grown in stem cell maintenance media (to promote possible re-programming) compared to SMC maintenance medium using single gene ChIP-PCR and correlate any changes with *Myh11* gene expression using qRT-PCR.

5. To examine the role of the DNA demethylase, Tet-2 in regulating histone modifications at the *Myh11* locus in mouse vascular SMCs, S100β resident vascular mVSCs, and their myogenic progeny following Short interfering RNA (siRNA) knockdown of Tet-2 using single gene ChIP-PCR and correlate any changes with *Myh11* gene expression using qRT-PCR.

In Chapter 4 the following objectives were addressed:

1. To determine whether a common epigenetic profile exists at the *Myh11* locus in mouse S100β resident vascular mVSCs when they specialise down various cell lineages (myogenic, adipogenic, osteogenic and vasculogenic) using single gene ChIP-PCR and correlate any changes with *Myh11* gene expression using qRT-PCR
2. To determine whether a common epigenetic profile exists at the *MYH11* locus in human S100β hiPSC-derived neuroectodermal progenitor stem cells when they specialise down various cell lineages (myogenic, adipogenic, osteogenic and

vasculogenic) using single gene ChIP-PCR and correlate any changes with *MYH11* gene expression using qRT-PCR.

In Chapter 5 the following objectives were addressed:

1. To determine whether a common epigenetic profile exists at the *Myh11* locus in human S100β hiPSC-derived neuroectodermal progenitor stem cells when they specialise down various cell lineages (myogenic, adipogenic, osteogenic and vasculogenic) using bulk ChIP-seq analysis.

2. To perform *in silico* analysis of published bulk ChIP-seq datasets to determine whether a common epigenetic profile exists at the *Myh11* locus in undifferentiated mouse and human mesenchymal stromal stem cells (MSCs) and embryonic stem cells (hESCs) when they specialise down various cell lineages (myogenic, adipogenic, osteogenic and vasculogenic).

Chapter 2

Materials and Methods

2.1 Materials

2.1.1 Primers

2.1.1.1 QIAGEN primers

Table 2.1. QIAGEN primers

Primer	**Product Name**	**Product No.**
Hprt	Mm_Hprt_1_SG QuantiTect Primer Assay	QT00166768
Myh11	Mm_ Myh11 _1_SG QuantiTect Primer Assay	QT01060843
Cnn1	Mm_Cnn1_1_SG QuantiTect Primer Assay	QT00105420
Tet2	Mm_Tet2_1_SG QuantiTect Primer Assay	QT00198058
S100β	Mm_S100b_1_SG QuantiTect Primer Assay	QT00151536
Sox10	Mm_Sox10_1_SG QuantiTect Primer Assay	QT00295204
Gapdh	Mm_Gapdh_3_SG QuantiTect Primer Assay	QT01658692
PECAM1	Hs_PECAM1_1_SG QuantiTect Primer Assay	QT00081172
GAPDH	Hs_GAPDH_1_SG QuantiTect Primer Assay	QT00079247
HPRT	Hs_HPRT1_1_SG QuantiTect Primer Assay	QT00059066
ALPL	Hs_ALPL_1_SG QuantiTect Primer Assay	QT00012957
SOST	Hs_SOST_1_SG QuantiTect Primer Assay	QT00219968
LPL	Hs_LPL_1_SG QuantiTect Primer Assay	QT00036771
FABP4	Hs_FABP4_1_SG QuantiTect Primer Assay	QT00055517

Alpl	Mm_Alpl_1_SG QuantiTect Primer Assay	QT00157717
Sost	Mm_Sost_1_SG QuantiTect Primer Assay	QT00294322
Lpl	Mm_Lpl_1_SG QuantiTect Primer Assay	QT01046017
Fabp4	Mm_Fabp4_1_SG QuantiTect Primer Assay	QT00091532

2.1.1.2 IDT primers

Table 2.2. IDT primers

Primer	**Sequence**
Mouse *Myh11*	(R) CCAGATCCTGGGTCCTTACA, (F) CCCTCCCTTTGCTAAACACA,
Human *MYH11*	(R)GTGAGTATTGCAGGCAGCCA (F)TGGCTGCCTGCAATACTCAC

2.1.2 Chemical and Biological agents

Table 2.3. Chemical and biological agents

Supplier	**Product and Catalogue No**
Seralab	Chick Embryo Extract (CE-650-J)
R&D System	Recombinant Mouse TGF-beta 1 Protein, CF (7666-MB-005/CF), Recombinant Mouse FGF basic Protein (3139-FB-025), Recombinant Rat PDGF-BB Protein (520-BB-050), Recombinant Rat Jagged 1 Fc Chimera Protein, CF (599-JG-100)
QIAGEN	RNase-Free DNase Set (50) (79254), Rotor-Gene SYBR® Green RT-PCR Kit (204174),
Gibco	B-27® Supplement (50X) serum free (17504044), 2-Mercaptoethanol (50 mM) (31350010), CTS™

	(Cell Therapy Systems) N-2 Supplement (A1370701), TrypLE™ Select Enzyme (1X), MEM α nucleosides GlutaMAX™ Supplement (32571036), Fungizone® Antimycotic (20mL) (15290018), Gibco™ StemPro™ Adipogenesis Differentiation Kit (A1007001), Gibco™ StemPro™ Osteogenesis Differentiation Kit (A1007201)
Bioline	SensiMix™ SYBR® No-ROX Kit (QT650-05)
Sigma-Aldrich	Water (W4502), Sodium bicarbonate solution (S8761), Sodium pyruvate solution (S8636), 2-mercaptoethanol (M-7154), 30% bis/acrylamide solution (A3699), APS (A3678), Collagenase (C6885), Dulbecco's Modified Essential Medium (DMEM) (D5796), Dimethyl Sulfoxide (DMSO) (C6164), Elastase from porcine pancreastype III (E0127), Bovine Serum Albumin (BSA)(A4503), Glycine (G8898), L-Glutamine Solution (G7513), Penicillin-Streptomycin (P4333), Ponceau S stain (P7170), Protease inhibitor (P8340), Retinoic acid (100nM) (R2656), Radioimmunoprecipitation assay RIPA (R0278), Soybean Trypsin inhibitor (10109886001, Roche), TMB (T0565), Triton X-100 (T8787), Trypan Blue (T8154), Trypsin (T4174), TWEEN® 20 (P1379), Minimum Essential Medium Eagle (M0644), Fluoromount™ Aqueous Mounting Medium (F4680), Trypsin Inhibitor from Soybean (10109886001 Roche), 2-Propanol (I9516), , Oil Red O O0625, Alizarin Red A5533, Formaldehyde F-8775
ATCC	Fetal Bovine Serum, ES Cell Qualified (ATCC® SCRR-30-2020™),
Mirus	TransIT-X2® Dynamic Delivery System (MIR6000)

Abcam	Chromatin Extraction Kit (ab223876)
Active Motif	Products provided by Express^{TM} HT kit (53018)
Promega	Products provided by ReliaPrep^{TM} RNA Cell Miniprep System Kit (Z6012)
Stem cell	VitronectinXF (07180)
Promo Cell	Endothelial cell growth medium MV Supplement Pack C-39220

2.1.3 Antibodies

Antibodies and their corresponding dilutions used in immunocytochemistry. Antibodies were diluted in antibody solution [2.5% bovine serum albumin (BSA), 0.3M Glycine and 1% Tween in Dulbecco's Phosphate Buffered Saline (DPBS)].

Table 2.4. Antibodies and their corresponding dilutions used in immunocytochemistry.

Antibody/Product Name	**Supplier/Product Number**	**Dilutions**
Rabbit anti-mouse Calponin [EP798Y]	Abcam (ab46794)	1/200
Goat anti-mouse/rat/human smooth muscle Myosin heavy chain	Santa Cruz (sc-79079)	1/200
Mouse anti-human/rat SOX10	R&D System (MAB28641/100)	1/100
Anti-Nestin Antibody (196908)	Abcam (ab6320)	1/100
Rabbit Anti-mouse/rat S100 beta [EP1576Y]	Abcam (ab52642)	1/100
Alexa Fluor 488 Goat anti-mouse Immunoglobulin (IgG)	Invitrogen (A-11001)	1/1000
Alexa Fluor 488 Goat anti-rabbit IgG	Invitrogen (A-11008)	1/1000

Table 2.5. Antibodies used in Chromatin Immunoprecipitation

Antibody/Product Name	**Supplier/Product Number**
Tri-Methyl-Histone H3 (Lys27) (C36B11) Rabbit mAb	Cell signalling technology
Di-Methyl-Histone H3 (Lys4) (C64G9) Rabbit mAb	Cell signalling technology
Normal Rabbit IgG (2729S)	Cell signalling technology
Rabbit Anti-Tet2 (ab94580)	Abcam

2.1.4 Tissue Culture

2.1.4.1 Cell lines

Commercial cell lines & tissue-derived cells

Table 2.6. Commercial cells used during the study

Cell line	**Supplier**
MOVAS	ATTC (CRL-2797™)
Embryonic stem cell	ATTC (ES-D3 ATCC® CRL1934™)
IPSCs	HipSci

Table 2.7. Tissue and cell-derived cells used during the study

Cells	**Cell origin**	**Description**
S100β mVSC	NE	mVSCs derived from the thoracic aortic medial layer by enzymatic dispersion
S100β SNEP	HiPSC	HiPSC-derived spontaneous NE progenitor cells (S100β SNEPs) are derived from iPSCs generated using a non-chemical stimulus
hSMC	SNEP	S100β SNEP-derived VSMCs (SNEP-SMCs) are derived from HiPSC-derived S100β SNEP

2.1.4.2 Growth medium

Table 2.8. Growth medium

Cell line	**Medium**
MOVAS	Roswell park memorial institute (RPMI)
S100β mVSCs	Maintenance medium type 1 (MM1)
Embryonic stem cell (ESC)	ESC medium
IPSCs	Essential 8 (E8)
S100β SNEP	E8
hSMC	Dulbecco's Modified Essential Medium (DMEM)

2.1.4.2.1 MOVAS maintenance medium

Table 2.9. RPMI

Components	**Volume**
RPMI 1640 With L-glutamine and sodium bicarbonate, liquid, sterile R8758 (Sigma)	44.5ml
Serum response factor F9665 (Sigma)	5ml
Penicillin-Streptomycin P4333 (Sigma)	0.5ml

2.1.4.2.2 S100β mVSC maintenance medium

Table 2.10. MM1

Stock solutions/powders	**Final concentrations or percentage**	**Volumes in 50 ml**
DMEM SLM-021-B (Sigma)	92.96%	46.48 ml
Chick Embryo Extract	2%	1 ml
Fetal Bovine Serum (FBS) embryonic qualified (ATCC®)	1%	500 µl
B-27® Supplement, serum free (50X)	1X	1 ml
CTSTM (Cell Therapy Systems) N-2 Supplement (100X)	1X	500 µl
Recombinant Mouse FGF basic Protein (100 µg/mL)	0.02 µg/mL	10 µl
Penicillin-Streptomycin (10000 units-10 mg /ml)	1%	500 µl
1:20 diluted 2-Mercaptoethanol	50 nM	5 µl
1:10 diluted Retinoic Acid	100 nM	5 µl

2.1.4.2.3 Mouse S100β mVSCs Differentiation medium

- Myogenic differentiation medium RPMI

  As described in section 2.1.4.2.1

- Endothelial cell medium kit P60104 (Innoprot)

Table 2.11. Endothelial cell medium

Endothelial cell medium	**Volume**
Basal Medium	500 ml
Fetal Bovine Serum (FBS)	25 ml
Endothelial Cell Growth Supplement	5 ml
penicillin/streptomycin solution (P/S solution)	5 ml

- StemPro® Adipogenesis Differentiation Kit A10070-01 (Invitrogen)

Table 2.12. StemPro® Adipogenesis Differentiation

Adipogenesis Differentiation Medium	**Concentration**	**Volume**
StemPro® Adipocyte Differentiation Basal Medium	1X	90 mL
StemPro® Adipocyte Supplement	1X	10 mL
Gentamicin reagent (10 mg/mL)	5 µg/mL	50 µL

- StemPro® Osteogenesis Differentiation Kit A10072-01 (Invitrogen)

Table 2.13. StemPro® Osteogenesis Differentiation

Osteogenesis Differentiation Medium	**Concentration**	**Volume**
StemPro® osteocyte Differentiation Basal Medium	1X	90 mL
StemPro® Osteogenesis Supplement	1X	10 mL
Gentamicin reagent (10 mg/mL)	5 µg/mL	50 µL

2.1.4.2.4 S100β SNEP Maintenance medium

Gibco™ Essential 8™ Flex Medium Kit A2858501

Table 2.14. Gibco™ Essential 8™ Flex Medium

Components	Volume
Essential 8™ Flex Basal Medium	48.5ML
Essential 8™ Flex Supplement (50X)	1ML
Penicillin-Streptomycin	0.5ML

2.1.4.2.5 Human S100β SNEPs Differentiation media

- Myogenic differentiation medium DMEM

Table 2.15. DMEM

Components	**Volume**
Dulbecco's Modified Eagle's medium – high Glucose D6429(Sigma)	44.5ml
Serum response factor F9665 (Sigma)	5ml
Penicillin-Streptomycin P4333 (Sigma)	0.5ml

- Endothelial cell growth medium MV Supplement Pack C-39220 (Promo Cell)

Table 2.16. Endothelial cell growth medium

Components	**Volume**
Endothelial Cell Growth Medium MV Kit	500 ml
Fetal Calf Serum	0.05ml/ml
Endothelial Cell Growth Factor	0.004ml/ml
Epidermal Growth Factor (recombinant human)	10ng/ml
Heparin	90μg/ml
Hydrocortisone	1μg/ml
Penicillin-Streptomycin	5ml

- StemPro® Adipogenesis Differentiation Kit A10070-01 (Invitrogen)

As described in section 2.1.4.2.3

- StemPro® Osteogenesis Differentiation Kit A10072-01 (Invitrogen)

As described in section 2.1.4.2.3

2.2 Methods

2.2.1 Cell culture

2.2.1.1 Mouse Aortic Smooth Muscle Cells (MOVAS)

Mouse aortic smooth muscle cells (mSMCs or MOVAS, ATCC® CRL-2797™) were bought commercially and cultured in RPMI supplemented with 10% Sigma-Aldrich FBS, and 1% of Penicillin and Streptomycin. Experiments were carried on till the cells reached passage 25. Myogenic markers Myosin Heavy-chain 11 (Myh11) and Calponin1 (Cnn1) were checked using immunocytochemistry (ICC) and quantitative real-time Polymerase Chain Reaction (qRT-PCR).

2.2.1.2 Isolation and culture of mouse vascular stem cells (vSCs) by explant and sequential seeding following enzymatic dispersion

The protocols for isolation of vascular stem cells (vSCs) from the tunica media of the aortic arch and thoracic aorta were performed as previously described, with some minor modifications (Tang et al., 2012). Isolated aortic vSCs were cultured in DMEM neuroectodermal-derived cells maintenance medium (NE-MM) as described by Tang and colleagues (Tang et al., 2012).

Removal of the adventitial layer

The use of animals in this study was carried out according to the EU legislation (Directive 2010/63/EU) for the protection of animals used in research. Mice strain C57BL and Thy1 were anesthetized with an overdose of pentobarbital sodium (0.1mg/g), and death was confirmed by exsanguination by an authorised professional. The rib cage was cut open at the front of the animal to expose internal organs. These were removed and the back of the rib cage was in view. The aorta was carefully excised using tweezers and scissors. The tweezers were carefully run along the side of the aorta to detach it from the backbone. The aorta tissue was harvested as fast as possible from the heart collecting it along the spine to the abdominal area. The tissue was placed in cold Phosphate Buffered Saline (PBS), and fatty tissue was removed with the use of two tweezers. A 2 ml syringe and a needle were used to wash the lumen area of the vessel and remove any trace of blood. Afterwards, the adventitia was enzymatically removed by incubation of the tissue in 2.5 mg/ml collagenase solution for

approx. 10-20 min at 37°C. Once the adventitia became detached, it was carefully removed using forceps under a dissection microscope as an intact layer.

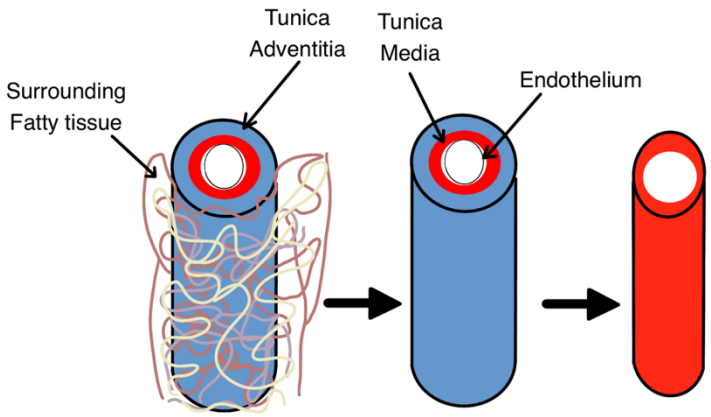

Figure 2.1. Adventitial removal.

Enzymatic Dispersion

The aorta was cut into small tissue pieces with a sterile blade, and placed in Elastase type III (Appendix) at 37°C. The tissues were vortexed every 15 min for approx. 2 hours or until the tissue was completely digested. Dispersed cells were centrifuged and washed twice in warm NE-MM and seeded on wells of a CELLstart™ pre-coated 6-well plate with 2mL of NE-MM (Figure 2.3). Cells were incubated at 37°C, 5% Carbon Dioxide (CO_2) for 1 week with minimal disturbance. All steps were carried out under aseptic conditions in a laminar flow hood. Surgical tools and a surgical platform were sterilised by autoclave. Solutions and culture vessels were all of cell-culture grade. Cells were split using Hank's balanced salt solution (HBSS) and 0.5 x TrypLE select. There was no need for CELLstart™ precoated vessels after P1, hence cells were maintained in adherent cell-culture-graded plates/flasks. Cells were healthy and proliferative when seeded at a cell density of 1 x 10^4 cells per cm2 or higher. Feeding was carried out every 3-4 days. Cells were grown in MM1 up to passage 20 stem cell markers SRY-box transcription 10 (Sox10) and S100 calcium-binding protein β (S100β) were monitored using ICC now and then to confirm stemness. These cells were generated in the lab and given to me to work with.

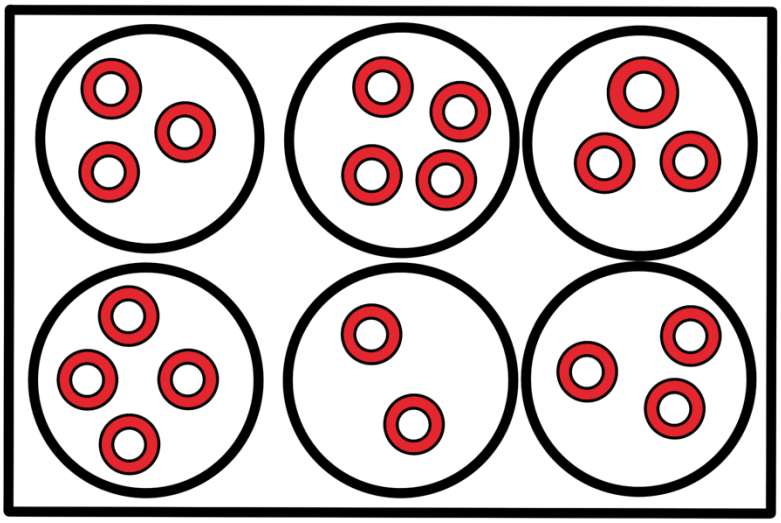

Figure 2.2. Tissue pieces on a CellStart pre-coated 6-well plate.

Table 2.17. CellStart Dilution for a 6-well plate.

Stock Solutions	**Final Concentrations**	**Volumes 5ml(750 µl/well)**
Dulbecco's Phosphate Buffered Saline (DPBS) with calcium and magnesium	1X	4410 µl
CTSTM CELLstartTM Substrate	1:50	90µl

The final solution was filtered using a 0.2 µm syringe end filter under sterile conditions.

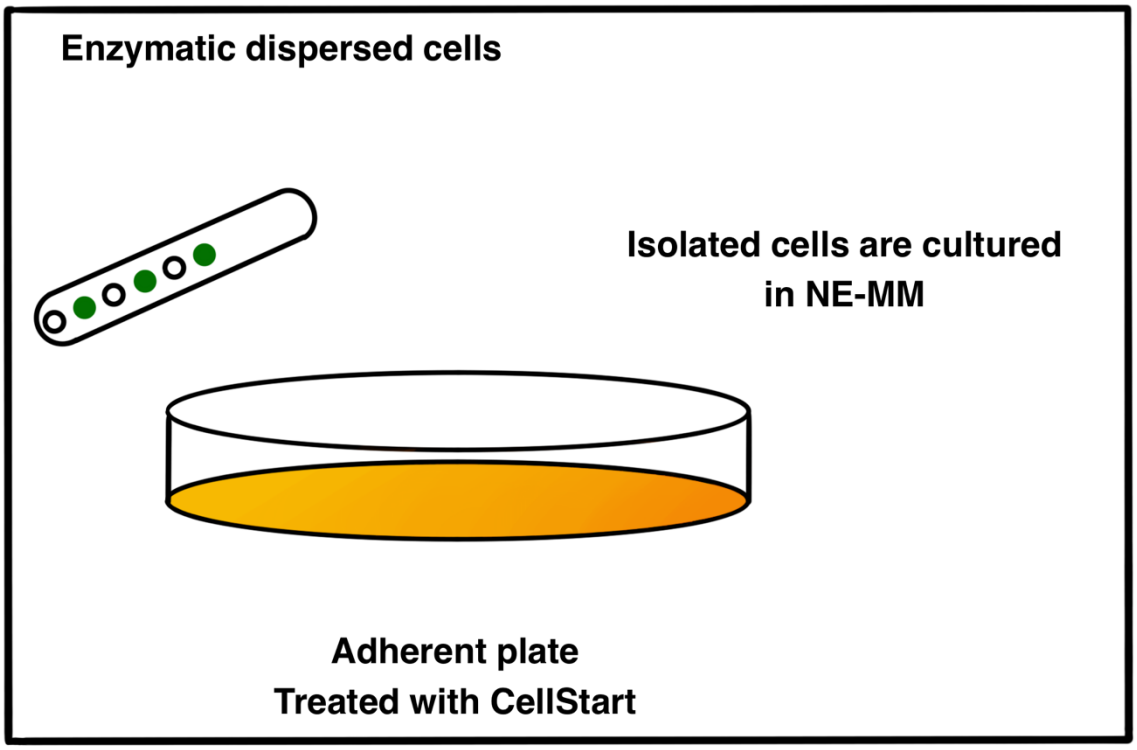

Figure 2.3. Schematic illustration of the seeding step on a CellStart pre-coated 6-well plate after cell enzymatic dissociation.

Generating S100β mVSCs in culture

All steps were carried out under aseptic conditions in a laminar flow hood. Surgical tools and a surgical platform were sterilised by autoclave. Solutions and culture vessels were all of cell-culture grade. Cells were split using HBSS and 0.5 x TrypLE select. There was no need for CELLstart™ precoated vessels after P1, hence cells were maintained in adherent cell-culture-graded plates/flasks. Cells were healthy and proliferative when seeded at a cell density of 1 x 10^4 cells per cm2 or higher. Feeding was carried out every 3-4 days. Cells grown in MM1 up to passage 20 stem cell markers Sox10 and S100β were monitored using ICC now and then to confirm stemness. These cells were generated in the lab and given to me to work with.

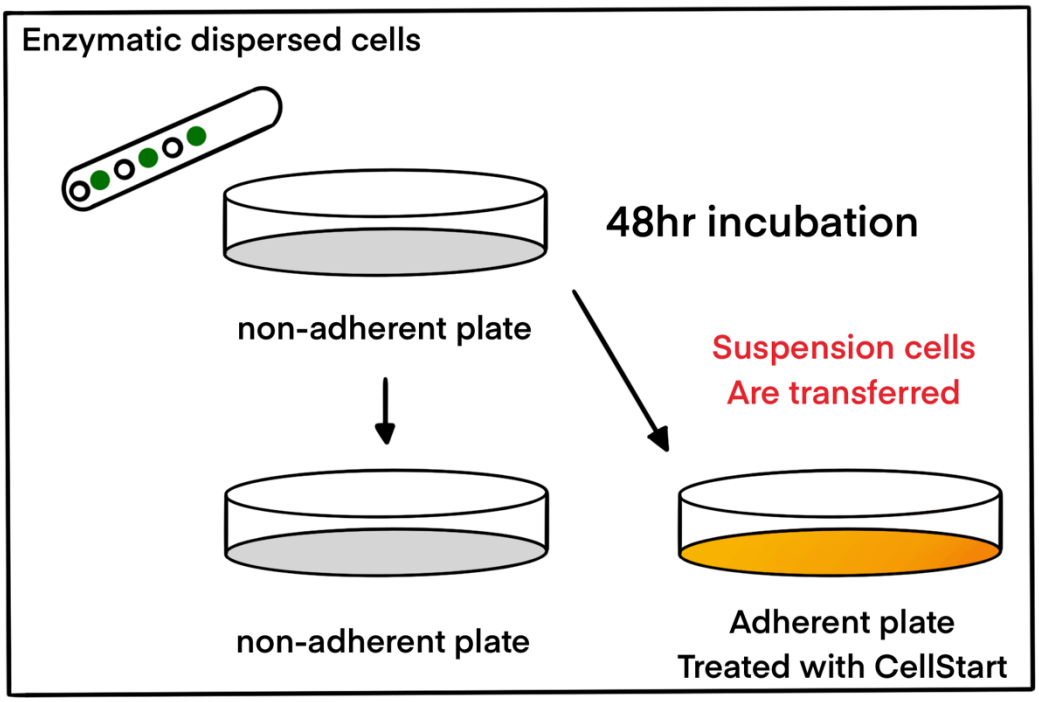

Figure 2.4. Schematic illustration of the seeding steps of the modified enzymatic dispersion protocol.

2.2.1.3 Mouse embryonic stem cells (mESC)

mESC (ES-D3 ATCC® CRL1934™) were bought commercially from ATTC and cultured in ESC medium supplemented with 15% ATCC- FBS, 1% of Penicillin and Streptomycin and 0.05 mmol/L 2-mercaptoethanol. Experiments were carried on till cells reached passage 20.

2.2.1.4 Mouse Aorta

The use of animals in this study was carried out according to the EU legislation (Directive 2010/63/EU) for the protection of animals used in research. Mice were anesthetized with an overdose of pentobarbital sodium (0.1mg/g), and death was confirmed by exsanguination by an authorised professional. The rib cage was cut open at the front of the animal to expose internal organs which were removed so the back of the rib cage was in view. The aorta was carefully excised using tweezers and scissors. The tweezers were carefully run along the side of the aorta to detach it from the backbone. The aorta tissue was harvested as fast as possible from the heart collecting it along the spine to the abdominal area. The tissue was placed in cold PBS, and fatty tissue was removed with the use of two tweezers. A 2 ml syringe and a needle were used to wash the lumen area of the vessel and remove any trace of blood. Afterwards, the adventitia was enzymatically removed by incubation of the tissue in 2.5

mg/ml collagenase solution (Appendix) for approx. 10-20 min at 37°C. Once the adventitia became detached, it was carefully removed using forceps under a dissection microscope as an intact layer. DNA and RNA After removing the adventitia the media layer was Snap frozen in liquid nitrogen and then with a mortar and pestle it was polarized to powder and then resuspended in the extraction buffer. In order to confirm the removal of the aventail liar the expression level of *Myh11* mRNA levels was measured.

2.2.1.5 Human-induced pluripotent stem cells (HiPSCs)

HiPSCs were cultured as per the manufacturer's protocol HipSci company. Briefly, the surface of the culture wear was pre-coated using Vitronectin (10µg/ml) and incubated at room temperature for 1 hour before seeding the cells. Cells were grown and maintained in feeder-free conditions in xeno-free, serum-free, complete Essential 8^{TM} medium (E8) media replacing 95% of the medium daily. Cells were subcultured by washing once with sterile PBS, incubated with EDTA (ethylenediaminetetraacetic acid) (0.5mM) for 4-8 minutes at room temperature while being observed under phase-contrast microscopy until bright halos around the edges and small holes appeared throughout the colonies. The EDTA was aspirated, and 2ml of E8 was added to the well. The dislodged cell colonies were then gently washed from the culture dish by pipetting the medium around the well using a 5ml/10 stripette until the desired cell aggregates were achieved. The resulting cell solution was then seeded into as many wells as were required. ROCK inhibitor (10mM) was added to optimize colony growth after subculturing. The culture was then agitated gently within the tissue culture incubator, ensuring an even distribution of cells across the culture plate was achieved. In this thesis hiPSCs were only used to generate SNEP.

2.2.1.6 Generation of HiPSCs-derived NE progenitors (SNEP)

HiPSCs were cultured as described in Section 2.2.1.5 until reaching 70% confluency. Cells were then split at a ratio of 1:10 and left at 37°C, 5 %CO_2 for 24 hours. 24 hours later, cells were incubated in E8 and left for 4-5 days. After this time period HiPSC colonies began to lose their typical defined borders which is followed by cell migration from the colonies. In order to promote proliferation of the migrated cells, HiPSC colonies were manually removed using a sterile glass picker. The remaining cells were subcultured at 60% confluency using EDTA solution (1:1000) for 4-8 minutes at room temperature while observed under phase-contrast

microscopy until cells displayed bright halos. EDTA solution was aspirated, and the recommended volume of E8 medium was added to the well. The dislodged cell colonies were then gently washed from the culture-wear by pipetting the medium around the well three times until a single cell suspension was obtained. Cells were centrifuged at 300 x g for 3 minutes and supernatant was removed, and the required amount of E8 media was added. Cells were then titrated into single cells using a 1ml syringe and 0.22µm gauge needle. The cells were used between passages 2-15 or till they lose their elongated morphology. These cells were generated in the lab and given to me to work with.

2.2.1.7 Human iPSC-derived smooth muscle cells (hSMC)

SNEP cells were cultured in the medium (E8) that was taken out at room temperature for an hour while coating the flask with Vitronectin, (cat no. 7180 stem cell), (40ul of Vitronectin 960ul of sterile PBS) 1ml for a well, 2ml for a T25 flask and 3ml for a T75 flask (Cheung et al., 2014). When cells were confluent, a flask was coated with 0,1% gelatine solution (cat no. G1393 Sigma), for 15 minutes in the incubator. After that it was coated with MEF medium for 24 hours in the incubator. MEF was aspirated before the cells were seeded in a flask with DMEM medium. The cells were resuspended with a needle and a syringe and the cells were treated with platelet-derived growth factor-BB (PDGF-BB), 10 ng/ml and transforming growth factor Beta 1 (TGF- β1), 2 ng/ml. The DMEM was replaced every third day and PDGF-BB, 10 ng/ml and TGF- β1, 2 ng/ml were added each time before the cells were harvested after 12 days.

A gelatin mixture heated at 56 °C for about 30 min was prepared until gelatin was dissolved and 0.5ml of 2% gelatine solution stock was prepared in 9.5ml of sterile PBS. The MEF preparation 500ml was combined with 450 ml of advanced DMEM F12, 50 ml of FBS, 5 ml of l-glutamine and 3.5 ml of β-Mercaptoethanol. An additional 5 ml of penicillin-streptomycin is also added. The medium was sterilised with a 500-ml vacuum filter unit and stored at 4 °C for up to 4 weeks (Cheung et al., 2014).

2.2.1.8 Cell Culture Methods

All cell culture techniques were carried out aseptically in a Biosciences Air 2000 Mac laminar flow cabinet. Cells were maintained in a Hera water jacketed cell culture incubator at 37°C and 5% CO_2. A Nikon Eclipse TS100 phase-contrast Microscope was used to visualize the cells.

2.2.1.9 Cell Subculture and Expansion

All cell lines used were adherent therefore detachment from their surface was required for cell subculture. Cells were subcultured using either 1X Trypsin (for mouse aortic smooth muscle cells, mSMCs) or 0.5X TrypLE select (for stem cells). Once they reached approx. 70-80% confluency, the cell growth medium was removed from the flasks/culture dishes and washed twice in HBSS to facilitate the removal of α-2-macroglobulin, a component of FBS which inhibits the action of trypsin or TrypLE.

Detachment solution was added to the culture vessel just to cover the surface area and cells were incubated at 37°C for 2-5 minutes (depending on cell type). Warm fresh maintenance medium was added to neutralise the detaching agent. Cells were pelleted by centrifugation at 300 x g for 5 minutes at room temperature. Cells were resuspended in the appropriate volume of maintenance medium and counted using a haemocytometer (Section 2.2.1.11). Cells were split at a cell density of 1-4 x 10^4 cells per cm^2 according to the specifications of individual cell lines.

2.2.1.10 Cryopreservation

Cells were trypsinized and pelleted as previously described. Following that cell pellet was resuspended in freezing media which varied depending on the cell line with 10% dimethyl sulfoxide (DMSO). This cell suspension was divided into 1mL aliquots in sterile cryopreservation vials. These vials were placed in a Mr. Frosty freezing container which was then stored overnight at -80°C. The vials were later transferred to liquid nitrogen for long-term storage.

2.2.1.11 Viable Cell Counting

After trypsinization and centrifugation, the cell pellet was resuspended in 1-3 mL of fresh growth media. 20µL of this cell suspension was diluted 1:1 with 0.4% Trypan Blue which was incubated at room temperature for 2 minutes. 20µL of this dilution was added to the counting chamber of a haemocytometer. The haemocytometer was then viewed under the microscope at 20x magnification. Trypan blue can enter and stain the cytoplasm of a dead cell but cannot cross the membrane of a viable cell. Due to this, dead cells appeared stained dark blue while live cells were unstained. Viable cells were counted in four of the major grid boxes on the haemocytometer and an average cell count was calculated. The following equation was used to estimate the viable cell concentration in the total cell suspension:

Average cell count x 10^4 (area under the cover slip) x 2 (dilution factor) = no. of viable cells/mL

2.2.2 Differentiation

2.2.2.1 Myogenic differentiation

2.2.2.1.1 Myogenic differentiation of S100β mVSC

Cells were seeded at a density of 1 x 10^3cells/cm^2 in their maintenance medium and left for 24 hr before being washed with HBSS twice, followed by feeding with the appropriate medium. Firstly, a population of cells were cultured in a maintenance medium as a control. Another population was cultured in a differentiation medium with TGF-β1 and PDGF-BB. The maintenance medium of each cell type is outlined in section 2.1.4.2. The dose used to treat cells was decided upon by a trial and error approach where the dose that elicited a significant effect was used for all similar experiments. The time chosen for myogenic differentiation was dependent on the output data – transcript levels were measured after 7 days whereas protein expression takes the most time and was measured after 7 days following treatment with 2ng/mL TGF-β1 and 10 ng/mL PDGF-BB. Cells were cultured in their RPMI medium for 7 days. And myogenic differentiation was confirmed with expression level of *Myh11* using qRT-PCR.

To immobilise Jagged-1 to a cell culture plate, each well was first immobilised with protein G (MSC 21193) (20µg/ml) overnight at 4^{o}C. Following the overnight incubation, the wells were washed three times with sterile PBS and then blocked with 1% BSA for 2 hours at room temperature. This was later removed and the wells were washed before the addition of 2µg/ml control Fc (R&D, 110-HG-100) or Jagged-1 and further incubation for 2 hours. The chosen dose to treat cells was decided by a trial and error approach where the dose that elicited a significant effect was used for all similar experiments. The time chosen for myogenic differentiation was dependent on the experimental readout; RNA or protein expression. This solution was removed and the wells were washed again before cells were seeded at a density of 20,000 cells/well directly onto the treated plates and incubated at 37^{o}C for 7 days myogenic differentiation was confirmed with expression level of Myh11 using qRT-PCR.

2.2.2.1.2 Myogenic differentiation of S100β SNEP

A flask was coated with 0,1% gelatin solution (cat co. G1393 Sigma) for 15 minutes in the incubator before they were coated with MEF medium for 24 hours in the incubator. MEF was aspired before the S100β SNEPs were seeded in a flask with DMEM medium. Cells were resuspended with a needle and a syringe and the cells were treated straight away with PDGF-BB, 10 ng/ml and TGF-β1, 2 ng/ml. The medium DMEM was changed every third day and PDGF-BB, 10 ng/ml and TGF-β1, 2 ng/ml were added every time medium was changed the cells were harvested after 12 days. Myogenic differentiation was confirmed with expression levels of *MYH11* and *CNN1* using qRT-PCR.

2.2.2.2 Vasculogenic Differentiation

2.2.2.2.1 Vasculogenic Differentiation of S100β mVSC

Innoprot Endothelial cell medium kit (P60104) was used to differentiate S100β mVSC to endothelial cells. Cells were seeded at a density of 1 x 10^3cells/cm^2 in their maintenance medium and left for 24 hours before being washed with HBSS twice, followed by feeding with the appropriate medium. a population of cells was cultured in a maintenance medium as a control for 21 days.

2.2.2.2.2 Vasculogenic Differentiation of S100β SNEP

Endothelial cell growth medium MV Supplement Pack C-39220 (Promo Cell) was used to differentiate S100β SNEP to endothelial cells. Cells were seeded at a density of 1 x 10^3cells/cm^2 in their maintenance medium and left for 24 hours before being washed with HBSS twice, followed by feeding with the Endothelial cell growth medium MV Supplement. A population of cells were cultured in a maintenance medium as a control for 21 days. Vasculogenic differentiation was confirmed by qRT-PCR measuring the expression level of platelet endothelial cell adhesion molecule 1 *(PECAM1)* and compared to SNEP controls.

2.2.2.3 Adipogenesis Differentiation

2.2.2.3.1 Adipogenesis Differentiation of S100β mVSC

StemPro® adipogenesis differentiation medium was used to differentiate mouse multipotent vascular stem cells into adipocytes. Cells were treated in accordance with the manufacturer's recommendations. briefly, cells were seeded at a density of 1 x 10^4 cells/cm^2 in their maintenance medium and left for two days before being washed with PBS twice followed by feeding with StemPro® adipogenesis differentiation med. A population of cells were cultured in maintenance medium as a control while the remaining cells were cultured in adipogenesis medium for 14 days, with medium replacement occurring every 3 – 4 days. On day 14, cells were harvested and adipogenic differentiation was shown using qRT-PCR to measure the expression level of Lipoprotein lipase *(Lpl)* and Fatty acid binding protein 4 (*Fabp4)* and Oil red O dye staining of lipids.

2.2.2.3.2 Adipogenesis Differentiation of S100β SNEP

StemPro® adipogenesis differentiation medium was used to differentiate mouse multipotent vascular stem cells into adipocytes. Cells were treated in accordance with the manufacturer's recommendations. Briefly, cells were seeded at a density of 1 x 10^4 cells/cm^2 in their maintenance medium and left for two days before being washed with PBS twice followed by feeding with StemPro® adipogenesis differentiation med. A population of cells were cultured in maintenance medium as a control while the remaining cells were cultured in adipogenesis medium for 14 days, with medium replacement occurring every 3 – 4 days. On day 14, cells

were harvested and adipogenic differentiation was shown using qRT-PCR to measure the expression level of *LPL* and *FABP4* and Oil red O dye absorbance at OD510nm.

2.2.2.4 Osteogenesis Differentiation

2.2.2.4.1 Osteogenesis Differentiation of S100β mVSC

StemPro® osteogenesis differentiation medium was used to differentiate mouse multipotent vascular stem cells into osteocytes. Cells were treated in accordance with the manufacturer's recommendations. Briefly, cells were seeded at a density of 5 x 10^3 cells/cm^2 in their maintenance medium and left for two days before being washed with PBS twice, followed by feeding with StemPro® osteogenesis differentiation medium. A population of cells were cultured in maintenance medium as a control while the remaining cells were cultured in osteogenesis medium for 21 days, with medium replacement occurring every 3 – 4 days. On day 21, cells were harvested and osteogenic differentiation was shown using qRT-PCR to measure the expression level of alkaline phosphatase (*Alpl*) and Sclerostin *(Sost)* and Alizarin red dye.

2.2.2.4.2 Osteogenesis Differentiation of S100β SNEP

StemPro® osteogenesis differentiation medium was used to differentiate SNEP into osteocytes. Cells were treated in accordance with the manufacturer's recommendations. Briefly, cells were seeded at a density of 5 x 10^3 cells/cm^2 in their maintenance medium and left for two days before being washed with PBS twice, followed by feeding with StemPro® osteogenesis differentiation medium. A population of cells were cultured in maintenance medium as a control while the remaining cells were cultured in osteogenesis medium for 21 days, with medium replacement occurring every 3 – 4 days. On day 21, cells were harvested and Osteogenic differentiation was shown using qRT-PCR to measure the expression level of *ALPL* and *SOST* and Alizarin red dye absorbance at OD 405nm.

2.2.3 Transient Transfections

2.2.3.1 Short interfering (siRNA) transfection

The Mirus TransIT-X2 Dynamic Delivery System was used for all siRNA transfections and was carried out as per the manufacturer's instructions. Briefly, approximately 2 x 10^3 cells/cm^2 were seeded on 6-well plates 24 hours prior to transfection. On the day of transfection, all the reagents were thawed at room temperature and then 25 nm of Silencer® Select siRNA (103015) was added to 250µL of opti-MEM I reduced serum media and 7.5µL of TransIT-X2. This was left for 30 minutes to allow complexes to form. The complexes were then added and incubated for up to 72 hours before RNA was isolated for gene expression analysis.

Table 2.18. Volume for siRNA Complex Tube setup with Mirus TransIT-X2

	Volume of media that is already seeded	**Serum-free medium**	**siRNA (10µM stock) 25nM final 4390771 (Bio-sciences)**	**TransIT-X2 MIR6003 (MSC)**
1 well	1.5 ml	150µl	4.2µl	4.5µl
T25 flask	2.5ml	250µl	6.8µl	7.5µl
T75 flask	7.5ml	750µl	20.4µl	22.5µl

The master mix was incubated at room temperature for 30 minutes before it was added to the cells in their inductive medium. Cells were harvested between 48-72 hours after. Transfection efficiency of the siRNA was confirmed using tye563Trans. Control (cat no. 51012019) the same volume of the tye563Trans. Control was added as the siRNA.

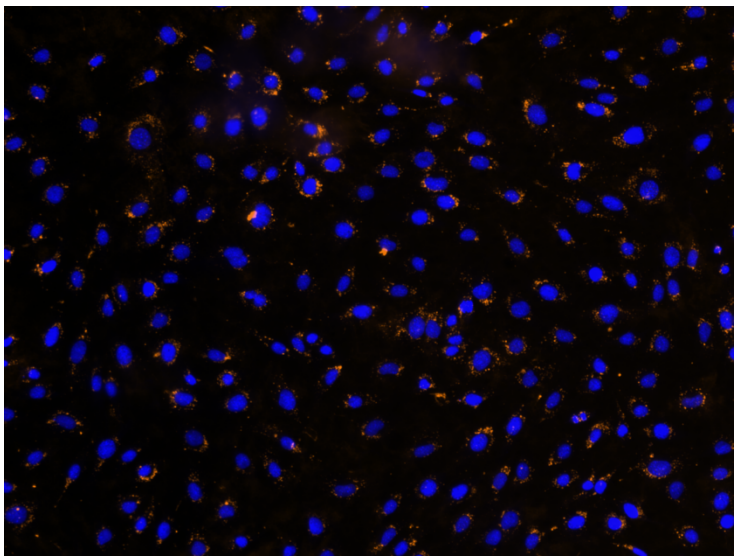

Figure 2.5. siRNA Transfection efficiency by Eoin Corcoran

2.2.4 Chromatin immunoprecipitation (ChIP) followed by polymerase chain reaction (PCR) – (ChiP-PCR)

ChIP-PCR was carried out using three different kits for chromatin extraction, immunoprecipitation and PCR. The protocols provided by the kits were followed and any variation from the protocol was noted as outlined below. ChIP—IT Express HT Kit (53018) from Active Motif Was used. In order to start ChIP a T75 flask must be between 70-90% confluent. Cells were harvested using cell scrapers and then were taken to the fixation process using ABCAM Chromatin Extraction Kit ab223876.

2.2.4.1 Chromatin Extraction

Chromatin extraction was carried out using the Chromatin Extraction Kit from Abcam. The provided protocol was divided into the different steps as follow: Starting material preparation – Adherent cells were detached using cell scraper and pelleted down. Cell pellets were washed once in cold HBSS and resuspended in cold HBSS (1 ml per 2-5 x 10^6 cells). Each 1 ml was transferred into a RNA/DNA-free 1.5 ml tube and centrifuged at 200 x g at 4°C for 5 min. Supernatant was discarded and pellets were ready for fixation. Aortas were harvested from the animals and cleaned. Tissues were weighed and cut into small pieces. Approx. 20 mg of Aorta tissue was transferred into RNA/DNA-free 1.5 ml tubes.

Cross-linking – Cell pellets (2-5 x 10^6 cells/pellet) or tissue pieces (20 mg) were resuspended in 1 ml of 1% formaldehyde for 10 min at room temperature with mixing on a seesaw platform. Samples were centrifuged at 1000 x g at 4°C for 3 min. Supernatant was discarded and samples resuspended in 1 ml of 1X Formaldehyde Quenching Solution in. Samples were incubated for 5 min at room temperature with mixing on a seesaw platform followed by a centrifugation step at 1000 x g at 4°C for 3 min. Supernatant was discarded and samples were washed twice in 1 ml of cold PBS. Centrifugations were carried out at 1000 x g at 4°C for 3 min. After the last centrifugation, PBS was removed and samples were stored at -80°C for the next step.

Chromatin extraction – frozen samples were always used for this step to minimize any variability between the usage of fresh or frozen material. The volume of lysis buffer (LB) was prepared according to the number of cells and quantity of tissue samples to be processed. 1 ml of LB: 5 µl of 200X protease inhibitor cocktail + 995 µl of extraction and LB. Fixed cell samples (2-5 x 10^6 cells) or tissue pieces (20 mg) were resuspended in 500µl or 300 µl of LB, respectively and incubated at room temperature for 30 min with mixing on a rotator wheel. Tissue pieces were homogenized using a Dounce tissue homogenizer prior to incubation. Cell samples were then centrifuged at 1000 x g at room temperature for 3 min and supernatant discarded. The pellets were resuspended in 300 µl of fresh LB. Samples were ready for sonication.

Sonication optimization was done for each cell line in order to apply the proper sonication conditions for the cells to get the required fragment sizes after running the samples on Agarose gel. Sonication shearing chromatin was performed at 0°C (ice water). The power of the sonicator and time were adjusted according to each sample type:

Table 2.19. Sonication conditions for each cell line

Cell line	AMP	Cycles	Seconds on and off
Mouse aortic tissue	35	9	10 on 10 off
MOVAS	15	7	10 on 10 off
S100β mVSCs	15	7	10 on 10 off
Mouse embryonic stem cells	15	7	10 on 10 off
S100β SNEP	15	7	10 on 10 off

After DNA fragmentation, 10 µl of IP Buffer Concentrate was added to every 100 µl of sonicated chromatin. DNA concentration was measured using the NanoDrop® ND-1000 Spectrophotometer (Thermo Scientific). Samples were stored at -80°C for the next step.

2.2.4.2 Chromatin Immunoprecipitation (ChIP)

ChIP assay was performed using the ChIP-IT Express HT kit from Active Motif. The protocol kit was followed in detail and any deviation was specified as outlined below: Chromatin lysates were thawed and their concentration of chromatin was adjusted to the limiting sample in order to work with the same concentration in all samples.
10 µl of each sample was transferred to a 0.2 ml tube and labelled as the Input DNA. Input samples are stored at -20°C and used later in the Reverse Cross-linking step.

The immunoprecipitation reaction was set up according to the company recommendation in 0.2 ml tubes (Table 2.20). For 60 µl of sheared chromatin, 3 µl of antibody was added to the reaction (Table 2.20). Incubation was carried out on an end-to-end rotator overnight at 4°C. On the following day, samples were briefly spun down, and placed on a magnetic stand to pellet the beads. The supernatant was carefully removed to avoid any disturbance to the pellet. It is important to note that beads are kept hydrated at all times to ensure the beads do not become damaged or degraded. The beads were washed twice with 200µl of ChIP Buffer 1 were performed followed by one more wash with 200µl of ChIP Buffer 2. Following

the final wash, the supernatant was discarded and the beads were resuspended in 50µl of Elution Buffer AM2. Samples were incubated on an end-to-end rotator for 15 min. Samples were briefly spun down preceded by a reverse cross-linking step. 50µl of the Reverse Cross-Linking Buffer was added to each 50µl of eluted chromatin sample (IP samples) and then mixed by pipetting. Tubes were placed on a magnetic stand to pellet the beads. The supernatants containing the eluted chromatin were carefully transferred to clean 0.2 ml tubes. The 10µl Input samples saved at the beginning of the protocol were thawed and the following reagents were added: 88µl of ChIP buffer 2 and 2µl of 5M NaCl. All the samples (IP and Input) were incubated at 65°C for 15 min. Samples were briefly spun down and allowed to reach room temperature before the addition of 2µl of Proteinase K. Samples were mixed and incubated at 37°C for 1 hour. Samples were briefly spun down and returned to room temperature before the addition of 2µL of Proteinase K Stop Solution. DNA concentration was measured using the NanoDrop® ND-1000 Spectrophotometer (Thermo Scientific), and stored at -20°C.

Table 2.20. ChIP reaction components.

Reagent	**Volumes (µl)**
Protein G Magnetic Beads	25
ChIP Buffer 1	10
Sheared Chromatin	60
Protease Inhibitor Cocktail	1
RNA/DNA-free water	1
Antibody	3
Total Volume	100

2.2.4.3 Real-Time Polymerase Chain Reaction (RT-PCR)

RT-PCR was performed using the SensiMix™ SYBR® No-ROX Kit from BioLine (QT650-05). The gene-specific primers for this PCR were adopted from Gomez et al. (Table 2.21) (Gomez et al., 2013). Optimization of the PCR cycling conditions was carried out for each specific pair of primers.

Bioline primer sets were supplied separately in tubes at a concentration of 50 µM.

Table 2.21. Preparation of a single Reaction Tube for RT-PCR.

Components	**Volume**	**Final Concentration**
2x SensiMixTM SYBR® No-ROX	12.5µl	1X
25 µM Forward Primer	0.25µl	200nM
25 µM Reverse Primer	0.25µl	200nM
Diethylpyrocarbonate (DEPC) water	7µl	
Template (IP or Input)	5µl	
Total reaction volume	25µl	

Table 2.22. Cycling Condition Setup for RT-PCR.

Step	**Time**	**Temperature**	**Cycles**
Polymerase Activation	10 min	95°C	1 cycle
Cycling Steps Denaturation Annealing Extension	 15 sec 15 sec 45 sec	 95°C 52°C 72°C	40 cycles

2.2.4.4 ChIP fold enrichment normalization

For ChIP analysis, a fold enrichment normalization method called also 'signal over background' or 'relative to the Immunoglobulin G (IgG) antibody control' was employed. With this method, the ChIP signals are divided by the IgG antibody signals, representing the ChIP signal as the fold increase in signal relative to the background signal. The assumption of this method is that the level of background signal is reproducible between different primer sets, samples, and replicate experiments. Background signal levels do vary between primer sets, samples, and experiments. First the nonspecific adjustment is calculated (Ct IP) - (Ct mock) and then the fold enrichment (2-DDCt). Ratio is calculated after fold enrichment first the nonspecific adjustment is calculated (Ct IP) - (Ct mock) and then the fold enrichment (2-DDCt). Following that the fold enrichment of H3K4me2 was divided by the fold enrichment of H3K27me3. Transcriptional analysis data were analysed using the Comparative CT method (ΔΔCT), described by Livak and Schmittgen (2001).

2.2.5 Total RNA Extraction from tissue and cultured cell samples.

Total RNA extraction from tissue and cultured cell samples is processed using the ReliaPrep RNA Cell Miniprep System kit from Promega Z6010. The provided protocol was followed in detail for both sample types. Lysates from tissue were prepared differently when compared to cell samples due to the need to first homogenise the specimens. In order to do so, tissues were weighed and pulverised by snap-freezing in liquid nitrogen and crushed using a clean pestle and mortar. Cells were harvested, counted and washed in HBSS twice to remove any trace of growth medium. A cell pellet was obtained following centrifuging the cell suspension at 300 x g for 5 min at room temperature and a lysis buffer (1:100 1-thioglycerol: BLbuffer) was added to samples. The volume of the lysis buffer was dependent on the number of cells and the weight of the tissue. The subsequent lysate was mixed by vortexing and/or pipetting. 100% Isopropanol was added to the samples according to the volume of lysis buffer and vortexed to homogenize the solution. And volumes were then transferred to pre-assembled filtered minicolumns. Samples were centrifuged at 12,000 – 14,000 x g for 30 sec at room temperature. The flow-throughs were discarded from the collection tubes and 500 µl of RNA wash buffer was added to the minicolumns. Samples were centrifuged at 12,000 – 14,000 x g for 30 sec at room temperature. The flow-throughs were discarded from the collection tubes,

and 30 µl of DNase I solution was added to the minicolumns followed by 15 min incubation. 200 µl of column wash solution was added to each minicolumn and tubes were centrifuged at 12,000 – 14,000 x g for 15 sec at room temperature. Two more washes in the RNA wash buffer were carried out before eluting the purified RNA. The filtered minicolumns were placed in nuclease-free tubes and nuclease-free water was added. The volume of nuclease-free water added to elute the RNA from the filter membrane depended on the cell/tissue input. Samples were centrifuged twice using the same flow-through at 12,000 – 14,000 x g for 1 min at room temperature. RNA concentration was determined using the NanoDrop ND-1000 Spectrophotometer (Thermo Scientific). Samples were aliquoted in small volumes and stored at -80°C.

2.2.6 DNA Isolation

Isolate II Genomic DNA kit BIO-52067 was used for DNA isolation as the provided protocol. Lysis Buffer G3 was added to the samples before incubating at 70°C for 10 min followed by ethanol in order to adjust the DNA binding. And then centrifuging before proceeding to a two-step wash with Wash Buffer GW1 and GW2. The Elution Buffer was added to the samples after being preheated at 70°C. This technique was used for sending the samples to be sequenced to confirm the binding of the primers and that they target the required gene.

2.2.7 Quantitation of Nucleic Acid Concentration

Quantitation of both RNA and DNA concentrations were carried out using the Nanodrop® ND-1000 Spectrophotometer. The solution that the DNA or RNA had been eluted in was used to blank the instrument. 1 µL of a sample was added to the stage and the absorbance of the sample was read at 260nm and 280nm. This gave a concentration of DNA/RNA in ng/µL. The ratio of OD260:OD280 provided an indication of the purity of the sample. It is accepted that a ratio of 1.8 indicates pure DNA while a ratio of 2.0 indicates pure RNA is fine to work with.

2.2.8 Real-Time Reverse-Transcriptase Polymerase Reaction Chain

RT-PCR for relative quantification of messenger RNA (mRNA) was performed. Rotor-Gene SYBR Green RT-PCR (QIAGEN, 204174) protocol was used for Real-Time One-Step RT-PCR

using the Real Time RotorGeneRG-3000™ lightcycler from Corbett Research. Real-Time One-Step RT-PCR protocols are designed to perform the reverse transcription and PCR reactions together in one tube. This protocol has Advantages over the two-step RT-PCR protocols as it is, less manipulation of the samples as everything is added in a single tube, and the minus reverse transcriptase (-RT) sample ran per primer in order to identify genomic DNA contamination present in the RNA samples.

The principle behind this method is that the fluorescence, emitted by the SYBR Green Dye complementary DNA (cDNA) complex in the reaction tube, is directly proportional to the start amount of gene-specific mRNA in the desired sample. Hence, the higher the fluorescence the greater the expression of gene-specific mRNA in the cell type of interest. In order to amplify the desired mRNA targets, gene-specific primers are needed. These primers are not included in the used kits, and therefore, they need to be supplied separately.

In order to carry out this analysis, a reference gene commonly known as housekeeping gene was selected to ensure that changes in the gene of interest were due to treatment and not secondary to other changes within the cells owing to the environmental stimulus. Housekeeping genes are usually involved in metabolic activities, therefore, they are constitutively expressed as they seem fundamental to cell survival (Salimnia et al., 2010). According to the cell/tissue type one of the following two housekeeping genes was used to carry out real-time RT-PCR in this Thesis:

Hypoxanthine Phosphoribosyltransferase (HPRT) – used as the housekeeping gene in mouse vascular stem cells, mSMCs and mNE-4Cs.

Glyceraldehyde-3-phosphate dehydrogenase (GAPDH) – used as the housekeeping gene in mouse vascular aortic stem cells, mSMCs, mNE-4Cs and mouse aortic tissue without tunica adventitia.

2.2.9 Real-Time One-Step RT-PCR by QIAGEN

Rotor-Gene SYBR®Green RT-PCR Kit (QIAGEN, 204174) was used in the study to perform QIAGEN Real-Time One-Step RT-PCR. This kit is provided with all the necessary components apart from the gene-specific primers.

Table 2.23. Components supplied in the Rotor-Gene SYBR® Green RT-PCR Kit (QIAGEN, 204174)

Components	**Description**
2x Rotor-Gene SYBR Green RTPCR Master Mix	HotStarTaq Plus DNA Polymerase (DNA poly) - it is new version of the QIAGEN HotStarTaq DNA Polymerase, which has been modified to reduce the hot activation time. It is activated by an incubation step of 5 min at 95°C, avoiding any activity while sitting in the reaction tube, and during reverse transcription reaction increases the affinity of the HotStarTaq Plus DNA Polymerase to single stranded DNA oligonucleotides. Additionally, a unique balanced combination of KCl and (NH4)2SO4 salts are present in the buffer as well as mgCl2 in order to increasing the ration of specific to non-specific primer binding during annealing step. This buffer is designed to shorten cycling times (denaturation, annealing of primers and extension) Deoxynucleoside triphosphate (dNTP)mix - dATP, dCTP, dGTP, dTTP
Rotor-Gene RT Mix	An optimal blend of two RT enzymes capable of transcribing through

	secondary structures, and a wide range of RNA amounts present in the samples: • Omniscript® RT - RNA amounts ≥ 50 ng. • Sensiscript® RT - RNA amounts < 50 ng
Fluorescent Dye	SYBR Green I - the dye binds to double-stranded DNA during extension step. The dye has a maximum excitation light of 494 nm wavelength, and its emission light is optimally detected at 521 nm. These requirements are compatible with the optic system of the Real Time Rotor-GeneRG-3000TMlightcycler from Corbett Research used in this study.
RNase-Free Water	PCR-grade

The Protocol used was the one provided in the Rotor-Gene SYBR Green Handbook by QIAGEN. A Table for preparation of reaction tubes (Table 2.24), and a Table for how to set up the cycling conditions of the Real-Time Rotor-GeneRG-3000™ lightcycler (Table 2.25).

Table 2.24. A Table for preparation of reaction tubes for the Rotor-Gene SYBR® Green RT-PCR Kit (QIAGEN, 204174)

Components	**Volume**	**Final Concentration**
2x Rotor-Gene SYBR Green RT-PCR Master Mix	12.5 µl	1X
Primer	2.5 µl	1 µM
Rotor-Gene RT Mix	0.25 µl	
RNase-Free Water or DEPC water	4.75 µl	
Template RNA (2ng/µl)	5 µl	
Total reaction volume	25 µl	

QIAGEN primer sets were supplied in separate tubes at a concentration of 25 µM. **Nano Dropped RNA samples were equally brought to the same concentration in the PCR.

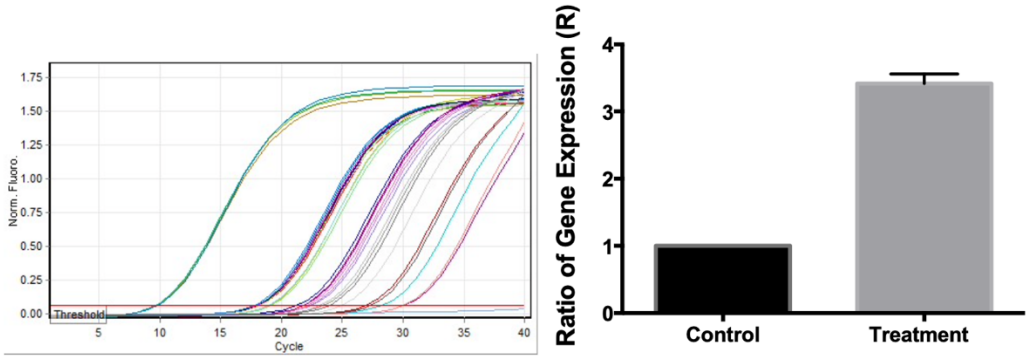

Figure 2.6. qRT-PCR. Relative levels of gene expression were measured by converting mRNA to cDNA and amplifying this cDNA using fluorescently-tagged primers specific to the target gene sequence. Fluorescence intensity data (sample on left) could be interpreted to allow gene expression ratios to be calculated and graphed (sample on right).

Table 2.25. Cycling Condition Setup for the Rotor-Gene SYBR® Green RT-PCR Kit (QIAGEN, 204174)

Step	**Time**	**Temperature**	**Comments**
Reverse transcription	10 min	55°C	Linear conversion of mRNAs into their cDNA molecules
PCR activation Step	5 min	95°C	During this initial step the HotStarTaq Plus DNA Polymerase (DNA poly) is activated
Cycling Steps Denaturation Annealing and Extension	 5 sec 10 sec	 95° C 60° C	35-40 cycles Double-stranded DNA melts away Primers annealed to their complementary DNA sequences, and the DNA poly extends the target gene sequences. SYBR Green I binds to the newly formed double stranded DNA products, becoming excited by the flashing light (494 nm). Fluorescence is then emitted at 521 nm

**NanoDropped RNA samples were equally optimized to be in the same concentration before use.

2.2.9.1 Relative expression ratio analysis by the REST© tool

In order to calculate relative changes in the expression of a target gene of interest an improvement of the 2ΔΔCTmethod was used in the study. The Comparative Ct method (ΔΔCt) described by Livak and Schmittgen (2001) is considered one of the most used to calculate relative mRNA expressions of target genes between target and reference (control) samples. In this method, the difference in cycle number (Ct) values between target and reference genes in a control sample (ΔCtcontrol) is then subtracted from the difference of Ct values between the same target and reference genes in the target sample (ΔCttarget), which results in the ΔΔCt(ΔCttarget - ΔCtcontrol). However, in order to compare these values with each other, an amplification efficiency of 100% is assumed across the different genes and samples. This assumption is practical but the real situation is reflected by this assumption. Amplification efficiency varies due to the nature of the components present in the reaction tubes, for instance, the presence of PCR inhibitor, RNA extraction (operator handling differences), different SYBR Green Mix, primers, probes, and enzymes. Therefore, PCR amplification efficiency needs to be determined to correct this assumption (Bustin et al, 2009) (Pfaffl, 2000). In this study, a software tool known as the REST© (relative expression software tool) Tool, is used to calculate relative gene expression ratios within a sample group (different target samples against the control) including the PCR implication efficiency (Pfafflet al, 2002). This software utilised a mathematical model including the PCR amplification efficiency (E) developed by Pfaffl,M.W. in 2001.

Real-time PCR amplification efficiencies were not calculated by QIAGEN RT-PCR reactions, as the company guaranteed a PCR amplification efficiency of 2 for every primer. Therefore, when no PCR amplification efficiency was calculated, the REST tool assumed an E = 2.

2.2.10 Immunocytochemistry (ICC)

Cells were seeded at a very low density (5 x 10^3 cells/well) for ICC to allow proper visualisation of the cells. They were seeded onto 6 well plates containing sterile coverslips. The 6-well plates containing the coverslips were placed under UV light for 30 min to ensure sterile conditions. Fluorochrome-conjugated antibody control samples were prepared to optimise the imagining parameters thus excluding false positive readouts due to secondary antibody non-specific binding. Hence, one control sample was prepared per type used during the experiment (Goat, mouse and rabbit).

The protocol was divided into different steps as follow:
Fixation and Permeabilization – 3 to 4 days after seeding, medium was discarded from the wells. For intracellular staining, cells were also permeabilized with a 3.7-4% Formaldehyde/0.1% Triton X-100 solution and incubated for 15 min at room temperature. Cells were washed 3 times in DPBS.

Blocking – Samples were blocked for non-specific binding sites using a blocking buffer for 1 hour at room temperature with gentle agitation. The blocking solution was made of 5% BSA, 0.3M Glycine and 1% Tween-20 in a DPBS solution. Cells were washed 3 times in DPBS.

Immunolabeling – Antibodies were diluted at a desired concentration in antibody solution, which consisted of 2.5% BSA, 0.3M Glycine and 1% Tween-20 in DPBS. The primary antibody (1° Ab) dilution was added to the coverslips. Cells were then allowed to incubate overnight at 4°C. From now on, all steps were carried out in darkened conditions to protect samples from the light. On the proceeding day, washing steps were carried out followed by incubation of the corresponding fluorochrome-conjugated antibody which is known as the secondary antibody (2° Ab) for 1-2 hours at room temperature with gentle agitation. Cells were washed 3 times in DPBS. Lastly, cells were incubated in a 4',6-diamidino-2-phenylindole (DAPI) dilution (1:1000 in 1 % Tween-20 DPBS) for 15 min at room temperature in order to stain the nuclei. For preparation of the 2° Ab controls, cells were subjected to the entire immunolabeling protocol except for the primary antibody incubation step. Instead, antibody solution was used to replace the primary antibody dilution.

Mounting – Coverslips were mounted onto microscope slides for fluorescent microscopy analysis. 25 µl of a water-based mounting medium was added to each glass slide. The coverslips were carefully placed (tissue-face down) onto the mounting medium-containing slide avoiding the formation of bubbles. The samples were cured overnight at 4°C protected in the dark to allow the mounting media to solidify.

Analysis – All images were taken and compiled using Olympus BX51 Fluorescence Microscope and CellF Multi-fluorescence and Imaging Software.

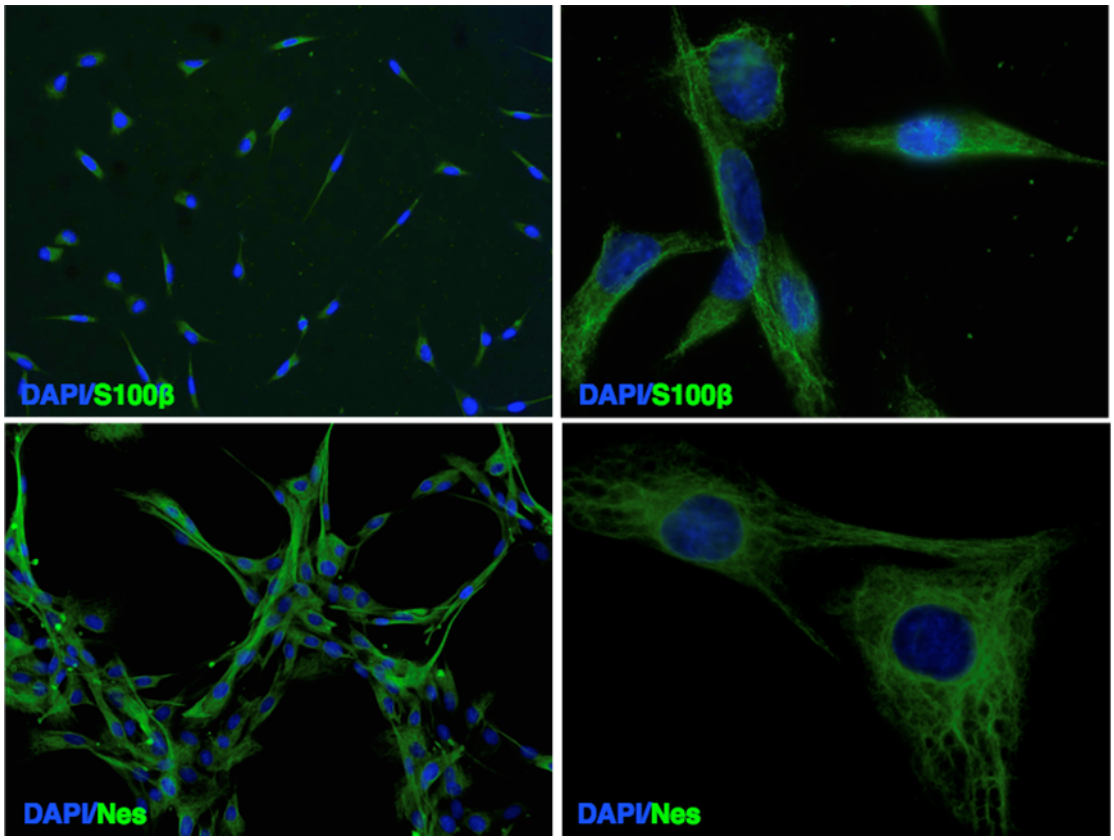

Figure 2.7. Isolated rfmVSC3T cells in maintenance media type 1 positively stained for S100β and Nestin proteins, astrocyte, and neuroectoderm markers.

2.2.11 Protein Manipulation

2.2.11.1 Protein Storage

All protein samples were stored in a Radioimmunoprecipitation assay (RIPA) buffer plus a Protease inhibitor cocktail at -80°C. Protein was always manipulated carefully and placed on ice outside the -80°C freezer.

2.2.11.2 Whole Protein Lysate Extraction

Adherent cells and mouse tissue were used as sources for protein extraction. Protein samples were harvested using RIPA lysis buffer (composed of; 20mM Tris, 150mM NaCl; 1mM Na2EDTA; 1mM EGTA; 1% Triton X-100 (v/v); 2.5mM sodium pyrophosphate; 1mM-glycerophosphate; 1mM sodium orthovanadate; 1µg/ml leupeptin) supplemented with protease (phosphate inhibitor cocktails: 1 µl per 100 µl of RIPA buffer).

2.2.11.3 Preparation of protein from adherent cells samples

Prior to isolation, cells were washed twice with ice-cold PBS, and the cells were scraped into 1 mL of PBS to detach the cells from the plate surface. The cells were collected and centrifuged for 5 minutes at 300 G. The PBS was removed and an appropriate volume of Protease-RIPA buffer (depending on pellet/sample size) was added to the pellet to lyse the cells. The amount that is added was 100µl for a T25 flask to ensure a high concentration (mg/ml) of protein was achieved. The protein samples were then placed on ice and vortexed every 10 min for an hour. The lysates were clarified by centrifugation at 300 x g for 5 min at 4°C. The supernatants (whole protein extract) were aliquoted into a clean tube and stored in an -80°C freezer.

2.2.11.4 Bicinchoninic acid Protein Assay

Pierce Bicinchoninic acid Protein Assay kit (23225) from Thermo Scientific was used to know the concentration of the proteins in the samples through different dilutions of Albumin Standard Ampules (2mg/ml). Pipette 25 µl of each standard or unknown sample replicates into a microplate well. Followed by adding 200 µl of the WR mix to each used well. The plate was placed on a plate shaker for 30 sec before incubation for 30 min at 37°C. The absorbance was measured at 562 nm on a plate reader.

2.2.11.5 Western blot

Transfer of protein to nitrocellulose membrane using a wet transfer system

Samples were prepared for SDS-PAGE. 5µL of 1X sample buffer (Laemmli Buffer containing β-mercaptoethanol) was added to 15µL of the sample. This mixture was incubated at 70°C for 10 minutes before transferring the full 20µL to a precast SDS 10% polyacrylamide gel to perform electrophoresis. This gel was run at 50mA for approx. 90 minutes.

Following gel electrophoresis, gels were equilibrated in a cold transfer buffer for at least 15 minutes. Equilibration facilitated the removal of electrophoresis salts and detergents. Salts, if not removed, increase the conductivity of the transfer and the amount of heat generated during transfer. Pre-cut nitrocellulose membranes (A19020 MyBio) were used along with sheets of Whatman filter paper that were required for the gel/membrane sandwich. These were then soaked in a transfer buffer. Protein transfer was carried out on a Bio-Rad Wet Transfer Criterion™. Build the transfer on the black side of the cassette where a pre-soaked sheet of filter paper was placed. A pipette was rolled over the surface of the filter paper to exclude all air bubbles. This step was repeated with two more sheets of filter paper. The SDS-PAGE gel was placed next and following this the nitrocellulose membrane and 3 more sheets of filter paper. These were of course rolled each time so as not to introduce bubbles. The cassette was closed up and then put into the rig with the black side on the inside. Gels were transferred at 100V for 30 minutes.

Staining of proteins immobilised on nitrocellulose filters

Ponceau S staining was employed to determine whether uniform transfer of proteins to the nitrocellulose membrane had taken place and to normalize for variations in protein loading. Transferred proteins were detected as red bands on a white background. This staining technique is reversible to allow further immunological analysis. Ponceau S is a negative stain, which binds to positively charged amino acid groups of proteins. It also binds non-covalently to non-polar regions of proteins. Following electrophoretic transfer, the nitrocellulose membrane was immersed in 20 ml Ponceau S solution (Sigma-Aldrich) and stained for 5 minutes with constant agitation. After proteins were visualised, the membrane was washed

in several changes of dH_2O until all the stain had been washed away. The membrane was later used for immunological probing.

Immunological probing

Following Ponceau S staining, the membrane was incubated at constant agitation in blocking buffer for 1 hour at room temperature or overnight at 4 °C. The membrane was then washed three times for 5 minutes a piece with fresh 1X Tris-Buffered Saline, 0.1% Tween (TBS-T). Incubation with the appropriate primary antibody (diluted in blocking buffer) at 4 °C overnight followed this. {Sodium azide can be added to each antibody solution to a final concentration of 0.02 % (w/v) as a preservative thus permitting reuse of the antibody}. After primary antibody incubation, the membrane was washed three times for 5 minutes a piece in fresh TBS-T. The membrane was then incubated at constant agitation with the appropriate peroxidase-conjugated secondary antibody (diluted in blocking buffer) for 1 hour at room temperature or overnight at 4 °C. Following this incubation, the membrane was then washed three times for 5 minutes a piece with fresh TBS-T. The membrane was then placed in a clean container and covered with 3,3',5,5'-tetramethylbenzidine (TMB, Sigma) which is used for the colorimetric detection of hydrogen peroxidase-conjugated molecules. When incubated, the peroxidase bound to the secondary antibody catalysed the production of a dark blue permanent-coloured product that was easily observable. The membrane was then rinsed in distilled water to stop the reaction and photographed.

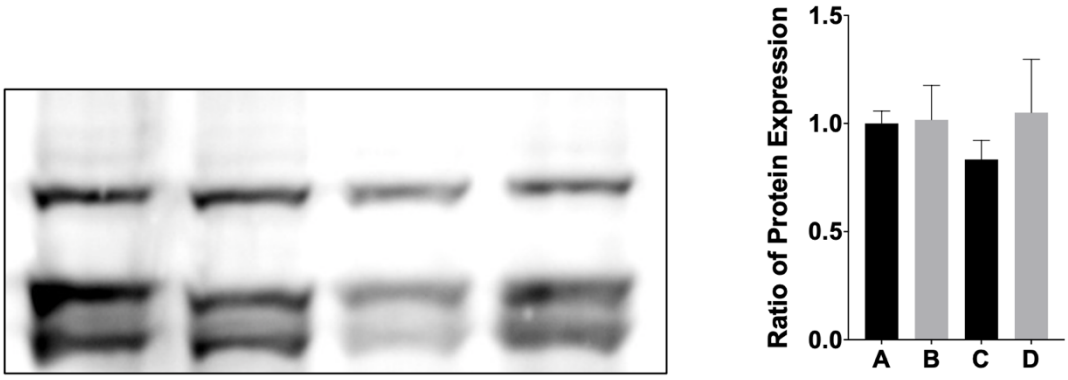

Figure 2.8. Western Blot. Relative protein expression levels were measured using Western Blot. Protein lysates were isolated and separated on an SDS-PAGE GEL before transfer to a nitrocellulose membrane. Sample lysates were then probed for specific markers using target-specific primary antibodies and host-specific secondary antibodies. Bands were visualized by chemiluminescence. This figure shows a sample image of the data output generated from Western Blot analysis. The blot image shows protein bands of similar molecular weight (left) and band intensities normalized to a loading control (right).

2.2.12 Running the DNA on 1.5% Agarose gel

The purpose of this experiment was to optimize the required sonication conditions for each cell line in order to embark on with the right size of fragments. All cells used in this study were characterised for the use of another kit. However, later Active Motif Express™ HT kit (53018) was used which recommended the use of less Amp and more cycles.

Sonication was done at different conditions considering cycles and Amp.

Table 2.26. 1.5% Agarose gel preparation

1,5% Agarose Gel, 50ml	
Compounds	***Volumes/Weight***
Tris-acetate (TAE) (50X)	*1ml*
Distilled water	*49ml*
Agarose	*0.75g*

All the compounds were boiled in a microwave for 1 min till the solution was clear. Once it is at body temperature the intercalating reagent (SYRB green or ethidium bromide) was added. The beaker was swirled carefully till it reached homogeneity, and the molten agarose was poured into the casting tray and left for 30min in the dark.

The loading buffer was added to each of the digested samples. which provides a visible dye that helps with gel loading and will also allow one to gauge how far the gel has run and it contains a high percentage of glycerol, so it increases the density of the DNA sample causing it to settle to the bottom of the gel well, instead of diffusing in the buffer. The gel was loaded in the casting tray in the electrophoresis box, and TAE(1X) was poured. 1KB DNA ladder was loaded into the first lane of the gel. The samples were loaded into the additional wells of the gel with the loading Buffer. The machine was turned on at 80-150 V until the dye line was approximately 75-80% of the way down the gel.

2.2.13 Oil Red O Dye

To confirm adipogenic differentiation of S100β mVSC and S100β SNEPs, 300mg of oil red O powder was added to 100ml of 99% isopropanol. In the fume hood 30ml of the oil red o stock was added to 20ml of Ultrapure Water (Merck Millipore). The solution was filtered with a 0.2µM filter and this solution was prepared before each experiment. Cells were fixed in 4% formaldehyde for 15 min, followed by 3 washes for 5min with Ultra-Pure Water (Merck Millipore). The formalin was removed, and oil red O working solution was filled into the culture plates to safely cover the plate bottom 1.25 ml per well for 6-well plates. The plates were incubated at room temperature for 30 min. They were then washed 5 times with Ultra-Pure Water (Merck Millipore). To elute the dye, 100% 2-propanol was added to the plates 2.5 ml per well for 6-well plates. The plates were incubated for 10 min at room temperature on an orbital shaker. The cells were then analysed using an Olympus CK30 microscope under phase contrast. In addition, absorption is measured in triplicate at 510 nm on a microtiter plate reader with a dynamic range of 0.000 O.D. to 3.200 O.D.

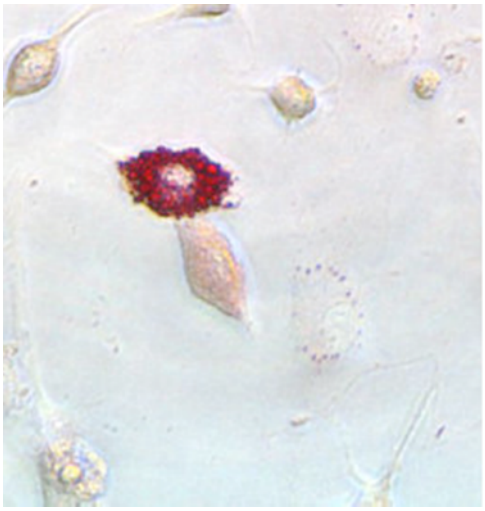

Figure 2.9. Positive Oil Red O on MSC-derived adipocyte under phase contrast.

2.2.14 Alizarin Red S Dye

To confirm osteogenic differentiation of S100β mVSC Alizarin red dye was prepared to a concentration of 2% in Ultra-Pure Water (Merck Millipore). The pH of the dye was adjusted to 4.1-4.3 if required using NH_4 OH. Afterwards, the dye was filtered using a 0.45µm pore filter and this solution was prepared before each experiment. After cell fixation the cells were stained with alizarin red dye and incubated for 30 minutes at room temperature. The cells were washed 5 times and left in PBS for analysis. The samples were visualised under Nikon microscope using phase contrast. Mineralized tissue nodules form where osteocytes (bone cells) are present, and calcium deposits stain bright red/orange by the Alizarin Red dye. To measure the absorbance 100 µl of 40 mM Alizarin Red S solution was added to 900 µl of standard dilution solution to make a 1 mL solution of 4 mM ARS. Mix well. In 8 1.5-mL microcentrifuge tubes 500 µl of standard dilution solution was added into each tube and labelled 1 to 8. 500 µl of the 4 mM ARS solution was added into tube #1 and mix well to get the 2 mM ARS standard. 500 µl of the 2 mM ARS standard was transferred from tube #1 to tube #2 and mix well to get the 1 mM ARS standard. This step was repeated for tubes #3-7 to serially dilute the ARS standards. Nothing was added to tube 8,which serves as the blank. In a 96-well plate, replicates were prepared (A, B, C) of each ARS standard by aliquoting 150 µl/well of each ARS standard into triplicate wells of the 96-well plate, according to the following plate.

Average the OD405nm of replicate wells of each ARS standard, blank and samples. Subtract the average OD405nm value of the blank from the average OD405nm values of others. Based on the calibrated OD405nm value of the ARS standard.

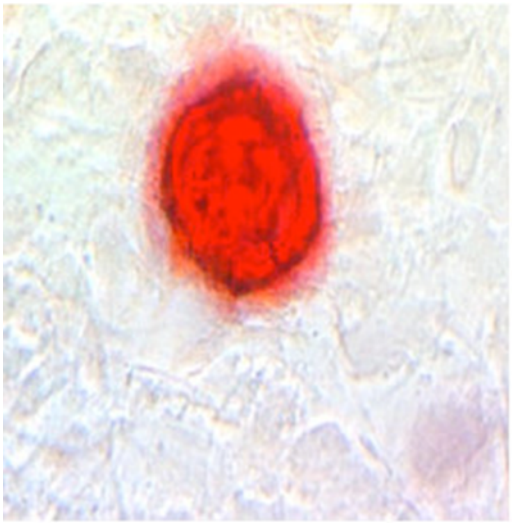

Figure 2.10. Positive Alizarin Red S on MSC-derived osteocyte under phase contrast

2.2.15 chromatin immunoprecipitation sequencing (ChIP-seq) analysis

2.2.15.1 In Silico ChIP-seq

Public bulk ChiP-seq datasets on mouse and human multipotent stem cells and their vasculogenic, adipogenic, osteogenic and myogenic progeny were sourced from the National Center for Biotechnology Information (NCBI at https://www.ncbi.nlm.nih.gov), the ChIP atlas (https://chip-atlas.org) and ENCODE project (https://www.encodeproject.org) by accession numbers. Various data types are available (e.g., reads, mapfiles, bigwig files, and peak lists), that are suitable for ChIP-seq analysis. The accession numbers were then used to access the datasets from the European Biotechnology Institute (EBI) (https://www.ebi.ac.uk) by downloading the Fastq file. These Fastq files were uploaded to Galaxy and Fast quality control (QC) quality reports were done to check the quality. FastQC is an open-source tool that simply provides a way to quality control raw sequence data. It provides a modular set of analyses which gives a quick impression of whether data has any problems of which we should be aware before doing any further analysis. Rather than looking at quality scores for each individual read, FastQC looks at quality collectively across all reads within a sample.

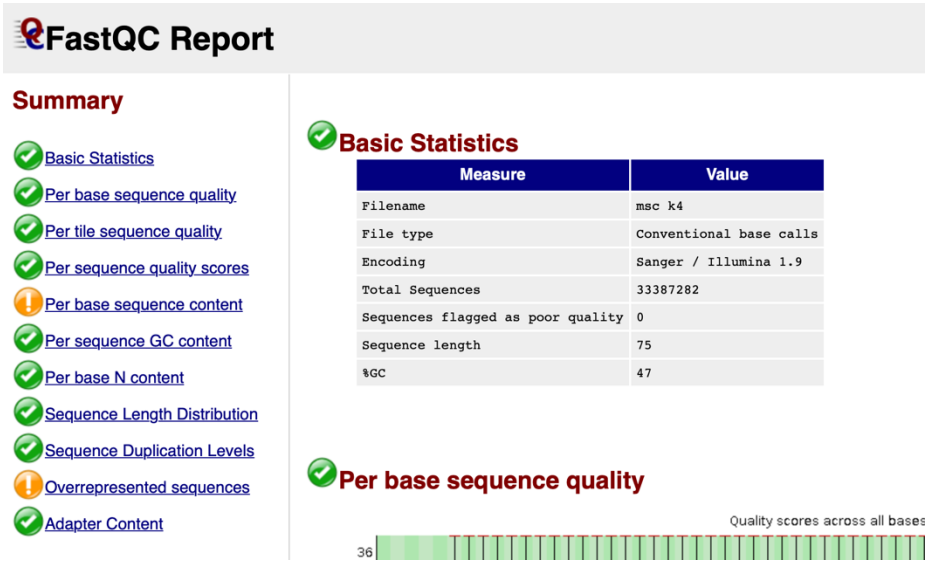

Figure 2.11. FastQC report on Galaxy

The Trim Galore!, a tool was used to remove the adapters from the data because they interfere with downstream analyses, such as alignment of reads to a reference. Then FastQc was performed to check the quality following trimming. The Bowtie2 tool is an ultrafast and memory-efficient tool for aligning sequencing reads to long reference sequences. It is particularly good at aligning to relatively long (e.g. mammalian) genomes. Bowtie 2 indexes the genome with an FM Index to keep its memory footprint small: for the human genome, its memory footprint is typically around 3.2 GB. In this study, Bowtie2 was performed for single-end reads. All the Bowtie2 produced Binary Alignment Map (BAM) files for each sample were merged as one file, if there were more than one file per sample. The Model-based Analysis of ChIP-seq (MACS) predicted tool was performed to predict fragment size from alignment results which was used for peak calling.

(a)

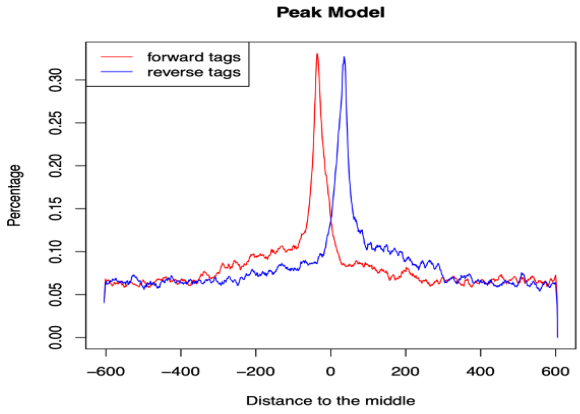

(b)

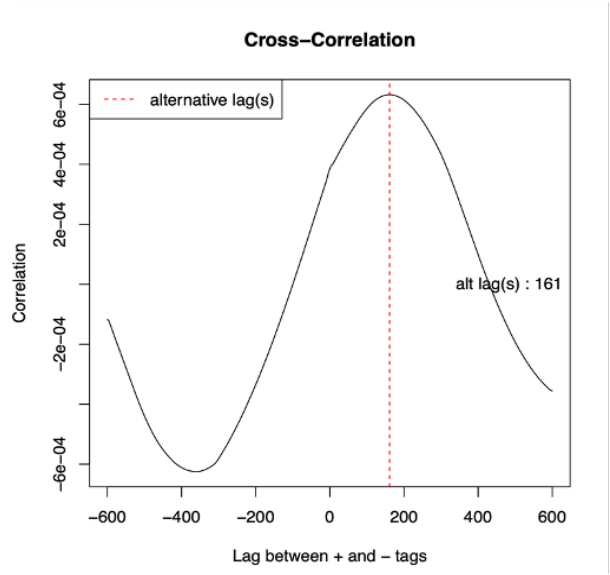

Figure 2.12. MACS predicted tool. (a) Peak model. (b) Cross-correlation.

MACS algorithm captures the influence of genome complexity to evaluate the significance of enriched ChIP regions. Although it was developed for the detection of transcription factor binding sites it is also suited for larger regions. MACS2 tool, which is the most common tool for peak calling, was used to generate peak calling from alignments. Peak calling is to filter out background noise and accurately identify the locations of peaks in the genome. An

integrated Genome Browser (IGB) was used to visualize the data and compare between different samples.

MACS2 peak calling generated a few files, one of which was Peaks in tabular format. This file shows the chromosome number start and end along with the peak score if there was a peak. To make these peak scores understandable and relate the peak score of a specific gene to the entire peaks across the genome, especially, as some samples and control files were not performed by the same group research or company.

Chrom	Start	End	Score
chr1	3671166	3671506	327
chr1	3671869	3672278	272
chr1	4785022	4786201	1159
chr1	4807449	4808507	311
chr1	4857707	4858608	615
chr1	5019508	5019836	67
chr1	5083109	5083849	807

Figure 2.13. MACS2 call peak showing chromosome number start and end of a peak with a Peak score**.**

Summary statistics were done to know the range of scores in the peaks on a specific column across the entire genome in a sample. Peak scoring is a way of assessing the importance of each peak relative to all other peaks across the genome. Having done that, it was necessary to use terminal Software that would allow us to generate a list of peaks if they were present at their location for the entire required genes. These commands were generated by someone in the school who is a professional at bioinformatics. And terminal generated files that were interrogated to determine the peak scores. If there were more than one peak score the one that is closer to the transcription starting site (TSS), was the one that is picked. The lower the percentage of the peak score the more significant the peak is.

Table 2.27. Summary of Peak scores

#sum	mean	stdev	0%	25%	50%	75%	100%
2.142850 6	107.665	100.566	1.565	19.5696	69.0161	184.047	437.331

Table 2.28. mouse MSC ChIP-seq accession numbers

Cell line	**Accession number**
mVSMC H3K27me3	SRR6907655
mVSMC H3K4me3	SRR6907654
mMSC Input	SRX1672919
mMSC H3K4me1	SRX1672802
mMSC H3K4me3	SRX1471729
mMSC myogenic differentiated H3K4me3	SRX770037
mMSC H3K27me3	SRR4040272
mMSC vasculogenic differentiated H3K4me3	SRR5249585
mMSC adipogenic differentiated H3K4me1	SRX1672907
mMSC osteogenic differentiated H3K4me3	SRX1672874

Table 2.29. human MSC ChIP-seq accession numbers

Cell line	**Accession number**
hMSC Input	SRR8810691
hESC H3K4me1	ENCFF681PBK
hMSC H3K4me1	ENCFF250JXU
hESC H3K4me2	ENCFF160HVH
hMSC H3K4me3	SRR7519602
hESC myogenic differentiated H3K4me2	SRR5339558
hVSMC H3K4me3	SRR11185364
hMSC H3K27me3	SRR1566130
hMSC vasculogenic differentiated H3K4me3	ENCFF721CUM
hMSC adipogenic differentiated H3K4me1	ENCFF985VXV
hESC osteogenic differentiated H3K4me1	ENCFF419QQN

2.2.15.2 Human SNEP ChIP-seq

Human S100β SNEP and their myogenic, vasculogenic, adipogenic and osteogenic progeny were prepared before ChIP was performed in the lab and the immunoprecipitated DNA was then shipped to Novogene Ltd to perform ChIP-seq on dry ice. Input and H3K4me2 for S100β SNEP and following lineage-specific differentiation and H3K27me3 for S100β SNEP. Sequencing of DNA libraries resulted in ~29–66 million reads per sample.

DNA samples to final data report, each step of sample QC, library preparation and sequencing can have an impact on the quality and quantity of data output, and the quality of data will directly affect the results of subsequent computational analysis. Therefore, obtaining high-quality data is the premise to ensure that bioinformatics analysis is correct, comprehensive and credible. In order to ensure the accuracy and reliability of sequencing data from the

beginning, Novogene strictly checked every experimental step that fundamentally ensured the output of high-quality data. Sample preparation, library construction, sequencing and bioinformatic analysis were all done by Novogene Company Ltd and were sent to me to visualise. The workflow was as follows:

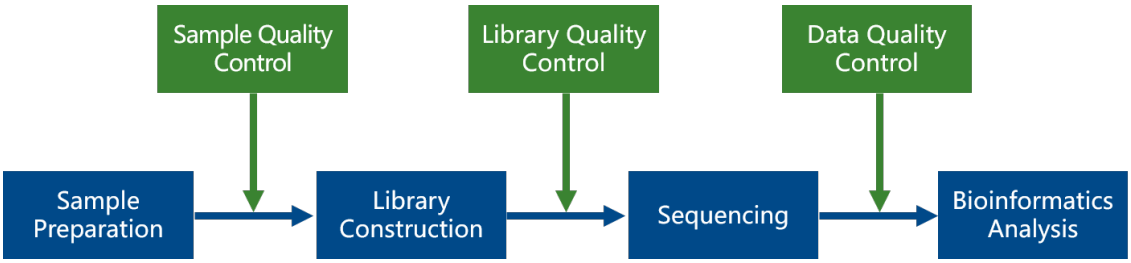

Figure 2.14. The workflow which was done by Novogene Company Ltd

The DNA samples were immunoprecipitated and purified before Novogene detection of these IPed DNA samples was assessed using Qubit to accurately quantify the DNA concentrations, and agarose gel electrophoresis analyses of DNA fragments for size distribution and detection of any contamination.

The Library was then prepared for sequencing as follow:

(1) The DNA fragments were repaired, dA-tailed.

(2) The DNA fragments with A tail were ligated to sequencing adaptors.

(3) The final DNA library was obtained by size selection and PCR amplification.

The workflow of library construction was as follows:

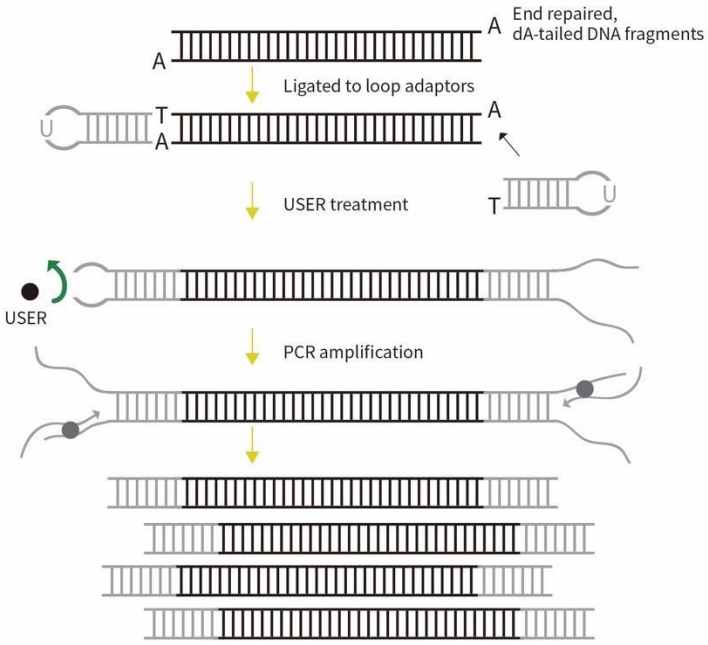

Figure 2.15. Library construction was done by Novogene Company Ltd

After the construction of the library, the initial quantification was performed with Qubit 2.0, and the library was diluted to 1ng/l. Then the insertion size of the library was detected with NGS3K. If meeting the expectation, the accurate concentration of the library was quantified by Q-PCR (library effective concentration > 2nM) to ensure the accurate molar amount that will be pooled for sequencing.

Sequencing was performed for different libraries according to the concentration and the demand of data amount on Illumina NovaSeq platform. The basic principle of sequencing is sequencing by synthesis. Four kinds of fluorescent labelled Deoxynucleoside triphosphate (dNTP), DNA polymerase and adapter primers are added to the flow cell for amplification. When each sequence cluster extends the complementary chain, each fluorescent labelled dNTP releases the corresponding fluorescence. The sequencer captures the fluorescent signal and converts the light signal into the sequencing peak through computer software to obtain the sequence information of the fragment to be detected.

The sequencing process is shown below.

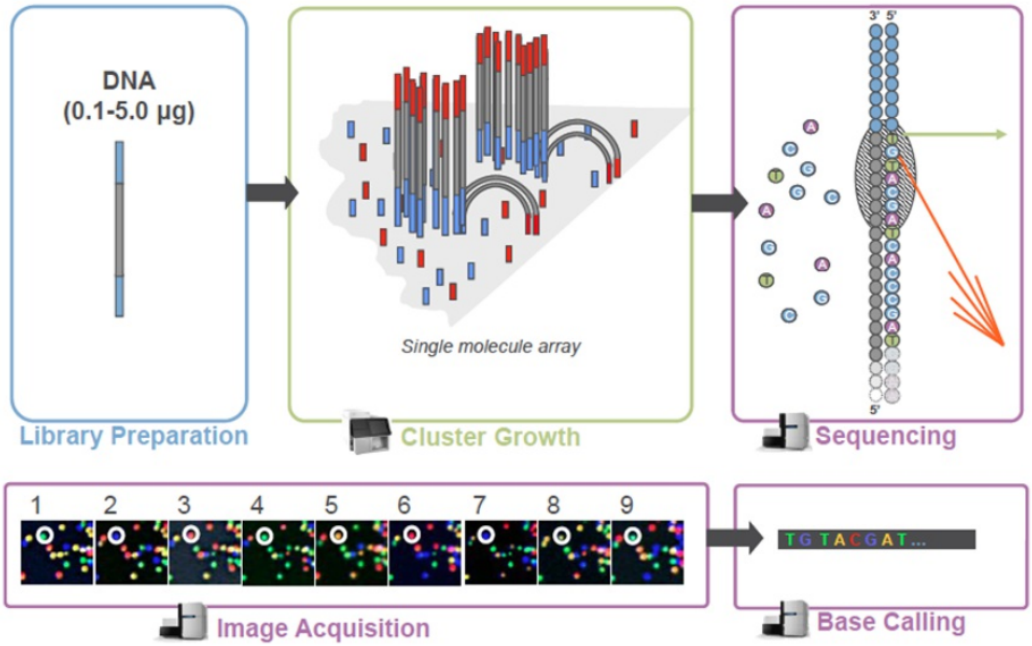

Figure 2.16. Sequencing was done by Novogene Company Ltd

The bioinformatics analysis workflow of raw sequencing data was as follows:

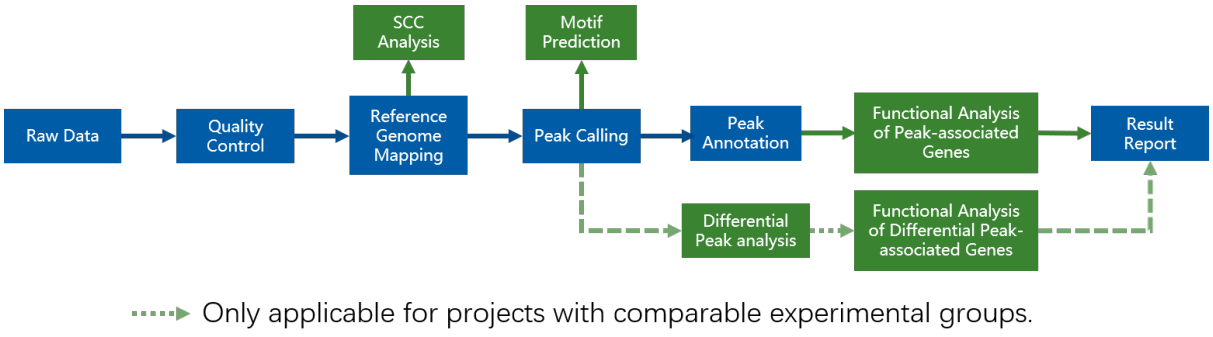

Figure 2.17. Bioinformatic analysis was done by Novogene Company Ltd

2.2.15.2.1 Data quality control

The original raw data from Illumina platform are transformed to Sequenced Reads, known as Raw Data or RAW Reads, by base calling of CASAVA. Raw data are recorded in a FASTQ file, which contains sequencing reads and corresponding sequencing quality.

FastQC of Raw reads

The massive raw data obtained by high-through sequencing technology must be qualified to guarantee the downstream bioinformatic data analysis. The popular tool for the quality control is software FastQC. Novogene uses it to get the basic quality of the raw reads.

Raw Data Trimming

For the raw data which pass the quality control, primer mismatch may result in nucleotidic composition bias at first several positions of the reads, which could lead to wrong bases insertion during sequencing. Because of the small fragment size of ChIP-Seq, there are often some adapter-appended reads. Trimming off the adapter sequences and low-quality bases is necessary. To ensure the quality of data analysis, raw data needs to be filtered to get clean data, and all the follow-up analyses are based on these clean data.

The procedure for data trimming is in the following:

(1) Discard the reads with low quality (proportion of low quality bases larger than 50%);

(2) Discard the reads with N ratio (unsure base) larger than 15%;

(3) Discard the reads with adaptor at the 5'-end;

(4) Discard the reads without adaptor and inserted fragment at the 3'-end;

(5) Trim the adapter sequence at the 3'-end;

(6) Discard the reads whose length are less than 18nt after trimming.

FastQC of Clean reads

Quality control of the clean reads after trimming is in the following:

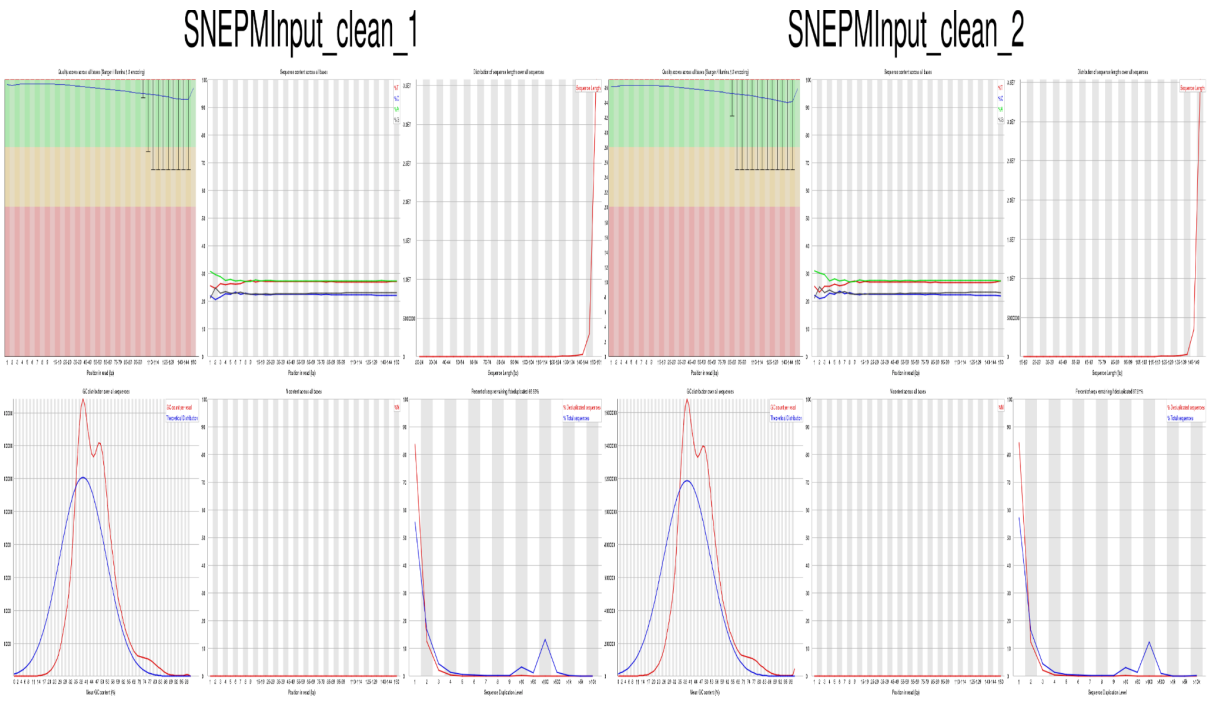

Figure 2.18. Quality control of the clean reads after trimming. Top-left: horizontal axis represents position in read (bp), vertical axis represents quality scores. Different colours represent different quality range. Top-middle: horizontal axis represents position in read (bp), vertical axis represents base percentage. Top-right: the distribution of read length. Bottom-left: GC distribution over all sequences. Red line is the actual GC content distribution, blue line is the theoretical distribution. Bottom-middle: N-ratio across all bases. Bottom-right: x-axis is the sequence duplication level. y-axis is the percent of the deduplicated reads.

2.2.15.2.2 Mapping

Summary of mapping

The common tools for mapping are Bowtie, BWA, MAQ, TOPhat, etc. A proper software and parameters were chosen according to different genome characters to do the genome mapping analysis for the filtered reads. Considering the small fragment size of ChIP-Seq, and the percentage of the unique sequence in the total sequence is the most important information, thus, reads can be mapped to the reference genome using BWA much more accurately (Li, H. and R. Durbin, 2009).

MAPQ

The most important thing during ChIP-Seq analysis is the percentage of the unique sequence in the total sequence number. Duplicates are labelled using SAMBLASTER (Faust and Hall, 2014) and mapping quality value is calculated by MAPQ. Proper quality value is chosen as the only threshold for mapping. Here 13 was chosen as the threshold, which means that the

mapping chance of the corresponding non-unique region is only 0.05. Only one read pair is kept for the duplicates in the following peak calling.

Genome-wide distribution of the mapped reads

Summary of the density of total mapped reads in different chromosomes (plus and minus). With a 5k slide window size, the medium of the number of reads mapped to each base within the window is calculated, and converted to log2. The longer the whole chromosome is, the more reads are mapped (Marquez et al. 2012). From the correlation of the number of the mapped reads and the length of the chromosome in the figure, we can see the correlation of the total number of the reads and the length of the chromosome much easier.

Distribution of the reads mapped to the gene

Since the binding sites of transcription factor and histone protein are important for gene regulation, analysis of relative mapping position distribution can help us predict the protein function. Each gene and its 2kb upstream and 2kb downstream are divided into 100 equal parts. Reads density is calculated in each part by the mapped reads and the ratio of the reads to total reads.

Sample correlation detection

Biological replicates are necessary for every experiment, same for high-throughput technology (Hansen et al.). Biological replicates mainly have two applications: One is to prove that the biological experiment can be replicated and there is no large variance. The other one is to make sure that following differential gene analysis can get reliable results. The correlation among samples is an important index to see whether the experiment design is reliable and whether the sampling is right. The correlation coefficient is much closer to 1, the similarity of the reads distribution pattern among samples is much higher.

Visualization of pileup signal

Novogene provides the visualization results of genome-wide reads mapping in bam format.

2.2.15.2.3 Fragment size prediction

Summary of fragment size

For a specific binding site, there is a significant read enrichment in the binding site. For single-end sequencing, MACS2 software to predict the frag sizes of IP experiments. The whole genome is scanned using a certain window size and the enrichment level of the reads in each window is calculated. Then proper windows (eg.1000) are extracted as the samples to build the enrichment model to predict the length of frag sizes. The predicted frag sizes are used for later peak calling.

2.2.15.2.4 Strand cross-correlation (SCC)

Summary of strand cross-correlation

As we know that the sequenced reads will be approximately evenly distributed on the plus and minus strands. By calculating the correlation of plus and minus strand (SCC), distance between two strands can be obtained. Through the SCC analysis of IP and input data, the correlation coefficient between plus and minus strands can be obtained, but also test the effect of the IP experiment.

SCC distribution between experimental groups

The ratio of the CC (Cross Correlation) value of the same experimental group (including IP and Input) to the lowest CC value of the whole SCC curve should be no less than 1.05. Besides, there is another shadow peak in the reads which is resulted from the sequencing read length. RSC value refers to the ratio of two differences: the difference between the CC value of fragment length and the lowest CC value, and the difference between CC value in the shadow peak and the lowest CC value.

2.2.15.2.5 Peak Calling

The annotation of transcription factor binding sites, histone binding sites is the important information for understanding the regulation mechanism and function. By mapping to the reference genome we can obtain the information of protein-DNA binding sites directly. By making use of MACS2 software (threshold q value = 0.05) to finish the peak calling, the

number of peaks are calculated, the peak width and its distribution, and find the peak related genes.

Quality assessment was based on the raw reads using the FASTQC quality control tool (v0.10.1). The sequence reads (single-end 51 bp) were mapped to the human reference genome (hg38) using Bowtie with default parameters. Ambiguously mapped reads were discarded from further analysis. Replicate BAM files were merged using SAMtools.

For signal detection (H3K4me2/H3K27me3) and peak calling, MACS was used which provides peaks and fitted signals. The shift size parameter was set according to the obtained fragment sizes. For peak detection a *P* value cut-off of 10^{-4} was used.

To assign the targeted peaks to genes and histone signals to TSS, RefSeq genes (hg38) from the IGB genome browser were used, containing 23,358 genes corresponding to 30,089 transcripts. Peaks were assigned to the genes if they are located within 10 kb upstream of the TSS or in the transcribed region. For the analysis of histone signals, we focused on unique transcripts with at least 4 kb in length. The filtering resulted in 19,904 TSS corresponding to 24,051 transcripts. For each TSS, ChIP-seq signals were assigned 2 kb upstream and 4 kb downstream. The resulting region of 6 kb length was further divided into 100 bp long non-overlapping windows and the total signal was calculated for each of these windows. Furthermore, signals were normalized (per million reads).

These were all the necessary steps done by Novogene to generate peak calling of the samples. Following that, I imaged the files using IGB.

2.16 Data Analysis and statistics

Results are expressed as mean ± SEM. Experimental points were performed in triplicate, with a minimum of three independent runs. A t-test was used for the comparison of two groups. A value of $p \leq 0.05$ was considered significant.

The mean and standard error margin was calculated for the sample replicates in every experiment and these values were used to plot the data. In order to determine the statistical significance of the data, a number of tests were carried out. The type of significance test used was determined by whether or not the data were normally distributed or not. The D'Agostino-Pearson omnibus normality test was used to analyse the spread of the data.

In data that contains only two samples, a paired or unpaired t-test (depending on matching of replicates) with Welch's correction was performed on normally distributed data. For non-parametric (skewed) data, the Mann-Whitney (paired) or Wilcoxon (unpaired) test was carried out to calculate statistical significance.

In the case of data containing more than two samples, ANOVA testing was used to perform multiple comparisons between all samples. This could be carried out using an ordinary one-way (one parameter to compare) or two-way (two parameters to compare) ANOVA for normalised data, or the Kruskal-Wallis test for non-parametric data. This would reveal the level of statistical significance for both the data as a whole and between each sample. immunocytochemistry and immunohistochemistry images were analysed using ImageJ, an image-analysis software(Schneider et al., 2012)

Chapter 3

The level of enrichment of H3K4me2, H3K27me3 and Tet-2 binding at the *Myh11* locus in de-differentiated murine vascular smooth muscle cells, resident S100β vascular stem cells and their myogenic progeny *in vitro*

3.1 Introduction:

Atherosclerotic lesions are characterized by the deposition of cholesterol within the arterial wall concurrent with the accumulation of intimal smooth muscle cell (SMC)-like cells and non-SMCs (Sanchez & Veith, 1998; Yia-Herttuala et al., 1989). A crucial hallmark of subclinical atherosclerosis is pathologic intimal thickening (PIT) defined as the initial progressive plaque responsible for the rise of advanced lesions (Virmani et al., 2000). Adaptive intimal thickening (AIT) composed primarily of infiltrating macrophage cells and intimal SMC-like cells is considered an important transitional non-atherosclerotic plaque that likely represents the earliest phase of lesion progression (Velican et al., 1981). The source of SMC-like cells contributing to AIT is a topic of much controversy. The two major sources that are the focus of this chapter include the de-differentiation of medial SMCs (Chappell et al., 2016) and the partial differentiation of resident S100 calcium-binding protein β (S100β) multipotent vascular stem cell mVSCs (Tang et al., 2012).

It has been widely reported that SMCs retain a high degree of plasticity both *in vitro* and *in vivo*. They are classically viewed as a unique cell type that has the ability to switch readily between two phenotypic states - 'contractile' and 'synthetic' dependent on the microenvironmental situation. Differentiated vascular SMCs exhibit the 'contractile phenotype' within adult blood vessels. However, these cells are purported to undergo phenotypic modulation in response to extracellular signals and de-differentiate to a more synthetic plastic phenotype (Campbell et al., 1992). One such instance is following endothelial injury, when inflammatory cells infiltrate and secrete various cytokines, which trigger de-differentiation, migration, and proliferation of medial SMCs (Jonasson et al., 1986). This process of de-differentiation and reprogramming is regularly associated with a significant loss in the expression of key SMC differentiation marker genes for a large number of proliferative vascular diseases *in vivo* and in sub-cultured cells *in vitro* (Yuan et al., 2017). Therefore, when remodelling is required, it has been proposed that SMC can switch their phenotypic state in order to respond to alterations in blood flow or when a wound healing response and vessel repair is required after vascular injury (Rensen, Doevendans and van Eys, 2007). Any disruption of this balance may lead to many cardiovascular diseases that involve neointimal formation (Liu et al., 2014). Indeed, SMCs are also capable of de-differentiation to a more

plastic synthetic state and undergo re-programming to myogenic, osteochondrogenic (Speer et al., 2009), and macrophage-like phenotypes (Shankman et al., 2015).

Previous reports suggest that lineage-specific SMC genes in de-differentiated SMC acquire key histone modifications at SMC-specific loci associated with a closed chromatin state and transcriptional silencing (Salmon et al., 2012). One such modification is histone 3 lysine 27 trimethylation (H3K27me3). Nevertheless, the retention of the histone 3 lysine 4 di-methylation (H3K4me2) histone mark that is widely associated with a differentiated phenotype remains stable at SMC-specific loci and is thought to facilitate re-differentiation during reversible phenotypic switching. Hence, H3K4me2 on the SMC gene loci is known to be a restricted and stable epigenetic signature of the SMC lineage distinguishing SMC from other cell types independently of their state of differentiation (McDonald et al., 2006). The presence of this mark at SMC-specific gene loci in a given cell is widely used to predict the origin of SMC-like cells and non-SMC within vascular lesions, irrespective of their phenotypic status. Indeed, it has been reported that the H3K4me2 mark at the myosin heavy-chain 11 *(Myh11)* locus is maintained in SMCs that had undergone transition to a macrophage-like state within mouse and human lesions (Shankman et al., 2015). Moreover, H3K4me2 is stably enriched on the *Myh11* and α-smooth muscle actin *(Acta2)* promoters in SMC treated with Platelet-derived Growth Factor-BB (PDGF-BB) (Liu et al., 2013) or oxidized phospholipids compared to untreated SMC (Gomez et al., 2013).

On the other hand, resident S100β mVSCs are negative for myogenic markers such as *Myh11* and Calponin1 (*Cnn1)* and demonstrate high levels of proliferation and telomerase activity indicative of stemness (Tang et al., 2012). Moreover, S100β mVSCs can undergo partial myogenic differentiation to become SMC-like cells in response to a number of different atherogenic stimuli, such as PDGF (Cheung et al., 2014; Xiao et al., 2007), transforming Growth Factor Beta (TGF-β) (Sinha et al., 2004, 2014; Wang et al., 2015; Xie et al., 2011) and Notch signalling (Kurpinski et al., 2010). H3K4me2 is known to be an epigenetic mark that directs multipotent progenitor cells toward SMC differentiation, both in normal vascular development and in vascular diseases. However, it is unclear how histone methyltransferases, which catalyse the formation of H3K4me2, are specifically addressed to SMC target genes and

how the H3K4me2-marked SMC genes switch from a silent to an active state during embryogenesis or adult homeostasis (McDonald et al., 2006).

H3K4 and H3K27 methylation are of interest as these modifications are catalysed, respectively, by trithorax- and polycomb-group proteins, which mediate mitotic inheritance of lineage-specific gene expression programs and have key developmental functions (Ringrose & Paro, 2004). H3K4me2 positively regulates transcription by recruiting nucleosome remodelling enzymes and histone acetylases (Pray-Grant et al., 2005; Santos-Rosa et al., 2003; Sims et al., 2005; Wysocka et al., 2005), while H3K27me3 regulates negatively transcription when a compact chromatin structure is promoted (Francis et al., 2004; Ringrose & Paro, 2004).

The mechanisms of DNA demethylation, albeit controversial have also been described during SMC differentiation and studies centre on the putative role of the ten-eleven-translocation (TET) family of enzymes that oxidise 5-methylcytosine (5-mC) to 5-hydroxymethylcytosine (5-hmC) in SMC (Liu et al., 2013). Through the DNA repair pathway and thymine-DNA glycosylase, 5hmC is later converted to unmethylated cytosine, leading to DNA demethylation and gene activation. TET-2 is the predominant isoform in human coronary artery SMC cultures, and is highly enriched in smooth muscle tissue (Liu et al., 2013).

One way of determining the origin of SMC-like cells has been to investigate the epigenetic profile at the *Myh11* locus in these cells since at least part of the SMC epigenetic programming established during SMC differentiation is retained during phenotypic switching and de-differentiation of SMCs *in vitro* (McDonald et al., 2006) and *in vivo* (Gomez et al., 2013) in response to pro-atherogenic stimuli. However, it is also possible that resident S100β mVSCs that have been cell fate mapped to SMC-like cells within vascular lesions (by our lab and others (Kramann et al., 2016; Tang et al., 2012; Wan et al., 2012)) also acquire this epigenetic signature following myogenic differentiation. Therefore, this Chapter addresses this key question *in vitro* by specifically examining the enrichment of H3K4me2 and H3K27me3 and Tet-2 binding at the SMC-specific *Myh11* locus in de-differentiated SMCs and resident S100β vascular mVSCs in response to pro-atherogenic stimuli and correlating any modifications with changes in *Myh11* gene expression. Furthermore, the role of Tet-2 demethylase in facilitating

any change in the enrichment of these histone marks at the *Myh11* locus is assessed at baseline and in response to pro-atherogenic stimuli both before and after specific Short interfering RNA (siRNA) knockdown of Tet-2. The repercussions of Tet-2 knockdown on pro-atherogenic stimulation of *Myh11* gene expression are also assessed.

Objectives:

The main aims of this chapter are to:-

1. To determine the level of enrichment of H3K4me2 and H3K27me3 (epigenetic profile) at the *Myh11* locus in de-differentiated mouse SMC *in vitro* and compare with differentiated mouse SMC isolated from freshly isolated aortic tissue *ex vivo* and mouse embryonic stem cells (mESC) *in vitro* using single gene Chromatin Immunoprecipitation followed by Polymerase Chain Reaction (ChIP-PCR) and correlate with *Myh11* gene expression using quantitative real-time Polymerase Chain Reaction (qRT-PCR).
2. Characterise the phenotype of resident mVSCs and mouse MOVAS™ SMCs in culture.
3. To determine the effects of atherogenic stimuli on the epigenetic profile at the *Myh11* locus in mouse SMCs using single gene ChIP-PCR and correlate any changes with *Myh11* gene expression using qRT-PCR.
4. To determine the effects of atherogenic stimuli on the epigenetic profile at the *Myh11* locus in resident S100β mVSCs *in vitro* using single gene ChIP-PCR and correlate any changes with *Myh11* gene expression using qRT-PCR.
5. To determine the epigenetic profile at the *Myh11* locus in de-differentiated mouse SMC *in vitro* when cells are grown in stem cell maintenance media (to promote possible re-programming) compared to SMC maintenance medium using single gene ChIP-PCR and correlate any changes with *Myh11* gene expression using qRT-PCR.

6. To examine the role of the DNA demethylase, Tet-2 in regulating histone modifications at the *Myh11* locus in mouse vascular SMCs, S100β resident vascular mVSCs, and their myogenic progeny following siRNA knockdown of Tet-2 using single gene ChIP-PCR and correlate any changes with *Myh11* gene expression using qRT-PCR.

3.2 Strategy

In order to investigate the epigenetic profile of de-differentiated vascular SMCs and S100β resident vascular mVSCs *in vitro*, the level of enrichment of two key histone modifications (H3K4me2 and H3K27me3) at the *Myh11* locus was assessed using chromatin immunoprecipitation (ChIP) as described in Chapter 2, Section 2.2.4 under baseline conditions and in response to known atherogenic stimuli (TGF-β1, PDGF-BB and the Notch ligand, Jagged1). Samples were fixed, sonicated and specific antibodies for H3K4me2 and H3K27me3 were used to immunoprecipitate H3K4me2, H3K27me3 and Tet-2 before the protein was removed and chr16:14,290,010-14,291,702 of the *Myh11* promoter was amplified by qRT-PCR using specific primers for this locus. The resultant amplicons were run on agarose gels to check for their predicted size before the bands were cut out, DNA purified and sequenced to confirm the correct sequence is amplified. Fresh mouse aortic tissue containing medial differentiated SMCs and undifferentiated mESCs were used as positive controls for assessing the epigenetic profile in differentiated SMCs and undifferentiated cells, respectively. S100β resident vascular mVSCs were isolated from the aortic arch region using enzymatic dispersion and sequential plating of cells following removal of the adventitia and endothelium, as described in Chapter 2, Section 2.2.1.2 and were grown and expanded in Maintenance Medium 1 (MM1). A de-differentiated SMC cell line, MOVAS, which is immortalised, and mESCs were purchased commercially. Immunocytochemistry (ICC) was then carried out in order to characterise the S100β mVSC population by probing for the calcium-binding protein, S100β and the neural stem cell marker, Nestin. ICC was also used to investigate the expression of SMC differentiation markers, such as Cnn1 and Myh11 in both MOVAS SMC and S100β mVSCs. Following characterization of S100β mVSCs and MOVAS SMCs, single gene ChIP-PCR was performed to investigate the level of enrichment of

H3K4me2 and H3K27me3 at the *Myh11* locus while qRT-PCR was performed to assess myogenic gene expression following treatment of cells with different atherogenic stimuli.

In order to assess the ability of MOVAS SMCs to lose their SMC-specific epigenetic mark, MOVAS SMCs are grown and expanded in stem cell maintenance medium (MM1) before single gene ChIP PCR of H3K4me2 and H3K27me3 at the *Myh11* locus was performed. In parallel, messenger RNA (mRNA) levels for stem cell genes, SRY-box transcription 10 *(Sox10)* and *S100β* and myogenic differentiation genes, *Myh11* and *Cnn1* were assessed using qRT-PCR to evaluate whether the transcriptional activity of myogenic or stem cell genes changed following this treatment.

As the demethylase, Tet-2 expression is necessary for SMC differentiation by binding to serum response factor *(SRF)*, MYOCD and *Myh11* promoters and directly modulating chromatin accessibility of target genes under myogenic differentiation conditions (Liu et al., 2013), the level of Tet-2 binding at the same *Myh11* locus in MOVAS SMC and S100β mVSCs treated with atherogenic stimuli (TGF-β1, PDGF-BB and the Notch ligand, Jagged1) before Tet-2 protein levels were evaluated by immunoblot using an anti-Tet-2 antibody and *Tet-2* mRNA levels by qRT-PCR.

In order to assess the role of Tet-2 in facilitating the changes in the epigenetic profile at the *Myh11* locus, Tet-2 knockdown using siRNA targeting *Tet-2* mRNA was performed before the level enrichment was assessed. The success of the Tet-2 knockdown was confirmed by first assessing the level of transfection of control fluorescently tagged siRNA duplexes before the levels of Tet-2 mRNA levels and protein were evaluated by qRT-PCR and immunoblot, respectively. Thus by comparing the level of enrichment of H3K4me2 and H3K27me3 at the *Myh11* gene locus in the absence and presence of Tet-2 DNA demethylation, the role of Tet-2 is evaluated.

Data for all experiments in this section was generated over at least three biological replicates. Normality tests were used to determine if data followed a parametric distribution pattern. Variation across samples was analysed by calculating p-values. The type of test used to calculate this was governed by the outcome of the normality test. Statistical significance was assigned to p-values <0.05.

3.3 Results

3.3.1 De-differentiated mouse aortic SMCs retain the H3K4me2 mark at the *Myh11* locus *in vitro* but it is dramatically reduced compared to differentiated aortic SMCs *in vitro*

De-differentiated MOVAS SMCs were seeded at a density of 15 x 10^4 cells/cm^2 to obtain a confluent T75 flask after 7 days. The cells were fixed and then sonicated before the level of enrichment of histone modifications H3K4me2 and H3K27me3 at the *Myh11* locus was assessed using single gene ChIP-PCR analysis as explained in section 2.2.4. and correlated with the transcriptional activity of the *Myh11* gene by measuring *Myh11* mRNA levels by qRT-PCR as explained in section 2.2.9.1.

The level of enrichment of H3K4me2 at the *Myh11* locus was first assessed in fresh aortic tissue, MOVAS SMCs and mESCs by measuring H3K4me2 binding to DNA against the Immunoglobulin G (IgG) control using a single gene ChIP-PCR assay. There was a significant enrichment of H3K4me2 in aortic tissue when compared to mESCs [Figure 3.1]. In contrast, the level of enrichment of H3K4me2 in MOVAS SMCs was significantly less than in fresh aortic tissue, albeit significantly higher than mESCs [Figure 3.1]. In parallel studies, the level of enrichment of H3K27me3 in aortic tissue, MOVAS and mESCs was also assessed by single gene ChIP-PCR assay at the same locus. There was a significant enrichment of H3K27me3 at the *Myh11* locus in mESCs when compared to aortic tissue [Figure 3.2]. The level of enrichment of H3K27me3 in MOVAS SMCs was not significantly different to fresh aortic tissue but was significantly less than mESCs [Figure 3.2]. Furthermore, the ratio of H3K4me2:H3K27me3 was significantly higher in fresh aortic tissue when compared to MOVAS and mESCs [Figure 3.3]. The ratio of H3K4me2:H3K27me3 was significantly higher in MOVAS compared to mESCs [Figure 3.3].

In parallel studies, the relative level of *Myh11* mRNA transcript was measured by qRT-PCR in aortic tissue, MOVAS SMC and mESCs. Aortic tissue had the highest level of *Myh11* mRNA which was significantly greater than mESC and MOVAS SMCs, respectively [Figure 3.4]. However, the level of *Myh11* mRNA in MOVAS SMCs was also significantly higher than mESCs [Figure 3.4].

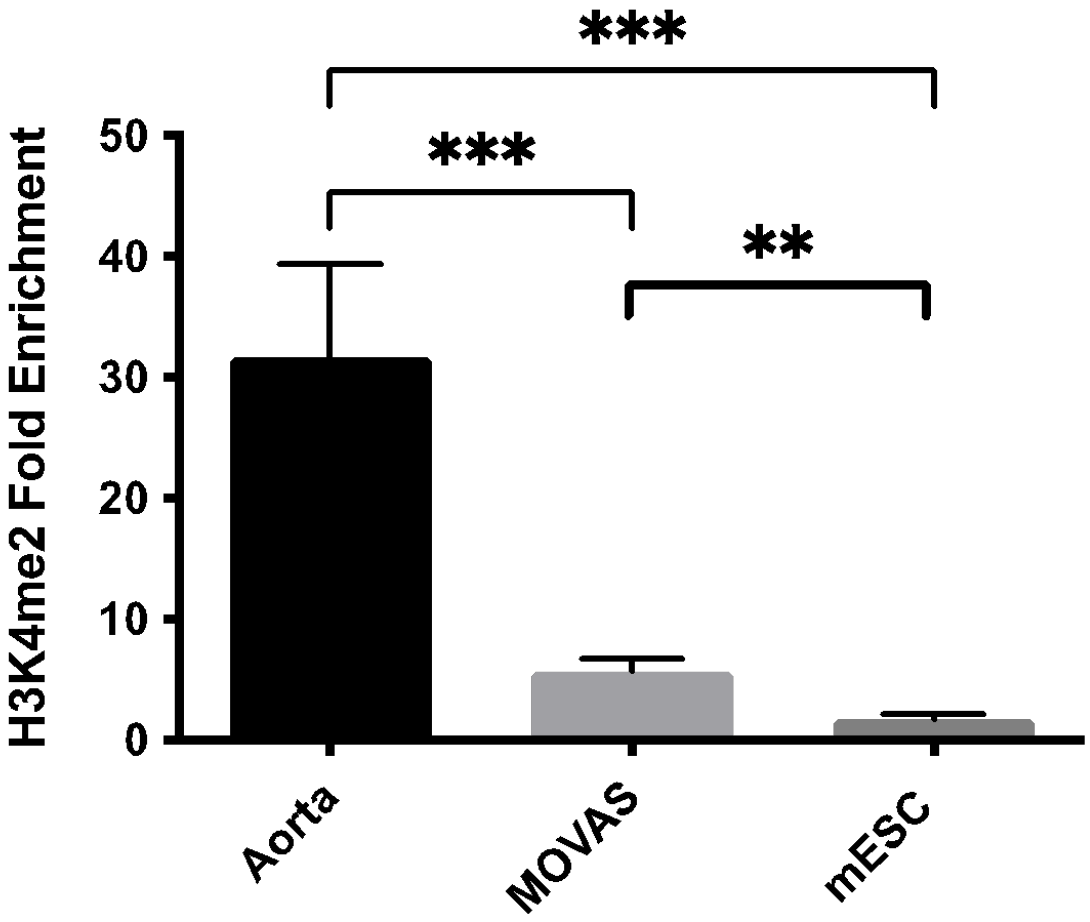

Figure 3.1. The level of enrichment of H3K4me2 at the *Myh11* locus in aortic tissue, MOVAS SMCs and mESCs. H3K4me2 binding at the *Myh11* locus was assessed by the single gene ChIP-PCR assay and corrected against the IgG control. Aorta tissue was used as a positive control and mESCs were a negative control. Fold enrichment was determined for each condition and the data are the mean ± SEM of 3 experiments performed in triplicate. ** $p<0.01$ *** $p<0.001$

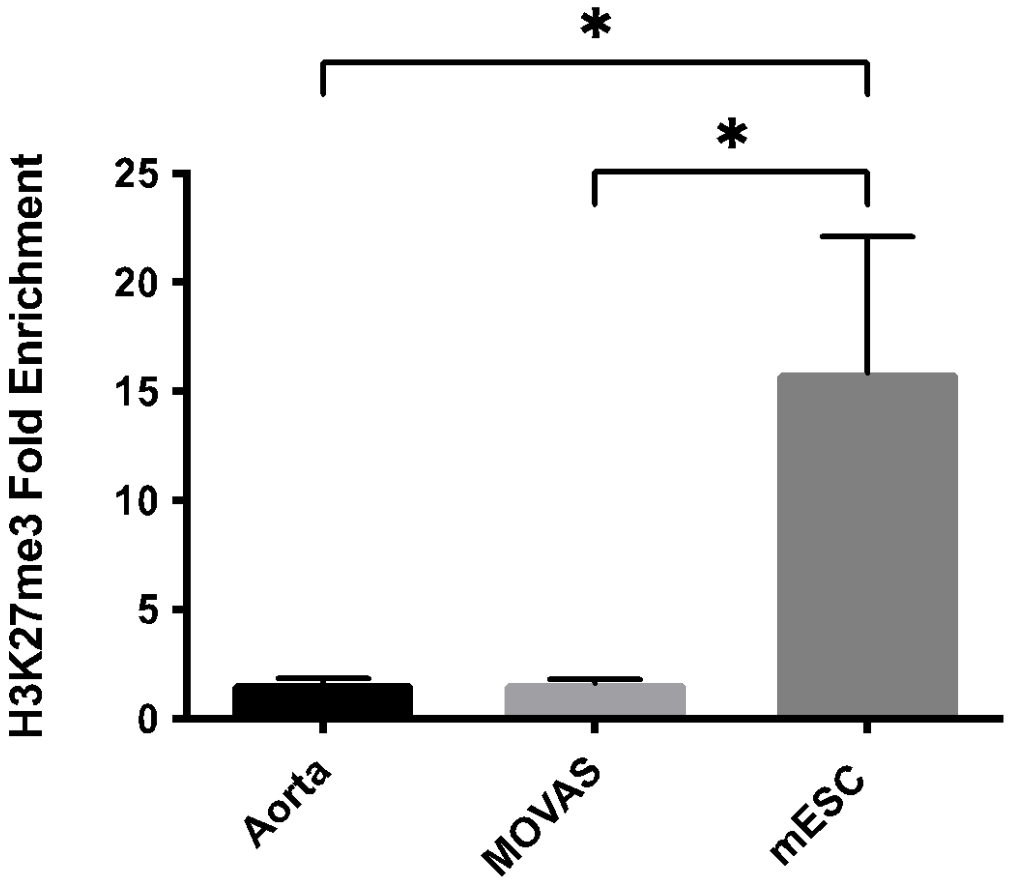

Figure 3.2. The level of enrichment of H3K27me3 at the *Myh11* locus in aortic tissue, MOVAS SMCs and mESCs. H3K27me3 binding at the *Myh11* locus was assessed by the single gene ChIP-PCR assay and corrected against the IgG control. Aorta tissue was used as a positive control and mESCs were a negative control. Fold enrichment was determined for each condition and the data are the mean ± SEM of 3 experiments performed in triplicate. * $p<0.01$

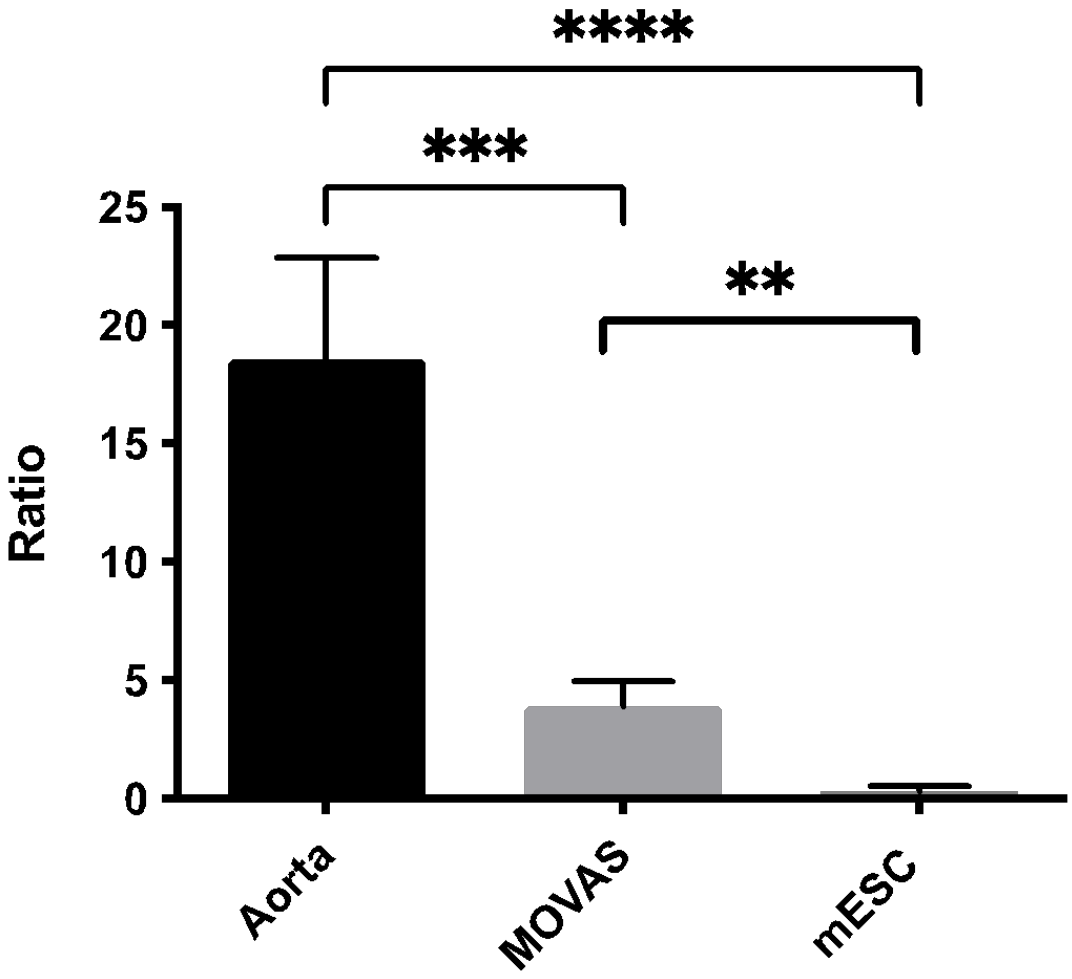

Figure 3.3. Ratio of H3K4me2/H3K27me3 levels in Aortic tissue, MOVAS and mESCs. The level of enrichment of H3K4me2 and H3K27me3 binding at the *Myh11* locus in aortic tissue, MOVAS SMCs and mESCs was assessed by the single gene ChIP-PCR assay and corrected against the IgG control. Aorta tissue was used as a positive control and mESCs were a negative control. The ratio of H3K4me2 and H3K27me3 binding was determined for each condition and the data are the mean ± SEM of 3 experiments performed in triplicate. ** $p<0.01$ *** $p<0.001$ **** $p<0.0001$

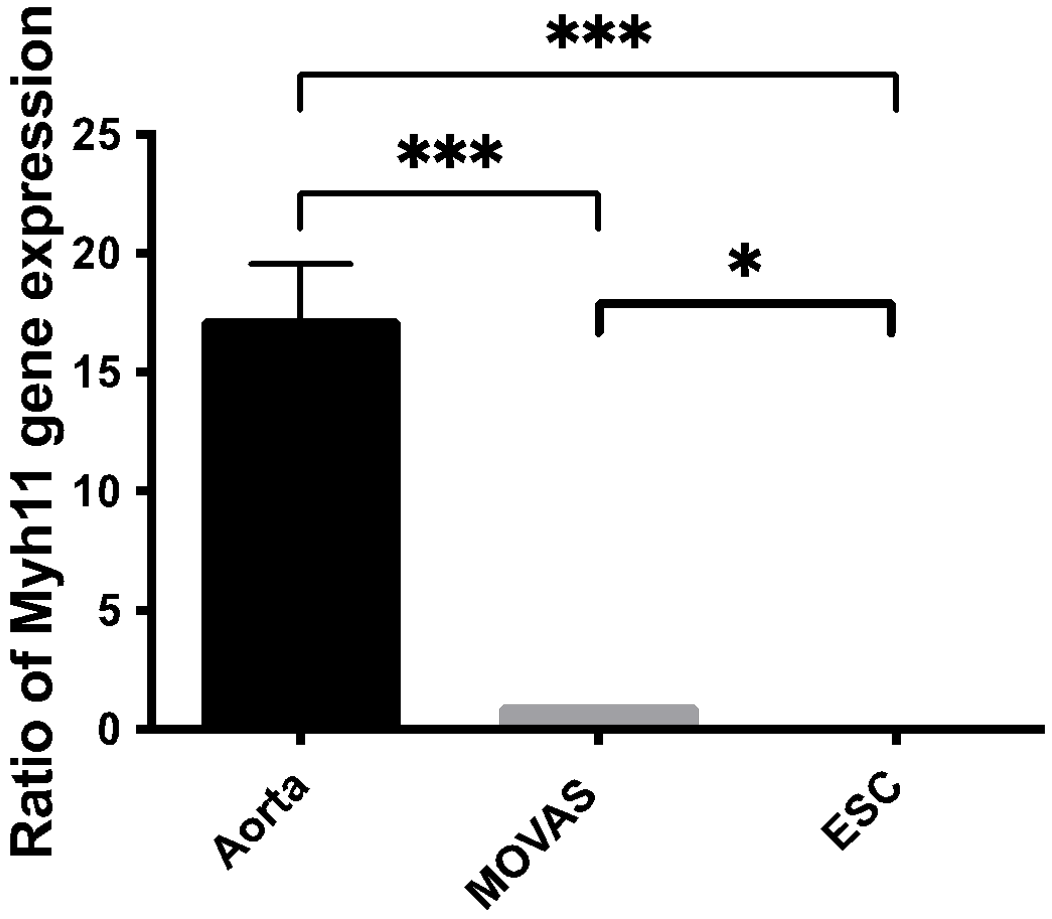

Figure 3.4. Relative expression of *Myh11* mRNA levels in fresh Aorta, MOVAS SMCs and mESCs. Total RNA was isolated from tissue and cells before the relative levels of *Myh11* transcript was measured by qRT-PCR with GAPDH as an internal control. Data are expressed as the ratio of gene expression (R) and represent the mean ± SEM of 3 experiments performed in triplicate. * $p<0.01$ *** $p<0.001$

The single gene ChIP-PCR results suggest that MOVAS SMCs are significantly enriched for H3K4me2 at *Myh11* locus. However, when the level of enrichment of MOVAS (which are thought to be de-differentiated SMCs) is compared to mouse aortic tissue (which is a differentiated SMC), MOVAS cells had much lower levels of enrichment. In contrast, both MOVAS SMC and aortic tissue have the same level of enrichment on H3K27me3 at the *Myh11* locus which is relatively low compared to the highly enriched mESCs. The ratio of H3K4me2:H3K27me3 in differentiated SMC from aortic tissue was significantly higher than the de-differentiated MOVAS SMCs concomitant with enhanced expression of *Myh11* mRNA levels in these cells and was correlated with ChIP-PCR results.

3.3.2 Mouse mVSCs and MOVAS SMCs express key phenotypic markers

Female Bl/tgtgt Thy1 YFP mice were anesthetized and culled as described in Material and Methods, Section 2.2.1.2 The aortic arch was extracted and washed with phosphate basic solution (PBS) and the adventitial layer was removed following collagenase treatment. In order to break down the elastic lamina and release cells, physical cutting of the tissue was combined with elastase treatment. Cells were then added to a non-adherent 6-well plate in MM1 and incubated at 37°C for 72 hours. Suspension cells were then transferred to an adherent 6-well plate and cultured in MM1. ICC was carried out on this cell population and also on MOVAS cells to confirm the presence of specific protein markers. Cells were seeded onto sterile coverslips in a 6-well plate at a low density (5 x 10^3 cells/well) and incubated at 37°C for 48 hours. Cells were fixed with 3.7% formaldehyde and stained with primary antibodies for S100β, Nestin, Stem Cell Antigen-1 (Sca1), Cnn1 or Myh11. In order to generate a fluorescent signal for staining, fluorophore-conjugated secondary antibodies were added and nuclei were stained with 4',6-diamidino-2-phenylindole (DAPI). Using a fluorescent microscope, these stains were visualised, imaged and analysed to determine the expression of each protein. An IgG control (secondary antibody probing without primary antibody staining) was used to account for background fluorescence or off-target binding of secondary IgGs. Cultured MOVAS SMCs were relatively positive for SMC differentiation marker expression (Cnn1 and Myh11) with some cells/hpf negative. S100β resident vascular mVSCs were found to be positive for S100β, Nestin and Sca1 expression (Figure 3.5) but negative for Cnn1 and Myh11 expression (Figure 3.5). Collectively, the ICC data on S100β mVSCs and

MOVAS SMCs indicated that these cells exhibit the expected expression of specific phenotypic markers for S100β mVSCs and SMCs *in vitro.*

(a)

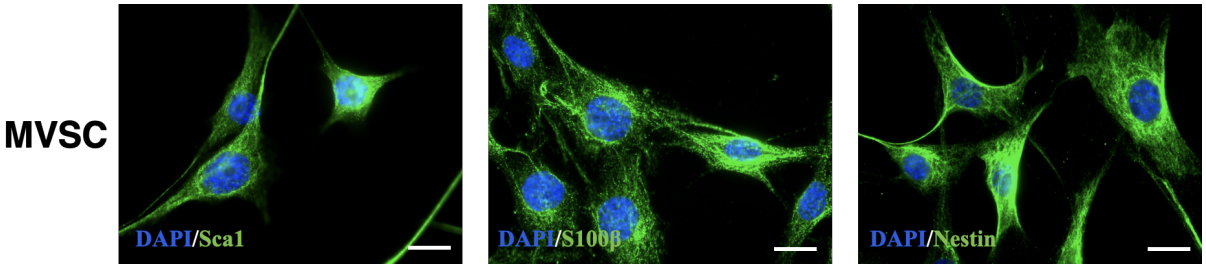

(b)

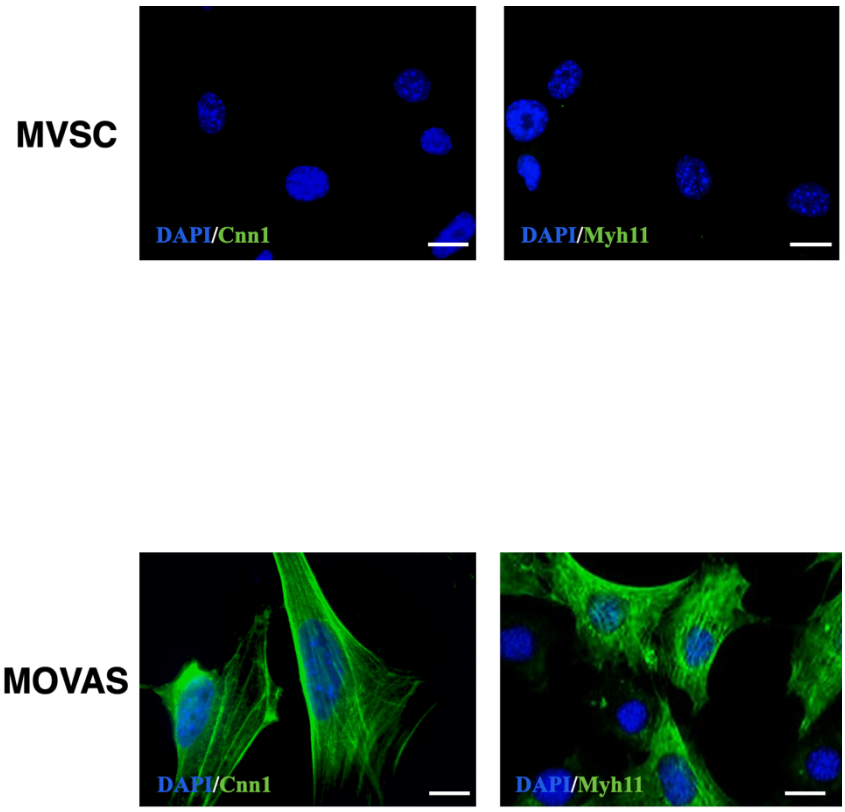

Figure 3.5. Characterisation of S100β mVSCs and MOVAS SMCs. (a) Representative ICC images of S100β mVSCs stained with DAPI, anti-S100β, anti-Sca1 or anti-Nestin primary antibody at 60X magnification. (b) Representative ICC images of S100β mVSCs and MOVAS SMCs stained with DAPI, anti-Cnn1 or anti-Myh11 primary antibody at 60X magnification. All images taken using Olympus DP-50 fluorescent microscope. Images representative of 10 images taken per sample. Alexa Fluor 488 secondary antibody used for visualisation of primary antibody binding. Control sample stained with secondary antibody but no primary antibody was used to determine level of background/off-target fluorescence. Scale bar = 10µm. Data are representative of n=3.

3.3.3 Atherogenic stimuli (PDGF-BB, TGF-β1 and Jagged1) differentially regulate H3K4me2 enrichment at the *Myh11* locus concomitant with changes to *Myh11* mRNA levels in mouse de-differentiated SMCs

De-differentiated MOVAS SMCs were seeded at a density of 15 x 10^4 cells/cm^2 to obtain a confluent T75 flask after 7 days. The cells were treated with different atherogenic stimuli including (i) 500 ng/ml Fc or Fc- Jag-1 (ii) 2ng/ml TGF-β1, (iii) 10ng/ml PDGF BB, or (iv) combination of both TGF-β and PDGF BB for 7 days. The DNA was then fixed and prepared for single gene ChIP-PCR analysis as described in Chapter 2, Section 2.2.4 and correlated with the transcriptional activity of the *Myh11* gene by measuring *Myh11* mRNA levels by qRT-PCR. Transcriptional activity of the *Myh11* gene was analysed as explained in section 2.2.9.1. De-differentiated MOVAS SMCs paired with each experiment.

The level of enrichment of H3K4me2 at the *Myh11* locus was first assessed by single gene ChIP-PCR in control non-treated MOVAS SMCs and MOVAS SMCs treated with Jag-1 or Fc control, TGF-β1, PDGF-BB, or a combination of both TGF-β1 and PDGF-BB, respectively by measuring H3K4me2 binding to DNA and comparing it to the IgG control. There was a significant enrichment of H3K4me2 in Jag-1 treated MOVAS SMC when compared to Fc control [Figure 3.6a]. In contrast, the level of enrichment of H3K4me2 in MOVAS SMC treated with TGF-β1 or TGF-β1/PDGF-BB was significantly less compared to control cells [Figure 3.6b] while no change was observed in PDGF-BB treated cells [Figure 3.6b]. In parallel studies, the level of enrichment of H3K27me3 in the same samples was also assessed by the single gene ChIP-PCR assay. There was a significant enrichment of H3K27me3 at the *Myh11* locus in cells treated with TGF-β1 when compared to control cells [Figure 3.7b]. The level of enrichment of H3K27me3 was not significantly different following treatment of cells with PDGF BB or Jag-1 and TGF-β1/ PDGF-BB (albeit TGF-β1/ PDGF-BB increased the level of enrichment of H3K27me3 but did not reach the level of significance) [Figure 3.7a&b]. However, the ratio of H3K4me2:H3K27me3 was significantly higher in Jag-1 treated cells when compared to control [Figure 3.8a]. In contrast, there was a significant decrease in the ratio of H3K4me2:H3K27me3 in TGF-β1, TGF-β1/PDGF-BB cells compared to control [Figure 3.8b]. There was no change in the ratio of H3K4me2:H3K27me3 observed in PDGF-BB and Fc treated cells in comparison with control [Figure 3.8b].

The relative level of *Myh11* mRNA transcript was also measured by qRT-PCR in untreated MOVAS SMC and MOVAS SMC treated with TGF-β1, PDGF BB, a combination of both TGF-β1 and PDGF-BB, and Jag-1 and its Fc control. There was a significant decrease in *Myh11* mRNA following treatment with PDGF-BB or a combination of PDGF-BB + TGF-β1 [Figure 3.9]. In contrast, the level of *Myh11* mRNA was not significantly different when cells were treated with TGF-β1 [Figure 3.9]. Moreover, there was no significant change in *Myh11* mRNA levels in Jag-1 treated cells when compared to its Fc control [Figure 3.9]. Collectively, the single gene ChIP and PCR data indicate that there is a disconnect between the epigenetic mark of H3K4me2 at the *Myh11* locus and the transcript level of *Myh11* mRNA levels following treatment of MOVAS SMCs with different atherogenic stimuli.

The single gene ChIP-PCR results suggest that MOVAS SMCs are significantly enriched for H3K4me2 at *Myh11* locus. This enrichment increased following treatment of cells with Jag-1 concomitant with a significant decrease in H3K27me3 mark at the same locus. The ratio of H3K4me2:H3K27me3 in Jag-1 treated MOVAS was significantly higher than MOVAS SMCs concomitant with no significant increase in *Myh11* mRNA levels. In contrast, TGF-β1 and TGF-β1/PDGF-BB decreased the H3K4me2 mark in these cells while decreasing the ratio of H3K4me2:H3K27me3 and *Myh11* mRNA levels in these cells. PDGF-BB alone failed to significantly alter the H3K4me2 or H3K27me3 mark or the ratio of H3K4me2:H3K27me3 while significantly reducing *Myh11* mRNA levels in these cells.

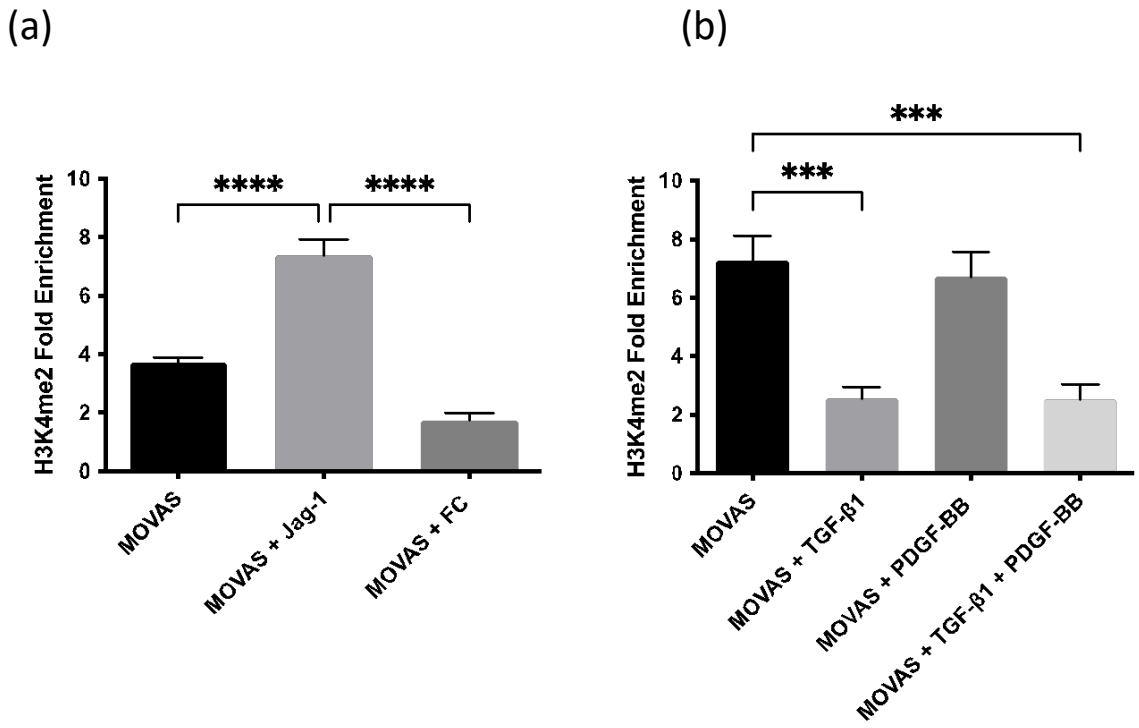

Figure 3.6. The level of enrichment of H3K4me2 at the *Myh11* locus in (a) MOVAS SMCs following treatment with Notch ligand, Jag-1. MOVAS SMC cells were treated with 500 ng/ml Fc or Fc- Jag-1 in Roswell park memorial institute (RPMI), 10% FBS (Sigma-Aldrich) for a week. A negative control sample cultured in SMC DM medium only was set up. (b) MOVAS SMCs following treatment with 2ng/ml TGF-β1, 10ng/ml PDGF BB and a combination of both TGF-β1 and PDGF-BB in RPMI, 10% FBS (Sigma-Aldrich) for 7 days. H3K4me2 binding at the *Myh11* locus was assessed by single gene ChIP-PCR assay and corrected against the IgG control. Fold enrichment was determined for each condition and the data are the mean ± SEM of 3 experiments performed in triplicate. ***p<0.001 **** p<0.0001

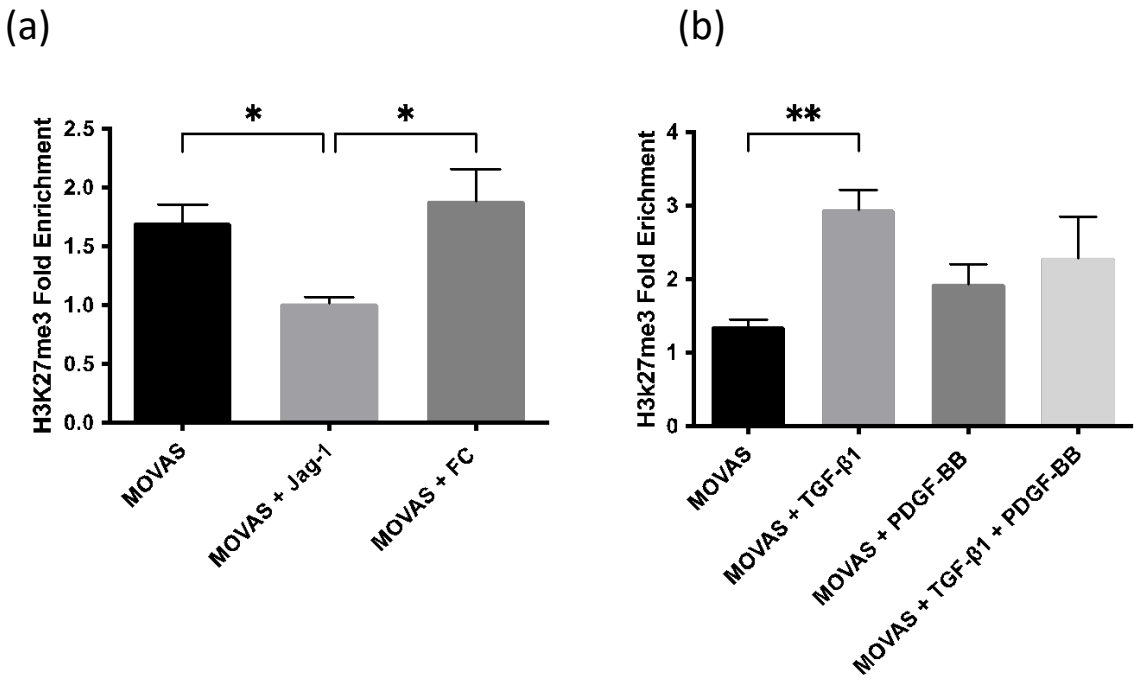

Figure 3.7. The level of enrichment of H3K27me3 at the *Myh11* locus in (a) MOVAS SMCs following treatment with Notch ligand, Jag-1. MOVAS SMCs were treated with 500 ng/ml Fc or Fc- Jag-1 in RPMI, 10% FBS (Sigma-Aldrich) for 7 days. (b) MOVAS SMCs treated with 2ng/ml TGF-β1, 10ng/ml PDGF BB and a combination of both TGF-β1 and PDGF-BB in RPMI, 10% FBS (Sigma-Aldrich) for a week. H3K27me3 binding at the *Myh11* locus was assessed by the single gene ChIP-PCR assay and corrected against the IgG control. Fold enrichment was determined for each condition and the data are the mean ± SEM of 3 experiments performed in triplicate. * $p<0.05$ ** $p<0.01$

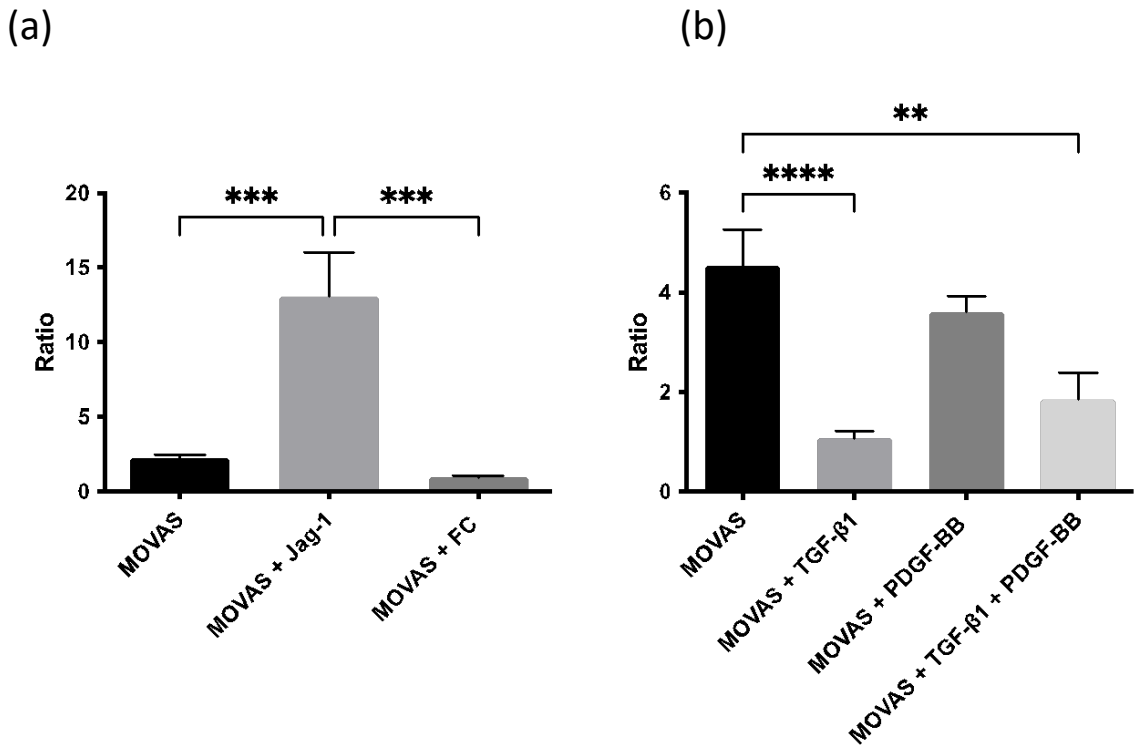

Figure 3.8. H3K4me2/H3K27me3 ratio at the *Myh11* locus (a) MOVAS SMCs following treatment with Notch ligand, Jag-1. MOVAS SMCs were treated with 500 ng/ml Fc or Fc- Jag-1 in RPMI, 10% FBS (Sigma-Aldrich) for 7 days. (b) MOVAS SMCs treated with 2ng/ml TGF-β1, 10ng/ml PDGF BB and a combination of both TGF-β1 and PDGF-BB in RPMI, 10% FBS (Sigma-Aldrich) for a week. H3K27me3 binding at the *Myh11* locus was assessed by the single gene ChIP-PCR assay and corrected against the IgG control. Fold enrichment was determined for each condition and the data are the mean ± SEM of 3 experiments performed in triplicate. ** $p<0.01$ *** $p<0.001$ **** $p<0.0001$

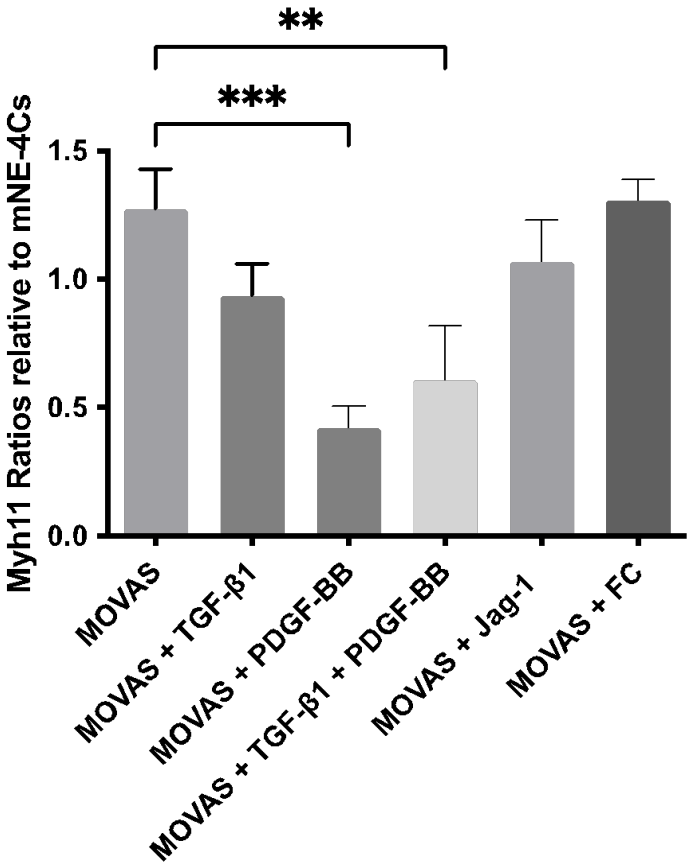

Figure 3.9. Expression of *Myh11* mRNA in MOVAS SMCs following treatment with Notch ligand, Jag-1, PDGF-BB and TGF-β1. *Myh11* expression was measured in MOVAS SMCs in their maintenance medium (RPMI) and compared to MOVAS SMC that was grown in RPMI supplemented with atherogenic stimuli 2ng/ml TGF-β1, 10ng/ml PDGF BB, 500 ng/ml Fc or Fc- Jag-1 and a combination of both TGF-β1 and PDGF-BB in RPMI, 10% FBS (Sigma-Aldrich) for 7 days. Total RNA was isolated before the relative levels of *Myh11* transcript was measured by qRT-PCR with GAPDH as an internal control. Data are expressed as the ratio of gene expression (R) and represent the mean ± SEM of 3 experiments performed in triplicate. * $p<0.05$ ** $p<0.01$

3.3.4 Atherogenic stimuli (PDGF-BB, TGF-β1 and Jagged1) enhance the enrichment of H3K4me2 at the *Myh11* locus and increase *Myh11* mRNA levels in resident mouse S100β mVSCs *in vitro.*

Resident S100β vascular mVSCs were seeded at the density of 5 x 10^3 cells/cm^2 to obtain a confluent T75 flask after 7 days. The cells were treated with different stimuli including (i) 500 ng/ml Fc or Fc- Jag-1 (ii) 2ng/ml TGF-β1 and (iii) 10ng/ml PDGF BB. The DNA was then fixed and prepared for single gene ChIP-PCR analysis as described in Chapter 2, Section 2.2.4 and correlated with the transcriptional activity of the *Myh11* gene by measuring *Myh11* mRNA levels by qRT-PCR and analysed as explained in section 2.2.9.

The level of enrichment of H3K4me2 at the *Myh11* locus was first assessed by the single gene ChIP-PCR analysis in control non-treated S100β mVSCs and S100β mVSCs treated with TGF-β1, PDGF-BB and Jag-1 by measuring H3K4me2 binding to DNA compared to the IgG control. There was a significant enrichment of H3K4me2 following treatment with the atherogenic stimuli Jag-1, TGF-β1, and PDGF-BB when compared to control [Figure 3.10]. In parallel studies, the level of enrichment of H3K27me3 in the same samples was also assessed by the single gene ChIP-PCR assay. There was a significant reduction in the level of enrichment of H3K27me3 at the *Myh11* locus in S100β mVSCs treated with Jag-1, TGF-β1, and PDGF-BB when compared to control [Figure 3.11]. Furthermore, the ratio of H3K4me2:H3K27me3 was significantly higher in Jag-1, TGF-β1 and PDGF-BB treated cells when compared to control [Figure 3.12]. The relative level of *Myh11* mRNA transcript was measured by qRT-PCR in control untreated S100β mVSCs and S100β mVSCs treated with Jag-1, TGF-β1, and PDGF-BB. There was a significant increase in *Myh11* mRNA following treatment with Jag-1, TGF-β1 and PDGF BB [Figure 3.13]. The increase in the enrichment level of H3K4me2 at the *Myh11* locus and the gene expression of *Myh11* in S100β mVSCs following treatment with all three atherogenic stimuli indicate myogenic differentiation of S100β mVSCs. Concomitant with a loss in the enrichment level of H3K27me3 at the *Myh11* locus.

The single gene ChIP-PCR results suggest that S100β mVSCs are highly enriched for H3K27me3 but not H3K4me2 at the *Myh11* locus. The enrichment of H3K4me2 increased significantly

following treatment of cells with Jag-1, TGF-β1 and PDGF-BB concomitant with a significant decrease in the H3K27me3 mark at the same locus. The ratio of H3K4me2:H3K27me3 in S100β mVSCs treated with atherogenic stimuli was significantly higher concomitant with a significant increase in *Myh11* mRNA levels following treatment.

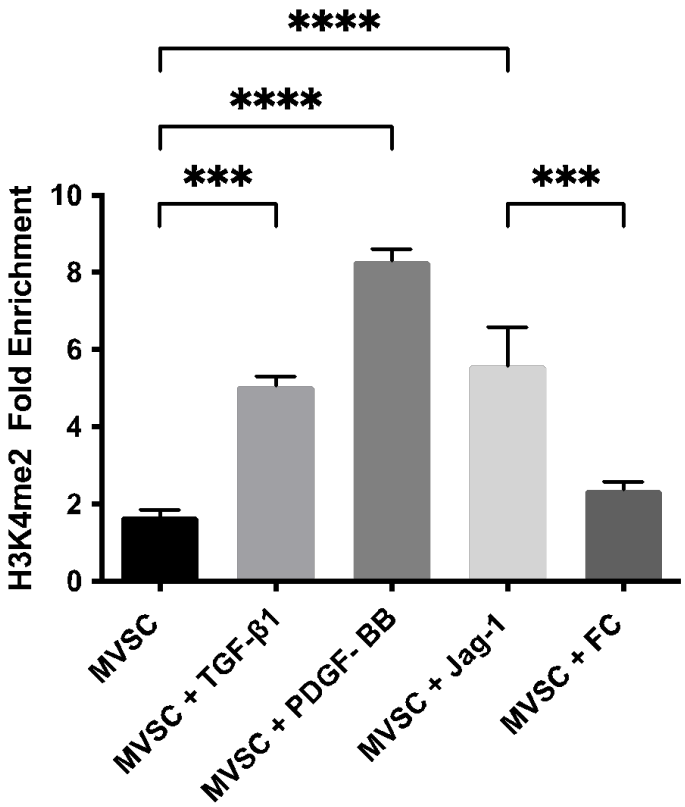

Figure 3.10. The level of enrichment of H3K4me2 at the *Myh11* locus in S100β mVSCs following treatment with Notch ligand, Jag-1, PDGF-BB and TGF-β1. S100β mVSCs were seeded at the required density in order to obtain a confluent T75 flask, and treated with 2ng/ml TGF-β1, 10ng/ml PDGF BB, 500 ng/ml Fc or Fc- Jag-1 in MM1 for 7 days. H3K4me2 binding at the *Myh11* locus was assessed by the single gene ChIP-PCR assay and corrected against the IgG control. Fold enrichment was determined for each condition and the data are the mean ± SEM of 3 experiments performed in triplicate. ** $p<0.01$ *** $p<0.001$ **** $p<0.0001$

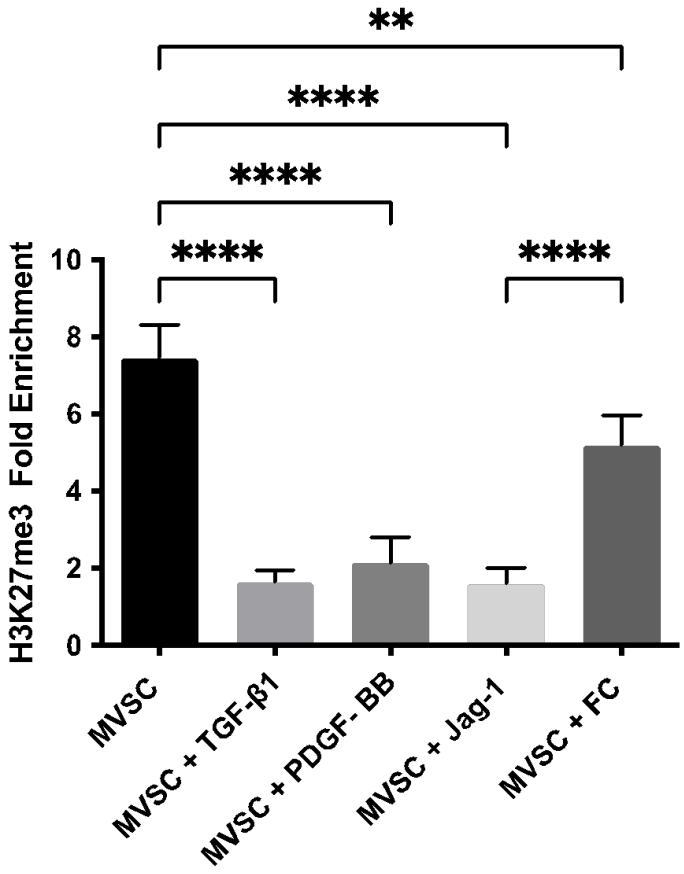

Figure 3.11. The level of enrichment of H3K27me3 at the *Myh11* locus in S100β mVSCs following treatment with Notch ligand, Jag-1, PDGF-BB and TGF-β1. S100β mVSCs treated with 2ng/ml TGF-β1, 10ng/ml PDGF BB, 500 ng/ml Fc or Fc- Jag-1 in MM1 for 7 days. H3K4me2 binding at the *Myh11* locus was assessed by the single gene ChIP-PCR assay and corrected against the IgG control. Fold enrichment was determined for each condition and the data are the mean ± SEM of 3 experiments performed in triplicate. ** $p<0.01$ **** $p<0.0001$

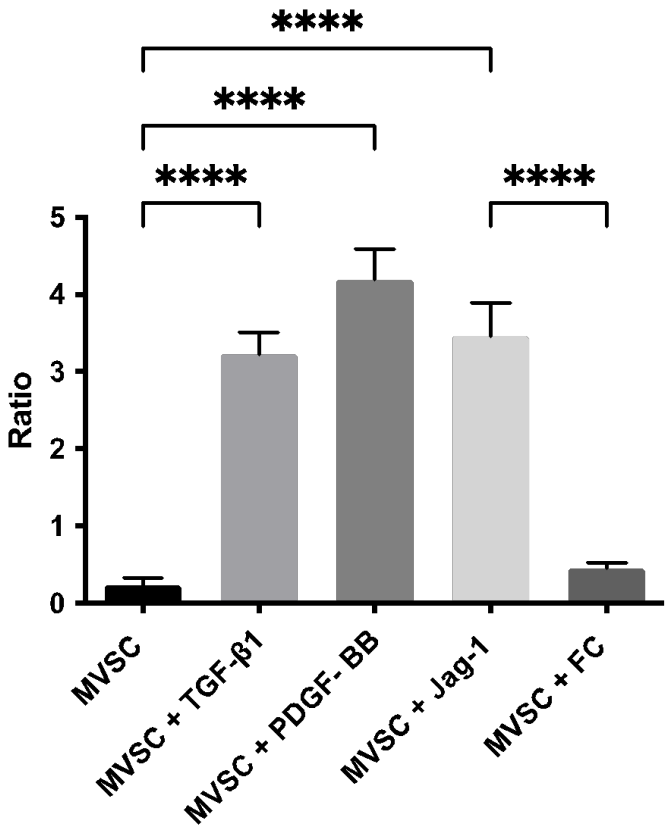

Figure 3.12. H3K4me2/H3K27me3 ratio at the *Myh11* locus in S100β mVSCs following treatment with Notch ligand, Jag-1, PDGF-BB and TGF-β1. S100β mVSCs were treated with 2ng/ml TGF-β1, 10ng/ml PDGF BB, 500 ng/ml Fc or Fc- Jag-1 in MM1 for 7 days. The level of enrichment of H3K4me2 and H3K27me3 binding at the *Myh11* locus in control untreated S100β mVSc and S100β mVSCs were treated with different atherogenic stimuli was assessed by the single gene ChIP-PCR assay and corrected against the IgG control. The ratio of H3K4me2 and H3K27me3 binding was determined for each condition and the data are the mean ± SEM of 3 experiments performed in triplicate. **** p<0.0001

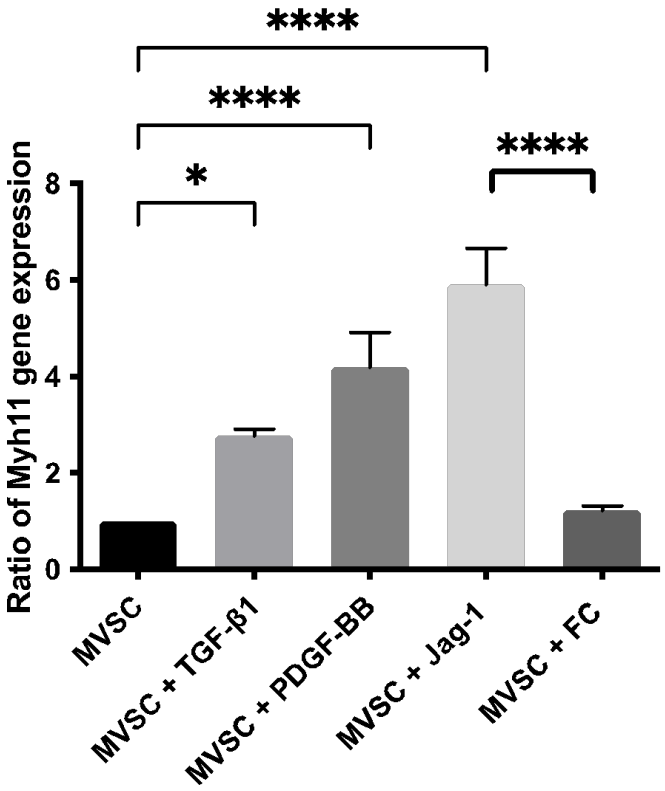

Figure 3.13. Expression of *Myh11* mRNA in S100β mVSCs following treatment with Notch ligand, Jag-1, PDGF-BB and TGF-β1. *Myh11* expression was measured in S100β mVSCs in their maintenance medium (MM1) and compared to S100β mVSCs that were grown in MM1 supplemented with atherogenic stimuli 2ng/ml TGF-β1, 10ng/ml PDGF BB, 500 ng/ml Fc and Fc- Jag-1 in MM1, 1% FBS (ATCC) for 7 days. Total RNA was isolated before the relative levels of *Myh11* transcript was measured by qRT-PCR with GAPDH as an internal control. Data are expressed as the ratio of gene expression (R) and represent the mean ± SEM of 3 experiments performed in triplicate. * $p<0.05$ ** $p<0.01$ **** $p<0.0001$

3.3.5 Stem cell maintenance media failed to change the H3K4me2 and H3K27me3 mark at the *Myh11* locus or *Myh11* mRNA levels in murine de-differentiated SMCs *in vitro.*

De-differentiated MOVAS SMCs were seeded at the density of 15 x 10^4 cells/cm^2 to obtain a confluent T75 flask after 21 days with normal splitting every 4 to 5 days. After 48 hours, medium was removed and the cells were washed twice with PBS to remove residual serum from the cells before either SMC growth medium or S100β mVSC stem cell maintenance medium was added to the cells, respectively for a further 21 days. The DNA was then fixed and prepared for single gene ChIP-PCR analysis as described in Chapter 2, Section 2.2.4 and correlated with the transcriptional activity of the *Myh11* gene by measuring *Myh11* mRNA levels by qRT-PCR and analysed as explained in section 2.2.9.

When MOVAS SMCs were grown in stem cell maintenance medium (MM1) over time, there was a notable change in their morphology as the cells became more stem-like when compared to their morphology in their own growth medium. Specifically, in their normal growth medium, MOVAS SMCs exhibit a classic round spindle -shaped morphology, typical of these cells in culture. However, when the cells were grown in MM1 media, the cells became more multipotent vascular stem-like, less round and more elongated after 5 and 15 days in culture, respectively [Figure 3.14]. Low power, not high-resolution images. From these low-resolution images there is an apparent change in morphology of MOVAS SMC grown in MM1 media these MOVAS SMC have dedifferentiated back towards stem cells, but higher magnification images are required to confirm that.

The level of enrichment of H3K4me2 at the *Myh11* locus in MOVAS SMC was assessed when cells were grown in their own growth medium (DM) or stem cell maintenance medium (MM1) by single gene ChIP-PCR. There was no significant difference in the level of enrichment of H3K4me2 between both conditions [Figure 3.15]. Similarly, the level of enrichment of H3K27me3 at the *Myh11* locus remained unchanged between both conditions [Figure 3.16]. Furthermore, the ratio of H3K4me2:H3K27me3 under both conditions remained unchanged [Figure 3.17].

In parallel studies, the relative levels of SMC differentiation marker genes, *Cnn1* and *Myh11* and stem cell marker genes, *S100β* and *Sox10* were measured by qRT-PCR in MOVAS SMCs when grown in differentiation growth medium (DM) and stem cell maintenance medium (MM1). No significant changes in the transcript levels were observed [Figure 3.18]. Stem cell maintenance medium did not change the epigenetic profile or the transcript level of MOVAS SMCs.

The single gene ChIP-PCR results suggest that MOVAS SMCs are enriched for H3K4me2 at the *Myh11* locus. However, there was no difference in the level enrichment of H3K4me2 between MOVAS SMCs grown and expanded in their normal growth medium compared to stem cell maintenance medium. The cells had a very low level of enrichment of H3K27me3 at the *Myh11* locus which remained unchanged in stem cell maintenance medium, despite a difference in morphology. The transcript levels of SMC differentiation genes and stem cell marker genes in MOVAS SMC remained unchanged in the stem cell maintenance medium.

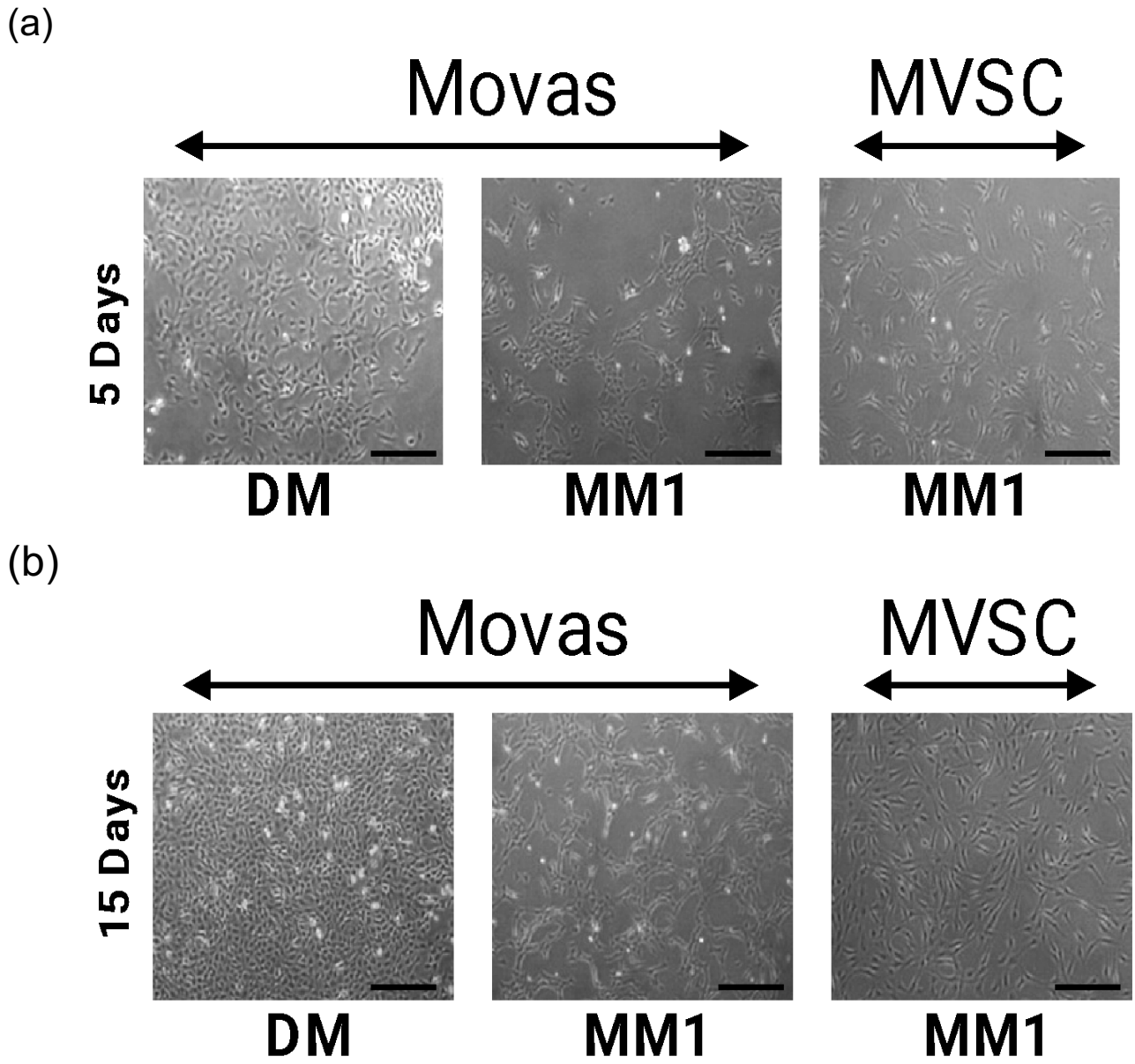

Figure 3.14. The effect of growth media on the morphological characteristics of MOVAS SMCs. (a) MOVAS SMC were cultured in their RPMI growth medium (DM) and a stem cell maintenance medium (MM1) for 5 days. Phase contrast images of MOVAS SMC. (b) MOVAS SMC were cultured in their RPMI growth medium (DM) and a stem cell maintenance medium (MM1) for 15 days. Phase contrast images of MOVAS SMC. Scale bar is 100µm.

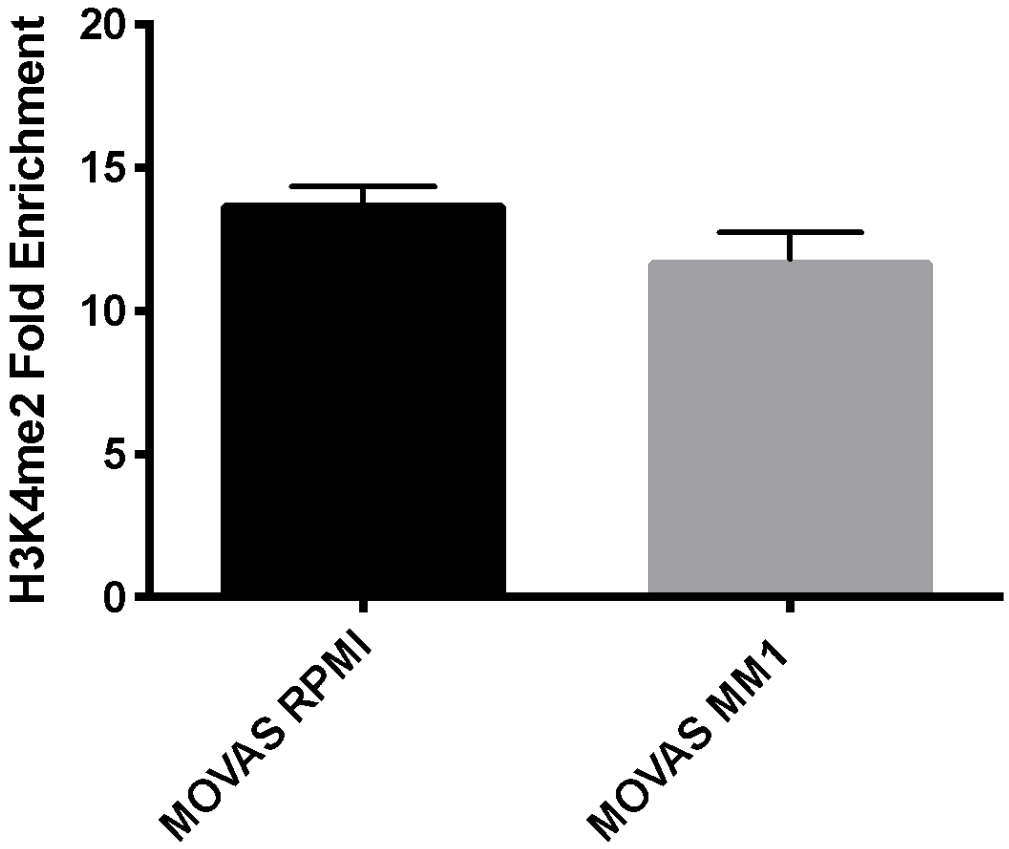

Figure 3.15. The effect of growth media on the level of enrichment of H3K4me2 at the *Myh11* locus in MOVAS SMC. MOVAS SMC were cultured in their RPMI growth medium (DM) and a stem cell maintenance medium (MM1) for 21 days. H3K4me2 binding at the *Myh11* locus was assessed by the single gene ChIP-PCR assay and corrected against the IgG control. Fold enrichment was determined for each condition and the data are the mean ± SEM of 3 experiments performed in triplicate.

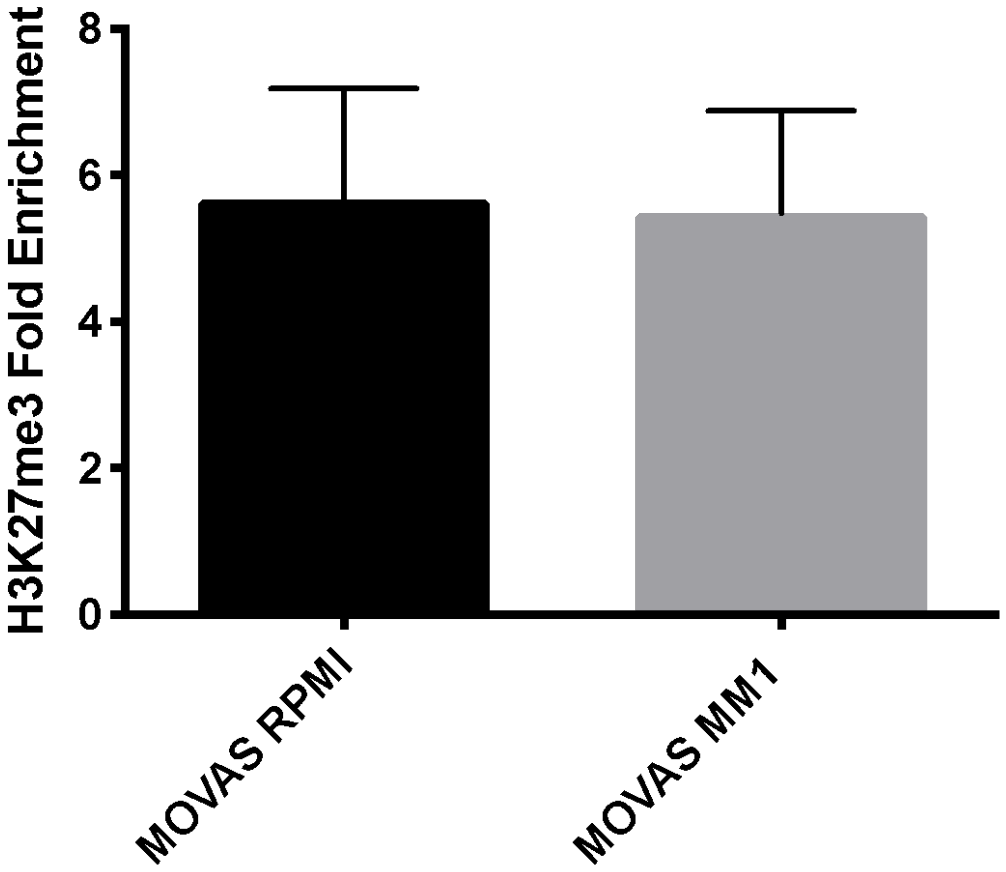

Figure 3.16 . The effect of growth media on the level of enrichment of H3K27me3 at the *Myh11* locus in MOVAS SMC. MOVAS SMC were cultured in their RPMI growth medium (DM) and a stem cell maintenance medium (MM1) for 21 days. H3K27me3 binding at the *Myh11* locus was assessed by the single gene ChIP-PCR assay and corrected against the IgG control. Fold enrichment was determined for each condition and the data are the mean ± SEM of 3 experiments performed in triplicate.

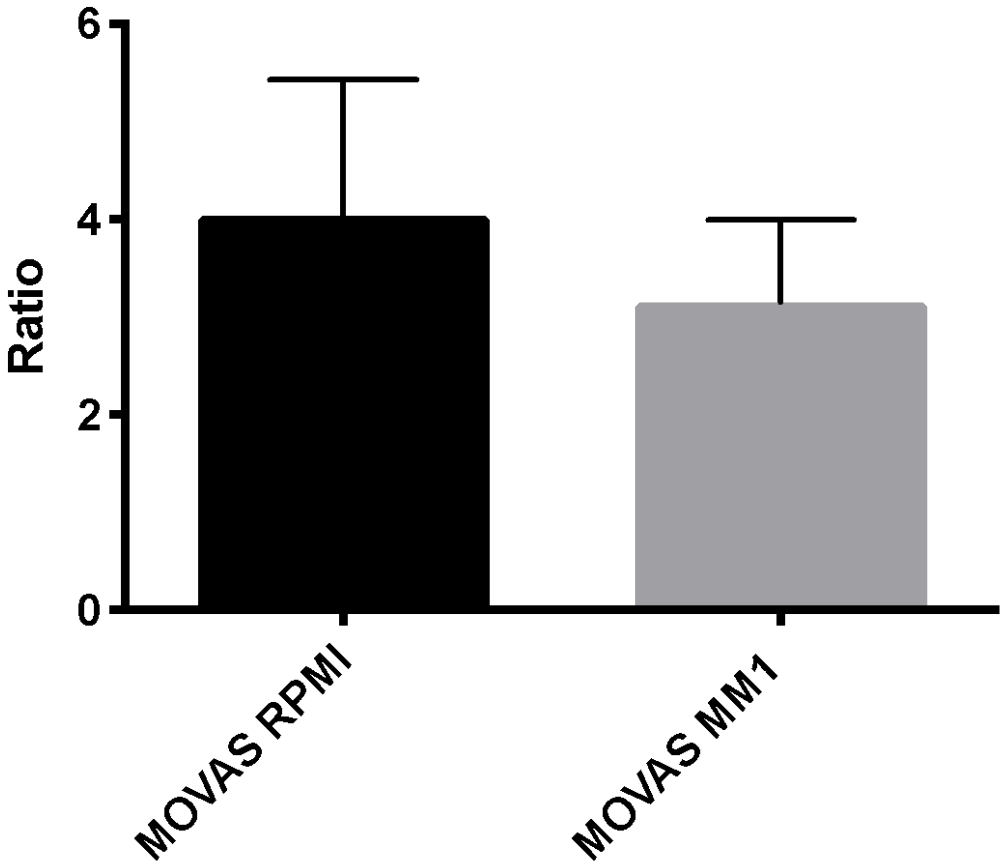

Figure 3.17. The effect of growth media on H3K4me2/H3K27me3 ratio at the *Myh11* locus in MOVAS SMC. MOVAS SMC were cultured in their RPMI growth medium (DM) and a stem cell maintenance medium (MM1) for 21 days. H3K4me2 and H3K27me3 binding at the *Myh11* locus was assessed by the single gene ChIP-PCR assay and corrected against the IgG control. Fold enrichment was determined for each condition before the H3K4me2/H3K27me3 ratio was evaluated. The data are the mean ± SEM of 3 experiments performed in triplicate.

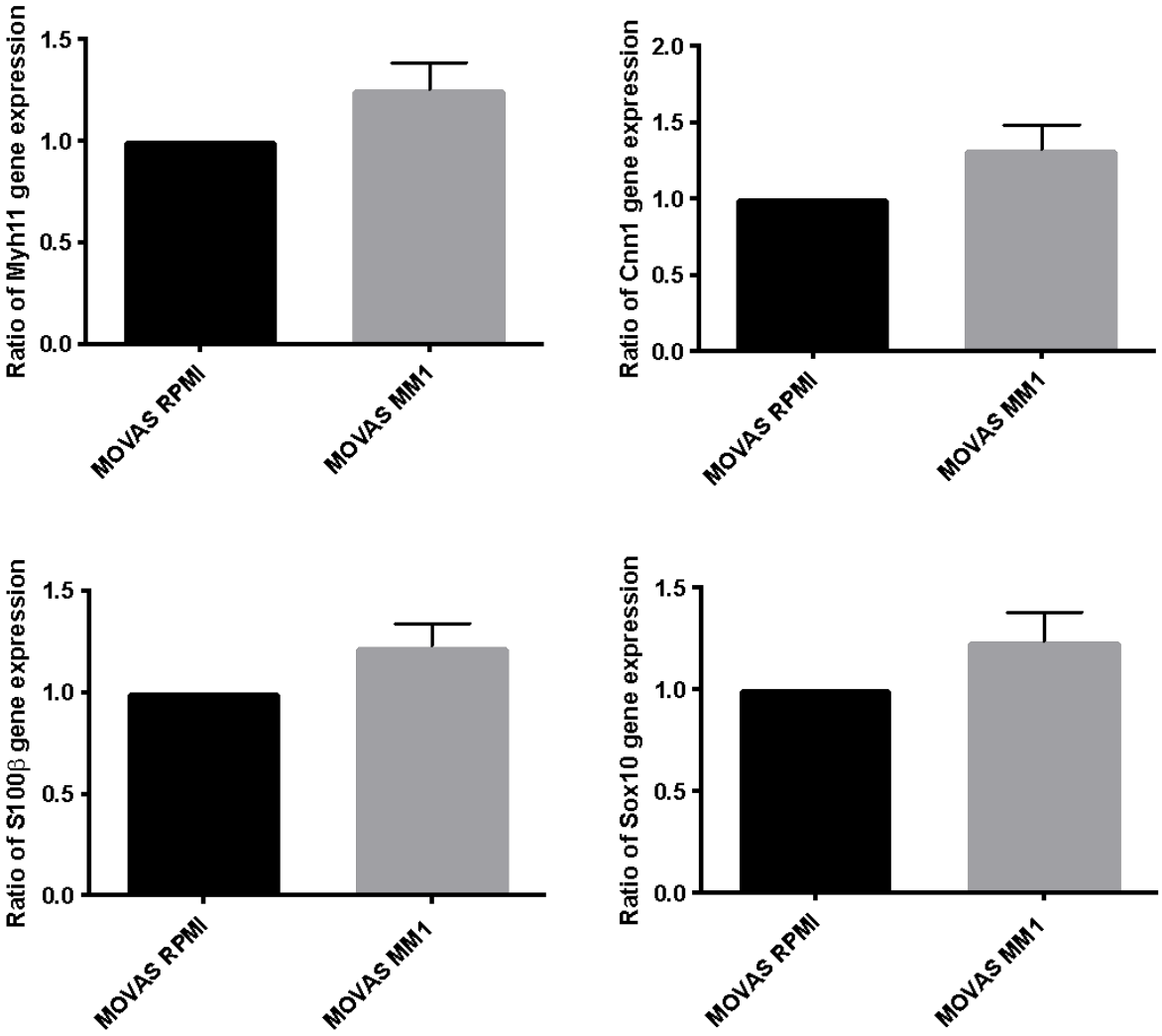

Figure 3.18. The effect of growth media on mRNA levels of SMC differentiation markers and stem cell markers in MOVAS SMC. MOVAS was grown for 3 weeks in their RPMI growth medium (DM) and a stem cell maintenance medium (MM1). Total RNA was isolated from cells before the relative levels of *Cnn1*, *Myh11*, *S100β* and *Sox10* transcript were measured by qRT-PCR with GAPDH as an internal control. Data are expressed as the ratio of gene expression (R) and represent the mean ± SEM of 3 experiments performed in triplicate.

3.3.6 The DNA demethylase, Tet-2 regulates H3K4me2 and H3K27me3 enrichment at *Myh11* locus and *Myh11* mRNA levels in de-differentiated aortic SMCs and resident S100β mVSCs *in vitro*

Cells were seeded at the density of 15 x 10^4 cells/cm^2 for MOVAS and 25 x 10^4 cells/cm^2 for S100β mVSC to obtain a confluent T75 flask after 7 days. After 24 h, MOVAS SMCs and S100β mVSCs were treated with 2ng/ml TGF-β1 or 10ng/ml PDGF BB for 7 days before the DNA was fixed and prepared for single gene ChIP-PCR analysis as described in Chapter 2, Section 2.2.4 and correlated with the transcriptional activity of the *Myh11* gene by measuring *Myh11* mRNA levels by qRT-PCR.

Tet-2 knockdown was performed as described in section 2.2.3.1 using a targeted siRNA duplex (with a scrambled duplex as a control) for 48 hours. The knockdown was confirmed by measuring *Tet-2* mRNA levels by qRT-PCR and Tet-2 protein levels by immunoblot using an anti-Tet-2 antibody before the DNA was prepared for single gene ChIP-PCR analysis and correlated with the transcriptional activity of the *Myh11* gene by measuring *Myh11* mRNA levels by qRT-PCR.

The level of enrichment of Tet-2 binding at the *Myh11* locus was assessed by single gene ChIP-PCR analysis. Tet-2 binding decreased in MOVAS SMCs treated with TGF-β1 and PDGF-BB, respectively, when compared to untreated control cells [Figure 3.19]. Jag1 failed to alter Tet-2 binding when compared to the Fc control [Figure 3.19].

The level of Tet-2 binding at the *Myh11* locus was also assessed by single gene ChIP-PCR analysis in non-treated S100β mVSCs and S100β mVSCs treated with TGF-β1, PDGF-BB and Jag-1 and compared to the IgG control. There was a significant enrichment of Tet-2 binding with all three stimuli when compared to untreated control S100β mVSCs [Figure 3.20].

The siRNA transfection efficiency in MOVAS SMCS and S100β mVSCs was first confirmed using microscopic analysis of fluorescence-tagged Tye563 dsiRNA transfected over 48 hours period. (Figure 3.21). Tet-2 knockdown was then validated by measuring *Tet-2* mRNA and Tet-2 protein levels in MOVAS SMCs treated with Tet-2 siRNA and scrambled siRNA control

duplexes, respectively. The level of *Tet-2* mRNA was significantly reduced in Tet-2 siRNA treated cells when compared to scrambled controls [Figure 3.22]. In parallel cultures, the level of Tet-2 protein was significantly reduced in Tet-2 siRNA treated cells when compared to scrambled controls [Figure 3.23].

The level of enrichment of H3K4me2 at the *Myh11* locus in MOVAS SMC was significantly decreased after the knockdown of Tet-2 when compared to the scrambled control [Figure 3.24]. In contrast, the enrichment of H3K27me3 at the *Myh11* locus was significantly increased in MOVAS SMCs after Tet-2 knockdown when compared to the scrambled sample [Figure 3.25]. Furthermore, the ratio of H3K4me2:H3K27me3 was significantly lower in MOVAS SMCs following Tet-2 knockdown when compared to scrambled control [Figure 3.26]. In parallel studies, *Myh11* and *Cnn1* gene expression was measured in MOVAS SMC following the knockdown of Tet-2 and compared to the scrambled control. While there was a tendency towards lower *Myh11* mRNA levels following Tet-2 knockdown, it was not significant [Figure 3.27]. In contrast, there was a significant decrease in *Cnn1* mRNA levels following Tet-2 knockdown when compared to the scrambled control [Figure 3.27]. Tet-2 knockdown was sufficient to alter the enrichment level of H3K4me2 at the *Myh11* locus in MOVAS SMCs.

Tet-2 knockdown was also validated in S100β mVSCs by measuring *Tet-2* mRNA in cells treated with Tet-2 siRNA and scrambled siRNA control duplexes, respectively. The level of *Tet-2* mRNA was significantly reduced in Tet-2 siRNA treated cells following treatment with TGF-β1 + PDGF-BB, when compared to scrambled controls [Figure 3.28]. In parallel cultures, the level of Tet-2 protein was not significantly reduced in Tet-2 siRNA treated cells when compared to scrambled controls [Figure 3.28].

The level of enrichment of H3K4me2 at the *Myh11* locus in S100β mVSCs at baseline was higher after the Tet-2 knockdown, compared to the scrambled control. [Figure 3.29]. Treatment of the cells with TGF-β1 and PDGF-B significantly increased the enrichment of H3K4me2, an effect that was significantly reduced following Tet-2 knockdown, when compared to the treated scrambled control [Figure 3.29]. In parallel studies, the level of enrichment of H3K27me3 at the *Myh11* locus was significantly decreased in S100β mVSCs at baseline after Tet-2 knockdown when compared to the scrambled control [Figure 3.30]. These

levels remained lower following treatment of S100β mVSCs with TGF-β1 and PDGF-BB, and did not change after Tet-2 knockdown, when compared to the treated scrambled control [Figure 3.30]. Moreover, the H3K4me2:H3K27me3 ratio was significantly increased after Tet-2 knockdown at baseline when compared to the scrambled control [Figure 3.31]. Treatment of the cells with TGF-β1 and PDGF-B significantly increased this ratio, an effect that was significantly reduced following Tet-2 knockdown, when compared to the treated scrambled control [Figure 3.31]. Tet-2 knockdown was sufficient to alter the level of enrichment of H3K4me2 at the *Myh11* locus in S100β mVSCs at baseline and following treatment with TGF-β1 and PDGF-BB.

The level of *Myh11* mRNA levels in S100β mVSCs were significantly lower at baseline following Tet-2 knockdown, when compared to the scrambled control [Figure 3.32]. The levels significantly increased following treatment with TGF-β1 and PDGF-BB, an effect that was significantly attenuated following Tet-2 knockdown, when compared to the treated scrambled control [Figure 3.32]. The level of *Myh11* mRNA levels in S100β mVSC at baseline and following treatment with TGF-β1 and PDGF-BB correlates with Tet-2.

The level of *Cnn1* mRNA levels in S100β mVSCs was not significantly lower at baseline following Tet-2 knockdown, when compared to the scrambled control [Figure 3.33]. The levels significantly increased following treatment with TGF-β1 and PDGF-BB, an effect that was significantly attenuated following Tet-2 knockdown, when compared to the treated scrambled control [Figure 3.33].

In summary, the single gene ChIP-PCR results for Tet-2 binding in de-differentiated MOVAS SMCs suggest that these cells are enriched for Tet-2 at the *Myh11* locus at baseline. This level of Tet-2 binding is modestly reduced in response to atherogenic stimuli, TGF-β1 and PDGF-BB, with little effect noted for the Notch ligand, Jag-1. Tet-2 knockdown significantly decreased the H3K4me2 mark at baseline concurrent with an increase in the H3K27me3 at the *Myh11* locus, a change in the ratio that had a minimal effect on the expression of *Myh11* gene expression.

In contrast, the single gene ChIP-PCR results for Tet-2 binding in S100β mVSCs suggest that these cells are not highly enriched at baseline for Tet-2 at the *Myh11* locus. However, the level of Tet-2 binding is increased significantly in response to atherogenic stimuli. Tet-2 knockdown significantly attenuated this enrichment of H3K4me2 at the *Myh11* locus in response to atherogenic stimuli without any significant effect on the observed reduction of the H3K27me3 mark in response to the same atherogenic stimuli. These data suggest that Tet-2 binding to the *Myh11* locus impacts the level of enrichment of H3k4me2 and H3K27me3 in both cell populations.

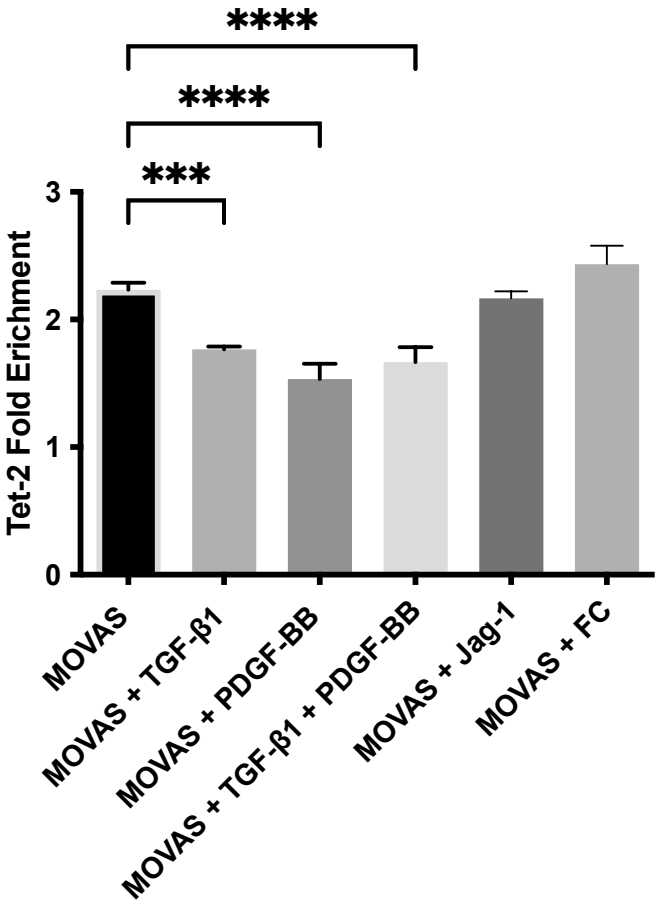

Figure 3.19. The effect of Notch ligand, Jag-1, TGF-β1 and PDGF-BB on Tet-2 binding to the *Myh11* locus in MOVAS SMC. MOVAS cells were treated with 2ng/ml TGF-β1 or 10ng/ml or PDGF-BB, 500 ng/ml Fc or Fc- Jag-1, in RPMI supplemented with 10% FBS for 7 d. Tet-2 protein binding at the *Myh11* locus was assessed by the single gene ChIP-PCR assay and corrected against the IgG control. Fold enrichment was determined for each condition and the data are the mean ± SEM of a representative experiment performed in triplicate. *** p<0.001, , **** p<0.0001

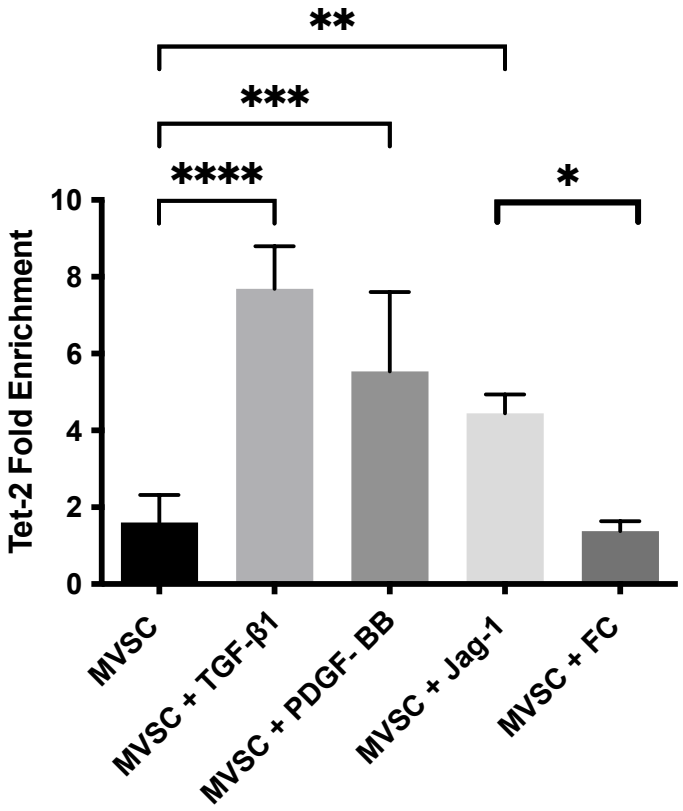

Figure 3.20. The effect of Notch ligand, Jag-1, TGF-β1 and PDGF-BB on Tet-2 binding to the *Myh11* locus in S100β mVSCs. S100β mVSCs were seeded and treated with 2ng/ml TGF-β1 or 10ng/ml or PDGF-BB in MM1 for 7 days. Tet-2 protein binding at the *Myh11* locus was assessed by the single gene ChIP-PCR assay and corrected against the IgG control. Fold enrichment was determined for each condition and the data are the mean ± SEM of 3 experiments performed in triplicate. * $p<0.05$ ** $p<0.01$, **** $p<0.0001$

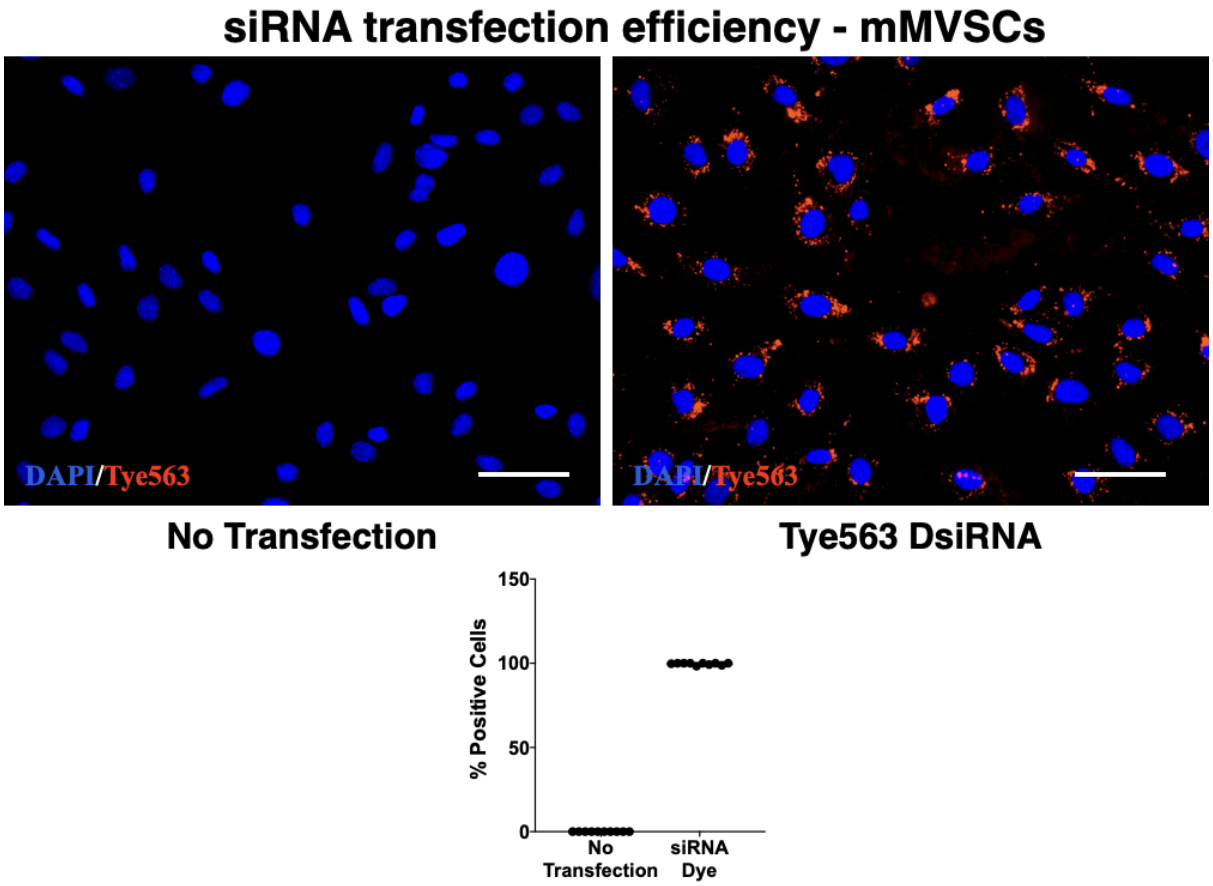

Figure 3.21. Transfection Efficiency of siRNA in S100β mVSCs. Fluorescence microscopic analysis of S100β mVSCs transfected with Tye563 DsiRNA for 48 h. DAPI was used to stain nuclei. Tye563+ cells were counted and compared against total cell count. (a) Representative fluorescence images of Tye563 expression in both transfected and non-transfected samples. Scale bar = 25µm. (b) Mean percentage of Tye563+ cells plotted for each sample. Error bars based on SEM. Data representative of n=3

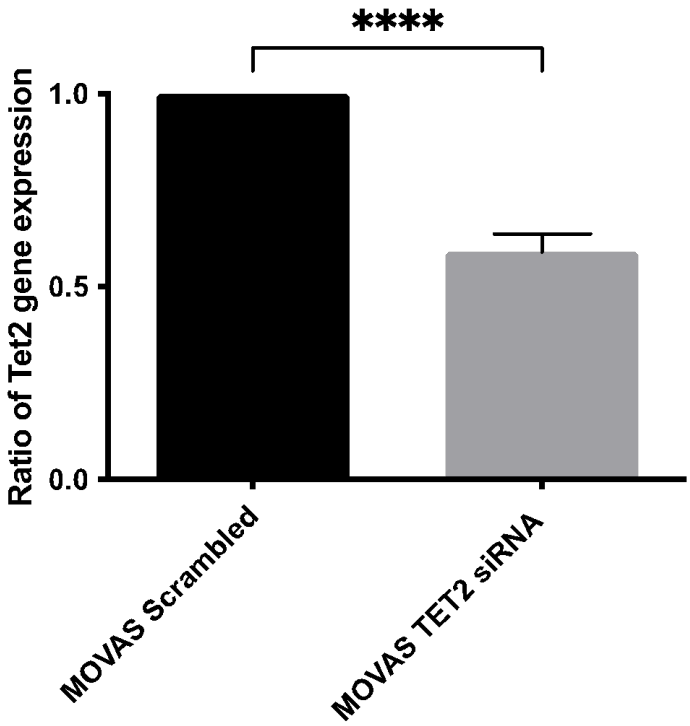

Figure 3.22. Tet-2 knockdown in MOVAS SMCs compared to scrambled control. *Tet-2* mRNA expression was measured MOVAS SMCs after Tet-2 siRNA knockdown after 48 h. Total RNA was isolated from cells before the relative levels of *Tet-2* mRNA was measured by qRT-PCR with *Gapdh* as an internal control. Data are expressed as the ratio of gene expression (R) and represent the mean ± SEM of 3 experiments performed in triplicate. **** $p<0.0001$

(a)

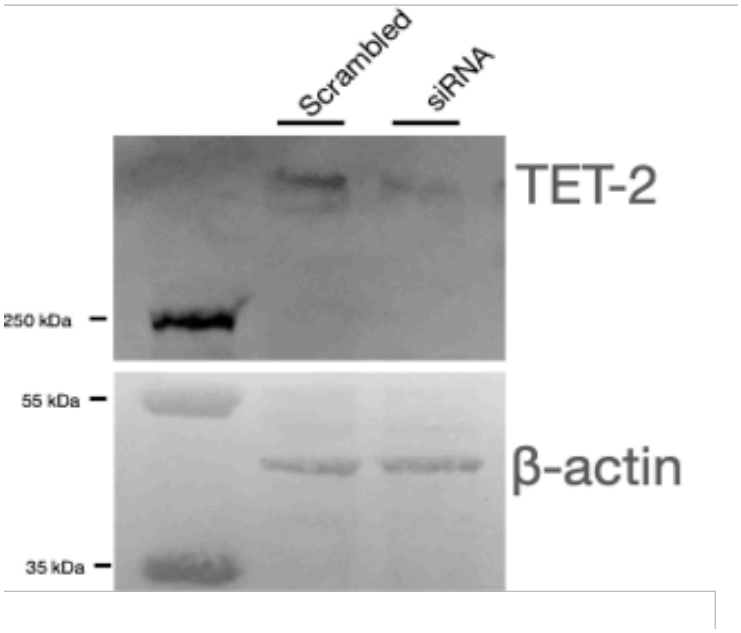

(b)

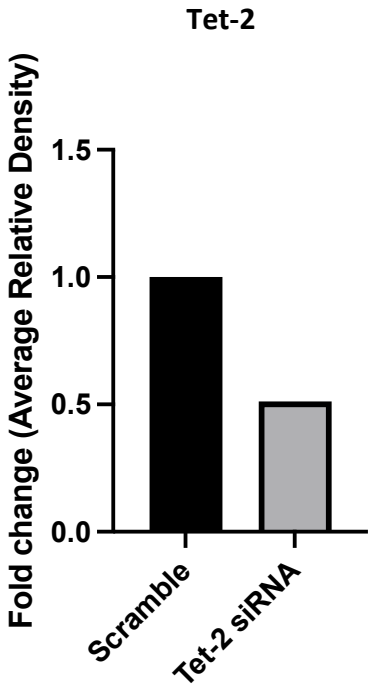

Figure 3.23 Tet-2 knockdown in MOVAS SMCs compared to scrambled control. (a) Tet-2 protein levels were measured in MOVAS SMCs following Tet-2 siRNA knockdown after 48 h. Cell lysates (~40µg/lane) from scrambled siRNA and Tet-2 siRNA treated MOVAS SMCs were prepared, separated by SDS-PAGE and analysed by western blot. Mock transfected MOVAS SMC and control cell lysates were also analysed. β-actin served as an internal control. Data are representative of one experiment. (b) Tet-2 knockdown in MOVAS SMCs compared to scrambled control. Tet-2 protein levels were measured in MOVAS SMCs following Tet-2 siRNA knockdown after 48 h. Densitometric data was analysed using ImageJ software with β-actin serving as an internal control. Data are representative of one experiment.

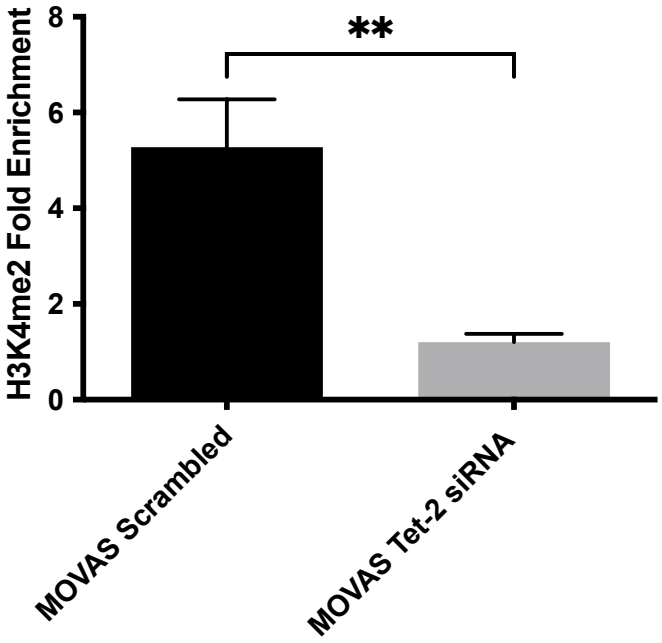

Figure 3.24. The level of enrichment of H3K4me2 at the *Myh11* locus in Tet-2 siRNA treated MOVAS SMCs compared to scrambled control. H3K4me2 binding at the *Myh11* locus was assessed by the single gene ChIP-PCR assay and corrected against the IgG control after Tet-2 siRNA knockdown for 48 h and compared to the scrambled control. Fold enrichment was determined for each condition and the data are the mean ± SEM of 3 experiments performed in triplicate. ** $p<0.01$

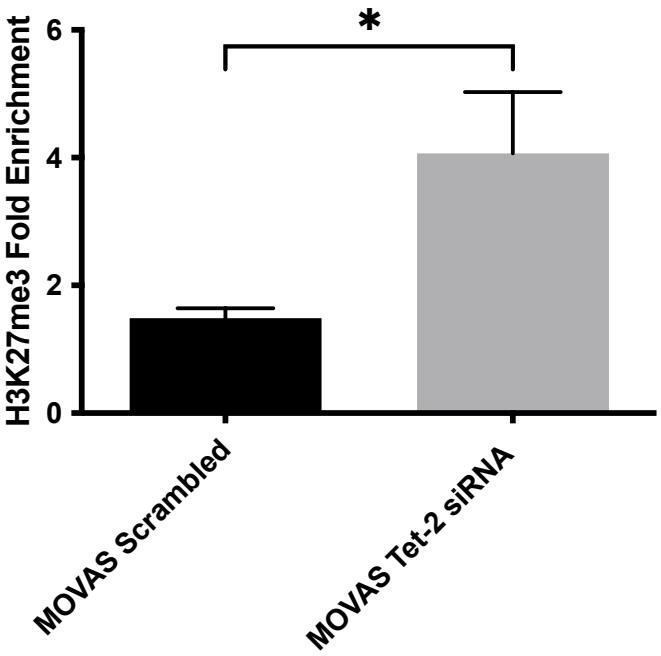

Figure 3.25. The level of enrichment of H3K27me3 at the *Myh11* locus in Tet-2 siRNA treated MOVAS SMCs compared to scrambled control. H3K27me3 binding at the *Myh11* locus was assessed by the single gene ChIP-PCR assay and corrected against the IgG control after Tet-2 siRNA knockdown for 48 h and compared to the scrambled control. Fold enrichment was determined for each condition and the data are the mean ± SEM of 3 experiments performed in triplicate. * $p<0.05$

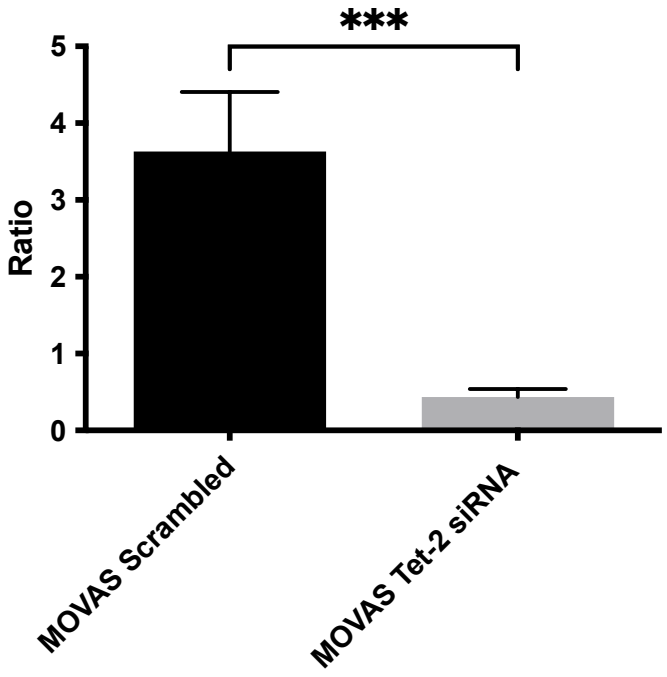

Figure 3.26. The combined H3K4me2/H3K27me3 ratio at the *Myh11* locus in MOVAS SMCs following siRNA knockdown of Tet-2 compared to scrambled control. The level of enrichment of H3K4me2 and H3K27me3 binding at the *Myh11* locus following Tet-2 siRNA knockdown compared to the scrambled control after 48 h was assessed by the single gene ChIP-PCR assay and corrected against the IgG control. The ratio of H3K4me2 and H3K27me3 binding was determined for each condition and the data are the mean ± SEM of 3 experiments performed in triplicate. *** $p<0.001$

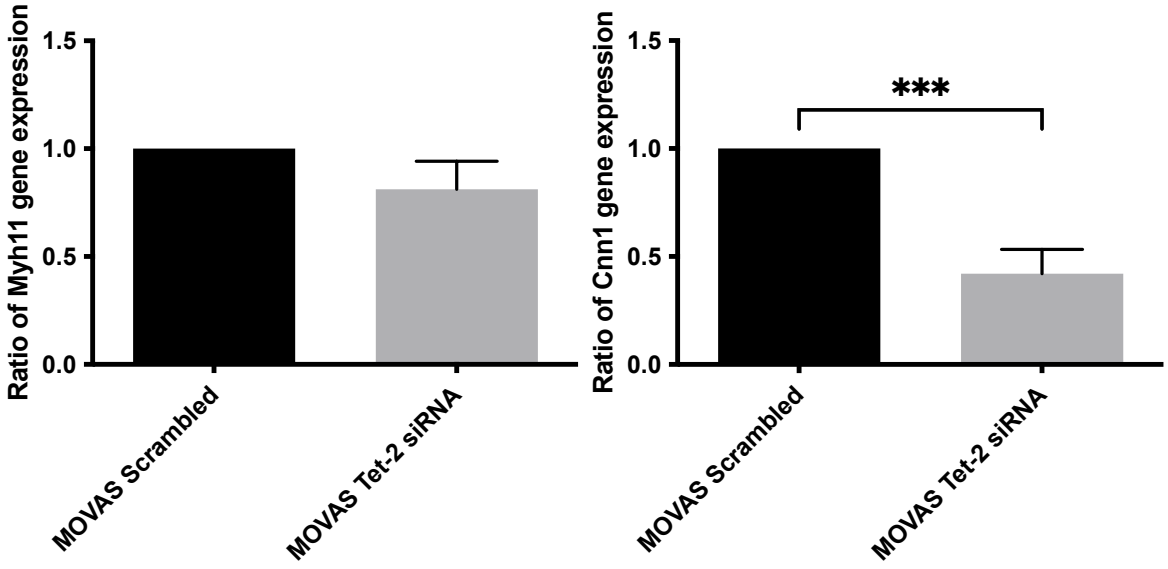

Figure 3.27. Expression of *Myh11* and *Cnn1* mRNA in MOVAS SMC compared to scrambled control. *Myh11* and *Cnn1* expression was measured in MOVAS Tet-2 siRNA in their maintenance medium (RPMI) and compared to scramble MOVAS after Tet-2 siRNA knockdown after 48 h. Total RNA was isolated from cells before the relative levels of *Tet-2* mRNA was measured by qRT-PCR with *Gapdh* as an internal control. Data are expressed as the ratio of gene expression (R) and represent the mean ± SEM of 3 experiments performed in triplicate. *** $p<0.001$

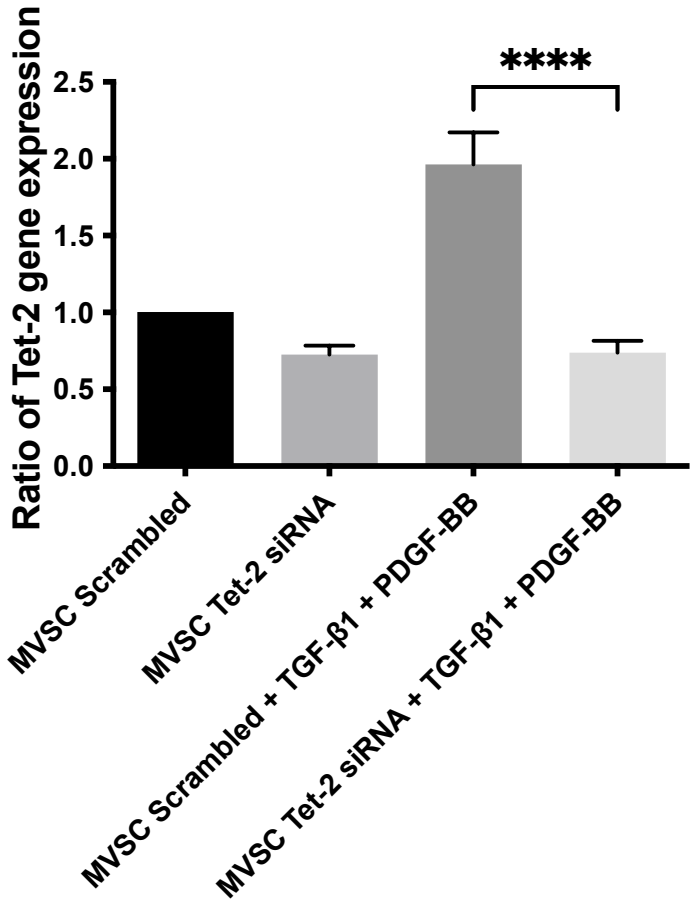

Figure 3.28. Tet-2 knockdown in S100β mVSCs compared to scrambled control before and following treatment. *Tet-2* mRNA expression was measured untreated and treated S100β mVSCs after Tet-2 siRNA knockdown after 48 h. Total RNA was isolated from cells before the relative levels of *Tet-2* mRNA was measured by qRT-PCR with *Gapdh* as an internal control. Data are expressed as the ratio of gene expression (R) and represent the mean ± SEM of 3 experiments performed in triplicate. **** $p<0.0001$

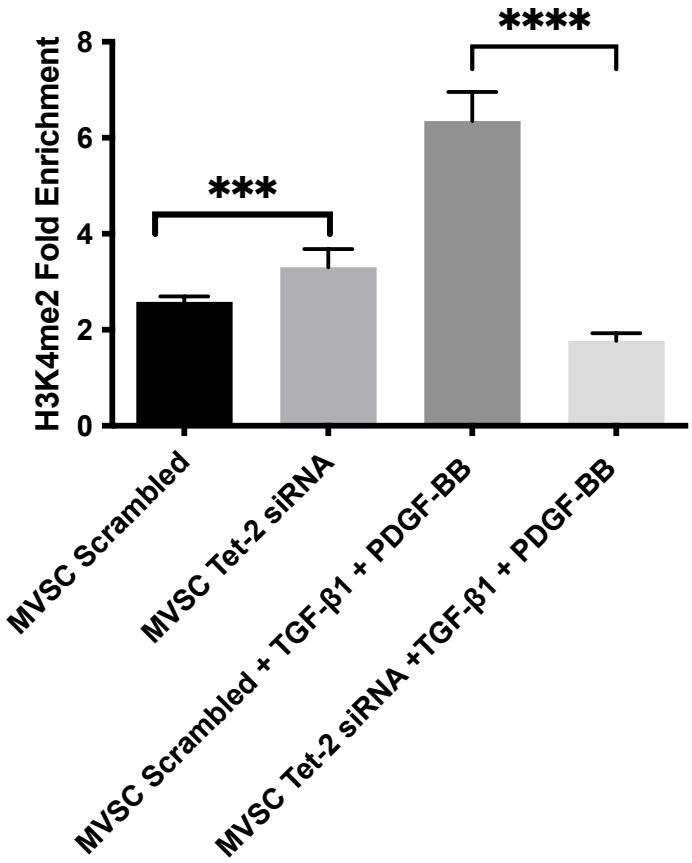

Figure 3.29. The level of enrichment of H3K4me2 at the *Myh11* locus in Tet-2 siRNA control S100β mVSCs compared to scrambled control and treated S100β mVSCs compared to treated scrambled. H3K4me2 binding at the *Myh11* locus was assessed by the single gene ChIP-PCR assay and corrected against the IgG control after Tet-2 siRNA knockdown for 48 h and compared to the related scrambled. Fold enrichment was determined for each condition and the data are the mean ± SEM of 3 experiments performed in triplicate. *** $p<0.001$ **** $p<0.0001$

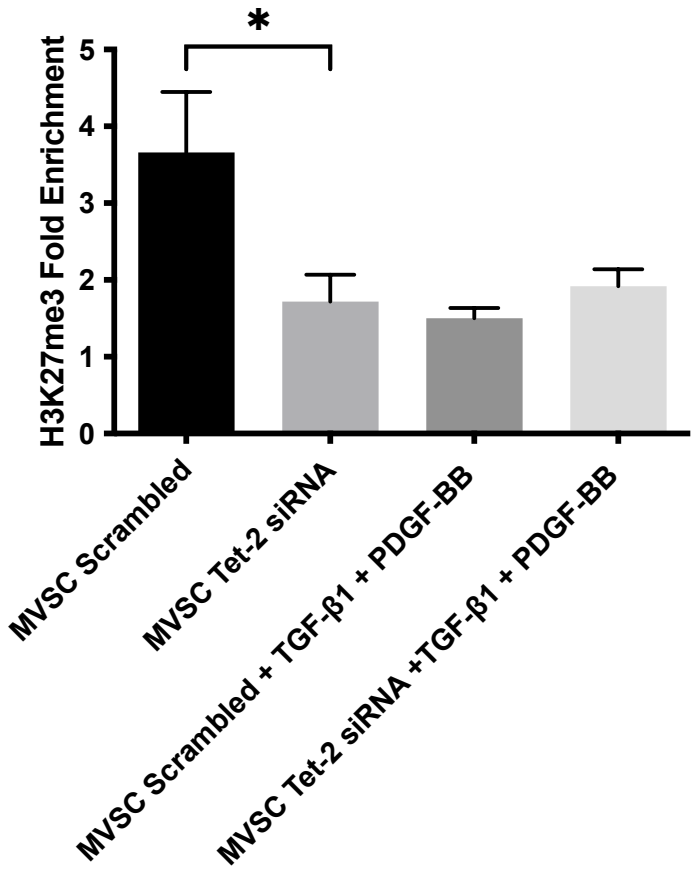

Figure 3.30. The level of enrichment of H3K27me3 at the *Myh11* locus in Tet-2 siRNA control S100β mVSCs compared to scrambled control and treated S100β mVSCs compared to treated scrambled. H3K27me3 binding at the *Myh11* locus was assessed by the single gene ChIP-PCR assay and corrected against the IgG control after Tet-2 siRNA knockdown for 48 h and compared to the related scrambled. Fold enrichment was determined for each condition and the data are the mean ± SEM of 3 experiments performed in triplicate. * $p<0.05$

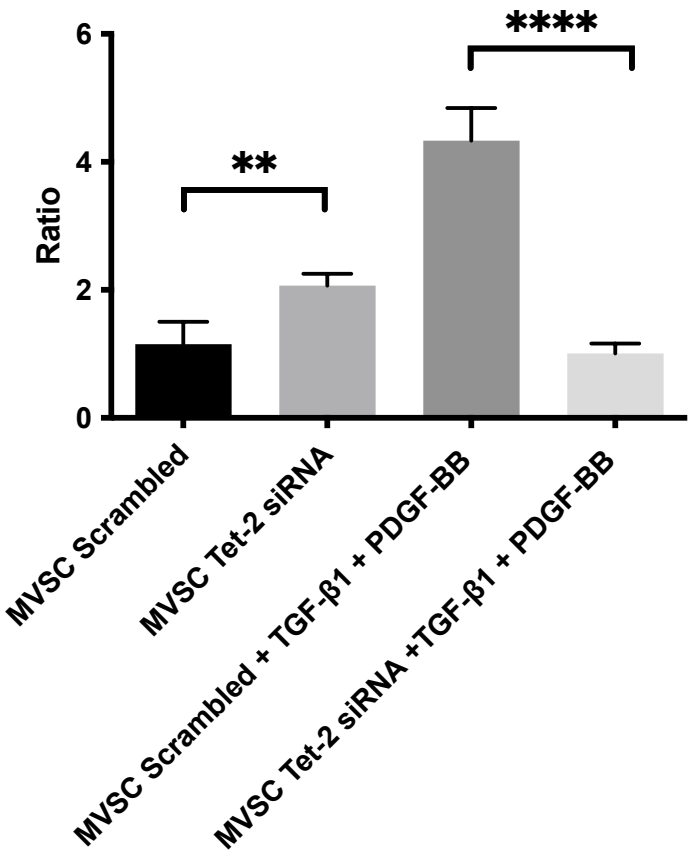

Figure 3.31. The combined H3K4me2/H3K27me3 ratio at the *Myh11* locus in Tet-2 siRNA control S100β mVSCs compared to scrambled control and treated S100β mVSCs compared to treated scrambled. The level of enrichment of H3K4me2 and H3K27me3 binding at the *Myh11* locus following Tet-2 siRNA knockdown compared to the scrambled control after 48 h was assessed by the single gene ChIP-PCR assay and corrected against the IgG control. The ratio of H3K4me2 and H3K27me3 binding was determined for each condition and the data are the mean ± SEM of 3 experiments performed in triplicate. ** $p<0.01$ **** $p<0.0001$.

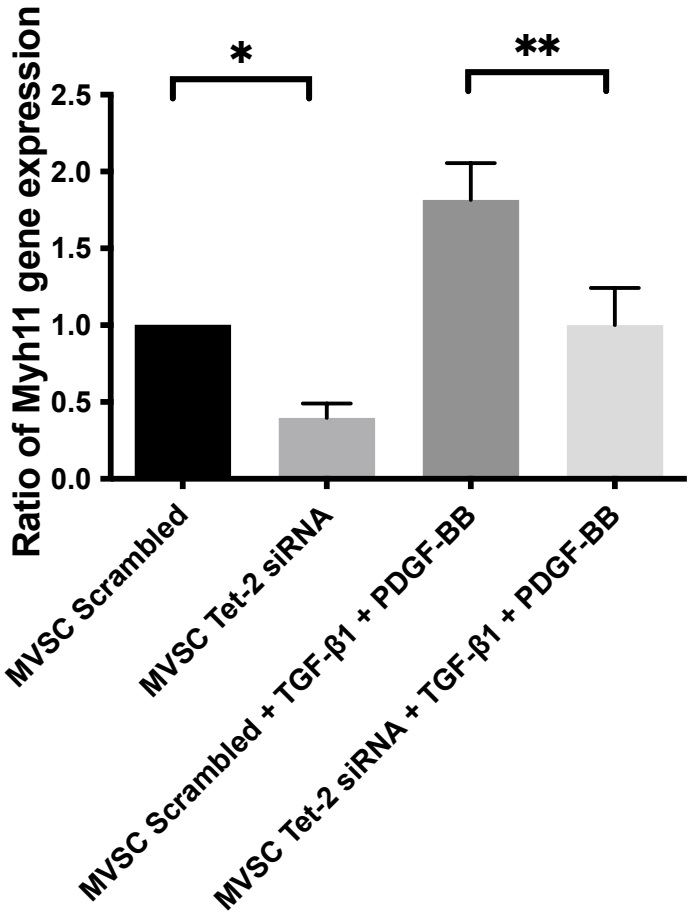

Figure 3.32. Expression of *Myh11* mRNA in S100β mVSC compared to scrambled control before and following treatment. *Myh11* expression was measured in S100β mVSCs Tet-2 siRNA in their maintenance medium (MM1) and compared to scramble S100β mVSCs also a scramble S100β mVSCs with differentiation stimuli with 2ng/ml TGF-β1, 10ng/ml PDGF BB was measured and compared to S100β mVSCs Tet-2 siRNA with differentiation stimuli. S100β mVSCs after Tet-2 siRNA knockdown after 48 h. Total RNA was isolated from cells before the relative levels of *Tet-2* mRNA was measured by qRT-PCR with *Gapdh* as an internal control. Data are expressed as the ratio of gene expression (R) and represent the mean ± SEM of 3 experiments performed in triplicate. * $p<0.05$ ** $p<0.01$

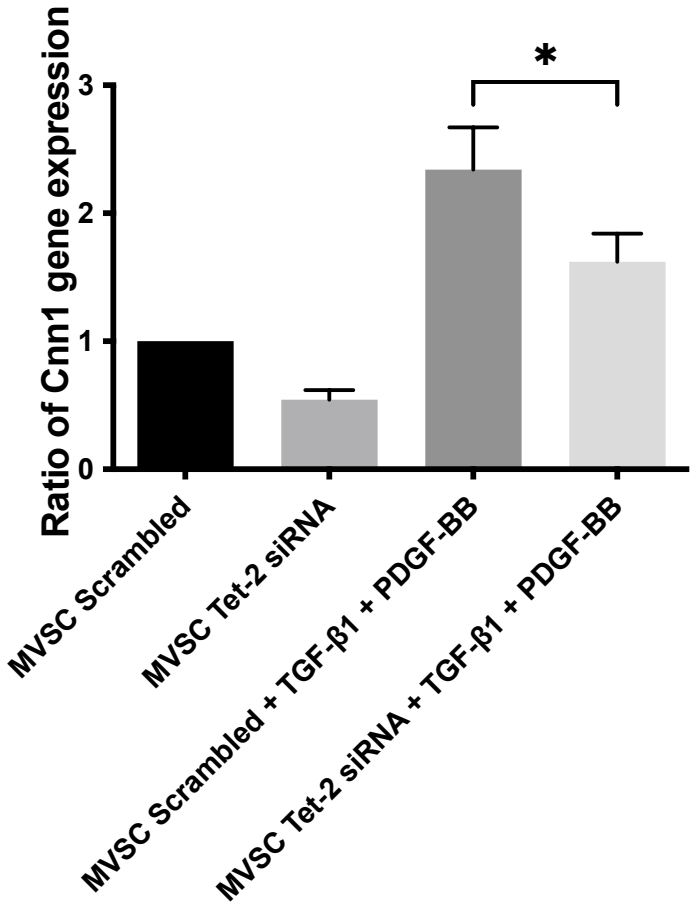

Figure 3.33. Expression of *Cnn1* mRNA in S100β mVSC compared to scrambled control before and following treatment. *Cnn1* expression was measured in S100β mVSCs Tet-2 siRNA in their maintenance medium (MM1) and compared to scramble S100β mVSCs also a scramble S100β mVSCs with differentiation stimuli with 2ng/ml TGF-β1, 10ng/ml PDGF BB was measured and compared to S100β mVSCs Tet-2 siRNA with differentiation stimuli. S100β mVSCs after Tet-2 siRNA knockdown after 48 h. Total RNA was isolated from cells before the relative levels of *Tet-2* mRNA was measured by qRT-PCR with *Gapdh* as an internal control. Data are expressed as the ratio of gene expression (R) and represent the mean ± SEM of 3 experiments performed in triplicate. * $p<0.05$

3.4 Discussion

A hallmark of arterial pathology in cardiovascular disease (CVD) is the accumulation of neointimal cells, primarily SMC-like cells within lesions, leading to intimal thickening and subclinical atherosclerosis (Benditt & Benditt, 1973). This accumulation leads to the development of early adaptive lesions (Velican et al., 1981) and an essential marker of subclinical disease yet the fundamental aspects of vascular cell accumulation, proliferation and the phenotypic changes within the vessel wall remain unresolved (Benditt & Benditt, 1973).

Substantial evidence exists over many years for the involvement of de-differentiated SMC-like cells in vascular lesions that have been 'reprogrammed' from medial differentiated SMCs through a process of phenotypic modulation or switching (Albarrán-Juárez et al., 2016; Chappell et al., 2016; Herring et al., 2014; Nemenoff et al., 2011). Although the field has made tremendous progress in characterising the phenotypic changes in vascular SMCs, our understanding of phenotypic transition dynamics (spatio-temporal information and interdependence) and their respective contribution in subclinical atherosclerosis remains limited. Compelling evidence of SMC phenotypic and functional diversity has recently been provided through lineage tracing and single-cell RNA transcriptomics studies (scRNAseq) studies, or a combination of both (Dobnikar et al., 2018; Wirka et al., 2019). A rare number of medial Sca1 positive SMCs are thought to de-differentiate and populate atherosclerotic lesions by their selective expansion and investment concomitant with profound and diverse modifications of their original phenotype and function (Dobnikar et al., 2018). It is postulated that this subgroup of differentiated medial SMCs could transiently transition to a "pioneer" or "first responder" state due to priming by atherogenic stimuli or environmental selection.

In addition, an SMC-specific epigenetic repertoire of histone modifications is acquired when SMCs develop from ESCs, including H3K4me2 at SMC gene loci such as *Acta2* and *Myh11*, the latter being the most specific marker of SMC lineage (Manabe & Owens, 2001; McDonald et al., 2006; Miano et al., 1994). Notably, it has been suggested that the histone modification H3K4me2 at these gene-specific promoters is restricted to vascular SMCs, while is absent in non-SMC lineages. In addition, H3K4me2 enrichment at these genes persists when SMCs are induced to undergo phenotypic switching to a less differentiated de-differentiated state

typical of SMCs in cultured (McDonald et al., 2006) and SMC-like cells in vascular lesions (Dobnikar et al., 2018) when assessed by single gene ChIP-PCR analysis.

Several further studies have provided evidence that DNA methylation may occur during SMC de-differentiation and in subclinical atherosclerosis with an associated altered SMC phenotype within SMC-like cells (Liu et al., 2015). While the mechanisms of DNA methylation have been widely studied, the mechanism of DNA demethylation in mammals remains poorly characterized and somewhat controversial. Recently, the TET family of enzymes have been shown to oxidize 5mC to 5hmC in cultured SMCs. TET-2 is the predominant isoform in human coronary artery SMCs, and *TET-2* expression is highly enriched in vascular tissues. It increases with rapamycin-induced SMC differentiation, and decreases following PDGF-BB-induced SMC de-differentiation. Ectopic expression of TET-2 or knockdown approaches has revealed the role of TET-2 in SMCs. TET-2 overexpression promoted all aspects of SMC differentiation in cultured SMC, including induction of many SMC differentiation-specific and anti-proliferative genes, reduced proliferation, and an overall differentiated morphology. In contrast, the loss of TET-2 impaired SMC differentiation while increasing expression of SMC synthetic genes such as Krüppel-like factor 4 (KLF4) and non-muscle myosin heavy chain (MYH10).

In the wider context of epigenetic changes in SMCs, bulk ChIP-PCR and chromatin immunoprecipitation sequencing (ChIP-seq) assays have contributed significantly to our understanding of the role of histone modifications in SMC gene regulation. However, they do not permit analysis with single-cell resolution, thus confounding analyses of heterogeneous cell populations. To address this issue, a method was developed that permits visualization of histone modifications of single genomic loci with single-cell resolution in formaldehyde-fixed paraffin-embedded tissue sections based on combined use of *in situ* hybridization and proximity ligation assays (ISH-PLA) (Gomez et al., 2013). Using this novel technique, the authors reported that the H3K4me2 mark at the *MYH11* locus is restricted to the SMC lineage in human and mouse tissue sections and that the mark persists even in phenotypically modulated SMC in atherosclerotic lesions that show no detectable expression of SMC marker genes. Moreover, using this technique in combination with lineage tracing analysis, this group went further and demonstrated that medial SMC-derived cells exhibit phenotypes of several other cell lineages, including macrophages, osteoblasts and MSCs (Shankman et al., 2015).

More recently, elegant studies have emerged suggesting that H3K4me2 at the *Myh11* locus is necessary for the maintenance of their lineage identity and functions by employing gene- and cell-specific chromatin editing (Liu et al., 2021). Selective removal of H3K4me2 on the SMC gene repertoire led to a marked loss of contractility and alteration of the SMC adaptive response during vascular remodelling. Rather than presenting intrinsic gene activation properties, H3K4me2 serves as a stable hub for the dynamic recruitment of the DNA demethylase, TET-2. The H3K4me2/TET-2 complex controls the transcriptional activity of the SMC-specific gene repertoire, including contractile genes and miR-145, a key microRNA promoting SMC differentiation. Hence, these studies identified H3K4me2 imprinting as the central epigenetic mechanism controlling retention of lineage identity and cellular memory of SMC during adaptive processing requiring their transient dedifferentiation and phenotypic modulation (Liu et al., 2021).

Collectively, the studies suggest that together with DNA methylation/demethylation, histone modifications, in particular H3K4me2, represents classic interdependent epigenetic mechanisms controlling SMC gene expression in cultured cells and in vascular lesions. Since a common feature of SMC-like and non-SMCs within vascular lesions is the persistence of the H3K4me2 mark at the *Myh11* gene locus, despite this gene being transcriptionally silent, most studies have used the presence of this mark in a given cell of any phenotype as compelling evidence of that cell originating from a differentiated medial SMC. In contrast to SMCs, ESCs do not enrich for the H3K4me2 modification at the specific SMC gene promoters. Instead, the H3K27me3 histone modification, known to be involved in gene silencing, is present at these loci. Similar to ESCs, non-SMC somatic cells, for instance endothelial cells, skeletal muscle myotubes and leukocytes also contain high levels of H3K27me3 at the SMC gene promoters (McDonald et al., 2006). While originally thought to facilitate de-differentiated SMCs remaining permissive for re-differentiation during reversible phenotypic switching via retention of lineage identity and cellular memory of SMC, an alternative explanation cannot be ruled out.

In this context, the first objective of this study was to determine whether differentiated medial SMCs and/or de-differentiated MOVAS SMC enrich for the H3K4me2 mark at the *Myh11* gene locus when compared to undifferentiated ESCs. It has been known for some

time that chromatin is more open at CC(A/T)-rich GG (CArG)-containing regions of SMC gene loci where contractile proteins are highly expressed, compared to non-SMCs, where Myh11 and other smooth muscle-specific markers are not expressed (McDonald et al., 2006). Unlike the acetylation of histones which is diminished during the de-differentiation process, H3K4me2 persists through SMC phenotypic modulation and de-differentiation, despite reduced *Myh11* gene expression. The methylation of H3K4 is partially attributed to the recruitment of WD Repeat Domain 5 (WDR5) and the associated histone lysine methyltransferase SET/MLL by pituitary homeobox 2 (Pitx2) to SMC promoters in early stages of differentiation (Gan et al., 2011). In agreement with previous studies, the H3K4me2 mark is maintained in de-differentiated SMCs but at a significantly lower level compared to differentiated medial aortic SMCs. The level of enrichment of H3K4me2 at *Myh11* locus in mouse SMC in culture (MOVAS SMC) relative to mouse aorta tissue and mESC *in vitro* also revealed that while de-differentiated MOVAS SMCs retain the H3K4me2 mark, they are much less enriched for H3K4me2 at the *Myh11* locus compared to differentiated SMCs from within the medial layer. After removing the adventitial and endothelial layer, medial aortic segments consist primarily of differentiated SMCs which explains why they are highly enriched for H3K4me2 at this locus (Gomez et al., 2013). While mESCs can differentiate into SMC when they are not kept in their required maintenance medium, the data suggest that cultured mESCs maintained enrichment of the specific histone H3K27me3 mark at this locus which is to be expected and is widely associated with gene repression across multiple gene loci (Barski et al., 2007). In contrast, MOVAS SMCs, while enriched for the H3K4me2 mark albeit to a much lesser extent than aortic SMCs, had similar levels of enrichment of H3K27me3. Moreover, these levels were significantly less than observed in mESCs. Nevertheless, the presence of similar levels of enrichment of H3K4me2 and H3K27me3 at the *Myh11* locus in de-differentiated MOVAS SMCs may explain the lack of robust *Myh11* gene expression in these cells, compared to differentiated SMCs. The balance of these histone modifications is believed to alter the higher order chromatin structure through attraction or repelling of charged histone tails thereby regulating nucleosome density and the “accessibility” of various cis promoter-enhancer control elements (Gomez et al., 2015).

In this context, the second objective of this study was to determine whether MOVAS SMC lose the H3K4me2 mark at the *Myh11* gene locus in response to known atherogenic stimuli *in vitro*.

Interestingly, TGF-β1 treated MOVAS SMCs had lower levels of enrichment of H3K4me2 and Tet-2 binding concomitant with higher enrichment levels on H3K27me3 compared to untreated MOVAS SMCs. This may be due to the TGF-β1 stimulus promoting apoptosis of H3K4me2 enriched cells and stimulating a population of less differentiated cells within these cultures to differentiate into SMC as TGF-β1 is known to promote smooth muscle differentiation (Chen & Lechleider, 2004). Indeed, TGF-β1 did not reduce the levels of *Myh11* mRNA compared to MOVAS control. In contrast, PDGF-BB, which is purported to promote de-differentiation (Yoshida et al., 2007), did not change the levels of enrichment for both histone modifications at the *Myh11* locus (Liu et al., 2013) but did reduce Tet-2 binding (Torella et al., 2011). In agreement with previous studies, the H3K4me2 epigenetic mark at the *Myh11* locus persists through SMC phenotypic modulation in PDGF-BB treated MOVAS (Gomez et al., 2013) at a lower level when compared to fresh aorta with a reduction in the expression of the SMC differentiation marker, *Myh11* (Molony et al., 2018). Furthermore, the combination of both TGF-β1/ PDGF-BB treatment on MOVAS SMCs suggests the dominant stimulus prevails resulting in a lower level of enrichment of H3K4me2 and *Myh11* expression. Jagged-1 treatment of MOVAS SMCs, which is known to stimulate Notch signalling and promote myogenic differentiation (Kurpinski et al.,2010), did not increase *Myh11* expression but did increase the enrichment of H3K4me2 and the H3K4me2/H3K27me3 ratio suggesting that Jagged-1 is sufficient to activate epigenetic changes that promote SMC differentiation but was unable to ultimately determine a change in the phenotypic fate of these cells. Hence, we can conclude that the effects of TGF-β1 and Jagged-1 on SMC gene expression may be dependent on the differentiation state of the cells.

A summary of the effects of atherogenic stimuli on histone modifications in MOVAS SMC is presented in Table 3.1. When the level of enrichment of H3K4me2 at the *Myh11* locus is analysed following treatment of MOVAS SMCs with Jagged-1, TGF-β1, PDGF-BB and TGF-β1 /PDGF-BB, it is clear that these atherogenic stimuli differentially affect H3K4me2 enrichment and *Myh11* gene expression. Specifically, there was no change in the expression level of *Myh11* in Jag-1 or TGF-β1 treated cells despite significant changes in the level of H3K4 enrichment. In contrast, PDGF-BB did not affect H3K4me2 enrichment consistent with the reported stable H3K4me2 mark in PDGF-BB treated cells (Gomez et al., 2015) despite causing a significant decrease in *Myh11* gene expression. This suggests that once a cell is enriched

with H3K4me2 at the *Myh11* locus, this mark remains stable following PDGF-BB treatment even though there is a decrease in *Myh11* gene expression. This is not the case with TGF-β1, which significantly decreased the H3K4me2 mark with a concomitant increase in H3K27me3 despite no effect on *Myh11* gene expression.

In conclusion, it is clear that selective stimuli have a significant impact on the H3K4me2/H3K27me3 epigenetic signature with little effect on the transcript levels of *Myh11* in de-differentiated MOVAS SMCs. In contrast, the classic de-differentiation stimulus, PDGF-BB can move the transcript levels of the *Myh11* gene but fails to drive any changes in the H3k4me2 epigenetic signature.

Table 3.1. The level of enrichment of H3K27me3 and H3K27me3 at the *Myh11* locus and the level of *Myh11* expression in MOVAS SMCs following treatment with Notch ligand, Jag-1, PDGF-BB and TGF-β1 in relation to untreated MOVAS.

	Jagged-1	**TGF-β1**	**PDGF-BB**	**TGF-β1 /PDGF-BB**
H3K4me2	↑	↓	–	↓
H3K27me3	↓	↑	–	–
Myh11	–	–	↓	↓

For many years, lineage tracing studies have also provided compelling evidence that resident vascular stem cell-derived progeny may also play a significant role in initiating and progressing adaptive intimal thickening (Kramann et al., 2016; Tang et al., 2012; Wan et al., 2012). Recent lineage tracing studies from our own research group have recently provided further compelling evidence that S100β mVSCs and their progeny significantly contribute to lesion formation in murine models (Di Luca et al., 2021, Molony et al., 2021). These S100β cells may become activated, clonally proliferate and differentiate down vascular and non-vascular lineages that subsequently dictate, in part, lesion formation.

Enzymatic dispersion was used to isolate a population of stem cells from the medial layer of a mouse aortic arch. The aortic arch was chosen as this is a high risk area for arteriosclerotic lesion formation (Redheuil et al., 2010). The aortic arch has its embryological origin in the neuroectoderm and so many of the cells present in this area still express markers related to that origin (Bacakova et al., 2018). These cells are referred to as multipotent vascular stem cells (mVSCs) and express neural stem cell markers. Using ICC, S100β mVSCs expressed S100β and Nestin. While Sca1 has been previously reported to be upregulated in SMC phenotypic switching (Dobnikar et al., 2018) and a number of stem cell populations in both the adventitial and medial layers of the artery have been shown to express Sca1 (Sainz et al., 2006; Tang et al., 2020; Torsney et al., 2005). Interestingly, while S100β mVSCs were originally reported to be Sca1 negative (Tang et al., 2012), this could be due to the growth media which consisted of Dulbecco's modified essential medium (DMEM) with 10% fetal bovine serum (FBS), as opposed to the 1% FBS MM1 maintenance media used in this study. This could have led to a loss of Sca1 expression as these cells leave their undifferentiated state. These cells are Sca1 positive when grown and maintained in MM1 media with a low 1% FBS content (Di Luca et al., 2021). Neural crest stem cells have been previously shown to differentiate down a myogenic SMC lineage (High et al., 2007). In this study, S100β mVSCs express a range of neural stem cell markers (Di Luca et al., 2021) and are negative for SMC markers, such as *Myh11* and *Cnn1*. Clearly, the ratio of H3K4me2:H3K27me3 enrichment and the level of Tet-2 binding at the *Myh11* locus in cultured undifferentiated S100β mVSCs isolated from the aortic arch suggests that these cells also have a different epigenetic profile compared to freshly isolated differentiated medial SMCs and de-differentiated MOVAS SMCs in culture. Moreover, given that these cells do not enrich for the stable H3K4me2 mark at the *Myh11* locus, it is unlikely that they are derived from medial SMCs in general, or indeed, the rare population of Sca1/Myh11 positive medial SMCs that are thought to de-differentiate and populate atherosclerotic lesions, as both these medial cell populations are known to retain the H3K4me2 mark at this locus (Gomez et al., 2013; Shankman et al., 2015). In contrast, S100β mVSCs were enriched for the H3K27me3 mark, albeit not to the same extent as ESCs, further indicating their stem-like undifferentiated state. Like many other non-SMCs including endothelial cells, fibroblasts and ESCs in culture, this marked enrichment of H3K27me3 at the *Myh11* gene locus is consistent with transcriptional silencing of this gene in undifferentiated S100β cells (Tang et al., 2012, Di Luca et al., 2021). Therefore, this data clearly indicates that

the S100β mVSCs isolated from the mouse aortic arch are phenotypically undifferentiated stem cells derived from a neuroectodermal origin.

In this context, the third objective of this study was to determine whether S100β-derived myogenic SMC-like progeny acquire the H3K4me2 mark at the *Myh11* gene locus in response to known atherogenic stimuli *in vitro*. Therefore, the effects of three different pro-atherogenic stimuli (PDGF-BB, TGF-β1 and Notch ligand, Jag-1) known to be involved in subclinical atherosclerosis, SMC differentiation/de-differentiation and driving epigenetic changes in SMCs were assessed. The presence of the H3K4me2 mark at the *Myh11* locus on SMC-like cells within lesions that have not been cell fate mapped to a parent Myh11/Sca1 medial SMC (Tang et al., 2012, Di Luca et al., 2021) would therefore be consistent with the appearance of S100β-derived myogenic progeny (SMC-like cells) within vascular lesions. This parent S100β mVSC that resides in the adventitial and/or medial layer may become activated by pro-atherogenic stimuli, promoting the initial stages of subclinical atherosclerosis (Di Luca et al., 2021, Molony et al., 2021). In this context, the ratio of enrichment of H3K4me2 and H3K27me3 and Tet-2 binding at the *Myh11* promoter in S100β mVSCs was first determined before the repercussions on *Myh11* gene expression were evaluated. Notably, all three pro-atherogenic stimuli increased the ratio of H3K4me2:H3K27me3 enrichment and Tet-2 binding in S100β mVSCs to a similar extent with a concomitant increase in the expression of *Myh11* mRNA levels (Table 3.2). The levels of H3K4me2 and Tet-2 binding were similar to the levels observed in de-differentiated MOVAS SMC and were significantly lower than those observed in freshly isolated differentiated SMCs. It is clear that H3K4me2 is an important epigenetic mark that directs multipotent vascular progenitors toward SMC myogenic differentiation, and may play an important role in normal vascular development and during vascular disease progression. However, it is unclear how histone methyltransferases, which catalyse the methylation of H3K4me2, are specifically targeted to SMC target genes following pro-atherogenic stimulation and how the H3K4me2-marked SMC genes switch from silent to active state during embryogenesis or adult homeostasis. Therefore, while the H3K4me2 mark on SMC marker gene, *Myh11* is known to be restricted and a stable epigenetic signature of the SMC lineage distinguishing SMC from other cell types independently of their state of differentiation, the acquisition of this mark by S100β mVSCs suggests that S100β-derived

myogenic progeny could be responsible for the appearance of this mark in SMC-like cells within lesions.

Numerous studies have indicated that the manner by which stem cells contribute to lesion formation is through differentiation of these cells to become SMC-like cells (Wang et al., 2018). This differentiation is likely controlled in some part by Notch signalling, as several elements of that pathway have been reported to be upregulated during injury-induced vascular remodelling and Notch target genes have the ability to induce myogenic differentiation in stem cells (Morrow et al., 2005). Also published data from our research group suggested that both Jag-1 and TGF-β1 promoted myogenic differentiation of mesenchymal stromal stem cells (MSCs) *in vitro* by inducing specific epigenetic changes at the *Myh11* promoter leading to *Myh11* promoter transactivation, increased expression of transcript for SMC differentiation markers (*Myh11* and *Cnn1*) concomitant with a significant increase in the number of Myh11, Acta2 and Cnn1 positive cells (Molony et al., 2018). Data from this Chapter provides further evidence that S100β mVSCs that reside within the vessel wall can be stimulated by pro-atherogenic stimuli to undergo myogenic differentiation and acquire the H3K4me2 mark at the *Myh11* locus.

Table 3.2 The level of enrichment of H3K27me3 and H3K27me3 at the *Myh11* locus and the level of *Myh11* expression in S100β mVSCs following treatment with Notch ligand, Jag-1, PDGF-BB and TGF-β1 in relation to untreated S100β mVSCs.

	Jagged-1	**TGF-β1**	**PDGF-BB**
H3K4me2	↑	↑	↑
H3K27me3	↓	↓	↓
Myh11	↑	↑	↑
Tet-2	↑	↑	↑

In conclusion, the appearance of the H3K4me2 mark at the *Myh11* locus in S100β-derived progeny that are cell fate mapped to vascular lesions supports the overall hypothesis that S100β mVSCs may undergo differentiation to become SMC-like cells in response to pro-atherogenic stimuli typical of vascular injury *in vivo*, thus contributing to the formation of a neointimal lesion.

The fourth objective of the study was to determine whether the transcriptional and epigenetic profile of de-differentiated MOVAS SMC in culture is altered when these cells were grown and expanded in stem cell maintenance media (MM1 medium) compared to normal SMC growth media. SMCs are known to be plastic and undergo phenotypic switching and reprogramming (Gomez et al., 2013), so it was of interest to determine whether the epigenetic profile of de-differentiated SMCs would remain stable when cells were grown in media that maintains and promotes a stem-like phenotype. Using ChIP analysis and *S100*β, *Sox10*, *Myh11* and *Cnn1* mRNA levels, no change was observed in the ratio of H3K4me2:H3K27me3 enrichment or the transcript levels of any of the genes. While MOVAS SMCs are an immortalised SMC cell line that may not be capable of switching backwards towards a stem-like phenotype, pro-atherogenic stimuli were capable of differentially driving changes in the epigenetic profile and expression of SMC genes in these cells. It is known that the phenotype of differentiated vascular SMCs can be maintained by seeding cells on various extracellular matrices including laminin and supplementing the serum-free growth media with insulin or insulin-like growth factor-1. However, when these cells dedifferentiate and proliferative following treatment with serum, PDGF-BB, or lysophosphatidic acid (LPA), they fail to redifferentiate back to differentiated cells despite being cultured on laminin with media supplemented with insulin/ insulin-like growth factor-1. These published studies suggest that SMC dedifferentiation is regulated by the extracellular environment and that extracellular signaling is an important factor in this differentiation and dedifferentiation process. However, extracellular signaling is insufficient at driving redifferentiation of these dedifferentiated cells. In a similar manner, stem cell maintenance media appears insufficient at driving the epigenetic profile of de-differentiated SMCs to a more stem-like epigenetic phenotype.

The last objective of the study was to examine the putative role of the DNA demethylase, Tet-2 on the levels of enrichment of H3K4me2 and H3K27me3 at *Myh11* locus in de-differentiated

MOVAS SMC and undifferentiated S100β mVSCs using siRNA knockdown of Tet-2 expression before determining the repercussions on *Myh11* gene expression. Tet-2 has a major role in maintaining hematopoietic stem cell differentiation and is found to be frequently mutated in various forms of myeloid malignancies (Ko et al., 2010; Moran-Crusio et al., 2011; Valle et al., 2012). Robust expression of Tet-2 is also associated with the mature, contractile differentiated SMC phenotype (Liu et al., 2013). In agreement with previous studies (Liu et al., 2013), Tet-2 binding at the *Myh11* locus was reduced in MOVAS SMCs following treatment with the pro-atherogenic stimulus, PDGF-BB concomitant with a decrease in *Myh11* mRNA levels. However, the ratio of H3K4me2:H3K27me3 remained stable. In contrast, TGF-β1 decreased both Tet-2 binding and the ratio of H3K4me2:H3K27me3 at the *Myh11* locus without affecting Myh11 gene expression. Moreover, Jag-1 did not affect Tet-2 binding but increased the ratio of H3K4me2:H3K27me3 at the *Myh11* locus without affecting gene expression (Table 3.3). These data suggest that there is a significant disconnect between the level of Tet-2 following treatment with pro-atherogenic stimuli and the ratio of H3K4me2:H3K27me3 and *Myh11* gene expression in de-differentiated MOVAS SMCs. The ratio of H3K4me2:H3K27me3 can change independent of any baseline changes in Tet-2 binding suggesting that the relationship between Tet-2 and these specific histone modifications is not directly quantitatively correlated in de-differentiated SMCs following treatment with atherogenic stimuli. As histone methylation, a reversible post-translational modification, is written by histone methyltransferase enzymes (HMTs) and erased by histone demethylases (HDMTs), it is likely that other factors could be at play (Xie et al, 2020).

Table 3.3 The effect of Notch ligand, Jag-1, TGF-β1 and PDGF-BB on Tet-2 binding to the *Myh11* locus in MOVAS SMC in relation to MOVAS.

	Notch ligand, Jag-1	**TGF-β1**	**PDGF-BB**
Tet-2	–	↓	↓
H3K4me2/H3K27me3	↑	↓	–

Methylation of H3 is one chromatin modification that defines distinct regulatory states of euchromatin. Mammals express 6 main HMTs that modify H3K4 by mono-, di-, or tri-methylation that include three pairs of SET/MLL paralogs (SETD1A/SETD1B, MLL1/MLL2, and MLL3/MLL4). All HMTs exhibit H3K4me activity when in complex with their protein partners, which include WDR5, Retinoblastoma binding protein 5 (RbBP5), Absent, small or homeotic 2-like protein (ASH2L) and Protein DPY-30 homolog (DPY30) ("WRAD"), critical for the enzymatic activity of the Su(var)3–9/Enhancer of Zeste/Trithorax (SET), or catalytic domain of MLL1-4 and the SET proteins (Yang et al., 2017). In addition to these core component differences, there are differences in transiently interacting proteins among these family members, due to the unique sequences of each of the six enzymes. The expression of MLL1-4 and SET proteins are all fairly ubiquitous, resulting in co-expression of most enzymes in most tissues. Correspondingly, the ε-amine group of lysine can be marked with monomethylation (me1), dimethylation (me2), and trimethylation (me3) by suppressor of variegation, enhancer of Zeste (Ezh), Trithorax (SET) domain-containing protein lysine methyltransferases or non-SET-domain-containing protein lysine methyltransferases. Therefore it remains to be seen if pro-atherogenic stimuli differentially control these key regulatory enzymes that modify H3K4 in dedifferentiated SMCs. The main principle emerging from murine knockout studies is that despite similarity between paralogs and co-expression in many of the same tissues, each H3K4 HMT has mainly unique, non-redundant functions, although one can find examples of redundancy. In this context, previous studies have shown that the histone methyltransferase EZH2 may play an important role in lesion formation *in vivo* and PDGF-BB markedly increased H3K27me3 and Ezh2 levels *in vitro* (Liang et al., 2019). Inhibition of Ezh2/1 activity by UNC1999 significantly suppressed PDGF-BB-induced SMC proliferation and neointima formation following wire-guided common carotid injury, which was mediated by increasing the transcription of the cyclin-dependent kinase inhibitor (p16INK4A).

To address the specific contribution of the DNA demethylase, Tet-2 in co-ordinating the methylation of histones by HMTs, Tet-2 knockdown studies were performed. Using transcript and western blot analysis, a significant knockdown of Tet-2 was confirmed after siRNA treatment of MOVAS SMCs. In MOVAS SMC, the level of enrichment of H3K4me2 at the *Myh11* locus at baseline was dramatically decreased in the Tet-2 knockdown cells concomitant with a significant rise in the level of enrichment of H3K27me3 (Table 3.4). While

the ratio of H3K4me2:H3K27me3 enrichment was significantly reduced following Tet-2 knockdown, the repercussions of Tet-2 knockdown on *Myh11* and *Cnn1* gene expression were less clear. The expression of *Cnn1* was significantly reduced following Tet-2 knockdown but *Myh11* levels remained relatively stable. The reason for this at present is unclear but may be due to the partial nature of the knockdown (~50%). Nevertheless, it is clear that reducing Tet-2 in MOVAS SMCs reduced the methylation of H3K4me2 concomitant with a reduction in some SMC-specific genes. The functional consequences of modifying H3K4me2 on SMC phenotype has also recently been addressed where H3K4me2 editing induced a profound alteration of SMC lineage identity by redistributing H3K4me2 toward genes associated with stemness and developmental programs (Liu et al., 2021).

Table 3.4 The level of enrichment of H3K27me3, H3K27me3 at the *Myh11* locus and ratio H3K27me3/H3K27me3 in Tet-2 siRNA treated MOVAS SMCs compared to scrambled control.

	Tet-2 siRNA
H3K4me2	↓
H3K27me3	↑
Ratio	↓

For S100β mVSCs, the specific contribution of the DNA demethylase, Tet-2 in co-ordinating the methylation of H3 histones by HMTs was also assessed. The level of Tet-2 expression was lower in S100β cells compared to MOVAS SMC. Tet-2 binding at the *Myh11* locus was increased in S100β mVSCs following treatment with pro-atherogenic stimuli (Table 3.5). In particular, PDGF-BB treatment increased *Myh11* mRNA levels concomitant with an increase in the ratio of H3K4me2:H3K27me3 and Tet-2 binding at the *Myh11* locus. Similar profiles were evident for TGF-β1 and Jag-1. These data suggest that, unlike MOVAS SMCs, there is a direct correlation between the level of Tet-2 following treatment with pro-atherogenic stimuli and the ratio of H3K4me2:H3K27me3 and *Myh11* gene expression in S100β mVSCs.

Table 3.5 The effect of Notch ligand, Jag-1, TGF-β1 and PDGF-BB on Tet-2 binding to the *Myh11* locus in S100β mVSCs in relation to untreated S100β mVSCs.

	Notch ligand, Jag-1	**TGF-β1**	**PDGF-BB**
Tet-2	↑	↑	↑
H3K4me2/H3K27me3	↑	↑	↑

To address this relationship, Tet-2 knockdown studies using siRNA were also performed on S100β mVSCs before and after treatment with TGF-β1/PDGF-BB and confirmed by measuring baseline and stimulated Tet-2 mRNA levels. While the knockdown of Tet-2 was less robust than MOVAS SMCs at baseline, this is most likely due to the fact that the baseline levels of Tet-2 are low in these cells. When stimulated with TGF-β1/PDGF-BB, the levels of Tet-2 increased, an effect that was attenuated following Tet-2 knockdown. The repercussion of Tet-2 knockdown on the epigenetic profile following TGF-β1/PDGF-BB treatment suggests there is a direct correlation between the ability of TGF-β1/PDGF-BB to stimulate enrichment of H3K4me2 at the *Myh11* locus and *Tet-2* expression and Tet-2 binding at the same locus (Table 3.6). Moreover, the loss of *Tet-2* expression, binding and enrichment of H3K4me2 at the Myh11 locus results in attenuation of TGF-β1/PDGF-BB activation of SMC genes, *Myh11* and *Cnn1.* It is noteworthy that the change in the ratio of H3K4me2:H3K27me3 is a result of changes to H3K4me2 without a significant effect on H3K27me3 enrichment (Table 3.6). It has previously been reported that PDGF-BB markedly increased H3K27me3 and Ezh2 levels in SMCs, an effect also evident from this study using MOVAS SMCs, albeit modest. However, PDGF-BB decreased H3K27me3 enrichment at the *Myh11* locus in S100β mVSCs. This inhibition is unaffected following Tet-2 knockdown suggesting that the reduction in H3K27me3 by TGF-β1/PDGF-BB is independent of Tet-2 as it is not reversed when Tet-2 is diminished.

Table 3.6 The level of enrichment of H3K27me3, H3K27me3 at the *Myh11* locus and ratio H3K27me3/H3K27me3 in Tet-2 siRNA treated S100β mVSCs at baseline and following atherogenic stimuli compared to scrambled control.

	Tet-2 siRNA Baseline	**Tet-2 siRNA + atherogenic stimuli**
H3K4me2	↑	↓
H3K27me3	↓	–
Ratio	↑	↓

In summary, the data in this Chapter confirm that the level of enrichment of H3K4me2 at the *Myh11* gene locus in de-differentiated MOVAS SMC is reduced when compared with differentiated SMCs from fresh aortic tissue, but is never lost. S100β mVSCs isolated from the aortic arch are highly enriched for H3K27me3 at the *Myh11* locus. However, following treatment with different pro-atherogenic stimuli, S100β mVSCs acquire this SMC epigenetic signature of H3K4me2 at the *Myh11* gene locus and lose the H3K27me3 mark at the same locus. Many studies have indicated that the manner by which stem cells contribute to lesion formation is through partial differentiation to SMC-like cells (Wang et al., 2018). This differentiation is likely controlled in some part by TGF-β1, PFDG-BB and Notch signalling, as several elements of these pathways have been reported to be upregulated during injury-induced vascular remodelling (Morrow et al., 2005). The DNA demethylase, Tet-2 has an emerging role in changing the epigenetic signature of S100β mVSCs as it can specifically dictate the enrichment of H3K4me2 at the *Myh11* locus when these cells undergo myogenic differentiation in response to atherogenic stimuli. This is not the case for undifferentiated SMCs. The appearance of the H3K4me2 mark at the *Myh11* locus is consistent with the partial myogenic differentiation of S100β mVSCs to SMC-like cells and supports cell fate mapping studies that confirm the presence of S100β-derived myogenic progeny in significant numbers within vascular lesions (Di Luca et al., 2021). Taken together, these findings confirm that SMC-like cells typical of vascular lesions that have the H3K4me2 epigenetic mark at the *Myh11* locus are as likely to have been derived from an S100β parent cell population following activation by pro-atherogenic stimuli when compared to the more established paradigm that

these SMC-like cells are differentiated SMCs derived from differentiated medial SMCs. If this is indeed the case, the targeting of these pathways in stem cells may offer some therapeutic advantage in reducing the accumulation of SMC-like cells in vascular lesions.

It is clear that SMC-like cells within lesions that house the H3K4me2 signature at the *Myh11* locus may be derived from an S100β parent. However, previous *Myh11*-Cre-LoxP (cyclization recombinase)-(locus of x-over, P1) cell fate mapping studies in murine models of vascular injury and disease had also suggested that many of the non-SMC-like cells (osteocytes, myeloid-like cells, adipocytes and MSC-like cells) within these lesions may also be derived from differentiated medial SMCs. In this context, up to 40% of myeloid-like cells (macrophage-like) that are cell fate mapped to a Myh11 medial SMC also house the H3K4me2 signature at the *Myh11* locus despite displaying a non-SMC phenotype (Gomez et al., 2013). The next Chapter will address whether S100β mVSCs may also acquire the H3K4me2 epigenetic mark at the *Myh11* locus following differentiation into several non-SMC cell phenotypes and ultimately contribute to the accumulation of not only SMC-like cells but also non-SMCs within vascular lesions to obstruct blood flow.

Chapter 4

The level of enrichment of H3K4me2, H3K27me3 and Tet-2 binding at the *Myh11* locus in mouse and human S100β mVSCs following myogenic, osteogenic, adipogenic and vasculogenic differentiation *in vitro*

4.1 Introduction

Among the large variety of different post-translational modifications, methylation histone 3 lysine 4 (H3K4) position has been widely studied (Robertson et al., 2008). Depending on the number of methyl groups attached to the lysine residual, there are three common forms, namely H3K4me1, H3K4me2 and H3K4me3. It has been shown that while H3K4me1 preferentially exists around enhancer regions, H3K4me3 preferentially exists around gene promoter regions (Heintzman et al., 2007) whereas H3K4me2 exists in both enhancers and promoters regions with a positive role in facilitating gene transcription (Koch & Andrau, 2011; Pekowska et al., 2011). The previous Chapter of results confirmed that H3K4me2 is an important epigenetic mark at the myosin heavy-chain 11 *(Myh11)* locus that directs multipotent vascular progenitors toward smooth muscle cell (SMC) myogenic differentiation in a ten-eleven-translocation 2 (Tet-2)-dependent manner. This process may play an important role during vascular disease progression and the accumulation of SMC-like cells within lesions. This Chapter will address whether these multipotent resident vascular stem cells are also capable of differentiation towards non-SMC lineages such as osteogenic (osteocytes), adipogenic (adipocytes) and vasculogenic (endothelial cells) *in vitro.* In addition, whether these cells acquire the H3K4me2 epigenetic mark at the *Myh11* locus in that process of non-SMC lineage specification and whether this could account for the presence of this mark in non-SMCs within vascular lesions during vascular disease progression.

Several previous studies have suggested that differentiated SMCs are capable of dedifferentiation and redifferentiation into several discrete phenotypes within the vessel wall following injury and during disease progression (Espinosa-Diez et al, 2021). De-differentiated SMCs are considered prone to further differentiate into alternative phenotypes such as osteogenic-like, macrophage-like (myeloid) and MSC-like cells that have inherent tri-lineage multipotency capacity including adipogenic, osteogenic and chondrogenic differentiation.

Several *in vitro* studies have shown that SMCs can undergo phenotypic transition to osteoblasts in a calcified environment, determined by an increased expression of the osteocyte markers, including sclerostin *(Sost)* (Zhu et al., 2011). While no studies have reported SMC differentiation into adipogenic-like cells, several studies have shown that

adipocytes can differentiate into SMC-like cells (Wang et al., 2010). In the case of vasculogenic differentiation, SMCs have been shown to differentiate into endothelial-like cells and express endothelial markers, such as platelet endothelial cell adhesion molecule 1 (PECAM1) (Hong et al., 2017). When vascular SMCs were treated with oxidised low-density lipoprotein (LDL), cells gradually dedifferentiated into macrophage-like cells, with an increase in the macrophage marker, Cluster of differentiation 68 (CD68) (Yuan et al., 2022). Differentiation of SMCs to MSC-like cells has been reported and these mesenchymal stem cell (MSC)-like cells have the capacity to differentiate into osteogenic, adipogenic and chondrogenic-like cells if they acquire the tri-lineage multipotent capacity of classical MSCs (Pan et al., 2020).

Each lineage is determined by the upregulation of lineage-specific genes. When osteoblasts cells were maintained in 3D cultures for 10 days, there was a significant increase in the *Sost* and Alkaline phosphatase *(Alpl)* genes known for osteocytes (Sawa et al., 2019). Lipoprotein lipase *(LPL)* and fatty acid binding protein 4 (*FABP4)* both are related to adipogenesis during differentiation and both increased throughout the differentiation process from preadipocytes to adipocytes (Wang et al., 2018). Using immunocytochemistry vasculogenic differentiation of mouse embryonic stem Cells (ESC) was confirmed by checking for Pecam1-positive cells which were induced under vascular endothelial growth factor (VEGF) stimulation (Kanki et al., 2017).

Several studies have shown that the initiation and progression of vascular calcification likely involves both active and passive mechanisms (Montezano et al., 2010; Speer et al., 2009; Urry, 1971). Passive calcification relies on the natural affinity of elastin and collagen in the extracellular matrix (ECM) for calcium ions which eventually lead to vascular calcification (Urry, 1971). On the other hand, active vascular calcification resembles physiological bone mineralization. The cells in the vessel walls differentiate or transdifferentiate into osteoblast-like cells in the pro-calcific milieu of atherosclerosis. The osteoblast-like cells initiate vascular calcification by releasing matrix vesicles (MV) (Zazzeroni et al., 2018) that are loaded with mineral crystals and deposited in the ECM. Mineralized MVs have been detected in the calcified lesions of atherosclerosis (Kapustin et al., 2011, 2015).

Importantly, H3K4me2 at the *Myh11* locus is maintained in SMCs that have undergone transition to both SMC-like cells and a macrophage-like state within mouse and human lesions (Shankman et al., 2015). Allahverdian et al showed that 50% of foam cells within advanced human coronary artery lesions are positive for α-smooth muscle actin (ACTA2), CD68 and Oil Red O marks (Allahverdian et al., 2014). Taken together, SMCs appear to contain a much larger burden of the excess cholesterol in human coronary atherosclerosis than previously known, in part, because of their relative inability to release excess cholesterol via ATP-binding cassette transporter 1 in comparison with myeloid lineage and may indicate that many cells identified as monocyte-derived macrophages in human atherosclerotic lesions are in fact SMC-derived cells (Allahverdian et al., 2014; Shankman et al., 2015).

Two different studies concluded that differentiated medial SMCs are responsible for the accumulation of the majority of SMC-like cells and a sizable proportion of non-SMC (e.g., macrophage-like) cells within vascular lesions (Chappell et al., 2016; Feil et al., 2014). Moreover, all of these cells are also enriched with the H3K4me2 mark at the *Myh11* locus (Gomez et al., 2013).

However, the SMC differentiation towards non-SMC cells *in vitro* and *in vivo* have been questioned. Tang et al. provided data in vitro using cell culture and lineage tracing experiments indicating that differentiated vascular mature SMCs are incapable of proliferation either in vivo in response to injury or in vitro in cell culture. Instead, there exists a small population (<10%) of undifferentiated MSCs in the media that proliferate to completely reconstitute medial cells in response to vascular injury. This has been supported by a publication from our lab which concluded that SMCs in culture are derived from a non-SMC but from an S100 calcium-binding protein β (S100β) parent population following flow restriction (Di Luca et al., 2021). *In vivo*, it has been reported that Tamoxifen can remain in tissues and induce fluorescent tag expression in cells for up to four weeks after the last injection has taken place (Reinert *et al.*, 2012). This could result in stem cells following myogenic or non-myogenic differentiation being tagged as of SMC origin.

Several *in vitro* studies have also shown that undifferentiated S100β stem cells can undergo transition to osteogenic, adipogenic and vasculogenic progeny either directly or indirectly

through an MSC-like intermediate (Tang et al., 2012). MSCs have the capacity to develop into several cell types, i.e., adipocytes, myocytes, chondrocytes, and osteocytes (Covas et al., 2008; Huang et al., 2009; Lin et al., 2010; New et al., 2015). Model cell culture systems have been indispensable in identifying and characterising the steps in the commitment and differentiation programs. Myogenic differentiation is stimulated by the presence of transforming growth factor beta (TGF-β) (Park et al., 2013), neurogenic differentiation by the presence of forskolin and valproic acid (New et al., 2015), and osteogenic cell differentiation by the presence of β-glycerol phosphate, ascorbic acid, dexamethasone (Tirkkonen et al., 2013) and dihydroxyvitamin D_3 (Logovskaya et al., 2013). Bone marrow-derived MSCs may differentiate into multiple cell types that are involved in cardiovascular pathologies, including vascular calcification (Liao et al., 2012).

Sera et a., successfully generated adipocytes from mouse hematopoietic stem cells *in vivo* and were stained positively with *Fabp4* (Sera et al., 2009). When cultured in osteogenic media, MSCs express markers known to be expressed by bone forming osteoblasts, which are the cells responsible for laying down the matrix and mineral during new bone formation *in vivo* (Huang *et al*., 2007). Osteocyte marker gene expression increases following osteogenic differentiation, especially *Sost* (Feng et al., 2006; Poole et al., 2005). Maul *et al* successfully differentiated rat MSCs to endothelial cells and found an incline in expression levels of *Pecam1* (Maul et al., 2011).

Lineage tracing studies have provided compelling evidence for a role for both de-differentiated SMCs (Chappell et al., 2016) and S100β stem cell-derived myogenic progeny (Di Luca et al., 2021) in the accumulation of SMC-like cells within vascular lesions. Moreover, many non-SMC-like cells (osteogenic, adipogenic and myeloid-like cells) also appear to be derived from differentiated SMC as they track to Myh11 parent cells and importantly retain the H3K4me2 mark at the *Myh11* locus. While the data in Chapter 3 confirms that S100β stem cell-derived myogenic progeny [that originated from a stem cell antigen-1 (Sca1)/S100β parent cell accumulate in vascular lesions following injury (Di Luca et al., 2021)] acquire the H3K4me2 mark at the *Myh11* locus *in vitro*, the question remained whether S100β stem cell-derived progeny other than myogenic (adipogenic, osteogenic, vasculogenic) also acquire this mark at the same locus. This will be addressed in this Chapter by examining their epigenetic

signature at the *Myh11* locus following lineage-specific differentiation of S100β murine multipotent resident vascular stem cells (mVSCs) and human induced pluripotent stem cells (hiPSC) derived S100β progenitor stem cells to myogenic and non-SMC phenotypes.

Therefore the major aim of this Chapter was to determine whether S100β stem cells (mouse and human) acquire this H3K4me2 mark at the *Myh11* locus when these cells undergo adipogenic, osteogenic or vasculogenic differentiation *in vitro* and thus may be responsible for the presence of this signature in adipocyte-, osteocyte- and endothelial-like cells in lesions.

Objectives:

The main aims of this chapter were:

1. To determine the epigenetic profile of S100β murine multipotent resident vascular stem cells (mVSCs) following adipogenic, osteogenic and vasculogenic differentiation to determine whether a common epigenetic H3K4me2 mark exists at the *Myh11* locus when undifferentiated S100β mVSCs undergo chromatin remodelling as they specialise down various cell lineages.
2. To determine the epigenetic profile of S100β human multipotent neuroectoderm progenitor stem cells (SNEPs) following adipogenic, osteogenic and vasculogenic differentiation to determine whether a common epigenetic H3K4me2 mark exists at the *MYH11* locus when undifferentiated stem cells undergo chromatin remodelling as they specialise down various cell lineages.

4.2 Strategy

In order to investigate the multipotency of mouse S100β mVSCs and hiPSC-derived S100β SNEPs following differentiation down into myogenic, adipogenic, osteogenic and vasculogenic lineages *in vitro,* S100β mVSCs and S100β SNEPs were cultured in their maintenance medium and respective inductive media for each lineage as described in Chapter 2, Section 2.2.2. The expression level of specific genes for each lineage were measured to confirm lineage-specific

differentiation using quantitative real-time polymerase chain reaction (qRT-PCR) as described in Chapter 2, section 2.2.9. This included *Myh11* and Calponin1 *(Cnn1)* genes for myogenic differentiation, *Alpl* and *Sost* genes for osteogenic differentiation, *Lpl* and *Fabp4* genes for adipogenic differentiation and the *Pecam-1* gene for vasculogenic differentiation. Staining with alizarin Red S Dye and oil Red O Dye was performed as described in Chapter 2, sections 2.2.14 and 2.2.13, to assess osteogenic and adipogenic differentiation, respectively.

Data for all experiments in this section was generated over at least three biological replicates. Normality tests were used to determine if data followed a parametric distribution pattern. Variation across samples was analysed by calculating p-values. The type of test used to calculate this was governed by the outcome of the normality test. Statistical significance was assigned to p-values <0.05.

4.3 Results

4.3.1 Adipogenic and osteogenic progeny acquire the H3K4me2 mark at the *Myh11* locus independent of any change in *Myh11* mRNA levels in resident mouse S100β mVSCs *in vitro.*

S100β mVSCs were seeded at the required density before cells were treated with myogenic, vasculogenic and osteogenic differentiation medium for 21 days and adipogenic differentiation medium for 14 days as described in Chapter 2, Section 2.2.2. Specific changes in cell morphology and staining with alizarin Red S Dye and oil Red O Dye were performed to assess osteogenic and adipogenic differentiation, respectively.

The DNA was isolated, fixed and prepared to perform ChIP analysis as described in section 2.2.4. The transcript levels of *Myh11* and *Cnn1* were assessed by qRT-PCR as outlined in Chapter 2, Section 2.2.9.

When S100β mVSCs were grown in various differentiation media over time, there was a notable change in cell morphology as the cells lost their multipotent vascular stem-like shape and characteristics [Figure 4.1]. Myogenic cells become elongated and display typical 'hill and valley' characteristics, typical of vascular SMCs. Osteogenic cells become round, large, irregularly shaped cells typical of osteocytes in culture, while adipogenic cells become round

and irregularly shaped typical of adipocytes in culture. Vasculogenic cells adopt a cobblestone morphology typical of endothelial cells in culture. The morphology of S100β mVSCs following treatment with different differentiation media indicates differentiation of S100β mVSCs. Notably, S100β mVSCs grown in adipogenic differentiation medium also stained positively for Oil Red O while S100β mVSCs cultured in osteogenic differentiation medium stained positively for Alizarin Red [Figure 4.2]. Oil Red O and Alizarin Red stains indicate differentiation of S100β mVSCs into adipocytes and osteocytes respectively.

The level of *Myh11* and *Cnn1* gene expression in S100β mVSCs cultured in myogenic differentiation was significantly higher compared to S100β mVSCs grown in maintenance medium [Figure 4.3]. The expression of osteogenic genes, *Alpl* and *Sost,* were significantly increased in S100β mVSCs cultured in osteogenic differentiation medium when compared to S100β mVSCs grown in stem cell maintenance type 1 (MM1) medium [Figure 4.4]. The expression of adipogenic genes, *Lpl* and *Fabp4 were* significantly increased in S100β mVSCs cultured in adipogenic differentiation medium when compared to S100β mVSCs grown in stem cell maintenance (MM1) medium [Figure 4.5]. The expression of lineage-specific genes confirms the differentiation of S100β mVSCs.

The level of enrichment of H3K4me2 at the *Myh11* locus was first assessed by ChIP analysis using S100β mVSCs grown in their maintenance medium (MM1) and compared to S100β mVSCs grown in vasculogenic (endothelial), myogenic (smooth muscle), adipogenic (adipocyte) and osteogenic (bone) differentiation medium by measuring H3K4me2 binding to DNA compared to the Immunoglobulin G (IgG) control. There was a significant enrichment of H3K4me2 in S100β mVSCs grown in myogenic, adipogenic and osteogenic differentiation medium when compared to S100β mVSCs grown in stem cell maintenance medium [Figure 4.6]. In contrast, there was no significant enrichment of H3K4me2 in vasculogenic progeny when compared to undifferentiated cells [Figure 4.6]. Notably, myogenic, adipogenic and osteogenic differentiation media was sufficient for S100β mVSCs to acquire the epigenetic mark of H3K4me2 at the *Myh11* locus.

In parallel studies, the level of enrichment of H3K27me3 in the same samples was also assessed by ChIP assay. There was a significant reduction in the level of enrichment of

H3K27me3 at the *Myh11* locus in S100β mVSCs grown in myogenic and osteogenic differentiation medium compared to S100β mVSCs in stem cell maintenance medium [Figure 4.7]. There was no significant change in the enrichment of H3K27me3 in S100β mVSCs grown in vasculogenic and adipogenic differentiation medium when compared to maintenance medium [Figure 4.7]. Notably, myogenic and osteogenic differentiation media was sufficient for S100β mVSCs to lose the silent epigenetic mark of H3K27me3 at the *Myh11* locus. Furthermore, the ratio of H3K4me2:H3K27me3 was significantly higher in S100β mVSCs grown in myogenic and osteogenic differentiation medium when compared to S100β mVSCs in stem cell maintenance medium [Figure 4.8]. The ratio of H3K4me2:H3K27me3 was increased but did not reach the level of significance in S100β mVSCs grown in adipogenic differentiation medium when compared to S100β mVSCs in stem cell maintenance medium [Figure 4.8]. There was no significant difference in the ratio of H3K4me2:H3K27me3 in S100β mVSCs grown in vasculogenic differentiation media compared to undifferentiated S100β mVSCs [Figure 4.8]. The increase in the level of enrichment of H3K4me2 at the *Myh11* locus along with the reduction in the level of enrichment of H3K27me3 at the same locus resulted in an increased ratio S100β mVSCs-derived myogenic and osteogenic progeny.

The level of enrichment of Tet-2 binding at the *Myh11* locus was also assessed by ChIP analysis in S100β mVSCs grown in their maintenance medium and compared to S100β mVSCs grown in vasculogenic (endothelial), myogenic (smooth muscle), adipogenic (adipocyte) and osteogenic (bone) differentiation medium by measuring Tet-2 binding compared to the IgG control. There was a significant increase in the level of Tet-2 binding in S100β mVSCs grown in myogenic, adipogenic and osteogenic differentiation medium when compared to S100β mVSCs in stem cell MM1 medium [Figure 4.9]. There was no significant difference in Tet-2 binding in S100β mVSCs grown in vasculogenic differentiation media [Figure 4.9]. Collectively, myogenic, adipogenic and osteogenic differentiation media was sufficient for S100β mVSCs to increase the level of Tet-2 binding at the *Myh11* locus.

The relative level of *Myh11* and *Cnn1* messenger RNA (mRNA) transcript was measured by qRT-PCR in S100β mVSCs grown in maintenance medium (MM1) and compared to S100β mVSCs grown in vasculogenic (endothelial), myogenic (smooth muscle), adipogenic

(adipocyte) and osteogenic (bone) differentiation medium. There was a significant increase in *Myh11* and *Cnn1* mRNA in S100β mVSCs grown in myogenic differentiation medium [Figure 4.10 and Figure 4.11]. There was no significant change in *Myh11* and *Cnn1* mRNA levels in S100β mVSCs grown in vasculogenic, adipogenic and osteogenic differentiation medium, respectively, when compared to S100β mVSCs grown in cell maintenance medium. Collectively, SMC gene expressions increased only following myogenic differentiation media of S100β mVSCs.

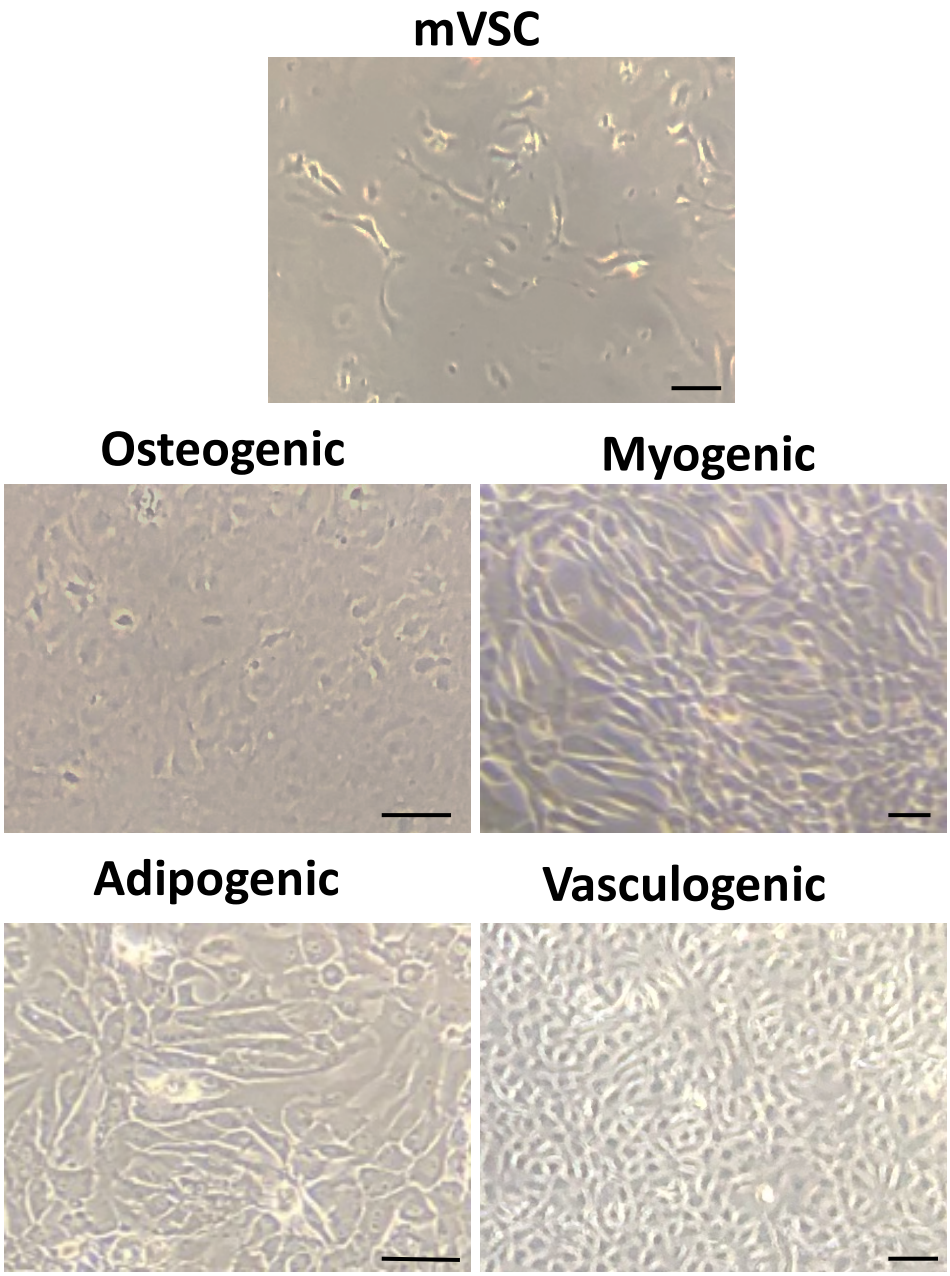

Figure 4.1. The effect of lineage-specific differentiation media on the morphological characteristics of S100β mVSCs and their derived progeny. Representative phase contrast images of S100β mVSCs grown in their growth maintenance medium (MM1) and compared to S100β mVSCs grown in vasculogenic (endothelial), myogenic (smooth muscle) and osteogenic (bone) for 21 days and adipogenic (adipocyte) for 14 days. Scale bar is 50µm.

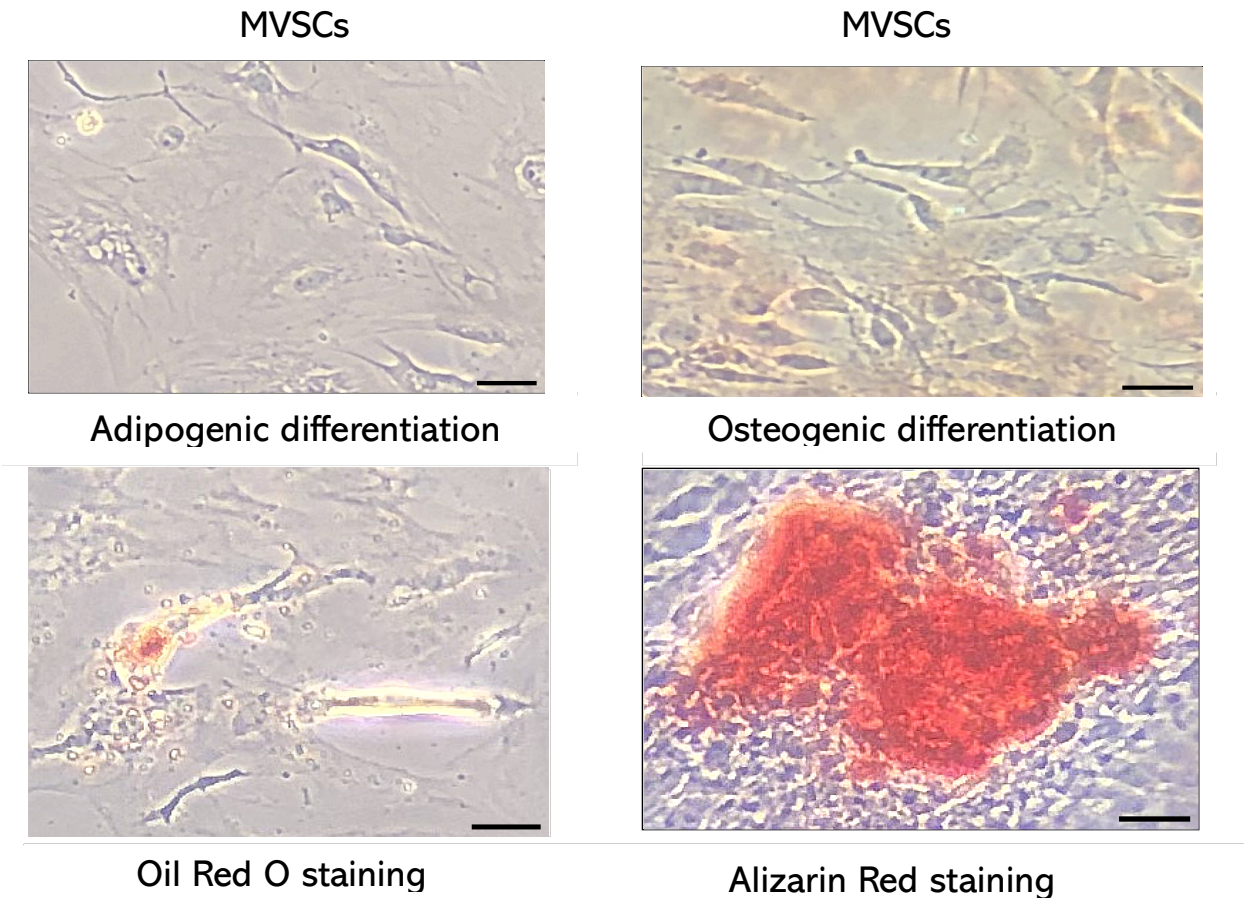

Figure 4.2 S100β mVSCs exhibit adipogenic and osteogenic potential. Representative phase contrast images of S100β mVSCs grown in adipogenic differentiation medium stained with Oil Red O (left panel) and osteogenic differentiation medium stained with Alizarin Red (right panel). Scale bar is 50µm.

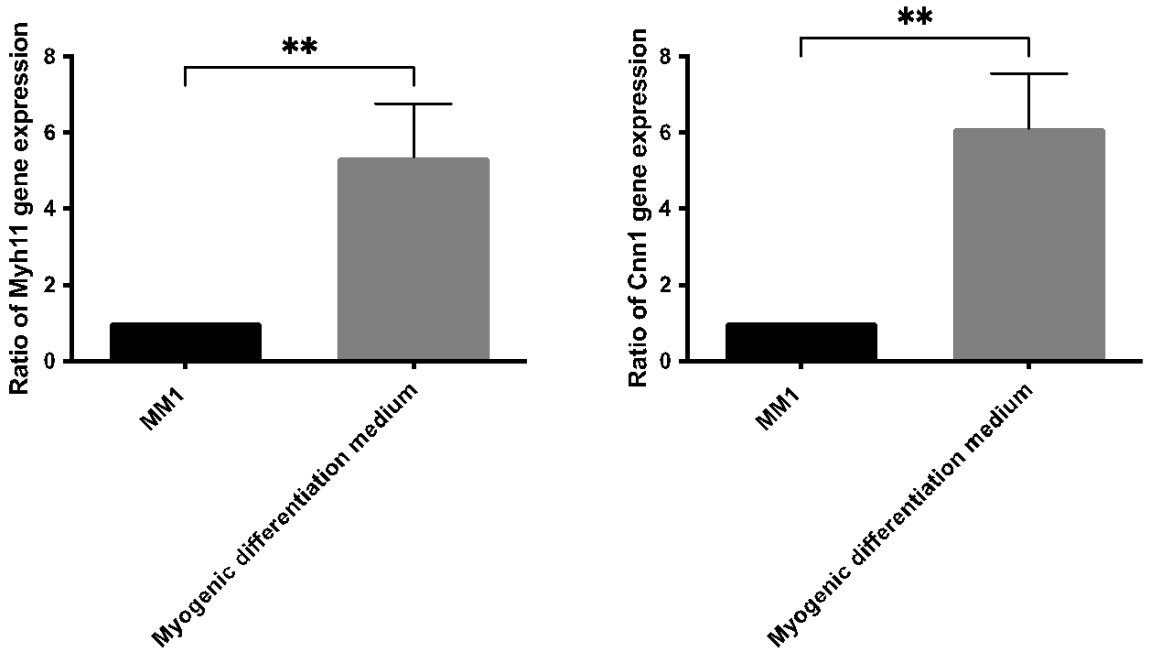

Figure 4.3. Expression of *Myh11* and *Cnn1* mRNA in S100β mVSCs following growth in their maintenance medium (MM1) compared to S100β mVSCs grown in myogenic differentiation medium. *Myh11 and Cnn1 expression* was measured in S100β mVSCs in their maintenance medium (MM1) and compared to S100β mVSCs grown in myogenic differentiation medium for 21 days. Total RNA was isolated from cells before the relative levels of *Myh11* and *Cnn1* transcript was measured by qRT-PCR with GAPDH as an internal control. Data are expressed as the ratio of gene expression (R) and represent the mean ± SEM of 3 experiments performed in triplicate.**p<0.01

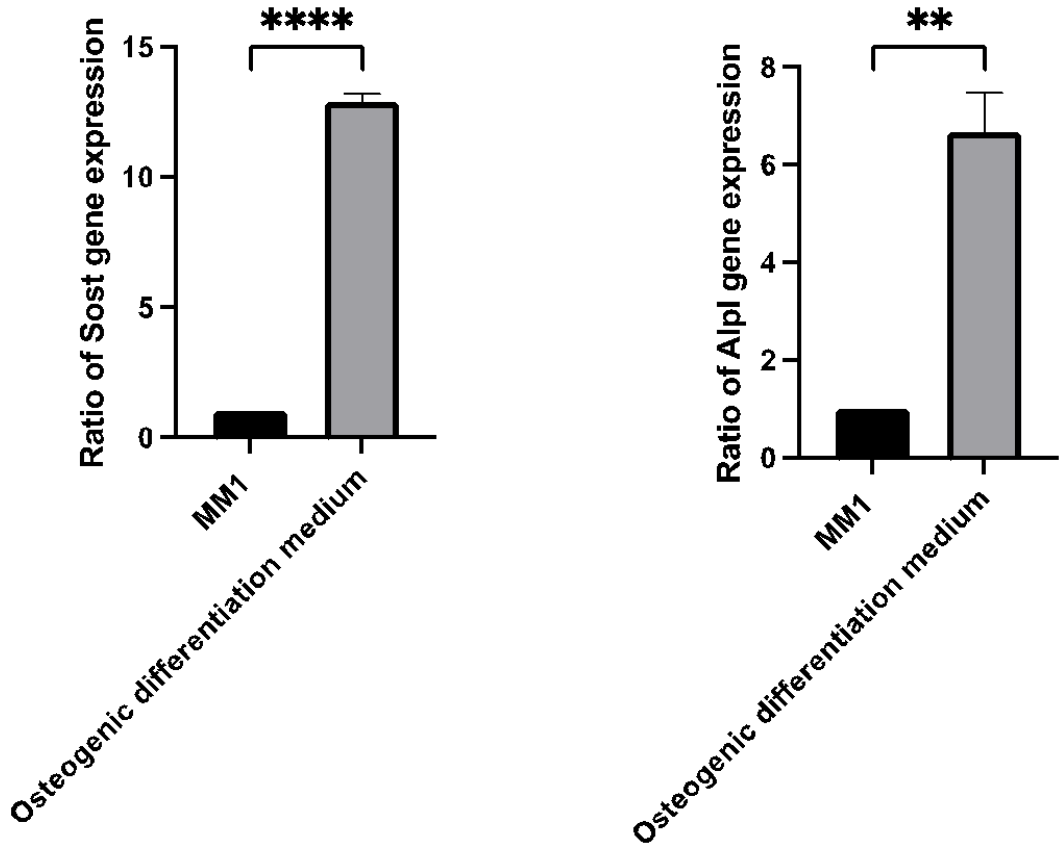

Figure 4.4. Expression of *Alpl* and *Sost* mRNA in S100β mVSCs following growth in their maintenance medium (MM1) compared to S100β mVSCs grown in osteogenic differentiation medium. *Alpl* and *Sost* expression was measured in S100β mVSCs in their maintenance medium (MM1) and compared to S100β mVSCs grown in osteogenic differentiation medium for 21 days. Total RNA was isolated from cells before the relative levels of *Alpl* and *Sost* transcript was measured by qRT-PCR with GAPDH as an internal control. Data are expressed as the ratio of gene expression (R) and represent the mean ± SEM of 3 experiments performed in triplicate. ** $p<0.01$ **** $p<0.0001$

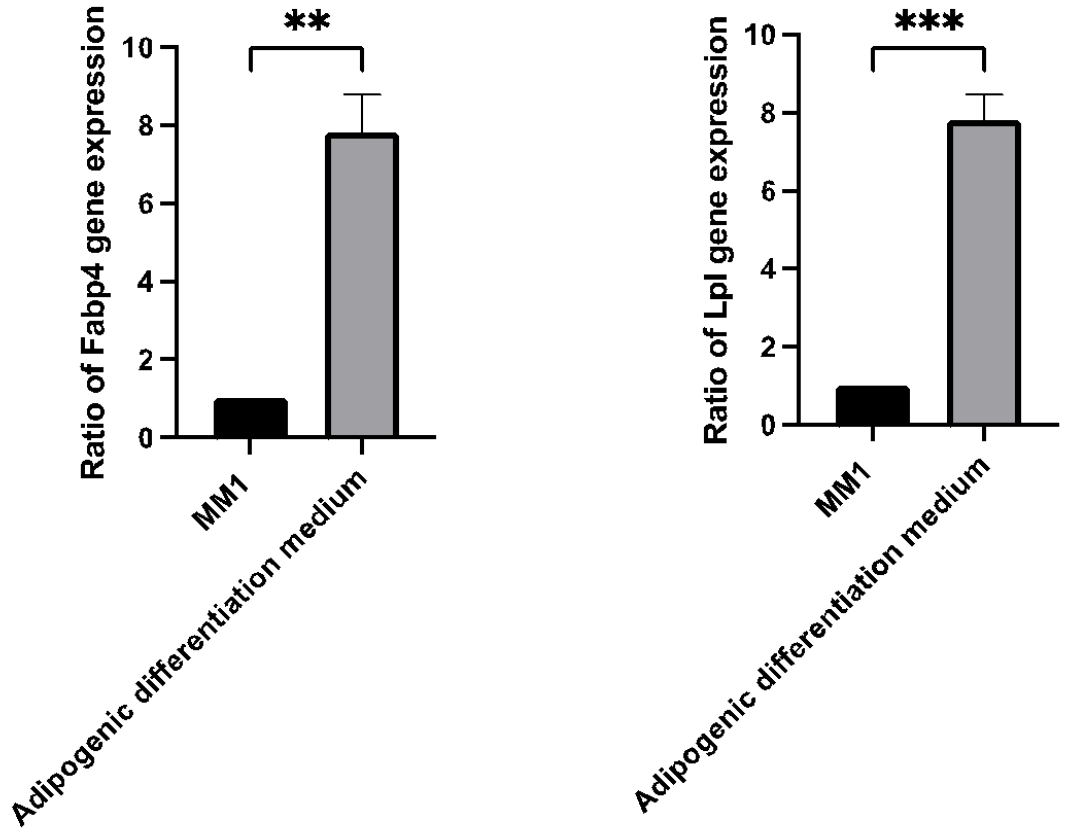

Figure 4.5. Expression of *Lpl* and *Fabp4* mRNA in S100β mVSCs following growth in their maintenance medium (MM1) compared to S100β mVSCs grown in adipogenic differentiation medium. *Lpl* and *Fabp4* expression was measured in S100β mVSCs in their maintenance medium (MM1) and compared to S100β mVSCs grown in adipogenic differentiation medium for 14 days. Total RNA was isolated from cells before the relative levels of *Lpl* and *Fabp4* transcript was measured by qRT-PCR with GAPDH as an internal control. Data are expressed as the ratio of gene expression (R) and represent the mean ± SEM of 3 experiments performed in triplicate. ** $p<0.01$ *** $p<0.001$

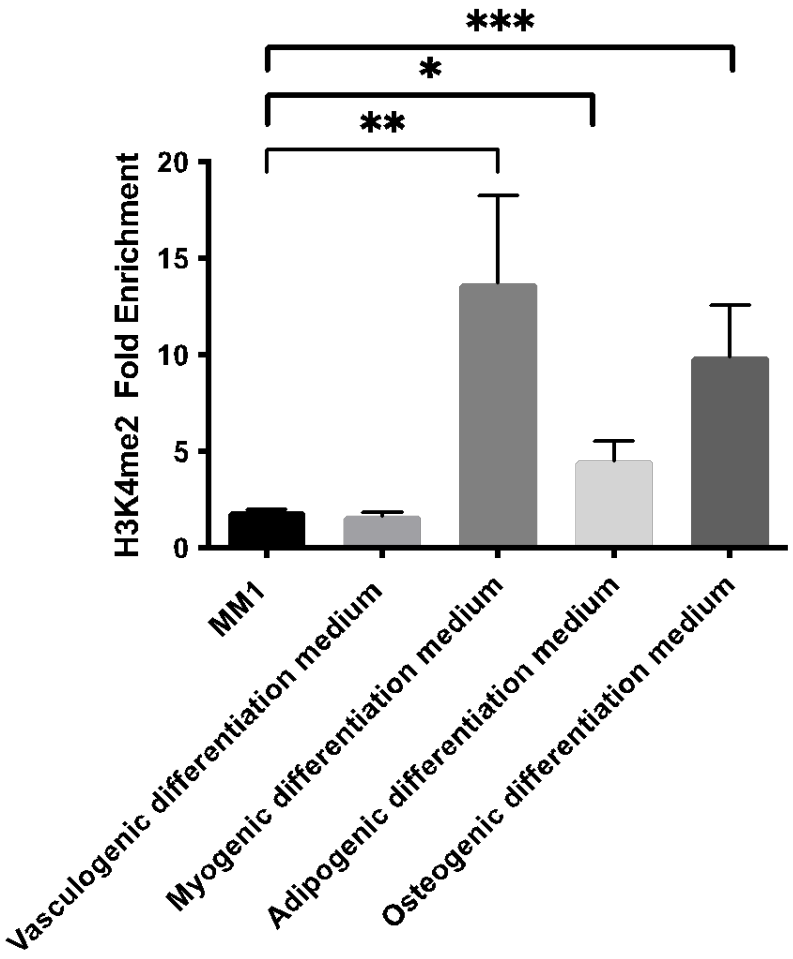

Figure 4.6. The level of enrichment of H3K4me2 at the *Myh11* locus in S100β mVSCs following growth in their maintenance medium (MM1) compared to S100β mVSCs grown in vasculogenic (endothelial), myogenic (muscle), adipogenic (fat) and osteogenic (bone) differentiation medium. S100β mVSCs were seeded at the required density in order to obtain a confluent T75 flask in 21 days. H3K4me2 binding at the *Myh11* locus was assessed by ChIP assay and corrected against the IgG control. Fold enrichment was determined for each condition and the data are the mean ± SEM of 3 experiments performed in triplicate. * $p<0.05$ ** $p<0.01$ *** $p<0.001$.

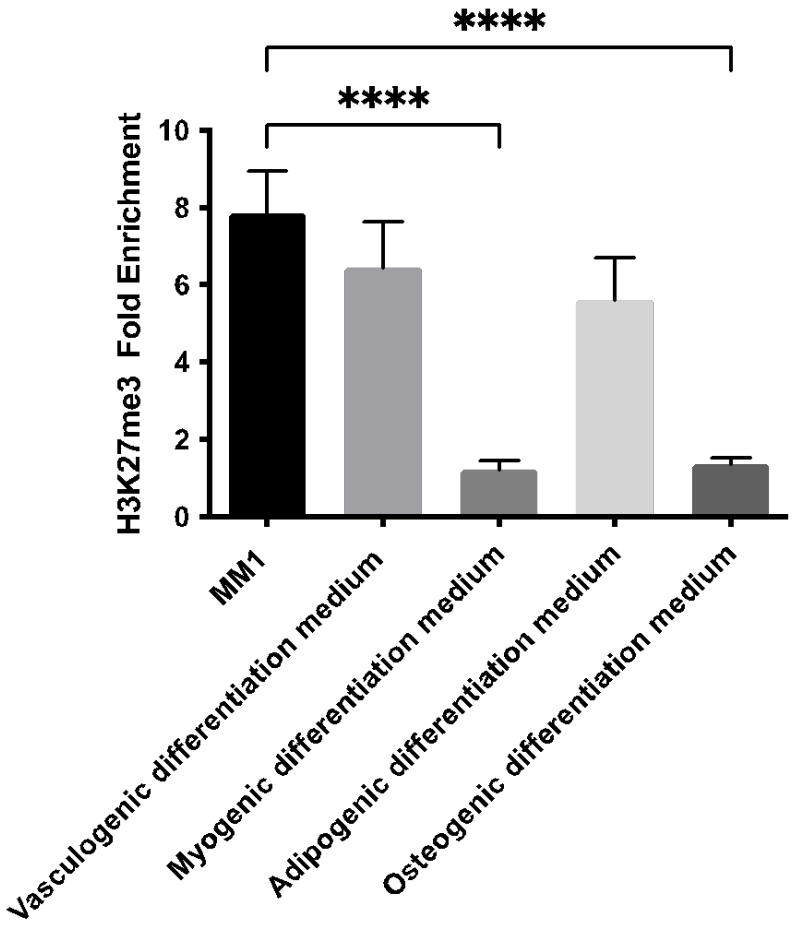

Figure 4.7. The level of enrichment of H3K27me3 at the *Myh11* locus in S100β mVSCs following growth in their maintenance medium (MM1) compared to cells grown in vasculogenic (endothelial), myogenic (muscle), adipogenic (fat) and osteogenic (bone) differentiation medium. H3K27me3 binding at the *Myh11* locus was assessed by ChIP assay and corrected against the IgG control. Fold enrichment was determined for each condition and the data are the mean ± SEM of 3 experiments performed in triplicate. **** $p<0.0001$

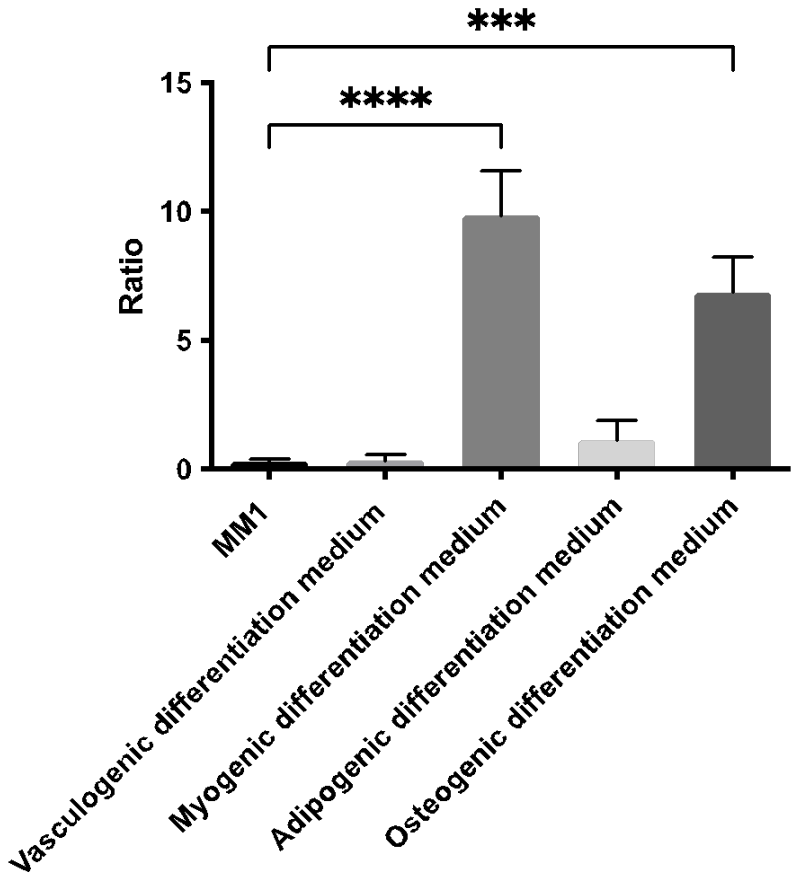

Figure 4.8. The ratio of H3K4me2/H3K27me3 enrichment at the *Myh11* locus in S100β mVSCs following growth in their maintenance medium (MM1) compared to cells grown in vasculogenic (endothelial), myogenic (muscle), adipogenic (fat) and osteogenic (bone) differentiation medium. The level of enrichment of H3K4me2 and H3K27me3 binding at the *Myh11* locus was assessed by ChIP assay and corrected against the IgG control. The ratio of H3K4me2 and H3K27me3 binding was determined for each condition and the data are the mean ± SEM of 3 experiments performed in triplicate. *** $p<0.001$ **** $p<0.0001$

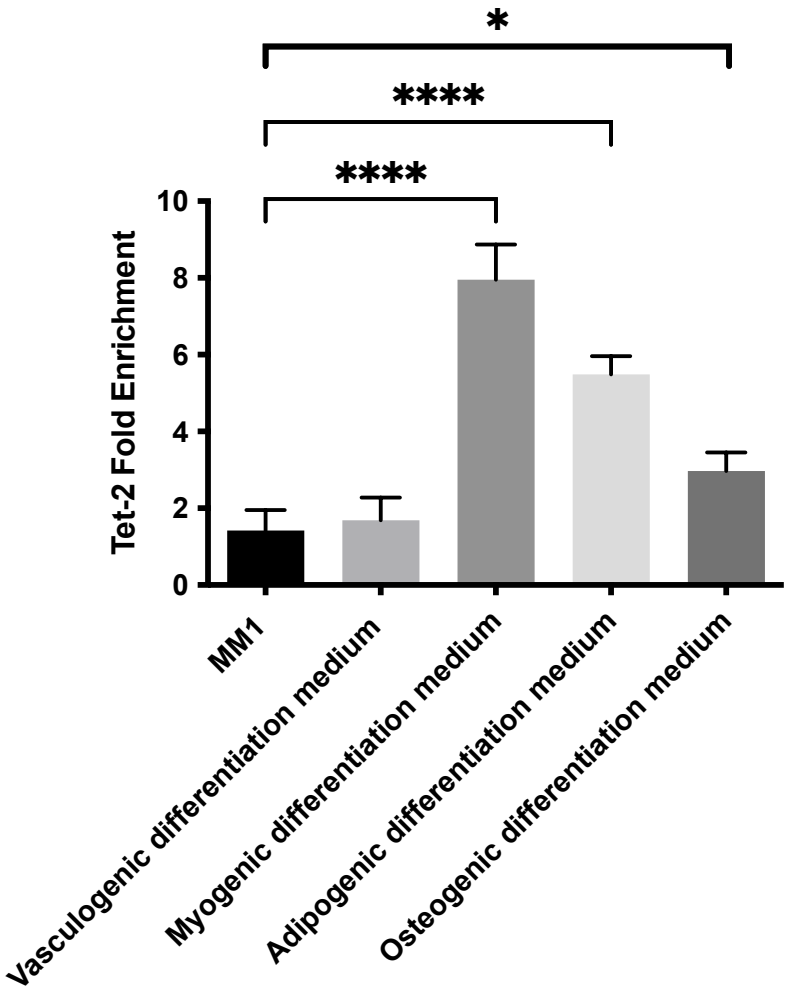

Figure 4.9. Tet-2 fold enrichment at the *Myh11* locus in S100β mVSCs following growth in their maintenance medium (MM1) compared to cells grown in vasculogenic (endothelial), myogenic (muscle), adipogenic (fat) and osteogenic (bone) differentiation medium. Tet-2 protein binding at the *Myh11* locus was assessed by ChIP assay and corrected against the IgG control. Fold enrichment was determined for each condition and the data are the mean ± SEM of 3 experiments performed in triplicate * $p<0.05$ **** $p<0.0001$

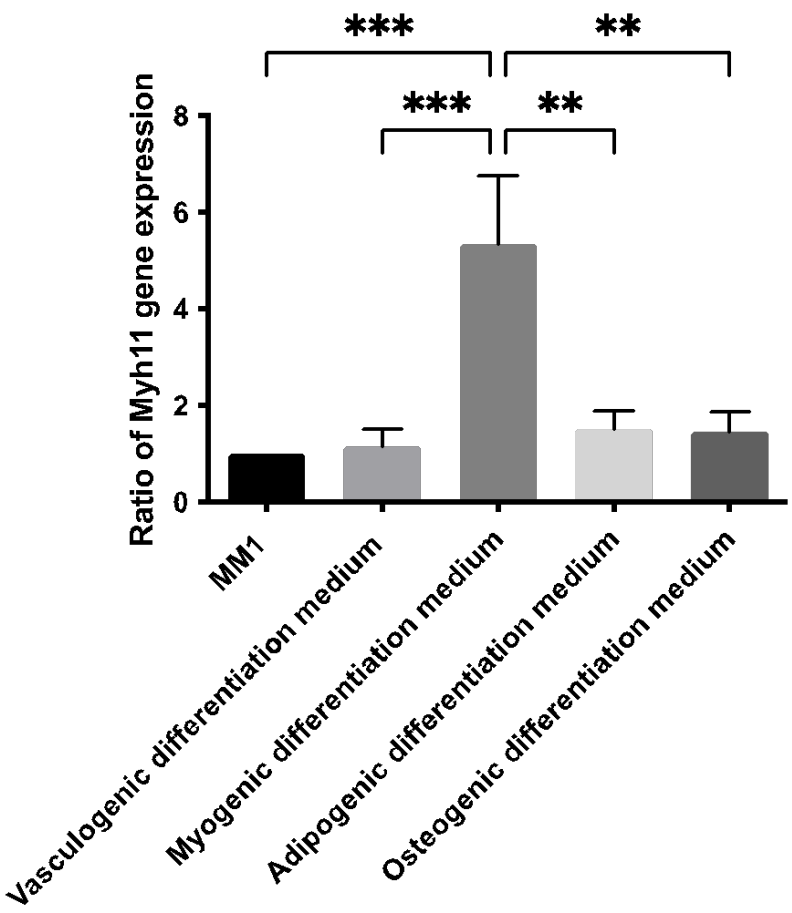

Figure 4.10. Expression of *Myh11* mRNA in S100β mVSCs following growth in their maintenance medium (MM1) compared to cells grown in vasculogenic (endothelial), myogenic (muscle), adipogenic (fat) and osteogenic (bone) differentiation medium. *Myh11* expression was measured after 21 days. Total RNA was isolated before the relative levels of *Myh11* transcript was measured by qRT-PCR with GAPDH as an internal control. Data are expressed as the ratio of gene expression (R) and represent the mean ± SEM of 3 experiments performed in triplicate. ** $p<0.01$ *** $p<0.001$ **** $p<0.0001$

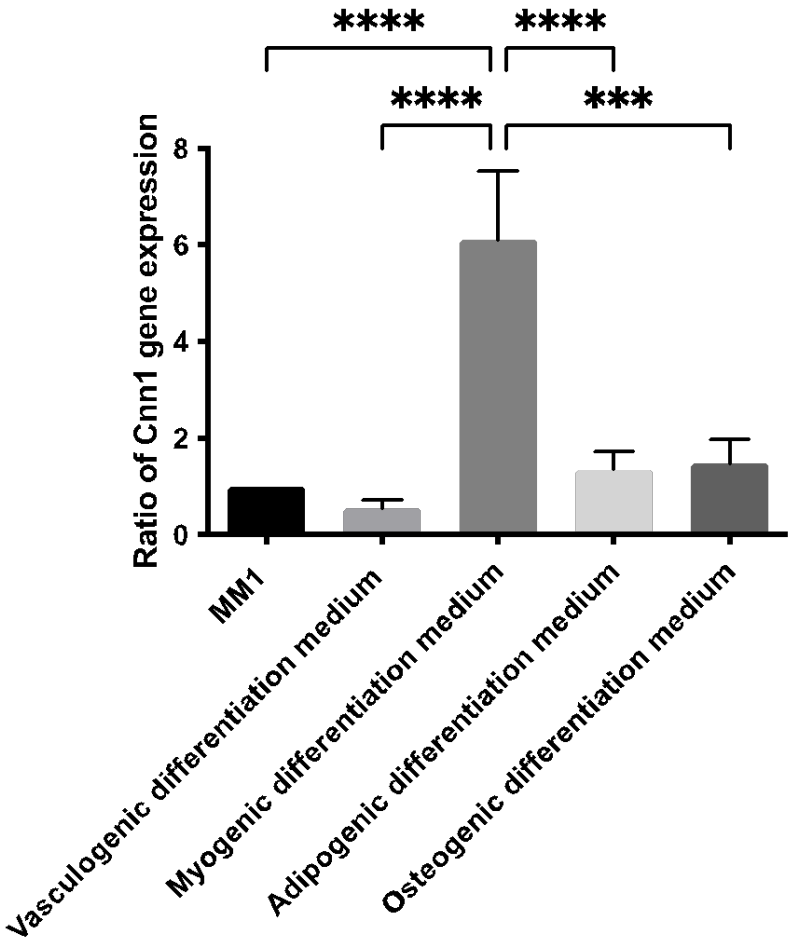

Figure 4.11. Expression of *Cnn1* mRNA in S100β mVSCs following growth in their maintenance medium (MM1) compared to cells grown in vasculogenic (endothelial), myogenic (muscle), adipogenic (fat) and osteogenic (bone) differentiation medium. Total RNA was isolated from cells before the relative levels of *Cnn1* transcript was measured by qRT-PCR with GAPDH as an internal control. Data are expressed as the ratio of gene expression (R) and represent the mean ± SEM of 3 experiments performed in triplicate. ** $p<0.01$ *** $p<0.001$ **** $p<0.0001$

4.3.1.1 Summary:

The ChIP results suggest that undifferentiated mouse S100β mVSCs grown in their maintenance medium (MM1) are not highly enriched for H3K4me2 at the *Myh11* locus. This enrichment increases significantly when S100β mVSCs undergo myogenic, adipogenic and osteogenic differentiation. Parallel studies revealed a significant decrease in H3K27me3 mark at the same locus when cells undergo myogenic and osteogenic differentiation. The ratio of H3K4me2:H3K27me3 was significantly increased in S100β mVSCs grown in myogenic and osteogenic differentiation medium despite the fact that *Myh11* and *Cnn1* mRNA levels did not increase in S100β mVSCs following osteogenic differentiation medium. Tet-2 binding levels increased when S100β mVSCs were grown in myogenic, adipogenic and osteogenic differentiation medium.

4.3.2 Adipogenic and osteogenic differentiation acquire the H3K4me2 mark at the *Myh11* locus independent of any change in *Myh11* mRNA levels in human iPSC derived S100β SNEP *in vitro.*

The hiPSC derived S100β SNEPs were seeded at the required density to obtain a confluent T75 flask were grown in myogenic differentiation medium for 12 days, vasculogenic and osteogenic differentiation medium for 21 days and adipogenic differentiation medium for 14 days, respectively, as described in Chapter 2, Section 2.2.2. Specific changes in cell morphology and staining with alizarin Red S Dye and oil Red O Dye was performed to assess osteogenic and adipogenic differentiation, respectively.

The DNA was isolated, fixed and prepared for ChIP analysis as described in Chapter 2, Section 2.2.4. The transcript levels of *MYH11* and *CNN1* were assessed by qRT-PCR as outlined in Chapter 2, Section 2.2.9.

The morphology of S100β SNEPs significantly changed over time when cells were grown in their respective myogenic, adipogenic, osteogenic and vasculogenic differentiation medium when compared to S100β SNEPs grown in their maintenance medium. There was a notable change in their morphology as the cells lost their multipotent vascular stem-like, and became less rounded and more elongated [Figure 4.12]. Myogenic cells become elongated and

display 'hill and valley' characteristics, typical of SMCs. Osteogenic progeny became round, large, irregularly shaped cells, typical of osteocytes in culture, while adipogenic cells became round and irregularly shaped typical of adipocytes in culture. Vasculogenic cells adopted a cobblestone morphology typical of endothelial cells in culture. The morphology of S100β SNEPs following treatment with different differentiation medium indicates differentiation of S100β SNEPs.

S100β SNEPs cultured in osteogenic differentiation medium stained positively with Alizarin Red and the absorbance measured 405 nm increased following osteogenic differentiation [Figure 4.13]. S100β SNEPs grown in adipogenic differentiation medium also stained positively with Oil Red O and the absorbance measured 510 nm increased following adipogenic differentiation [Figure 4.14]. Absorbance of the dyes indicate differentiation of S100β SNEPs into adipocytes and osteocytes.

The level of *MYH11* and *CNN1* gene expression in S100β SNEPs cultured in myogenic differentiation was significantly higher compared to undifferentiated cells grown in their maintenance medium [Figure 4.15]. The level of *PECAM1* gene expression in S100β SNEPs cultured in vasculogenic differentiation was significantly higher compared to undifferentiated cells [Figure 4.16]. Similarly, the level of *ALPL* and *SOST* gene expression in S100β SNEPs following culture in osteogenic differentiation medium was significantly higher when compared to undifferentiated cells [Figure 4.17]. The level of *LPL* and *FABP4* gene expression was also significantly higher in S100β SNEPs following culture in adipogenic differentiation medium when compared to undifferentiated cells [Figure 4.18]. The expression of lineage-specific genes confirms the differentiation of S100β SNEPs.

The level of enrichment of H3K4me2 at the *MYH11* locus was next assessed by ChIP analysis in S100β SNEPs grown in their respective differentiation medium by measuring H3K4me2 binding to DNA and compared to the IgG control. There was a significant enrichment of H3K4me2 in S100β SNEPs grown in myogenic and osteogenic progeny when compared to undifferentiated cells [Figure 4.19]. There was a notable increase in the enrichment of H3K4me2 (albeit that it did not reach the level of significance) in adipogenic progeny when compared to undifferentiated cells [Figure 4.19]. Notably, myogenic and osteogenic

differentiation media was sufficient for S100β SNEPs to acquire the epigenetic mark of H3K4me2 at the *MYH11* locus. In parallel studies, the level of enrichment of H3K27me3 in the same samples was also assessed by ChIP assay. There was a significant reduction in the level of enrichment of H3K27me3 at the *MYH11* locus in S100β SNEP-derived vasculogenic, myogenic, adipogenic and osteogenic progeny when compared to undifferentiated cells [Figure 4.20]. All four lineage differentiation media was sufficient for S100β SNEPs to lose the epigenetic mark of H3K27me3 at the *MYH11* locus. Furthermore, the ratio of H3K4me2:H3K27me3 was significantly higher in myogenic, adipogenic and osteogenic progeny [Figure 4.21]. There was no significant increase in the ratio of H3K4me2:H3K27me3 in S100β SNEP following vasculogenic differentiation [Figure 4.21]. Notably, changes in the two histones were sufficient for S100β SNEPs to increase the ratio following myogenic, adipogenic and osteogenic differentiation media.

The level of enrichment of TET-2 binding at the *MYH11* locus was next assessed by ChIP analysis in S100β SNEPs grown in their respective myogenic, adipogenic, osteogenic and vasculogenic medium by measuring TET-2 binding to DNA and compared to the IgG control. There was a significant increase in the level of TET-2 binding in myogenic and osteogenic progeny, when compared to undifferentiated cells [Figure 4.22]. There was a notable increase in the level of TET-2 binding in adipogenic progeny, albeit it did not reach a level of significance [Figure 4.22]. There was no significant increase in TET-2 binding in vasculogenic progeny [Figure 4.22]. Collectively, myogenic and osteogenic differentiation media was sufficient for S100β SNEPs to increase TET-2 binding at the *MYH11* locus.

The relative level of *MYH11* and *CNN1* mRNA transcript was measured by qRT-PCR in S100β SNEPs and their myogenic, adipogenic, osteogenic and vasculogenic progeny. There was a significant increase in *MYH11* and *CNN1* mRNA in myogenic progeny only [Figure 4.23 and Figure 4.24]. There was no significant change in *MYH11* and *CNN1*mRNA levels in S100β SNEPs grown in vasculogenic, adipogenic and osteogenic differentiation medium, respectively, when compared to S100β SNEPs grown in cell maintenance medium. Collectively, SMC gene expressions of *MYH11* and *CNN1* only increased following myogenic differentiation medium of S100β SNEPs.

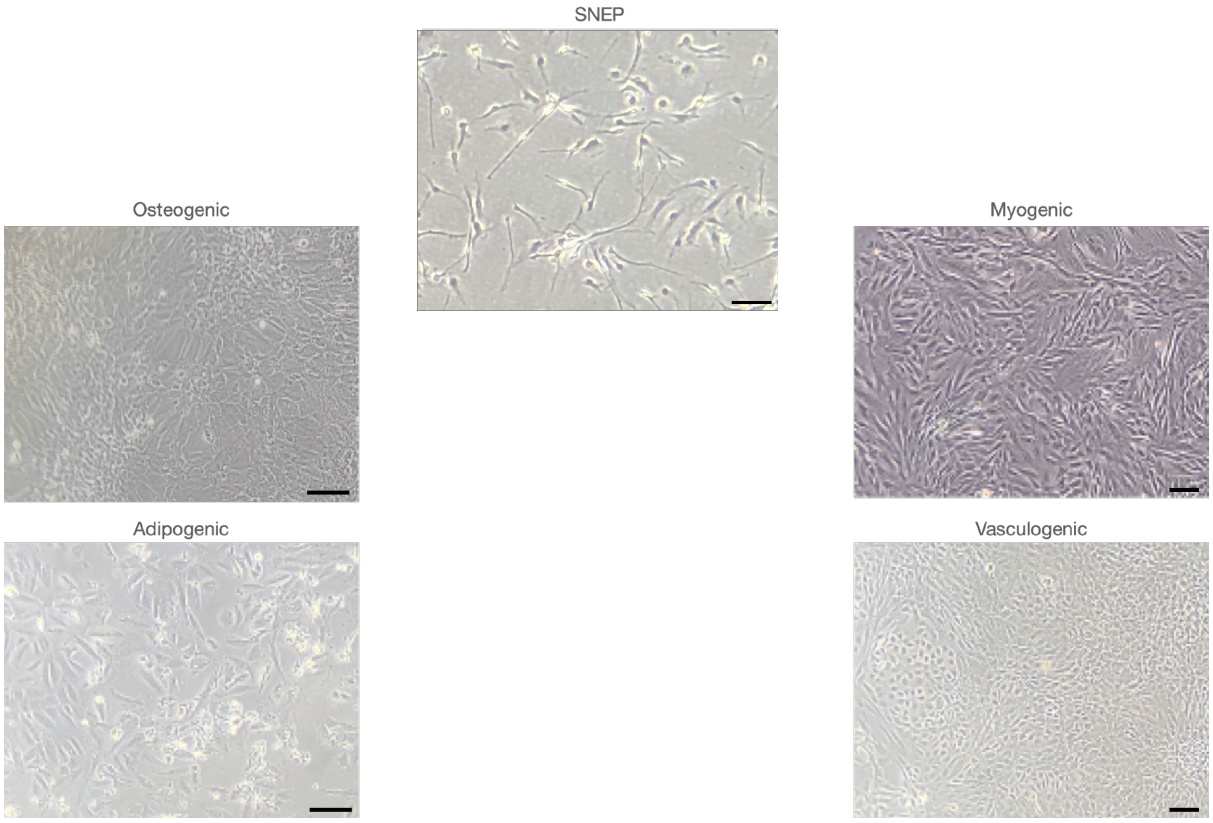

Figure 4.12. The effect of myogenic, adipogenic, osteogenic and vasculogenic differentiation media on the morphological characteristics of S100β SNEPs. Representative phase contrast images of SNEPs cultured in maintenance medium compared to S100β SNEPs grown in myogenic differentiation medium for 12 days, osteogenic and vasculogenic differentiation medium for 21 days and adipogenic differentiation medium for 14 days. Scale bar is 50µm.

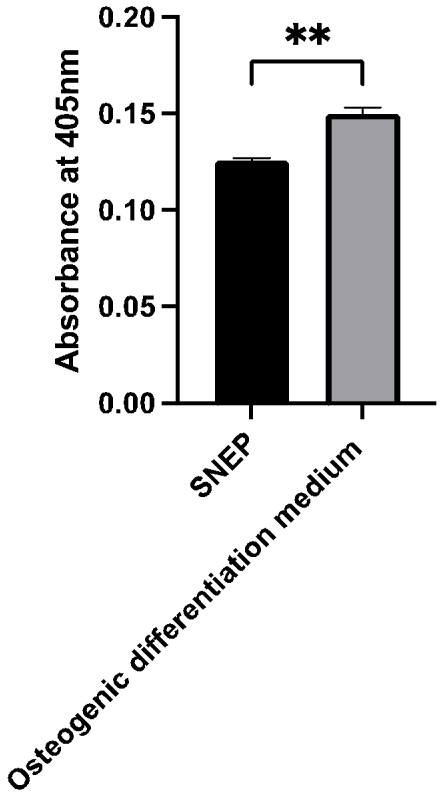

Figure 4.13. Osteogenic differentiation of S100β SNEPs. The level of Alizarin Red staining in S100β SNEPs following osteogenic differentiation. Osteogenic differentiation was determined by measuring absorbance at 405nm in S100β SNEPs grown in osteogenic differentiation medium for 21 days following staining with Alizarin Red. Data are expressed as the absorbance at 405nm and represent the mean ± SEM of an experiment performed in triplicate. ** $p<0.01$

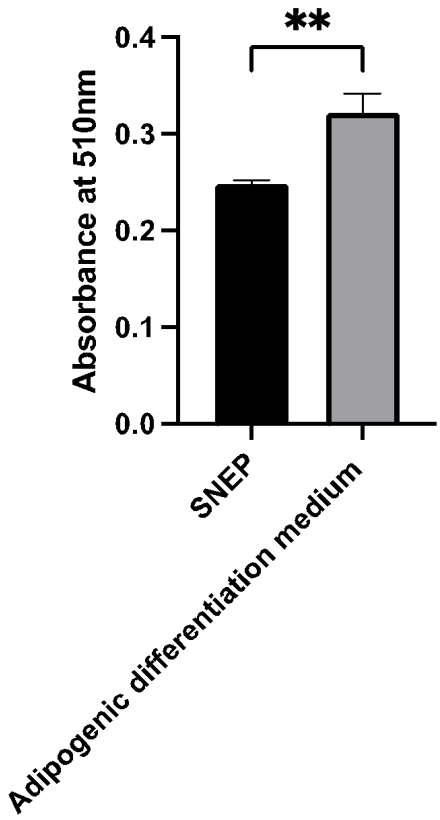

Figure 4.14. Adipogenic differentiation of S100β SNEPs. The level of Oil Red O staining in S100β SNEPs following adipogenic differentiation. Adipogenic differentiation was determined by measuring absorbance at 510nm in S100β SNEPs grown in adipogenic differentiation medium for 14 days following staining with Oil Red O. Data are expressed as the absorbance at 510nm and represent the mean ± SEM of an experiment performed in triplicate. ** $p<0.01$

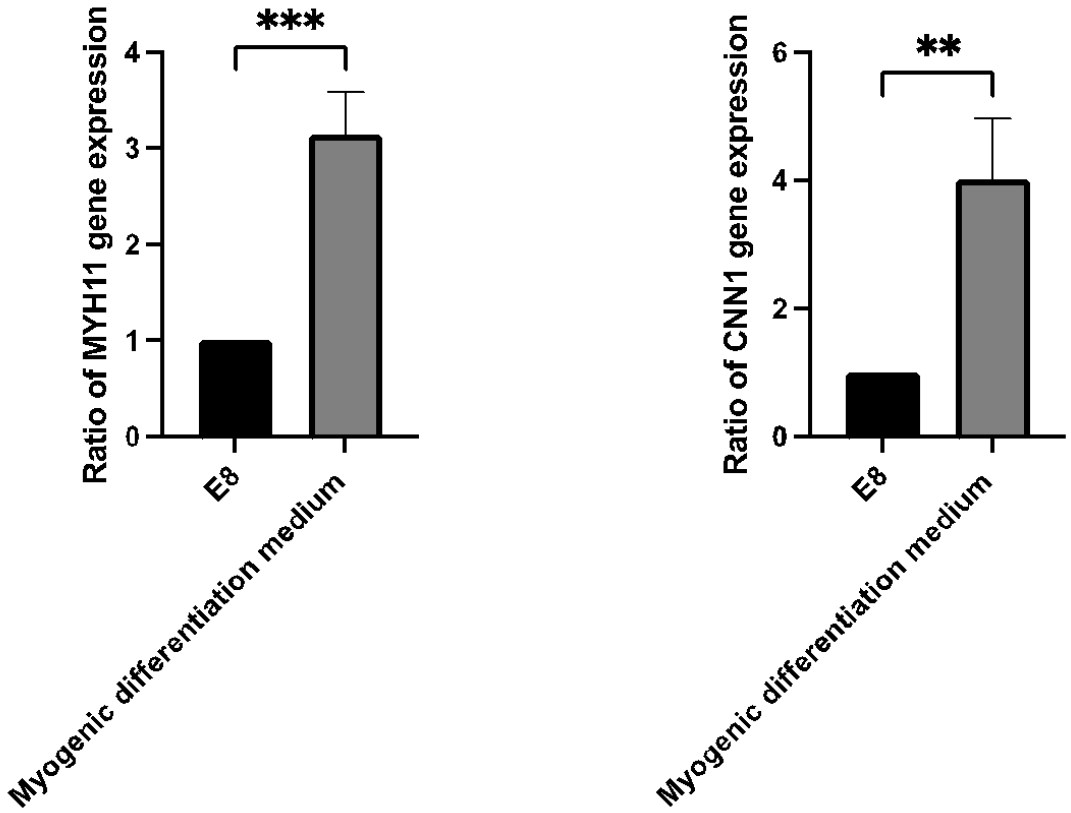

Figure 4.15. Expression of *MYH11* and *CNN1* mRNA in S100β SNEP following myogenic differentiation. *MYH11* and *CNN1* expression was measured in S100β SNEPs grown in their maintenance medium compared to S100β SNEPs grown in myogenic differentiation medium for 12 days. Total RNA was isolated from cells before the relative levels of *MYH11* and *CNN1* transcript was measured by qRT-PCR with *GAPDH a*s an internal control. Data are expressed as the ratio of gene expression (R) and represent the mean ± SEM of 3 experiments performed in triplicate. ** $p<0.01$ *** $p<0.001$

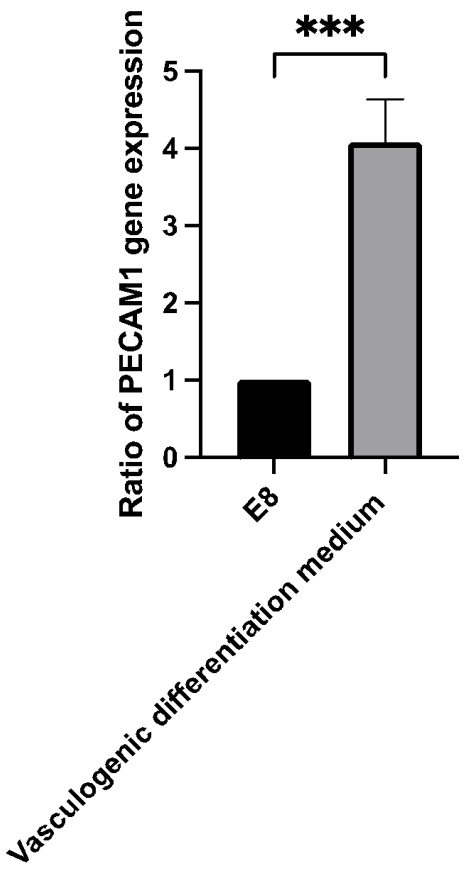

Figure 4.16. Expression of *PECAM-1* mRNA in S100β SNEP following vasculogenic differentiation. *PECAM-1* mRNA expression levels were measured in S100β SNEPs grown in maintenance media and compared to S100β SNEPs grown in vasculogenic differentiation medium for 21 days. Total RNA was isolated from cells before the relative levels of *PECAM-1* transcript was measured by qRT-PCR with *GAPDH* as an internal control. Data are expressed as the ratio of gene expression (R) and represent the mean ± SEM of 3 experiments performed in triplicate. *** $p<0.001$

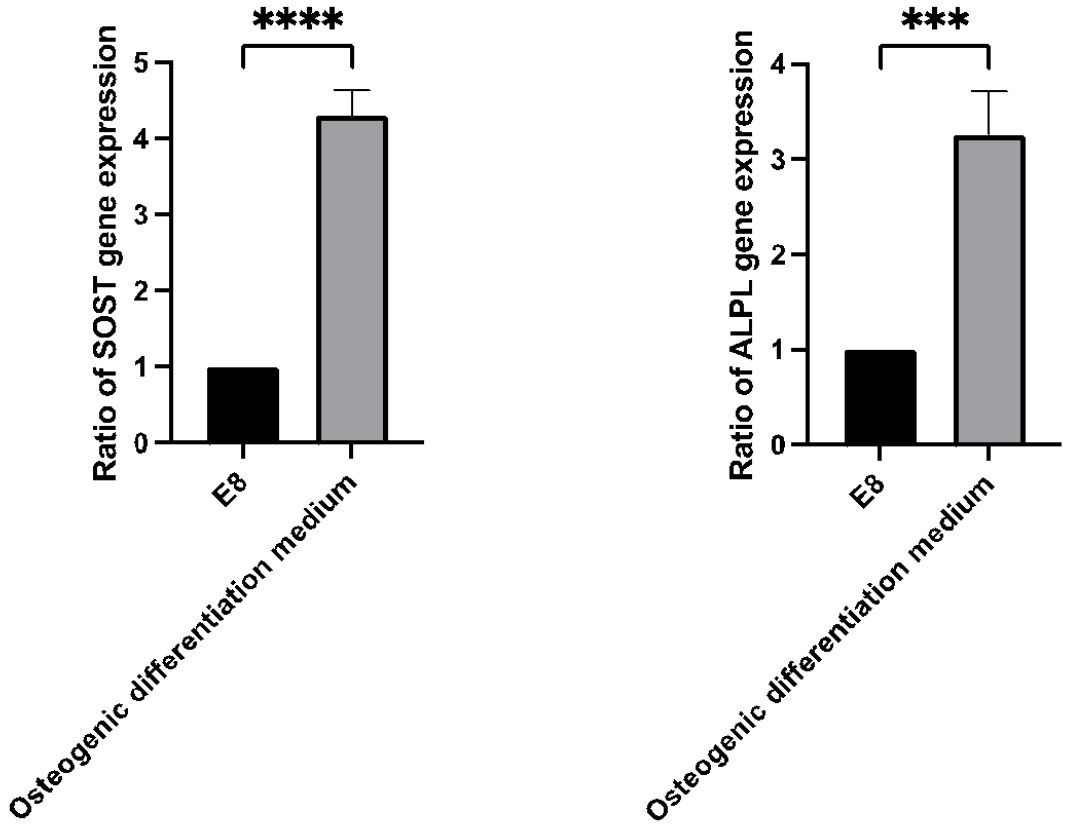

Figure 4.17. Expression of *ALPL* and *SOST* mRNA in S100β SNEP following osteogenic differentiation. *ALPL* and *SOST* expression was measured in S100β SNEPs grown in their maintenance medium compared to S100β SNEPs grown in osteogenic differentiation medium for 21 days. Total RNA was isolated from cells before the relative levels of *ALPL* and *SOST* transcript was measured by qRT-PCR with *GAPDH α*s an internal control. Data are expressed as the ratio of gene expression (R) and represent the mean ± SEM of 3 experiments performed in triplicate. *** $p<0.001$ **** $p<0.0001$

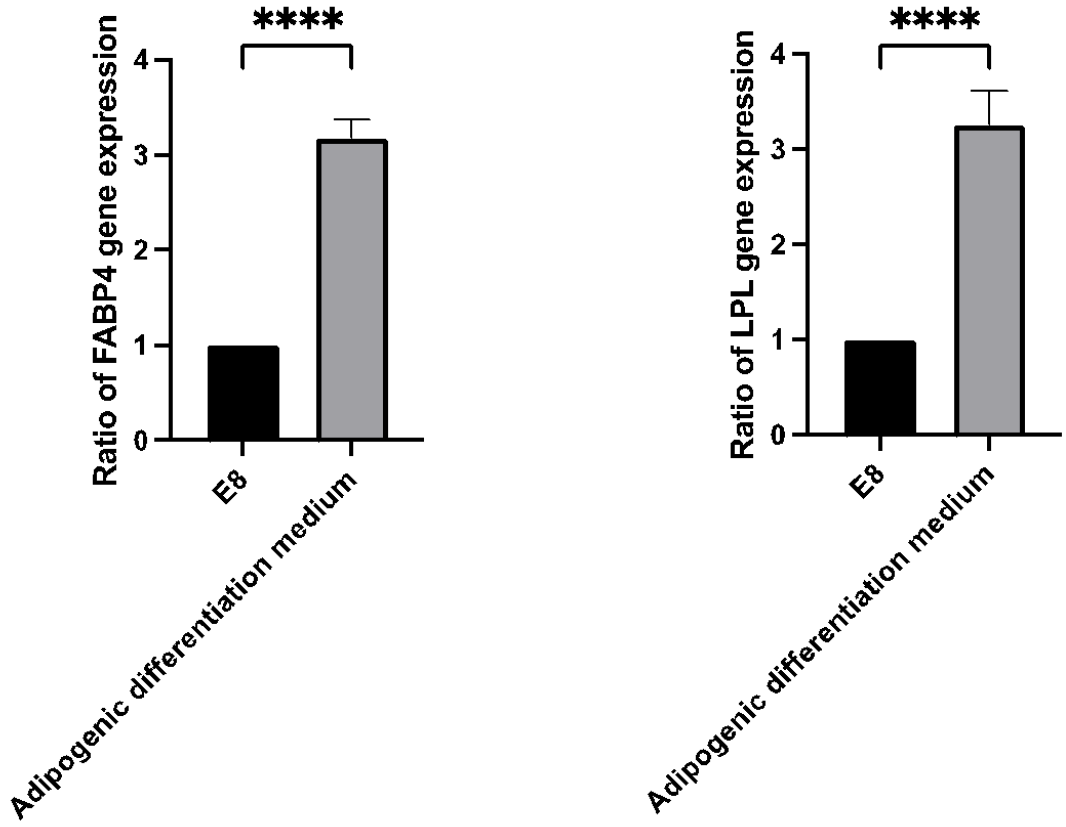

Figure 4.18. Expression of *LPL* and *FABP4* mRNA in S100β SNEP following adipogenic differentiation. *LPL* and *FABP4* expression was measured in S100β SNEPs grown in their maintenance medium compared to S100β SNEPs grown in adipogenic differentiation medium for 14 days. Total RNA was isolated from cells before the relative levels of *LPL* and *FABP4* transcript was measured by qRT-PCR with *GAPDH* as an internal control. Data are expressed as the ratio of gene expression (R) and represent the mean ± SEM of 3 experiments performed in triplicate. **** $p<0.0001$

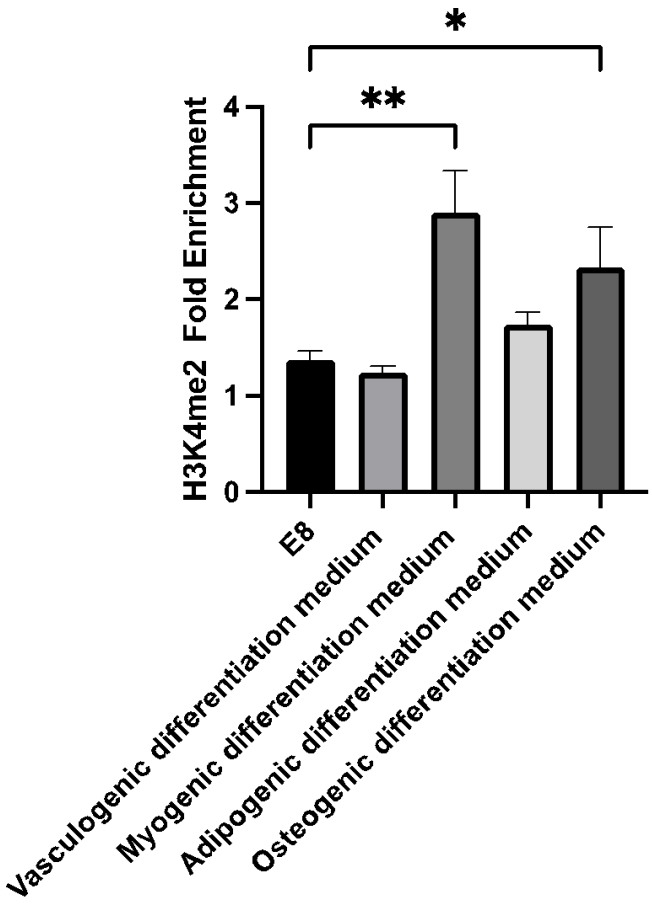

Figure 4.19. The level of enrichment of H3K4me2 at the *MYH11* locus in S100β SNEP following myogenic, vasculogenic, adipogenic and osteogenic differentiation. S100β SNEPs were seeded at the required density before cells were treated with myogenic differentiation medium for 12 days, vasculogenic and osteogenic differentiation medium for 21 days and adipogenic differentiation medium for 14 days. H3K4me2 binding at the *MYH11* locus was assessed by ChIP assay and corrected against the IgG control. Fold enrichment was determined for each condition and the data are the mean ± SEM of 3 experiments performed in triplicate. * $p<0.05$ ** $p<0.01$

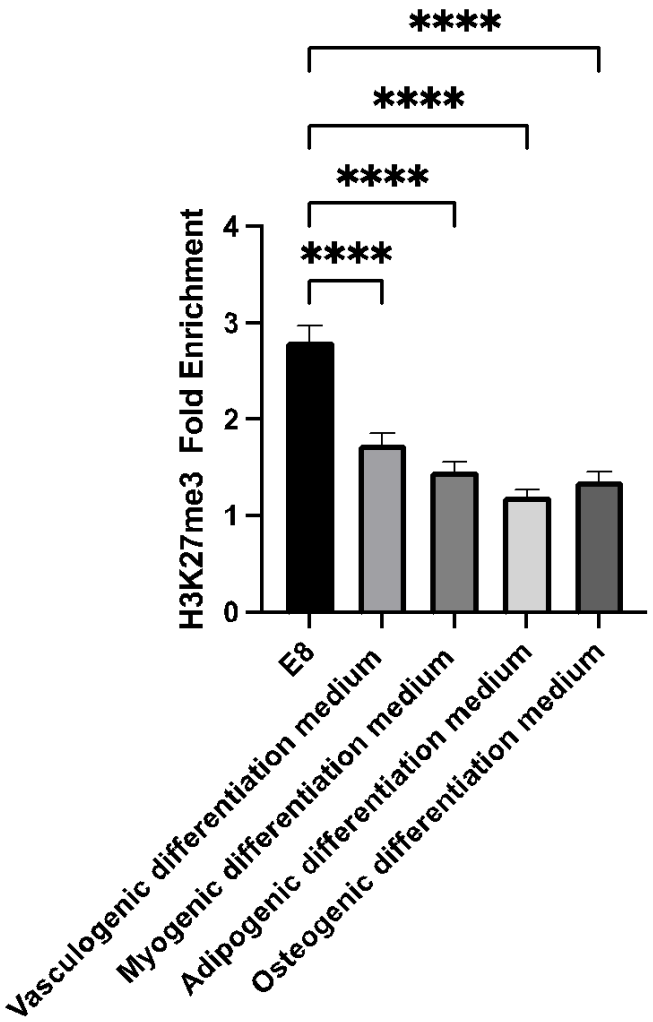

Figure 4.20. The level of enrichment of H3K27me3 at the *MYH11* locus in S100β SNEP following myogenic, vasculogenic, adipogenic and osteogenic differentiation. S100β SNEPs were seeded at the required density before cells were treated with myogenic differentiation medium for 12 days, vasculogenic and osteogenic differentiation medium for 21 days and adipogenic differentiation medium for 14 days. H3K27me3 binding at the *MYH11* locus was assessed by ChIP assay and corrected against the IgG control. Fold enrichment was determined for each condition and the data are the mean ± SEM of 3 experiments performed in triplicate. **** $p<0.0001$

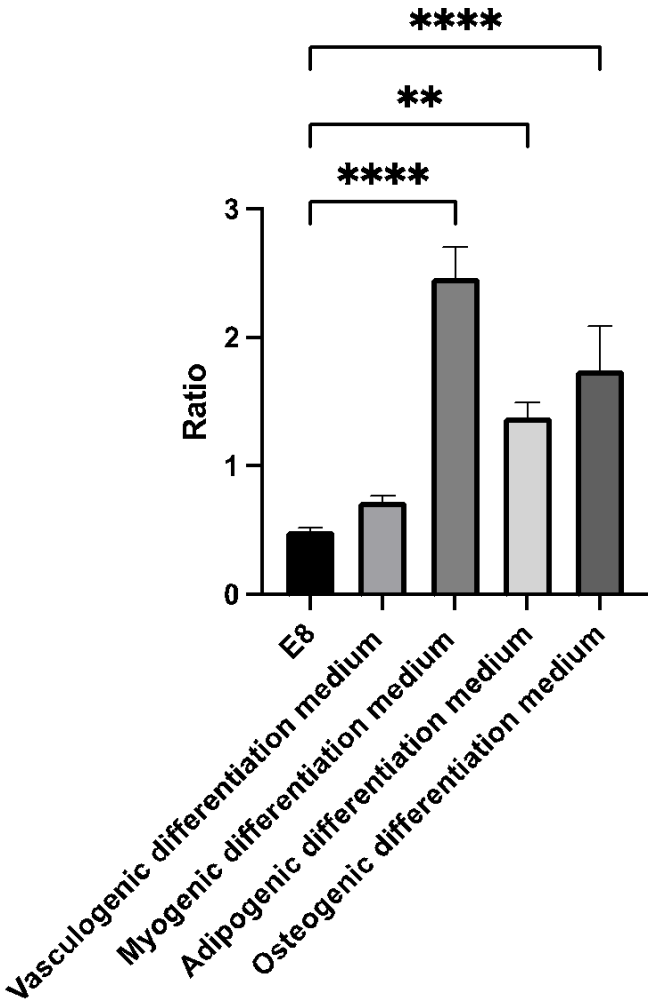

Figure 4.21. H3K4me2/H3K27me3 ratio at the *MYH11* locus in S100β SNEP following myogenic, vasculogenic, adipogenic and osteogenic differentiation. S100β SNEPs were seeded at the required density before cells were treated with myogenic differentiation medium for 12 days, vasculogenic and osteogenic differentiation medium for 21 days and adipogenic differentiation medium for 14 days. H3K27me3 binding at the *MYH11* locus was assessed by ChIP assay and corrected against the IgG control. The ratio of H3K4me2 and H3K27me3 binding was determined for each condition and the data are the mean ± SEM of 3 experiments performed in triplicate. ** $p<0.01$ **** $p<0.0001$

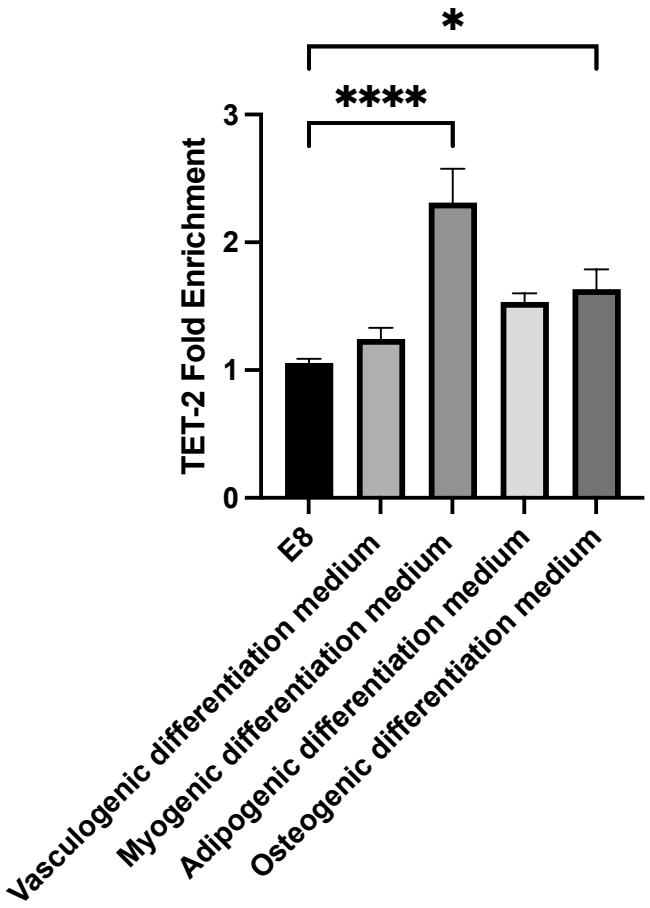

Figure 4.22. TET-2 fold enrichment at the *MYH11* locus in S100β SNEP following myogenic, vasculogenic, adipogenic and osteogenic differentiation. S100β SNEPs were seeded at the required density before cells were treated with myogenic differentiation medium for 12 days, vasculogenic and osteogenic differentiation medium for 21 days and adipogenic differentiation medium for 14 days. TET-2 protein binding at the *MYH11* locus was assessed by ChIP assay and corrected against the IgG control. Fold enrichment was determined for each condition and the data are the mean ± SEM of 3 experiments performed in triplicate * $p<0.05$ **** $p<0.0001$

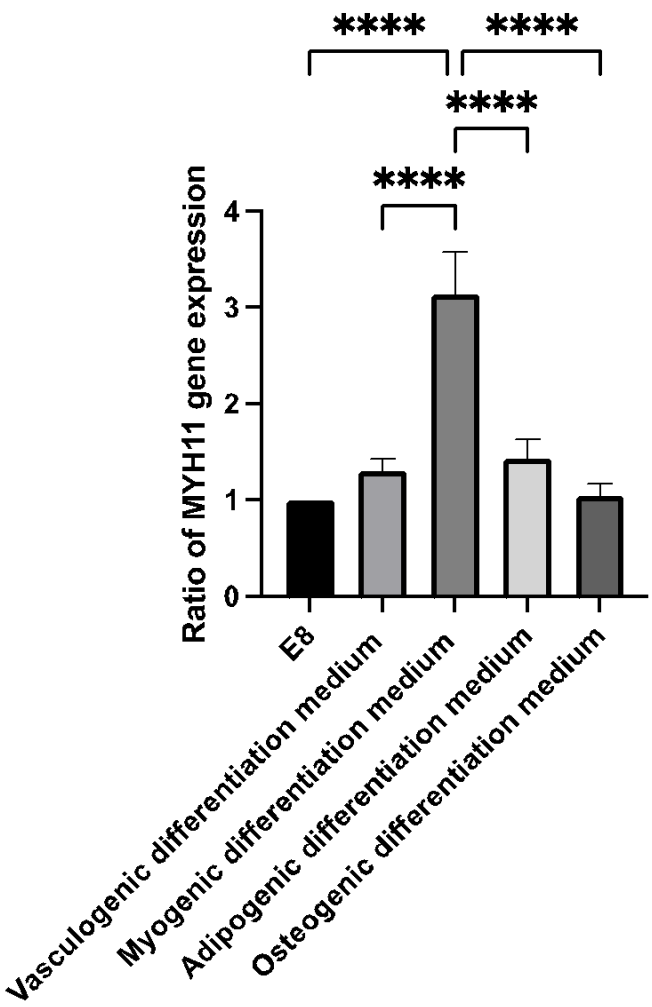

Figure 4.23. The expression of *MYH11* mRNA in S100β SNEP following myogenic, vasculogenic, adipogenic and osteogenic differentiation. S100β SNEPs were seeded at the required density before cells were treated with myogenic differentiation medium for 12 days, vasculogenic and osteogenic differentiation medium for 21 days and adipogenic differentiation medium for 14 days. Total RNA was isolated from cells before the relative levels of *MYH11* transcript was measured by qRT-PCR with *GAPDH* as an internal control. Data are expressed as the ratio of gene expression (R) and represent the mean ± SEM of 3 experiments performed in triplicate. *** $p<0.001$ **** $p<0.0001$

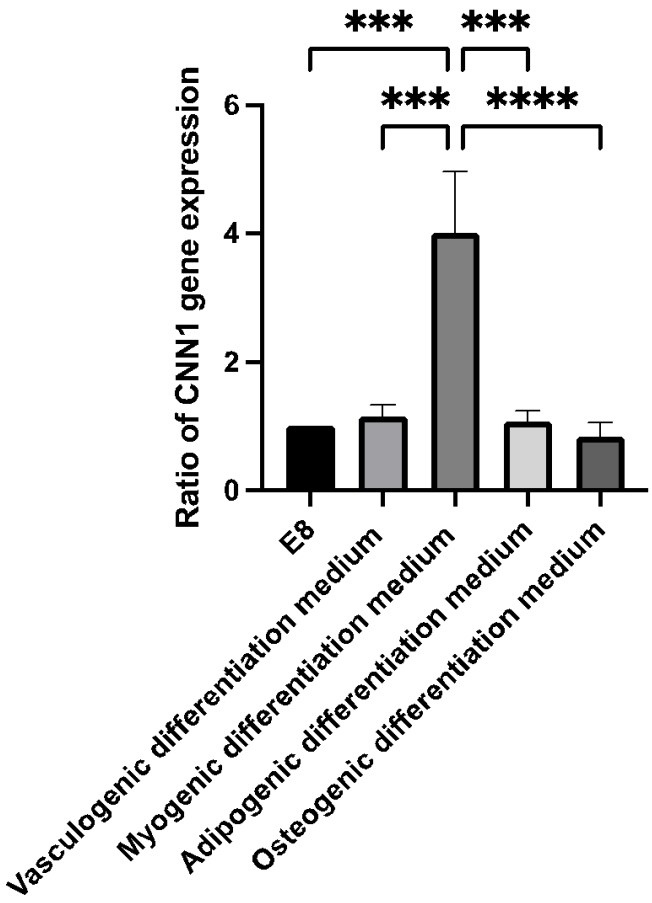

Figure 4.24. The expression of *CNN1* mRNA in S100β SNEP following myogenic, vasculogenic, adipogenic and osteogenic differentiation. S100β SNEPs were seeded at the required density before cells were treated with myogenic differentiation medium for 12 days, vasculogenic and osteogenic differentiation medium for 21 days and adipogenic differentiation medium for 14 days. Total RNA was isolated from cells before the relative levels of *CNN1* transcript was measured by qRT-PCR with *GAPDH* as an internal control Data are expressed as the ratio of gene expression (R) and represent the mean ± SEM of 3 experiments performed in triplicate. *** $p<0.001$ **** $p<0.0001$

4.3.2.1 Summary

The ChIP results suggest that undifferentiated S100β SNEPs are not highly enriched for H3K4me2 at *MYH11* locus. This enrichment increased significantly when S100β SNEPs were grown in myogenic and osteogenic differentiation medium, respectively. Parallel studies revealed a significant decrease in H3K27me3 mark at the same locus when cells undergo myogenic, osteogenic, adipogenic and vasculogenic differentiation. The ratio of H3K4me2:H3K27me3 was significantly increased in S100β SNEPs grown in myogenic, adipogenic and osteogenic differentiation medium but not vasculogenic differentiation medium despite the fact that *MYH11* and *CNN1* mRNA levels did not significantly increase in S100β SNEPs following adipogenic and osteogenic differentiation. TET-2 binding levels increased when S100β SNEPs grew in myogenic and osteogenic differentiation medium.

4.4 Discussion

The data from Chapter 3 reveal that the acquisition of the H3K4me2 epigenetic mark at the *Myh11* locus is an important factor that directs multipotent vascular progenitors toward SMC myogenic differentiation in a Tet-2-dependent manner. This Chapter addressed whether these same S100β multipotent resident vascular stem cells from mouse and human are also capable of differentiation towards non-SMC lineages such as osteogenic (osteocytes), adipogenic (adipocytes) and vasculogenic (endothelial cells) *in vitro.* Moreover, whether these S100β stem cells acquire the epigenetic signature of H3K4me2 at the *Myh11* locus when these cells undergo adipogenic, osteogenic or vasculogenic differentiation *in vitro* and thus be in part responsible for the reported presence of this key signature in non-SMCs typical of vascular lesions (Gomez et al., 2013).

The accumulation of SMC-like and non-SMCs plays an important role during vascular disease progression and lesion formation. Normal arterial vessels and lesions following injury or during disease progression are heterogeneous with a variety of cellular phenotypes found in the adventitial, medial and intimal layers of normal vessels and arteriosclerotic (carotid ligation/wire-induced injury etc) and atherosclerotic lesions (apolipoprotein e deficient mouse model (ApoE) or low-density lipoprotein receptor (LDLR) deficient mice fed a high fat diet) (Potente et al., 2017; Van Kuijk et al., 2019). Recent evidence suggests that most of the major cell types in atherosclerotic plaques, e.g. endothelial cells, macrophages, T-cells, and SMC-like cells are heterogeneous and/or plastic to some extent. Although endothelial cells, macrophages, T cells, and SMCs are the most discussed cells relating to disease progression, recent research in the field has shown that MSCs possibly also play a role. They may originate from an MSC-like cell type, which can give rise to various cell types like (myo)fibroblasts or SMC-like cells (El Agha et al., 2017).

For many years, it had been assumed that differentiated medial SMCs undergo phenotypic modulation and switching to become de-differentiated SMCs and contribute to the accumulation of both SMC-like cells, and more recently non-SMCs, within vascular lesions. Initial results from SMC lineage tracing system studies revealed that >95% of SMC-derived cells in atherosclerotic lesions from brachiocephalic arteries of SMC-*EYFP*$^{+/+}$ *ApoE*$^{-/-}$ mice

using Cre-LoxP (cyclization recombinase)-(locus of x-over, P1) were not detectable as being of SMC origin via Acta2 or Myh11 immunostaining (Gomez et al., 2013). However, a sizable proportion of *Myh11* marked non-SMC cells were enriched for the stable epigenetic mark, H3K4me2 on the *Myh11* locus using a proximity ligation assay (PLA) *in vitro*. The authors concluded that non-SMC phenotypes that include mesenchymal-like cells, fibroblasts, macrophage -, adipogenic - and osteogenic-like cells may be derived from *Myh11* marked SMCs. These data suggest that a substantial proportion of the non-SMCs within lesions that become enriched at the *Myh11* locus for H3K4me2 are derived from differentiated SMC. The central de-differentiated SMC type is classified as a mesenchymal-like phenotype. Mesenchymal-like cells subsequently seem to differentiate into fibroblast-like, macrophage-like, osteogenic-like, and adipocyte-like cells, which require the transcription factor Krüppel-like factor 4 (KLF4) and contribute differentially to vascular disease (Yap et al., 2021). Lesions are known to house a heterogenous population of SMC-like cells and non-SMCs that may be derived from differentiated SMCs since differentiated SMCs marked using Myh11-Cre-LoxP mice are tracked to lesions also enrich for H3K4me2 at the *Myh11* locus (Gomez et al., 2013).

Therefore upon injury, it has been reported that mesenchymal-like plastic SMCs proliferate and migrate into the media and intima, to support tissue repair, possibly leading to neointimal thickening (Tang et al., 2020). Vascular SMCs can acquire a macrophage-like phenotype switching from a contractile vascular SMC, via the mesenchymal-like to a macrophage-like vascular SMC, which is associated with development of atherosclerosis (Shankman et al., 2015). Using an *in vivo* fate mapping approach, with either a constitutive or an inducible *Myh11*-driven cyclization recombinase (Cre) mouse model, it has been demonstrated that SMCs are also able to adapt toward an adipocyte-like phenotype (Long et al., 2014). Single-cell RNA sequencing (ScRNA-Seq) studies have reported that a fibroblast-like SMC phenotype is also observed following vascular injury, such as during atherosclerotic progression or aortic aneurysm formation. This phenotype is also referred to as myofibroblasts-like SMCs or fibromyositis (Buam et al., 2011). ScRNAseq data also suggests that a Sca1 cell population within the medial layer of the vessel wall is a heterogeneous population that consists of endothelial cells, perivascular adipocytes, and platelet-derived growth factor receptor alpha or beta (PDGFRα)(PDGFRβ) stromal cells. An intersectional genetics strategy pinpointed the Sca1/PDGFRα cell population as the main source of de novo smooth muscle healing of severe

transversal arterial injury. These Sca1-derived SMCs possessed more propensity to expand compared with pre-existing SMCs, imparting them an important fraction of SMCs regeneration. Genetic Sca1 cell ablation supports their involvement in vessel repair and recovery (Tang et al., 2020).

Multipotent stem cells are able to migrate into sites of injury, self-renew, and differentiate as well as release trophic and growth factors (Dong et al., 2005; Pereira et al., 1995; Pittenger et al., 1999). These activities facilitate post-injury tissue regeneration, making stem cells the prime candidate for use in regenerative medicine, including repair of tissues such as bone and cartilage. Endogenous resident multipotent resident stem cells contribute to wound healing, in spite of being subjected to the harsh wound microenvironment, suggesting that these cells have an innate mechanism of adapting to an environment low in nutrients (Lu et al., 2011; Wang et al., 2013; Williams et al., 2013).

Several resident stem cells have been identified in the vasculature by a number of different research groups. Resident S100β vascular stem cells, like other multipotent stem cells, can differentiate *in vitro* into myogenic SMC-like cells, osteocytes, chondrocytes, and adipocytes *in vitro* (Dominici et al., 2006; Kennedy, Mooney, et al., 2014; Mortada et al., 2018; Tang et al., 2012). Furthermore, many groups have reported through lineage tracing studies that cells within vascular lesions may arise, at least in part, from a resident stem cell parent population (Tang et al., 2012; Yuan et al., 2017). In particular, our research group has shown using genetic lineage tracing of S100β stem cells using an inducible Cre-LoxP reporter system under the control of the S100β promoter that these S100β mVSCs contribute to vascular lesion formation (Di Luca et al., 2021, Molony et al., 2021).

In this context, it is clear that SMC-like and non-SMC cells within lesions are mapped through lineage tracing to a rare parent Sca1/Myh11 parent subpopulation of medial SMCs (Chappell et al., 2016, Dobnikar et al., 2018) that retain the H3K4me2 mark at the *Myh11* locus (Shankman et al., 2015; Gomez et al, 2013). While compelling, these data may overestimate the number of SMC-like and non-SMC-like cells that are derived from medial Sca1/Myh11 cells due to the manner in which these experiments were performed. The likelihood that

other cells were inadvertently marked is highlighted by studies examining the persistence of the cyclization recombinase estrogen receptor type 2 (CreERT2) recombinase inducer, tamoxifen, within tissues for up to 4 weeks after dosing is terminated (Reinert *et al.*, 2012). The repercussions of tamoxifen remaining within tissues is clearly important. These seminal studies suggest that tamoxifen doses commonly used to induce Cre-loxP recombination may continue to label significant numbers of cells for weeks after tamoxifen treatment, possibly confounding the interpretation of time-sensitive studies using tamoxifen-dependent models. As a result, experimental approaches using tamoxifen-inducible systems should consider both maximal recombination efficiency but also the length of time that tamoxifen-induced Cre-loxP recombination occurs. In this context, previous studies from our group using S100β-CreERT2-Td mice to track S100β mVSCs mitigated against this possibility by leaving a 4 week washout period after tamoxifen dosing before cells were cell fate mapped after vascular injury (Molony et al., 2021). In these studies and other studies, there is clear evidence that a significant proportion of SMC-like and non-SMC-like cells within vascular lesions are mapped through lineage tracing to a rare parent population of S100β/Nestin/Gli cells within the adventitial and/or medial layer of normal vessels (Molony et al., 2021, Wan et al., 2012, Kramann et al., 2015, He et al., 2020). If these data are indeed representative of the heterogeneity of lesional cells, the presence of the H3K4me2 mark at the *Myh11* locus in SMC-like cells and non-SMCs would also be predicted. The data in Chapter 3 confirmed that SMC-like cells derived from mouse S100β mVSCs following pro-atherogenic induced myogenic differentiation acquire the H3K4me2 mark at the *Myh11* locus, at least *in vitro*. This Chapter addressed whether human hiPSC-derived S100β stem cells also acquire this mark following myogenic differentiation. Furthermore, it addressed if mouse and human hiPSC derived S100β stem cells are also capable of undergoing osteogenic, adipogenic and vasculogenic differentiation (typical of non-SMCs in vascular lesions) and furthermore whether they also acquire the H3K4me2 mark at the *Myh11* locus irrespective of their final phenotype.

Multipotent stem cells can produce progeny with multiple phenotypes although they have some limitations in their capacity for differentiation (Pittenger et al., 2001). For example, the brain MSCs can generate neural and glial cells but haematopoietic stem cells, which differentiate into most of the blood cells, do not have the ability to produce neural cells. In contrast, bone marrow-derived MSCs can differentiate into all blood cell forms (Mundra et

al., 2012). As shown in the previous Chapter, atherogenic stimuli (TGF-β1, PDGF-BB and the Notch ligand, Jag-) all induced myogenic differentiation of S100β mVSCs cells *in vitro* concomitant with increased *Myh11* gene expression and enrichment of the epigenetic H3K4me2 mark at the *Myh11* gene locus.

Indeed, S100β mVSCs are believed to be multipotent via an MSC-like intermediate (Tang et al., 2012) and are capable of differentiating down several other lineages such as, adipogenic, osteogenic and vasculogenic. While previous studies have demonstrated the ability of multipotent stem cells in general to undergo lineage specification (Tange et al., 2012), this study is one of the first to demonstrate the ability of aortic arch-derived S100β mouse mVSCs and hiPSC-derived human SNEPs to undergo similar lineage-specification. There was a clear change of the morphology of S100β mVSCs and S100β SNEP following lineage specification in comparison to their morphology when grown in their maintenance medium. These initial data clearly indicate that these cells undergo lineage-specific differentiation. Changes in the level of lineage-specific genes in S100β mVSCs and S100β SNEP following osteogenic, adipogenic and vasculogenic differentiation, in addition with myogenic lineage-specific genes, further confirmed lineage-specification of both S100β mVSCs and S100β SNEP *in vitro*. In particular, for S100β stem cell-derived adipogenic cells, the expression levels of *FABP4* and *LPL* increased with induction, and maintained a high level of expression compared to their undifferentiated parent stem cell population in both mouse and human, confirming previous studies in preadipocytes (Wang et al., 2018). For S100β stem cell-derived osteogenic progeny in mouse and human, the expression levels of osteogenic lineage-specific genes, *ALPL* and *SOST* were also increased when compared to their undifferentiated parent population, in agreement with previous studies (Sawa et al., 2019). In SNEP-derived vasculogenic progeny, *PECAM1* gene expression was increased compared to SNEP in essential 8 (E8) medium in agreement with previous studies (Kanki et al., 2017). Adipogenic and osteogenic differentiation was further confirmed by oil red and alizarin red staining, respectively. These data clearly indicate that mouse S100β mVSCs and human S100β SNEPs are multipotent as they differentiate down vasculogenic, osteogenic, adipogenic and myogenic pathways *in vitro,* a process that depends on the respective inductive stimulus. This is not surprising as S100β mVSCs are known to differentiate to an MSC-like intermediate (Tang et al, 2012) and MSCs are capable of tri-lineage-specification (adipogenic, osteogenic and chondrogenic) when stimulated with the

corresponding inductive stimuli. The specification of S100β mVSCs to vasculogenic endothelial cells was not unexpected as these aortic arch S100β cells are also Sca1 positive (Di Luca et al., 2021) and Sca1 cells are capable of both myogenic and vasculogenic differentiation *in vitro* and *in vivo* (Tang et al., 2020, 2021; Hong and Gu, 2019). In addition, the calcium binding protein, S100β has been shown to trigger neointimal formation in injured arteries by maintaining the intermediate state of double-positive Sca-1 progenitor and SMCs, which were associated with direct activation of RAGE (The receptor for advanced glycosylation end products) by S100β and indirect induction of stromal cell-derived factor 1 α by activating Phosphoinositide-3-kinase/protein kinase B and nuclear factor kappa B. As the Sca1 gene is not expressed in humans (Holmes and Stanford, 2007), the ability of human S100β SNEPs to undergo vasculogenic differentiation is not dependent on this phenotype. However, previous studies have demonstrated concurrent vasculogenesis and neurogenesis from a common neural stem cell, suggesting that certain S100β/Nestin neural stem cells are fully capable of differentiating into not only somatic cells of identity but also into vascular cells for tissue regeneration (Li et al., 2009; Ryu et al., 2016).

The level of enrichment of H3K4me2 at the *Myh11* locus and binding of Tet-2 were both increased in osteogenic progeny derived from mouse S100β mVSCs which is associated with the mature, contractile SMC phenotype (Liu et al., 2013). This may also explain the decrease in the level of enrichment of H3K27me3 at the same locus. Similarly, adipogenic progeny exhibited enrichment of H3K4me2 and increased Tet-2 binding at the *Myh11* locus compared to undifferentiated S100β mVSCs. This enrichment of Tet-2 at lineage-specific promoters is in agreement with previous findings using embryonic stem cells (Ficz et al., 2011). While 5-hydroxymethylcytosine (5hmC) is known to be relatively enriched in euchromatic parts of the genome, including in cytosine phosphate guanine (CpG) islands (CGIs) and promoters, and its presence in promoters and exons is associated with increased levels of transcription, the observed enrichment of H3K4me2 and Tet-2 binding at the *Myh11* locus was not accompanied with the expression of myogenic genes namely, *Myh11* and *Cnn1* which remained similar to undifferentiated S100β mVSCs following adipogenic and osteogenic differentiation. While the ratio of H3K4me2:H3K27me3 was only significantly increased in S100β mVSC-derived osteogenic progeny, this is primarily due to the lack of change in H3K4me2 enrichment at this locus following adipogenic differentiation. While the levels of

H3K27me3 did not significantly decrease in adipogenic progeny to impact the ratio, the tendency was for an increase in the overall ratio. These data indicate that S100β mVSC-derived osteogenic and adipogenic progeny acquire the H3K4me2 mark at the *Myh11* gene locus irrespective of their phenotypic state and transcript level of myogenic genes *in vitro*. This raises the possibility that the appearance of the H3K4me2 mark at this locus in non-SMCs *in situ* could be a direct result of adipogenic and osteogenic differentiation of S100β mVSCs, rather than, or in addition to the de-differentiation of medial SMCs. In that context, S100β mVSC-derived adipogenic and osteogenic progeny could conceivably contribute to the accumulation of non-SMC-like cells within vascular lesions, in particular, as they are cell fate mapped to these lesions (Di Luca et a., 2021, Molony et al., 2021).

In contrast to S100β mVSC-derived adipogenic and osteogenic progeny, there was no change in the H3K4me2, H3K27me3 mark or Tet-2 binding at the *Myh11* locus in vasculogenic progeny, concomitant with no change in the level of *Myh11* and *Cnn1* gene expression. Previous studies have demonstrated that endothelial cells in culture contain high levels of H3K27me3 at the SMC gene loci (McDonald et al., 2006). S100β mVSC-derived vasculogenic progeny mimicked the levels of H3K4me3 at the *Myh11* locus in undifferentiated cells. This may indicate that S100β mVSC-derived endothelial cells are a distinct endothelial population and/or represent a partially differentiated or dysfunctional phenotype despite their morphological similarity to endothelial cells in culture. Indeed, H3K27me3 is methylated by Polycomb repressive complex 2 (PRC2) and is one of the most widely studied histone marks in these cells. EZH2 is the main active subunit of PRC2 that initiates and maintains H3K27me3 and can become downregulated in endothelial cells following dysfunction (Floris et al., 2015).

In hiPSC-derived S100β SNEPs, a similar epigenetic profile to mouse S100β mVSCs at the *MYH11* locus was observed in both adipogenic and osteogenic progeny. Namely, the ratio of the H3K4me2:H3K27me3 mark and TET-2 binding at the *MYH11* locus increased significantly concomitant with no discernible change in the expression levels of *MYH11* and *CNN1* compared to undifferentiated S100β SNEPs. While adipogenic progeny exhibited a tendency to enrich for H3K4me2 at the *MYH11* gene locus (albeit not significant), the ratio is increased overall due to a significant reduction in the level of enrichment of H3K27me3 in these progeny at the same locus. In contrast, the ratio of the H3K4me2:H3K27me3 mark and TET-2 binding

at the *MYH11* locus did not change in vasculogenic progeny nor did *MYH11* and *CNN1* gene expression despite a significant decline in the level of H3K27me3 enrichment at the *MYH11* locus. The level of enrichment of H3K4me2 again correlated with TET-2 binding level at the same locus in agreement with previous studies that suggest promoters that are high in 5hmC are enriched in the activating histone mark H3K4me3, whereas those enriched in 5-methylcytosine (5mC) are depleted of H3K4me3 which is affected by TET-2 (Ficz et al., 2011).

Clearly, as with S100β mVSCs, the ratio of H3K4me2:H3K27me3 increases in S100β SNEP-derived osteogenic and adipogenic progeny at the *MYH11* gene locus irrespective of their phenotypic state and transcript level of myogenic genes *in vitro*. This raises the possibility that the appearance of the H3K4me2 mark at this locus in non-SMCs within human vascular lesions *in situ* (Shankman et al., 2015, Gomez et al, 2013) could be a direct result of adipogenic and osteogenic differentiation of S100β mVSCs, rather than, or in addition to the de-differentiation of medial SMCs. On the other hand, vasculogenic progeny from S100β mVSCs and S100β SNEPs failed to enrich for the H3K4me2 mark at the *Myh11* locus. These data suggest that differentiation of these endothelial-like cells from S100β stem cells *in vitro* does not require acquisition of this mark. In agreement, previous lineage tracing studies that mark endothelial cells using Endotrack- YFP or -LacZ and the tamoxifen-inducible Ind.Endotrack-YFP confirm that endothelial-derived cells contribute to lesion formation through endothelial to mesenchymal transition, which is dependent upon early activation of the Smad2/3-Slug signaling pathway (Cooley et al., 2014).

The S100β mVSCs and their human counterpart, S100β SNEPs are a highly similar population of multipotent vascular stem cells that are involved in the formation of arteriosclerotic neointima (Di Luca et al., 2021; Tang et al., 2012). Numerous studies have indicated that the manner by which these stem cells contribute to lesion formation is through differentiation of these cells to become SMC-like cells (Wang et al., 2018). Based on their epigenetic profile *in vitro*, and our previous lineage tracing studies tracking these cells following injury *in vivo* (Molony et al., 2021; Di Luca et al., 2021), it is clear that non-SMCs that have the H3K4me2 mark within lesions and exhibit adipogenic and osteogenic phenotypes may also be derived from these cells.

In conclusion, single gene chromatin immunoprecipitation followed by polymerase chain reaction (ChIP-PCR) analysis confirms that mouse and human S100β multipotent stem cells acquire the H3K4me2 mark at the *Myh11* gene locus as they differentiate down SMC-like (myogenic) and non-SMC-like (adipogenic and osteogenic) lineages. These epigenetic changes at myogenic gene loci may represent a critical factor in dictating their initial multipotency commitment to lineage specification before they are fully cell-fated and determined following transcription factor regulation of lineage-specific gene expression. In this context, the next Chapter will perform genome-wide bulk chromatin immunoprecipitation sequencing (ChIP-seq) of these S100β SNEPs and interrogate parallel *in-silico* analysis of genome-wide ChIP-seq datasets from mouse and human stem cells before and after lineage specification (myogenic, adipogenic, osteogenic and vasculogenic). This will determine whether the mono-, di- and trimethylation of H3K4 occurs at numerous myogenic gene-specific loci as these cells undergo differentiation down specific lineages other than myogenic and vice versa.

Chapter 5

Genome-wide bulk ChIP-seq analysis of histone methylation in undifferentiated stem cells before and after myogenic, adipogenic, osteogenic and vasculogenic differentiation

5.1 Introduction:

The single gene chromatin immunoprecipitation followed by polymerase chain reaction (ChIP-PCR) data presented in Chapter 3 suggests that the acquisition of histone 3 lysine 4 di-methylation (H3K4me) mark at the Myosin Heavy Chain 11 *(Myh11)* locus is an important epigenetic signature of S100 calcium-binding protein β (S100β) multipotent vascular stem cell (mVSCs) during myogenic differentiation. The acquisition is ten-eleven-translocation 2 (Tet-2) dependent and controls subsequent *Myh11* gene expression in response to pro-atherogenic stimuli in these cells *in vitro*. As a result, the appearance of this histone mark at the *Myh11* locus in smooth muscle cell (SMC)-like cells within vascular lesions *in situ* may represent partial myogenic differentiation of resident S100β mVSCs in addition to, or instead of, dedifferentiation of differentiated medial SMCs (Gomez et al., 2013).

In Chapter 4, single gene ChIP-PCR data using human induced pluripotent stem cells (hiPSC)-derived S100β human multipotent neuroectoderm progenitor stem cells (SNEPs) confirmed that the acquisition of an H3K4me2 mark at the *MYH11* locus is also prevalent in human S100β stem cells and is an important epigenetic signature of these cells during myogenic differentiation *in vitro*. As a result, the appearance of this histone mark at the *MYH11* locus in SMC-like cells within human vascular lesions *in situ* (Gomez et al, 2013, Shankman et al, 2015) may also represent partial myogenic differentiation of resident S100β stem cells in human vessels (Tang et al., 2012). Moreover, the acquisition of an H3K4me2 mark at this locus in S100β mVSCs and human S100β SNEPs occurs not only in SMC-like myogenic progeny but also in adipogenic and osteogenic, but not vasculogenic, progeny *in vitro*. As a result, the appearance of this histone mark at this locus in non-SMCs within murine and human vascular lesions *in situ* (Gomez et al., 2013; Shankman et al, 2015) may represent differentiation of resident S100β stem cells in addition to, or instead of, dedifferentiation of differentiated medial SMCs.

This Chapter expands on this novel observation by performing genome-wide bulk chromatin immunoprecipitation sequencing (ChIP-seq) analysis of H3K4me2 and H3K27me3 enrichment at *MYH11* locus but also interrogating the loci of a panel of myogenic genes namely, calponin1

(CNN1), smoothelin *(SMTN)* and transgelin *(TAGLN)* following myogenic differentiation of a series of multipotent stem cells *in vitro.* In addition, *in-silico* analysis of previously published genome-wide ChIP-seq datasets from mouse and human stem cells before and after lineage specification (myogenic, adipogenic, osteogenic and vasculogenic) was also performed. Using this genome-wide ChIP-seq approach, the mono-, di- and trimethylation of H3K4 at numerous myogenic gene-specific loci in mouse and human stem cells was evaluated as they undergo lineage-specification other than myogenic and vice versa.

The rapid technological developments in next-generation sequencing (NGS) and the arsenal of genomic assays available to the biologist have been transformative (Bentley et al., 2006; Mardis et al., 2008; Shendure & Ji, 2008). The ability to sequence millions of short DNA fragments in a single run is enabling increasingly large experiments that could only be imagined a few years ago. NGS has already been applied in many areas. Such as, the sequencing of whole genomes (Hillier et al., 2008; Ley et al., 2008). Genome-wide mapping of protein–DNA interactions and epigenetic marks is an essential way for understanding transcriptional regulation. A map of binding sites for transcription factors, core transcriptional machinery and other DNA-binding proteins is vital for deciphering the gene regulatory networks that underlie various biological processes (Johnson et al., 2008; Valouev et al., 2008). The combination of nucleosome positioning and dynamic modification of DNA and histones has a key role in gene regulation (Cosgrove et al., 2004; Segal et al., 2006) and guides development and differentiation. States of chromatin can influence transcription directly by altering the packaging of DNA to allow or prevent access to DNA-binding proteins, or they can modify the nucleosome surface to enhance or impede recruitment of effector protein complexes. Recent advances suggest that this interplay between chromatin and transcription is dynamic and more complex than previously appreciated (Berger, 2007), and there is a growing recognition that systematic profiling of the epigenomes in multiple cell types and stages may be needed for understanding developmental processes and disease states (Bernstein et al., 2007).

ChIP–seq offers many advantages over ChIP–chip. First, its base pair resolution is probably the greatest improvement over ChIP–chip. Although arrays can be tiled at a high density, this requires a large number of probes and remains expensive for mammalian genomes (Kim et

al., 2005). Arrays also have fundamental limitations in resolution due to the uncertainties in the hybridization process. Second, ChIP–seq does not suffer from the noise generated by the hybridization step in ChIP–chip. Nucleic acid hybridization is complex and dependent on many factors, including the guanine-cytosine content, length, concentration and secondary structure of the target and probe sequences. Therefore, cross-hybridization between imperfectly matched sequences frequently occurs and contributes to the noise. Third, the intensity signal measured on arrays might not be linear over its entire range, and its dynamic range is limited below and above saturation points. In a recent study, distinct and biologically meaningful peaks seen in ChIP–seq were obscured when the same experiment was conducted with ChIP–chip (Alekseyenko et al., 2008). However, ChIP-seq and its variations (Policastro & Zentner, 2018) suffer from low signals, high backgrounds and epitope masking due to cross-linking, and low yields that require large numbers of cells (Policastro & Zentner, 2018; Teytelman et al., 2013) and also its current cost and availability.

In contrast to bulk ChIP-seq, which is unable to detect chromatin signatures of individual cells, single-cell ChIP-seq (scChIP-seq) helps study genetic diversity in heterogeneous cell populations and understand the evolution in a population of cells. Droplet-based single-cell ChIP-seq (Drop-ChIP) combines a microfluidic device with single-cell DNA barcoding, allowing researchers to obtain a relatively low-coverage map per cell (Rotem et al., 2015). Indeed, scChIP-seq enables the clustering of cell populations based on the diversity of the chromatin landscape and the identification of chromatin features specific to each population, such as the loss of H3K27me3 markers in some cells may associate with chemoresistance (Grosselin et al., 2019). However, because the data generated by Drop-ChIP of individual cells are too sparse, thousands of cells are required to obtain good results for clustering.

ChIP followed by sequencing was one of the early applications of NGS, and the first studies were published in 2007 (Barski et al., 2007; Johnson et al., 2007; Mikkelsen et al., 2007; Robertson et al., 2007). In ChIP–seq, the DNA fragments of interest are sequenced directly and not hybridized on an array. ChIP–seq has higher resolution, fewer artefacts, greater coverage and a larger dynamic range and therefore provides substantially improved data compared to ChIP–chip. Although the short reads (∼35 bp) generated by NGS platforms pose serious difficulties for certain applications — for example, *de novo* genome assembly — they

are acceptable for ChIP–seq. The more precise mapping of protein-binding sites provided by ChIP–seq allows an accurate list of targets for transcription factors and enhancers, in addition to better identification of sequence motifs (Johnson et al., 2007; Visel et al., 2009). Enhanced spatial resolution is particularly important for profiling histone variants, post-translational modifications of both chromatin and nucleosome positioning, and ChIP–seq has enabled enormous progress in these areas. ChIP-seq has been routinely deployed to measure the level of H3K4me2 distribution on the gene promoter across the whole genome and reveals the patterns of H3K4me2 distribution over certain genomic regions and can be related to gene transcriptional activities (Heintzman et al., 2007, 2009). Specifically, it has been shown that a "long tail" distribution pattern of H3K4me2 over the promoter regions is indicative of tissue-specific gene expression (Pekowska et al., 2010). Furthermore, it was observed that such long-tail patterns of H3K4me2 can be acquired at different stages of tissue differentiation including as early as the ESC stage (Pekowska et al., 2010).

Based on the single gene ChIP-PCR data presented in Chapter 4, where the H3K4me2 mark was observed on the *MYH11* gene locus in human hiPSC-derived S100β SNEPs and in resident S100β mVSCs following lineage specification, the focus of this Chapter was to perform genome-wide bulk ChIP-seq on hiPSC-derived S100β SNEPs. This was done to confirm the H3K4me2/H3K27me3 marks at the *MYH11* locus in myogenic progeny before further investigating whether similar epigenetic changes were present on the *MYH11* locus following the same tri-lineage-specification (adipogenic, osteogenic and vasculogenic) of these multipotent stem cells. ChIP-seq was performed on S100β hiPSC-derived SNEPs using a commercial ChIP-seq service (Novogene Ltd) to specifically investigate whether the H3K4me2/H3K27me3 marks at the *MYH11* gene locus following vasculogenic, adipogenic and/or osteogenic differentiation of these human stem cells. Parallel *in silico* analysis of published genome-wide bulk ChIP-seq datasets from mouse and human multipotent stem cells were also analysed. In this instance, the mono-, di- or trimethylation of H3K4 and H3K27me3 marks were analysed at several SMC gene loci and tri-lineage-specific gene loci following vasculogenic, adipogenic and/or osteogenic differentiation of these mouse and human multipotent stem cells. In both cases, the interrogation was performed by assessing peak calling to determine the peak of each gene at a specific histone and peak scoring to determine the significance of that peak across the entire genome for a given sample.

Objectives:

The main aims of this chapter were:

1. *In-silico* analysis of published bulk ChIP-seq datasets of mono- di- and trimethylation of H3K4 and H3K27me3 at SMC-specific gene loci in undifferentiated murine MSCs and their myogenic, adipogenic, osteogenic and vasculogenic progeny to determine whether H3K4 methylation occurs at SMC gene loci following non-SMC tri-lineage-specification.
2. *In-silico* analysis of published bulk ChIP-seq datasets of mono- di- and trimethylation of H3K4 and H3K27me3 at SMC-specific gene loci in undifferentiated human MSCs and hESCs and their respective myogenic, adipogenic, osteogenic and vasculogenic progeny to determine whether H3K4 methylation occurs at SMC gene loci following non-SMC tri-lineage-specification
3. Bulk-ChIP-seq analysis of H3K4me2 and H3K27me3 marks at the MYH11 gene locus in undifferentiated hiPSC-derived S100β SNEPs and their myogenic, adipogenic, osteogenic and vasculogenic progeny to determine whether H3K4me2 enrichment occurs at this locus following non-SMC tri-lineage-specification.

5.2 Strategy

5.2.1 *In-silico* ChIP-seq analysis of H3K4 methylation histone marks at SMC-specific gene loci from published data in undifferentiated murine and human MSCs and hESCs and their respective myogenic, adipogenic, osteogenic and vasculogenic progeny.

In-silico analysis of published ChIP-seq data for H3K4me1, H3K4me2 or H3K4me3 enrichment at SMC-specific loci depending on their availability was first assessed before and after myogenic (H3K4me2), vasculogenic (H3K4me3), adipogenic (H3K4me1) and osteogenic (H3K4me1) differentiation of murine and human mesenchymal stem cells (MSCs) using the

Galaxy Training Network (GTN). The annotation of H3K4me1/2/3 histone binding sites on the *Myh11*, *Cnn1*, *Smtn and Tagln* locus was assessed by mapping to the reference genome to obtain the information of protein-DNA binding sites directly. In-silico analysis was performed as described in Chapter 2 Section, 2.2.15.1.

5.2.2 Bulk ChIP-seq analysis of H3K4me2 histone marks at the *MYH11* gene locus in undifferentiated hiPSC-derived S100β SNEPs and their myogenic, adipogenic, osteogenic and vasculogenic progeny *in vitro.*

In order to investigate whether H3K4me2 histone marks are present at the *MYH11* gene locus in S100β SNEPs following myogenic differentiation, ChIP-seq was performed by Novogene as described in Chapter 2, Section 2.2.15.2. From DNA samples to final data reports, each step of sample quality control (QC), library preparation and sequencing can have an impact on the quality and quantity of data output, and the quality of data will directly affect the results of subsequent computational analysis. Therefore, obtaining high-quality data is the premise to ensure that bioinformatics analysis is correct, comprehensive and credible. In order to ensure the accuracy and reliability of sequencing data from the beginning, Novogene strictly checked every experimental step that fundamentally ensured the output of high-quality data. Sample preparation, library construction, sequencing and bioinformatic analysis were all done by Novogene Company Ltd and were sent to be visualised.

5.3 Results

5.3.1 *In-silico* genome-wide bulk ChIP-seq analysis confirms the enrichment for H3K4 methylation at the SMC gene loci following myogenic, osteogenic and adipogenic differentiation of mouse MSC *in vitro.*

In-silico analysis of published ChIP-seq data on H3K4me1, H3K4me2 or H3K4me3 marks at SMC-specific and lineage-specific gene loci (depending on availability) before and after myogenic (H3K4me3), vasculogenic (H3K4me3), adipogenic (H3K4me1) and osteogenic (H3K4me3) differentiation of mouse MSCs was performed using the GTN. The data was downloaded using its accession number from the published papers and GTN was used to perform the in-silico analysis as outlined in Chapter 2, Section 2.2.15.1 Differentiation of each

lineage was confirmed by checking peak calling of H3K4me1, H4K4me2 or H3K4me3 at their respective lineage-specific gene loci. Specifically, *Myh11, Cnn1, Smtn* and *Tagln* for MSC-derived myogenic progeny, lipoprotein lipase *(Lpl)* for MSC-derived adipogenic progeny, sclerostin *(Sost)* for MSC-derived osteogenic progeny and platelet endothelial cell adhesion molecule 1 *(Pecam1)* for MSC derived vasculogenic progeny. An integrated Genome Browser (IGB) was used to visualise and image the peaks, as described previously in Chapter 2, Section 2.2.15.1. Peak scores were generated by Galaxy and the terminal was used to look at the required locations for each gene of interest. Peak scores for each gene were compared to the overall peak scores across the genome for a given sample where the lower the percentage score, the more significant the peak.

To address the epigenetic profile of H3K27me3 and H3K4me3 at SMC gene-specific loci, peak calling was first assessed in mouse vascular smooth muscle cells (mVSMC) in culture. There was notable enrichment for H3K4me3 at SMC-specific gene loci (*Myh11, Cnn1, Tagln* and *Smtn*) in these cells compared to a lack of enrichment of H3K27me3 at the same SMC-specific gene loci [Figure 5.1]. In contrast, in undifferentiated mMSCs, there were notable peaks for H3K27me3 enrichment at different myogenic gene loci compared to INPUT [Figure 5.2]. Collectively, undifferentiated mMSCs enrich on H3K27me3 at SMC gene-specific loci while mVSMC enriches on H3K4me3 at the same loci.

In order to address whether H3K4me3 was enriched at SMC gene-specific loci following myogenic differentiation of mMSCs, peak calling was assessed using IGB. There was a notable peak for H3K4me3 enrichment at the *Myh11* and *Tagln* locus in mMSC-derived myogenic progeny compared to undifferentiated mMSC [Figure 5.3]. However, while there were notable peaks for H3K4me3 enrichment at the *Cnn1 and Smtn* gene loci in mMSC-derived myogenic progeny, these peaks appear less pronounced compared to undifferentiated mMSCs [Figure 5.3]. Therefore, peak scores for each gene were generated and compared before and after myogenic differentiation, where the lower the percentage peak score, the more significant the peak across the genome.

The change in the peak scoring for H3K4me3 enrichment at the *Myh11* locus following myogenic differentiation of mMSCs was significant and in the top 75% of all peaks, when

compared to undifferentiated mMSCs [Figure 5.4]. Similarly, the change in peak scores for H3K4me3 enrichment at the *Tagln* locus was also significant and in the top 75% of all peaks in mMSC-derived myogenic when compared to undifferentiated mMSCs [Figure 5.4]. In contrast, the opposite was observed for H3K4me3 enrichment at both the *Cnn1* and *Smtn* locus following myogenic differentiation of mMSCs where peak scores rose significantly from 25% of all peaks in undifferentiated mMSCs [Figure 5.4].

To confirm lineage-specific differentiation of MSCs, methylation of H3K4 was assessed at lineage-specific loci following vasculogenic, osteogenic and adipogenic differentiation, respectively. Peak calling was determined at each lineage-specific loci (*Pecam1*, *Lpl* and *Sost)* following lineage-specific differentiation using IGB. There was a notable peak for H3K4me3 enrichment at the *Pecam1* locus in MSC-derived vasculogenic progeny compared to undifferentiated mMSC [Figure 5.5]. Similarly, there was notable enrichment of H3K4me3 on the *Sost* locus and H3K4me1 on the *Lpl locus* in mMSC-derived osteogenic and adipogenic progeny, respectively, when compared to in undifferentiated mMSC [Figure 5.6, Figure 5.7]. Peaks at lineage-specific genes indicate differentiation of mMSC.

In order to determine whether the H3K4me3 mark was enriched at SMC gene-specific loci following vasculogenic, osteogenic and adipogenic differentiation, respectively, peak calling at these loci was next assessed using IGB.

In undifferentiated mMSCs, there was no discernible peak for H3K4me3 enrichment at the *Myh11* locus whereas there were notable peaks at the *Cnn1*, *Tagln* and *Smtn* locus in these undifferentiated mMSCs [Figure 5.8]. Similarly, there were no discernible peaks for H3K4me3 at the *Myh11* locus in vasculogenic progeny and the H3K4me3 peaks at the *Cnn1*, *Tagln* and *Smth* locus appeared less pronounced than undifferentiated mMSCs [Figure 5.8].

There were notable peaks for H3K4me3 enrichment at the *Myh11* locus in osteogenic progeny while the H3K4me3 peaks at the *Cnn1*, *Tagln* and *Smth* locus appeared less pronounced than undifferentiated mMSCs [Figure 5.8]. There were also notable peaks for H3K4me1 enrichment at the *Myh11* locus in adipogenic progeny compared to undifferentiated mMSCs

whilst the H3K4me1 peaks at the *Cnn1, Tagln* and *Smth* locus appeared similar or less pronounced than undifferentiated mMSCs [Figure 5.9].

Peak scores were again generated for each histone mark at gene-specific loci and compared before and after lineage specification, where the lower the percentage peak score, the more significant the peak across the genome. Peak scoring for H3K4me3 and H3K4me1 enrichment was assessed at the lineage-specific gene loci following specification [Figure 5.10, 5.11 and 5.12] and confirmed the peak calling data profiling for vasculogenic, adipogenic and osteogenic progeny [Figures 5.5, 5.6 and 5.7].

The change in the peak score for H3K4me3 at the lineage-specific *Pecam1* gene locus in vasculogenic progeny was significant and in the top 50% when compared to the insignificant peak score in undifferentiated mMSCs [Figure 5.10]. However, the change in the peak score for H3K4me3 enrichment at the *Myh11* locus in both undifferentiated mMSCs and their vasculogenic progeny was not significant when compared to similar peaks across the genome [Figure 5.10]. Similarly, the change in the peak score for H3K4me3 enrichment at the *Cnn1* and *Smtn* locus in vasculogenic progeny was not significant compared to similar peaks across the genome in undifferentiated mMSCs [Figure 5.10]. Only the peak score for H3K4me3 at the *Tagln* locus became more significant in vasculogenic progeny when compared to similar peaks across the genome [Figure 5.10].

The change in the peak score for H3K4me3 enrichment at the lineage-specific *Sost* locus in osteogenic progeny was significant and in the top 50% of peaks compared to similar peaks across the genome in undifferentiated mMSCs [Figure 5.11]. The change in the peak score for H3K4me3 enrichment at the *Myh11* locus in osteogenic progeny was also significant and in the top 25% of all peaks when compared to similar peaks across the genome and undifferentiated mMSCs [Figure 5.11]. The peak score for H3K4me3 enrichment at the *Smtn* locus in osteogenic progeny did not change from the top 25% of all peaks while the peak scores for H3K4me3 enrichment at the *Cnn1 and Tagln* loci were less significant following osteogenic differentiation [Figure 5.11].

The change in the peak score for H3K4me1 enrichment at the lineage-specific *Lpl* locus in adipogenic progeny was significant and in the top 25% of peaks compared to similar peaks across the genome and in undifferentiated mMSCs [Figure 5.12]. Similarly, the change in the peak score for H3K4me1 enrichment at the *Myh11* locus in adipogenic progeny was also significant and in the top 25% of all peaks when compared to similar peaks across the genome and in undifferentiated mMSCs [Figure 5.12]. The change in the peak score for H3K4me1 enrichment at the *Smtn* locus in adipogenic progeny was also significant and in the top 75% of all peaks when compared to undifferentiated mMSCs [Figure 5.12]. The change in the peak score for H3K4me1 enrichment at the *Cnn1*and *Smtn loci* in adipogenic progeny was less significant when compared to the peak score of 75% and 50%, respectively, of all peaks in undifferentiated mMSCs [Figure 5.12]. Peak scores for H3K4me1 enrichment at the *Tagln* locus in adipogenic progeny did not change from the top 75% of all peaks when compared to undifferentiated mMSCs [Figure 5.12].

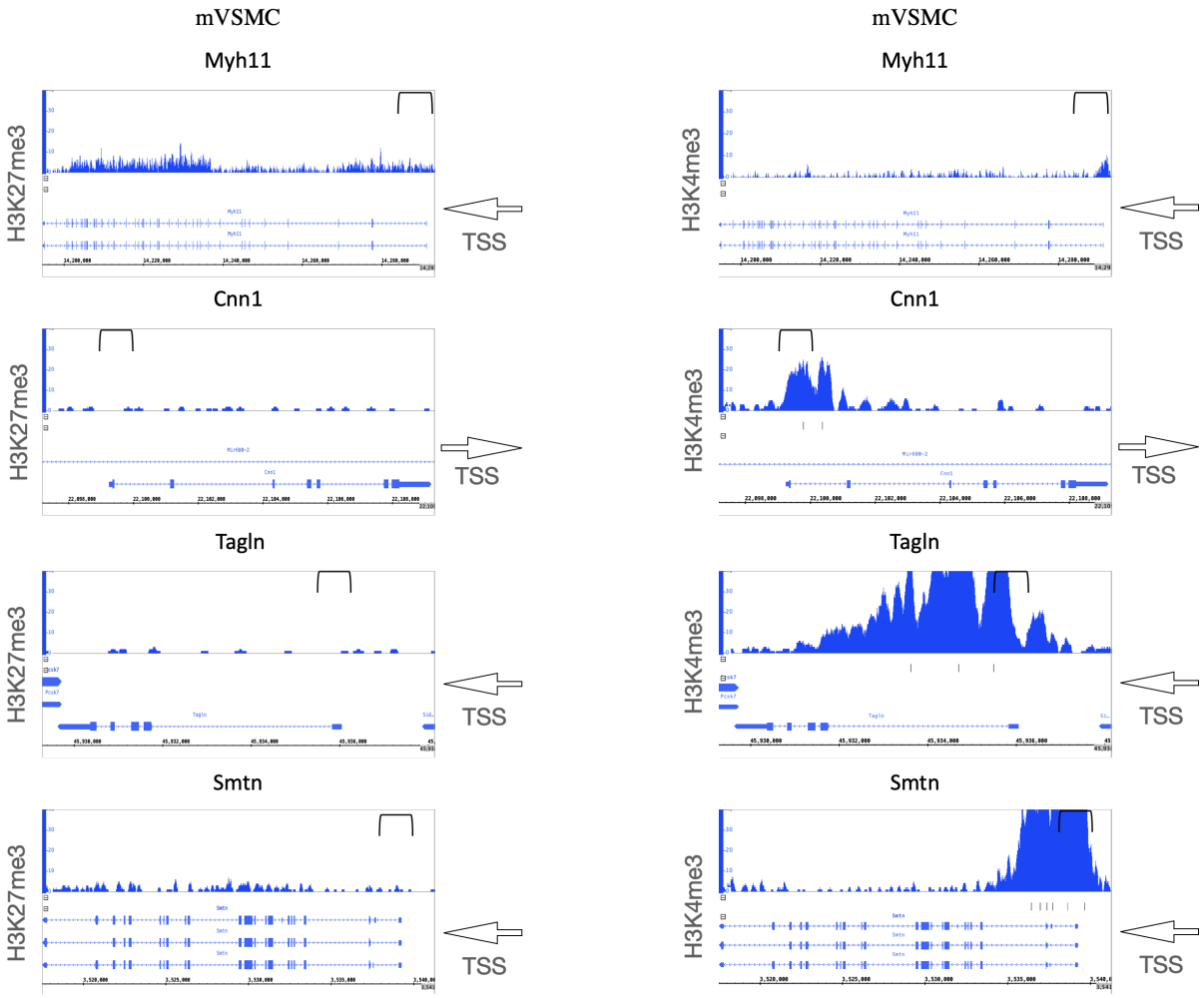

Figure 5.1. ChIP-seq peak calling for H3K27me3 and H3K4me3 at *Myh11, Cnn1, Tagln* and *Smtn* gene loci in cultured mouse vascular smooth muscle cells (mVSMC).

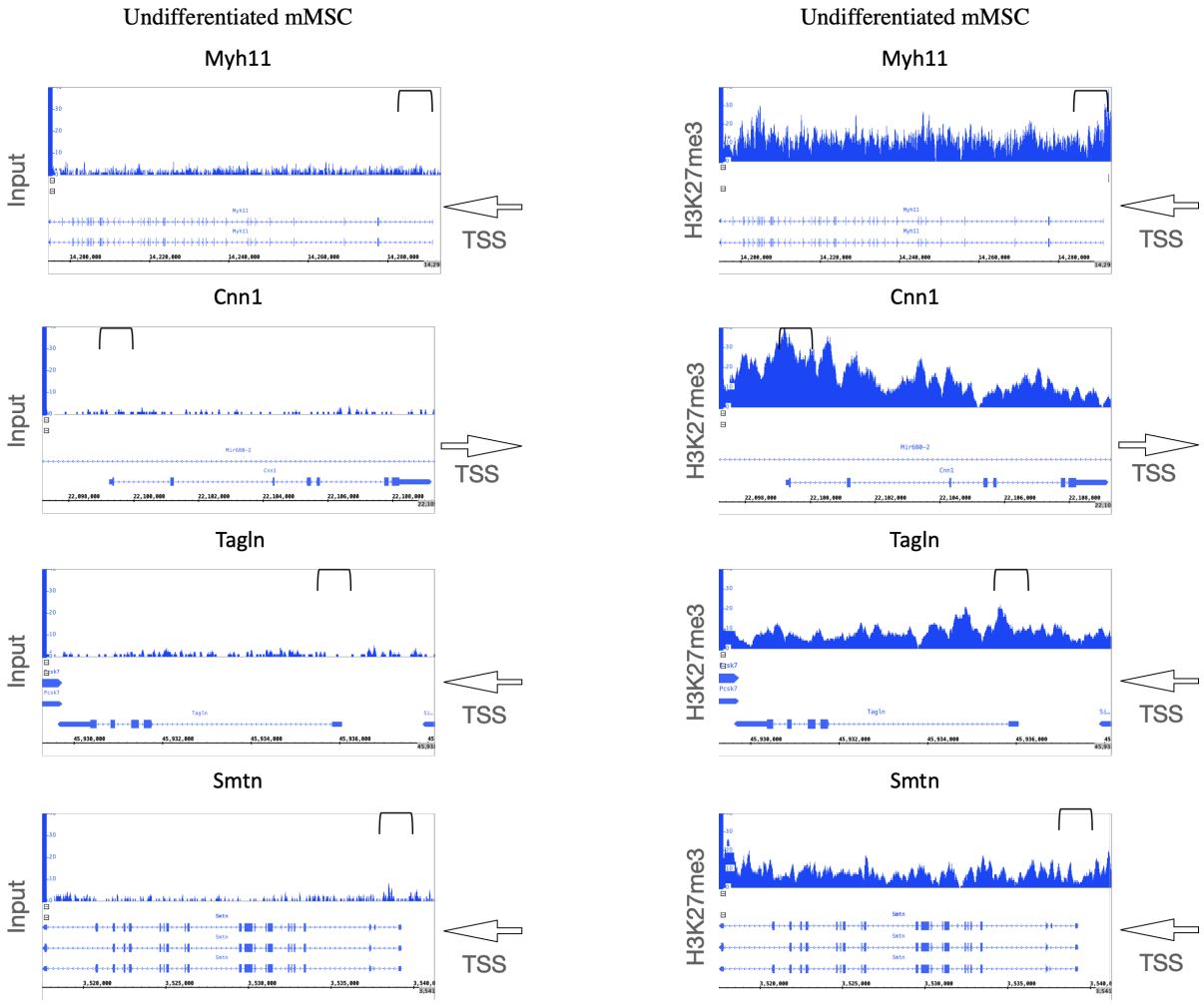

Figure 5.2. ChIP-seq peak calling for Input and H3K27me3 at the *Myh11, Cnn1, Tagln* and *Smtn* gene loci in undifferentiated mMSC grown in their maintenance medium.

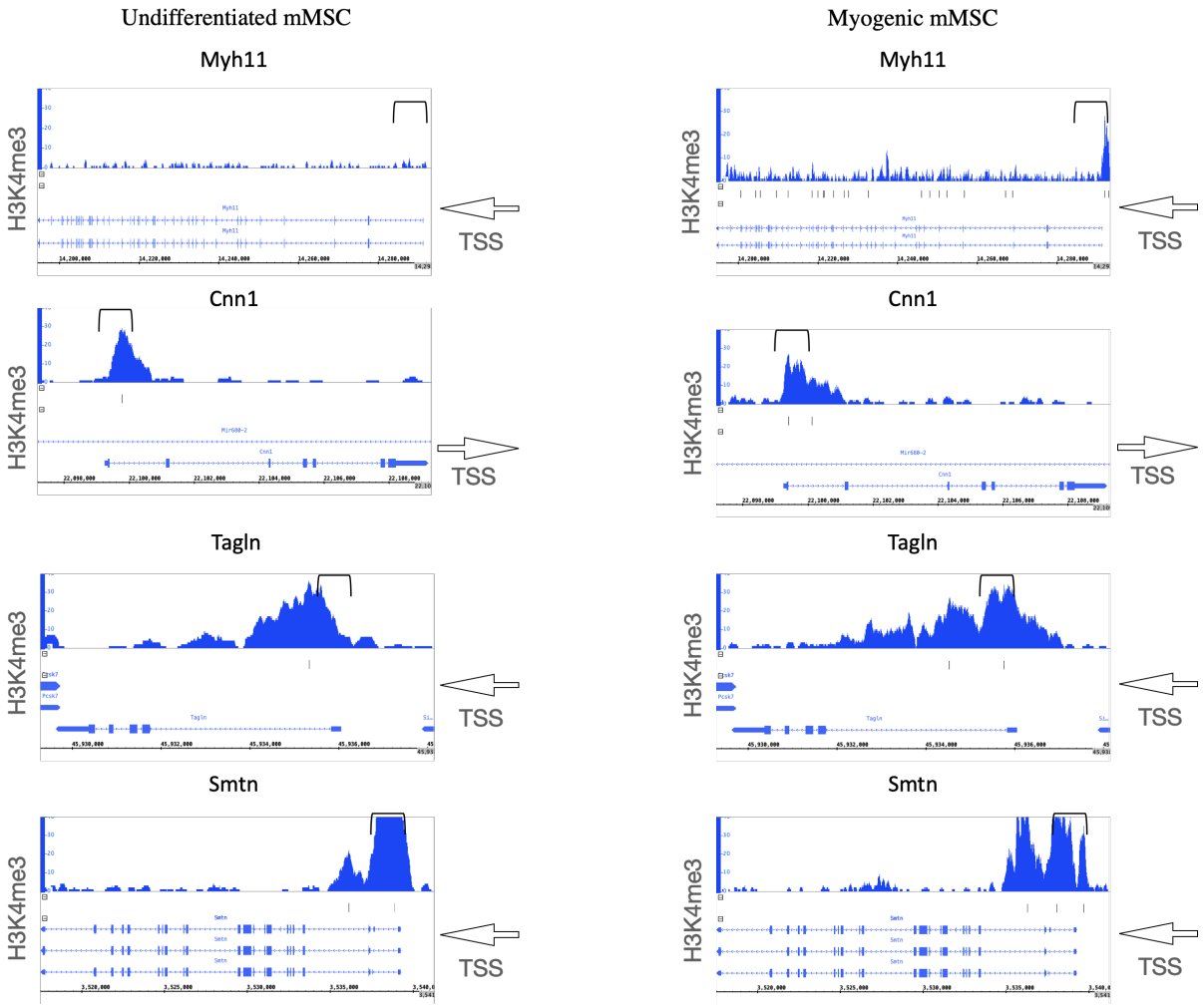

Figure 5.3. ChIP-seq peak calling for H3K4me3 at the *Myh11, Cnn1*, *Tagln* and *Smtn* gene loci in undifferentiated mMSC and mMSCs following myogenic differentiation.

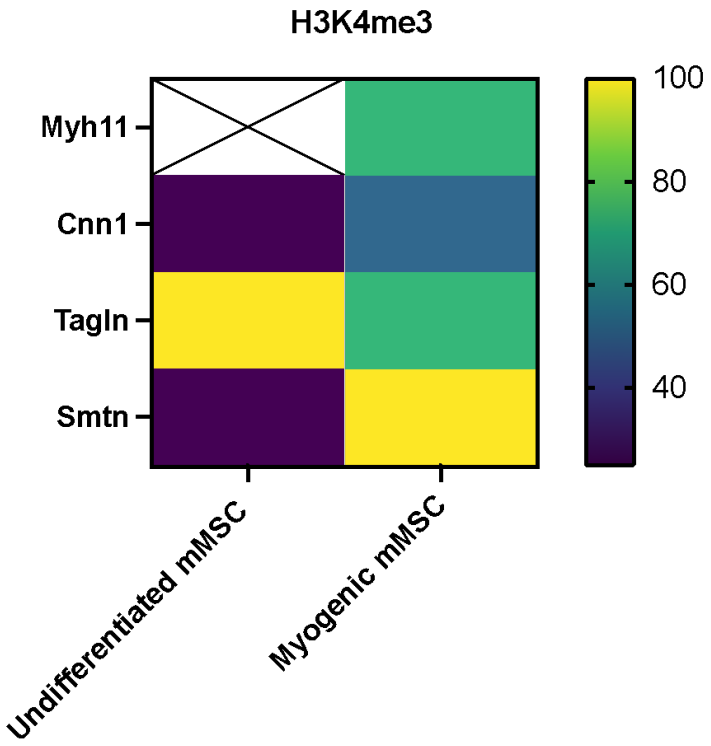

Figure 5.4. ChIP-seq peak scores for H3K4me3 at different gene loci *(Myh11, Cnn1, Smtn* and *Tagln*) in mMSC derived myogenic progeny compared to undifferentiated mMSCs.

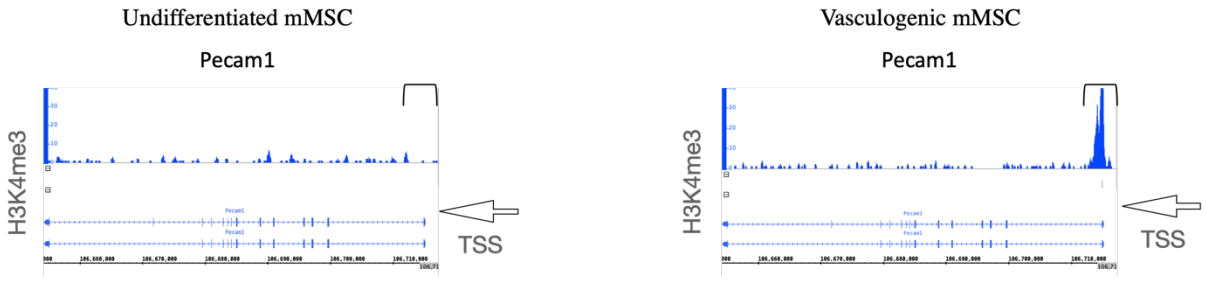

Figure 5.5. ChIP-seq peak calling for H3K4me3 at the *Pecam1* gene locus in undifferentiated mMSC and vasculogenic differentiated mMSC

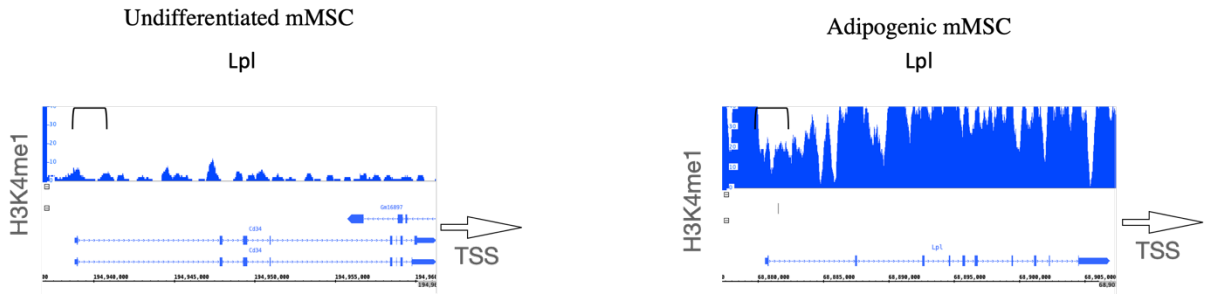

Figure 5.6. ChIP-seq peak calling for H3K4me1 at *Lpl* gene locus in undifferentiated mMSC and adipogenic differentiated mMSC

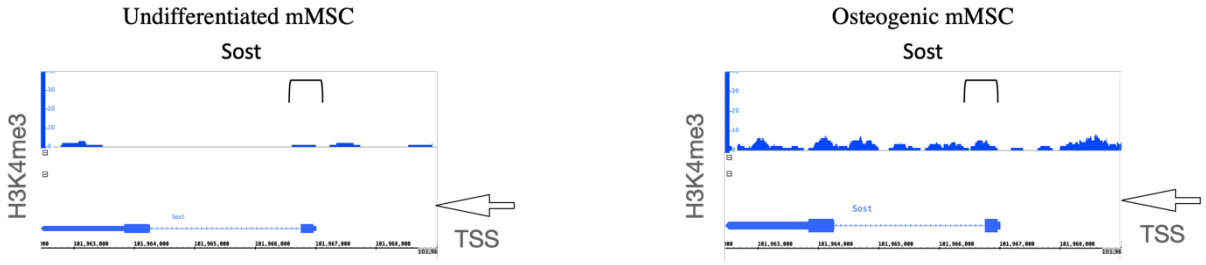

Figure 5.7. ChIP-seq peak calling for H3K4me3 at *Sost* gene locus in undifferentiated mMSC and osteogenic differentiated mMSC

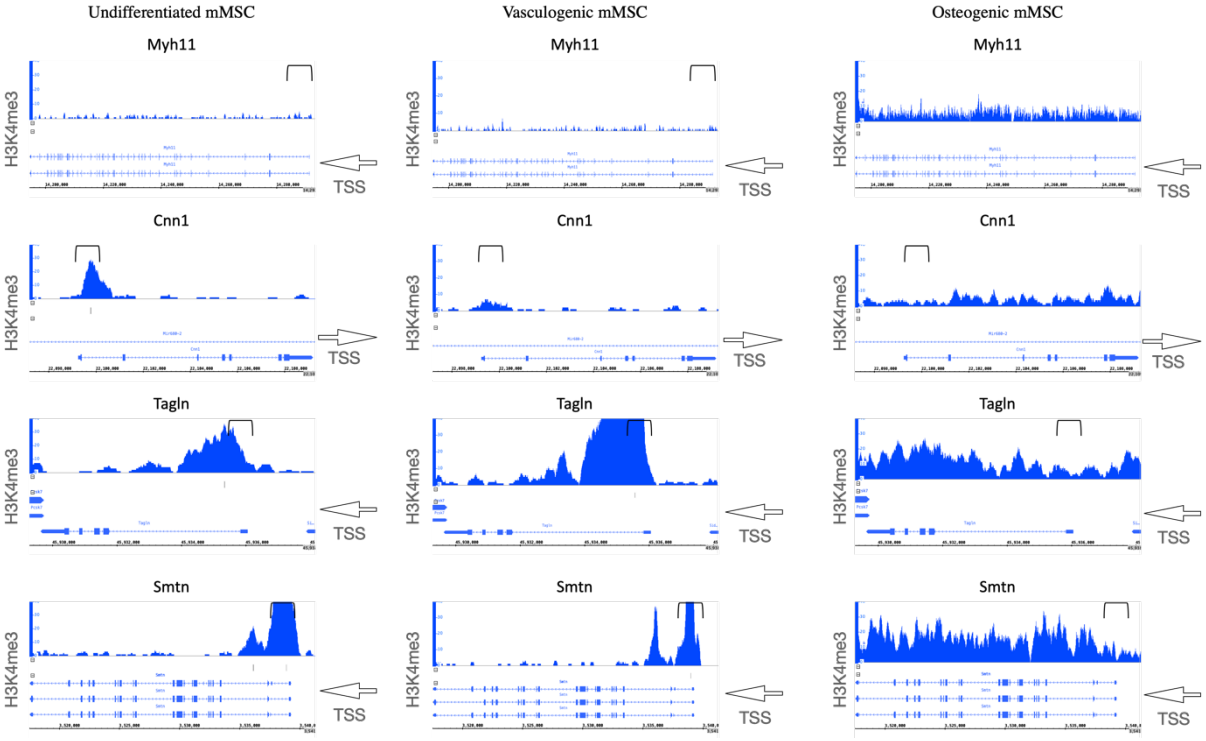

Figure 5.8. ChIP-seq peak calling for H3K4me3 at *Myh11, Cnn1, Tagln* and *Smtn* gene loci in undifferentiated mMSC and following vasculogenic and osteogenic differentiation of mMSC.

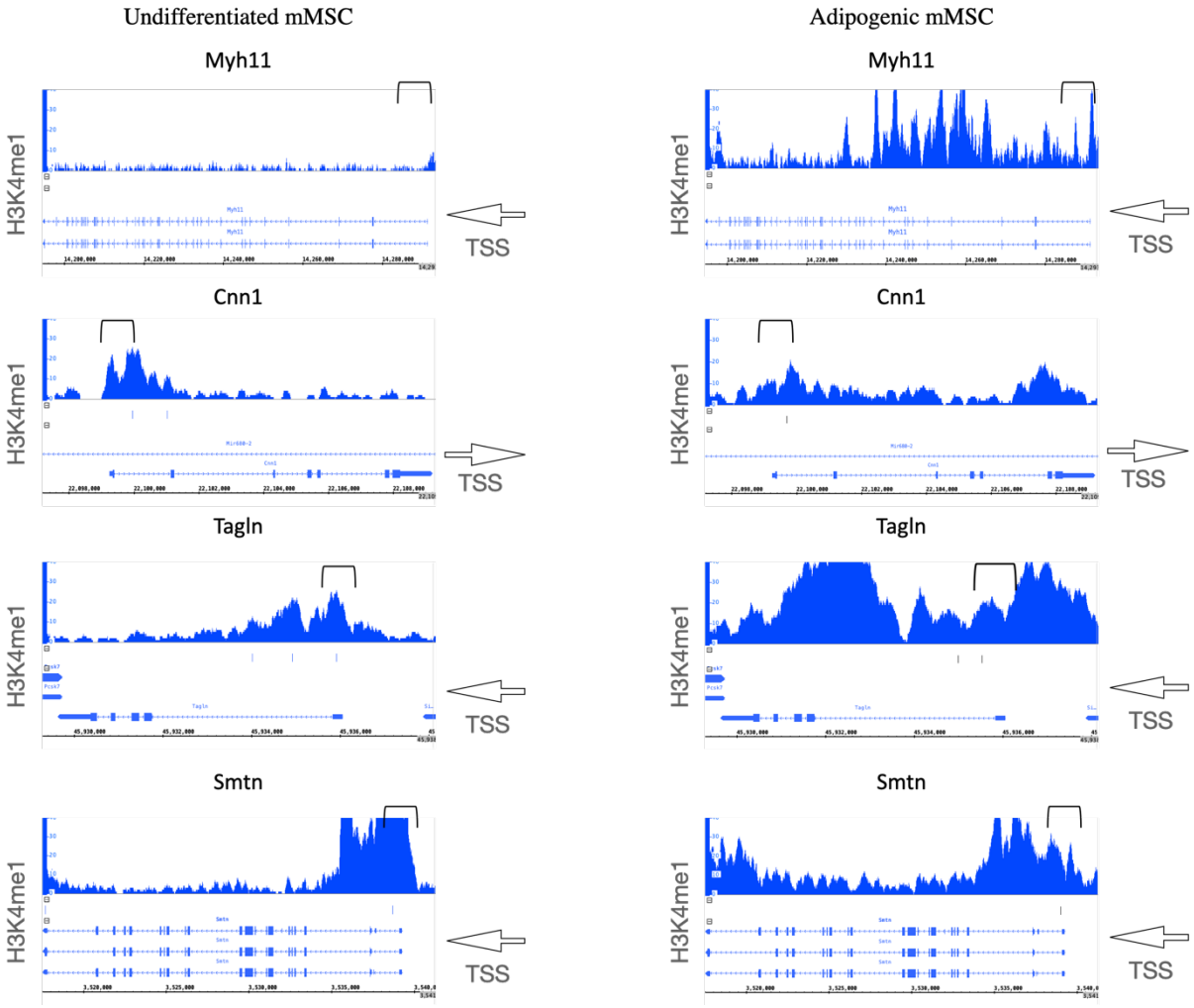

Figure 5.9. ChIP-seq peak calling for H3K4me1 at *Myh11, Cnn1, Tagln* and *Smtn* gene loci in undifferentiated mMSC and following adipogenic differentiation of mMSC.

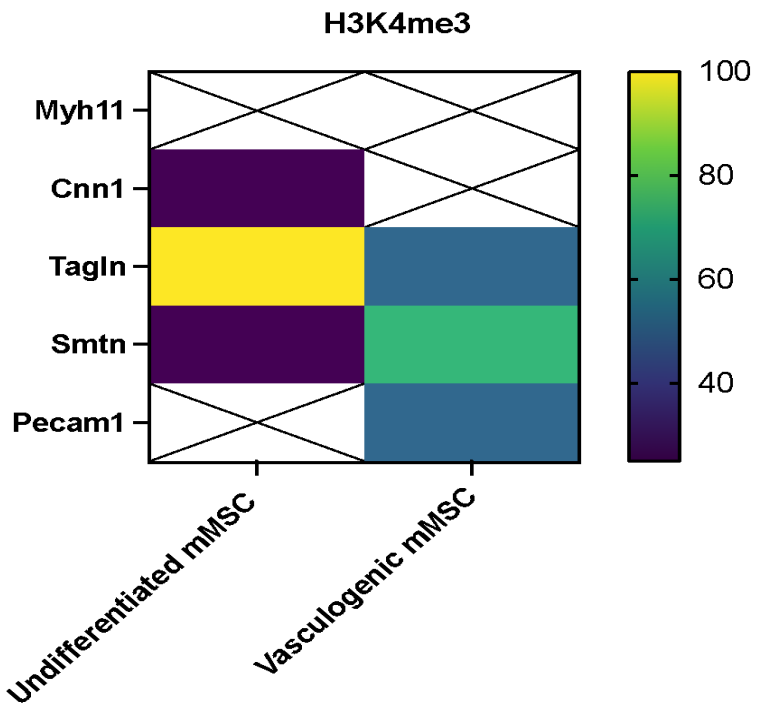

Figure 5.10. ChIP-seq peak scores of H3K4me3 at SMC gene loci (*Myh11, Cnn1, Smtn, Tagln)* and the *Pecam1* locus in mMSC derived vasculogenic progeny compared to undifferentiated MSCs.

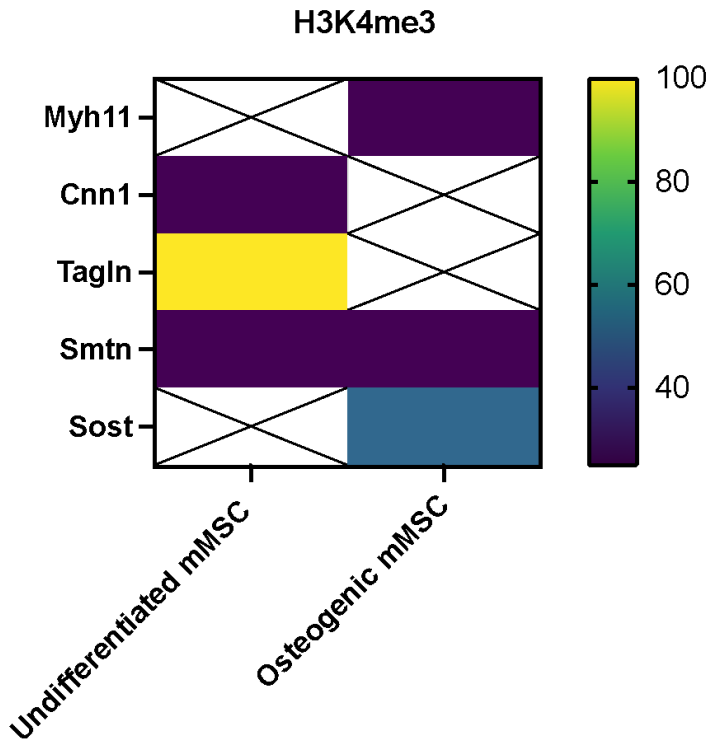

Figure 5.11. ChIP-seq peak scores of H3K4me3 at SMC gene loci (*Myh11, Cnn1, Smtn, Tagln)* and the *Sost* locus in mMSC derived osteogenic progeny compared to undifferentiated MSCs.

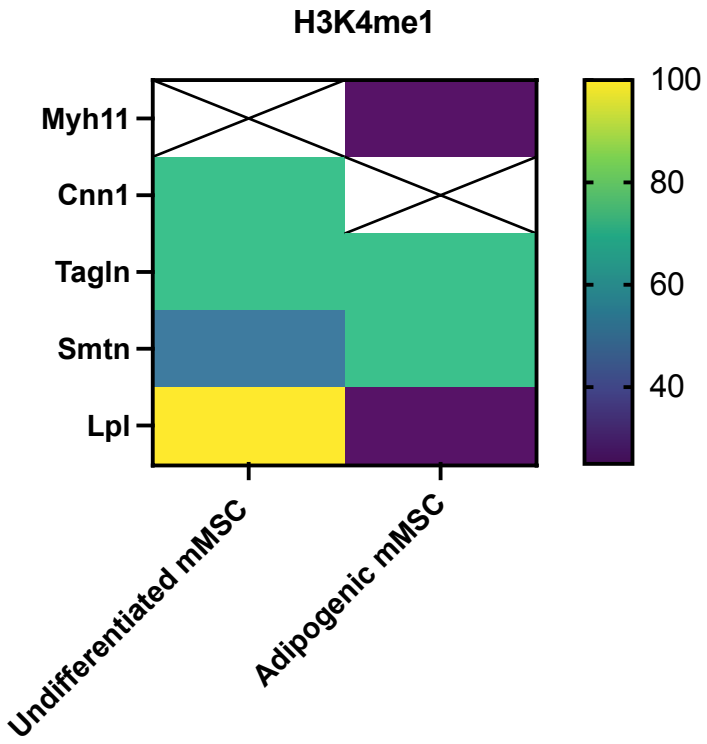

Figure 5.12. ChIP-seq peak scores of H3K4me1 at SMC gene loci (*Myh11, Cnn1, Smtn, Tagln)* and the *Lpl* locus in mMSC derived adipogenic progeny compared to undifferentiated MSCs.

5.3.2 *In-silico* genome-wide bulk ChIP-seq analysis reveals the enrichment for H3K4 methylation at the SMC gene loci following myogenic, osteogenic and adipogenic differentiation of human MSC and human embryonic stem cells (H9 ESCs) *in vitro.*

In-silico analysis of published ChIP-seq data on H3K4me1, H3K4me2 or H3K4me3 marks at SMC-specific loci and lineage-specific loci (depending on availability) before and after myogenic (H3K4me2), vasculogenic (H3K4me3), adipogenic (H3K4me1) and osteogenic (H3K4me1) differentiation of human MSCs or human H9 ESCs were first performed using the GTN. The data was downloaded using its accession number from the published papers and GTN was used to perform the *in-silico analysis* as outlined in Chapter 2, Section 2.2.15.1.

Differentiation of each lineage was first checked by peak calling of H3K4me1, H4K4me2 or H3K4me3 enrichment at their respective lineage-specific gene loci. Specifically, *MYH11, CNN1, SMTN* and *TAGLN* were interrogated in H9 ESCs-derived myogenic progeny, while *LPL* was assessed for hMSC-derived adipogenic progeny, *SOST fo*r H9 ESCs-derived osteogenic progeny and cluster of differentiation 34 *(CD34)* for MSC-derived vasculogenic progeny. IGB was used to visualise and image the peaks as described previously in Chapter 2, Section 2.2.15.1. Peak scores were generated by Galaxy and the terminal was used to look at the required locations for each gene of interest. Peak scores for each gene were compared to the overall peak scores across the genome for a given sample where the lower the percentage score, the more significant the peak.

Peak calling for the repressive H3K27me3 mark at SMC gene-specific loci (*MYH11, CNN1, TAGLN* and *SMTN*) was first assessed in undifferentiated hMSCs using IGB. There were notable peaks for H3K27me3 enrichment in undifferentiated hMSC at *MYH11, CNN1* and *TAGLN* gene loci compared to INPUT [Figure 5.13].

In order to address whether H3K4me2 was enriched at SMC gene-specific loci in H9 ESCs-derived myogenic progeny, peak calling was again assessed using IGB. H3K4me2 was notably enriched at SMC-specific gene loci (*MYH11*, *CNN1*, *TAGLN* and *SMTN)* around the transcription starting site (TSS) following myogenic differentiation when compared to undifferentiated H9 ESCs [Figure 5.14]. The change in peak score for H3K4me2 enrichment

at the *MYH11* locus was significant in myogenic progeny and in the top 25% of all peaks when compared to similar peaks across the genome and compared to undifferentiated H9 ESCs [Figure 5.15]. Similarly, the change in peak score for H3K4me2 enrichment at the *CNN1* locus in myogenic progeny was significant and in the top 50% of all peaks when compared to undifferentiated H9 ESCs [Figure 5.15]. The change in peak score for H3K4me2 enrichment at the *TAGLN* locus was also significant and in the top 25% of all peaks in myogenic progeny when compared to similar peaks across the genome and undifferentiated H9 ESCs [Figure 5.15]. However, the peak score for H3K4me2 enrichment at the S*MTN* locus did not change from the top 75% in myogenic progeny when compared to undifferentiated H9 ESCs [Figure 5.15].

In order to address whether methylation of H3K4me was enriched at lineage-specific loci following vasculogenic, osteogenic and adipogenic differentiation of hMSCs, peak calling of H3K4me1, 2 or 3 at lineage-specific loci was assessed using IGB. There was a notable peak for H3K4me3 enrichment at the *CD34* locus in vasculogenic progeny compared to undifferentiated hMSC [Figure 5.16]. Similarly, there was notable enrichment for H3K4me1 on the *SOST* and *LPL* loci in H9 ESCs and hMSC-derived osteogenic and adipogenic progeny, respectively when compared to in undifferentiated cells [Figure 5.17, Figure 5.18]. Peaks at lineage-specific genes indicate differentiation of H9 ESCs and hMSC.

In order to assess whether H3K4me3 was enriched at SMC gene-specific loci following vasculogenic differentiation of hMSCs, peak calling was assessed using IGB. There were notable peaks for H3K4me3 enrichment at the *SMTN and TAGLN* locus in hMSC-derived vasculogenic progeny when compared to undifferentiated hMSCs [Figure 5.19]. In contrast, there was no discernible observed difference in the peaks for H3K4me3 enrichment at the *MYH11 and CNN1* locus in hMSC-derived vasculogenic progeny when compared to undifferentiated hMSCs [Figure 5.19].

In order to assess whether H3K4me1 was enriched at SMC gene-specific loci following adipogenic and osteogenic differentiation, peak calling was assessed using IGB. There were notable peaks for H3K4me1 enrichment at the *MYH11*, *CNN1,* and *TAGLN* gene loci in hMSCs-derived adipogenic when compared to undifferentiated hMSCs [Figure 5.20]. While *SMTN*

locus appeared similar or less pronounced than undifferentiated hMSCs There were notable peaks for H3K4me1 enrichment at the *MYH11*, *CNN1, TAGLN* and *SMTN* gene loci in H9 hESCs-derived osteogenic progeny when compared to undifferentiated H9 hESCs [Figure 5.21].

The change in peak score for H3K4me3 enrichment at the lineage-specific *CD34* vasculogenic gene locus following vasculogenic differentiation of hMSCs was significant and in the top 50% of all peaks compared to undifferentiated hMSCs [Figure 5.22]. The change in peak scores for H3K4me3 enrichment at the *TAGLN* and *SMTN* locus in vasculogenic progeny were also significant and in the top 25% and 50% of all peaks, respectively, when compared to similar peaks across the genome and compared to undifferentiated hMSCs [Figure 5.22]. In contrast, the peak scores for H3K4me3 enrichment at the *MYH11* and *CNN1* locus in vasculogenic progeny were insignificant with no significant difference in peak scores when compared to undifferentiated hMSCs [Figure 5.22].

The change in the peak score for H3K4me1 enrichment at the lineage-specific *LPL* adipogenic gene locus following adipogenic differentiation of hMSCs was significant and in the top 50% of all peaks compared to undifferentiated hMSCs [Figure 5.23]. The peak scores for H3K4me1 enrichment in adipogenic progeny at the *MYH11* and *SMTN* loci did not change from the top 25% of all peaks when compared to undifferentiated hMSCs [Figure 5.23]. The change in the peak score for H3K4me1 enrichment at the *CNN1* and *TAGLN* loci in adipogenic progeny was significant and in the top 25% of all peaks when compared to undifferentiated hMSCs [Figure 5.23].

The change in peak score for H3K4me1 enrichment at the lineage-specific *SOST* osteogenic gene locus following osteogenic differentiation of H9 ESCs was significant when compared to undifferentiated H9 ESCs [Figure 5.24]. The change in the peak score for H3K4me1 enrichment at the *MYH11 l*ocus in osteogenic progeny was significant and in the top 25% of all peaks when compared to undifferentiated H9 hESCs [Figure 5.24]. The change in the peak score for H3K4me1 enrichment at the *CNN1* locus in the same osteogenic progeny was significant and in the top 25% of all peaks when compared to undifferentiated H9 hESCs [Figure 5.24]. Peak scores for H3K4me1 enrichment at the *TAGLN* and *SMTN* locus in osteogenic progeny did not

change from the top 75% of all peaks when compared to undifferentiated H9 hESCs [Figure 5.24].

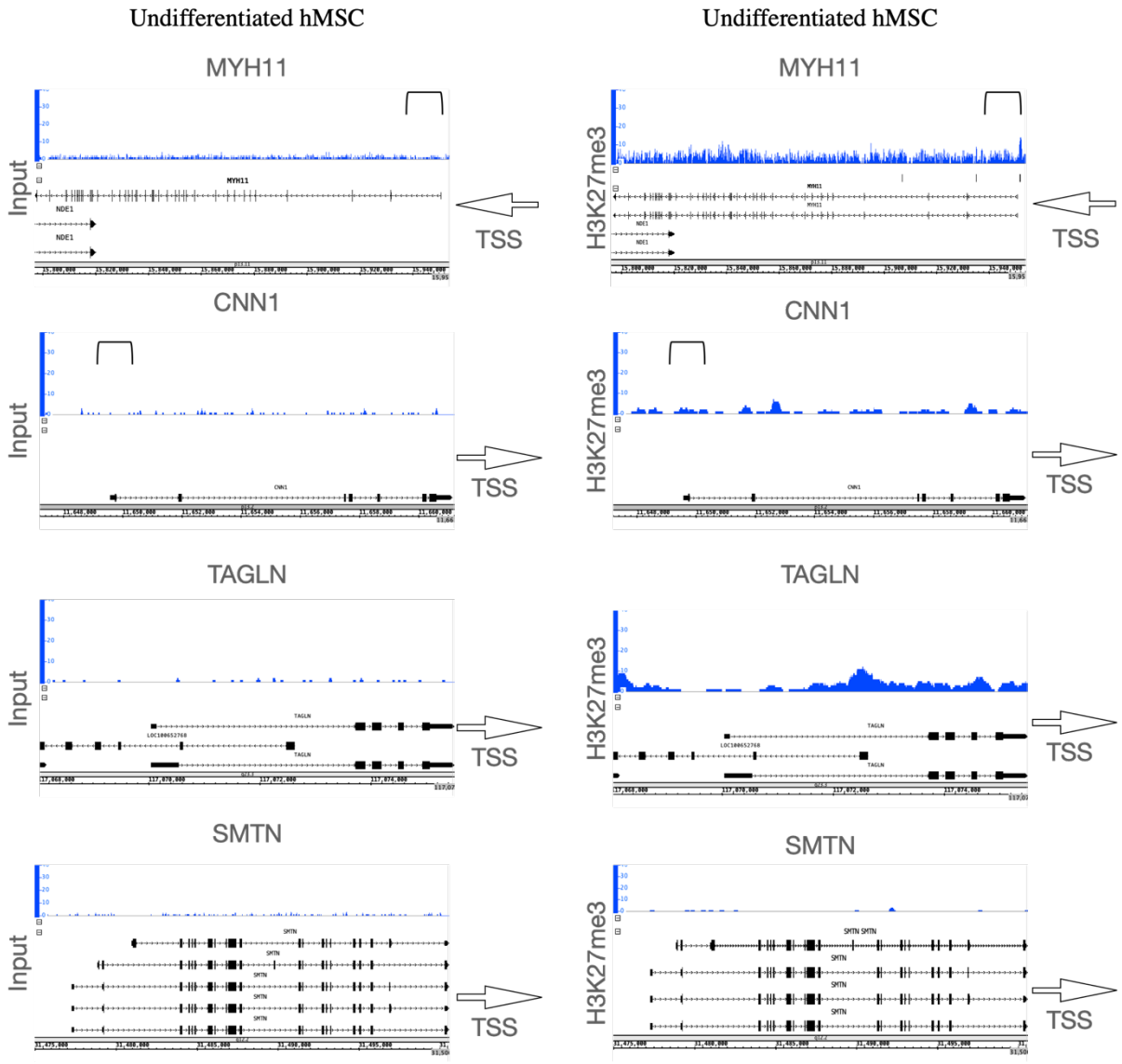

Figure 5.13. ChIP-seq peak calling for Input and H3K27me3 at *MYH11, CNN1, TAGLN* and *SMTN g*ene loci in undifferentiated hMSC grown in their maintenance medium.

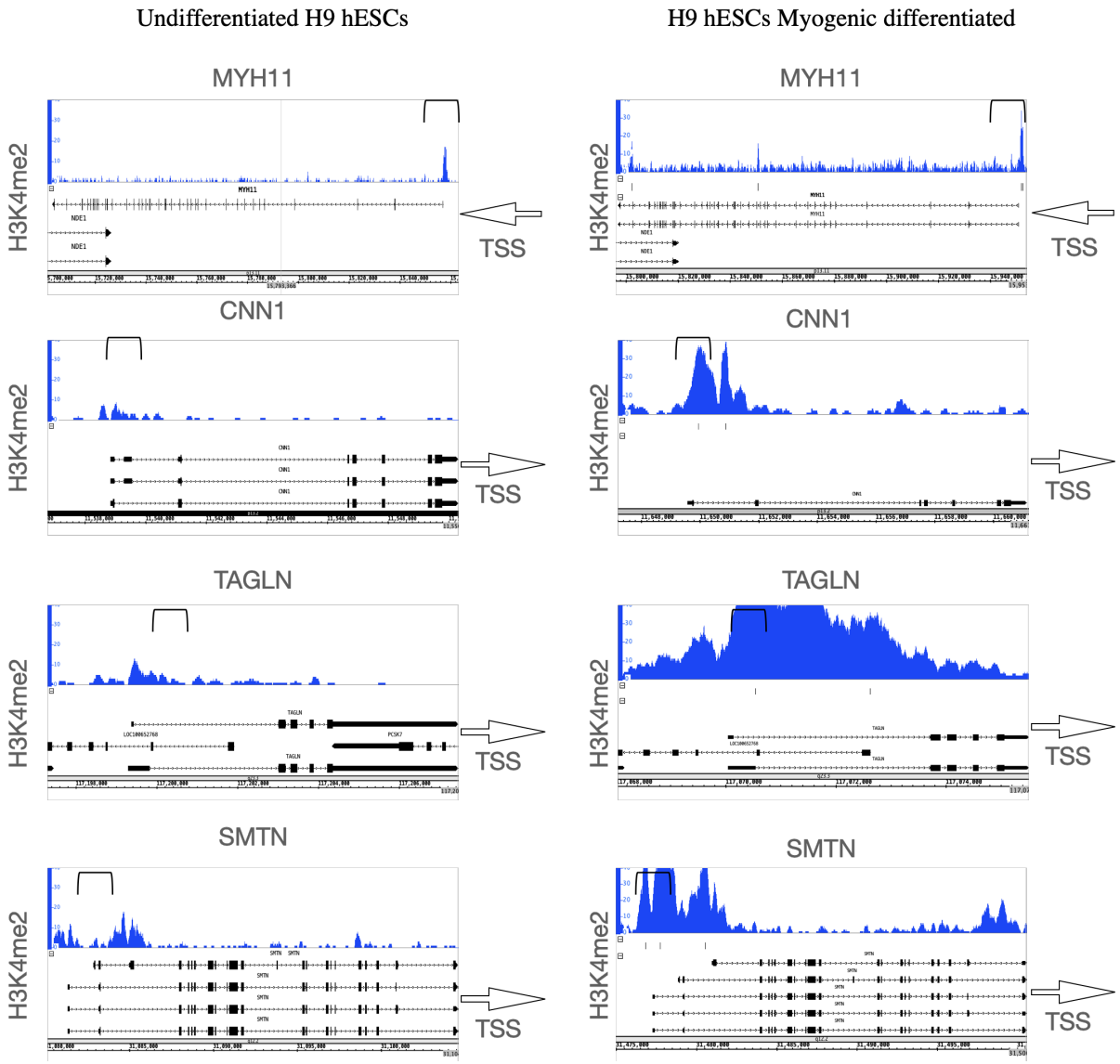

Figure 5.14. ChIP-seq peak calling for H3K4me2 at *MYH11, CNN1, TAGLN* and *SMTN* gene loci in undifferentiated H9 hESCs and following myogenic differentiation of H9 hESCs.

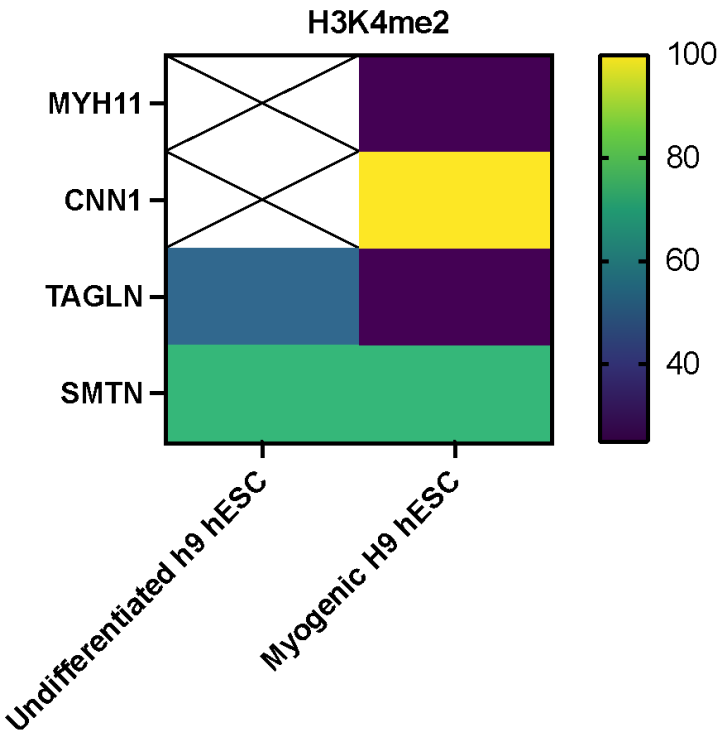

Figure 5.15. ChIP-seq peak scores of H3K4me2 at SMC gene loci (*MYH11, CNN1, SMTN, TAGLN)* in H9 hESCs derived myogenic progeny compared to undifferentiated H9 hESCs.

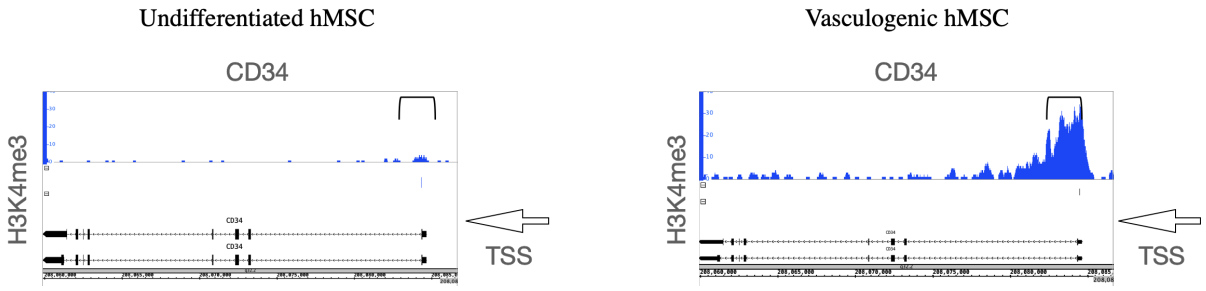

Figure 5.16. ChIP-seq peak calling for H3K4me3 at the *CD34* gene locus in in undifferentiated hMSC and following vasculogenic differentiation of hMSCs.

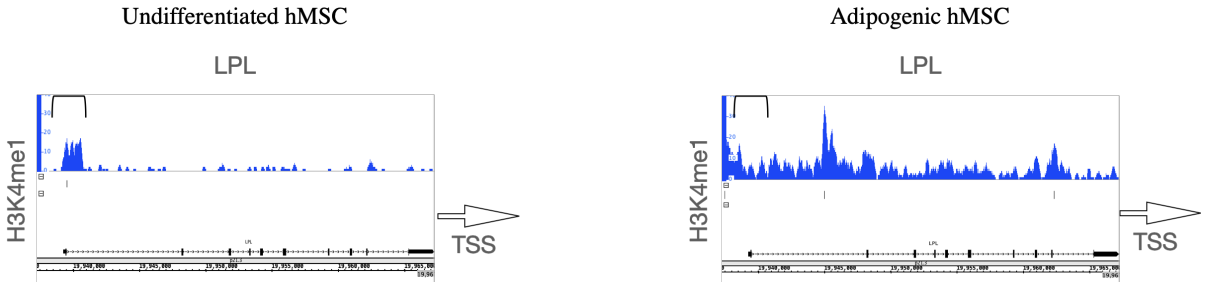

Figure 5.17. ChIP-seq peak calling for H3K4me1 at the *LPL* gene locus in undifferentiated hMSC and following adipogenic differentiation of hMSCs.

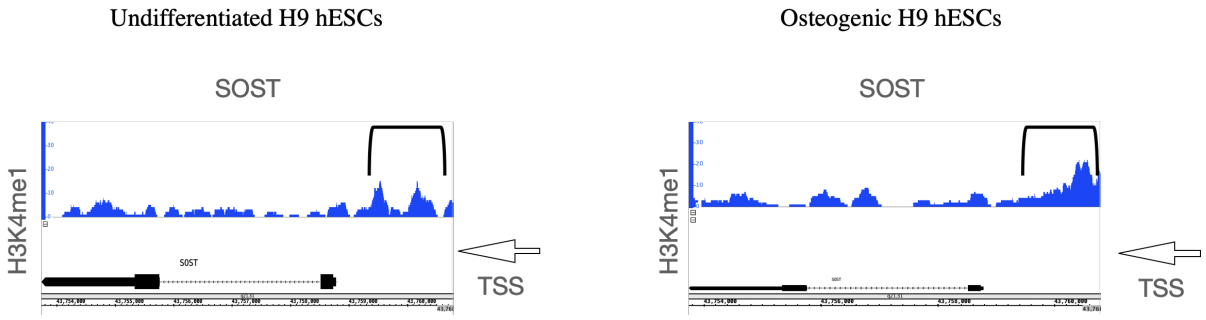

Figure 5.18. ChIP-seq peak calling for H3K4me1 at *SOST* gene locus in undifferentiated H9 hESCs and following osteogenic differentiation of H9 hESCs.

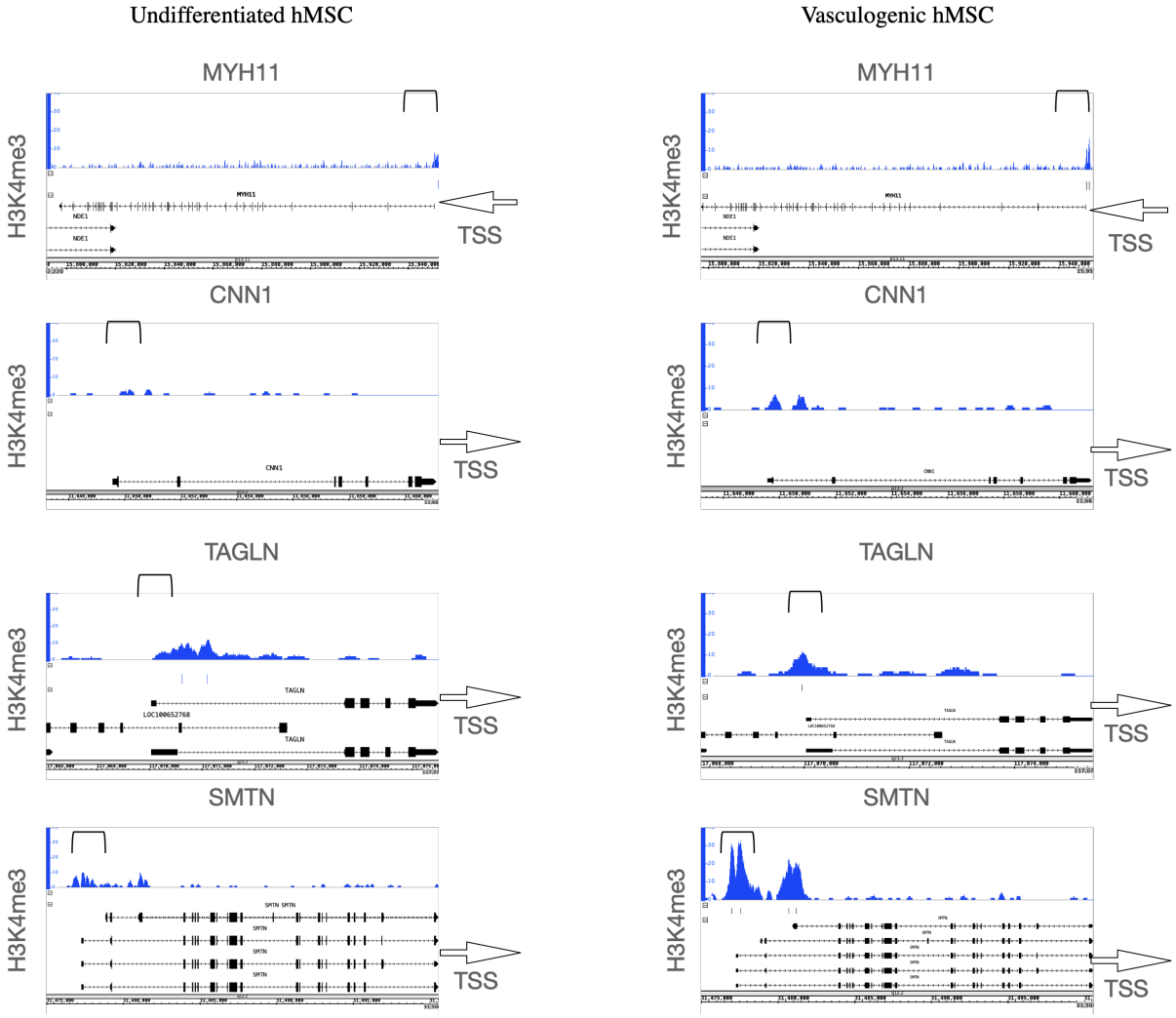

Figure 5.19. ChIP-seq peak calling for H3K4me3 at SMC gene loci (*MYH11, CNN1, TAGLN* and *SMTN)* in undifferentiated hMSC and following vasculogenic differentiation of hMSCs.

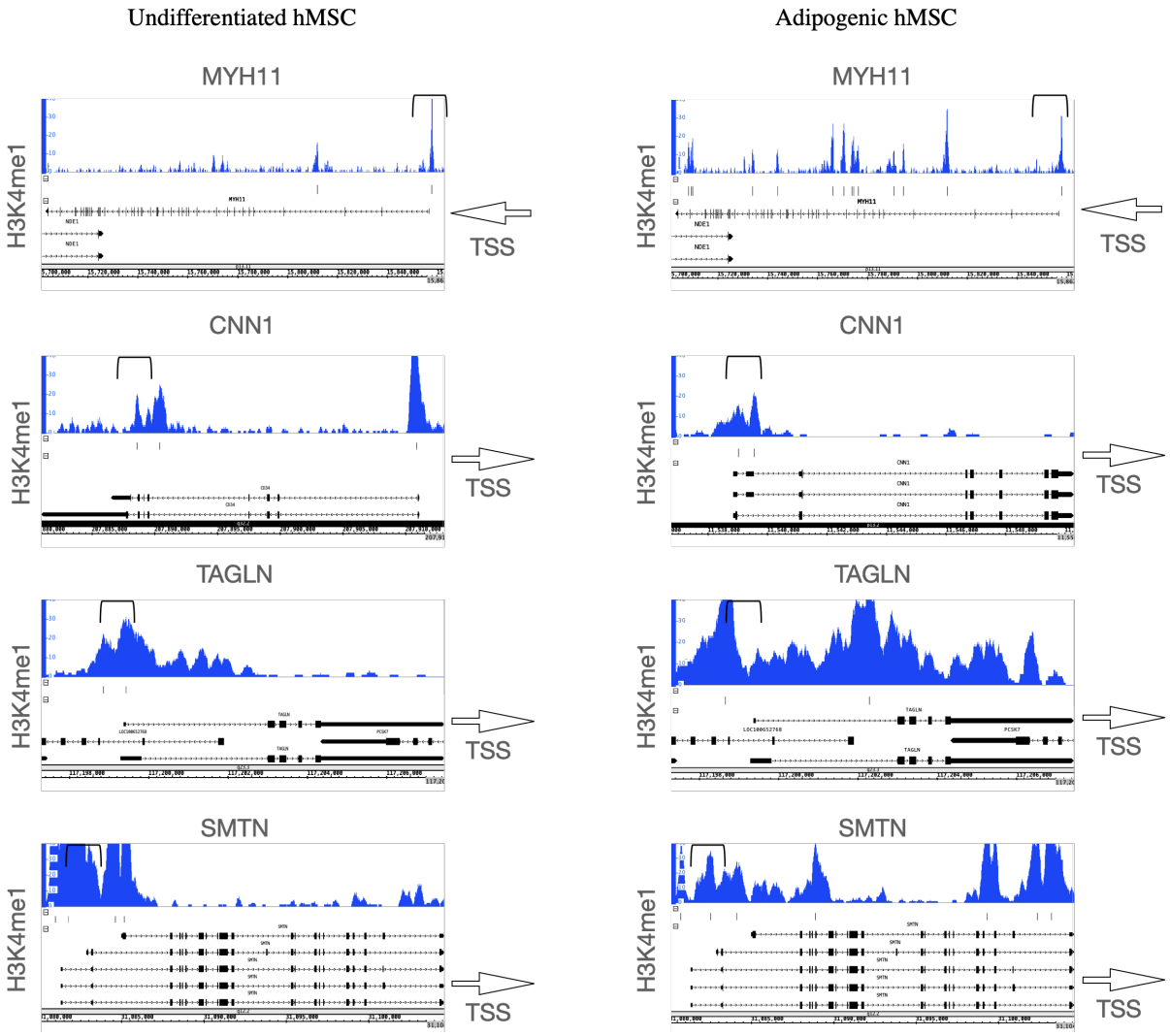

Figure 5.20. ChIP-seq peak calling for H3K4me1 at SMC gene loci (*MYH11, CNN1, TAGLN* and *SMTN)* in undifferentiated hMSC and following adipogenic differentiation of hMSCs.

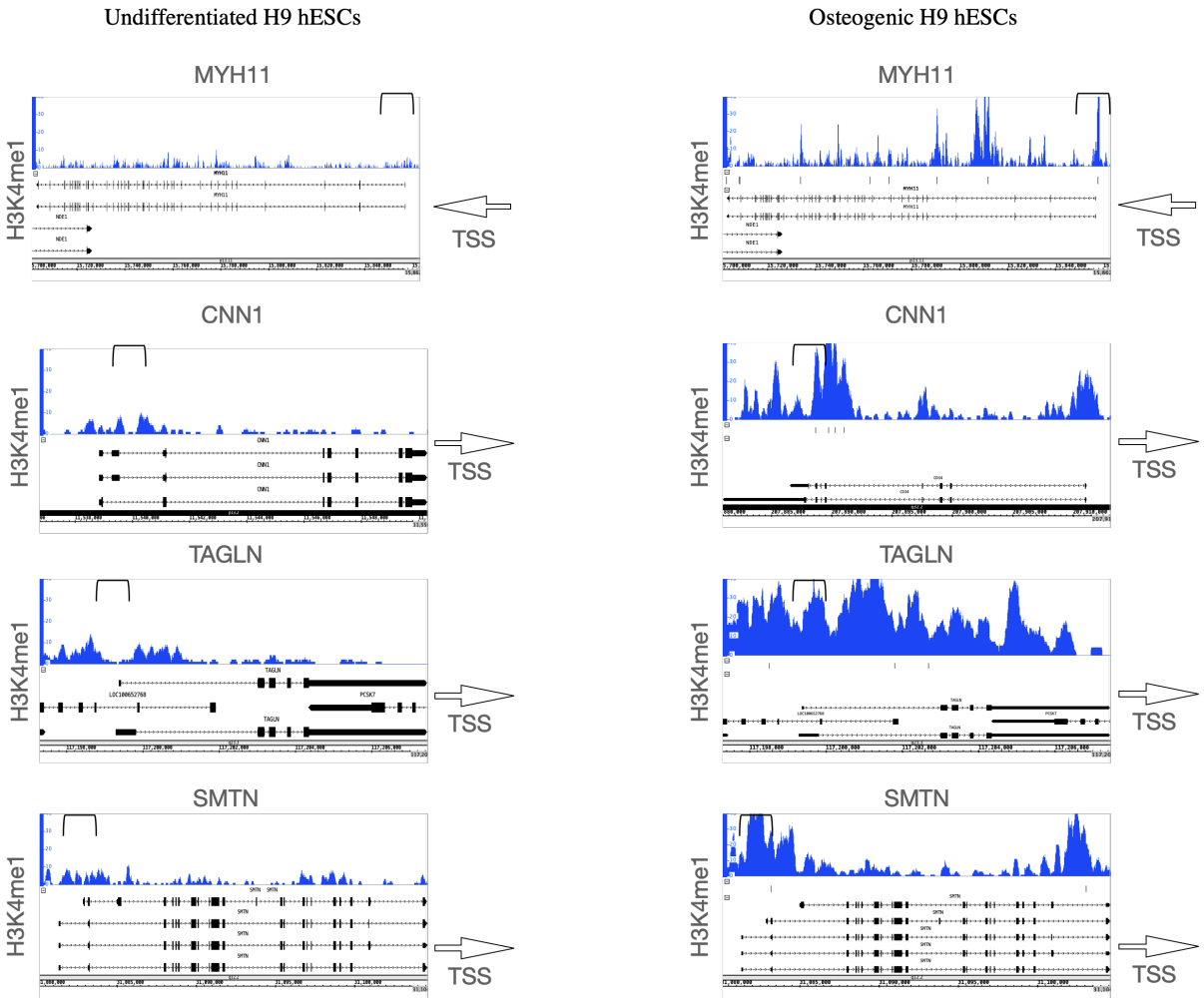

Figure 5.21. ChIP-seq peak calling for H3K4me1 at SMC gene loci (*MYH11, CNN1, TAGLN* and *SMTN)* in undifferentiated H9 hESCs and following osteogenic differentiation of H9 hESCs.

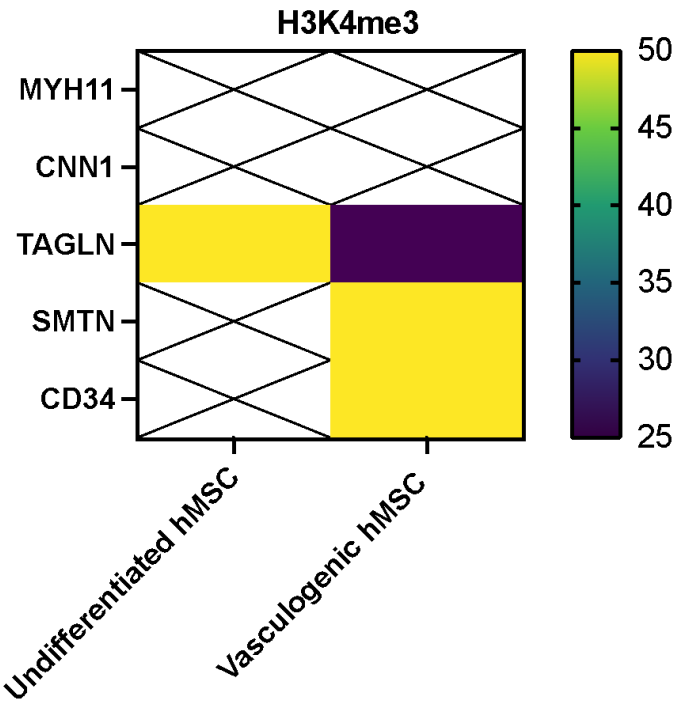

Figure 5.22. ChIP-seq peak scores of H3K4me3 at SMC gene loci (*MYH11, CNN1, TAGLN* and *SMTN)* and the *CD34* locus for H3K4me3 in hMSC derived vasculogenic progeny compared to undifferentiated hMSCs.

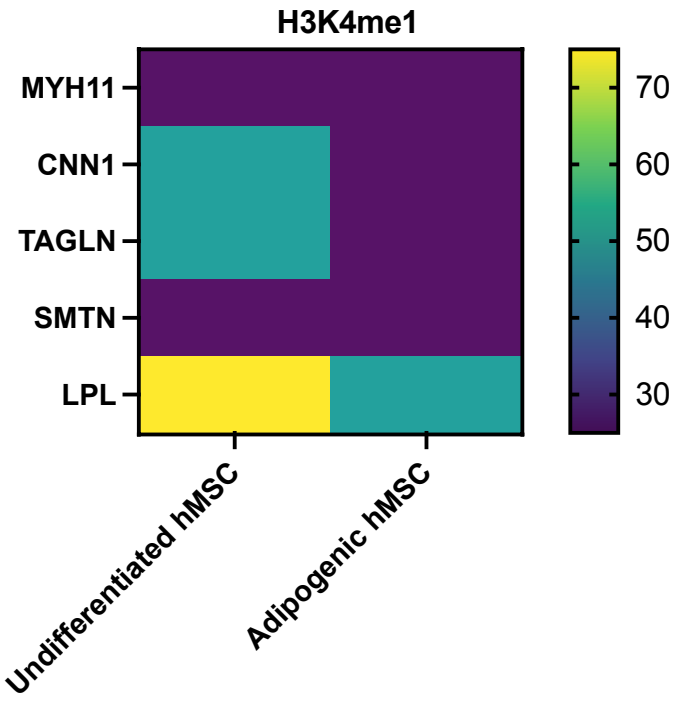

Figure 5.23. ChIP-seq peak scores of H3K4me1 at SMC gene loci (*MYH11, CNN1, TAGLN* and *SMTN)* and the *LPL* locus in hMSC derived adipogenic progeny compared to undifferentiated hMSCs.

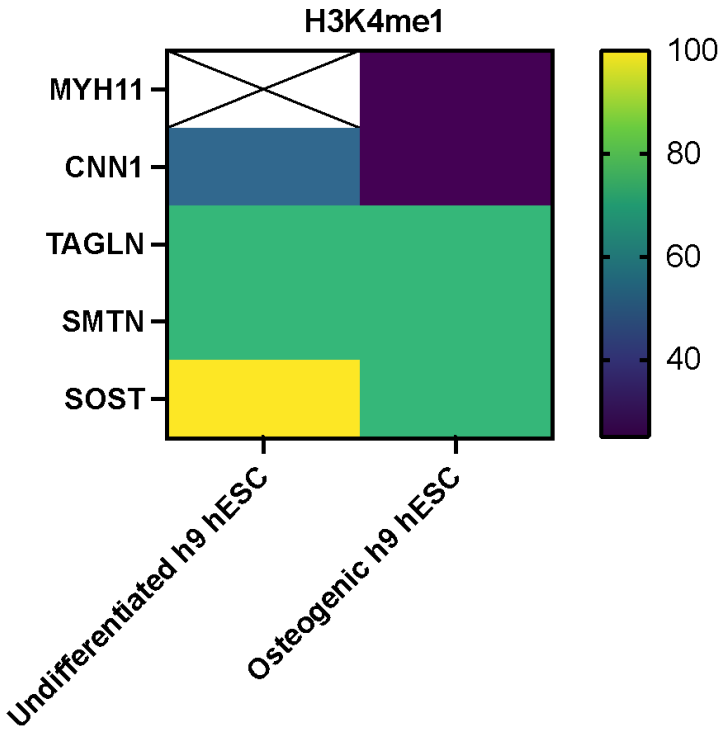

Figure 5.24. ChIP-seq peak scores of H3K4me1 at SMC gene loci (*MYH11, CNN1, TAGLN* and *SMTN)* and the *SOST* locus in H9 hESCs. derived osteogenic progeny compared to undifferentiated H9 hESCs.

5.3.3 Bulk ChIP-seq analysis reveals the acquisition of the H3K4me2 mark at the *MYH11* locus following myogenic, osteogenic and adipogenic differentiation of hiPSC-derived S100β SNEPs *in vitro.*

Myogenic, vasculogenic, osteogenic and adipogenic differentiation of hiPSC-derived S100β SNEPs was performed as outlined in Chapter 2, Section 2.2.4 before H4K4me2 ChIP analysis was executed and the DNA samples sequenced by Novogene Company Ltd as outlined in Chapter 2 Section 2.2.15.2. The company concluded that the quality of the samples did not pass the QC following FastQC but suggested preparing libraries for the samples which were then created. Sample preparation, library construction, sequencing and bioinformatic analysis were all done by Novogene Company Ltd. The data generated were then analysed *in silico* by peak calling of H4K4me2 enrichment at specific differentiation gene loci - *MYH11* locus for S100β SNEP-derived myogenic progeny; *LPL* locus for S100β SNEP-derived adipogenic progeny, *SOST* locus for S100β SNEP-derived osteogenic progeny and *PECAM1* locus for SNEP-derived vasculogenic progeny.

There was a notable peak for the repressive H3K27me3 mark at the *MYH11* locus in undifferentiated S100β SNEPs compared to INPUT [Figure 5.25]. Upon myogenic differentiation, there were notable peaks for H4K4me2 enrichment at the *MYH11* locus around the TSS in myogenic progeny, compared to undifferentiated S100β SNEPs [Figure 5.26]. Upon vasculogenic differentiation, there was a notable peak for H3K4me2 enrichment at the *PECAM1* locus in vasculogenic progeny compared to undifferentiated S100β SNEPs [Figure 5.27]. Similarly, upon osteogenic and adipogenic differentiation, there were notable peaks for H3K4me2 enrichment at the *SOST and LPL* locus in osteogenic and adipogenic progeny, respectively compared to undifferentiated S100β SNEPs [Figure 5.28, 5.29]. Collectively, Peaks at lineage-specific differentiation genes indicate differentiation of SNEPs.

When the level of enrichment of H3K4me2 at the *MYH11* locus was analysed by peak calling following vasculogenic, osteogenic and adipogenic differentiation of S100β SNEPs, there were notable peaks observed upstream from the TSS in osteogenic and adipogenic progeny, but not vasculogenic, when compared to undifferentiated S100β SNEPs [Figure 5.30]. ChIP-seq indicates that S100β SNEPs derived osteogenic and adipogenic progeny acquired the SMC-specific mark of H3K4me2 at the *MYH11* locus.

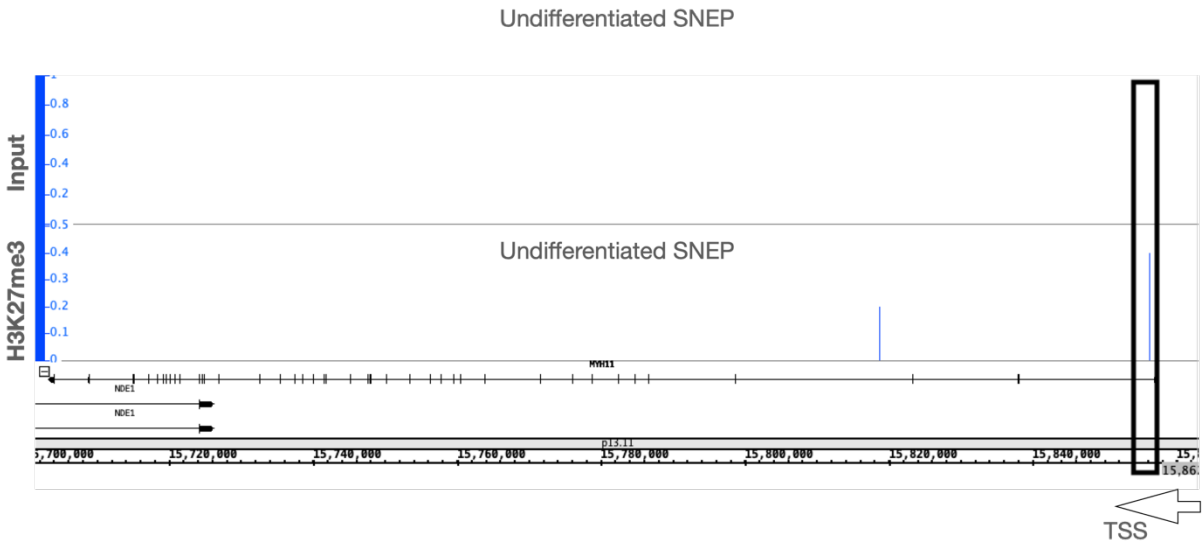

Figure 5.25. ChIP-seq peak calling for Input and H3K27me3 at the *MYH11* locus in undifferentiated S100β SNEP grown in their maintenance medium.

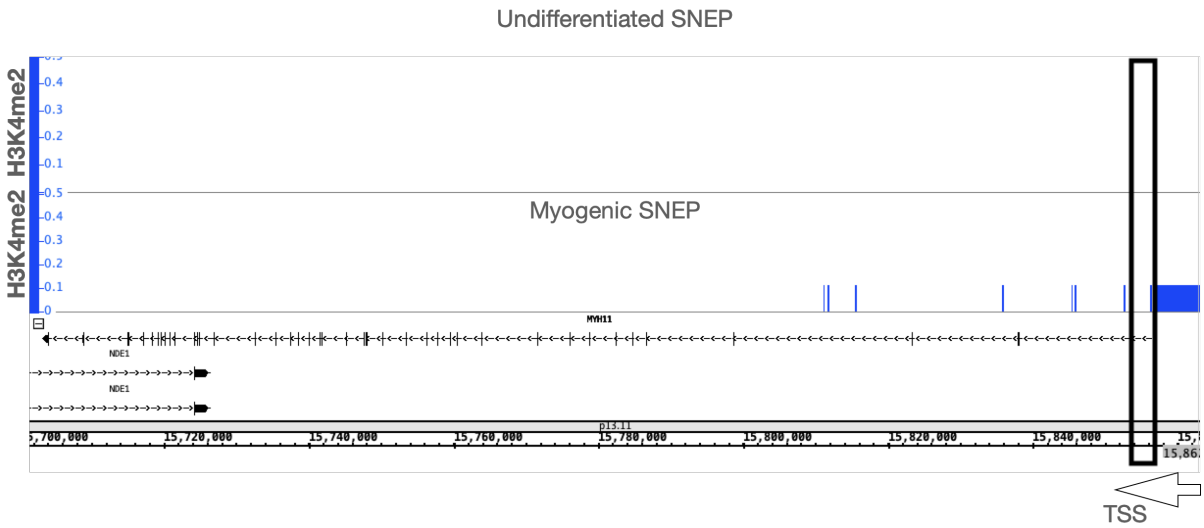

Figure 5.26. ChIP-seq peak calling for H3K4me2 at the *MYH11* locus in undifferentiated S100β SNEP and following myogenic differentiation of S100β SNEPs.

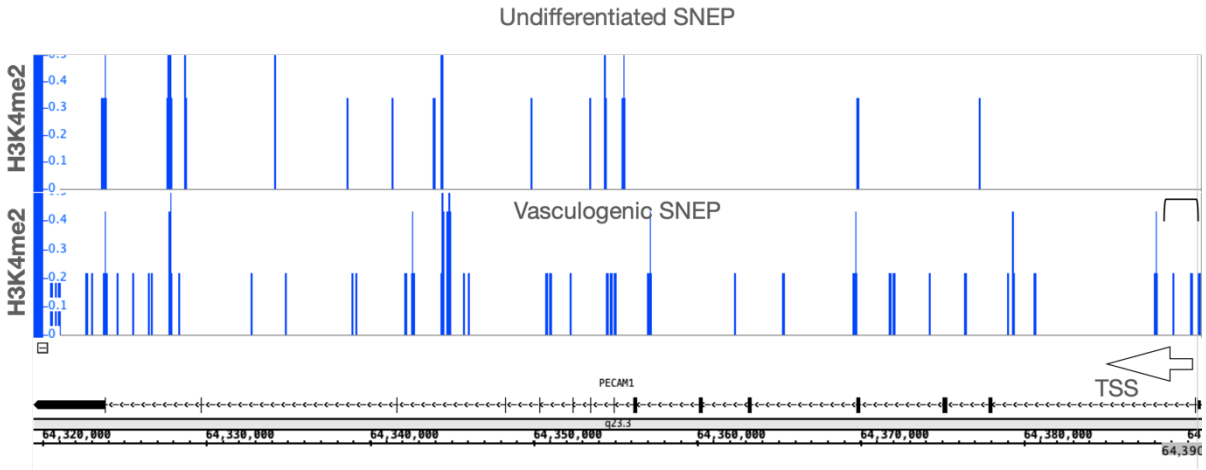

Figure 5.27. ChIP-seq peak calling for H3K4me2 at the *PECAM1* locus in undifferentiated S100β SNEP and following vasculogenic differentiation of S100β SNEPs.

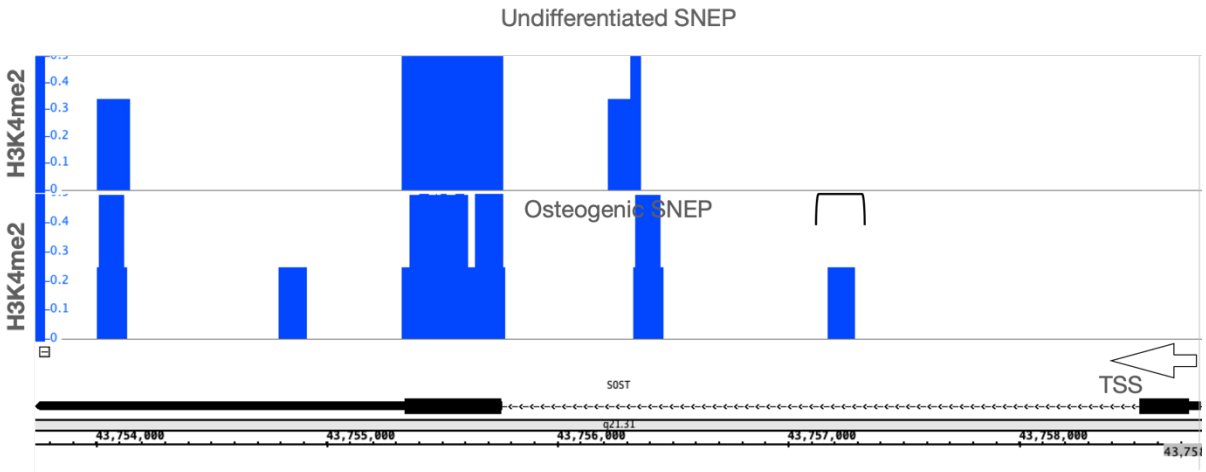

Figure 5.28. ChIP-seq peak calling for H3K4me2 at *SOST* gene locus in undifferentiated S100β SNEP and following osteogenic differentiation of S100β SNEPs.

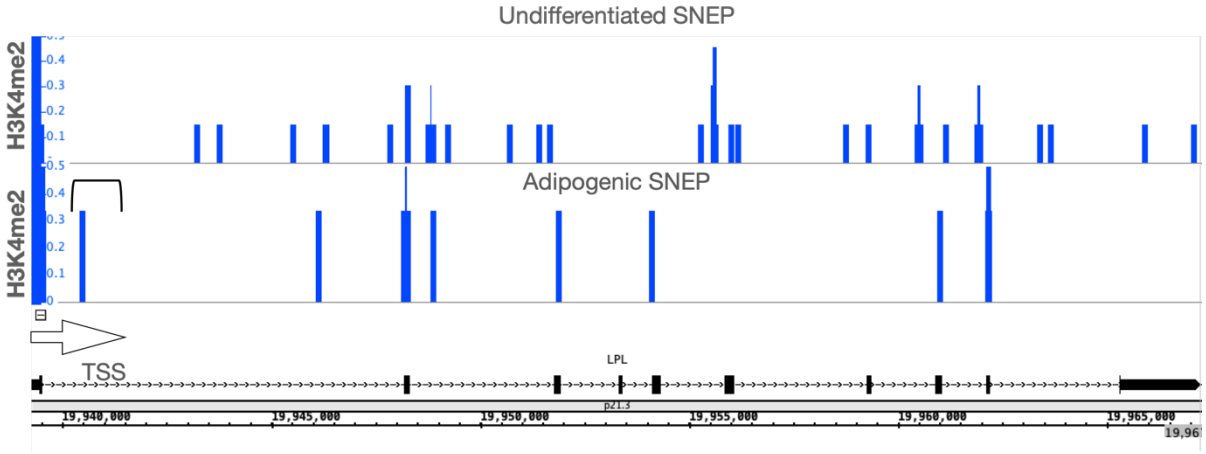

Figure 5.29. ChIP-seq peak calling for H3K4me2 at *LPL* gene locus in undifferentiated S100β SNEP and following adipogenic differentiation of S100β SNEPs.

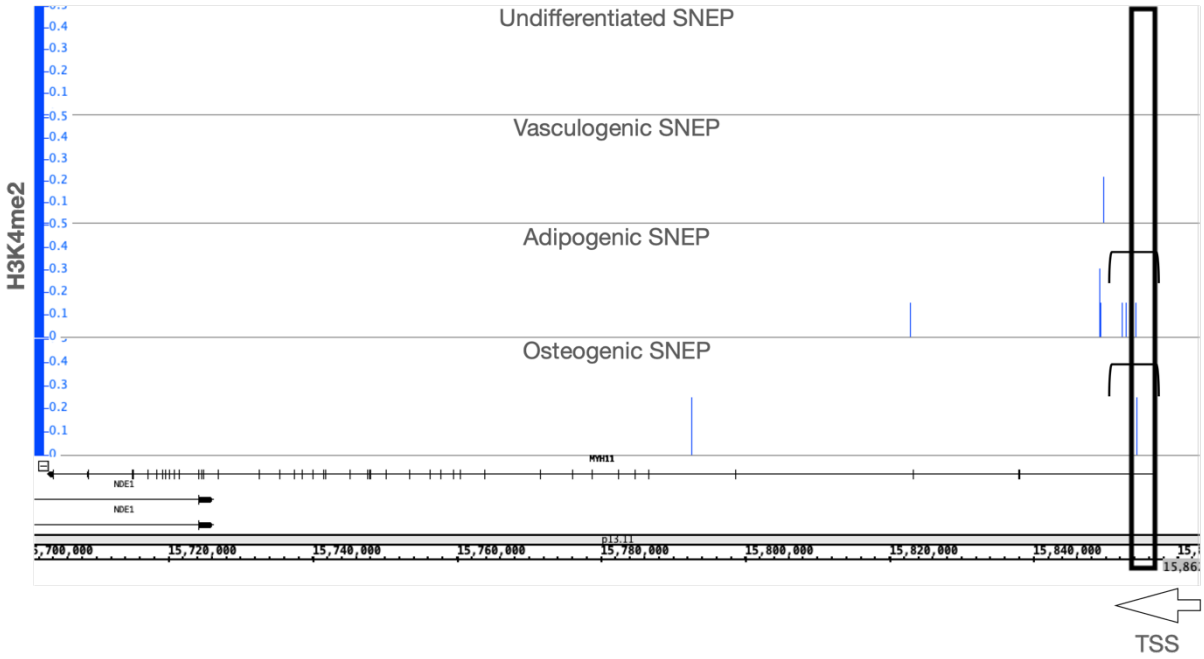

Figure 5.30. ChIP-seq peak calling for H3K4me2 at *MYH11* gene locus in undifferentiated S100β SNEP and following vasculogenic, adipogenic and osteogenic differentiation of S100β SNEPs.

5.4 Discussion

The results from Chapter 4 using single gene ChIP-PCR revealed that S100β vascular stem cells from mouse and human acquire the H3K4me2 mark at the *Myh11* locus when these cells undergo myogenic, adipogenic and osteogenic, but not vasculogenic, differentiation *in vitro.* In this Chapter, genome-wide bulk ChiP-seq analysis was performed on human S100β SNEPs to determine whether the same H3K4me2/H3K27me3 marks at the *MYH11* gene locus were present in these cells before and after the same lineage specification *in vitro*. In addition, parallel *in silico* analysis of published genome-wide bulk ChIP-seq datasets for mono-, di- and trimethylation of H3K4 was performed in mouse and human S100β multipotent stem cells at several SMC gene loci, including *Myh11* and at lineage-specific gene loci before lineage specification. This analysis determined whether similar epigenetic changes that occur at the *Myh11* locus were also evident at other SMC loci during SMC-like and non-SMC lineage-specification. In all cases, the interrogation was performed by assessing peak calling to determine the peak of each gene at a specific histone and peak scoring to determine the significance of that peak across the entire genome for a given sample. The data clearly further confirm that human S100β SNEPs and mouse and human MSCs and hESCs acquire the H3K4me2 mark at the *Myh11* locus when these cells undergo myogenic, adipogenic and osteogenic, but not vasculogenic, differentiation *in vitro.* A similar trend was observed at other SMC loci but this was dependent on whether the undifferentiated stem cell was already marked with H3K4 modifications prior to lineage specification. Overall, these findings provide further evidence that the H3K4me2 signature at the *Myh11* locus in stem cell-derived progeny may be in part responsible for the reported presence of this key signature in SMC-like and non-SMCs typical of vascular lesions *in situ* (Gomez et al., 2013).

Transcription factors bind to the genome in a punctate pattern and are vital mediators of external cellular stimuli. These events can be preceded by, or are an effect of, the chromatin landscape in which they reside; therefore, histone modifications can be accurate predictors of genomic transitions (Lee & Workman, 2007). Lineage specification is determined by integrating microenvironmental cues with intracellular signalling pathways, transcriptional regulatory networks, and chromatin remodelling (Abdallah et al., 2015). Indeed, it has been reported in a number of studies that key epigenetic modifications could affect key

transcriptional factors shaping gene expression and lineage-specific differentiation potentials of ESCs (Hattori et al., 2004; Kimura et al., 2004; O'Neill et al., 2006). Multipotent S100β mVSCs are adult stem cells that have the ability to differentiate into distinct mesodermal (Bianco et al., 2001) and neuroectoderm lineage cells (Luk et al., 2005), such as adipocytes, osteoblasts, chondrocytes, and myocytes (Bianco et al., 2001) through an MSC-like intermediate (Tang et al., 2012). Hence, it is not surprising that S100β mVSCs and hiPSC-derived S100β SNEPs are capable of tri-lineage-specification (Woods et al., 2021).

In this chapter, human S100β SNEPs were treated with different differentiation inductive media to specify myogenic, vasculogenic, adipogenic and osteogenic lineages before S100β SNEPs, public murine and human MSC and hESC ChIP-seq datasets were interrogated and the level of enrichment of either H3K4me1, 2 or 3 and H3K27me3 at four SMC gene loci (*Myh11, Cnn1, Smtn* and *Tagln)* assessed. The level of H3K4 methylation was also confirmed at their lineage-specific gene loci in vasculogenic, adipogenic and osteogenic progeny. The enrichment of H3K4me2 of SMC CC(A/T)-rich GG(CArG)-containing promoter regions was considered specific to SMCs and this epigenetic mark persists even when cultured SMCs are induced to undergo phenotypic switching (McDonald et al., 2006). The presence of H3K4me2 on the *Myh11* promoter was completely restricted to SMC within all mouse and human tissues examined, including numerous arteries and arterioles (Gomez et al., 2013). Using an *in situ* hybridization-proximity ligation assay (ISH-PLA) method for detecting the H3K4me2 mark in single cells *in situ* in conjunction with SMC lineage tracing in mice, previous studies had suggested that the H3K4me2 mark is retained in 'phenotypically modulated SMC' within arteriosclerotic and atherosclerotic lesions that lack detectable expression of SMC marker genes (Gomez et al., 2013). ChIP-seq data on mouse SMCs confirms that differentiated vascular SMCs enrich for H3K4me3 not only at the *Myh11* locus but also at *Tagln, Cnn1* and *Smtn* loci confirming that differentiated SMCs enrich for H3K4me3 at early, mid and late SMC gene loci.

Having confirmed that mouse and human stem cell-derived myogenic, vasculogenic, adipogenic and osteogenic progeny enrich for H3K4 methylation at specific gene loci for each lineage, the level of enrichment of H3K27me3, H3K4me1, H3K4me2 or H3K4me3 at SMC-specific gene loci was next assessed. Analysis of ChIP-seq data for both peak calling and peak

scoring in human hMSC and hESCs suggests that the H3K27me3 mark occurs at all SMC gene loci in undifferentiated cells without any enrichment of H3K4me2 at the same loci. This is to be expected as these genes are transcriptionally silent in undifferentiated cells. In contrast, the enrichment of H3K4me2 mark was robust in all SMC gene loci in hESC-derived myogenic progeny, concomitant with lower peak scores at MYH11, CNN1 and TAGLN loci, confirming that these peaks were significant and more pronounced in these progeny. This ChIP-seq data confirmed the previous single gene ChIP-PCR data that these undifferentiated stem cells enrich for H3K27me3 at the *MYH11* locus which also correlates with the low level of transcript for the *MYH11* gene. This is also supported by reported data from our group that noted undifferentiated murine S100β mVSCs enriched for H3K27me3 and do not contain the SMC-specific signature of H3K4me2 at the *Myh11* locus (Di Luca et al., 2021). However, on myogenic differentiation to an SMC-like cell, H3K4me2 becomes enriched at the same locus.

While ChIP-seq data on mouse and human SMCs confirms that differentiated cells enrich for H3K4 methylation not only at the *Myh11* locus but also at *Tagln, Cnn1* and *Smtn* loci, It is widely accepted that some SMC differentiation marker genes are also expressed in a variety of circumstances in other cell types. Specifically, *Tagln* (Zhang et al., 2001) which is expressed in skeletal and cardiac muscle during development, and within activated fibroblasts under a variety of conditions (Kim et al., 1997; Li et al., 1996; Sartore et al., 2001) and *Smtn* which is expressed at high levels in a variety of organs and tissues such as, prostate stromal cells in culture in response to basic fibroblast growth factor (Wang et al., 2002). As a result, the observed presence of H3K4 methylation at SMC loci in undifferentiated mouse MSCs might reflect the baseline differentiation state where there may have been some partial differentiation of these cells in culture prior to lineage-directed specification using inductive cues. This is borne out by the presence of H3K4 methylation marks at SMC loci in undifferentiated cells. Nevertheless, the presence of lower peak scores at these SMC gene loci in adipogenic, osteogenic and myogenic progeny suggests that these cells further enrich for H3K4 methylation marks when they undergo lineage specification. In particular, the presence of lower peak scores for H3K4me1 at *MYH11* and *CNN1* loci in hESC-derived osteogenic progeny compared to undifferentiated hESCs suggests these cells enrich for this mark at SMC-specific loci as they differentiate down osteogenic lineages.

In this context, there is growing evidence that posttranslational modification of histones is a dynamic process that shows many correlations with gene expression. For example, when the genome-wide distribution of H3K4me2 and H3K27me3 was mapped during late mouse retinal development, genes expressed only in mature rod photoreceptors have a unique signature consisting of *de-novo* accumulation of H3K4me2, both at the site TSS and over the whole gene. This correlated with the increase in transcription, but no accumulation of H3K27me3 at any stage. *In silico* analysis further suggested that the distribution of H3K4me2 and H3K27me3 on the genes widely expressed is not always associated with their transcriptional levels (Popova et al., 2012). It is clear that different histone signatures for genes with the same gene expression pattern highlight the diversities of epigenetic regulation. In the case of S100β multipotent stem cells, SMC genes with the H3K27me3 mark at the TSS represented a large group of transcripts never expressed. Importantly, the epigenetic signatures defined by H3K4me2 and H3K27me3 can distinguish cell-type specific genes from widespread transcripts and may be reflective of cell specificity during cell maturation (Popova et al., 2012).

One advantage of using ChIP-seq is the ability to assess for the same histone mark at multiple lineage-specific genes to determine whether multipotent stem cells can have enrichment at their lineage-specific loci and SMC gene loci. The epigenetic changes that occur at other lineage-specific gene loci were confirmed for each lineage. Vasculogenic differentiation of undifferentiated ESC cells is associated with the upregulation of *Pecam1* in endothelial cells (Kanki et al., 2017). These data not only agree with vasculogenic differentiation from the previous chapter where the expression level of *PECAM1* was upregulated in S100β SNEP derived vasculogenic progeny but also the ChIP-seq data for H3K4me at vasculogenic gene loci in mouse and human cells. Enrichment of H3K4me marks at *Pecam1* and especially *CD34* locus in mouse and human stem cells correlates with an increase in their transcription levels. Similarly, enrichment of H3K4me1 at the *Lpl* locus was indicative of adipogenic differentiation while osteogenic progeny showed enrichment of H3K4me1 at *SOST* locus. Previous studies have demonstrated that *Lpl* gene expression was upregulated in mMSC-derived adipogenic progeny (Ali & Hamam, 2016) while mMSC-derived osteogenic progeny have increased levels of *Sost* transcript concomitant with enrichment of H3K4me at these gene-specific loci (Glemžaite & Navakauskiene, 2016). Clearly, these data confirm undifferentiated stem cells

acquire H3K4me marks at lineage-specific loci following myogenic, vasculogenic, adipogenic and osteogenic differentiation, respectively *in vitro.*

Collectively, these data indicate that H3K4 methylation at specific SMC gene loci can occur in human and mouse progeny when these cells do not undergo myogenic differentiation *in vitro*. Indeed, the human MSC and hESC ChIP-seq data confirms that enrichment of H3K4me1 at SMC gene loci occurs at *MYH11* and *CNN1* promoters following osteogenic and adipogenic differentiation, respectively, indicating H3K4 methylation at SMC gene loci in cells that were not SMC. In contrast, following vasculogenic differentiation, there was no enrichment of H3K4 methylation marks at these same SMC loci in these progeny when compared to undifferentiated cells. While enrichment for H3K4me3 at early SMC gene loci was observed (*TAGLN and SMTN*), these two early myogenic genes have been reported to be upregulated in non-SMC (Zhang et al., 2001). Analysis of the S100β SNEP ChIP-seq data further supported the single gene ChIP-PCR data from the previous Chapter and the additional analysis of public datasets for these histone modifications at the *MYH11* locus. In particular, H3K4me2 peaks were present at this locus in myogenic progeny but also in adipogenic and osteogenic progeny compared to undifferentiated S100β SNEPs. This enrichment of H3K4me2 at the *MYH11* locus is unlikely to be due to the presence of fetal bovine serum (FBS) in both the adipogenic and osteogenic differentiation media. These media are supplemented with 1% FBS which is the same as the maintenance medium for undifferentiated mouse S100β mVSCs and human S100β SNEPs, respectively. In contrast, there was no enrichment for H3K4me2 at the *MYH11* locus in vasculogenic progeny, when compared to undifferentiated cells.

The enrichment of the mark at the MYH11 locus was too specific for cytosine phosphate guanine (CpG) islands (CGIs). As the precise regulation of gene transcription is required to establish and maintain cell type-specific gene expression programs during multicellular development, chemical modification plays a central role in regulating gene expression. In vertebrates, DNA is pervasively methylated at CG dinucleotides, a modification that is repressive to transcription. However, approximately 70% of vertebrate gene promoters are associated with DNA elements called CGIs that are refractory to DNA methylation (Hughes et al., 2020). CGIs integrate the activity of a range of chromatin-regulating factors that can post-translationally modify histones and modulate gene expression. This is specifically true for the

H3K4me3 mark, which is enriched at CGI-associated gene promoters and correlates with transcriptional activity. It is clear that the presence of the H3K4me3 mark at CGIs can shape the distribution of H3K4me3 and, in turn, H3K4me3 influences the chromatin landscape at CGIs. In the current study, a similar relationship between CGIs and the H3K4me2 mark is evident in S100β SNEP-derived myogenic progeny where the presence of this mark at CGIs on the MYH11 locus is indicative of transcription activity for this lineage. However, the presence of this mark on the MYH11 locus in S100β SNEP-derived adipogenic and osteogenic progeny is not associated with transcription activity for these lineages. The reason(s) for this is unclear but gene transcription is not only dictated by chemical modification of DNA at CGIs but also by the presence and abundance of key transcription factor(s), which may well be absent in adipogenic and osteogenic progeny. Moreover, while the enrichment of H3K4me3 at gene promoters is conserved across all eukaryotes, in vertebrates H3K4me1 is more broadly distributed and enriched at enhancers, while H3K4me2 tends to be elevated in regions flanking peaks of H3K4me3 (Hughes et al., 2020). In recent studies, removal of H3K4me2 via selective editing in cultured vascular SMCs and in murine arterial vasculature led to loss of myogenic differentiation and reduced contractility due to impaired recruitment of TET-2 at CGIs. H3K4me2 editing also induced a profound alteration of SMC lineage identity by redistributing H3K4me2 marks toward genes associated with stemness and developmental programs (Liu et al., 2021).

Previous studies have also demonstrated the presence of H3K4me2 on the *Myh11* promoter is maintained in cells that transitioned from medial SMCs to macrophage-like cells (myeloid lineage) within mouse and human vascular lesions (Shankman et al., 2015). Using ISH-PLA, the same group provided evidence that approximately 20% of macrophage marker positive cells within advanced human coronary artery lesions were of SMC, and not myeloid origin, and moreover, >35% of cells dual positive for Galectin3 and α-smooth muscle actin (Acta2) were of SMC origin (Shankman et al., 2015). However, the CHiP-seq data from this Chapter and the previous single gene ChiP-PCR studies confirm that non-SMCs can also acquire the H3K4me2 mark at the *Myh11* locus in the absence of any changes in SMC gene transcription. Whether this is also true for stem-derived myeloid-like progeny is yet to be determined. Ongoing studies within the laboratory have shown that S100β mVSC and S100β SNEPs are capable of differentiating to a Cluster of differentiation 68 (CD68) myeloid-like cell in response

to lipid atherogenic stimulation (cholesterol and low-density lipoprotein (LDL)). However, it does not exclude the possibility that multipotent vascular stem cells which differentiate into myeloid-like progeny following exposure to these stimuli enrich for H3K4me2 at the *Myh11* promoter.

This concept of epigenetic control of lineage determination and maintenance of lineage epigenetic memory has been proposed (Zhu et al., 2013). In support, several studies have demonstrated that H3K4me2 is preferentially distributed on genes related to lineage identity and cell-specific functions in multiple cell types and tissues (Zhang et al., 2012). While the comparison of the genome-wide epigenetic landscape by ChIP-seq is primarily descriptive and does address the putative causality between histone modifications, gene expression, and changes to cellular phenotype, this Chapter provides further evidence that multipotent mouse and human MSCs, hESCs and S100β SNEPs are capable of myogenic, adipogenic and osteogenic differentiation concomitant with enrichment of H3K4 methylation at gene-specific loci. Moreover, non-SMC progeny acquire H3K4me marks at the Myh11 locus following adipogenic and osteogenic differentiation.

SMC phenotypic switching has been classically described as a de-differentiation process due to the loss of expression of SMC contractile genes. Phenotypically modulated SMC do not lose their H3K4me2 epigenetic signature nor their lineage identity (Gomez et al., 2013). Moreover, the ability of SMCs to undergo reversible loss of contractility is considered a fundamental and epigenetically programmed property of medial differentiated SMCs (Liu et al., 2021). Furthermore, SMC reversible phenotypic modulation in response to modifications of the environment is purported to be an evolutionarily conserved process necessary for the maintenance of vascular homeostasis where H3K4me2 is considered pivotal in facilitating this reversible loss of contractility. However, the results in this Chapter from the ChIP-seq data of H3K4me2 in S100β SNEPs in addition with interrogation of available public datasets for H3K4 methylation in murine mMSCs and human MSCs and hESCs strongly suggest that this paradigm may need to be revisited.

It has been widely assumed that H3K4 methylation is a mechanism of gene activation based on the correlation between the distribution of H3K4 methylated residues and actively transcribed genes (Buratowski and Kim, 2010; Sims et al., 2003). However, the data from this

Chapter provides evidence contradicting this paradigm as H3K4me2 enrichment was also found on transcriptionally poised and inactive genes, suggesting that presence of H3K4me2 at the Myh11 locus is not sufficient to induce gene activation, at least in adipogenic and osteogenic progeny. While H3K4me2 enrichment on the *Myh11* gene locus is stably retained during SMC de-differentiation and repression of these genomic loci *in vitro* and *in vivo* (Gomez et al., 2013; McDonald et al., 2006; Shankman et al., 2015), the presence of this mark in SMC-like and non-SMC cells on transcriptionally poised and inactive genes could be attributable to lineage-specification of multipotent vascular stem cells (rather than repression of SMC genomic loci). The present studies support a model by which H3K4me2 may serve as a mechanism for priming lineage-specific genes for dynamic activation and ensuring appropriate gene expression once the key transcription factor(s) are present within these cells.

Chapter 6

General Discussion

Cardiovascular Disease (CVD), such as atherosclerosis, is a chronic progressive inflammatory disease widely regarded as one of the leading causes of death worldwide (Lockhart et al., 2012). A hallmark of atherosclerosis is the accumulation of vascular smooth muscle cell SMC-like and non-SMC neointimal cells leading to intimal medial thickening, lipid accumulation, plaque formation and the obstruction to blood flow that may result in a heart attack or stroke (Benditt & Benditt, 1973). The origin of SMC-like and non-SMC neointimal cells is controversial. Recent lineage tracing studies, single-cell RNA sequencing (scRNA-seq) and single-cell chromatin Immunoprecipitation (ChIP) analysis *in situ* have provided compelling evidence in various animal models for the involvement of a rare population of differentiated Myosin Heavy-chain 11/ stem cell antigen-1 (Myh11/Sca1) medial SMCs that undergo de-differentiation and phenotypic switching (Chappell et al., 2016). Contrasting lineage tracing studies from our lab and others suggest a role for resident S100 calcium-binding protein β (S100β) adventitial and/or medial multipotent vascular stem cell (mVSCs) that undergo lineage-specification including myogenic, adipogenic and osteogenic differentiation. (Kramann et al., 2016; Tang et al., 2012; Wan et al., 2012; Di Luca et al., 2021, Molony et al., 2021).

This thesis assessed whether murine S100β mVSCs and human S100β progenitors acquire the histone 3 lysine 4 di-methylation (H3K4me2) mark at SMC *MYH11* gene-specific locus when treated with atherogenic stimuli associated with SMC de-differentiation and phenotypic switching *in vitro.* In doing so, these epigenetic changes may serve to facilitate their myogenic differentiation to SMC-like cells typical of arteriosclerotic lesions. Using quantitative chromatin immunoprecipitation followed by polymerase chain reaction (ChIP-PCR) assays, SMC differentiation assays and messenger RNA (mRNA) analysis, the role of H3K4me2 and H3K27me3 histone modifications and their modulation by ten-eleven-translocation 2 (Tet-2) demethylases at similar loci on stem cell transition to SMC were evaluated in mouse and human models *in vitro.* Furthermore, the project addressed whether these same epigenetic marks at SMC-specific loci were evident following vasculogenic, adipogenic and/or osteogenic differentiation of (i) murine and human S100β mVSCs *in vitro* using quantitative chromatin immunoprecipitation followed by polymerase chain reaction (ChIP-PCR) and bulk chromatin immunoprecipitation sequencing (ChIP-seq) assays and (ii)

mouse and human mesenchymal stromal stem (MSCs) cells using published bulk ChIP-seq datasets.

CVD is the leading cause of morbidity and mortality (Murray & Lopez, 1996; Yusuf et al., 2001). Atherosclerosis is the underlying pathology, which develops insidiously over years and is usually advanced by the time symptoms occur (De Backer et al., 2003). Subclinical atherosclerosis defines the initiation and progression of early atherosclerotic plaques and can be present in a number of different forms (DIT, AIT and PIT). Diffuse intimal thickening (DIT) occurs at the beginning of the atherosclerosis stage, lipids accumulate in the extracellular space. Subsequently, macrophages infiltrate into the thickened intima and become foam cells to form an early lesion together with intimal SMCs and extracellular lipids (Nakashima et al., 2007; Tabas et al., 2007). Adaptive intimal thickening (AIT) is often seen as a precursor to pathologic intimal thickening (PIT) as it allows for increased lipid retention in the vessel wall (Otsuka et al., 2015). PIT is one of the most widespread forms of subclinical atherosclerosis and is widely reported to give rise to more advanced plaque lesions. It involves infiltration of the macrophages, loss of intimal SMCs and the formation of an extracellular lipid pool (Kolodgie et al., 2007). Treatment options for atherosclerosis following PIT progression into late atherosclerotic plaques include balloon angioplasty and stent deployment (Farooq et al., 2011). However, In-stent restenosis (ISR) can prevail leading to neointimal hyperplasia which is characterised by extensive proliferation and migration of SMC-like cells into the intimal space of the stented artery resulting in the formation of a neointima (Indolfi et al., 2003). A notable hallmark of subclinical atherosclerosis and ISR is the accumulation of SMC-like and non-SMC cells within these developing lesions.

The source of SMC-like cells contributing to subclinical atherosclerosis, ISR and neointimal hyperplasia is a topic of much controversy. The sources reported so far are de-differentiated SMCs (Chappell et al., 2016), resident vascular stem cells (Tang et al., 2012), bone marrow-derived stem cells (Sata, 2003; Shimizu et al., 2001) and endothelial mesenchymal transition (Cooley et al, 2014; Zeisberg et al., 2007). However, some of the most recent evidence comes from studies that describe the myogenic differentiation of resident vascular stem cells in response to vessel injury (Di Luca et al., 2021; Molony et al., 2021; Roostalu et al., 2018; Tang et al., 2012; Torsney et al., 2005). Stem cell populations have been

identified not only in the medial but also in the adventitial layer of the artery. Recent data from lineage tracing studies, scRNA-Seq and single-cell photonics have provided compelling evidence that neointimal cells within lesions are derived from an S100β and/or Sca1 stem cell parent population within the vessel wall (Di Luca et al., 2021; Molony et al., 2021; Roostalu et al., 2018; Tang et al., 2012; Torsney et al., 2005).

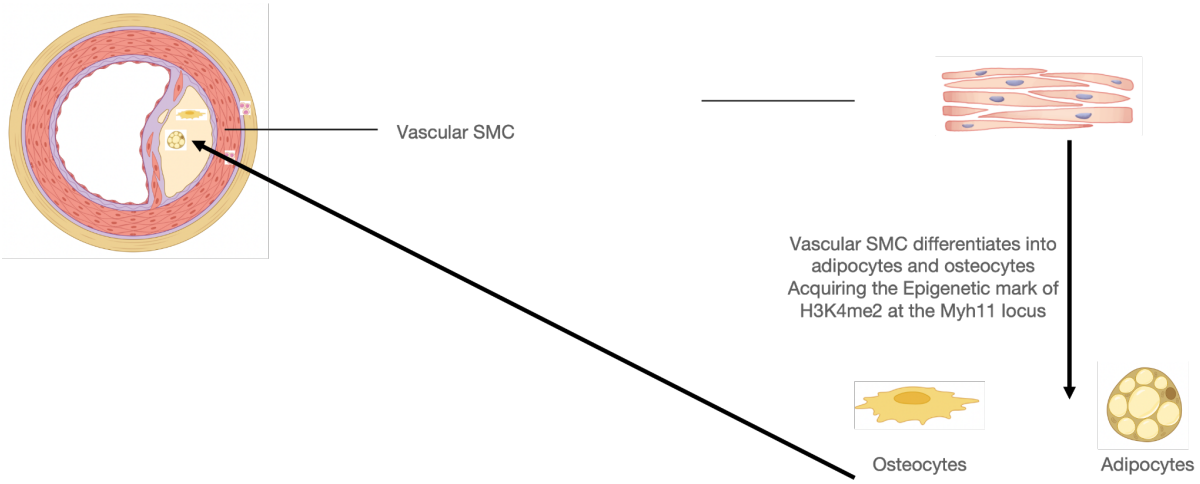

Figure 6.1 Non-SMC-like cells (fibroblasts, macrophage -, adipogenic - and osteogenic-like cells) in vascular lesions could arise from SMC that retain the epigenetic profile of H3K4me2 at the *Myh11* locus following progeny differentiation.

A lineage tracing study carried out by our own research group was analysed and the resulting data confirmed the presence of neointimal cells in an injured vessel which were derived from an S100β parent population. Moreover, this lineage tracing model, which used an inducible S100β-controlled Cre system, was the first of its kind to incorporate a 4-week tamoxifen washout period to ensure that the potential for mislabelling neointimal cells was kept to a minimum. These findings supported previous evidence from our research group which used both lineage tracing and single cell photonics to identify a subpopulation of multipotent vascular stem cells mVSCs which are S100β and, following vascular injury, can migrate and differentiate to become SMC-like cells in the neointima (Molony *et al.*, 2020; Di Luca *et al.*, 2021).

6.1. De-differentiated murine vascular SMC-like cells typical of vascular lesions retain the H3K4me2 mark at the *Myh11* locus

A common feature of de-differentiation and phenotypic switching of medial SMCs in vascular lesions is the persistence of H3K4me2 at the *Myh11* gene promoter locus despite this gene being transcriptionally silenced due to the loss of serum response factor (SRF)-myocardin binding, the formation of heterochromatin, and the loss of H3/H4 hyperacetylation. This raises the possibility that H3K4me2 serves as a mechanism of epigenetic cell lineage memory, i.e., a mechanism for phenotypically modulated SMCs to remain permissive for re-differentiation into SMCs during reversible phenotypic switching. However, the possibility that these changes in histone patterning may reflect myogenic differentiation of S100β mVSCs cannot be ruled out. Vascular stem cells within the vessel wall remain quiescent until their function is required to actively drive vascular regeneration following injury when symmetric and asymmetric cell division maintains a balance between stem cell self-renewal and myogenic SMC differentiation. During SMC differentiation, myogenic master regulator transcription factors are activated and drive progression through a myogenic differentiation programme, involving transforming Growth factor beta 1 (TGF-β1), platelet-derived growth factor-BB (PDGF-BB) and the Notch ligand, Jagged 1. Involvement of epigenetic regulators during stem cell self-renewal and differentiation, as well as changes in DNA methylation/demethylation patterns during myogenic differentiation, are also specifically indicated.

Many groups have sought to determine the molecular pathways that stimulate stem cell populations to undergo myogenic differentiation to SMC-like cells. In embryonic and adult stem cells, PDGF-BB promotes myogenic differentiation to an SMC-like phenotype (Cheung et al., 2014; Xiao et al., 2007). Human embryonic stem cells (hESCs) and human induced pluripotent stem cells (hiPSCs) were driven towards the SMC phenotype by transitioning through embryological lineage-specific progenitors that involved the treatment of neuroectodermal or (paraxial and lateral plate) mesodermal progenitors with recombinant TGF-β1 protein confirming the involvement of TGF-β signalling in SMC maturation from embryonic cells *in vitro* (Cheung et al., 2014). The Notch signalling pathway, and the Notch1

receptor in particular, have an important role in both the process of arterial remodelling and the myogenic differentiation of stem cells (Kurpinski et al., 2010).

An SMC-specific epigenetic repertoire of histone modifications is acquired when vascular SMCs develop from hESCs, including H3K4me2 at myogenic gene loci such as α-smooth muscle actin *(ACTA2)* and *MYH11*, the latter being the most specific marker of SMC lineage (Manabe & Owens, 2001; McDonald et al., 2006; Miano et al., 1994). Notably, It has been shown that the epigenetic modification H3K4me2 at these gene promoters is restricted to SMCs, while is absent in non-SMC lineages. In addition, H3K4me2 enrichment at these genes may persist when cultured SMCs are induced to undergo phenotypic switching to a less differentiated state (Figure 6.1) (McDonald et al., 2006), a process of dedifferentiation. In contrast to SMCs, ESCs do not enrich for the H3K4me2 modification at the specific SMC gene promoters. Instead, the H3K27me3 histone modification, known to be involved in gene silencing, is present at these SMC-specific loci. Similar to ESCs, non-SMC somatic cells, for instance endothelial cells, skeletal muscle myotubes and leukocytes also contain high levels of H3K27me3 at the SMC gene promoters (McDonald et al., 2006).

The first aim of this thesis was to determine whether the H3K4me2 mark at the *Myh11* locus is retained in de-differentiated SMCs in culture and further whether changes in that specific signature can occur following treatment of different pro-atherogenic stimuli. Treatment of MOVAS SMCs with pro-atherogenic stimuli suggests that these cells are enriched for H3K4me2 at the *Myh11* locus and have a high gene expression of *Myh11* in comparison with undifferentiated cells. MOVAS SMCs enrich for H3K4me2 at the *Myh11* locus when compared to endothelial cells or other non-somatic cells (Gomez et al., 2013). However, this level of enrichment in MOVAS SMCs in culture, which is believed to be an immortalised de-differentiated SMC, is extremely low when compared to differentiated SMCs freshly isolated from aorta. Previous studies suggest that SMC in culture have reduced expression of *Myh11* defining them as de-differentiated 'modulated' cells (McDonald et al., 2006; Gomez et al., 2013). The baseline expression levels of *Myh11* in MOVAS SMCs are much lower than differentiated SMCs and could be dictated by the reduction in the H3K4me2 epigenetic mark at the *Myh11* locus. However, the differential effects of the atherogenic stimuli on the level of H3K4me2 at the *Myh11* locus and the *Myh11* transcript reveal that the correlation between

H3K4me2 mark and the *Myh11* transcript level is not maintained following treatment with atherogenic stimuli. PDGF-BB can change the transcript level (Liu et al., 2013) but not the epigenetic mark (McDonald et al., 2006; Gomez et al., 2013) and vice versa for Notch ligand, Jag-1 and TGF-β1. In this context, Cheng *et al.* identified a putative role of microRNA-145 (miR-145) as a critical modulator of SMC phenotype both *in vitro* and *in vivo*. Vascular SMC differentiation marker genes such as *Acta2*, calponin1 *(Cnn1)*, and *Myh11* were downregulated by miR-145 downregulation and upregulated by miR-145 upregulation (Cheng et al., 2009). Hence, there could be a direct correlation between the effect of the atherogenic stimuli and miR-143, 145 and the subsequent effects of these atherogenic stimuli on the expression levels of *Myh11,* independent of changes in the histone mark. Indeed, PDGF-BB treated vascular SMC have decreased expression of *Myh11* and *miR-145* concomitant with a stable H3K4me2 mark (Cheng et al., 2009). This indicates that there may be a correlation between miR-145 levels and the expression level *Myh11* following PDGF-BB treatment.

The overall lack of correlation between histone modifications and gene expression in MOVAS SMCs following exposure to atherogenic stimuli may therefore involve the putative role of microRNAs (miRs). Indeed, several studies have reported a regulatory role for miRs in vascular lesion formation (Lu et al., 2018). While histone modifications control the accessibility of the chromatin and transcriptional activities inside a cell, miRs are small RNA molecules, ∼22 nucleotides long that can negatively control their target gene expression post transcriptionally. Short interfering RNAs (siRNAs), often considered to be closely related to miRNAs, have been shown to be involved in both DNA methylation and histone modifications (He and Hannon, 2004). The processing pathways of siRNAs and miRNAs share many of the enzymes involved in the RNA interference (RNAi) pathway. Evidence also suggests that they affect histone modifications. RNase treatment can abolish the localisation of methylated H3 lysine 9 and HP1 to pericentromeric chromatin (Maison et al., 2002). Dicer-related RNAi machinery is also necessary for the formation of heterochromatin structure (Fukagawa et al.,2004). In the context of SMC biology, the H3K4me2/TET2 complex controls the transcriptional activity of the many SMC-specific genes, including contractile genes and miR-145, a key miR promoting SMC differentiation (Liu et al., 2021). Atherogenic stimuli are also known to control miR expression while regulation of miRs has been reported in murine models of vascular lesions formation (Chen et al., 2018; Sun et al., 2011).

The presence of the H3K4me2 mark at the *Myh11* locus could also be dependent on the activity of the Tet-2 demethylase (Xu et al., 2019). Tet-2 binding level seems to be correlated with the H3K4me2 mark at the *Myh11* locus following TGF-β1 treatment where both decrease without any effect on the *Myh11* transcript level. However, there is no correlation between Tet-2 and H3K4me2 at the *Myh11* locus following treatment with Notch ligand, Jag-1 and PDGF-BB in MOVAS SMC. Increases in the epigenetic mark are not associated with any changes in Tet-2 binding or the *Myh11* transcript level. While decreases in the level of Tet-2 binding and *Myh11* expression are not associated with changes in epigenetic mark (Torella et al., 2011). The functional consequences of modifying Tet-2 on SMC phenotype have previously been addressed where Tet-2 knockdown induced a profound alteration of SMC lineage identity by redistributing the enrichment of H3K4me2 at the *MYH11* gene locus (Liu et al., 2013). Tet-2 knockdown in MOVAS SMC supports these studies by demonstrating that Tet-2 knockdown and the enrichment of H3K4me2 are correlated. A recent study also shows that H3K4me2 knockdown leads to TET-2 decline (Liu et al., 2021).

Histone deacetylase 3-deficient macrophages acquire an anti-inflammatory phenotype and exhibit less foam cell formation. Furthermore, histone deacetylase 3 deletion leads to a pro-fibrotic program via epigenetic regulation of TGF-β1, which allows vascular SMCs to generate collagen to stabilize the plaques (Hoeksema et al., 2014). A regulation between miR-143 and DNA-methyltransferase 3 a (DNMT3a) has been reported to mediate vascular SMC proliferation induced by homocysteine. miR-143 directly targets DNMT3a. However, increased DNMT3a expression causes the hypermethylation of miR-143 in homocysteine-induced vascular SMC proliferation (Zhang et al., 2016). In addition, a recent study reported that higher methylation levels of cyclin-dependent kinase inhibitor 2A/2B increases the risk for aortic arch and coronary artery calcification in patients with Ischemic stroke (Zhou et al., 2016, 2017). TET-2 depletion in vascular SMCs activates de-differentiation programmes and induces krüppel-like factor 4 (KLF4). Most importantly, TET-2 negatively regulates intimal hyperplasia in response to arterial injury *in vivo* (Zhuang et al., 2017).

To conclude, data here show that the epigenetic mark of H3Kme2 at the *Myh11* locus is not retained in de-differentiated SMC to the same level as in freshly isolated aortic differentiated

medial SMCs. Moreover, the mark could be downregulated following TGF-β1 treatment suggesting that the mark could be altered by specific atherogenic stimuli. This raises the question of how accurate it is to conclude that every SMC-like cell or non-SMC-like cell that acquires that mark is indeed generated from a parent medial differentiated SMC.

6.2. Murine resident vascular S100β mVSCs and spontaneous S100β human iPSC-derived neuroectoderm progenitor stem cells (SNEPs) acquire the H3K4me2 mark at the *Myh11* locus following myogenic differentiation into SMC-like cells typical of vascular lesions.

While lineage tracing studies have provided compelling evidence for de-differentiated SMC-like cells originating from medial differentiated SMCs as the source of SMC-like cells in vascular lesions in murine injury models (Chappell et al., 2016), the efficiency of the inducible CreERT2-LoxP (cyclization recombinase estrogen receptor type 2-Locus of x-over, P1) system to exclusively mark *Myh11* tracked cells has been questioned. In order for lineage tracing studies to be reliable, it is important that the cell labelling approach only mark the desired cell population and their progeny. Unfaithful expression of reporter genes in other cell types or unintended labelling of even the correct cell population at an undesired time point can lead to wrong conclusions (Alvarez-Aznar et al., 2020). In particular, the reliance on tamoxifen to induce the Cre-ERT2 as it may remain in tissues long after tamoxifen withdrawal. This could result in inadvertent marking of non-SMCs that acquire an active *Myh11* promoter following myogenic differentiation during disease progression (Reinert et al., 2012). As a result, stem cells undergoing myogenic differentiation could be marked, thus misleading the origin of these SMC-like neointimal cells. Therefore, it was important to establish whether S100β mVSCs and S100β SNEPs acquire the H3K4me2 mark at the *Myh11* locus when these cells differentiate to an SMC-like phenotype. Moreover, whether this acquisition of H3K4me2 was associated with an increase in Tet-2 binding. Therefore, the second aim of this thesis was to determine whether S100β resident mouse vascular mVSCs and human S100β SNEPs can acquire the SMC signature of H3K4me2 at the *Myh11* locus following treatment with different atherogenic stimuli and further to determine a role if any for Tet-2 in controlling this process.

The data suggest that the presence of the H3K4me2 mark at the SMC *Myh11* locus in SMC-like cells (typical of vascular lesions) in response to atherogenic stimuli is a direct result of myogenic differentiation of S100β resident mVSCs cells and S100β SNEPs to a SMC-like phenotype. Moreover, the presence of this mark is dependent on the activity of the Tet-2 demethylase. These data are in agreement with previous studies demonstrating a role for Tet-2 binding in controlling the appearance of the H3K4me2 mark at this locus, at least in human SMCs (Liu et al., 2013). The data are also consistent with numerous studies that have indicated the manner by which stem cells contribute to lesion formation is through differentiation of these cells to become SMC-like cells (Wang et al., 2018). The data further provide evidence that S100β mVSCs and S100β SNEPs can be stimulated by atherogenic stimuli to undergo myogenic differentiation and acquire the histone mark. In particular, in resident mouse S100β mVSCs, there was a strong correlation between the acquisition of the H3K4me2 mark at the *Myh11* locus in response to atherogenic stimuli and the increase in *Myh11* gene expression, an effect that is attenuated following Tet-2 knockdown, at least following exposure to TGF-β1/PDGF-BB.

The importance of this finding is supported by recent publications from our lab group that demonstrated the majority of cells within ligated arteriosclerotic vessels were classified as S100β mVSC or their myogenic progeny (~65%) using both lineage tracing of S100β mVSCs and supervised machine learning following interrogation of single cell photonic signatures of cells within normal 'sham' vessels and cell within arteriosclerotic lesions following carotid artery ligation (Di Luca et al., 2021; Molony et al., 2021). Specifically, when cells isolated from normal 'sham' vessels were interrogated, most cells from normal vessels were classified as SMCs. In contrast, in arteriosclerotic vessels, the majority of cells were classified as S100β mVSC-derived SMC-like progeny on a cross-validated leave-one-out basis. Taken together, these data confirm that a significant proportion of cells within ligated/arteriosclerotic vessels share a photonic profile similar to S100β mVSC-derived myogenic progeny (Molony et al., 2021). These data further suggest that the presence of the H3K4me2 mark at the *Myh11* locus within these SMC-like cells in lesions is likely to be due in part to the presence of S100β mVSC myogenic progeny which acquire this mark on differentiation. This data does not exclude the possible contribution of SMCs that de-differentiate to SMC-like cells and, thus contribute to the formation of neointimal cells in the lesion. However, the data provide supportive evidence

for a role of resident vascular stem cells in the formation of neointimal SMC-like cells in lesions.

In order to further confirm the single gene ChIP data at the *MYH11* locus, ChIP-seq data on S100β SNEPs were generated and interrogated to confirm H3K4me2 and H3K27me3 enrichment patterns at this locus. The data are in full agreement with the single gene ChIP assay in that these undifferentiated S100β stem cells are enriched for H3K27me3 at the *MYH11* locus concomitant with a low level of transcript for the *MYH11* gene (Di Luca et al., 2021). However, on myogenic differentiation, enrichment of H3K4me2 occurs at the same locus. These data are in agreement with previous studies on the epigenetic profile of SMCs in culture (McDonald et al., 2006). This enrichment occurred on the CpG islands (CGIs) in non-coding regions upstream of transcription starting site (TSS). Indeed, roughly 80% of DNA methylation occurs at CGIs within gene promoters and this region is where the enrichment of H3K4 methylation was most pronounced in *Myh11* and other SMC loci (Toghill et al., 2015). *In silico* analysis of previously published mouse MSCs, human hESC and MSCs bulk ChIP-seq datasets further confirm the enrichment of H3K4 methylation at the same specific SMC gene locus.

While the presence of H3K4 methylation marks at other SMC gene loci was evident in some undifferentiated mMSCs, this could be due to partial differentiation of these stem cells prior to specific myogenic induction. Indeed, transgelin *(Tagln)* is expressed in skeletal and cardiac muscle during development, and within activated fibroblasts under a variety of conditions (Kim et al., 1997; Li et al., 1996; Sartore et al., 2001) and smoothelin *(Smtn)* is expressed in a variety of organs and tissues such as prostate stromal cells in culture (Wang et al., 2002).

Unlike single-cell ChIP-seq, bulk ChIP-seq may not provide an accurate account of the percentage of the cells that acquired H3K4me2 at the *Myh11* gene locus (Rotem et al., 2015). A limitation of chromatin mapping technologies is that they require large amounts of input material and yield ‘averaged’ profiles that are insensitive to cellular heterogeneity. This is a major shortcoming given that cell-to-cell variability is inherent to most tissues and cell populations. In particular, bulk ChIP-seq profiles are insensitive to cell-to-cell variation. While the data obtained from single cells is sparse, comprising on the order of 1000 unique reads, by assaying thousands of cells, a spectrum of sub-populations defined by differences in

chromatin signatures of pluripotency and differentiation priming can be obtained. When corroborated by comparing the single-cell ChIP-seq to orthogonal single-cell gene expression data, aspects of epigenetic heterogeneity not captured by transcriptional analysis alone are realised. Nevertheless, in the current study, the nascent population of undifferentiated cells that acquired enrichment of H3K4me2 at the *Myh11* gene locus was significant when compared to the undifferentiated control.

6.3. Murine resident vascular S100β mVSCs and spontaneous S100β human iPSC-derived neuroectoderm progenitor stem cells (SNEPs) acquire the H3K4me2 mark at the *Myh11* locus following adipogenic and osteogenic differentiation into non-SMC-like cells typical of vascular lesions.

Using lineage tracing in *Myh11-CreER/Apoe-/- (*apolipoprotein e deficient mouse model) mice, it has been reported that macrophage-like cells, fibroblast-like cells, MSCs and other cell phenotypes in arteriosclerotic/atherosclerotic lesions are derived from medial SMCs, a process mediated by KLF4 (Shankman et al., 2015). A similar result was observed using *Myh11-CreER;Rosa26-Confetti* mice where non-SMCs that expressed the macrophage marker, Galectin3 during neointima formation were tracked to a parent Myh11/Sca1 subpopulation of medial SMCs (Chappell et al., 2016). Both studies confirm that medial SMCs can simultaneously form the fibrous cap and the plaque core are characterized by ACTA2 modulated SMC-like cells and macrophage-like non-SMC, respectively (Chappell et al., 2016; Feil et al., 2014). Importantly, the H3K4me2 mark at the *Myh11* locus was also present in these SMC-like and non-SMC lesional cells that were tracked to a parent medial SMC (Gomez et al., 2013; Shankman et al., 2015) (Figure 6.1). However, unfaithful expression of reporter genes in other cell types or unintended labelling of even the correct cell population at an undesired time point can lead to wrong conclusions (Alvarez-Aznar et al., 2020). In addition, the use of tamoxifen to induce the Cre-ERT2 could again result in inadvertent marking of non-SMCs that acquire an active *Myh11* promoter during lineage specification (Reinert et al., 2012). As a result, stem cells undergoing lineage specification could again be marked, thus misleading the origin of these non-SMC-like neointimal cells. If this is a real possibility, it would require resident vascular stem cells that undergo lineage specification other than myogenic to acquire the H3K4me2 mark at the *Myh11* locus. Therefore, it was important to

establish whether S100β mVSCs and S100β SNEPs acquire the H3K4me2 mark at this locus when these cells differentiate to several non-SMC phenotypes (adipogenic, osteogenic and vasculogenic). Indeed, histone marks on several lysine residues are deposited on particular areas of the genome and associated with distinct states of gene transcription, and these patterns are generally conserved from yeast to humans. Promoters of transcriptionally active genes are associated with enriched H3K4me3 and lysine acetylation on histone H3 and H4, while actively transcribing genes tend to have higher levels of H3K36me3 and H3K79me3 in the gene body (Gates et a., 2017). In this context, the third aim of this thesis was to determine whether S100β resident vascular mVSCs and S100β SNEPs can acquire the H3K4me2 mark at the *Myh11* locus following differentiation into non-SMC lineages (adipogenic, osteogenic and vasculogenic).

It has been reported in a number of studies that epigenetic changes affect key transcriptional factors shaping gene expression and differentiation potentials of stem cells (Hattori et al., 2004; Kimura et al., 2004; O'Neill et al., 2006). Epigenetic signatures defined by H3K4me2 and H3K27me3 during development can distinguish cell-type specific genes from genes with different cell types and cell lineage patterns of expression (Popova et al., 2012). This data suggests that upregulation of gene expression for specific lineages is usually correlated with a discrete epigenetic profile at the lineage-specific gene loci. Enrichment of histone modifications has been observed on SMC marker gene loci, including *Myh11, Acta2,* and *Tagln*, in mature SMC and SMC progenitor cells committed to differentiate into SMCs. In contrast, this enrichment was not seen in hESC and non-SMC somatic cells (Barski et al., 2007). While H3K27 mono-, di- and tri- methylation are histone marks of transcriptionally silent chromatin, multiple non-SMCs including ECs, fibroblasts and hESCs in culture show marked enrichment of H3K27me3 at the *MYH11* gene locus as determined by single gene ChIP assays, consistent with its transcriptional silencing of this gene in these cells (McDonald et al., 2006).

In the current study, *in silico* analysis confirmed a similar enrichment for H3K27me3 at *SMC* gene loci in undifferentiated S100β mVSCs and S100β SNEPs as well as mMSC, hMSC and hESCs. This H3K27me3 mark was also present at adipogenic and osteogenic genes loci (data not shown) in agreement with previous studies (Hemming et al., 2014). However, following differentiation, SMC loci in mouse SMCs lose this enrichment before these loci become

enriched for H3K4 methylation marks. Previous studies have shown that several transcription factors essential for lineage specification are not expressed in undifferentiated mouse ESCs but their respective promoters are enriched for both H3K4me3 and H3K27me3 (Azuara et al., 2006).

In mouse S100β mVSCs, the level of enrichment of H3K4me2 at the *Myh11* locus and binding of Tet-2 were both increased in osteogenic progeny derived from and may also explain the decrease in the level of enrichment of H3K27me3 at the same locus. Similarly, adipogenic progeny exhibited enrichment of H3K4me2 and increased Tet-2 binding at the *Myh11* locus compared to undifferentiated S100β mVSCs. This enrichment of Tet-2 at lineage-specific promoters is in agreement with previous findings using embryonic stem cells (Ficz et al., 2011). While 5-hydroxymethylcytosine (5hmC) is known to be relatively enriched in euchromatic parts of the genome, including in CGIs and promoters, and its presence in promoters and exons is associated with increased levels of transcription, the observed enrichment of H3K4me2 and Tet-2 binding at the *Myh11* locus was not accompanied with the expression of myogenic genes namely, *Myh11* and *Cnn1,* which remained similar to undifferentiated S100β mVSCs following adipogenic and osteogenic differentiation. While the ratio of H3K4me2:H3K27me3 was only significantly increased in S100β mVSC-derived osteogenic progeny, this is primarily due to the lack of change in H3K27me3 enrichment at this locus following adipogenic differentiation.

In hiPSC-derived S100β SNEPs, a similar epigenetic profile at the *MYH11* locus was observed for both adipogenic and osteogenic progeny. Namely, the ratio of the H3K4me2:H3K27me3 mark at the *MYH11* locus increased significantly concomitant with no discernible change in the expression levels of *MYH11* and *CNN1* compared to undifferentiated SNEPs. While adipogenic progeny exhibited a tendency to enrich for H3K4me2, it did not reach significance. However, the ratio increased overall due to a significant reduction in the level of enrichment of H3K27me3 in these progeny at the same locus. In S100β SNEP-derived osteogenic progeny, the level of enrichment of H3K4me2 again correlated with TET-2 binding level at the same locus in agreement with previous studies that suggest promoters that are high in 5hmC are enriched in the activating histone mark H3K4me3, whereas those enriched in 5-methylcytosine (5mC) are depleted of H3K4me3 which is affected by TET-2 (Ficz et al., 2011).

Clearly, as with S100β mVSCs, the ratio of H3K4me2:H3K27me3 increases in S100β SNEP-derived osteogenic and adipogenic progeny at the *MYH11* gene locus irrespective of their phenotypic state and transcript level of myogenic genes *in vitro*.

Analysis of ChIP-seq data for both peak calling and peak scoring in adipogenic and osteogenic progeny from mouse mMSCs, human hESC and hMSCs suggest that enrichment of H3K4 methylation marks occurs not only at their respective lineage-specific loci but also at the *Myh11* locus. Collectively, these data indicate that enrichment for H3K4 methylation at the *Myh11* locus is not specific to SMC as osteocytes and adipocytes generated from stem cells also acquire that mark. In contrast, there was no enrichment for H3K4 methylation marks at the *Myh11* locus in vasculogenic progeny using either single gene ChIP-PCR or ChIP-seq. This is consistent with previous studies that confirm the lack of enrichment of this mark at this locus in mature endothelial cells *in situ* (Gomez et al., 2013) or in culture (McDonald et al., 2007).

One question that arises is why would multiple histone modifications at different loci be employed in parallel to control transcription? Previous studies have suggested that histone lysine methylation is regarded as an active chromatin mark in many organisms, and is implicated in mediating active euchromatin. H3K4me3 was predominantly enriched at TSSs of the majority of protein-coding genes (85%). Genome-wide CHiP-seq analysis revealed that the likelihood of a gene being marked by H3K4me3 correlated with it being transcribed at one or more time points during the cell cycle but importantly not necessarily by continuous active transcription (Strenkert et al., 2022). This may explain why the *Myh11* transcripts levels remained unchanged in adipogenic and osteogenic progeny. Partially redundant functions of histone marks in chromatin might confer robustness on epigenetic regulation. Thus, transcriptional responses might be largely independent of small changes in any single modification and the cell might have several options to induce transcriptional changes (changes in transcription can be elicited by inhibition or activation of one of several different histone-modification pathways). Whether the enrichment of H3K4 methylation histone marks at the *Myh11* locus in adipogenic and osteogenic progeny with parallel enrichment at lineage-specific loci contributes to overall lineage specification in these progeny remains unclear. However, it is known that particular chromatin modifications are associated with different

states of gene transcription, yet our understanding of which modifications are causal 'drivers' in promoting transcription is incomplete. Histone tails are extensively post-translationally modified ('marked') by the balance of writers and erasers. Genome-wide localisation of histone marks occurs at distinct genic regions (e.g., promoters, enhancers, or gene bodies), often correlating with different functional impacts on Pol II transcription. The interplay between histone marks in specifying the 'next step' of transcription remains unclear. The observation that histone marks may not always correlate with distinct genomic regions and states of gene expression raises questions regarding their functional role in different steps of the Pol II transcription cycle. Previous studies have highlighted clear roles for H3K4me3, H3K9ac, H3K36me3, and other lysine marks in the context of particular stages of transcription. Moreover, there are many histone marks observed that correlate with transcription for which mechanistic functions are not yet elucidated. (Gates et al., 2017). Given the large number of different histone modifications, the potential combinatorial complexity is considerable. Advances in technology over the past decade such as ChIP-sequencing have facilitated the mapping, distribution and co-localisation of histone marks at high-resolution genome-wide, while mass spectrometry, often in combination with stable isotope labelling has enabled the analysis of histone marks and dynamics at the level of a single histone tail. Mass spectrometric data has provided evidence for many combinations of modifications that are either more likely to occur together, or are mutually exclusive, suggesting crosstalk between these marks. Such crosstalk can occur in cis between distinct modifications on the same histone tail, or in trans either on neighbouring histones within the same nucleosome or on neighbouring nucleosomes in a chromatin domain (Zhang et al., 2015).

Notwithstanding the potentially important role of combinatorial histone marks, it is clear from data presented in this thesis that the mere presence of an H3K4me2 epigenetic mark at the *Myh11* gene locus in adipogenic and osteogenic progeny does not imply transcriptional activity for this gene. The reason for this is presently unknown but may indicate local induction of histone methylation is sufficient to allow re-expression of silenced target genes in various cell types but writing of the mark overcomes epigenetic silencing in a sustained but context-dependent manner (Cano-Rodriguez et al., 2016). Maintenance of the re-expression is achieved, but strongly depends on the chromatin microenvironment (i.e., DNA methylation status). Moreover, H3K79me appears to be essential in allowing stable gene re-expression,

confirming its role in epigenetic crosstalk for stable reactivation (Cano-Rodriguez et al., 2016). In any case, the presence of the H3K4me2 mark is not definitive evidence to conclude that a given cell is derived from a differentiated SMC since stem cell-derived osteogenic and/or adipogenic progeny can also have this mark independent of re-expression of this silenced gene. These data suggest that the presence of this epigenetic mark in non-SMCs within vascular lesions does not necessarily prove that these lesional cells are derived from an SMC parent cell.

This finding may also have implications for macrophage-like cells present in vascular lesions that exhibit the SMC-specific *MYH11* H3K4me2 epigenetic signature (Gomez et al., 2013; Shankman et al., 2015). The data from single gene ChIP-PCR and ChIP-seq demonstrate that a multipotent stem cell is fully capable of acquiring the H3K4me2 mark at the *Myh11* locus when undergoing osteogenic and adipogenic differentiation (Figure 6.2). Ongoing studies are currently investigating whether myeloid differentiation of S100β mVSCs and S100β SNEPs to macrophage-like Cluster of differentiation 68 (CD68) cells in response to oxidised low-density lipoprotein (LDL) and cholesterol is accompanied by an increase in the level of enrichment for H3K4me2 at this locus.

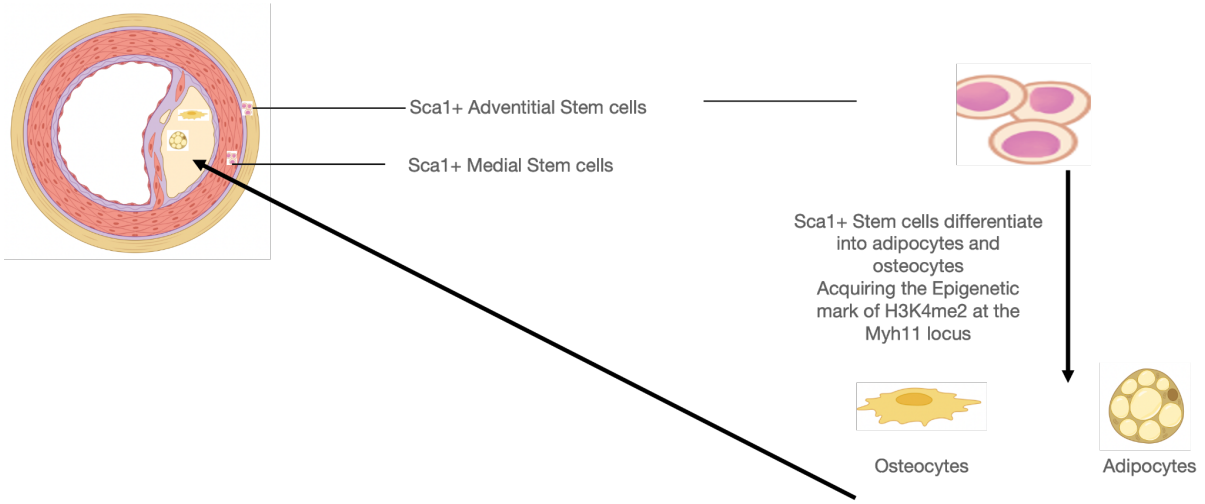

Figure 6.2 Non-SMC-like cells (fibroblasts, macrophage -, adipogenic - and osteogenic-like cells) in vascular lesions could arise from S100β resident vascular mVSCs that acquire the epigenetic profile of H3K4me2 at the *Myh11* locus following progeny differentiation.

6.4 H3K4 methylation marks at lineage-specific loci may define commitment of multipotent stem cells before cell fate is determined by transcriptional activity

Histone methylation has important functions throughout development in every cell and tissue type (Jambhekar et al., 2019). This epigenetic process regulates key developmental gene networks dictating when genes are switched on and off in a highly dynamic fashion in accordance with developmental signals (Peters et al., 2003; Rea et al., 2000; Rice et al., 2003). Regulatory genes that promote access to alternative fates are either expressed or inducible in the precursors but end up not only repressed but irreversibly silenced as a result of commitment.

The mechanisms of recruitment of H3K4 methyltransferases to the target genes may (1) be recruited, directly or indirectly, by sequence-specific DNA binding factors (2) directly associated with basal transcriptional machinery (3) associated with chromatin through histone modification readers, or (4) be recruited by RNA. The existing literature suggests that a combination of all four mechanisms is likely to operate *in vivo* (Ruthenburg et al., 2007). The third mechanism is supported by the discovery of a histone tail "presenter module" within the MLL core complex (Wysocka et al., 2005), also with the general observation that H3K4 methyltransferase proteins themselves contain a wealth of potential histone modification binding domains.

In vivo, histone methyltransferases and demethylases often operate in large protein complexes, and their genomic targets are often influenced by the presence of reader proteins or domains that recognize various histone modifications. Although the members of a family of readers can recognize different degrees of methylation at different sites, each reader typically recognizes a single or a few closely related methylation marks (Lan et al., 2007; Li et al., 2006; Peña et al., 2006; Shi et al., 2006; Wysocka et al., 2006). It has been reported that individual histone marks and their regulatory enzymes often show distinct effects on ESC differentiation towards different lineages. For example, MLL4 loss led to deficits in differentiation towards endoderm, an increase in mesodermal markers, but relatively few effects on differentiation into embryoid bodies and ectoderm (Wan et al., 2014).

The mechanisms responsible for these regulatory changes in S100β stem cells are unknown but some studies have begun to address this phenomenon in other cell systems. For example, during T-cell development, a stepwise process of cell fate choices for descendants of multipotent stem cells is apparent. Sequential events that exclude alternative lineages occur at phenotypically well-defined stages within the thymus, providing a revealing model for the kinds of events needed to channel multipotent stem cells into a single developmental path (Rothenberg, 2011). The molecular mechanisms involved were addressed by probing five stages spanning the commitment process using RNA-seq and ChIP-seq to track genome-wide shifts in transcription, cohorts of active transcription factor genes, histone modifications at diverse classes of cis-regulatory elements, and binding repertoire of key transcription factors with complementary roles in T cell development (Zhang et al., 2012). These data highlighted potential promoter-distal cis-regulatory elements in play and reveal both activation sites and diverse mechanisms of repression that silence genes used in alternative lineages. Of note, histone marking was dynamic and reversible, and though permissive marks anticipate, repressive marks often lag behind changes in transcription. Moreover, *in vivo* binding of key transcription factors relative to epigenetic marking reveals distinctive factor-specific rules for recruitment of these crucial transcription factors to different subsets of their potential sites, dependent on dose and developmental context (Zhang et al., 2012).

In a similar manner, epigenetic mechanisms are fundamental regulators of lineage specification and cell fate decisions of multipotent MSCs, and as such, the question of which epigenetic modifications characterise the transition of nascent MSCs to tissue-specific MSC-derived progeny has recently been addressed (Wu et al., 2017). By profiling the temporal changes of seven histone marks correlated to gene expression during proliferation, early commitment, matrix deposition, and mineralization stages, distinct epigenetic mechanisms that regulate transcriptional programs necessary for tissue-specific phenotype development were revealed (Figure 6.3). Patterns of stage-specific enrichment of histone modifications revealed distinct modes of repression and activation of gene expression. At commitment, H3K27me3 is removed from genes that are upregulated and is not acquired on downregulated genes. Additionally, the absence of H3K4me3 modification at promoters defined a subset of osteoblast-specific upregulated genes, indicating that acquisition of acetyl modifications may

drive activation of these genes. Significantly, loss or gain of H3K36me3 was the primary predictor of dynamic changes in temporal gene expression (Wu et al., 2017).

It is unclear how genes are activated when multipotent S100β stem cells undergo lineage specification and whether only lineage-specific genes are enriched for H3K4 methylation marks when undergoing specific differentiation. Based on the *in silico* analysis of human and mouse MSC and hESCs from published work, and single gene ChIP-PCR analysis of S100β mVSCs and S100β SNEPs, specific enrichment of histone modifications revealed distinct modes of repression and activation of gene expression. For example, at commitment, mMSC-derived adipogenic progeny acquire peaks of enrichment for H3K4me1 at alkaline phosphatase *(Alpl)* (osteogenic gene) gene locus while mMSC-derived osteogenic progeny enrich for H3K4me3 at fatty acid binding protein 4 *(Fabp4)* (adipogenic gene) gene locus with a corresponding increase in the expression of these lineage-specific genes. However, mMSC-derived adipogenic and osteogenic progeny also acquire peaks of enrichment for H3K4me1 and H3K4me3, respectively, at the myogenic *Myh11* gene locus without a corresponding increase in *Myh11* gene expression. A similar profile of enrichment for H3K4 methylation and H3K27me3 is observed for hMSCs and hESCs at lineage-specific loci. Hence, in an undifferentiated state, H3K27me3 is present on lineage-specific genes that are downregulated while H3K4 methylation marks are absent. The absence of H3K4 methylation at lineage-specific loci confirms a distinct mode of repression and activation of gene expression. However, when the same population of undifferentiated multipotent stem cells receive an inductive cue to differentiate down a specific lineage, the cells become committed and acquire the H3K4 methylation marks not only at gene loci associated with that lineage but also at other lineage-specific loci without a corresponding change in gene expression for these genes. Clearly, the subsequent binding of key transcription factors relative to epigenetic marking is important for recruitment of these crucial transcription factors to gene-specific promoter and enhancer regions that drive gene expression. Moreover, regulatory genes that promote access to alternative fates are either expressed or inducible in the precursors but end up not only repressed but irreversibly silenced as a result of commitment. In this context, it is therefore of interest to determine whether the acquisition of the H3K4 methylation marks at the *Myh11* locus in adipogenic and osteogenic progeny is closely associated with a parallel enrichment of H3K27me3 at this locus, thereby facilitating repression of *Myh11* gene

expression in these non-myogenic progeny. Studies to address this possibility are currently ongoing.

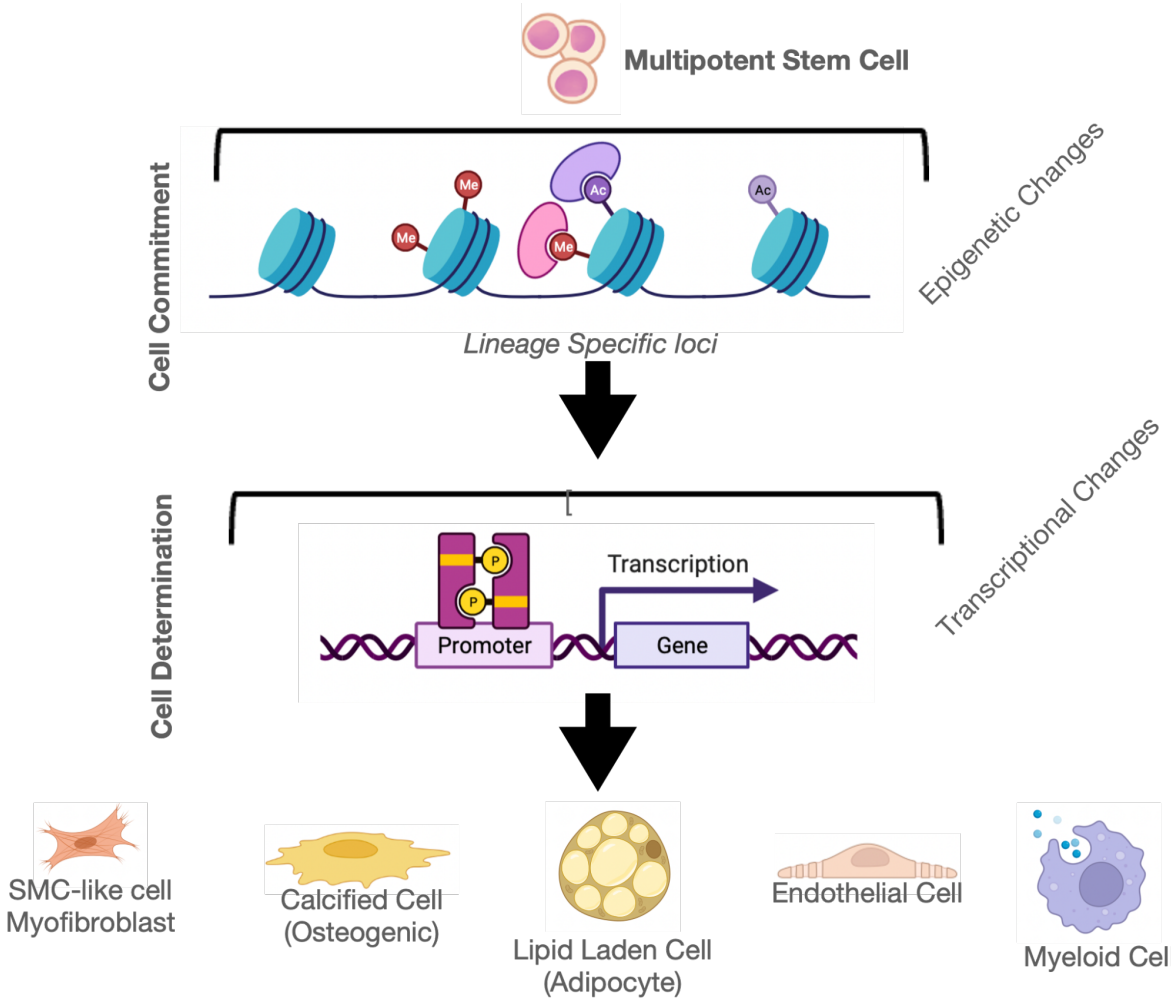

Figure 6.3 When MSC differentiation requires cell commitment and epigenetic changes before the differentiation of these cells is determined and the transcript level is upregulated for a specific lineage.

6.5 Future work

As bulk ChIP-seq does not provide an accurate account of the percentage of cells that acquire the H3K4me2 epigenetic signature at the *Myh11* gene locus within a given cell population, single-cell ChIP-seq may provide a more accurate analysis of the percentage of stem cells that acquire this mark following adipogenic and osteogenic differentiation.

While H3K4me2 was enriched at the *MYH11* locus in myogenic, adipogenic and osteogenic progeny, further examination of the presence of the H3K4me2 mark at other SMC loci (CNN1, SM22α etc) is required to determine whether this observation is specific for the MYH11 locus or prevails across all myogenic lineage specific loci in S100β SNEP derived adipogenic and osteogenic progeny using the same bulk ChIP-seq dataset.

Moreover, while the data provide compelling evidence that adipogenic and osteogenic progeny are enriched for H3K4me2 at the *MYH11* locus, it is unclear whether osteogenic and adipogenic lineage specific loci are also enriched for H3K4me2 in SNEPs following myogenic differentiation. Therefore, it would be of interest to interrogate the same genome-wide bulk ChIP-seq datasets of SNEPs used in this study for H3K4 methylation marks at adipogenic and osteogenic specific gene loci in myogenic progeny. Specifically, ChIP-seq analysis of H3K4me2 marks at several adipogenic and osteogenic loci following myogenic differentiation would confirm that the aforementioned relationship between H3K4me2 at the myogenic Myh11 locus in adipogenic and osteogenic progeny is reciprocated in myogenic progeny at specific adipogenic and osteogenic loci. This would support the hypothesis that specific histone marks occur at several lineage specific loci once a undifferentiated stem cell undergoes lineage specification irrespective of the final lineage, at least for myogenic, adipogenic and osteogenic. Whether a similar lack of the H3K4me2 mark is also apparent following vasculogenic differentiation could also be revealed.

Further examination of the presence of the H3K27me3 mark at the MYH11 locus in adipogenic and osteogenic progeny might help to explain whether the persistence of this mark in adipogenic and osteogenic progeny despite the enrichment of H3K4me2 at the same locus could be responsible for the silencing of the *MYH11* gene in these cells. Indeed, previous studies have suggested that the presence of this H3K27me3 mark at the MYH11 locus is a hallmark of de-differentiated SMCs that retain the H3K4me2 mark (Gomez et al., 2013). Therefore, it would be of interest to interrogate H3K27me3 enrichment at the MYH11 gene locus in adipogenic and osteogenic progeny using the genome-wide bulk ChIP-seq datasets for SNEPs. Moreover, it would also reveal whether the presence of H3K27me3 at myogenic

loci, despite the presence of the H3K4me2 mark at the same loci, is responsible for the lack of SMC transcription in adipogenic and osteogenic progeny.

While it is clear that the DNA demethylase, TET-2 controls the enrichment of H3K4me2 at CpG islands on myogenic specific loci (Liu et al., 2013), the reciprocal role of H3K4me2 in facilitating TET-2 binding has also been reported. Previous studies uncovered that H3K4me2 serves as a stable hub for selective recruitment of the methylcytosine dioxygenase TET2 on SMC gene repertoire (Liu et al., 2021). Indeed, H3K4me2-mediated TET2 binding promotes activation of SMC pro-differentiation gene program via DNA demethylation and hydroxymethylation. It would therefore be of interest to assess whether removal of H3K4me2 via selective editing in S100β derived myogenic progeny led to loss of differentiation due to impaired recruitment of the DNA methylcytosine dioxygenase TET2.

Finally, as the number of bulk ChIP-seq datasets were from a limited number of studies, there is a requirement for more data generation on H3K4 methylation marks in osteogenic, adipogenic and myogenic progeny. These studies would further address whether the presence of the H3K4me2/H3K27m3 marks are key to determining activation or repression of lineage and non-lineage-specific genes in each progeny.

6.6 Conclusions

Collectively, the data presented in this thesis suggest that the presence of the H3K4me2 mark at the *Myh11* locus in cells typical of SMC-like cells and non-SMCs within vascular lesions is not exclusive to de-differentiation of medial SMCs. Moreover, the presence of this histone mark at multiple lineage-specific loci following differentiation may reflect the overall 'commitment status' of S100β mVSCs and ultimately dictate their capacity to proceed and be fully determined and fated down specific lineages.

References

Abdallah, B. M., Jafari, A., Zaher, W., Qiu, W., & Kassem, M. (2015). Skeletal (stromal) stem cells: An update on intracellular signaling pathways controlling osteoblast differentiation. *Bone*, *70*, 28–36. https://doi.org/10.1016/j.bone.2014.07.028

Ailawadi, G., Moehle, C. W., Pei, H., Walton, S. P., Yang, Z., Kron, I. L., Lau, C. L., & Owens, G. K. (2009). Smooth muscle phenotypic modulation is an early event in aortic aneurysms. *Journal of Thoracic and Cardiovascular Surgery*, *138*(6), 1392–1399. https://doi.org/10.1016/j.jtcvs.2009.07.075

Aird, W. C. (2007). Phenotypic heterogeneity of the endothelium: II. Representative vascular beds. *Circulation Research*, *100*(2), 174–190. https://doi.org/10.1161/01.RES.0000255690.03436.ae

Akhurst, R. J., Lehnert, S. A., Faissner, A., & Duffie, E. (1990). TGF beta in murine morphogenetic processes: The early embryo and cardiogenesis. *Development*, *108*(4), 645–656. https://doi.org/10.1242/dev.108.4.645

Albarrán-Juárez, J., Kaur, H., Grimm, M., Offermanns, S., & Wettschureck, N. (2016). Lineage tracing of cells involved in atherosclerosis. *Atherosclerosis*, *251*, 445–453. https://doi.org/10.1016/j.atherosclerosis.2016.06.012

Alexander, M. R., Murgai, M., Moehle, C. W., & Owens, G. K. (2012). Interleukin-1β modulates smooth muscle cell phenotype to a distinct inflammatory state relative to PDGF-DD via NF-κB-dependent mechanisms. *Physiological Genomics*, *44*(7), 417–429. https://doi.org/10.1152/physiolgenomics.00160.2011

Alexander, M. R., & Owens, G. K. (2011). Epigenetic Control of Smooth Muscle Cell Differentiation and Phenotypic Switching in Vascular Development and Disease. *Annual Review of Physiology*, *74*(1), 13–40. https://doi.org/10.1146/annurev-physiol-012110-142315

Alekseyenko, A. A. et al. A sequence motif within chromatin entry sites directs MSL establishment on the *Drosophila* X chromosome. *Cell* 134, 599–609 (2008). https://doi.org/10.1016/j.cell.2008.06.033

Ali, D., Chalisserry, E. P., Manikandan, M., Hamam, R., Alfayez, M., Kassem, M., Aldahmash, A., & Alajez, N. M. (2018). Romidepsin promotes osteogenic and adipocytic

differentiation of human mesenchymal stem cells through inhibition of histondeacetylase activity. *Stem Cells International*, *2018*. https://doi.org/10.1155/2018/2379546

Allahverdian, S., Chehroudi, A. C., McManus, B. M., Abraham, T., & Francis, G. A. (2014). Contribution of intimal smooth muscle cells to cholesterol accumulation and macrophage-like cells in human atherosclerosis. *Circulation*, *129*(15), 1551–1559. https://doi.org/10.1161/CIRCULATIONAHA.113.005015

Álvarez-Aznar, A., Martínez-Corral, I., Daubel, N., Betsholtz, C., Mäkinen, T., & Gängel, K. (2020). Tamoxifen-independent recombination of reporter genes limits lineage tracing and mosaic analysis using CreERT2 lines. *Transgenic research*, *29*(1), 53-68. https://doi.org/10.1007/s11248-019-00177-8

Anderson, J. P., Dodou, E., Heidt, A. B., De Val, S. J., Jaehnig, E. J., Greene, S. B., Olson, E. N., & Black, B. L. (2004). HRC Is a Direct Transcriptional Target of MEF2 during Cardiac, Skeletal, and Arterial Smooth Muscle Development In Vivo. *Molecular and Cellular Biology*, *24*(9), 3757–3768. https://doi.org/10.1128/mcb.24.9.3757-3768.2004

Asmar, R. G., Brunel, P. C., Pannier, B. M., Lacolley, P. J., & Safar, M. E. (1988). Arterial distensibility and ambulatory blood pressure monitoring in essential hypertension. *The American journal of cardiology*, *61*(13), 1066-1070. https://doi.org/10.1016/0002-9149(88)90127-0

Azuara, V., Perry, P., Sauer, S., Spivakov, M., Jørgensen, H. F., John, R. M., Gouti, M., Casanova, M., Warnes, G., Merkenschlager, M., & Fisher, A. G. (2006). Chromatin signatures of pluripotent cell lines. *Nature Cell Biology*, *8*(5), 532–538. https://doi.org/10.1038/ncb1403

Bacakova, L., Zarubova, J., Travnickova, M., Musilkova, J., Pajorova, J., Slepicka, P., Kasalkova, N. S., Svorcik, V., Kolska, Z., Motarjemi, H., & Molitor, M. (2018). Stem cells: their source, potency and use in regenerative therapies with focus on adipose-derived stem cells – a review. *Biotechnology Advances*, *36*(4), 1111–1126. https://doi.org/10.1016/j.biotechadv.2018.03.011

Baccarelli, A., Rienstra, M., & Benjamin, E. J. (2010). Cardiovascular epigenetics: Basic concepts and results from animal and human studies. *Circulation: Cardiovascular Genetics*, *3*(6), 567–573. https://doi.org/10.1161/CIRCGENETICS.110.958744

Bailey, T., Krajewski, P., Ladunga, I., Lefebvre, C., Li, Q., Liu, T., Madrigal, P., Taslim, C., &

Zhang, J. (2013). Practical Guidelines for the Comprehensive Analysis of ChIP-seq Data. *PLoS Computational Biology*, *9*(11), 5–12. https://doi.org/10.1371/journal.pcbi.1003326

Barski, A., Cuddapah, S., Cui, K., Roh, T. Y., Schones, D. E., Wang, Z., Wei, G., Chepelev, I., & Zhao, K. (2007). High-Resolution Profiling of Histone Methylations in the Human Genome. *Cell*, *129*(4), 823–837. https://doi.org/10.1016/j.cell.2007.05.009

Bazzoni, G., & Dejana, E. (2004). Endothelial cell-to-cell junctions: Molecular organization and role in vascular homeostasis. *Physiological Reviews*, *84*(3), 869–901. https://doi.org/10.1152/physrev.00035.2003

Benditt, E. P., & Benditt, J. M. (1973). Evidence for a monoclonal origin of human atherosclerotic plaques. *Proceedings of the National Academy of Sciences of the United States of America*, *70*(6), 1753–1756. https://doi.org/10.1073/pnas.70.6.1753

Benjamin, E. J., Muntner, P., Alonso, A., Bittencourt, M. S., Callaway, C. W., Carson, A. P., Chamberlain, A. M., Chang, A. R., Cheng, S., Das, S. R., Delling, F. N., Djousse, L., Elkind, M. S. V., Ferguson, J. F., Fornage, M., Jordan, L. C., Khan, S. S., Kissela, B. M., Knutson, K. L., … Virani, S. S. (2019). Heart Disease and Stroke Statistics-2019 Update: A Report From the American Heart Association. In *Circulation* (Vol. 139, Issue 10). https://doi.org/10.1161/CIR.0000000000000659

Bennett, M. R., Sinha, S., & Owens, G. K. (2016). Vascular Smooth Muscle Cells in Atherosclerosis. *Circulation Research*, *118*(4), 692–702. https://doi.org/10.1161/CIRCRESAHA.115.306361

Bentley, D. R. (2006). Whole-genome re-sequencing. *Current Opinion in Genetics and Development*, *16*(6), 545–552. https://doi.org/10.1016/j.gde.2006.10.009

Berger, S. L. (2007). The complex language of chromatin regulation during transcription. *Nature*, *447*(7143), 407–412. https://doi.org/10.1038/nature05915

Berk, B. C., Abe, J. I., Min, W., Surapisitchat, J., & Yan, C. (2001). Endothelial atheroprotective and anti-inflammatory mechanisms. *Annals of the New York Academy of Sciences*, *947*, 93–111. https://doi.org/10.1111/j.1749-6632.2001.tb03932.x

Bernstein, B. E., Humphrey, E. L., Erlich, R. L., Schneider, R., Bouman, P., Liu, J. S., Kouzarides, T., & Schreiber, S. L. (2002). Methylation of histone H3 Lys 4 in coding regions of active genes. *Proceedings of the National Academy of Sciences of the United States of America*, *99*(13), 8695–8700. https://doi.org/10.1073/pnas.082249499

Bernstein, B. E., Kamal, M., Lindblad-Toh, K., Bekiranov, S., Bailey, D. K., Huebert, D. J., McMahon, S., Karlsson, E. K., Kulbokas, E. J., Gingeras, T. R., Schreiber, S. L., & Lander, E. S. (2005). Genomic maps and comparative analysis of histone modifications in human and mouse. *Cell*, *120*(2), 169–181. https://doi.org/10.1016/j.cell.2005.01.001

Bernstein, B. E., Meissner, A., & Lander, E. S. (2007). The Mammalian Epigenome. *Cell*, *128*(4), 669–681. https://doi.org/10.1016/j.cell.2007.01.033

Bianco, P., Riminucci, M., Gronthos, S., & Robey, P. G. (2001). Bone Marrow Stromal Stem Cells: Nature, Biology, and Potential Applications. *Stem Cells*, *19*(3), 180–192. https://doi.org/10.1634/stemcells.19-3-180

Blahnik, K. R., Dou, L., O'Geen, H., McPhillips, T., Xu, X., Cao, A. R., Iyengar, S., Nicolet, C. M., Ludäscher, B., Korf, I., & Farnham, P. J. (2009). Sole-Search: An integrated analysis program for peak detection and functional annotation using ChIP-seq data. *Nucleic Acids Research*, *38*(3), 1–17. https://doi.org/10.1093/nar/gkp1012

Bobik, A. (2006). Transforming growth factor-βs and vascular disorders. *Arteriosclerosis, Thrombosis, and Vascular Biology*, *26*(8), 1712–1720. https://doi.org/10.1161/01.ATV.0000225287.20034.2c

Bobik, A., Agrotis, A., Kanellakis, P., Dilley, R., Krushinsky, A., Smirnov, V., Tararak, E., Condron, M., & Kostolias, G. (1999). Distinct patterns of transforming growth factor-β isoform and receptor expression in human atherosclerotic lesions: Colocalization implicates TGF- β in fibrofatty lesion development. *Circulation*, *99*(22), 2883–2891. https://doi.org/10.1161/01.CIR.99.22.2883

Boettger, T., Beetz, N., Kostin, S., Schneider, J., Krüger, M., Hein, L., & Braun, T. (2009). Acquisition of the contractile phenotype by murine arterial smooth muscle cells depends on the Mir143/145 gene cluster. *Journal of Clinical Investigation*, *119*(9), 2634–2647. https://doi.org/10.1172/JCI38864

Boeva, V., Lermine, A., Barette, C., Guillouf, C., & Barillot, E. (2012). Nebula-a web-server for advanced ChIP-seq data analysis. *Bioinformatics*, *28*(19), 2517–2519. https://doi.org/10.1093/bioinformatics/bts463

Bohlander, S. K., Espinosa, R., Le Beau, M. M., Rowley, J. D., & Díaz, M. O. (1992). A method for the rapid sequence-independent amplification of microdissected chromosomal material. *Genomics*, *13*(4), 1322–1324. https://doi.org/10.1016/0888-7543(92)90057-Y

Bornfeldt, K. E., Raines, E. W., Nakano, T., Graves, L. M., Krebs, E. G., & Ross, R. (1994).

Insulin-like growth factor-I and platelet-derived growth factor-BB induce directed migration of human arterial smooth muscle cells via signaling pathways that are distinct from those of proliferation. *Journal of Clinical Investigation*, *93*(3), 1266–1274. https://doi.org/10.1172/JCI117081

Boucher, J. M., Peterson, S. M., Urs, S., Zhang, C., & Liaw, L. (2011). The miR-143/145 cluster is a novel transcriptional target of Jagged-1/Notch signaling in vascular smooth muscle cells. *Journal of Biological Chemistry*, *286*(32), 28312–28321. https://doi.org/10.1074/jbc.M111.221945

Buratowski, S., Kim T.m The role of cotranscriptional histone methylations Cold Spring Harb. Symp. Quant. Biol., 75 (2010), pp. 95-102, 10.1101/sqb.2010.75.036

Bray, S. (1998). Notch signalling in Drosophila: Three ways to use a pathway. *Seminars in Cell and Developmental Biology*, *9*(6), 591–597. https://doi.org/10.1006/scdb.1998.0262

Bray, S. J. (2016). Notch signalling in context. *Nature Reviews Molecular Cell Biology*, *17*(11), 722–735. https://doi.org/10.1038/nrm.2016.94

Brobeil, A., Bobrich, M., Graf, M., Kruchten, A., Blau, W., Rummel, M., Oeschger, S., Steger, K., & Wimmer, M. (2011). PTPIP51 is phosphorylated by Lyn and c-Src kinases lacking dephosphorylation by PTP1B in acute myeloid leukemia. *Leukemia Research*, *35*(10), 1367–1375. https://doi.org/10.1016/j.leukres.2011.03.024

Bruneau, B. G. (2008). The developmental genetics of congenital heart disease. *Nature*, *451*(7181), 943–948. https://doi.org/10.1038/nature06801

Campbell, K. A., Lipinski, M. J., Doran, A. C., Skaflen, M. D., Fuster, V., & McNamara, C. A. (2012). Lymphocytes and the adventitial immune response in atherosclerosis. *Circulation Research*, *110*(6), 889–900. https://doi.org/10.1161/CIRCRESAHA.111.263186

Cano-Rodriguez, D., Gjaltema, R., Jilderda, L. et al. Writing of H3K4Me3 overcomes epigenetic silencing in a sustained but context-dependent manner. Nat Commun 7, 12284 (2016). https://doi.org/10.1038/ncomms12284

Cao, T., Zhang, L., Yao, L. L., Zheng, F., Wang, L., Yang, J. Y., Guo, L. Y., Li, X. Y., Yan, Y. W., Pan, Y. M., Jiang, M., Chen, L., Tang, J. M., Chen, S. Y., & Wang, J. N. (2017). S100B promotes injury-induced vascular remodeling through modulating smooth muscle phenotype. *Biochimica et Biophysica Acta - Molecular Basis of Disease*, *1863*(11), 2772–2782. https://doi.org/10.1016/j.bbadis.2017.07.002

Caplice, N. M., Bunch, T. J., Stalboerger, P. G., Wang, S., Simper, D., Miller, D. V., Russell, S. J., Litzow, M. R., & Edwards, W. D. (2003). Smooth muscle cells in human coronary atherosclerosis can originate from cells administered at marrow transplantation. *Proceedings of the National Academy of Sciences of the United States of America*, *100*(8), 4754–4759. https://doi.org/10.1073/pnas.0730743100

Carthew, R. W., & Sontheimer, E. J. (2009). Origins and Mechanisms of miRNAs and siRNAs. *Cell*, *136*(4), 642–655. https://doi.org/10.1016/j.cell.2009.01.035

Catravas, J. D., Callow, A. D., & Ryan, U. S. (Eds.). (1999). *Vascular endothelium: mechanisms of cell signaling* (Vol. 308). IOS Press.

Cawley, S., Bekiranov, S., Ng, H. H., Kapranov, P., Sekinger, E. A., Kampa, D., Piccolboni, A., Sementchenko, V., Cheng, J., Williams, A. J., Wheeler, R., Wong, B., Drenkow, J., Yamanaka, M., Patel, S., Brubaker, S., Tammana, H., Helt, G., Struhl, K., & Gingeras, T. R. (2004). Unbiased Mapping of Transcription Factor Binding Sites along Human Chromosomes 21 and 22 Points to Widespread Regulation of Noncoding RNAs. *Cell*, *116*(4), 499–509. https://doi.org/10.1016/S0092-8674(04)00127-8

Chamley-Campbell, J., Campbell, G. R., & Ross, R. (1979). The smooth muscle cell in culture. *Physiological reviews*, *59*(1), 1-61. https://doi.org/10.1152/physrev.1979.59.1.1

Chappell, J., Harman, J. L., Narasimhan, V. M., Yu, H., Foote, K., Simons, B. D., Bennett, M. R., & Jørgensen, H. F. (2016). Extensive Proliferation of a Subset of Differentiated, yet Plastic, Medial Vascular Smooth Muscle Cells Contributes to Neointimal Formation in Mouse Injury and Atherosclerosis Models. *Circulation Research*, *119*(12), 1313–1323. https://doi.org/10.1161/CIRCRESAHA.116.309799

Chen C, Yan Y, Liu X. microRNA-612 is downregulated by platelet-derived growth factor-BB treatment and has inhibitory effects on vascular smooth muscle cell proliferation and migration via directly targeting AKT2. Exp Ther Med. 2018 Jan;15(1):159-165. doi: 10.3892/etm.2017.5428. Epub 2017 Nov 1. PMID: 29399059; PMCID: PMC5768077.

Chen, D., Zhang, C., Chen, J., Yang, M., Afzal, T. A., An, W., Maguire, E. M., He, S., Luo, J., Wang, X., Zhao, Y., Wu, Q., & Xiao, Q. (2021). miRNA-200c-3p promotes endothelial to mesenchymal transition and neointimal hyperplasia in artery bypass grafts. *Journal of Pathology*, *253*(2), 209–224. https://doi.org/10.1002/path.5574

Chen, J., Kitchen, C. M., Streb, J. W., & Miano, J. M. (2002). Myocardin: A component of a

molecular switch for smooth muscle differentiation. *Journal of Molecular and Cellular Cardiology*. https://doi.org/10.1016/S0022-2828(02)92086-9

Chen, P. Y., Qin, L., Baeyens, N., Li, G., Afolabi, T., Budatha, M., Tellides, G., Schwartz, M. A., & Simons, M. (2015). Endothelial-to-mesenchymal transition drives atherosclerosis progression. *Journal of Clinical Investigation*, *125*(12), 4514–4528. https://doi.org/10.1172/JCI82719

Chen, Q., Yang, M., Wu, H., Zhou, J., Wang, W., Zhang, H., Zhao, L., Zhu, J., Zhou, B., Xu, Q., & Zhang, L. (2018). Genetic lineage tracing analysis of c-kit+ stem/progenitor cells revealed a contribution to vascular injury-induced neointimal lesions. *Journal of Molecular and Cellular Cardiology*, *121*(July), 277–286. https://doi.org/10.1016/j.yjmcc.2018.07.252

Chen, S., Kulik, M., & Lechleider, R. J. (2003). Smad proteins regulate transcriptional induction of the SM22α gene by TGF-β. *Nucleic Acids Research*, *31*(4), 1302–1310. https://doi.org/10.1093/nar/gkg224

Chen, S., & Lechleider, R. J. (2004). Transforming growth factor-β-induced differentiation of smooth muscle from a neural crest stem cell line. *Circulation Research*, *94*(9), 1195–1202. https://doi.org/10.1161/01.RES.0000126897.41658.81

Chen, Z., Karaplis, A. C., Ackerman, S. L., Pogribny, I. P., Melnyk, S., Lussier-Cacan, S., Chen, M. F., Pai, A., John, S. W. M., Smith, R. S., Bottiglieri, T., Bagley, P., Selhub, J., Rudnicki, M. A., James, S. J., & Rozen, R. (2001). Mice deficient in methylenetetrahydrofolate reductase exhibit hyperhomocysteinemia and decreased methylation capacity, with neuropathology and aortic lipid deposition. *Human Molecular Genetics*, *10*(5), 433–443. https://doi.org/10.1093/hmg/10.5.433

Cheng Y, Liu X, Yang J, Lin Y, Xu D, Lu Q, Deitch EA, Huo Y, Delphin E, Zhang C: MicroRNA-145, a novel smooth muscle cell phenotypic marker and modulator, controls vascular neointimal lesion formation. Circ Res. 2009, 105: 158-166. 10.1161/CIRCRESAHA.109.197517

Cherepanova, O. A., Gomez, D., Shankman, L. S., Swiatlowska, P., Williams, J., Sarmento, O. F., Alencar, G. F., Hess, D. L., Bevard, M. H., Greene, E. S., Murgai, M., Turner, S. D., Geng, Y. J., Bekiranov, S., Connelly, J. J., Tomilin, A., & Owens, G. K. (2016). Activation of the pluripotency factor OCT4 in smooth muscle cells is atheroprotective. *Nature Medicine*, *22*(6), 657–665. https://doi.org/10.1038/nm.4109

Cheung, C., Bernardo, A. S., Pedersen, R. A., & Sinha, S. (2014). Directed differentiation of embryonic origin-specific vascular smooth muscle subtypes from human pluripotent stem cells. *Nature Protocols*, *9*(4), 929–938. https://doi.org/10.1038/nprot.2014.059

Chih, L. L., Kaplan, T., Kim, M., Buratowski, S., Schreiber, S. L., Friedman, N., & Rando, O. J. (2005). Single-nucleosome mapping of histone modifications in S. cerevisiae. *PLoS Biology*, *3*(10). https://doi.org/10.1371/journal.pbio.0030328

Cho, H. J., Cho, H. J., Lee, H. J., Song, M. K., Seo, J. Y., Bae, Y. H., Kim, J. Y., Lee, H. Y., Lee, W., Koo, B. K., Oh, B. H., Park, Y. B., & Kim, H. S. (2013). Vascular Calcifying Progenitor Cells Possess Bidirectional Differentiation Potentials. *PLoS Biology*, *11*(4). https://doi.org/10.1371/journal.pbio.1001534

Choi, K.-D., Yu, J., Smuga-Otto, K., Salvagiotto, G., Rehrauer, W., Vodyanik, M., Thomson, J., & Slukvin, I. (2009). Hematopoietic and Endothelial Differentiation of Human Induced Pluripotent Stem Cells. *Stem Cells*, *27*(3), 559–567. https://doi.org/10.1634/stemcells.2008-0922

Cines, D. B., Pollak, E. S., Buck, C. A., Loscalzo, J., Zimmerman, G. A., McEver, R. P., ... & Stern, D. M. (1998). Endothelial cells in physiology and in the pathophysiology of vascular disorders. *Blood, The Journal of the American Society of Hematology*, *91*(10), 3527-3561. https://doi.org/10.1182/blood.V91.10.3527

Cohn, J. (2001). Arterial compliance to stratify cardiovascular risk: more precision in therapeutic decision making. *American Journal of Hypertension*, *14*(8), S258–S263. https://doi.org/10.1016/s0895-7061(01)02154-9

Clough, E., & Barrett, T. (2016). The gene expression omnibus database. In *Statistical genomics* (pp. 93-110). Humana Press, New York, NY. https://doi.org/10.1007/978-1-4939-3578-9_5

Colazzo, F., Alrashed, F., Saratchandra, P., Carubelli, I., Chester, A. H., Yacoub, M. H., Taylor, P. M., & Somers, P. (2014). Shear stress and VEGF enhance endothelial differentiation of human adipose-derived stem cells. *Growth Factors*, *32*(5), 139–149. https://doi.org/10.3109/08977194.2014.945642

Cooley BC, Nevado J, Mellad J, Yang D, St Hilaire C, Negro A, Fang F, Chen G, San H, Walts AD, Schwartzbeck RL, Taylor B, Lanzer JD, Wragg A, Elagha A, Beltran LE, Berry C, Feil R, Virmani R, Ladich E, Kovacic JC, Boehm M. TGF-β signaling mediates endothelial-to-mesenchymal transition (EndMT) during vein graft remodeling. Sci Transl Med. 2014

Mar 12;6(227):227ra34. doi: 10.1126/scitranslmed.3006927

Cordes, K. R., Sheehy, N. T., White, M. P., Berry, E. C., Morton, S. U., Muth, A. N., Lee, T. H., Miano, J. M., Ivey, K. N., & Srivastava, D. (2009). MiR-145 and miR-143 regulate smooth muscle cell fate and plasticity. *Nature*, *460*(7256), 705–710. https://doi.org/10.1038/nature08195

Corjay, M. H., Thompson, M. M., Lynch, K. R., & Owens, G. K. (1989). Differential effect of platelet-derived growth factor- versus serum-induced growth on smooth muscle α-actin and nonmuscle β-actin mRNA expression in cultured rat aortic smooth muscle cells. *Journal of Biological Chemistry*, *264*(18), 10501–10506. https://doi.org/10.1016/S0021-9258(18)81649-0

Cosgrove, M. S., Boeke, J. D., & Wolberger, C. (2004). Regulated nucleosome mobility and the histone code. *Nature Structural and Molecular Biology*, *11*(11), 1037–1043. https://doi.org/10.1038/nsmb851

Cosma, M. P., Tanaka, T., & Nasmyth, K. (1999). Ordered recruitment of transcription and chromatin remodeling factors to a cell cycle- and developmentally regulated promoter. *Cell*, *97*(3), 299–311. https://doi.org/10.1016/S0092-8674(00)80740-0

Covas, D. T., Panepucci, R. A., Fontes, A. M., Silva, W. A., Orellana, M. D., Freitas, M. C. C., Neder, L., Santos, A. R. D., Peres, L. C., Jamur, M. C., & Zago, M. A. (2008). Multipotent mesenchymal stromal cells obtained from diverse human tissues share functional properties and gene-expression profile with CD146+ perivascular cells and fibroblasts. *Experimental Hematology*, *36*(5), 642–654. https://doi.org/10.1016/j.exphem.2007.12.015

Dalia Ali, Rimi Hamam, Musaed Alfayez, Moustapha Kassem, Abdullah Aldahmash, N. M. A. (2016). *Epigenetic Library Screen Identifies Abexinostat as Novel Regulator of Adipocytic and Osteoblastic Differentiation of Human Skeletal (Mesenchymal) Stem Cells*. 754–763. https://doi.org/10.5966/sctm.2015-0331

Dawlaty, M. M., Breiling, A., Le, T., Barrasa, M. I., Raddatz, G., Gao, Q., Powell, B. E., Cheng, A. W., Faull, K. F., Lyko, F., & Jaenisch, R. (2014). Loss of tet enzymes compromises proper differentiation of embryonic stem cells. *Developmental Cell*, *29*(1), 102–111. https://doi.org/10.1016/j.devcel.2014.03.003

De Backer, G., Ambrosioni, E., Borch-Johnsen, K., Brotons, C., Cifkova, R., Dallongeville, J., Ebrahim, S., Faergeman, O., Graham, I., Mancia, G., Cats, V. M., Orth-Gomér, K., Perk,

J., Pyörälä, K., Rodicio, J. L., Sans, S., Sansoy, V., Sechtem, U., Silber, S., … Wood, D. (2003). European guidelines on cardiovascular disease prevention in clinical practice: Third Joint Task Force of European and other Societies on Cardiovascular Disease Prevention in clinical practice. *European Heart Journal*, *24*(17), 1601–1610. https://doi.org/10.1016/S0195-668X(03)00347-6

Della Vittoria Scarpati, G., Calura, E., Di Marino, M., Romualdi, C., Beltrame, L., Malapelle, U., Troncone, G., De Stefano, A., Pepe, S., De Placido, S., D'Incalci, M., Marchini, S., & Carlomagno, C. (2014). Analysis of differential miRNA expression in primary tumor and stroma of colorectal cancer patients. *BioMed Research International*, *2014*. https://doi.org/10.1155/2014/840921

Deruiter, M. C., Poelmann, R. E., Vanmunsteren, J. C., Mironov, V., Markwald, R. R., & Gittenberger-de Groot, A. C. (1997). Embryonic endothelial cells transdifferentiate into mesenchymal cells expressing smooth muscle alpha actin in vivo and in vitro. *Circulation Research*, *80*(4), 444–451. https://doi.org/10.1161/01.RES.80.4.444

Derynck, R., & Zhang, Y. E. (2003). *Smad-dependent and Smad-independent pathways in TGF-*. *4*. https://doi.org/10.1038/nature02006

Di Luca, M., Fitzpatrick, E., Burtenshaw, D., Liu, W., Helt, J. C., Hakimjavadi, R., Corcoran, E., Gusti, Y., Sheridan, D., Harman, S., Lally, C., Redmond, E. M., & Cahill, P. A. (2021). The calcium binding protein S100β marks hedgehog-responsive resident vascular stem cells within vascular lesions. *Npj Regenerative Medicine*, *6*(1), 1–15. https://doi.org/10.1038/s41536-021-00120-8

Dobnikar, L., Taylor, A. L., Chappell, J., Oldach, P., Harman, J. L., Oerton, E., Dzierzak, E., Bennett, M. R., Spivakov, M., & Jørgensen, H. F. (2018). Disease-relevant transcriptional signatures identified in individual smooth muscle cells from healthy mouse vessels. *Nature Communications*, *9*(1). https://doi.org/10.1038/s41467-018-06891-x

Doi, H., Iso, T., Sato, H., Yamazaki, M., Matsui, H., Tanaka, T., Manabe, I., Arai, M., Nagai, R., & Kurabayashi, M. (2006). Jagged1-selective notch signaling induces smooth muscle differentiation via a RBP-Jκ-dependent pathway. *Journal of Biological Chemistry*, *281*(39), 28555–28564. https://doi.org/10.1074/jbc.M602749200

Dominici, M., Le Blanc, K., Mueller, I., Slaper-Cortenbach, I., Marini, F. C., Krause, D. S., Deans, R. J., Keating, A., Prockop, D. J., & Horwitz, E. M. (2006). Minimal criteria for defining multipotent mesenchymal stromal cells. The International Society for Cellular

Therapy position statement. *Cytotherapy*, *8*(4), 315–317. https://doi.org/10.1080/14653240600855905

Dong, H. K., Keon, H. Y., Kyung, S. C., Choi, J., Choi, S. Y., Yang, S. E., Yang, Y. S., Ho, J. I., Kye, H. K., Hye, L. J., Ki, W. S., & Hong, H. K. (2005). Gene expression profile of cytokine and growth factor during differentiation of bone marrow-derived mesenchymal stem cell. *Cytokine*, *31*(2), 119–126. https://doi.org/10.1016/j.cyto.2005.04.004

Driessens, G., Beck, B., Caauwe, A., Simons, B. D., & Blanpain, C. (2012). Defining the mode of tumour growth by clonal analysis. *Nature*, *488*(7412), 527–530. https://doi.org/10.1038/nature11344

Du, K. L., Ip, H. S., Li, J., Chen, M., Dandre, F., Yu, W., Lu, M. M., Owens, G. K., & Parmacek, M. S. (2003). Myocardin Is a Critical Serum Response Factor Cofactor in the Transcriptional Program Regulating Smooth Muscle Cell Differentiation. *Molecular and Cellular Biology*, *23*(7), 2425–2437. https://doi.org/10.1128/mcb.23.7.2425-2437.2003

Duan, L., Liu, C., Hu, J., Liu, Y., Wang, J., Chen, G., Li, Z., & Chen, H. (2017). *Epigenetic mechanisms in coronary artery disease: The current state and prospects*. https://doi.org/10.1016/j.tcm.2017.12.012

Duggan, D. J., Bittner, M., Chen, Y., Meitzer, P., & Trent, J. M. (1999). Expression profiling using cdna microarrays. *Nature Genetics*, *21*(1S), 14. https://doi.org/10.1038/4434

Dulak, J., Szade, K., Szade, A., Nowak, W., & Józkowicz, A. (2015). Adult stem cells: Hopes and hypes of regenerative medicine. *Acta Biochimica Polonica*, *62*(3), 329–337. https://doi.org/10.18388/abp.2015_1023

Dunn, J., Simmons, R., Thabet, S., & Jo, H. (2015). The role of epigenetics in the endothelial cell shear stress response and atherosclerosis. *International Journal of Biochemistry and Cell Biology*, *67*, 167–176. https://doi.org/10.1016/j.biocel.2015.05.001

El Agha E, Kramann R, Schneider RK, Li X, Seeger W, Humphreys BD, Bellusci S. Mesenchymal stem cells in fibrotic disease. Cell Stem Cell 2017;21:166–177.

Espinosa-Diez C, Mandi V, Du M, Liu M, Gomez D. Smooth muscle cells in atherosclerosis: clones but not carbon copies. JVS Vasc Sci. 2021 May 15;2:136-148. doi: 10.1016/j.jvssci.2021.02.002. PMID: 34617064; PMCID: PMC8489213.

Farooq, V., Gogas, B. D., & Serruys, P. W. (2011). Restenosis: Delineating the numerous causes of drug-eluting stent restenosis. *Circulation: Cardiovascular Interventions*, *4*(2), 195–205. https://doi.org/10.1161/CIRCINTERVENTIONS.110.959882

Feil, S., Fehrenbacher, B., Lukowski, R., Essmann, F., Schulze-Osthoff, K., Schaller, M., & Feil, R. (2014). Transdifferentiation of vascular smooth muscle cells to macrophage-like cells during atherogenesis. *Circulation Research*, *115*(7), 662–667. https://doi.org/10.1161/CIRCRESAHA.115.304634

Feng, J. Q., Ward, L. M., Liu, S., Lu, Y., Xie, Y., Yuan, B., Yu, X., Rauch, F., Davis, S. I., Zhang, S., Rios, H., Drezner, M. K., Quarles, L. D., Bonewald, L. F., & White, K. E. (2006). Loss of DMP1 causes rickets and osteomalacia and identifies a role for osteocytes in mineral metabolism. *Nature Genetics*, *38*(11), 1310–1315. https://doi.org/10.1038/ng1905

Ficz, G., Branco, M. R., Seisenberger, S., Santos, F., Krueger, F., Hore, T. A., Marques, C. J., Andrews, S., & Reik, W. (2011). Dynamic regulation of 5-hydroxymethylcytosine in mouse ES cells and during differentiation. *Nature*, *473*(7347), 398–404. https://doi.org/10.1038/nature10008

Fishbein, G. A., & Fishbein, M. C. (2009). Rethinking the Current Classification. *Arch Pathol Lab Med.*, *133*, 1309–1316.

Floris I, Descamps B, Vardeu A, Mitic T, Posadino AM, Shantikumar S, et al. Gestational diabetes mellitus impairs fetal endothelial cell functions through a mechanism involving microrna-101 and histone methyltransferase enhancer of zester homolog-2. Arterioscler Thromb Vasc Biol. 2015;35(3):664–674. doi: 10.1161/ATVBAHA.114.304730

Francis, N. J., Kingston, R. E., & Woodcock, C. L. (2004). Chromatin compaction by a polycomb group protein complex. *Science*, *306*(5701), 1574–1577. https://doi.org/10.1126/science.1100576

Fredriksson, S., Gullberg, M., Jarvius, J., Olsson, C., Pietras, K., Gústafsdóttir, S. M., Östman, A., & Landegren, U. (2002). Protein detection using proximity-dependent DNA Ligation Assays. *Nature Biotechnology*, *20*(May), 473–477. https://www.wakopyrostar.com/blog/post/the-detection-of-endotoxins-via-the-lal-test-the-chromogenic-method/

Frid, M. G., Kale, V. A., & Stenmark, K. R. (2002). Mature vascular endothelium can give rise to smooth muscle cells via endothelial-mesenchymal transdifferentiation: In vitro analysis. *Circulation Research*, *90*(11), 1189–1196. https://doi.org/10.1161/01.RES.0000021432.70309.28

Frostegård, J., Ulfgren, A. K., Nyberg, P., Hedin, U., Swedenborg, J., Andersson, U., &

Hansson, G. K. (1999). Cytokine expression in advanced human atherosclerotic plaques: Dominance of pro-inflammatory (Th1) and macrophage-stimulating cytokines. *Atherosclerosis*, *145*(1), 33–43. https://doi.org/10.1016/S0021-9150(99)00011-8

Fujiki, K., Shinoda, A., Kano, F., Sato, R., Shirahige, K., & Murata, M. (2013). PPARγ-induced PARylation promotes local DNA demethylation by production of 5-hydroxymethylcytosine. *Nature Communications*, *4*. https://doi.org/10.1038/ncomms3262

Fukagawa T, Nogami M, Yoshikawa M, Ikeno M, Okazaki T, Takami Y, Nakayama T, Oshimura M 2004 Dicer is essential for formation of the heterochromatin structure in vertebrate cells. Nat Cell Biol 6: 784–791

Galkina, E., Kadl, A., Sanders, J., Varughese, D., Sarembock, I. J., & Ley, K. (2006). Lymphocyte recruitment into the aortic wall before and during development of atherosclerosis is partially L-selectin dependent. *Journal of Experimental Medicine*, *203*(5), 1273–1282. https://doi.org/10.1084/jem.20052205

Gan, Q., Thiébaud, P., Thézé, N., Jin, L., Xu, G., Grant, P., & Owens, G. K. (2011). WD repeat-containing protein 5, a ubiquitously expressed histone methyltransferase adaptor protein, regulates smooth muscle cell-selective gene activation through interaction with pituitary homeobox 2. *Journal of Biological Chemistry*, *286*(24), 21853-21864. DOI:https://doi.org/10.1074/jbc.M111.233098

Gates LA, Foulds CE, O'Malley BW. Histone Marks in the 'Driver's Seat': Functional Roles in Steering the Transcription Cycle. Trends Biochem Sci. 2017 Dec;42(12):977-989. doi: 10.1016/j.tibs.2017.10.004. Epub 2017 Nov 6. PMID: 29122461; PMCID: PMC5701853.

Gazave, E., Lapébie, P., Richards, G. S., Brunet, F., Ereskovsky, A. V., Degnan, B. M., Borchiellini, C., Vervoort, M., & Renard, E. (2009). Origin and evolution of the Notch signalling pathway: An overview from eukaryotic genomes. *BMC Evolutionary Biology*, *9*(1), 1–27. https://doi.org/10.1186/1471-2148-9-249

Gerton, J. L., DeRisi, J., Shroff, R., Lichten, M., Brown, P. O., & Petes, T. D. (2000). Global mapping of meiotic recombination hotspots and coldspots in the yeast Saccharomyces cerevisiae. *Proceedings of the National Academy of Sciences of the United States of America*, *97*(21), 11383–11390. https://doi.org/10.1073/pnas.97.21.11383

Gertz, J., Savic, D., Varley, K. E., Partridge, E. C., Safi, A., Jain, P., Cooper, G. M., Reddy, T. E., Crawford, G. E., & Myers, R. M. (2013). Distinct properties of cell-type-specific and

shared transcription factor binding sites. *Molecular Cell*, *52*(1), 25–36. https://doi.org/10.1016/j.molcel.2013.08.037

Giangreco, A., Arwert, E. N., Rosewell, I. R., Snyder, J., Watt, F. M., & Stripp, B. R. (2009). Stem cells are dispensable for lung homeostasis but restore airways after injury. *Proceedings of the National Academy of Sciences of the United States of America*, *106*(23), 9286–9291. https://doi.org/10.1073/pnas.0900668106

Gimbrone, M. A., Topper, J. N., Nagel, T., Anderson, K. R., & Garcia-Cardeña, G. (2000). Endothelial dysfunction, hemodynamic forces, and atherogenesis. *Annals of the New York Academy of Sciences*, *902*, 230–240. https://doi.org/10.1111/j.1749-6632.2000.tb06318.x

Glemžaite, M., & Navakauskiene, R. (2016). Osteogenic Differentiation of Human Amniotic Fluid Mesenchymal Stem Cells Is Determined by Epigenetic Changes. *Stem Cells International*, *2016*. https://doi.org/10.1155/2016/6465307

Gomez, D., & Owens, G. K. (2012). Smooth muscle cell phenotypic switching in atherosclerosis. *Cardiovascular Research*, *95*(2), 156–164. https://doi.org/10.1093/cvr/cvs115

Gomez, D., Shankman, L. S., Nguyen, A. T., & Owens, G. K. (2013). Detection of histone modifications at specific gene loci in single cells in histological sections. *Nature methods*, *10*(2), 171. https://doi.org/10.1038/NMETH.2332

Gomez, D., Swiatlowska, P., & Owens, G. K. (2015). Epigenetic Control of Smooth Muscle Cell Identity and Lineage Memory. *Arteriosclerosis, Thrombosis, and Vascular Biology*, *35*(12), 2508–2516. https://doi.org/10.1161/ATVBAHA.115.305044

Gräbner, R., Lötzer, K., Döpping, S., Hildner, M., Radke, D., Beer, M., Spanbroek, R., Lippert, B., Reardon, C. A., Getz, G. S., Fu, Y. X., Hehlgans, T., Mebius, R. E., Van Wall, M. Der, Kruspe, D., Englert, C., Lovas, A., Hu, D., Randolph, G. J., … Habenicht, A. J. R. (2009). Lymphotoxin β receptor signaling promotes tertiary lymphoid organogenesis in the aorta adventitia of aged ApoE -/- mice. *Journal of Experimental Medicine*, *206*(1), 233–248. https://doi.org/10.1084/jem.20080752

Grosselin K, Durand A, Marsolier J, Poitou A, Marangoni E, Nemati F, et al. High-throughput single-cell ChIP-seq identifies heterogeneity of chromatin states in breast cancer. Nat Genet. 2019;51(6):1060–6. https://doi.org/10.1038/s41588-019-0424-9

Gullberg, M., Gústafsdóttir, S. M., Schallmeiner, E., Jarvius, J., Bjarnegård, M., Betsholtz, C.,

Landegren, U., & Fredriksson, S. (2004). Cytokine detection by antibody-based proximity ligation. *Proceedings of the National Academy of Sciences of the United States of America*, *101*(22), 8420–8424. https://doi.org/10.1073/pnas.0400552101

Guo, X. (2012). Transforming growth factor-β and smooth muscle differentiation. *World Journal of Biological Chemistry*, *3*(3), 41. https://doi.org/10.4331/wjbc.v3.i3.41

Guzik, T. J., Hoch, N. E., Brown, K. A., McCann, L. A., Rahman, A., Dikalov, S., Goronzy, J., Weyand, C., & Harrison, D. G. (2007). Role of the T cell in the genesis of angiotensin II-induced hypertension and vascular dysfunction. *Journal of Experimental Medicine*, *204*(10), 2449–2460. https://doi.org/10.1084/jem.20070657

Handy, D. E., Castro, R., & Loscalzo, J. (2011). Epigenetic modifications: Basic mechanisms and role in cardiovascular disease. *Circulation*, *123*(19), 2145–2156. https://doi.org/10.1161/CIRCULATIONAHA.110.956839

Hao, H., Gabbiani, G., & Bochaton-Piallat, M. L. (2003). Arterial smooth muscle cell heterogeneity: Implications for atherosclerosis and restenosis development. *Arteriosclerosis, Thrombosis, and Vascular Biology*, *23*(9), 1510–1520. https://doi.org/10.1161/01.ATV.0000090130.85752.ED

Hattori, N., Nishino, K., Ko, Y. G., Hattori, N., Ohgane, J., Tanaka, S., & Shiota, K. (2004). Epigenetic Control of Mouse Oct-4 Gene Expression in Embryonic Stem Cells and Trophoblast Stem Cells. *Journal of Biological Chemistry*, *279*(17), 17063–17069. https://doi.org/10.1074/jbc.M309002200

He S, Yang F, Yang M, An W, Maguire EM, Chen Q, Xiao R, Wu W, Zhang L, Wang W, Xiao Q. miR-214-3p-Sufu-GLI1 is a novel regulatory axis controlling inflammatory smooth muscle cell differentiation from stem cells and neointimal hyperplasia. Stem Cell Res Ther. 2020 Nov 3;11(1):465. doi: 10.1186/s13287-020-01989-w. PMID: 33143723; PMCID: PMC7640405.

He L, Hannon GJ 2004 MicroRNAs: small RNAs with a big role in gene regulation. Nat Rev Genet 5: 522–531

Heintzman, N. D., Hon, G. C., Hawkins, R. D., Kheradpour, P., Stark, A., Harp, L. F., Ye, Z., Lee, L. K., Stuart, R. K., Ching, C. W., Ching, K. A., Antosiewicz-Bourget, J. E., Liu, H., Zhang, X., Green, R. D., Lobanenkov, V. V., Stewart, R., Thomson, J. A., Crawford, G. E., … Ren, B. (2009). Histone modifications at human enhancers reflect global cell-type-specific gene expression. *Nature*, *459*(7243), 108–112. https://doi.org/10.1038/nature07829

Heintzman, N. D., Stuart, R. K., Hon, G., Fu, Y., Ching, C. W., Hawkins, R. D., Barrera, L. O., Van Calcar, S., Qu, C., Ching, K. A., Wang, W., Weng, Z., Green, R. D., Crawford, G. E., & Ren, B. (2007). Distinct and predictive chromatin signatures of transcriptional promoters and enhancers in the human genome. *Nature Genetics*, *39*(3), 311–318. https://doi.org/10.1038/ng1966

Heinz, S., Benner, C., Spann, N., Bertolino, E., Lin, Y. C., Laslo, P., Cheng, J. X., Murre, C., Singh, H., & Glass, C. K. (2010). Simple Combinations of Lineage-Determining Transcription Factors Prime cis-Regulatory Elements Required for Macrophage and B Cell Identities. *Molecular Cell*, *38*(4), 576–589. https://doi.org/10.1016/j.molcel.2010.05.004

Hellström, M., Kalén, M., Lindahl, P., Abramsson, A., & Betsholtz, C. (1999). Role of PDGF-B and PDGFR-β in recruitment of vascular smooth muscle cells and pericytes during embryonic blood vessel formation in the mouse. *Development*, *126*(14), 3047–3055. https://doi.org/10.1242/dev.126.14.3047

Hemming, S., Cakouros, D., Isenmann, S., Cooper, L., Menicanin, D., Zannettino, A., & Gronthos, S. (2014). EZH2 and KDM6A act as an epigenetic switch to regulate mesenchymal stem cell lineage-specification. *Stem cells*, *32*(3), 802-815. https://doi.org/10.1002/stem.1573

Hempleman, S. C., & Warburton, S. J. (2013). Comparative Embryology of the Carotid Body. *Respiratory Physiology and Neurobiology*, *185*(1), 3–8. https://doi.org/10.1016/j.resp.2012.08.004

Herring, B. P., Hoggatt, A. M., Burlak, C., & Offermanns, S. (2014). Previously differentiated medial vascular smooth muscle cells contribute to neointima formation following vascular injury. *Vascular Cell*, *6*(1). https://doi.org/10.1186/2045-824X-6-21

High, F. A., Zhang, M., Proweller, A., Tu, L. L., Parmacek, M. S., Pear, W. S., & Epstein, J. A. (2007). An essential role for Notch in neural crest during cardiovascular development and smooth muscle differentiation. *Journal of Clinical Investigation*, *117*(2), 353–363. https://doi.org/10.1172/JCI30070

Hillier, L. D. W., Marth, G. T., Quinlan, A. R., Dooling, D., Fewell, G., Barnett, D., Fox, P., Glasscock, J. I., Hickenbotham, M., Huang, W., Magrini, V. J., Richt, R. J., Sander, S. N., Stewart, D. A., Stromberg, M., Tsung, E. F., Wylie, T., Schedl, T., Wilson, R. K., & Mardis, E. R. (2008). Whole-genome sequencing and variant discovery in C. elegans. *Nature*

Methods, *5*(2), 183–188. https://doi.org/10.1038/nmeth.1179

Hinck, A. P. (2012). Structural studies of the TGF-βs and their receptors - Insights into evolution of the TGF-β superfamily. *FEBS Letters*, *586*(14), 1860–1870. https://doi.org/10.1016/j.febslet.2012.05.028

Hinck, A. P., & Huang, T. (2013). TGF-β antagonists: Same knot, but different hold. *Structure*, *21*(8), 1269–1270. https://doi.org/10.1016/j.str.2013.07.015

Hirschi, K. K., Lai, L., Belaguli, N. S., Dean, D. A., Schwartz, R. J., & Zimmer, W. E. (2002). Transforming growth factor-β induction of smooth muscle cell phenotype requires transcriptional and post-transcriptional control of serum response factor. *Journal of Biological Chemistry*, *277*(8), 6287–6295. https://doi.org/10.1074/jbc.M106649200

Hoeksema, M. A., Gijbels, M. J., Van den Bossche, J., Velden, S., Sijm, A., Neele, A. E., Seijkens, T., Stöger, J. L., Meiler, S., Boshuizen, M. C., Dallinga-Thie, G. M., Levels, J. H., Boon, L., Mullican, S. E., Spann, N. J., Cleutjens, J. P., Glass, C. K., Lazar, M. A., Vries, C. J., … Winther, M. P. (2014). Targeting macrophage Histone deacetylase 3 stabilizes atherosclerotic lesions. *EMBO Molecular Medicine*, *6*(9), 1124–1132. https://doi.org/10.15252/emmm.201404170

Holmes C, Stanford WL. Concise review: stem cell antigen-1: expression, function, and enigma. Stem Cells. 2007 Jun;25(6):1339-47. doi: 10.1634/stemcells.2006-0644. Epub 2007 Mar 22. PMID: 17379763.

Hong, X., Margariti, A., Le Bras, A., Jacquet, L., Kong, W., Hu, Y., & Xu, Q. (2017). Transdifferentiated human vascular smooth muscle cells are a new potential cell source for endothelial regeneration. *Scientific reports*, *7*(1), 1-17. DOI:10.1038/s41598-017-05665-7

Hoofnagle, M. H., Thomas, J. A., Wamhoff, B. R., & Owens, G. K. (2006). Origin of neointimal smooth muscle: We've come full circle. *Arteriosclerosis, Thrombosis, and Vascular Biology*, *26*(12), 2579–2581. https://doi.org/10.1161/01.ATV.0000249623.79871.bc

Hu, B., Wu, Z., & Phan, S. H. (2003). Smad3 mediates transforming growth factor-β-induced α-smooth muscle actin expression. *American Journal of Respiratory Cell and Molecular Biology*, *29*(3 I), 397–404. https://doi.org/10.1165/rcmb.2003-0063OC

Hu, Y., Zhang, Z., Torsney, E., Afzal, A. R., Davison, F., Metzler, B., & Xu, Q. (2004). Abundant progenitor cells in the adventitia contribute to atherosclerosis of vein grafts in ApoE-deficient mice. *Journal of Clinical Investigation*, *113*(9), 1258–1265.

https://doi.org/10.1172/JCI19628

Huang, H., Song, T. J., Li, X., Hu, L., He, Q., Liu, M., Lane, M. D., & Tang, Q. Q. (2009). BMP signaling pathway is required for commitment of C3H10T1/2 pluripotent stem cells to the adipocyte lineage. *Proceedings of the National Academy of Sciences of the United States of America*, *106*(31), 12670–12675. https://doi.org/10.1073/pnas.0906266106

Huang, J., Cheng, L., Li, J., Chen, M., Zhou, D., Min, M. L., Proweller, A., Epstein, J. A., & Parmacek, M. S. (2008). Myocardin regulates expression of contractile genes in smooth muscle cells and is required for closure of the ductus arteriosus in mice. *Journal of Clinical Investigation*, *118*(2), 515–525. https://doi.org/10.1172/JCI33304

Huang, S. X. L., Islam, M. N., O'Neill, J., Hu, Z., Yang, Y. G., Chen, Y. W., Mumau, M., Green, M. D., Vunjak-Novakovic, G., Bhattacharya, J., & Snoeck, H. W. (2014). Efficient generation of lung and airway epithelial cells from human pluripotent stem cells. *Nature Biotechnology*, *32*(1), 84–91. https://doi.org/10.1038/nbt.2754

Huang, Z., Nelson, E. R., Smith, R. L., & Goodman, S. B. (2007). The sequential expression profiles of growth factors from osteroprogenitors to osteoblasts in vitro. *Tissue engineering*, *13*(9), 2311-2320. https://doi.org/10.1089/ten.2006.0423

Hughes AL, Kelley JR, Klose RJ. Understanding the interplay between CpG island-associated gene promoters and H3K4 methylation. Biochim Biophys Acta Gene Regul Mech. 2020 Aug;1863(8):194567. doi: 10.1016/j.bbagrm.2020.194567. Epub 2020 Apr 29. PMID: 32360393; PMCID: PMC7294231.

Humphrey, J. D. (2008). Mechanisms of arterial remodeling in hypertension coupled roles of wall shear and intramural stress. *Hypertension*, *52*(2), 195–200. https://doi.org/10.1161/HYPERTENSIONAHA.107.103440

Ihrie, R. A., & Alvarez-Buylla, A. (2008). Cells in the astroglial lineage are neural stem cells. *Cell and Tissue Research*, *331*(1), 179–191. https://doi.org/10.1007/s00441-007-0461-z

Impey, S., McCorkle, S. R., Cha-Molstad, H., Dwyer, J. M., Yochum, G. S., Boss, J. M., McWeeney, S., Dunn, J. J., Mandel, G., & Goodman, R. H. (2004). Defining the CREB regulon: A genome-wide analysis of transcription factor regulatory regions. *Cell*, *119*(7), 1041–1054. https://doi.org/10.1016/j.cell.2004.10.032

Indolfi, C., Mongiardo, A., Curcio, A., & Torella, D. (2003). Molecular mechanisms of in-stent restenosis and approach to therapy with eluting stents. *Trends in Cardiovascular Medicine*, *13*(4), 142–148. https://doi.org/10.1016/S1050-1738(03)00038-0

Iso, T., Kedes, L., & Hamamori, Y. (2003). HES and HERP families: Multiple effectors of the Notch signaling pathway. *Journal of Cellular Physiology*, *194*(3), 237–255. https://doi.org/10.1002/jcp.10208

Ito, S., Dalessio, A. C., Taranova, O. V., Hong, K., Sowers, L. C., & Zhang, Y. (2010). Role of tet proteins in 5mC to 5hmC conversion, ES-cell self-renewal and inner cell mass specification. *Nature*, *466*(7310), 1129–1133. https://doi.org/10.1038/nature09303

Iwata, H., Manabe, I., Fujiu, K., Yamamoto, T., Takeda, N., Eguchi, K., Furuya, A., Kuro-O, M., Sata, M., & Nagai, R. (2010). Bone marrow-derived cells contribute to vascular inflammation but do not differentiate into smooth muscle cell lineages. *Circulation*, *122*(20), 2048–2057. https://doi.org/10.1161/CIRCULATIONAHA.110.965202

Iyer, V. R., Horak, C. E., Scafe, C. S., Botstein, D., Snyder, M., & Brown, P. O. (2001). Genomic binding sites of the yeast cell-cycle transcription factors SBF and MBF. *Nature*, *409*(6819), 533–538. https://doi.org/10.1038/35054095

Jafar-Nejad, H., Leonardi, J., & Fernandez-Valdivia, R. (2010). Role of glycans and glycosyltransferases in the regulation of Notch signaling. *Glycobiology*, *20*(8), 931–949. https://doi.org/10.1093/glycob/cwq053

Jambhekar, A., Dhall, A., & Shi, Y. (2019). Roles and regulation of histone methylation in animal development. *Nature Reviews Molecular Cell Biology*, *20*(10), 625–641. https://doi.org/10.1038/s41580-019-0151-1

Johnson, C. P., Baugh, R., Wilson, C. A., & Burns, J. (2001). Age related changes in the tunica media of the vertebral artery: Implications for the assessment of vessels injured by trauma. *Journal of Clinical Pathology*, *54*(2), 139–145. https://doi.org/10.1136/jcp.54.2.139

Johnson, D. S., Li, W., Gordon, D. B., Bhattacharjee, A., Curry, B., Ghosh, J., Brizuela, L., Carroll, J. S., Brown, M., Flicek, P., Koch, C. M., Dunham, I., Bieda, M., Xu, X., Farnham, P. J., Kapranov, P., Nix, D. A., Gingeras, T. R., Zhang, X., … Liu, X. S. (2008). Systematic evaluation of variability in ChIP-chip experiments using predefined DNA targets. *Genome Research*, *18*(3), 393–403. https://doi.org/10.1101/gr.7080508

Johnson, D. S., Mortazavi, A., Myers, R. M., & Wold, B. (2007). Genome-wide mapping of in vivo protein-DNA interactions. *Science*, *316*(5830), 1497-1502 DOI: 10.1126/science.1141319

Jonasson, L., Holm, J., Skalli, O., Bondjers, G., & Hansson, G. K. (1986). Regional

accumulations of T cells, macrophages, and smooth muscle cells in the human atherosclerotic plaque. *Arteriosclerosis*, *6*(2), 131–138. https://doi.org/10.1161/01.atv.6.2.131

Kanki, Y., Nakaki, R., Shimamura, T., Matsunaga, T., Yamamizu, K., Katayama, S., Suehiro, J. I., Osawa, T., Aburatani, H., Kodama, T., Wada, Y., Yamashita, J. K., & Minami, T. (2017). Dynamically and epigenetically coordinated GATA/ETS/SOX transcription factor expression is indispensable for endothelial cell differentiation. *Nucleic Acids Research*, *45*(8), 4344–4358. https://doi.org/10.1093/nar/gkx159

Kaplan-Albuquerque, N., Van Putten, V., Weiser-Evans, M. C., & Nemenoff, R. A. (2005). Depletion of serum response factor by RNA interference mimics the mitogenic effects of platelet-derived growth factor-BB in vascular smooth muscle cells. *Circulation Research*, *97*(5), 427–433. https://doi.org/10.1161/01.RES.0000179776.40216.a9

Kapustin, A. N., Chatrou, M. L. L., Drozdov, I., Zheng, Y., Davidson, S. M., Soong, D., Furmanik, M., Sanchis, P., De Rosales, R. T. M., Alvarez-Hernandez, D., Shroff, R., Yin, X., Muller, K., Skepper, J. N., Mayr, M., Reutelingsperger, C. P., Chester, A., Bertazzo, S., Schurgers, L. J., & Shanahan, C. M. (2015). Vascular smooth muscle cell calcification is mediated by regulated exosome secretion. *Circulation Research*, *116*(8), 1312–1323. https://doi.org/10.1161/CIRCRESAHA.116.305012

Kapustin, A. N., Davies, J. D., Reynolds, J. L., McNair, R., Jones, G. T., Sidibe, A., Schurgers, L. J., Skepper, J. N., Proudfoot, D., Mayr, M., & Shanahan, C. M. (2011). Calcium regulates key components of vascular smooth muscle cell-derived matrix vesicles to enhance mineralization. *Circulation Research*, *109*(1). https://doi.org/10.1161/CIRCRESAHA.110.238808

Kaya-Okur, H. S., Janssens, D. H., Henikoff, J. G., Ahmad, K., & Henikoff, S. (2020). Efficient low-cost chromatin profiling with CUT&Tag. *Nature Protocols*, *15*(10), 3264–3283. https://doi.org/10.1038/s41596-020-0373-x

Kaya-Okur, H. S., Wu, S. J., Codomo, C. A., Pledger, E. S., Bryson, T. D., Henikoff, J. G., Ahmad, K., & Henikoff, S. (2019). CUT&Tag for efficient epigenomic profiling of small samples and single cells. *Nature Communications*, *10*(1), 1–10. https://doi.org/10.1038/s41467-019-09982-5

Kennedy, E., Hakimjavadi, R., Greene, C., Mooney, C. J., Fitzpatrick, E., Collins, L. E., Loscher, C. E., Guha, S., Morrow, D., Redmond, E. M., & Cahill, P. A. (2014). Embryonic rat

vascular smooth muscle cells revisited - A model for neonatal, neointimal SMC or differentiated vascular stem cells? *Vascular Cell*, *6*(1). https://doi.org/10.1186/2045-824X-6-6

Kennedy, E., Mooney, C. J., Hakimjavadi, R., Fitzpatrick, E., Guha, S., Collins, L. E., Loscher, C. E., Morrow, D., Redmond, E. M., & Cahill, P. A. (2014). Adult vascular smooth muscle cells in culture express neural stem cell markers typical of resident multipotent vascular stem cells. *Cell and Tissue Research*, *358*(1), 203–216. https://doi.org/10.1007/s00441-014-1937-2

Khan, R., Agrotis, A., & Bobik, A. (2007). Understanding the role of transforming growth factor-β1 in intimal thickening after vascular injury. *Cardiovascular Research*, *74*(2), 223–234. https://doi.org/10.1016/j.cardiores.2007.02.012

Kim, H. J., Yi, S. W., Oh, H. J., Lee, J. S., Park, J. S., & Park, K. H. (2018). Transfection of gene regulation nanoparticles complexed with pDNA and shRNA controls multilineage differentiation of hMSCs. *Biomaterials*, *177*, 1–13. https://doi.org/10.1016/j.biomaterials.2018.05.035

Kim, K., Doi, A., Wen, B., Ng, K., Zhao, R., Cahan, P., Kim, J., Aryee, M. J., Ji, H., Ehrlich, L. I. R., Yabuuchi, A., Takeuchi, A., Cunniff, K. C., Hongguang, H., McKinney-Freeman, S., Naveiras, O., Yoon, T. J., Irizarry, R. A., Jung, N., … Daley, G. Q. (2010). Epigenetic memory in induced pluripotent stem cells. *Nature*, *467*(7313), 285–290. https://doi.org/10.1038/nature09342

Kim, K., Zhao, R., Doi, A., Ng, K., Unternaehrer, J., Cahan, P., Hongguang, H., Loh, Y. H., Aryee, M. J., Lensch, M. W., Li, H., Collins, J. J., Feinberg, A. P., & Daley, G. Q. (2011). Donor cell type can influence the epigenome and differentiation potential of human induced pluripotent stem cells. *Nature Biotechnology*, *29*(12), 1117–1119. https://doi.org/10.1038/nbt.2052

Kim, S., Ip, H. S., Lu, M. M., Clendenin, C., & Parmacek, M. S. (1997). A serum response factor-dependent transcriptional regulatory program identifies distinct smooth muscle cell sublineages. *Molecular and Cellular Biology*, *17*(4), 2266–2278. https://doi.org/10.1128/mcb.17.4.2266

Kim, T. H., Barrera, L. O., Zheng, M., Qu, C., Singer, M. A., Richmond, T. A., Wu, Y., Green, R. D., & Ren, B. (2005). A high-resolution map of active promoters in the human genome. *Nature*, *436*(7052), 876–880. https://doi.org/10.1038/nature03877

Kim van Kuijk, Christoph Kuppe, Christer Betsholtz, Michael Vanlandewijck, Rafael Kramann, Judith C Sluimer, Heterogeneity and plasticity in healthy and atherosclerotic vasculature explored by single-cell sequencing, Cardiovascular Research, Volume 115, Issue 12, 1 October 2019, Pages 1705–1715, https://doi.org/10.1093/cvr/cvz185

Kimura, H., Tada, M., Nakatsuji, N., & Tada, T. (2004). Histone Code Modifications on Pluripotential Nuclei of Reprogrammed Somatic Cells. *Molecular and Cellular Biology*, *24*(13), 5710–5720. https://doi.org/10.1128/mcb.24.13.5710-5720.2004

Ko, M., Huang, Y., Jankowska, A. M., Pape, U. J., Tahiliani, M., Bandukwala, H. S., An, J., Lamperti, E. D., Koh, K. P., Ganetzky, R., Liu, X. S., Aravind, L., Agarwal, S., MacIejewski, J. P., & Rao, A. (2010). Impaired hydroxylation of 5-methylcytosine in myeloid cancers with mutant TET2. *Nature*, *468*(7325), 839–843. https://doi.org/10.1038/nature09586

Koch, F., & Andrau, J. C. (2011). Initiating RNA polymerase II and TIPs as hallmarks of enhancer activity and tissue-specificity. *Transcription*, *2*(6), 263–268. https://doi.org/10.4161/trns.2.6.18747

Kockx, M. M. (2013). *Spontaneous and induced intima formation in blood vessels*. Springer Science & Business Media.

Koh, K. P., Yabuuchi, A., Rao, S., Huang, Y., Cunniff, K., Nardone, J., Laiho, A., Tahiliani, M., Sommer, C. A., Mostoslavsky, G., Lahesmaa, R., Orkin, S. H., Rodig, S. J., Daley, G. Q., & Rao, A. (2011). Tet1 and Tet2 regulate 5-hydroxymethylcytosine production and cell lineage-specification in mouse embryonic stem cells. *Cell Stem Cell*, *8*(2), 200–213. https://doi.org/10.1016/j.stem.2011.01.008

Kolodgie, F. D., Burke, A. P., Nakazawa, G., & Virmani, R. (2007). Is pathologic intimal thickening the key to understanding early plaque progression in human atherosclerotic disease? *Arteriosclerosis, Thrombosis, and Vascular Biology*, *27*(5), 986–989. https://doi.org/10.1161/ATVBAHA.0000258865.44774.41

Kopan, R., & Ilagan, M. X. G. (2009). The Canonical Notch Signaling Pathway: Unfolding the Activation Mechanism. *Cell*, *137*(2), 216–233. https://doi.org/10.1016/j.cell.2009.03.045

Korshunov, V. A., & Berk, B. C. (2003). Flow-Induced Vascular Remodeling in the Mouse: A Model for Carotid Intima-Media Thickening. *Arteriosclerosis, Thrombosis, and Vascular Biology*, *23*(12), 2185–2191. https://doi.org/10.1161/01.ATV.0000103120.06092.14

Koyanagi-Aoi, M., Ohnuki, M., Takahashi, K., Okita, K., Noma, H., Sawamura, Y., Teramoto, I.,

Narita, M., Sato, Y., Ichisaka, T., Amanoa, N., Watanabe, A., Morizane, A., Yamada, Y., Sato, T., Takahashi, J., & Yamanaka, S. (2013). Differentiation-defective phenotypes revealed by large-scale analyses of human pluripotent stem cells. *Proceedings of the National Academy of Sciences of the United States of America*, *110*(51), 20569–20574. https://doi.org/10.1073/pnas.1319061110

Koyanagi, M., Baguet, A., Martens, J., Margueron, R., Jenuwein, T., & Bix, M. (2005). EZH2 and histone 3 trimethyl lysine 27 associated with Il4 and Il13 gene silencing in TH1 cells. *Journal of Biological Chemistry*, *280*(36), 31470–31477. https://doi.org/10.1074/jbc.M504766200

Kramann, R., Goettsch, C., Wongboonsin, J., Iwata, H., Schneider, R. K., Kuppe, C., Kaesler, N., Chang-Panesso, M., Machado, F. G., Gratwohl, S., Madhurima, K., Hutcheson, J. D., Jain, S., Aikawa, E., & Humphreys, B. D. (2016). Adventitial MSC-like Cells Are Progenitors of Vascular Smooth Muscle Cells and Drive Vascular Calcification in Chronic Kidney Disease. *Cell Stem Cell*, *19*(5), 628–642. https://doi.org/10.1016/j.stem.2016.08.001

Kramann, R., Schneider, R. K., Dirocco, D. P., Machado, F., Fleig, S., Bondzie, P. A., Henderson, J. M., Ebert, B. L., & Humphreys, B. D. (2015). Perivascular Gli1+ progenitors are key contributors to injury-induced organ fibrosis. *Cell Stem Cell*, *16*(1), 51–66. https://doi.org/10.1016/j.stem.2014.11.004

Kubota, K., Okazaki, J., Louie, O., Kent, K. C., & Liu, B. (2003). TGF-β stimulates collagen (I) in vascular smooth muscle cells via a short element in the proximal collagen promoter. *Journal of Surgical Research*, *109*(1), 43–50. https://doi.org/10.1016/S0022-4804(02)00037-9

Kurdistani, S. K., & Grunstein, M. (2003). In vivo protein-protein and protein-DNA crosslinking for genomewide binding microarray. *Methods*, *31*(1), 90–95. https://doi.org/10.1016/S1046-2023(03)00092-6

Kurpinski, K., Lam, H., Chu, J., Wang, A., Kim, A., Tsay, E., Agrawal, S., Schaffer, D. V., & Li, S. (2010). Transforming growth factor-β and notch signaling mediate stem cell differentiation into smooth muscle cells. *Stem Cells*, *28*(4), 734–742. https://doi.org/10.1002/stem.319

Lan, F., Collins, R. E., De Cegli, R., Alpatov, R., Horton, J. R., Shi, X., Gozani, O., Cheng, X., & Shi, Y. (2007). Recognition of unmethylated histone H3 lysine 4 links BHC80 to LSD1-

mediated gene repression. *Nature*, *448*(7154), 718–722. https://doi.org/10.1038/nature06034

Landt, S. G., Marinov, G. K., Kundaje, A., Kheradpour, P., Pauli, F., Batzoglou, S., Bernstein, B. E., Bickel, P., Brown, J. B., Cayting, P., Chen, Y., DeSalvo, G., Epstein, C., Fisher-Aylor, K. I., Euskirchen, G., Gerstein, M., Gertz, J., Hartemink, A. J., Hoffman, M. M., … Snyder, M. (2012). ChIP-seq guidelines and practices of the ENCODE and modENCODE consortia. *Genome Research*, *22*(9), 1813–1831. https://doi.org/10.1101/gr.136184.111

Laukkanen, M. O., Mannermaa, S., Hiltunen, M. O., Aittomäki, S., Airenne, K., Jänne, J., & Ylä-Herttuala, S. (1999). Local hypomethylation in atherosclerosis found in rabbit ec-sod gene. *Arteriosclerosis, Thrombosis, and Vascular Biology*, *19*(9), 2171–2178. https://doi.org/10.1161/01.ATV.19.9.2171

Leask, A., & Abraham, D. J. (2004). TGF-β signaling and the fibrotic response. *The FASEB Journal*, *18*(7), 816–827. https://doi.org/10.1096/fj.03-1273rev

Lee, K. K., & Workman, J. L. (2007). Histone acetyltransferase complexes: One size doesn't fit all. *Nature Reviews Molecular Cell Biology*, *8*(4), 284–295. https://doi.org/10.1038/nrm2145

Lee, Y. S., & Mrksich, M. (2002). Protein chips: from concept to practice. *Trends in biotechnology*, *20*(12), s14-s18. https://doi.org/10.1016/S1471-1931(02)00200-8

Ley, T. J., Mardis, E. R., Ding, L., Fulton, B., McLellan, M. D., Chen, K., Dooling, D., Dunford-Shore, B. H., McGrath, S., Hickenbotham, M., Cook, L., Abbott, R., Larson, D. E., Koboldt, D. C., Pohl, C., Smith, S., Hawkins, A., Abbott, S., Locke, D., … Wilson, R. K. (2008). DNA sequencing of a cytogenetically normal acute myeloid leukaemia genome. *Nature*, *456*(7218), 66–72. https://doi.org/10.1038/nature07485

Li M, Nishimura H, Sekiguchi H, Kamei N, Yokoyama A, Horii M, Asahara T. Concurrent vasculogenesis and neurogenesis from adult neural stem cells. Circ Res. 2009 Oct 23;105(9):860-8. doi: 10.1161/CIRCRESAHA.109.199299. Epub 2009 Sep 17. PMID: 19762683.

Li, E. (2002). Chromatin modification and epigenetic reprogramming in mammalian development. *Nature Reviews Genetics*, *3*(9), 662–673. https://doi.org/10.1038/nrg887

Li, H., Ilin, S., Wang, W., Duncan, E. M., Wysocka, J., Allis, C. D., & Patel, D. J. (2006). Molecular basis for site-specific read-out of histone H3K4me3 by the BPTF PHD finger of NURF. *Nature*, *442*(7098), 91–95. https://doi.org/10.1038/nature04802

Li, J., Huang, N. F., Zou, J., Laurent, T. J., Lee, J. C., Okogbaa, J., Cooke, J. P., & Ding, S. (2013). Conversion of human fibroblasts to functional endothelial cells by defined factors. *Arteriosclerosis, Thrombosis, and Vascular Biology*, *33*(6), 1366–1375. https://doi.org/10.1161/ATVBAHA.112.301167

Li, L., Miano, J. M., Cserjesi, P., & Olson, E. N. (1996). SM22α, a marker of adult smooth muscle, is expressed in multiple myogenic lineages during embryogenesis. *Circulation Research*, *78*(2), 188–195. https://doi.org/10.1161/01.RES.78.2.188

Li, S., Wang, D. Z., Wang, Z., Richardson, J. A., & Olson, E. N. (2003). The serum response factor coactivator myocardin is required for vascular smooth muscle development. *Proceedings of the National Academy of Sciences of the United States of America*, *100*(16), 9366–9370. https://doi.org/10.1073/pnas.1233635100

Liang, G., & Zhang, Y. (2013). Genetic and epigenetic variations in iPSCs: Potential causes and implications for application. Cell Stem Cell, 13(2), 149–159. https://doi.org/10.1016/j.stem.2013.07.001

Liang J, Li Q, Cai W, Zhang X, Yang B, Li X, Jiang S, Tian S, Zhang K, Song H, Ai D, Zhang X, Wang C, Zhu Y. Inhibition of polycomb repressor complex 2 ameliorates neointimal hyperplasia by suppressing trimethylation of H3K27 in vascular smooth muscle cells. Br J Pharmacol. 2019 Sep;176(17):3206-3219. doi: 10.1111/bph.14754.

Liao, J., Chen, X., Li, Y., Ge, Z., Duan, H., Zou, Y., & Ge, J. (2012). Transfer of bone-marrow-derived mesenchymal stem cells influences vascular remodeling and calcification after balloon injury in hyperlipidemic rats. *Journal of Biomedicine and Biotechnology*, *2012*. https://doi.org/10.1155/2012/165296

Libby, P., Ridker, P. M., & Hansson, G. K. (2011). Progress and challenges in translating the biology of atherosclerosis. *Nature*, *473*(7347), 317–325. https://doi.org/10.1038/nature10146

Lin, C. S., Xin, Z. C., Deng, C. H., Ning, H., Lin, G., & Lue, T. F. (2010). Defining adipose tissue-derived stem cells in tissue and in culture. *Histology and Histopathology*, *25*(6), 807–815. https://doi.org/10.14670/HH-25.807

Li, H., Ilin, S., Wang, W. *et al.* Molecular basis for site-specific read-out of histone H3K4me3 by the BPTF PHD finger of NURF. *Nature* 442**,** 91–95 (2006). https://doi.org/10.1038/nature04802

Liu, C. L., Schreiber, S. L., & Bernstein, B. E. (2003). Development and validation of a T7 based linear amplification for genomic DNA. *BMC genomics*, *4*(1), 1-11. https://doi.org/10.1186/1471-2164-4-19

Liu, M., Espinosa-Diez, C., Mahan, S., Du, M., Nguyen, A. T., Hahn, S., Chakraborty, R., Straub, A. C., Martin, K. A., Owens, G. K., & Gomez, D. (2021). H3K4 di-methylation governs smooth muscle lineage identity and promotes vascular homeostasis by restraining plasticity. *Developmental Cell*, *56*(19), 2765-2782.e10. https://doi.org/10.1016/j.devcel.2021.09.001

Liu, M., & Gomez, D. (2019). Smooth Muscle Cell Phenotypic Diversity. *Arteriosclerosis, Thrombosis, and Vascular Biology*, *39*(9), 1715–1723. https://doi.org/10.1161/ATVBAHA.119.312131

Liu, R., Jin, Y., Tang, W. H., Qin, L., Zhang, X., Tellides, G., Hwa, J., Yu, J., & Martin, K. A. (2013). Ten-eleven translocation-2 (TET2) is a master regulator of smooth muscle cell plasticity. *Circulation*, *128*(18), 2047–2057. https://doi.org/10.1161/CIRCULATIONAHA.113.002887

Liu, R., Leslie, K. L., & Martin, K. A. (2015). Epigenetic regulation of smooth muscle cell plasticity. In *Biochimica et Biophysica Acta - Gene Regulatory Mechanisms* (Vol. 1849, Issue 4, pp. 448–453). https://doi.org/10.1016/j.bbagrm.2014.06.004

Liu, T., Ortiz, J. A., Taing, L., Meyer, C. A., Lee, B., Zhang, Y., Shin, H., Wong, S. S., Ma, J., Lei, Y., Pape, U. J., Poidinger, M., Chen, Y., Yeung, K., Brown, M., Turpaz, Y., & Liu, X. S. (2011). Cistrome: An integrative platform for transcriptional regulation studies. *Genome Biology*, *12*(8), R83. https://doi.org/10.1186/gb-2011-12-8-r83

Lockhart, P. B., Bolger, A. F., Papapanou, P. N., Osinbowale, O., Trevisan, M., Levison, M. E., ... & Baddour, L. M. (2012). Periodontal disease and atherosclerotic vascular disease: does the evidence support an independent association? A scientific statement from the American Heart Association. Circulation, 125(20), 2520-2544. https://doi.org/10.1161/CIR.0b013e31825719f3

Logovskaya, L. V., Bukharova, T. B., Volkov, A. V., Vikhrova, E. B., Makhnach, O. V., & Goldshtein, D. V. (2013). Induction of osteogenic differentiation of multipotent mesenchymal stromal cells from human adipose tissue. *Bulletin of Experimental Biology and Medicine*, *155*(1), 145–150. https://doi.org/10.1007/s10517-013-2100-x

Long, J. Z., Svensson, K. J., Tsai, L., Zeng, X., Roh, H. C., Kong, X., ... & Spiegelman, B. M. (2014). A smooth muscle-like origin for beige adipocytes. *Cell metabolism*, *19*(5), 810-820. https://doi.org/10.1016/j.cmet.2014.03.025

Long, X., Bell, R. D., Gerthoffer, W. T., Zlokovic, B. V., & Miano, J. M. (2008). Myocardin is sufficient for a smooth muscle-like contractile phenotype. *Arteriosclerosis, Thrombosis, and Vascular Biology*, *28*(8), 1505–1510. https://doi.org/10.1161/ATVBAHA.108.166066

Lu, D., Chen, B., Liang, Z., Deng, W., Jiang, Y., Li, S., Xu, J., Wu, Q., Zhang, Z., Xie, B., & Chen, S. (2011). Comparison of bone marrow mesenchymal stem cells with bone marrow-derived mononuclear cells for treatment of diabetic critical limb ischemia and foot ulcer: A double-blind, randomized, controlled trial. *Diabetes Research and Clinical Practice*, *92*(1), 26–36. https://doi.org/10.1016/j.diabres.2010.12.010

Lu, Y., Thavarajah, T., Gu, W., Cai, J., & Xu, Q. (2018). Impact of miRNA in atherosclerosis. *Arteriosclerosis, thrombosis, and vascular biology*, *38*(9), e159-e170. https://doi.org/10.1161/ATVBAHA.118.310227

Luger, K., Mäder, A. W., Richmond, R. K., Sargent, D. F., & Richmond, T. J. (1997). Crystal structure of the nucleosome core particle at 2.8 Å resolution. *Nature*, *389*(6648), 251–260. https://doi.org/10.1038/38444

Luk, J. M., Wang, P. P., Lee, C. K., Wang, J. H., & Fan, S. T. (2005). Hepatic potential of bone marrow stromal cells: Development of in vitro co-culture and intra-portal transplantation models. *Journal of Immunological Methods*, *305*(1), 39–47. https://doi.org/10.1016/j.jim.2005.07.006

Lund, G., Andersson, L., Lauria, M., Lindholm, M., Fraga, M. F., Villar-Garea, A., Ballestar, E., Esteller, M., & Zaina, S. (2004). DNA methylation polymorphisms precede any histological sign of atherosclerosis in mice lacking apolipoprotein E. *Journal of Biological Chemistry*, *279*(28), 29147–29154. https://doi.org/10.1074/jbc.M403618200

Maherali, N., Sridharan, R., Xie, W., Utikal, J., Eminli, S., Arnold, K., Stadtfeld, M., Yachechko, R., Tchieu, J., Jaenisch, R., Plath, K., & Hochedlinger, K. (2007). Directly Reprogrammed Fibroblasts Show Global Epigenetic Remodeling and Widespread Tissue Contribution. *Cell Stem Cell*, *1*(1), 55–70. https://doi.org/10.1016/j.stem.2007.05.014

Mintz, B. (1965). Genetic mosaicism in adult mice of quadriparental lineage. *Science*, *148*(3674), 1232-1233. DOI: 10.1126/science.148.3674.1232

Maison C, Bailly D, Peters AH, Quivy JP, Roche D, Taddei A, Lachner M, Jenuwein T, Almouzni G 2002 Higher-order structure in pericentric heterochromatin involves a distinct pattern of histone modification and an RNA component. Nat Genet 30: 329–334 https://doi.org/10.1038/ng843

Majesky, M. W. (2007). Developmental basis of vascular smooth muscle diversity. *Arteriosclerosis, Thrombosis, and Vascular Biology*, *27*(6), 1248–1258. https://doi.org/10.1161/ATVBAHA.107.141069

Majesky, M. W., Dong, X. R., Hoglund, V., Mahoney, W. M., & Daum, G. (2011). The adventitia: A dynamic interface containing resident progenitor cells. *Arteriosclerosis, Thrombosis, and Vascular Biology*, *31*(7), 1530–1539. https://doi.org/10.1161/ATVBAHA.110.221549

Majesky, M. W., Horita, H., Ostriker, A., Lu, S., Regan, J. N., Bagchi, A., Dong, X. R., Poczobutt, J., Nemenoff, R. A., & Weiser-Evans, M. C. M. (2017). Differentiated Smooth Muscle Cells Generate a Subpopulation of Resident Vascular Progenitor Cells in the Adventitia Regulated by Klf4. *Circulation Research*, *120*(2), 296–311. https://doi.org/10.1161/CIRCRESAHA.116.309322

Manabe, I., & Owens, G. K. (2001). *Recruitment of Serum Response Factor and Hyperacetylation of Histones at Smooth Muscle – Specific Regulatory Regions During Differentiation of a Novel P19-Derived In Vitro Smooth Muscle Differentiation System*. 1127–1134. https://doi.org/10.1161/hh1101.091339

Mardis, E. R. (2008). Next-generation DNA sequencing methods. *Annual Review of Genomics and Human Genetics*, *9*, 387–402. https://doi.org/10.1146/annurev.genom.9.081307.164359

Margariti, A., Winkler, B., Karamariti, E., Zampetaki, A., Tsai, T. N., Baban, D., Ragoussis, J., Huang, Y., Han, J. D. J., Zeng, L., Hu, Y., & Xu, Q. (2012). Direct reprogramming of fibroblasts into endothelial cells capable of angiogenesis and reendothelialization in tissue-engineered vessels. *Proceedings of the National Academy of Sciences of the United States of America*, *109*(34), 13793–13798. https://doi.org/10.1073/pnas.1205526109

Massagué, J. (2012). TGFβ signalling in context. *Nature Reviews Molecular Cell Biology*, *13*(10), 616–630. https://doi.org/10.1038/nrm3434

Masui, S., Nakatake, Y., Toyooka, Y., Shimosato, D., Yagi, R., Takahashi, K., Okochi, H.,

Okuda, A., Matoba, R., Sharov, A. A., Ko, M. S. H., & Niwa, H. (2007). Pluripotency governed by Sox2 via regulation of Oct3/4 expression in mouse embryonic stem cells. *Nature Cell Biology*, *9*(6), 625–635. https://doi.org/10.1038/ncb1589

Maul, T. M., Chew, D. W., Nieponice, A., & Vorp, D. A. (2011). Mechanical stimuli differentially control stem cell behavior: Morphology, proliferation, and differentiation. *Biomechanics and Modeling in Mechanobiology*, *10*(6), 939–953. https://doi.org/10.1007/s10237-010-0285-8

McClellan, M., Brown, N., Califf, R. M., & Warner, J. J. (2019). Call to Action: Urgent Challenges in Cardiovascular Disease: A Presidential Advisory from the American Heart Association. *Circulation*, *139*(9), E44–E54. https://doi.org/10.1161/CIR.0000000000000652

Mcdonald, O. G., & Owens, G. K. (2007). *Programming Smooth Muscle Plasticity With Chromatin Dynamics*. 1428–1441. https://doi.org/10.1161/01.RES.0000266448.30370.a0

McDonald, O. G., Wamhoff, B. R., Hoofnagle, M. H., & Owens, G. K. (2006). Control of SRF binding to CArG box chromatin regulates smooth muscle gene expression in vivo. *Journal of Clinical Investigation*, *116*(1), 36–48. https://doi.org/10.1172/JCI26505

Meissner, A., Mikkelsen, T. S., Gu, H., Wernig, M., Hanna, J., Sivachenko, A., Zhang, X., Bernstein, B. E., Nusbaum, C., Jaffe, D. B., Gnirke, A., Jaenisch, R., & Lander, E. S. (2008). Genome-scale DNA methylation maps of pluripotent and differentiated cells. *Nature*, *454*(7205), 766–770. https://doi.org/10.1038/nature07107

Meshorer, E., & Misteli, T. (2006). Chromatin in pluripotent embryonic stem cells and differentiation. *Nature Reviews Molecular Cell Biology*, *7*(7), 540–546. https://doi.org/10.1038/nrm1938

Meshorer, E., Yellajoshula, D., George, E., Scambler, P. J., Brown, D. T., & Misteli, T. (2006). Hyperdynamic plasticity of chromatin proteins in pluripotent embryonic stem cells. *Developmental Cell*, *10*(1), 105–116. https://doi.org/10.1016/j.devcel.2005.10.017

Métivier, R., Penot, G., Carmouche, R. P., Hübner, M. R., Reid, G., Denger, S., Manu, D., Brand, H., Koš, M., Benes, V., & Gannon, F. (2004). Transcriptional complexes engaged by apo-estrogen receptor-α isoforms have divergent outcomes. *EMBO Journal*, *23*(18), 3653–3666. https://doi.org/10.1038/sj.emboj.7600377

Metzger, D., & Feil, R. (1999). Engineering the mouse genome by site-specific

recombination. *Current opinion in biotechnology*, *10*(5), 470-476. https://doi.org/10.1016/S0958-1669(99)00012-9

Mezger, A., Klemm, S., Mann, I., Brower, K., Mir, A., Bostick, M., Farmer, A., Fordyce, P., Linnarsson, S., & Greenleaf, W. (2018). High-throughput chromatin accessibility profiling at single-cell resolution. *Nature Communications*, *9*(1), 6–11. https://doi.org/10.1038/s41467-018-05887-x

Miano, J. M. (2003). Serum response factor: Toggling between disparate programs of gene expression. *Journal of Molecular and Cellular Cardiology*, *35*(6), 577–593. https://doi.org/10.1016/S0022-2828(03)00110-X

Miano, J. M. (2015). Myocardin in biology and disease. *Journal of Biomedical Research*, *29*(1), 3–19. https://doi.org/10.7555/jbr.29.20140151

Miano, J. M., Cserjesi, P., Ligon, K. L., Periasamy, M., & Olson, E. N. (1994). Smooth muscle myosin heavy chain exclusively marks the smooth muscle lineage during mouse embryogenesis. *Circulation Research*, *75*(5), 803–812. https://doi.org/10.1161/01.RES.75.5.803

Mikkelsen, T. S., Ku, M., Jaffe, D. B., Issac, B., Lieberman, E., Giannoukos, G., Alvarez, P., Brockman, W., Kim, T. K., Koche, R. P., Lee, W., Mendenhall, E., O'Donovan, A., Presser, A., Russ, C., Xie, X., Meissner, A., Wernig, M., Jaenisch, R., … Bernstein, B. E. (2007). Genome-wide maps of chromatin state in pluripotent and lineage-committed cells. *Nature*, *448*(7153), 553–560. https://doi.org/10.1038/nature06008

Millan, F. A., Denhez, F., Kondaiah, P., & Akhurst, R. J. (1991). Embryonic gene expression patterns of TGF β1, β2 and β3 suggest different developmental functions in vivo. *Development*, *111*(1), 131–143. https://doi.org/10.1242/dev.111.1.131

Millette, E., Rauch, B. H., Defawe, O., Kenagy, R. D., Daum, G., & Clowes, A. W. (2005). Platelet-derived growth factor-BB-induced human smooth muscle cell proliferation depends on basic FGF release and FGFR-1 activation. *Circulation Research*, *96*(2), 172–179. https://doi.org/10.1161/01.RES.0000154595.87608.db

Mokry, M., Hatzis, P., Schuijers, J., Lansu, N., Ruzius, F. P., Clevers, H., & Cuppen, E. (2012). Integrated genome-wide analysis of transcription factor occupancy, RNA polymerase II binding and steady-state RNA levels identify differentially regulated functional gene classes. *Nucleic Acids Research*, *40*(1), 148–158. https://doi.org/10.1093/nar/gkr720

Molony, C., King, D., Di Luca, M., Kitching, M., Olayinka, A., Hakimjavadi, R., Julius, L. A. N.,

Fitzpatrick, E., Gusti, Y., Burtenshaw, D., Healy, K., Finlay, E. K., Kernan, D., Llobera, A., Liu, W., Morrow, D., Redmond, E. M., Ducrée, J., & Cahill, P. A. (2021). Disease-Relevant Single Cell Photonic Signatures Identify S100β Stem Cells and their Myogenic Progeny in Vascular Lesions. *Stem Cell Reviews and Reports*, *17*(5), 1713–1740. https://doi.org/10.1007/s12015-021-10125-x

Molony, C., McIntyre, J., Maguire, A., Hakimjavadi, R., Burtenshaw, D., Casey, G., Di Luca, M., Hennelly, B., Byrne, H. J., & Cahill, P. A. (2018). Label-free discrimination analysis of de-differentiated vascular smooth muscle cells, mesenchymal stem cells and their vascular and osteogenic progeny using vibrational spectroscopy. *Biochimica et Biophysica Acta - Molecular Cell Research*, *1865*(2), 343–353. https://doi.org/10.1016/j.bbamcr.2017.11.006

Montezano, A. C., Zimmerman, D., Yusuf, H., Burger, D., Chignalia, A. Z., Wadhera, V., Van Leeuwen, F. N., & Touyz, R. M. (2010). Vascular smooth muscle cell differentiation to an osteogenic phenotype involves TRPM7 modulation by magnesium. *Hypertension*, *56*(3), 453–462. https://doi.org/10.1161/HYPERTENSIONAHA.110.152058

Mooney, C. J., Hakimjavadi, R., Fitzpatrick, E., Kennedy, E., Walls, D., Morrow, D., Redmond, E. M., & Cahill, P. A. (2015). Hedgehog and Resident Vascular Stem Cell Fate. *Stem Cells International*, *2015*. https://doi.org/10.1155/2015/468428

Moran-Crusio, K., Reavie, L., Shih, A., Abdel-Wahab, O., Ndiaye-Lobry, D., Lobry, C., Figueroa, M. E., Vasanthakumar, A., Patel, J., Zhao, X., Perna, F., Pandey, S., Madzo, J., Song, C., Dai, Q., He, C., Ibrahim, S., Beran, M., Zavadil, J., … Levine, R. L. (2011). Tet2 Loss Leads to Increased Hematopoietic Stem Cell Self-Renewal and Myeloid Transformation. *Cancer Cell*, *20*(1), 11–24. https://doi.org/10.1016/j.ccr.2011.06.001

Morrow, D., Scheller, A., Birney, Y. A., Sweeney, C., Guha, S., Cummins, P. M., Murphy, R., Walls, D., Redmond, E. M., & Cahill, P. A. (2005). Notch-mediated CBF-1/RBP-Jκ-dependent regulation of human vascular smooth muscle cell phenotype in vitro. *American Journal of Physiology - Cell Physiology*, *289*(5 58-5), 1188–1196. https://doi.org/10.1152/ajpcell.00198.2005

Mortada, I., Mortada, R., & Al Bazzal, M. (2018). Dental pulp stem cells and the management of neurological diseases: An update. *Journal of Neuroscience Research*, *96*(2), 265–272. https://doi.org/10.1002/jnr.24122

Movassagh, M., Choy, M. K., Goddard, M., Bennett, M. R., Down, T. A., & Foo, R. S. Y. (2010).

Differential DNA methylation correlates with differential expression of angiogenic factors in human heart failure. *PLoS ONE*, *5*(1). https://doi.org/10.1371/journal.pone.0008564

Muiño, J. M., Kaufmann, K., van Ham, R. C. H. J., Angenent, G. C., & Krajewski, P. (2011). ChIP-seq Analysis in R (CSAR): An R package for the statistical detection of protein-bound genomic regions. *Plant Methods*, *7*(1), 1–8. https://doi.org/10.1186/1746-4811-7-11

Mundra, V., Gerling, I. C., & Mahato, R. I. (2013). Mesenchymal stem cell-based therapy. *Molecular pharmaceutics*, *10*(1), 77-89. https://doi.org/10.1021/mp3005148

Munger, J. S., Harpel, J. G., Giancotti, F. G., & Rifkin, D. B. (1998). Interactions between growth factors and integrins: latent forms of transforming growth factor-β are ligands for the integrin αvβ1. *Molecular biology of the cell*, *9*(9), 2627-2638. https://doi.org/10.1091/mbc.9.9.2627

Murray, C. J. ., & Lopez, A. D. (1996). Global Burden of Disease and Injur Y Series the Global Burden of Disease. *Lancet, 349, 15* https://doi.org/10.1088/1742-6596/707/1/012025

Mymryk, J. S., Fryer, C. J., Jung, L. A., & Archer, T. K. (1997). Analysis of chromatin structure in vivo. *Methods: A Companion to Methods in Enzymology*, *12*(1), 105–114. https://doi.org/10.1006/meth.1997.0452

Nagy, P. L., Cleary, M. L., Brown, P. O., & Lieb, J. D. (2003). Genomewide demarcation of RNA polymerase II transcription units revealed by physical fractionation of chromatin. *Proceedings of the National Academy of Sciences of the United States of America*, *100*(11), 6364–6369. https://doi.org/10.1073/pnas.1131966100

Nakagawa, K., & Nakashima, Y. (2018). Pathologic intimal thickening in human atherosclerosis is formed by extracellular accumulation of plasma-derived lipids and dispersion of intimal smooth muscle cells. *Atherosclerosis*, *274*, 235–242. https://doi.org/10.1016/j.atherosclerosis.2018.03.039

Nakagawa, M., Koyanagi, M., Tanabe, K., Takahashi, K., Ichisaka, T., Aoi, T., Okita, K., Mochiduki, Y., Takizawa, N., & Yamanaka, S. (2008). Generation of induced pluripotent stem cells without Myc from mouse and human fibroblasts. *Nature Biotechnology*, *26*(1), 101–106. https://doi.org/10.1038/nbt1374

Nakagawa, M., Takizawa, N., Narita, M., Ichisaka, T., & Yamanaka, S. (2010). Promotion of direct reprogramming by transformation-deficient Myc. *Proceedings of the National*

Academy of Sciences of the United States of America, *107*(32), 14152–14157. https://doi.org/10.1073/pnas.1009374107

Nelson, J. D., Denisenko, O., Sova, P., & Bomsztyk, K. (2006). Fast chromatin immunoprecipitation assay. *Nucleic Acids Research*, *34*(1), 1–7. https://doi.org/10.1093/nar/gnj004

Nemenoff, R. A., Horita, H., Ostriker, A. C., Furgeson, S. B., Simpson, P. A., Vanputten, V., Crossno, J., Offermanns, S., & Weiser-Evans, M. C. M. (2011). SDF-1α induction in mature smooth muscle cells by inactivation of PTEN is a critical mediator of exacerbated injury-induced neointima formation. *Arteriosclerosis, Thrombosis, and Vascular Biology*, *31*(6), 1300–1308. https://doi.org/10.1161/ATVBAHA.111.223701

New, S. E. P., Alvarez-Gonzalez, C., Vagaska, B., Gomez, S. G., Bulstrode, N. W., Madrigal, A., & Ferretti, P. (2015). A matter of identity - Phenotype and differentiation potential of human somatic stem cells. *Stem Cell Research*, *15*(1), 1–13. https://doi.org/10.1016/j.scr.2015.04.003

Newby, A. C., & Zaltsman, A. B. (2000). Molecular mechanisms in intimal hyperplasia. *Journal of Pathology*, *190*(3), 300–309. https://doi.org/10.1002/(SICI)1096-9896(200002)190:3<300::AID-PATH596>3.0.CO;2-I

Nguyen, A. T., Gomez, D., Bell, R. D., Campbell, J. H., Clowes, A. W., Gabbiani, G., Giachelli, C. M., Parmacek, M. S., Raines, E. W., Rusch, N. J., Speer, M. Y., Sturek, M., Thyberg, J., Towler, D. A., Weiser-Evans, M. C., Yan, C., Miano, J. M., & Owens, G. K. (2013). Smooth muscle cell plasticity: fact or fiction? *Circulation Research*, *112*(1), 17–22. https://doi.org/10.1161/CIRCRESAHA.112.281048

Ni, Z., Deng, J., Potter, C. M. F., Nowak, W. N., Gu, W., Zhang, Z., Chen, T., Chen, Q., Hu, Y., Zhou, B., Xu, Q., & Zhang, L. (2019). Recipient c-kit lineage cells repopulate smooth muscle cells of transplant arteriosclerosis in mouse models. *Circulation Research*, *125*(2), 223–241. https://doi.org/10.1161/CIRCRESAHA.119.314855

Niwa, H., Ogawa, K., Shimosato, D., & Adachi, K. (2009). A parallel circuit of LIF signalling pathways maintains pluripotency of mouse ES cells. *Nature*, *460*(7251), 118–122. https://doi.org/10.1038/nature08113

O'Neill, L. P., VerMilyea, M. D., & Turner, B. M. (2006). Epigenetic characterization of the early embryo with a chromatin immunoprecipitation protocol applicable to small cell populations. *Nature Genetics*, *38*(7), 835–841. https://doi.org/10.1038/ng1820

Otsuka, F., Kramer, M. C. A., Woudstra, P., Yahagi, K., Ladich, E., Finn, A. V., de Winter, R. J., Kolodgie, F. D., Wight, T. N., Davis, H. R., Joner, M., & Virmani, R. (2015). Natural progression of atherosclerosis from pathologic intimal thickening to late fibroatheroma in human coronary arteries: A pathology study. *Atherosclerosis*, *241*(2), 772–782. https://doi.org/10.1016/j.atherosclerosis.2015.05.011

Owens, G. K., Kumar, M. S., & Wamhoff, B. R. (2004). Molecular regulation of vascular smooth muscle cell differentiation in development and disease. *Physiological Reviews*, *84*(3), 767–801. https://doi.org/10.1152/physrev.00041.2003

Pan, H., Xue, C., Auerbach, B. J., Fan, J., Bashore, A. C., Cui, J., ... & Reilly, M. P. (2020). Single-cell genomics reveals a novel cell state during smooth muscle cell phenotypic switching and potential therapeutic targets for atherosclerosis in mouse and human. *Circulation*, *142*(21), 2060-2075. https://doi.org/10.1161/CIRCULATIONAHA.120.048378

Pan, X. X., Ruan, C. C., Liu, X. Y., Kong, L. R., Ma, Y., Wu, Q. H., Li, H. Q., Sun, Y. J., Chen, A. Q., Zhao, Q., Wu, F., Wang, X. J., Wang, J. G., Zhu, D. L., & Gao, P. J. (2019). Perivascular adipose tissue-derived stromal cells contribute to vascular remodeling during aging. *Aging Cell*, *18*(4), 1–13. https://doi.org/10.1111/acel.12969

Papakonstanti, E. A., & Stournaras, C. (2008). Cell responses regulated by early reorganization of actin cytoskeleton. *FEBS Letters*, *582*(14), 2120–2127. https://doi.org/10.1016/j.febslet.2008.02.064

Park, W. S., Heo, S. C., Jeon, E. S., Hong, D. H., Son, Y. K., Ko, J. H., Kim, H. K., Lee, S. Y., Kim, J. H., & Han, J. (2013). Functional expression of smooth muscle-specific ion channels in TGF-β1-treated human adipose-derived mesenchymal stem cells. *American Journal of Physiology - Cell Physiology*, *305*(4), 377–391. https://doi.org/10.1152/ajpcell.00404.2012

Passman, J. N., Dong, X. R., Wu, S. P., Maguire, C. T., Hogan, K. A., Bautch, V. L., & Majesky, M. W. (2008). A sonic hedgehog signaling domain in the arterial adventitia supports resident Sca1+ smooth muscle progenitor cells. *Proceedings of the National Academy of Sciences of the United States of America*, *105*(27), 9349–9354. https://doi.org/10.1073/pnas.0711382105

Pekowska, A., Benoukraf, T., Ferrier, P., & Spicuglia, S. (2010). A unique H3K4me2 profile marks tissue-specific gene regulation. *Genome Research*, *20*(11), 1493–1502.

https://doi.org/10.1101/gr.109389.110

Pekowska, A., Benoukraf, T., Zacarias-Cabeza, J., Belhocine, M., Koch, F., Holota, H., Imbert, J., Andrau, J. C., Ferrier, P., & Spicuglia, S. (2011). H3K4 tri-methylation provides an epigenetic signature of active enhancers. *EMBO Journal*, *30*(20), 4198–4210. https://doi.org/10.1038/emboj.2011.295

Peña, P. V., Davrazou, F., Shi, X., Walter, K. L., Verkhusha, V. V., Gozani, O., Zhao, R., & Kutateladze, T. G. (2006). Molecular mechanism of histone H3K4me3 recognition by plant homeodomain of ING2. *Nature*, *442*(7098), 100–103. https://doi.org/10.1038/nature04814

Pereira, R. F., Halford, K. W., O'Hara, M. D., Leeper, D. B., Sokolov, B. P., Pollard, M. D., Bagasra, O., & Prockop, D. J. (1995). Cultured adherent cells from marrow can serve as long-lasting precursor cells for bone, cartilage, and lung in irradiated mice. *Proceedings of the National Academy of Sciences of the United States of America*, *92*(11), 4857–4861. https://doi.org/10.1073/pnas.92.11.4857

Perera, A., Eisen, D., Wagner, M., Laube, S. K., Künzel, A. F., Koch, S., Steinbacher, J., Schulze, E., Splith, V., Mittermeier, N., Müller, M., Biel, M., Carell, T., & Michalakis, S. (2015). TET3 is recruited by REST for context-specific hydroxymethylation and induction of gene expression. *Cell Reports*, *11*(2), 283–294. https://doi.org/10.1016/j.celrep.2015.03.020

Peters, A. H. F. M., Kubicek, S., Mechtler, K., O'Sullivan, R. J., Derijck, A. A. H. A., Perez-Burgos, L., Kohlmaier, A., Opravil, S., Tachibana, M., Shinkai, Y., Martens, J. H. A., & Jenuwein, T. (2003). Partitioning and Plasticity of Repressive Histone Methylation States in Mammalian Chromatin. *Molecular Cell*, *12*(6), 1577–1589. https://doi.org/10.1016/S1097-2765(03)00477-5

Pidkovka, N. A., Cherepanova, O. A., Yoshida, T., Alexander, M. R., Deaton, R. A., Thomas, J. A., Leitinger, N., & Owens, G. K. (2007). Oxidized phospholipids induce phenotypic switching of vascular smooth muscle cells in vivo and in vitro. *Circulation Research*, *101*(8), 792–801. https://doi.org/10.1161/CIRCRESAHA.107.152736

Pipes, G. C. T., Creemers, E. E., & Olson, E. N. (2006). The myocardin family of transcriptional coactivators: Versatile regulators of cell growth, migration, and myogenesis. *Genes and Development*, *20*(12), 1545–1556. https://doi.org/10.1101/gad.1428006

Pittenger, M. F., Mackay, A. M., Beck, S. C., Jaiswal, R. K., Douglas, R., Mosca, J. D.,

Moorman, M. A., Simonetti, D. W., Craig, S., & Marshak, D. R. (1999). Multilineage potential of adult human mesenchymal stem cells. *Science*, *284*(5411), 143–147. https://doi.org/10.1126/science.284.5411.143

Pittenger, M. F., & Marshak, D. R. (2001). Mesenchymal stem cells of human adult bone marrow. *COLD SPRING HARBOR MONOGRAPH SERIES*, *40*, 349-374.

Poduri, A., Rateri, D. L., Howatt, D. A., Balakrishnan, A., Moorleghen, J. J., Cassis, L. A., & Daugherty, A. (2015). Fibroblast Angiotensin II type 1a receptors contribute to Angiotensin II-induced medial hyperplasia in the ascending aorta. *Arteriosclerosis, Thrombosis, and Vascular Biology*, *35*(9), 1995–2002. https://doi.org/10.1161/ATVBAHA.115.305995

Pokholok, D. K., Harbison, C. T., Levine, S., Cole, M., Hannett, N. M., Tong, I. L., Bell, G. W., Walker, K., Rolfe, P. A., Herbolsheimer, E., Zeitlinger, J., Lewitter, F., Gifford, D. K., & Young, R. A. (2005). Genome-wide map of nucleosome acetylation and methylation in yeast. *Cell*, *122*(4), 517–527. https://doi.org/10.1016/j.cell.2005.06.026

Policastro, R. A., & Zentner, G. E. (2018). Enzymatic methods for genome-wide profiling of protein binding sites. *Briefings in Functional Genomics*, *17*(2), 138–145. https://doi.org/10.1093/bfgp/elx030

Poole, K. E. S., Van Bezooijen, R. L., Loveridge, N., Hamersma, H., Papapoulos, S. E., Löwik, C. W., & Reeve, J. (2005). Sclerostin is a delayed secreted product of osteocytes that inhibits bone formation. *The FASEB Journal*, *19*(13), 1842–1844. https://doi.org/10.1096/fj.05-4221fje

Popova, E. Y., Xu, X., DeWan, A. T., Salzberg, A. C., Berg, A., Hoh, J., Zhang, S. S., & Barnstable, C. J. (2012). Stage and Gene-specific Signatures Defined by Histones H3K4me2 and H3K27me3 Accompany Mammalian Retina Maturation In Vivo. *PLoS ONE*, *7*(10). https://doi.org/10.1371/journal.pone.0046867

Potente, M., Mäkinen, T. Vascular heterogeneity and specialization in development and disease. Nat Rev Mol Cell Biol 18, 477–494 (2017). https://doi.org/10.1038/nrm.2017.36

Potter, C. M. F., Lao, K. H., Zeng, L., & Xu, Q. (2014). Role of biomechanical forces in stem cell vascular lineage differentiation. *Arteriosclerosis, Thrombosis, and Vascular Biology*, *34*(10), 2184–2190. https://doi.org/10.1161/ATVBAHA.114.303423

Pray-Grant, M. G., Daniel, J. A., Schieltz, D., Yates, J. R., & Grant, P. A. (2005). Chd1

chromodomain links histone H3 methylation with SAGA- and SLIK-dependent acetylation. *Nature*, *433*(7024), 434–438. https://doi.org/10.1038/nature03242

Proweller, A., Pear, W. S., & Parmacek, M. S. (2005). Notch signaling represses myocardin-induced smooth muscle cell differentiation. *Journal of Biological Chemistry*, *280*(10), 8994–9004. https://doi.org/10.1074/jbc.M413316200

Psaltis, P. J., Harbuzariu, A., Delacroix, S., Witt, T. A., Holroyd, E. W., Spoon, D. B., Hoffman, S. J., Pan, S., Kleppe, L. S., Mueske, C. S., Gulati, R., Sandhu, G. S., & Simari, R. D. (2012). Identification of a monocyte-predisposed hierarchy of hematopoietic progenitor cells in the adventitia of postnatal murine aorta. *Circulation*, *125*(4), 592–603. https://doi.org/10.1161/CIRCULATIONAHA.111.059360

Puig, O., Caspary, F., Rigaut, G., Rutz, B., Bouveret, E., Bragado-Nilsson, E., Wilm, M., & Séraphin, B. (2001). The tandem affinity purification (TAP) method: A general procedure of protein complex purification. *Methods*, *24*(3), 218–229. https://doi.org/10.1006/meth.2001.1183

Qin, Q., Mei, S., Wu, Q., Sun, H., Li, L., Taing, L., Chen, S., Li, F., Liu, T., Zang, C., Xu, H., Chen, Y., Meyer, C. A., Zhang, Y., Brown, M., Long, H. W., & Liu, X. S. (2016). ChiLin: A comprehensive ChIP-seq and DNase-seq quality control and analysis pipeline. *BMC Bioinformatics*, *17*(1), 1–13. https://doi.org/10.1186/s12859-016-1274-4

Qiu, P., Feng, X. H., & Li, L. (2003). Interaction of Smad3 and SRF-associated complex mediates TGF-β1 signals to regulate SM22 transcription during myofibroblast differentiation. *Journal of Molecular and Cellular Cardiology*, *35*(12), 1407–1420. https://doi.org/10.1016/j.yjmcc.2003.09.002

Rantala, J. K., Pouwels, J., Pellinen, T., Veltel, S., Laasola, P., Mattila, E., Potter, C. S., Duffy, T., Sundberg, J. P., Kallioniemi, O., Askari, J. A., Humphries, M. J., Parsons, M., Salmi, M., & Ivaska, J. (2011). SHARPIN is an endogenous inhibitor of β1-integrin activation. *Nature Cell Biology*, *13*(11), 1315–1324. https://doi.org/10.1038/ncb2340

Rea, S., Eisenhaber, F., O'Carroll, D., Strahl, B. D., Sun, Z. W., Schmid, M., Opravil, S., Mechtier, K., Ponting, C. P., Allis, C. D., & Jenuwein, T. (2000). Regulation of chromatin structure by site-specific histone H3 methyltransferases. *Nature*, *406*(6796), 593–599. https://doi.org/10.1038/35020506

Redheuil, A., Yu, W. C., Wu, C. O., Mousseaux, E., De Cesare, A., Yan, R., ... & Lima, J. A. (2010). Reduced ascending aortic strain and distensibility: earliest manifestations of

vascular aging in humans. *Hypertension*, *55*(2), 319-326. https://doi.org/10.1161/HYPERTENSIONAHA.109.141275

Reinert, R. B., Kantz, J., Misfeldt, A. A., Poffenberger, G., Gannon, M., Brissova, M., & Powers, A. C. (2012). Tamoxifen-induced cre-loxp recombination is prolonged in pancreatic islets of adult mice. *PLoS ONE*, *7*(3). https://doi.org/10.1371/journal.pone.0033529

Ren, B., Robert, F., Wyrick, J. J., Aparicio, O., Jennings, E. G., Simon, I., Zeitlinger, J., Schreiber, J., Hannett, N., Kanin, E., Volkert, T. L., Wilson, C. J., Bell, S. P., & Young, R. A. (2000). Genome-wide location and function of DNA binding proteins. *Science*, *290*(5500), 2306–2309. https://doi.org/10.1126/science.290.5500.2306

Rensen, S. S. M., Doevendans, P. A. F. M. and van Eys, G. J. J. M. (2007) 'Regulation and characteristics of vascular smooth muscle cell phenotypic diversity.', *Netherlands heart journal : monthly journal of the Netherlands Society of Cardiology and the Netherlands Heart Foundation*. Springer, 15(3), pp. 100–8. DOI: 10.1007/BF03085963

Rice, J. C., Briggs, S. D., Ueberheide, B., Barber, C. M., Shabanowitz, J., Hunt, D. F., Shinkai, Y., & Allis, C. D. (2003). Histone Methyltransferases Direct Different Degrees of Methylation to Define Distinct Chromatin Domains. *Molecular Cell*, *12*(6), 1591–1598. https://doi.org/10.1016/S1097-2765(03)00479-9

Ringrose, L., & Paro, R. (2004). Epigenetic regulation of cellular memory by the polycomb and trithorax group proteins. *Annual Review of Genetics*, *38*, 413–443. https://doi.org/10.1146/annurev.genet.38.072902.091907

Robertson, A. G., Bilenky, M., Tam, A., Zhao, Y., Zeng, T., Thiessen, N., Cezard, T., Fejes, A. P., Wederell, E. D., Cullum, R., Euskirchen, G., Krzywinski, M., Birol, I., Snyder, M., Hoodless, P. A., Hirst, M., Marra, M. A., & Jones, S. J. M. (2008). Genome-wide relationship between histone H3 lysine 4 mono- and tri-methylation and transcription factor binding. *Genome Research*, *18*(12), 1906–1917. https://doi.org/10.1101/gr.078519.108

Robertson, G., Hirst, M., Bainbridge, M., Bilenky, M., Zhao, Y., Zeng, T., Euskirchen, G., Bernier, B., Varhol, R., Delaney, A., Thiessen, N., Griffith, O. L., He, A., Marra, M., Snyder, M., & Jones, S. (2007). Genome-wide profiles of STAT1 DNA association using chromatin immunoprecipitation and massively parallel sequencing. *Nature Methods*, *4*(8), 651–657. https://doi.org/10.1038/nmeth1068

Robertson, I. B., Horiguchi, M., Zilberberg, L., Dabovic, B., Hadjiolova, K., & Rifkin, D. B. (2015). Latent TGF-β-binding proteins. *Matrix Biology*, *47*, 44–53. https://doi.org/10.1016/j.matbio.2015.05.005

Robyr, D., Suka, Y., Xenarios, I., Kurdistani, S. K., Wang, A., Suka, N., & Grunstein, M. (2002). Microarray deacetylation maps determine genome-wide functions for yeast histone deacetylases. *Cell*, *109*(4), 437-446. https://doi.org/10.1016/S0092-8674(02)00746-8

Roostalu, U., Aldeiri, B., Albertini, A., Humphreys, N., Simonsen-Jackson, M., Wong, J. K. F., & Cossu, G. (2018). Distinct cellular mechanisms underlie smooth muscle turnover in vascular development and repair. *Circulation Research*, *122*(2), 267–281. https://doi.org/10.1161/CIRCRESAHA.117.312111

Rosamond, W., Flegal, K., Friday, G., Furie, K., Go, A., Greenlund, K., Haase, N., Ho, M., Howard, V., Kissela, B., Kittner, S., Lloyd-Jones, D., McDermott, M., Meigs, J., Moy, C., Nichol, G., O'Donnell, C. J., Roger, V., Rumsfeld, J., … Hong, Y. (2007). Heart disease and stroke statistics - 2007 Update: A report from the American Heart Association Statistics Committee and Stroke Statistics Subcommittee. In *Circulation* (Vol. 115, Issue 5). https://doi.org/10.1161/CIRCULATIONAHA.106.179918

Rose, G. (1964). Familial Patterns in Ischaemic Heart Disease. *British Journal of Preventive & Social Medicine*, *18*, 75–80. https://doi.org/10.1136/jech.18.2.75

Rotem A, Ram O, Shoresh N, Sperling RA, Goren A, Weitz DA, et al. Single-cell ChIP-seq reveals cell subpopulations defined by chromatin state. Nat Biotechnol. 2015;33(11):1165–72. https://doi.org/10.1038/nbt.3383.

Rothenberg E.V. T cell lineage commitment: identity and renunciation. J. Immunol. 2011; 186: 6649-6655 DOI: https://doi.org/10.4049/jimmunol.1003703

Rouhi, A., Mager, D. L., Humphries, R. K., & Kuchenbauer, F. (2008). MiRNAs, epigenetics, and cancer. *Mammalian Genome*, *19*(7–8), 517–525. https://doi.org/10.1007/s00335-008-9133-x

Ross, R. (1999) 'Atherosclerosis - An Inflammatory Disease', *The New England Journal of Medicine*, 340(2), pp. 115–126. doi: 10.1056/NEJM199901143400207.

Ross, R. (1993). The pathogenesis of atherosclerosis: a perspective for the 1990s. *Nature*, *362*(6423), 801-809.

Rufaihah, A. J., Huang, N. F., Jamé, S., Lee, J. C., Nguyen, H. N., Byers, B., De, A., Okogbaa, J., Rollins, M., Reijo-Pera, R., Gambhir, S. S., & Cooke, J. P. (2011). Endothelial cells derived

from human iPSCS increase capillary density and improve perfusion in a mouse model of peripheral arterial disease. *Arteriosclerosis, Thrombosis, and Vascular Biology*, *31*(11), 72–79. https://doi.org/10.1161/ATVBAHA.111.230938

Ruthenburg, A. J., Allis, C. D., & Wysocka, J. (2007). Methylation of Lysine 4 on Histone H3: Intricacy of Writing and Reading a Single Epigenetic Mark. *Molecular Cell*, *25*(1), 15–30. https://doi.org/10.1016/j.molcel.2006.12.014

Ryu S, Lee SH, Kim SU, Yoon BW. Human neural stem cells promote proliferation of endogenous neural stem cells and enhance angiogenesis in ischemic rat brain. Neural Regen Res. 2016 Feb;11(2):298-304. doi: 10.4103/1673-5374.177739. PMID: 27073384; PMCID: PMC4810995.

Sainz, J., Zen, A. A. H., Caligiuri, G., Demerens, C., Urbain, D., Lemitre, M., & Lafont, A. (2006). Isolation of "side population" progenitor cells from healthy arteries of adult mice. *Arteriosclerosis, Thrombosis, and Vascular Biology*, *26*(2), 281–286. https://doi.org/10.1161/01.ATV.0000197793.83391.91

Sakamoto, A., Torii, S., Jinnouchi, H., Finn, A. V., Virmani, R., & Kolodgie, F. D. (2018). Pathologic intimal thickening: Are we any closer to understand early transitional plaques that lead to symptomatic disease? *Atherosclerosis*, *274*, 227–229. https://doi.org/10.1016/j.atherosclerosis.2018.04.033

Salimnia, H., Patel, D., Lephart, P. R., Fairfax, M. R., & Chandrasekar, P. H. (2010). Listeria grayi: Vancomycin-resistant, gram-positive rod causing bacteremia in a stem cell transplant recipient. *Transplant Infectious Disease*, *12*(6), 526–528. https://doi.org/10.1111/j.1399-3062.2010.00539.x

Salmon, M., Gomez, D., Greene, E., Shankman, L., & Owens, G. K. (2012). Cooperative binding of KLF4, pELK-1, and HDAC2 to a G/C repressor element in the SM22α promoter mediates transcriptional silencing during SMC phenotypic switching in vivo. *Circulation Research*, *111*(6), 685–696. https://doi.org/10.1161/CIRCRESAHA.112.269811

Sanchez, L. A., & Veith, F. J. (1998). Diagnosis and treatment of chronic lower extremity ischemia. *Vascular Medicine*, *3*(4), 291–299. https://doi.org/10.1191/135886398672364993

Santos-Rosa, H., Schneider, R., Bernstein, B. E., Karabetsou, N., Morillon, A., Weise, C., Schreiber, S. L., Mellor, J., & Kouzarides, T. (2003). Methylation of histone H3 K4

mediates association of the Isw1p ATPase with chromatin. *Molecular Cell*, *12*(5), 1325–1332. https://doi.org/10.1016/S1097-2765(03)00438-6

Sarkar, D., Gentleman, R., Lawrence, M., & Yao, Z. (2013). chipseq: A package for analyzing chipseq data. *R package*

Sartore, S., Chiavegato, A., Faggin, E., Franch, R., Puato, M., Ausoni, S., & Pauletto, P. (2001). Contribution of adventitial fibroblasts to neointima formation and vascular remodeling: From innocent bystander to active participant. *Circulation Research*, *89*(12), 1111–1121. https://doi.org/10.1161/hh2401.100844

Sata, M. (2003). Circulating vascular progenitor cells contribute to vascular repair, remodeling, and lesion formation. *Trends in Cardiovascular Medicine*, *13*(6), 249–253. https://doi.org/10.1016/S1050-1738(03)00106-3

Sata, M., Saiura, A., Kunisato, A., Tojo, A., Okada, S., Tokuhisa, T., Hirai, H., Makuuchi, M., Hirata, Y., & Nagai, R. (2002). Hematopoietic stem cells differentiate into vascular cells that participate in the pathogenesis of atherosclerosis. *Nature Medicine*, *8*(4), 403–409. https://doi.org/10.1038/nm0402-403

Sawa, N., Fujimoto, H., Sawa, Y., & Yamashita, J. (2019). Alternating Differentiation and Dedifferentiation between Mature Osteoblasts and Osteocytes. *Scientific Reports*, *9*(1), 1–9. https://doi.org/10.1038/s41598-019-50236-7

Sawicka, A., & Seiser, C. (2012). Histone H3 phosphorylation - A versatile chromatin modification for different occasions. *Biochimie*, *94*(11), 2193–2201. https://doi.org/10.1016/j.biochi.2012.04.018

Schmid, M., Rè Se Durussel, T., & Laemmli, U. K. (2004). Technique ChIC and ChEC: Genomic Mapping of Chromatin Proteins ble, and significant amounts are lost into the pellet dur-ing centrifugation. While ChIP is highly successful when applied to solu. *Molecular Cell*, *16*, 147–157.

Schneider, C. A., Rasband, W. S., & Eliceiri, K. W. (2012). NIH Image to ImageJ: 25 years of image analysis. *Nature Methods*, *9*(7), 671–675. https://doi.org/10.1038/nmeth.2089

Schwartz, S. M., deBlois, D., & O'Brien, E. R. (1995). The intima: soil for atherosclerosis and restenosis. *Circulation research*, *77*(3), 445-465. https://doi.org/10.1161/01.RES.77.3.445

Segal, E., Fondufe-Mittendorf, Y., Chen, L., Thåström, A., Field, Y., Moore, I. K., Wang, J. P. Z., & Widom, J. (2006). A genomic code for nucleosome positioning. *Nature*, *442*(7104),

772–778. https://doi.org/10.1038/nature04979

Serbedzija, G. N., Bronner-Fraser, M., & Fraser, S. E. (1989). A vital dye analysis of the timing and pathways of avian trunk neural crest cell migration. *Development*, *106*(4), 809–816. https://doi.org/10.1242/dev.106.4.809

Seri, B., García-Verdugo, J. M., Collado-Morente, L., McEwen, B. S., & Alvarez-Buylla, A. (2004). Cell types, lineage, and architecture of the germinal zone in the adult dentate gyrus. *Journal of Comparative Neurology*, *478*(4), 359–378. https://doi.org/10.1002/cne.20288

Sera, Y., LaRue, A. C., Moussa, O., Mehrotra, M., Duncan, J. D., Williams, C. R., ... & Ogawa, M. (2009). Hematopoietic stem cell origin of adipocytes. *Experimental hematology*, *37*(9), 1108-1120. https://doi.org/10.1016/j.exphem.2009.06.008

Shankman, L. S., Gomez, D., Cherepanova, O. A., Salmon, M., Alencar, G. F., Haskins, R. M., Swiatlowska, P., Newman, A. A. C., Greene, E. S., Straub, A. C., Isakson, B., Randolph, G. J., & Owens, G. K. (2015). KLF4-dependent phenotypic modulation of smooth muscle cells has a key role in atherosclerotic plaque pathogenesis. *Nature Medicine*, *21*(6), 628–637. https://doi.org/10.1038/nm.3866

Shaw, L. J., Bairey Merz, C. N., Pepine, C. J., Reis, S. E., Bittner, V., Kelsey, S. F., Olson, M., Johnson, B. D., Mankad, S., Sharaf, B. L., Rogers, W. J., Wessel, T. R., Arant, C. B., Pohost, G. M., Lerman, A., Quyyumi, A. A., & Sopko, G. (2006). Insights from the NHLBI-sponsored Women's Ischemia Syndrome Evaluation (WISE) study. Part I: Gender differences in traditional and novel risk factors, symptom evaluation, and gender-optimized diagnostic strategies. *Journal of the American College of Cardiology*, *47*(3 SUPPL.), S4–S20. https://doi.org/10.1016/j.jacc.2005.01.072

Shendure, J., & Ji, H. (2008). Next-generation DNA sequencing. *Nature Biotechnology*, *26*(10), 1135–1145. https://doi.org/10.1038/nbt1486

Shi, H., Wang, Q., Zhang, Q., Leng, L., & Li, H. (2010). Tissue expression characterization of chicken adipocyte fatty acid-binding protein and its expression difference between fat and lean birds in abdominal fat tissue. *Poultry Science*, *89*(2), 197–202. https://doi.org/10.3382/ps.2009-00397

Shi, N., & Chen, S. Y. (2016). Smooth Muscle Cell Differentiation: Model Systems, Regulatory Mechanisms, and Vascular Diseases. *Journal of Cellular Physiology*, *231*(4), 777–787.

https://doi.org/10.1002/jcp.25208

Shi, X., Hong, T., Walter, K. L., Ewalt, M., Michishita, E., Hung, T., Carney, D., Peña, P., Lan, F., Kaadige, M. R., Lacoste, N., Cayrou, C., Davrazou, F., Saha, A., Cairns, B. R., Ayer, D. E., Kutateladze, T. G., Shi, Y., Côté, J., … Gozani, O. (2006). ING2 PHD domain links histone H3 lysine 4 methylation to active gene repression. *Nature*, *442*(7098), 96–99. https://doi.org/10.1038/nature04835

Shimizu, K., Sugiyama, S., Aikawa, M., Fukumoto, Y., Rabkin, E., Libby, P., & Mitchell, R. N. (2001). Host bone-marrow cells are a source of donor intimal smoothmuscle-like cells in murine aortic transplant arteriopathy. *Nature Medicine*, *7*(6), 738–741. https://doi.org/10.1038/89121

Shin, H., Liu, T., Duan, X., Zhang, Y., & Liu, X. S. (2013). Computational methodology for ChIP-seq analysis. *Quantitative Biology*, *1*(1), 54–70. https://doi.org/10.1007/s40484-013-0006-2

Shin, M., Nagai, H., & Sheng, G. (2009). Notch mediates Wnt and BMP signals in the early separation of smooth muscle progenitors and blood/endothelial common progenitors. *Development*, *136*(4), 595–603. https://doi.org/10.1242/dev.026906

Sims, R. J., Chen, C. F., Santos-Rosa, H., Kouzarides, T., Patel, S. S., & Reinberg, D. (2005). Human but not yeast CHD1 binds directly and selectively to histone H3 methylated at lysine 4 via its tandem chromodomains. *Journal of Biological Chemistry*, *280*(51), 41789–41792. https://doi.org/10.1074/jbc.C500395200

Sims III, R. J., Nishioka, K., & Reinberg, D. (2003). Histone lysine methylation: a signature for chromatin function. *TRENDS in Genetics*, *19*(11), 629-639. https://doi.org/10.1016/j.tig.2003.09.007

Sinha, S., Hoofnagle, M. H., Kingston, P. A., McCanna, M. E., & Owens, G. K. (2004). Transforming growth factor-β1 signaling contributes to development of smooth muscle cells from embryonic stem cells. *American Journal of Physiology - Cell Physiology*, *287*(6 56-6), 1560–1568. https://doi.org/10.1152/ajpcell.00221.2004

Sinha, S., Iyer, D., & Granata, A. (2014). Embryonic origins of human vascular smooth muscle cells: Implications for in vitro modeling and clinical application. *Cellular and Molecular Life Sciences*, *71*(12), 2271–2288. https://doi.org/10.1007/s00018-013-1554-3

Skene, P. J., Henikoff, J. G., & Henikoff, S. (2018). Targeted in situ genome-wide profiling with high efficiency for low cell numbers. *Nature Protocols*, *13*(5), 1006–1019.

https://doi.org/10.1038/nprot.2018.015

Skene, P. J., & Henikoff, S. (2017). An efficient targeted nuclease strategy for high-resolution mapping of DNA binding sites. *ELife*, *6*, 1–35. https://doi.org/10.7554/eLife.21856

Söderberg, O., Gullberg, M., Jarvius, M., Ridderstråle, K., Leuchowius, K. J., Jarvius, J., Wester, K., Hydbring, P., Bahram, F., Larsson, L. G., & Landegren, U. (2006). Direct observation of individual endogenous protein complexes in situ by proximity ligation. *Nature Methods*, *3*(12), 995–1000. https://doi.org/10.1038/nmeth947

Söderberg, O., Leuchowius, K. J., Gullberg, M., Jarvius, M., Weibrecht, I., Larsson, L. G., & Landegren, U. (2008). Characterizing proteins and their interactions in cells and tissues using the in situ proximity ligation assay. *Methods*, *45*(3), 227–232. https://doi.org/10.1016/j.ymeth.2008.06.014

Solomon, M. J., & Varshavsky, A. (1985). Formaldehyde-mediated DNA-protein crosslinking: A probe for in vivo chromatin structures. *Proceedings of the National Academy of Sciences of the United States of America*, *82*(19), 6470–6474. https://doi.org/10.1073/pnas.82.19.6470

Speer, M. Y., Yang, H. Y., Brabb, T., Leaf, E., Look, A., Lin, W. L., Frutkin, A., Dichek, D., & Giachelli, C. M. (2009). Smooth muscle cells give rise to osteochondrogenic precursors and chondrocytes in calcifying arteries. *Circulation Research*, *104*(6), 733–741. https://doi.org/10.1161/CIRCRESAHA.108.183053

Spin, J. M., Maegdefessel, L., & Tsao, P. S. (2012). Vascular smooth muscle cell phenotypic plasticity: Focus on chromatin remodelling. In *Cardiovascular Research*. https://doi.org/10.1093/cvr/cvs098

Spin, J. M., Nallamshetty, S., Tabibiazar, R., Ashley, E. A., King, J. Y., Chen, M., Tsao, P. S., & Quertermous, T. (2005). Transcriptional profiling of in vitro smooth muscle cell differentiation identifies specific patterns of gene and pathway activation. *Physiological Genomics*, *19*(30), 292–302. https://doi.org/10.1152/physiolgenomics.00148.2004

Spin, J. M., Quertermous, T., & Tsao, P. S. (2010). Chromatin remodeling pathways in smooth muscle cell differentiation, and evidence for an integral role for p300. *PLoS ONE*, *5*(12). https://doi.org/10.1371/journal.pone.0014301

Ss, V., Alonso, A., Hj, A., Ej, B., Ms, B., & Cw, C. (2021). Heart Disease and Stroke Statistics-2021 Update A Report from the American Heart Association. *Circulation*, E254–E743. https://doi.org/10.1161/CIR.0000000000000950

Strenkert, D., Yildirim, A., Yan, J., Yoshinaga, Y., Pellegrini, M., O'Malley, R.C., Merchant, S.S. and Umen, J.G. (2022), The landscape of Chlamydomonas histone H3 lysine 4 methylation reveals both constant features and dynamic changes during the diurnal cycle. Plant J. https://doi.org/10.1111/tpj.15948

Stocker, R., & Keaney, J. F. (2004). Role of Oxidative Modifications in Atherosclerosis. *Physiological Reviews*, *84*(4), 1381–1478. https://doi.org/10.1152/physrev.00047.2003

Strahl, B. D., & Allis, C. D. (2000). The language of covalent histone modifications. *Nature*. https://doi.org/10.1038/47412

Sun SG, Zheng B, Han M, Fang XM, Li HX, Miao SB, Su M, Han Y, Shi HJ, Wen JK. miR-146a and Krüppel-like factor 4 form a feedback loop to participate in vascular smooth muscle cell proliferation. EMBO Rep. 2011;12:56–62. doi: 10.1038/embor.2010.172

Tabas, I., Williams, K. J., & Borén, J. (2007). Subendothelial Lipoprotein Retention as the Initiating Process in Atherosclerosis. *Circulation*, *116*(16), 1832–1844. https://doi.org/10.1161/circulationaha.106.676890

Tanabe, K., Nakamura, M., Narita, M., Takahashi, K., & Yamanaka, S. (2013). Maturation, not initiation, is the major roadblock during reprogramming toward pluripotency from human fibroblasts. *Proceedings of the National Academy of Sciences of the United States of America*, *110*(30), 12172–12179. https://doi.org/10.1073/pnas.1310291110

Tang, J., Wang, H., Huang, X., Li, F., Zhu, H., Li, Y., He, L., Zhang, H., Pu, W., Liu, K., Zhao, H., Bentzon, J. F., Yu, Y., Ji, Y., Nie, Y., Tian, X., Zhang, L., Gao, D., & Zhou, B. (2020). Arterial Sca1+ Vascular Stem Cells Generate De Novo Smooth Muscle for Artery Repair and Regeneration. *Cell Stem Cell*, *26*(1), 81-96.e4. https://doi.org/10.1016/j.stem.2019.11.010

Tang, Z., Wang, A., Yuan, F., Yan, Z., Liu, B., Chu, J. S., Helms, J. A., & Li, S. (2012). Differentiation of multipotent vascular stem cells contributes to vascular diseases. *Nature Communications*, *3*. https://doi.org/10.1038/ncomms1867

Tao, H., Shi, K. H., Yang, J. J., & Li, J. (2016). Epigenetic mechanisms in atrial fibrillation: New insights and future directions. *Trends in Cardiovascular Medicine*, *26*(4), 306–318. https://doi.org/10.1016/j.tcm.2015.08.006

Targets, S., & Targets, D. (2015). 8. Cardiovascular Disease and Risk Management. *Diabetes Care*, *39*(Supplement 1), S60–S71. https://doi.org/10.2337/dc16-s011

Taura, D., Noguchi, M., Sone, M., Hosoda, K., Mori, E., Okada, Y., Takahashi, K., Homma, K.,

Oyamada, N., Inuzuka, M., Sonoyama, T., Ebihara, K., Tamura, N., Itoh, H., Suemori, H., Nakatsuji, N., Okano, H., Yamanaka, S., & Nakao, K. (2009). Adipogenic differentiation of human induced pluripotent stem cells: Comparison with that of human embryonic stem cells. *FEBS Letters*, *583*(6), 1029–1033. https://doi.org/10.1016/j.febslet.2009.02.031

Taura, D., Sone, M., Homma, K., Oyamada, N., Takahashi, K., Tamura, N., Yamanaka, S., & Nakao, K. (2009). Induction and isolation of vascular cells from human induced pluripotent stem cells - Brief report. *Arteriosclerosis, Thrombosis, and Vascular Biology*, *29*(7), 1100–1103. https://doi.org/10.1161/ATVBAHA.108.182162

Ten Dijke, P., & Arthur, H. M. (2007). Extracellular control of TGFβ signalling in vascular development and disease. *Nature Reviews Molecular Cell Biology*, *8*(11), 857–869. https://doi.org/10.1038/nrm2262

Ten Dijke, P., & Hill, C. S. (2004). New insights into TGF-β-Smad signalling. *Trends in Biochemical Sciences*, *29*(5), 265–273. https://doi.org/10.1016/j.tibs.2004.03.008

Tesfamariam, B., & Cohen, R. A. (1992). Free radicals mediate endothelial cell dysfunction caused by elevated glucose. *American Journal of Physiology - Heart and Circulatory Physiology*, *263*(2 32-2). https://doi.org/10.1152/ajpheart.1992.263.2.h321

Teytelman, L., Thurtle, D. M., Rine, J., & Van Oudenaarden, A. (2013). Highly expressed loci are vulnerable to misleading ChIP localization of multiple unrelated proteins. *Proceedings of the National Academy of Sciences of the United States of America*, *110*(46), 18602–18607. https://doi.org/10.1073/pnas.1316064110

Tieu, B. C., Lee, C., Sun, H., LeJeune, W., Recinos, A., Ju, X., Spratt, H., Guo, D. C., Milewicz, D., Tilton, R. G., & Brasier, A. R. (2009). An adventitial IL-6/MCP1 amplification loop accelerates macrophage-mediated vascular inflammation leading to aortic dissection in mice. *Journal of Clinical Investigation*, *119*(12), 3637–3651. https://doi.org/10.1172/JCI38308

Tintut, Y., Alfonso, Z., Saini, T., Radcliff, K., Watson, K., Boström, K., & Demer, L. L. (2003). Multilineage Potential of Cells from the Artery Wall. *Circulation*, *108*(20), 2505–2510. https://doi.org/10.1161/01.CIR.0000096485.64373.C5

Tirkkonen, L., Haimi, S., Huttunen, S., Wolff, J., Pirhonen, E., Sándor, G., & Miettinen, S. (2013). Osteogenic medium is superior to growth factors in differentiation of human adipose stem cells towards bone-forming cells in 3D culture. *European Cells and*

Materials, *25*, 144–158. https://doi.org/10.22203/ecm.v025a10

Toghill, B. J., Saratzis, A., Harrison, S. C., Verissimo, A. R., Mallon, E. B., & Bown, M. J. (2015). The potential role of DNA methylation in the pathogenesis of abdominal aortic aneurysm. *Atherosclerosis*, *241*(1), 121–129. https://doi.org/10.1016/j.atherosclerosis.2015.05.001

Tokumoto, Y., Ogawa, S., Nagamune, T., & Miyake, J. (2010). Comparison of efficiency of terminal differentiation of oligodendrocytes from induced pluripotent stem cells versus embryonic stem cells in vitro. *Journal of Bioscience and Bioengineering*, *109*(6), 622–628. https://doi.org/10.1016/j.jbiosc.2009.11.013

Torella, D., Iaconetti, C., Catalucci, D., Ellison, G. M., Leone, A., Waring, C. D., Bochicchio, A., Vicinanza, C., Aquila, I., Curcio, A., Condorelli, G., & Indolfi, C. (2011). MicroRNA-133 controls vascular smooth muscle cell phenotypic switch in vitro and vascular remodeling in vivo. *Circulation Research*, *109*(8), 880–893. https://doi.org/10.1161/CIRCRESAHA.111.240150

Torsney, E., Hu, Y., & Xu, Q. (2005). Adventitial progenitor cells contribute to arteriosclerosis. *Trends in Cardiovascular Medicine*, *15*(2), 64–68. https://doi.org/10.1016/j.tcm.2005.02.003

Uchida, K., Sasahara, M., Morigami, N., Hazama, F., & Kinoshita, M. (1996). Expression of platelet-derived growth factor B-chain in neointimal smooth muscle cells of balloon injured rabbit femoral arteries. *Atherosclerosis*, *124*(1), 9–23. https://doi.org/10.1016/0021-9150(95)05742-0

Urnov, F. D., & Wolffe, A. P. (2001). Above and within the genome: Epigenetics past and present. *Journal of Mammary Gland Biology and Neoplasia*, *6*(2), 153–167. https://doi.org/10.1023/A:1011304606604

Urry, D. W. (1971). Neutral Sites for Calcium Ion Binding. *Proceedings of the National Academy of Sciences USA*, *68*(4), 810–814.mhttps://doi.org/10.1073/pnas.68.4.810

Valouev, A., Johnson, D. S., Sundquist, A., Medina, C., Anton, E., Batzoglou, S., Myers, R. M., & Sidow, A. (2008). Genome-wide analysis of transcription factor binding sites based on ChIP-Seq data. *Nature Methods*, *5*(9), 829–834. https://doi.org/10.1038/nmeth.1246

Velican, C., & Velican, D. (1981). Coronary intimal necrosis occurring as an early stage of atherosclerotic involvement. *Atherosclerosis*, *39*(4), 479-496. https://doi.org/10.1016/0021-9150(81)90006-X

Verrecchia, F., & Mauviel, A. (2002). Transforming growth factor-β signaling through the Smad pathway: Role in extracellular matrix gene expression and regulation. *Journal of Investigative Dermatology*, *118*(2), 211–215. https://doi.org/10.1046/j.1523-1747.2002.01641.x

Virmani, R., Kolodgie, F. D., Burke, A. P., Farb, A., & Schwartz, S. M. (2000). Lessons From Sudden Coronary Death. *Arteriosclerosis, Thrombosis, and Vascular Biology*, *20*(5), 1262–1275. https://doi.org/10.1161/01.atv.20.5.1262

Visel, A., Blow, M. J., Li, Z., Zhang, T., Akiyama, J. A., Holt, A., Plajzer-Frick, I., Shoukry, M., Wright, C., Chen, F., Afzal, V., Ren, B., Rubin, E. M., & Pennacchio, L. A. (2009). ChIP-seq accurately predicts tissue-specific activity of enhancers. *Nature*, *457*(7231), 854–858. https://doi.org/10.1038/nature07730

Waggoner, D. (2007). Mechanisms of Disease: Epigenesis. *Seminars in Pediatric Neurology*, *14*(1), 7–14. https://doi.org/10.1016/j.spen.2006.11.004

Wakil, S. J. (1989). Fatty Acid Synthase, A Proficient Multifunctional Enzyme. *Biochemistry*, *28*(11), 4523–4530. https://doi.org/10.1021/bi00437a001

Wan, M., Li, C., Zhen, G., Jiao, K., He, W., Jia, X., Wang, W., Shi, C., Xing, Q., Chen, Y. F., De Beur, S. J., Yu, B., & Cao, X. (2012). Injury-activated transforming growth factor β controls mobilization of mesenchymal stem cells for tissue remodeling. *Stem Cells*, *30*(11), 2498–2511. https://doi.org/10.1002/stem.1208

Wan, X., Liu, L., Ding, X., Zhou, P., Yuan, X., Zhou, Z., Hu, P., Zhou, H., Li, Q., Zhang, S., Xiong, S., & Zhang, Y. (2014). Mll2 Controls Cardiac Lineage Differentiation of Mouse Embryonic Stem Cells by Promoting H3K4me3 Deposition at Cardiac-Specific Genes. *Stem Cell Reviews and Reports*, *10*(5), 643–652. https://doi.org/10.1007/s12015-014-9527-y

Wang, C., Cen, L., Yin, S., Liu, Q., Liu, W., Cao, Y., & Cui, L. (2010). A small diameter elastic blood vessel wall prepared under pulsatile conditions from polyglycolic acid mesh and smooth muscle cells differentiated from adipose-derived stem cells. *Biomaterials*, *31*(4), 621-630. https://doi.org/10.1016/j.biomaterials.2009.09.086

Wang, D., Li, L. A. K., Dai, T., Wang, A., & Li, S. (2018). Adult stem cells in vascular remodeling. *Theranostics*, *8*(3), 815–829. https://doi.org/10.7150/THNO.19577

Wang, D. Z., Chang, P. S., Wang, Z., Sutherland, L., Richardson, J. A., Small, E., Krieg, P. A., &

Olson, E. N. (2001). Activation of cardiac gene expression by myocardin, a transcriptional cofactor for serum response factor. *Cell*, *105*(7), 851–862. https://doi.org/10.1016/S0092-8674(01)00404-4

Wang, G., Jacquet, L., Karamariti, E., & Xu, Q. (2015). Origin and differentiation of vascular smooth muscle cells. *Journal of Physiology*, *593*(14), 3013–3030. https://doi.org/10.1113/JP270033

Wang, H., Cao, R., Xia, L., Erdjument-Bromage, H., Borchers, C., Tempst, P., & Zhang, Y. (2001). Purification and functional characterization of a histone H3-lysine 4-specific methyltransferase. *Molecular Cell*, *8*(6), 1207–1217. https://doi.org/10.1016/S1097-2765(01)00405-1

Wang, L., Pasha, Z., Wang, S., Li, N., Feng, Y., Lu, G., Millard, R. W., & Ashraf, M. (2013). Protein Kinase G1 α Overexpression Increases Stem Cell Survival and Cardiac Function after Myocardial Infarction. *PLoS ONE*, *8*(3). https://doi.org/10.1371/journal.pone.0060087

Wang, S., Zhang, Y., Xu, Q., Yuan, X., Dai, W., Shen, X., Wang, Z., Chang, G., Wang, Z., & Chen, G. (2018). The differentiation of preadipocytes and gene expression related to adipogenesis in ducks (Anas platyrhynchos). *PLoS ONE*, *13*(5), 1–13. https://doi.org/10.1371/journal.pone.0196371

Weinmann, A. S., Yan, P. S., Oberley, M. J., Huang, T. H. M., & Farnham, P. J. (2002). Isolating human transcription factor targets by coupling chromatin immunoprecipitation and CpG island microarray analysis. *Genes and Development*, *16*(2), 235–244. https://doi.org/10.1101/gad.943102

Weissman, I. L. (2000). Stem cells: Units of development, units of regeneration, and units in evolution. *Cell*, *100*(1), 157–168. https://doi.org/10.1016/S0092-8674(00)81692-X

Westermark, B., Siegbahn, A., Heldin, C. H., & Claesson-Welsh, L. (1990). B-type receptor for platelet-derived growth factor mediates a chemotactic response by means of ligand-induced activation of the receptor protein-tyrosine kinase. *Proceedings of the National Academy of Sciences of the United States of America*, *87*(1), 128–132. https://doi.org/10.1073/pnas.87.1.128

Wick, G., Knoflach, M., & Xu, Q. (2004). Autoimmune and Inflammatory Mechanisms in Atherosclerosis. *Annual Review of Immunology*, *22*(1), 361–403. https://doi.org/10.1146/annurev.immunol.22.012703.104644

Williams, A. R., Suncion, V. Y., McCall, F., Guerra, D., Mather, J., Zambrano, J. P., Heldman, A. W., & Hare, J. M. (2013). Durable Scar Size Reduction Due to Allogeneic Mesenchymal Stem Cell Therapy Regulates Whole-Chamber Remodeling. *Journal of the American Heart Association*, *2*(3), 1–9. https://doi.org/10.1161/jaha.113.000140

Williams, R. R. E., Azuara, V., Perry, P., Sauer, S., Dvorkina, M., Jørgensen, H., Roix, J., McQueen, P., Misteli, T., Merkenschlager, M., & Fisher, A. G. (2006). Neural induction promotes large-scale chromatin reorganisation of the Mash1 locus. *Journal of Cell Science*, *119*(1), 132–140. https://doi.org/10.1242/jcs.02727

Woods K, Guezguez B. Dynamic Changes of the Bone Marrow Niche: Mesenchymal Stromal Cells and Their Progeny During Aging and Leukemia. Front Cell Dev Biol. 2021 Aug 10;9:714716. doi: 10.3389/fcell.2021.714716. PMID: 34447754; PMCID: PMC8383146.

Wu H, Gordon JA, Whitfield TW, Tai PW, van Wijnen AJ, Stein JL, Stein GS, Lian JB. Chromatin dynamics regulate mesenchymal stem cell lineage-specification and differentiation to osteogenesis. Biochim Biophys Acta Gene Regul Mech. 2017 Apr;1860(4):438-449. doi: 10.1016/j.bbagrm.2017.01.003. Epub 2017 Jan 8. PMID: 28077316; PMCID: PMC5385709.

Wysocka, J., Swigut, T., Milne, T. A., Dou, Y., Zhang, X., Burlingame, A. L., Roeder, R. G., Brivanlou, A. H., & Allis, C. D. (2005). WDR5 associates with histone H3 methylated at K4 and is essential for H3 K4 methylation and vertebrate development. *Cell*, *121*(6), 859–872. https://doi.org/10.1016/j.cell.2005.03.036

Wysocka, J., Swigut, T., Xiao, H., Milne, T. A., Kwon, S. Y., Landry, J., Kauer, M., Tackett, A. J., Chait, B. T., Badenhorst, P., Wu, C., & Allis, C. D. (2006). A PHD finger of NURF couples histone H3 lysine 4 trimethylation with chromatin remodelling. *Nature*, *442*(7098), 86–90. https://doi.org/10.1038/nature04815

Xi, J., Khalil, M., Shishechian, N., Hannes, T., Pfannkuche, K., Liang, H., Fatima, A., Haustein, M., Suhr, F., Bloch, W., Reppel, M., Šarić, T., Wernig, M., Jänisch, R., Brockmeier, K., Hescheler, J., & Pillekamp, F. (2010). Comparison of contractile behavior of native murine ventricular tissue and cardiomyocytes derived from embryonic or induced pluripotent stem cells. *The FASEB Journal*, *24*(8), 2739–2751. https://doi.org/10.1096/fj.09-145177

Xiang, C. C., Kozhich, O. A., Chen, M., Inman, J. M., Phan, Q. N., Chen, Y., & Brownstein, M. J. (2002). Amine-modified random primers to label probes for DNA microarrays. *Nature*

Biotechnology, *20*(7), 738–742. https://doi.org/10.1038/nb0702-738

Xiao, L., Liu, Y., & Wang, N. (2014). New paradigms in inflammatory signaling in vascular endothelial cells. In *American Journal of Physiology - Heart and Circulatory Physiology,* 306 (3). https://doi.org/10.1152/ajpheart.00182.2013

Xiao, Q., Zeng, L., Zhang, Z., Hu, Y., & Xu, Q. (2007). Stem cell-derived Sca-1+ progenitors differentiate into smooth muscle cells, which is mediated by collagen IV-integrin α1/β1/αv and PDGF receptor pathways. *American Journal of Physiology - Cell Physiology*, *292*(1), 342–352. https://doi.org/10.1152/ajpcell.00341.2006

Xie, C., Ritchie, R. P., Huang, H., Zhang, J., & Chen, Y. E. (2011). Smooth muscle cell differentiation in vitro: Models and underlying molecular mechanisms. *Arteriosclerosis, Thrombosis, and Vascular Biology*, *31*(7), 1485–1494. https://doi.org/10.1161/ATVBAHA.110.221101

Xie, D., Boyle, A. P., Wu, L., Zhai, J., Kawli, T., & Snyder, M. (2013). XDynamic trans-acting factor colocalization in human cells. *Cell*, *155*(3), 713. https://doi.org/10.1016/j.cell.2013.09.043

Xu, S., Kamato, D., Little, P. J., Nakagawa, S., Pelisek, J., & Jin, Z. G. (2019). Targeting epigenetics and non-coding RNAs in atherosclerosis: from mechanisms to therapeutics. *Pharmacology and Therapeutics*, *196*, 15–43. https://doi.org/10.1016/j.pharmthera.2018.11.003

Yamashita, J., Itoh, H., Hirashima, M., Ogawa, M., Nishikawa, S., Yurugi, T., Naito, M., Nakao, K., & Nishikawa, S. I. (2000). Flk1-positive cells derived from embryonic stem cells serve as vascular progenitors. *Nature*, *408*(6808), 92–96. https://doi.org/10.1038/35040568

Yan, F. fang, Liu, Y. F., Liu, Y., & Zhao, Y. X. (2008). KLF4: A novel target for the treatment of atherosclerosis. *Medical Hypotheses*, *70*(4), 845–847. https://doi.org/10.1016/j.mehy.2007.07.031

Yang W, Ernst P. Distinct functions of histone H3, lysine 4 methyltransferases in normal and malignant hematopoiesis. Curr Opin Hematol. 2017 Jul;24(4):322-328. doi: 10.1097/MOH.0000000000000346.

Yang, J., Corsello, T. R., & Ma, Y. (2012). Stem cell gene SALL4 suppresses transcription through recruitment of DNA methyltransferases. *Journal of Biological Chemistry*, *287*(3), 1996–2005. https://doi.org/10.1074/jbc.M111.308734

Yap, C., Mieremet, A., De Vries, C. J. M., Micha, D., & De Waard, V. (2021). Six shades of

vascular smooth muscle cells illuminated by klf4 (krüppel-like factor 4). *Arteriosclerosis, Thrombosis, and Vascular Biology*, *4*(November), 2693–2707. https://doi.org/10.1161/ATVBAHA.121.316600

Ye, T., Krebs, A. R., Choukrallah, M. A., Keime, C., Plewniak, F., Davidson, I., & Tora, L. (2011). seqMINER: an integrated ChIP-seq data interpretation platform. *Nucleic acids research*, *39*(6), e35-e35. https://doi.org/10.1093/nar/gkq1287

Yia-Herttuala, S., Palinski, W., Rosenfeld, M. E., Parthasarathy, S., Carew, T. E., Butler, S., Witztum, J. L., & Steinberg, D. (1989). Evidence for the presence of oxidatively modified low density lipoprotein in atherosclerotic lesions of rabbit and man. *Journal of Clinical Investigation*, *84*(4), 1086–1095. https://doi.org/10.1172/jci114271

Yoshida, T., Gan, Q., Shang, Y., & Owens, G. K. (2007). Platelet-derived growth factor-BB represses smooth muscle cell marker genes via changes in binding of MKL factors and histone deacetylases to their promoters. *American Journal of Physiology - Cell Physiology*, *292*(2), 886–895. https://doi.org/10.1152/ajpcell.00449.2006

Yu, H., Stoneman, V., Clarke, M., Figg, N., Xin, H. B., Kotlikoff, M., Littlewood, T., & Bennett, M. (2011). Bone marrow-derived smooth muscle-like cells are infrequent in advanced primary atherosclerotic plaques but promote atherosclerosis. *Arteriosclerosis, Thrombosis, and Vascular Biology*, *31*(6), 1291–1299. https://doi.org/10.1161/ATVBAHA.110.218578

Yuan, X., Xiao, H., Hu, Q., Shen, G., & Qin, X. (2022). RGMa promotes dedifferentiation of vascular smooth muscle cells into a macrophage-like phenotype in vivo and in vitro. *Journal of Lipid Research*, 100276.https://doi.org/10.1016/j.jlr.2022.100276

Yuan, F., Wang, D., Xu, K., Wang, J., Zhang, Z., Yang, L., Yang, G. Y., & Li, S. (2017). Contribution of vascular cells to neointimal formation. *PLoS ONE*, *12*(1), 1–11. https://doi.org/10.1371/journal.pone.0168914

Yusuf, S., Reddy, S., Ôunpuu, S., & Anand, S. (2001). Clinical Cardiology : New Frontiers Global Burden of Cardiovascular Diseases. *Circulation*, *104*(C), 2746–2753. https://doi.org/10.1161/hc4601.099487

Zachary, I., & Morgan, R. D. (2011). Therapeutic angiogenesis for cardiovascular disease: Biological context, challenges, prospects. *Heart*, *97*(3), 181–189. https://doi.org/10.1136/hrt.2009.180414

Zazzeroni, L., Faggioli, G., & Pasquinelli, G. (2018). Mechanisms of Arterial Calcification: The

Role of Matrix Vesicles. *European Journal of Vascular and Endovascular Surgery*, *55*(3), 425–432. https://doi.org/10.1016/j.ejvs.2017.12.009

Zeisberg, E. M., Tarnavski, O., Zeisberg, M., Dorfman, A. L., McMullen, J. R., Gustafsson, E., Chandraker, A., Yuan, X., Pu, W. T., Roberts, A. B., Neilson, E. G., Sayegh, M. H., Izumo, S., & Kalluri, R. (2007). Endothelial-to-mesenchymal transition contributes to cardiac fibrosis. *Nature Medicine*, *13*(8), 952–961. https://doi.org/10.1038/nm1613

Zhang T, Cooper S, Brockdorff N. The interplay of histone modifications - writers that read. EMBO Rep. 2015 Nov;16(11):1467-81. doi: 10.15252/embr.201540945. Epub 2015 Oct 15. PMID: 26474904; PMCID: PMC4641500.

Zhang JA, Mortazavi A, Williams BA, Wold BJ, Rothenberg EV. Dynamic transformations of genome-wide epigenetic marking and transcriptional control establish T cell identity. Cell. 2012 Apr 13;149(2):467-82. doi: 10.1016/j.cell.2012.01.056. PMID: 22500808; PMCID: PMC3336965.

Zhang, H. P., Wang, Y. H., Cao, C. J., Yang, X. M., Ma, S. C., Han, X. B., Yang, X. L., Yang, A. N., Tian, J., Xu, H., Zhang, M. H., & Jiang, Y. D. (2016). A regulatory circuit involving miR-143 and DNMT3a mediates vascular smooth muscle cell proliferation induced by homocysteine. *Molecular Medicine Reports*, *13*(1), 483–490. https://doi.org/10.3892/mmr.2015.4558

Zhang, J., Parvin, J., & Huang, K. (2012). Redistribution of H3K4me2 on neural tissue specific genes during mouse brain development. *BMC genomics*, *13*(8), 1-10. https://doi.org/10.1186/1471-2164-13-S8-S5

Zhang, J. C. L., Kim, S., Helmke, B. P., Yu, W. W., Du, K. L., Lu, M. M., Strobeck, M., Yu, Q.-C., & Parmacek, M. S. (2001). Analysis of SM22α-Deficient Mice Reveals Unanticipated Insights into Smooth Muscle Cell Differentiation and Function. *Molecular and Cellular Biology*, *21*(4), 1336–1344. https://doi.org/10.1128/mcb.2001.21.4.1336-1344.2001

Zhang, Q. J., Goddard, M., Shanahan, C., Shapiro, L., & Bennett, M. (2002). Differential gene expression in vascular smooth muscle cells in primary atherosclerosis and in stent stenosis in humans. *Arteriosclerosis, Thrombosis, and Vascular Biology*, *22*(12), 2030–2036. https://doi.org/10.1161/01.ATV.0000042206.98651.15

Zhang, Q., Zhao, K., Shen, Q., Han, Y., Gu, Y., Li, X., Zhao, D., Liu, Y., Wang, C., Zhang, X., Su, X., Liu, J., Ge, W., Levine, R. L., Li, N., & Cao, X. (2015). Tet2 is required to resolve inflammation by recruiting Hdac2 to specifically repress IL-6. *Nature*, *525*(7569), 389–

393. https://doi.org/10.1038/nature15252

Zheng, G. X. Y., Terry, J. M., Belgrader, P., Ryvkin, P., Bent, Z. W., Wilson, R., Ziraldo, S. B., Wheeler, T. D., McDermott, G. P., Zhu, J., Gregory, M. T., Shuga, J., Montesclaros, L., Underwood, J. G., Masquelier, D. A., Nishimura, S. Y., Schnall-Levin, M., Wyatt, P. W., Hindson, C. M., … Bielas, J. H. (2017). Massively parallel digital transcriptional profiling of single cells. *Nature Communications*, *8*. https://doi.org/10.1038/ncomms14049

Zhong, J., Agha, G., & Baccarelli, A. A. (2016). The Role of DNA Methylation in Cardiovascular Risk and Disease: Methodological Aspects, Study Design, and Data Analysis for Epidemiological Studies. *Circulation Research*, *118*(1), 119–131. https://doi.org/10.1161/CIRCRESAHA.115.305206

Zhou, J., & Herring, B. P. (2005). Mechanisms responsible for the promoter-specific effects of myocardin. *Journal of Biological Chemistry*, *280*(11), 10861–10869. https://doi.org/10.1074/jbc.M411586200

Zhou, S., Zhang, Y., Wang, L., Zhang, Z., Cai, B., Liu, K., Zhang, H., Dai, M., Sun, L., Xu, X., Cai, H., Liu, X., Lu, G., & Xu, G. (2016). CDKN2B methylation is associated with carotid artery calcification in ischemic stroke patients. *Journal of Translational Medicine*, *14*(1), 1–8. https://doi.org/10.1186/s12967-016-1093-4

Zhu, D., Mackenzie, N. C. W., Millan, J. L., Farquharson, C., & MacRae, V. E. (2011). The appearance and modulation of osteocyte marker expression during calcification of vascular smooth muscle cells. *PloS one*, *6*(5), e19595. https://doi.org/10.1371/journal.pone.0019595

Zhu, J. Adli, M. Zou, J.Y. G. Verstappen, M. Coyne, X. Zhang, T. Durham, M. Miri, V. Deshpande, P.L. De Jager, et al. Genome-wide chromatin state transitions associated with developmental and environmental cues Cell, 152 (2013), pp. 642-654, 10.1016/j.cell.2012.12.033

Zhuang, J., Luan, P., Li, H., Wang, K., Zhang, P., Xu, Y., & Peng, W. (2017). The yin-yang dynamics of DNA methylation is the key regulator for smooth muscle cell phenotype switch and vascular remodelling. *Arteriosclerosis, Thrombosis, and Vascular Biology*, *37*(1), 84–97. https://doi.org/10.1161/ATVBAHA.116.307923

Appendices

Appendix A

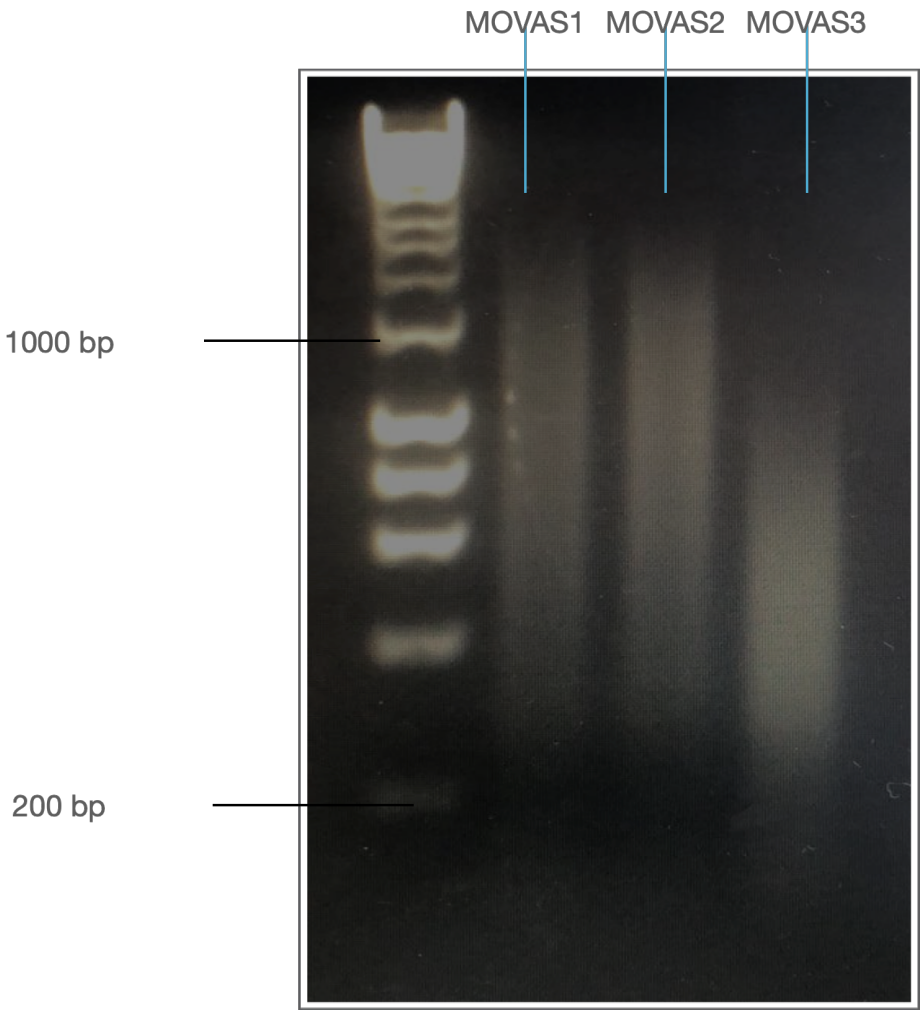

Supplementary Figure S1. Optimisation of DNA fragment size. Sheared chromatin from formaldehyde-crosslinked MOVAS cells was prepared by the following protocol. 5 µl of sheared chromatin was then electrophoresed through a 1.5% agarose gel stained with SYBR® Safe. Lane 1: MOVAS1 sonication conditions; 3 cycles, 10 seconds on 10 seconds off at 15% amp. Lane 2: MOVAS2 sonication conditions; 5 cycles 10 seconds on 10 seconds off at 15% amp. Lane 3: MOVAS3 sonication conditions; 7 cycles 10 seconds on 10 seconds off at 15% amp. Sonication was performed to test various parameters including cycles, time and amplitude. During sonication, cells are fragmented and broken open by hydrodynamic shearing by exposure to varying periods of sonication. This process sheared the chromatin to manageable-size DNA fragments (200-1000bp) (Sambrook & Russell 2001).

Appendix B

Bioinformatics Analysis

Primer Selection

B.1 Mouse primer

Myh11 myosin, heavy polypeptide 11, smooth muscle [*Mus musculus* (house mouse)]

Gene ID: 17880, updated on 16-Feb-2021

Download Datasets

Summary

Official Symbol	Myh11 provided by MGI
Official Full Name	myosin, heavy polypeptide 11, smooth muscle provided by MGI
Primary source	MGI:MGI:102643
See related	Ensembl:ENSMUSG00000018830
Gene type	protein coding
RefSeq status	VALIDATED
Organism	Mus musculus
Lineage	Eukaryota; Metazoa; Chordata; Craniata; Vertebrata; Euteleostomi; Mammalia; Eutheria; Euarchontoglires; Glires; Rodentia; Myomorpha; Muroidea; Muridae; Murinae; Mus; Mus
Also known as	SM; SM1; SM2; smMH; smMHC; AV071570
Expression	Biased expression in bladder adult (RPKM 911.5), colon adult (RPKM 71.0) and 1 other tissue See more
Orthologs	human all

Alignment

A BLAST search was carried out prior to alignment. The reverse complement of the Synthesized primer sequences was generated. The primer set was then aligned to the respective *MYH11* promoter sequence.

Description	Scientific Name	Max Score	Total Score	Query Cover	E value	Per. Ident	Acc. Len	Accession
PREDICTED: Mus musculus myosin, heavy polypeptide 11, smooth muscle (Myh1...	Mus musculus	36.2	36.2	100%	10.0	100.00%	7432	XM_006521844.2
PREDICTED: Mus musculus myosin, heavy polypeptide 11, smooth muscle (Myh1...	Mus musculus	36.2	36.2	100%	10.0	100.00%	7393	XM_006521843.2

>XM_006521844.2 PREDICTED: Mus musculus myosin, heavy polypeptide 11, smooth muscle (*Myh11*), transcript variant X2, mRNA

AGCTAGAGTGTAATGGAGAGTGTGTCAGGTCCGACAAAAGAGACAGGGAGACAGGGACCTAGATCCATACAGGGCTAAGGGAAAGAGATTGAGAAGTATCCCTTGCTGAGGGGGGACAGCTGTGAACTTGCGGGGGACCAGCAAGTACCCCGCATTC
TCTTAGGGTCTTAGCACGCATCCTCCAAGTGCCATAATGCACTCTTTCTCCAGCAGCACCCCGCTTTTCAACGATGTTCAGAGAAACCACGTTATTGGTTCCAGGCACCCTGGGATTATATTTAATTTTGGTTGTAGCATGAATGGAACTGCAAAGAACAAGT
TAGGAAAAACAAGTTTCCCTTTCTTTTCCCACACATTCCCAGCAGTCACTGGAGGATATGCGGTGACCTGCTTTGCACCTTGCAGAGTTCAAAAAAAAAAAAAAAAAAATCACCTTTCCCCTCCCTTTGCTAAACACAACCGCCCTCAGATCTAAGAGGTGGCA
GGTGAATGAAGAGGGGATGAAGGAGAGTGGGAGGTATCAAGCCTCCAGTATGTATGAACAGGAAGAGGTTAAAATCCAGCTGGAATGGACCTAGGGGGAGAAATTCTCACGTTTCCCTACAGACTCTGTATACCGGATTCCTTTTCTGTAAGGACCCAG
GATCTGGGTGGCTACAGGGAGCGAAGCCTGAGGCTGTGGGTCAGTGCGGCTCTGTTCCTCACCTGCAGGGGGCGCCGCGAAGGGAAGAGGATCCTCCCACTCTCGGACGTCCGACAGCCACCTCCCCTTTCCACTCTCAGATAGCGCTGACTCTATAAAG
CCAGGCGTCCGAAGCTTACAGAGAGATTTGGACCATCCCAGCCTGGGATCAGTGCCAGATCCGAGCTCTCCATCCGGTGTCCTCCTGCTAATCCACCCCCGGAGTAGATCTGGGACCACCAGACATCATGGCGCAGAAAGGGCAGCTCAGCGATGATGAG
AAGTTCCTCTTTGTGGATAAAAACTTCATGAACAGCCCAATGGCTCAGGCCGACTGGGTAGCCAAGAAGCTGGTGTGGGTCCCTTCAGAGAAGCAGGGCTTCGAAGCAGCCAGCATCAAGGAGGAGAAGGGCGATGAGGTGGTCGTGGAGTTGGTGGA
AAATGGAAAGAAGGTCACAGTTGGCAAAGATGACATCCAAAAAATGAACCCACCCAAGTTCTCTAAGGTGGAGGACATGGCAGAGCTGACGTGCCTCAATGAGGCCTCTGTGCTGCACAACCTGAGGGAGCGATACTTCTCAGGCCTCATCTATACCTAC
TCTGGCCTCTTCTGTGTGGTGGTCAACCCCTACAAGTACCTACCCATCTACTCAGAAAAGATCGTGGATATGTACAAGGGCAAGAAGAGGCATGAGATGCCGCCTCACATCTATGCCATTGCCGACACAGCCTACAGAAGCATGCTACAAGATCGTGAAGA
CCAGTCCATTCTGTGCACAGGTGAGTCTGGAGCCGGAAAGACAGAGAACACAAAGAAAGTCATACAGTACTTGGCTGTGGTGGCATCCTCCCACAAGGGCAAGAAAGACAGCAGCATCACGCAAGGTCCATCTTTTGCCTACGGGGAGCTGGAAAAGCA
GCTTCTACAGGCAAACCCAATCCTGGAGGCTTTCGGCAATGCGAAAACCGTCAAGAACGACAACTCCTCTCGCTTTGGCAAGTTCATTCGCATCAACTTCGATGTCACTGGTTACATTGTAGGTGCCAATATTGAAACATATCTTCTGGAAAAGTCTAGGGC
TATTCGACAGGCTAGGGATGAGAGAACATTTCACATCTTCTACTACCTGCTCGCCGGAGCCAAGGAAAAGATGAAAAGTGACCTGCTTTTGGAGAGCTTCAACAGCTACACATTTTTATCCAATGGCTTTGTGCCCATCCCAGCTGCACAAGATGATGAGAT
GTTCCAGGAGACACTGGAAGCCATGTCTATCATGGGCTTCAATGAAGAGGAACAGCTAGCCATCTTGAAGGTAGTATCATCTGTCCTTCAGCTTGGAAACATTGTCTTCAAGAAGGAGCGAAACACAGACCAGGCATCCATGCCTGATAACACAGCGGCTC
AGAAAGTTTGCCACCTCGTGGGGATTAATGTGACAGATTTCACTAGAGCCATCCTGACCCCACGTATCAAAGTTGGACGGGATGTGGTGCAGAAGGCTCAGACCAAAGAACAGGCTGACTTTGCCATCGAGGCCTTAGCCAAGGCCACCTATGAGCGCCT
TTTCCGATGGATTCTCAGCCGTGTAAACAAGGCCTTGGACAAGACCCATCGGCAGGGGGCCTCCTTCCTGGGCATTCTGGATATTGCTGGGTTTGAAATCTTTGAGGTAAACTCCTTCGAGCAGCTGTGCATCAACTACACCAACGAGAAGCTGCAGCAGC
TGTTCAACCACACGATGTTCATCCTGGAGCAGGAAGAGTACCAGCGAGAGGGCATCGAGTGGAACTTCATCGACTTCGGCCTGGACCTGCAGCCTTGTATTGAGCTGATTGAGCGGCCGAACAACCCTCCCGGTGTGCTGGCCCTGCTGGATGAAGAATG
CTGGTTCCCCAAAGCTACAGACAAGTCTTTTGTGGAGAAGCTATGCTCAGAGCAGGGAAATCACCCCAAATTTCAGAAGCCCAAGCAGCTAAAGGACAAAACAGAGTTCTCCATCATCCACTATGCTGGGAAGGTGGACTACAATGCAAGTGCCTGGCTG
ACCAAGAACATGGACCCGCTAAATGACAATGTGACATCACTCCTCAATGCCTCCTCTGACAAGTTTGTGGCTGACCTGTGGAAGGATGTGGACCGCATTGTGGGGCTGGACCAGATGGCCAAGATGACTGAGAGCTCACTGCCCAGTGCCTCCAAGACCA
AAAAGGGCATGTTCCGCACCGTGGGCCAGCTCTACAAAGAGCAGTTGGGGAAACTGATGACTACACTGCGCAATACCACGCCTAACTTTGTGCGCTGCATCATCCCCAACCATGAGAAGAGGTCTGGCAAGCTGGATGCATTTCTAGTGCTGGAACAGCT
GCGCTGCAACGGTGTGTTGGAAGGCATCCGCATCTGCCGTCAGGGCTTCCCCAACAGGATTGTCTTCCAAGAGTTCCGGCAACGCTATGAGATCCTGGCAGCGAACGCCATCCCCAAAGGCTTCATGGATGGAAAGCAAGCCTGCATTCTCATGATCAAA
GCCCTCGAACTTGACCCTAACCTGTACAGGATTGGGCAGAGCAAAATCTTCTTCCGAACGGGGGTCCTGGCCCACCTAGAGGAGGAACGAGACCTGAAAATTACTGATGTCATCATGGCCTTCCAGGCAATGTGTCGTGGCTACCTTGCCAGAAAGGCCTT
CACCAAGAGGCAGCAACAGCTGACAGCCATGAAGGTGATCCAGAGGAACTGCGCTGCCTACCTTAAGCTCCGCAACTGGCAATGGTGGCGGCTCTTCACCAAAGTAAAGCCATTGCTCCAGGTGACACGGCAGGAGGAGGAGATGCAGGCCAAGGAGG
AGGAGATGCAAAAGATCAAGGAGCGGCAGCAGAAGGCAGAGACTGAGTTGAAGGAGCTGGAGCAGAAGCACACTCAGCTGGCTGAGGAGAAGACTCTGCTGCAGGAGCAGTTGCAGGCAGAGACAGAGCTGTATGCTGAGGCTGAGGAGATGCGG
GTCCGGTTGGCAGCCAAGAAGCAGGAACTGGAGGAGATCCTACATGAGATGGAGGCCCGCCTGGAGGAAGAGGAAGACCGGGGCCAGCAACTACAGGCTGAGAGGAAGAAGATGGCTCAGCAGATGCTAGACCTGGAGGAGCAACTGGAGGAGGA
AGAGGCCGCCAGACAGAAACTACAGCTAGAGAAGGTCACGGCTGAGGCCAAGATCAAGAAACTGGAGGATGACATCTTGGTTATGGATGATCAGAACAGTAAACTTTCAAAAGAACGAAAACTCCTTGAAGAGAGGGTCAGCGACTTGACAACCAACC
TAGCAGAAGAGGAAGAAAAGGCTAAAAACCTCACAAAGCTGAAGAGCAAGCATGAGTCTATGATCTCAGAGCTGGAGGTGAGGCTGAAGAAAGAGGAGAAGAGCCGGCAGGAGCTGGAGAAACTCAAGAGGAAACTGGAGGGTGATGCCAGTGACT
TCCATGAGCAGATCGCTGACTTGCAGGCCCAGATTGCAGAGCTCAAGATGCAGCTGGCAAAGAAAGAGGAAGAGCTACAGGCAGCTCTAGCCAGGCTTGATGAAGAGATCGCCCAGAAAAACAATGCCCTAAAGAAGATTCGCGAGCTAGAGGGCCAT
ATCTCAGACCTACAAGAGGACCTAGACTCAGAGCGGGCTGCCAGGAACAAGGCCGAGAAGCAGAAGCGAGACCTGGGGGAGGAGCTGGAGGCACTCAAGACGGAGCTGGAGGATACGCTGGACAGCACAGCTACCCAGCAGGAGCTCAGAGCCAAG
AGGGAACAGGAGGTGACAGTGCTGAAGAAGGCCCTGGATGAGGAGACGCGGTCCCATGAGGCCCAGGTCCAGGAGATGAGGCAGAAGCACACACAGGCAGTGGAGGAACTCACAGAGCAGCTGGAGCAGTTCAAAAGGGCCAAGGCAAACCTGGA
CAAAAGCAAGCAGACACTGGAGAAGGAGAACGCGGACCTGGCTGGGGAGCTGCGTGTCCTGGGCCAGGCGAAGCAGGAGGTGGAACACAAGAAGAAGAAGCTGGAGGTGCAGCTGCAGGATCTGCAGTCCAAGTGCAGTGATGGGGAGCGTGCCC
GGGCTGAGCTCAGTGACAAGGTCCACAAGCTACAGAATGAAGTGGAGAGTGTCACTGGCATGCTCAATGAGGCAGAGGGCAAAGCCATCAAACTGGCCAAAGATGTGGCTTCCCTTGGATCCCAGCTTCAGGACACCCAAGAGCTGCTCCAAGAAGAAA
CCCGGCAGAAGCTCAATGTGTCTACCAAGCTGCGTCAGTTGGAAGATGAAAGGAACAGCCTGCAGGACCAGCTGGATGAGGAGATGGAGGCTAAGCAAAACCTGGAGCGCCATGTCTCAACACTGAACATTCAGCTCTCAGACTCTAAGAAGAAGCTGC
AGGACTTTGCAAGTACCATCGAGGTCATGGAGGAGGGGAAGAAGAGGTTACAGAAAGAGATGGAGGGCCTCAGCCAGCAGTATGAGGAGAAGGCGGCTGCCTATGACAAACTGGAGAAAACCAAGAACAGGCTCCAGCAGGAGCTGGATGACCTGG
TCGTGGACTTGGACAACCAGCGGCAACTGGTATCCAATCTGGAAAAGAAGCAGAAGAAATTTGACCAGTTGTTAGCTGAGGAGAAGAACATCTCCTCCAAGTATGCGGATGAGAGAGACCGAGCTGAAGCAGAGGCCAGGGAAAAGGAGACAAAGGC
TTTGTCTCTAGCCCGGGCCCTGGAGGAAGCCCTGGAAGCCAAAGAAGAGCTGGAGAGGACCAACAAGATGCTCAAAGCTGAGATGGAAGACCTGGTCAGCTCCAAGGATGATGTAGGCAAGAACGTGCATGAACTGGAGAAGTCCAAGCGTGCCTTGG
AGACCCAGATGGAAGAGATGAAAACCCAGCTGGAGGAGTTGGAGGATGAGCTGCAGGCCACTGAGGATGCCAAGCTGCGGCTAGAGGTCAACATGCAGGCCCTCAAGGGCCAGTTTGAACGCGATCTCCAGGCTCGGGATGAACAGAATGAGGAGAA
GAGGAGGCAGCTACAGCGGCAGCTGCACGAGTATGAGACAGAACTGGAAGATGAACGGAAGCAGAGAGCTCTGGCGGCGGCAGCTAAGAAGAAGCTGGAAGGGGACCTAAAAGACCTAGAGCTCCAGGCTGACTCAGCCATCAAAGGGAGGGAGG
AAGCCATCAAGCAGCTTCGAAAACTGCAGGCTCAGATGAAGGACTTCCAAAGAGAGCTGGATGATGCCCGTGCCTCCAGGGATGAGATCTTTGCCACCTCAAAAGAGAATGAGAAGAAAGCCAAGAGTCTGGAGGCAGACCTCATGCAGCTCCAAGAG
GACCTGGCAGCAGCTGAGAGAGCTCGCAAGCAAGCTGACCTGGAGAAGGAGGAGCTGGCCGAGGAGCTGGCTAGCAGCTTGTCAGGAAGGAATACACTGCAGGATGAGAAGCGCCGCCTGGAGGCAAGGATCGCCCAACTAGAGGAGGAGCTGGAG
GAAGAGCAGGGCAACATGGAGGCCATGAGTGATAGAGTACGCAAGGCCACACTGCAGGCTGAGCAACTGAGCAATGAGCTGGCCACAGAACGCAGCACGGCTCAGAAGAATGAGAGCGCACGGCAACAGCTGGAGCGCCAGAACAAGGAACTGCGA
AGCAAGTTGCAGGAGGTAGAAGGTGCTGTCAAAGCCAAGCTCAAGTCCACTGTTGCGGCGCTGGAGGCCAAGATTGCACAGCTGGAGGAGCAGGTTGAACAGGAGGCCAGAGAGAAACAGGCGGCCACCAAGTCGCTGAAGCAAAAGGACAAGAAG
CTAAAGGAGGTCCTGCTGCAGGTGGAGGATGAGCGCAAGATGGCAGAGCAGTACAAGGAGCAGGCAGAGAAAGGAAACACCAAGGTCAAGCAGCTGAAGAGGCAGCTGGAAGAGGCAGAGGAGGAGTCCCAGCGCATCAACGCCAACCGCAGGAA
GCTGCAGCGGGAGCTAGATGAGGCCACAGAGAGCAATGAGGCCATGGGCCGTGAGGTGAACGCCCTCAAGAGCAAACTCAGAGGGCCCCCCCCACAGGAAACTTCGCAGTGAGCCACCAGGAGAGGAAACGAGGCTTCATTTGTTCCTTCCAGAAGGG
CTGGGGGCCGTAGAGTTATTGAAAACACAGATGGTTCTGAAGAAGAAATGGACGCTCGGGACTCAGACTTCAATGGAACCAAAGCCAGTGAATAAATTCAGGATTGGACACCATGTCAGGGAAAACAGAACACTAAACGACAGCAGAGCCCAGCAGAC
TGCTTAGCACTTGTGTCCATTCGTTCTCAAGTCACAGAAATCACTCCACCCCTCACCAGGAGTCAACCACAGCCCTGCACAAAGGGTGTGAATTCAAGTTCTTAGATGGGCTATCAGAGAAAAATCCAAATAAGACGTACAGGTCAGGAGCCACAGTCACCA
GCAACTTTGTTTACATGAAATGAGGAAGTTACATGAATGGGTGCCACAGCCCCCAACCCACTCCCAACCTTTCCCTGACCTGCCTGACCTTCCAGTTTGGGAGGAAATCCCGTTTGAAAATTCCCTTCCCTTTCCTGCCTGCCACACCTCAGACACACAGTTCA
CTTCGCCCAAGTGACTTTTTTAGTCATCTGAATTAAAAAAAGAAACACTGCTCCCAGAGCGAGCGGAGCAGAGCAATCACACTTATTTGCACCCATGGTCACTTTCACTAATAAAAGGTTGTAAGTCACGAGAAA

B.2 Human primer

Homo sapiens myosin heavy chain 11 (MYH11), RefSeqGene on chromosome 16

Sequence ID: NG_009299.1 Length: 160896 Number of Matches: 1

Range 1: 24124 to 24143 GenBank Graphics ▼ Next Match ▲ Previous Match

Alignment

A BLAST search was carried out prior to alignment. The reverse complement of the Synthesized primer sequences was generated. The primer set was then aligned to the respective *MYH11* promoter sequence.

Homo sapiens myosin, heavy chain 11, smooth muscle isoform 1 (MYH11) gene, ...	Homo sapiens	40.1	40.1	100%	0.64	100.00%	157896	GU143399.1
Homo sapiens myosin heavy chain 11 (MYH11), RefSeqGene on chromosome 16	Homo sapiens	40.1	40.1	100%	0.64	100.00%	160896	NG_009299.1

-500 bp UST 5' MYH11 human
caaagttcaagaaatccccttccctaccttcacgctgcacagccggcc
ctctttccagacagtgcgatgccaataaaatgggaagtggggtgggagat
gtcaagtcagatccaccacagccccgacacggggaggaagaggttaaagc
ctttgcggccggaaccgactcagggaagacgttctcaagcatcccgcaca
gacactgcctgctcgacccccttttctctagggatccggagcgtctgcgac
cgcctggggccggggctgagactcccgtccctgtgcgcacctgttccgtg
cgcccttgtgcggtgcgcacctgttccgtgcacccttgtcccgagcgccc
cagctccttgcgctcccgccgggggtgcgccctgcaggggcgcggcgag
ggggccgcgagggaccctccccaactccacccccttcggcctcctcccctt
tcccagccgcgggcagctccgggtctataaagagaggcgtccgaggacgc

>*MYH11* Forward
GTGAGTATTGCAGGCAGCCA
>REVCOMPLEMENT
TGGCTGCCTGCAATACTCAC
>*MYH11* REVERSE
CTCCCAACACATTTCTAATGCCT
>Reverse-Complement of Reverse
AGGCATTAGAAATGTGTTGGGAG
CTCCCAACACATTTCTAATGCCT
GTGAGTATTGCAGGCAGCCAggtacctactcctggcctcataaggaaagt
AGGCATTAGAAATGTGTTGGGAG

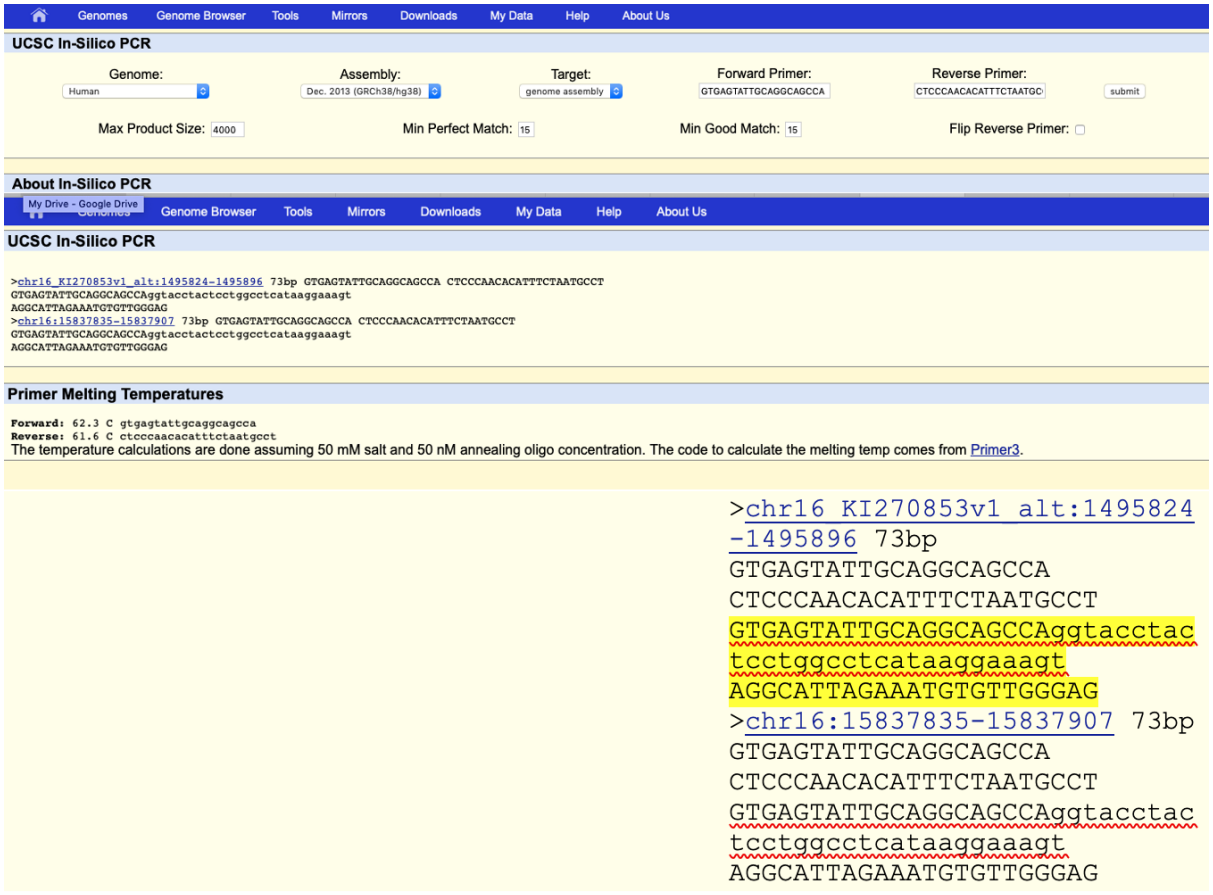

>chr16_KI270853v1_alt:1495824-1495896 73bp
GTGAGTATTGCAGGCAGCCA
CTCCCAACACATTTCTAATGCCT
GTGAGTATTGCAGGCAGCCAggtacctac
tcctggcctcataaggaaagt
AGGCATTAGAAATGTGTTGGGAG
>chr16:15837835-15837907 73bp
GTGAGTATTGCAGGCAGCCA
CTCCCAACACATTTCTAATGCCT
GTGAGTATTGCAGGCAGCCAggtacctac
tcctggcctcataaggaaagt
AGGCATTAGAAATGTGTTGGGAG

```
20401 acctcggcct cccacagtgt tgggtttaca ggtgtgagcc accttgtcca gccctacttc
20461 ctgcctcctg agcactgggt agtatttcac agtgtggaaa tagcatggct tatgtatcca
20521 gctgtatgtt ggtggacatt tgggttgtct gacttttggt attttaggcg atgacacaca
20581 tccctttctg aagggccttt gggtggtctc tgttctttga ccacatacac aatactgcag
20641 gtctttgtac ttggtgggat gtctctgcag accgagttcc tagacagggc aaggtgagtg
20701 gttggtctgt cttccgggct tggttgtggt ctgattctga ccctgttacc ttattccaca
20761 ggggaccaac aaggcaccat ggcgcagaag ggccaactca gtgacgatga gaagttcctc
20821 tttgtggaca aaaacttcat caacagccca gtggcccagg ctgactgggc cgccaagaga
20881 ctcgtctggg tcccctcgga gaagcagggc ttcgaggcag ccagcattaa ggaggagaag
20941 ggggatgagg tggttgtgga gctggtggag aatggcaaga aggtcacggt tgggaaagat
21001 gacatccaga agatgaaccc acccaagttc tccaaggtgg aggacatggc ggagctgacg
21061 tgcctcaacg aagcctccgt gctacacaac ctgagggagc ggtacttctc agggctaata
21121 tatgtgagta ttgcaggcag ccaggtacct actcctggcc tcataaggaa agtaggcatt
21181 agaaatgtgt tgggaggget gggcacagtg gctcatgcct gtactcccag cactttggga
21241 ggccgaggtg ggcagatcac ctgaggtcag aagttcgaga ccacgctggc caacatgatg
21301 aaatgccgtc tctactaaaa atacaaaaag tagccaaggg tggtggtgcg catctgtaat
21361 cccagctact ggggaggctg gggcagagga attgcttgaa tccaggaggt ggaggtgcag
21421 tgagccaaga ctgtaccact gcactccagc ctgggtgaca gaataagact ctgtctcaaa
21481 aaaaaaaaaa aaggaaatgg gaggctgaag gtttgatcga gggagattgc aagatgaggt
21541 ggaatcattc caaggtgggt tcacatctca gcccttgaag aggttatttc ctctctcgaa
21601 gccttggttt tcctatccgt aaaatgggaa taatcaccct cattacagac aggaggtgtg
21661 acaatcccat gtcatcacat gtgccaagtg ccaagacgta tgataaactc tcaacagatt
21721 tcattggcat cgttctctgt ccttccttcc tcttgaaagt aaagaagagc tcataaccac
21781 tttggaaagg ctggtttgtc ttggcagcca ggtgggtagg agacatgagg atgtggctag
21841 gttttaggga ggccttcctt gtcacagagg ggaatgttca ggttggtcgt aggactattt
21901 taggtagact tgcagaacag agtggactag agatggcaca atatggtagc cactggccac
```

Appendix C

C.1 mMSC ChIP-seq summary of peaks

Supplementary table S1. Peak scores for enrichment for H3K4me1 in Undifferentiated mMSC

#sum	mean	stdev	0%	25%	50%	75%	100%
2.561080 6	89.227	113.899	1.34979	5.26648	15.9051	169.594	546.296

Gene	**chr**	**start**	**end**	**-log10(qvalue)**
Tagln	chr9	45935325	45935077	24.57798
Cnn1	chr9	22099206	22100593	18.49409
Smtn	chr11	3535203	3540046	228.43732
Lpl	chr8	68880177	68882648	172.35774

Supplementary table S2. Peak scores for enrichment for H3K4me3 in Undifferentiated mMSC

#sum	mean	stdev	0%	25%	50%	75%	100%
2.490270 6	158.002	135.437	1.89637	32.7458	131.909	252.128	854.419

Gene	**chr**	**start**	**end**	**-log10(qvalue)**
Tagln	chr9	45934066	45936049	30.20814
Cnn1	chr9	22099461	22100632	21.70778
Smtn	chr11	3537282	3539890	268.50668

Supplementary table S3. Peak scores for enrichment for H3K4me3 in myogenic differentiated mMSC

#sum	mean	stdev	0%	25%	50%	75%	100%
2.336620 6	35.5222	60.9846	1.32584	5.67924	9.60949	31.8744	640.14

Gene	chr	start	end	-log10(qvalue)
Myh11	chr16	14292305	14293078	12.00682
Tagln	chr9	45935205	45937135	12.29926
Cnn1	chr9	22100867	22101781	9.43933
Smtn	chr11	3534882	3540115	140.54915

Supplementary table S4. Peak scores for enrichment for H3K4me3 in Vasculogenic differentiated mMSC

#sum	mean	stdev	0%	25%	50%	75%	100%
2.1428506	107.665	100.566	1.565	19.5696	69.0161	184.047	437.331

Gene	chr	start	end	-log10(qvalue)
Tagln	chr9	45934237	45935866	67.26181
Smtn	chr11	3538541	3539282	168.62691
Pecam1	chr11	106713791	106715221	58.73271

Supplementary table S5. Peak scores for enrichment for H3K4me1 in Adipogenic differentiated mMSC

#sum	mean	stdev	0%	25%	50%	75%	100%
883909	7.45186	4.68319	1.91961	4.53047	6.30528	9.07016	267.064

Gene	chr	start	end	-log10(qvalue)
Myh11	chr16	14280073	14280384	3.46915
Tagln	chr9	45931343	45933016	8.59474
Smtn	chr11	3536083	3536648	8.32917
Lpl	chr8	68878958	68879280	3.12909

Supplementary table S6. Peak scores for enrichment for H3K4me3 in Osteogenic differentiated mMSC

#sum	mean	stdev	0%	25%	50%	75%	100%
28933.3	14.1969	30.4018	1.65504	3.71819	5.221	9.48383	341.124

Gene	**chr**	**start**	**end**	**-log10(qvalue)**
My11	chr16	14316353	14316810	3.38687
Smtn	chr11	3536100	3536356	2.31603
Sost	chr11	101963847	101964360	4.43376

C.2 hMSC ChIP-seq summary of peaks

Supplementary table S7. Peak scores for enrichment for H3K4me1 in undifferentiated hMSC

hMSC H3K4me1

#sum	mean	stdev	0%	25%	50%	75%	100%
1.5852406	7.1762	4.12191	1.35141	4.19439	6.08812	9.04874	337.519

Gene	**chr**	**start**	**end**	**-log10(qvalue)**
MYH11	chr16	15790308	15790582	3.56540
TAGLN	chr11	117201710	117202493	5.18705
CNN1	chr19	11538708	11539018	4.21736
SMTN	chr22	31080515	31080896	5.15989
LPL	chr8	19961755	19963074	5.53061

Supplementary table S8. Peak scores for enrichment for H3K4me1 in undifferentiated H9 hESC

H9 hESC H3K4me1

#sum	mean	stdev	0%	25%	50%	75%	100%
465037	4.35204	1.89953	1.30302	3.11634	3.94418	5.16849	72.9255

Gene	chr	start	end	-log10(qvalue)
TAGLN	chr11	117198498	117198707	4.34637
CNN1	chr19	11540239	11540560	3.57255
SMTN	chr22	31096616	31096809	4.62993
SOST	chr17	43759416	43759596	5.39254

Supplementary table S9. Peak scores for enrichment for H3K4me2 in undifferentiated H9 hESC

H9 hESC H3K4me2

#sum	mean	stdev	0%	25%	50%	75%	100%
214641	7.24209	3.53286	1.30366	4.65799	6.39893	9.04559	36.6636

Gene	chr	start	end	-log10(qvalue)
TAGLN	chr11	117199367	117199580	5.66706
SMTN	chr22	31084536	31084738	7.19648

Supplementary table S10. Peak scores for enrichment for H3K4me3 in undifferentiated hMSC

#sum	mean	stdev	0%	25%	50%	75%	100%
1.4744111	7.643407	4.8244807	13133	3.5578707	7.5905307	11.1351908	100.9706808

Gene	chr	start	end	-log10(qvalue)
TAGLN	chr11	117071343	117071398	3.95380

Supplementary table S11. Peak scores for enrichment for H3K4me2 in Myogenic differentiated hMSC

hMSC myogenic differentiated H3K4me2

#sum	mean	stdev	0%	25%	50%	75%	100%
1.004390 6	8.80785	7.58457	1.36671	3.98499	6.00725	10.4987	189.836

Gene	**chr**	**start**	**end**	**-log10(qvalue)**
MYH11	chr16	15850716	15850968	3.98389
TAGLN	chr11	117072277	117072833	2.64583
CNN1	chr19	11649738	11650497	11.29840
SMTN	chr22	31480229	31480731	7.31818

Supplementary table S12. Peak scores for enrichment for H3K4me2 in Vasculogenic differentiated hMSC

#sum	mean	stdev	0%	25%	50%	75%	100%
31576 2	13.2679	7.40878	1.30163	7.37079	12.1662	17.9862	228.024

Gene	**chr**	**start**	**end**	**-log10(qvalue)**
TAGLN	chr11	117069786	117070195	6.82105
SMTN	chr22	31476852	31477184	9.94290
CD34	chr1	208083146	208084752	9.19971

Supplementary table S13. Peak scores for enrichment for H3K4me1 in Adipogenic differentiated hMSC

#sum	mean	stdev	0%	25%	50%	75%	100%
1.802030 6	7.95322	4.75426	1.58875	4.68607	6.61407	9.88484	274.094

Gene	chr	start	end	-log10(qvalue)
MYH11	chr16	15790452	15790786	3.43775
TAGLN	chr11	117201850	117202507	4.55016
CNN1	chr19	11538807	11539231	4.35392
SMTN	chr22	31082214	31082712	4.52316
LPL	chr8	19944871	19945237	10.07188

Supplementary table S14. Peak scores for enrichment for H3K4me1 in Osteogenic differentiated H9 hESC.

#sum	mean	stdev	0%	25%	50%	75%	100%
2.3910206	11.7521	8.45788	1.35994	5.88434	9.14939	14.8972	161.596

Gene	chr	start	end	-log10(qvalue)
MYH11	chr16	15835157	15835673	5.79385
TAGLN	chr11	117200654	117201510	8.54673
CNN1	chr19	11538357	11538745	6.69378
SMTN	chr22	31084319	31084606	4.32476
SOST	chr17	43755462	43755863	7.53916

Appendix D

D.1. mMSC ChIP-seq peaks for osteogenic gene loci following adipogenic stimuli.

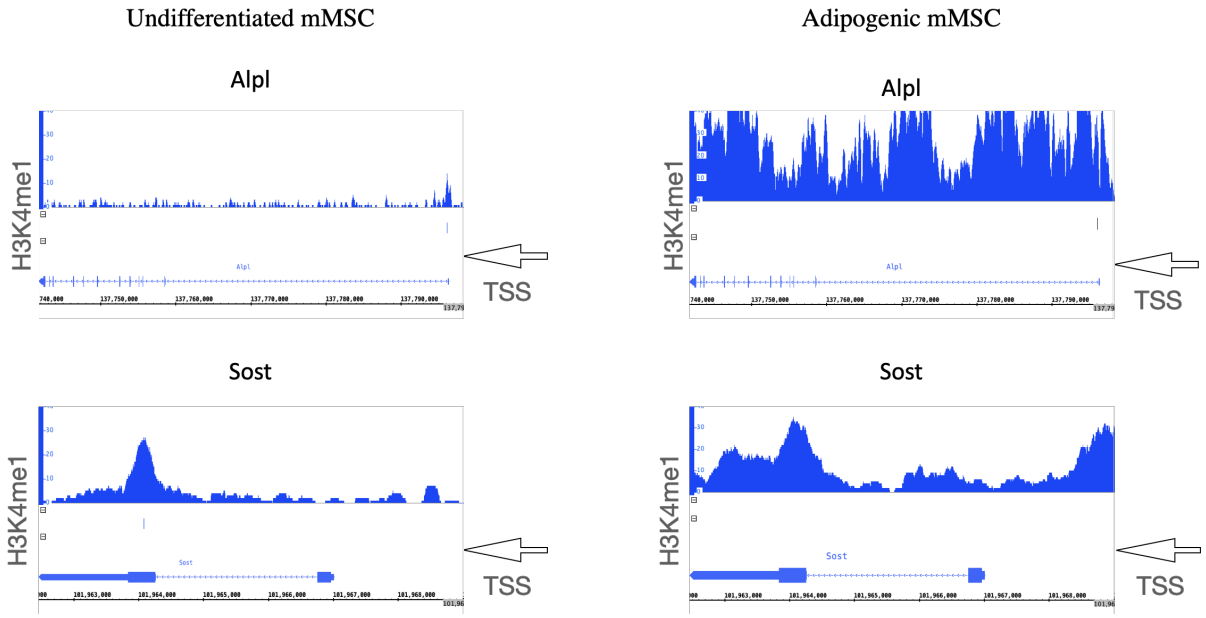

Supplementary Figure S2. ChIP-seq peak calling for H3K4me1 at the *Alpl and Sost* gene loci in undifferentiated mMSC and following adipogenic differentiation of mMSCs.

D.2. mMSC ChIP-seq peaks for adipogenic gene loci following osteogenic stimuli.

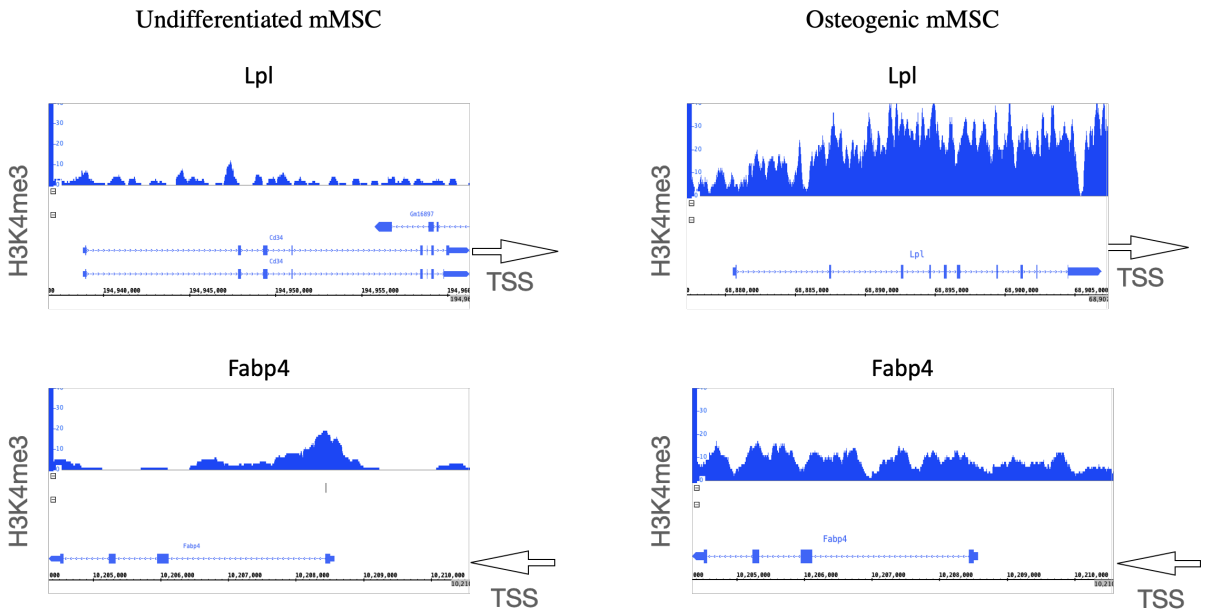

Supplementary Figure S3. ChIP-seq peak calling for H3K4me3 at the *Lpl and Fabp4* gene loci in undifferentiated mMSC and following osteogenic differentiation of mMSCs.

D.3. hMSC ChIP-seq peaks for osteogenic gene loci following adipogenic stimuli.

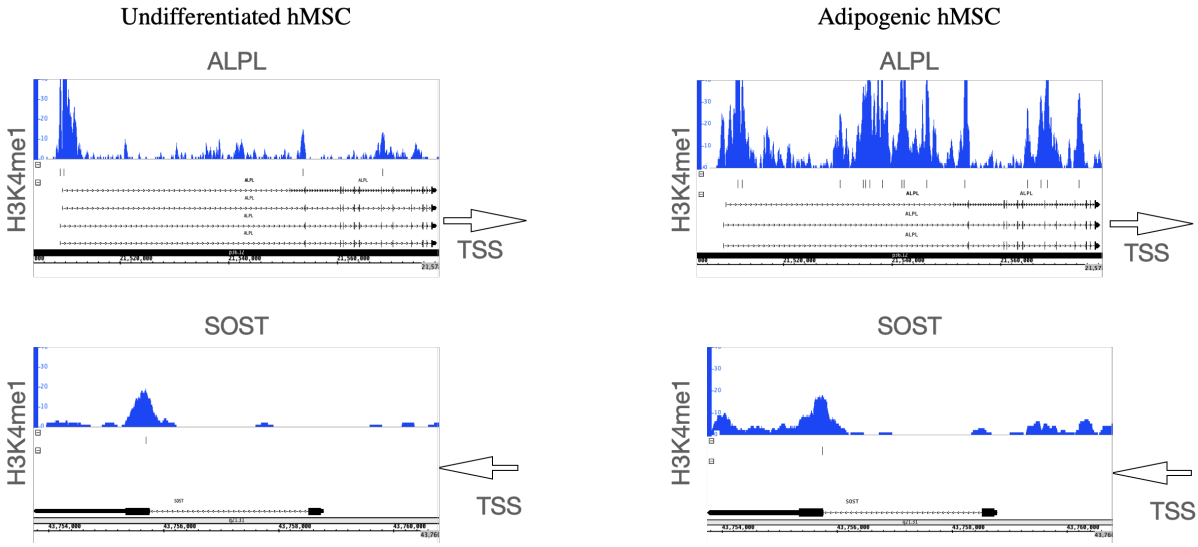

Supplementary Figure S4. ChIP-seq peak calling for H3K4me1 at the *ALPL and SOST* gene loci in undifferentiated hMSC and following adipogenic differentiation of hMSCs.

D.4. hESC ChIP-seq peaks for adipogenic gene loci following osteogenic stimuli.

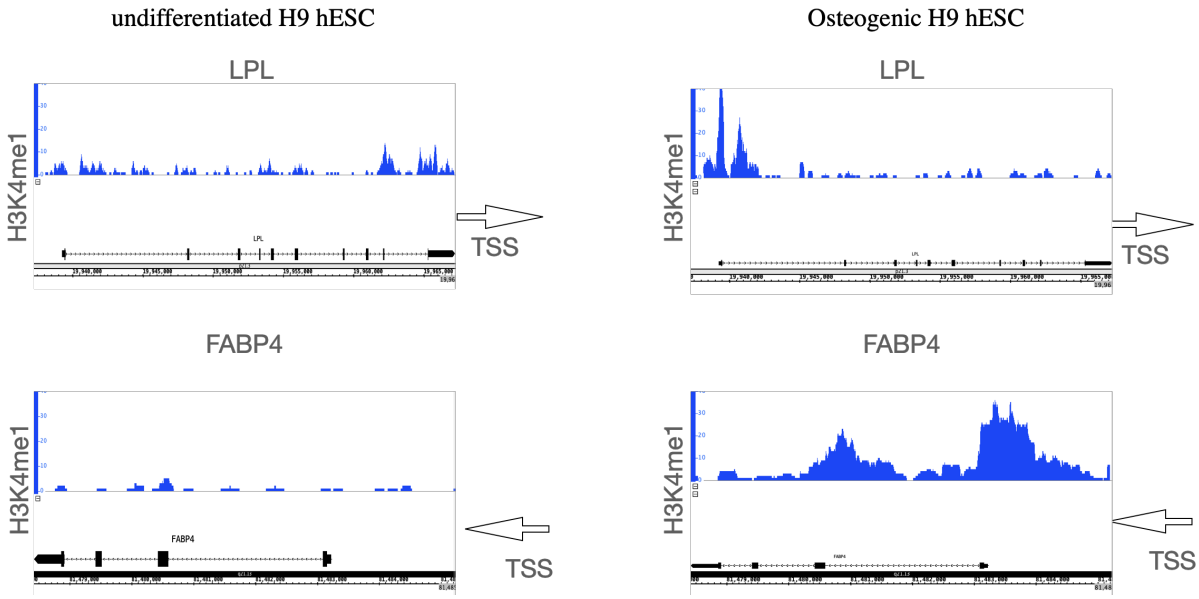

Supplementary Figure S5. ChIP-seq peak calling for H3K4me1 at the *LPL and FABP4* gene loci in undifferentiated H9 hESCs and following osteogenic differentiation of H9 hESCs.

Appendix E

Supplementary table S15. Collagenase/Elastase Solution.

Stock Solutions/Powders	**Final Concentrations**	**Volumes/Weights in 2ml**
MEM α nucleosides GlutaMAXTM Supplement		2 ml
Soybean Trypsin inhibitor (50 mg/ml)	0.4 mg/ml	16µl
Bovine Serum Albumin	1 mg/ml	2mg
Collagenase type 1A (125 Units/mg)	0.7 mg/ml	1.4 mg
Elastase Type III	0.25 mg/ml	0.5 mg